CLIMATE CHANGE
AGRICULTURE AND FOOD SECURITY

CGIAR Research Program on
Climate Change, Agriculture and Food Security (CCAFS)

Climate Change in West African Agriculture: Recent Trends, Current Projections, Crop-Climate Suitability, and Prospects for Improved Climate Model Information

February 2012

Richard Washington & Matt Hawcroft

CGIAR

Earth System Science Partnership
DIVERSITAS IGBP IHDP WCRP

UNIVERSITY OF OXFORD

Correct citation:

Richard Washington & Matt Hawcroft. 2012. Climate Change in West African Agriculture: Recent Trends, Current Projections, Crop-Climate Suitability, and Prospects for Improved Climate Model Information. CGIAR Research Program on Climate Change, Agriculture and Food Security (CCAFS). Copenhagen, Denmark. Available online at: www.ccafs.cgiar.org.

Published by the CGIAR Research Program on Climate Change, Agriculture and Food Security (CCAFS).

CCAFS Coordinating Unit - Department of Agriculture and Ecology, Faculty of Life Sciences, University of Copenhagen, Rolighedsvej 21, DK-1958 Frederiksberg C, Denmark. Tel: +45 35331046; Email: ccafs@cgiar.org

Abstract

The climate of West Africa is investigated and the implications of climate change on agriculture are assessed, with a particular focus on those aspects that may have greatest impact on the crops currently grown in the region. The ability of General Circulation Models (GCMs) to reproduce the observed climate was investigated, to establish how reliable future climate and associated crop growth projections might be. The influences and interactions that control the region's climate are complex and models have difficulty in simulating the observed climate. Projections for changes in crop cultivation limits are variable over space and time, and so the outlook for agriculture is highly uncertain, particularly in the vulnerable Sahel region. Insufficient observational records constrain the accuracy of reanalysis and gridded data, making the identification of local trends and mechanisms difficult. In addition, there is wide divergence in model projections for the region's climate by the end of this century. This poses a significant challenge to designing agricultural adaptation strategies.

Keywords

General Circulation Model; climate; crop suitability; Sahel; adaptation.

About the authors

Richard Washington is Professor of Climate Science at the School of Geography and the Environment and Fellow of Keble College, University of Oxford. His research interests are in climate change and variability, particularly in Africa and the global tropics. He has degrees from the University of Natal and University of Oxford and taught at the University of Natal and University of Cape Town. His doctorate was on African rainfall variability and change, which was undertaken jointly between the University of Oxford under Professor Alayne Street-Perrott and Chris Folland's group at the Hadley Centre of the UK Meteorological Office. He took up a University Lectureship position and Fellowship at Keble College in 1999, and a Readership in 2006. Richard is Co-Chair World Climate Research Program African Climate Variability Panel (CLIVAR-VACS) 2006-2010 and served as a panel member of CLIVAR-VACS from 2003-2006. Richard leads the development of the CLIVAR Africa Climate Atlas. **Contact:** richard.washington@ouce.ox.ac.uk

Matt Hawcroft has degrees in law from the University of Cambridge and geography from the University of Oxford. He co-authored this report whilst working as a research assistant in the School of Geography and the Environment, Oxford. He is now at the Department of Meteorology, Reading University where he is reading for a PhD analysing processes associated with latent heat release in mid-latitude cyclones. His broader interests remain widely focussed on many aspects of climate and climate change. **Contact:** M.K.Hawcroft@pgr.reading.ac.uk

Contents

Acronyms

5DD	5-or-more dry days
AMMA	African Monsoon Multidisciplinary Analysis
AMO	Atlantic Multidecadal Oscillation
CDD	Consecutive dry days
CRU	University of East Anglia's Climatic Research Unit
GCMs	General circulation models
GHG	Greenhouse gas
IPCC AR4	Intergovernmental Panel on Climate Change Fourth Assessment Report
IPO	Inter-decadal Pacific Oscillation
ITCZ	Intertropical convergence zone
RCM	Regional climate model
SST	Sea surface temperature
WAMME	West African Monsoon Modelling and Evaluation

1. Introduction

The region selected for this report is shown in Figure 1.1 and represents an area of approximately 7.5m km^2. The climate of the region varies, approximately meridionally, from the tropics of the Gulf of Guinea coastline in the south to the Sahara desert in the north. As such, the regional climate exhibits high spatial variability. Much research focus has been on the Sahel, a band of water stressed but populated land stretching across the southern boundary of the Sahara which has experienced severe drought conditions over much of the last 40 years (Hulme 1992; Nicholson et al. 1998, 2000; Dai et al. 2004).

Figure 1.1: The West Africa region covered by Benin, Burkina Faso, Chad, Cote D'Ivoire, Gambia, Ghana, Guinea Bissau, Guinea, Liberia, Mali, Mauritania, Niger, Nigeria, Senegal, Sierra Leone and Togo. Mask set at 1°x1° resolution.

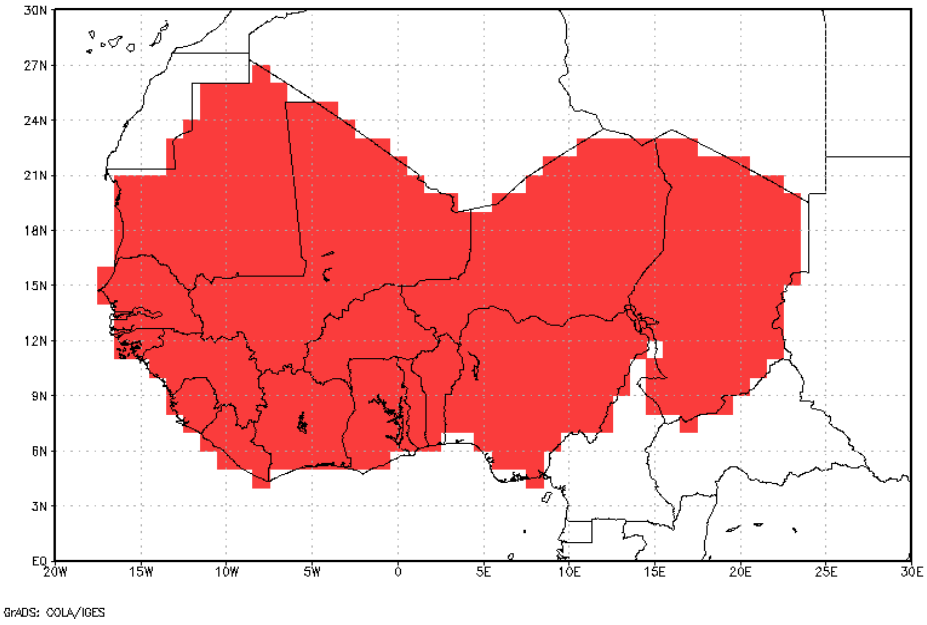

In Section 2, this report will begin by introducing the climate of the region, the seasonal cycle which characterises the climate and observed trends in both the overall climate and certain extremes of climate which are relevant to regional agriculture. The quality of observed gridded data and reanalysis data will also be assessed. In Section 3 the primary food crops produced in the region will be introduced and the current spatial extent of their production and the climatic thresholds which those crops are capable of withstanding will be discussed. The regions where, based on these thresholds, growth of these crops should be possible are

mapped to aid discussion. In Section 4 the ability of certain general circulation models (GCMs) taken from the CMIP3 dataset to reproduce the regional observed climatology, observed climatic variability and any key observed trends general circulation models is assessed. In Section 5, the thresholds identified in Section 3 are then applied to the model output to provide an assessment of the magnitude of model error in simulating the regional climate and the impact this has on the location and extent of the crop growth domains in comparison to those taken from observed and reanalysis data. In Section 6, projections of regional climate change are discussed. The robustness and uncertainty of projections derived from GCM and regional model experiments is interrogated, before the performance of the models used in this study is analysed. In Section 7, using data from 21st century climate scenarios of the selected GCMs, the threshold analysis applied in Sections 3 and 5 will be repeated. This will allow an assessment of the possible impact of climate change on food production in the region, specific to the primary crops, in addition to analysis of general trends in the climate which are relevant to food production. Any divergence in these projections due to model or emissions uncertainty will be highlighted. Section 8 will conclude by summarising the research outcomes of the report and the key conclusions which can be drawn from this work.

2. The Observed Climate of West Africa

In this section, the background climate of West Africa will be outlined, with particular focus on the seasonal cycle of precipitation—the dominant characteristic of the region's climate—and temperature. In addition, climatic variability will be discussed and observed trends in the climate will be analysed. The complex nature of the climate of West Africa makes it challenging for reanalysis and GCMs to accurately capture the temporal and spatial variability which is observed in the region (Cook and Vizy 2006; Turner et al. 2009), an issue that is further investigated in Section 4.

2.1 Description of datasets

Details of the observed and reanalysis datasets used in this study are in Table 2.1. Observed temperature data is taken from the University of East Anglia's Climatic Research Unit (CRU) gridded dataset which has a spatial distribution of 0.5°x0.5°, or just over 55 km at the

Equator. Initially, three reanalysis precipitation datasets were investigated. The paucity of station data, particularly in the Sahel and Sahara, make verification of the reanalysis data in this region challenging. As such, this introduces a degree of uncertainty into the analysis. The three datasets were analysed, with particular focus on their reproduction of Sahelian precipitation. It was found that the NCEP and JapRe datasets were the driest and wettest of the three datasets, respectively. In addition, the intraseasonal pattern of precipitation in the datasets was inhomogenous, with the greatest variability in the JapRe dataset and the most consistent precipitation across the key monsoon season in the NCEP dataset. In both cases, the ERA dataset was found to be the median product. As a result, the NCEP and JapRe datasets have been used for the remainder of this study, since they provide a degree of uncertainty with respect to the baseline climate state in the region which impacts both on model verification and future crop growth projections.

Table 2.1: Observed and reanalysis data used in this report

Data	Data set	Period available	Resolution	Key Papers
Land surface temperature	CRU TS2.1 (CRU)	1901-2002	0.5° x 0.5°	Mitchell and Jones 2005
Precipitation and temperature	National Centre for Environmental Prediction (NCEP)	1948-2010	1° x 1°	Kalnay et al. 1996
Precipitation	Japanese Reanalysis (JapRe)	1948-2006	0.5° x 0.5°	Hirabayashi et al. 2008
Precipitation	ERA-40 (ERA)	1960-2002	2.5° x 2.5°	Uppala et al. 2005

2.2 West African climate – the basic state

The climate of West Africa is dominated by the monsoon. Coastal regions experience a bi-modal precipitation season, with most intense precipitation at the start and end of the year, with more northerly, inland regions receiving greater precipitation during the summer monsoon months (Grist and Nicholson 2001; Le Barbe et al. 2002; Nicholson and Grist 2003). It has been debated whether the core monsoon rains are best characterised as a northward migration of the intertropical convergence zone (ITCZ) or are produced by a separate, independent feature (Zhang et al. 2006; Mohr and Thorncrof 2006; Nicholson 2009). What is clear is that the seasonal cycle is driven by a complex interplay between a variety of influences including sea surface temperatures (SSTs)—from local, regional and global

patterns of SST and the overall trend associated with global warming (Ward 1998; Vizy and Cook 2001, 2002; Gu and Adler 2004; Hoerling et al. 2006; Mohino et al. 2010), the evolution and variability of the Saharan heat low (Haarsma et al. 2005; Lavaysse et al. 2009; Biasutti et al. 2009), the African Easterly Jet and Tropical Easterly Jet (Sultan and Janicot 2003), the West African Westerly Jet (Godsky et al. 2003; Pu and Cook 2010) and regional dust fluxes (Nicholson 2000; Prospero and Lamb 2003; Yoshioka et al. 2007; Konare et al. 2008). These mechanisms are interdependent and provide feedbacks to other components of the regional climate (Webb et al. 2006; IPCC 2007; Wilby 2009). The mechanisms through which many of these different components are connected are also still open to debate, with, for example, the suggested mechanism for the interaction between the evolution of the Saharan heat low and the onset of the monsoon in the Sahel having several competing explanations (Sultan and Janicot 2003; Ramel et al. 2006; Sijikumar et al. 2006).

The monsoon period, from late June to September, provides 75–90% of the total annual precipitation in the Sahel (Lebel et al. 2003), with much of any remaining precipitation occurring in isolated events. The monsoon rains in this area are initiated by the so-called monsoon "jump" in late June, when the locus of intense precipitation rapidly switching from 5°N through 10°N at this time (Sultan and Janicot 2003; Hagos and Cook 2007), an event preceded by the migration of the heat low from 11–15°N to 20°N (Ramel et al. 2006).

In recent decades, decreased precipitation and drought in the Sahel has become a particular focus for research as it represents one of the largest recent observed climate changes of any region (Dai et al. 2004). This shift, which occurred in the late 1960s and is readily observed in Figure 2.5, the mechanisms which caused it, and the possibility that it may be coming to a conclusion remain a challenge to explain (Cook 2008) and will be further discussed below.

2.2.1 Temperature

Figure 2.1 shows plots of the wider regional temperature climatology for the period 1970–99 and the seasonal cycle. Within the study domain, the annual temperature cycle has greatest magnitude in the Sahara and is dictated by the northward migration of the most intense insolation towards boreal summer. Average temperatures during June and July exceed 35°C in the Sahara and the annual cycle is in excess of 10°C. In coastal regions the annual temperature cycle is far less pronounced, characterised by warmer temperatures in the spring and a cooler summer as the locus of intense precipitation (and the ITCZ) moves northward

with the monsoon. A second, smaller, temperature peak is observed as the monsoon retreats. The seasonal temperature cycle in much of the tropical coastal regions is less than 5°C with a climatological temperature of around 25°C.

Figure 2.1: Annual and monthly observed temperature climatology for the region

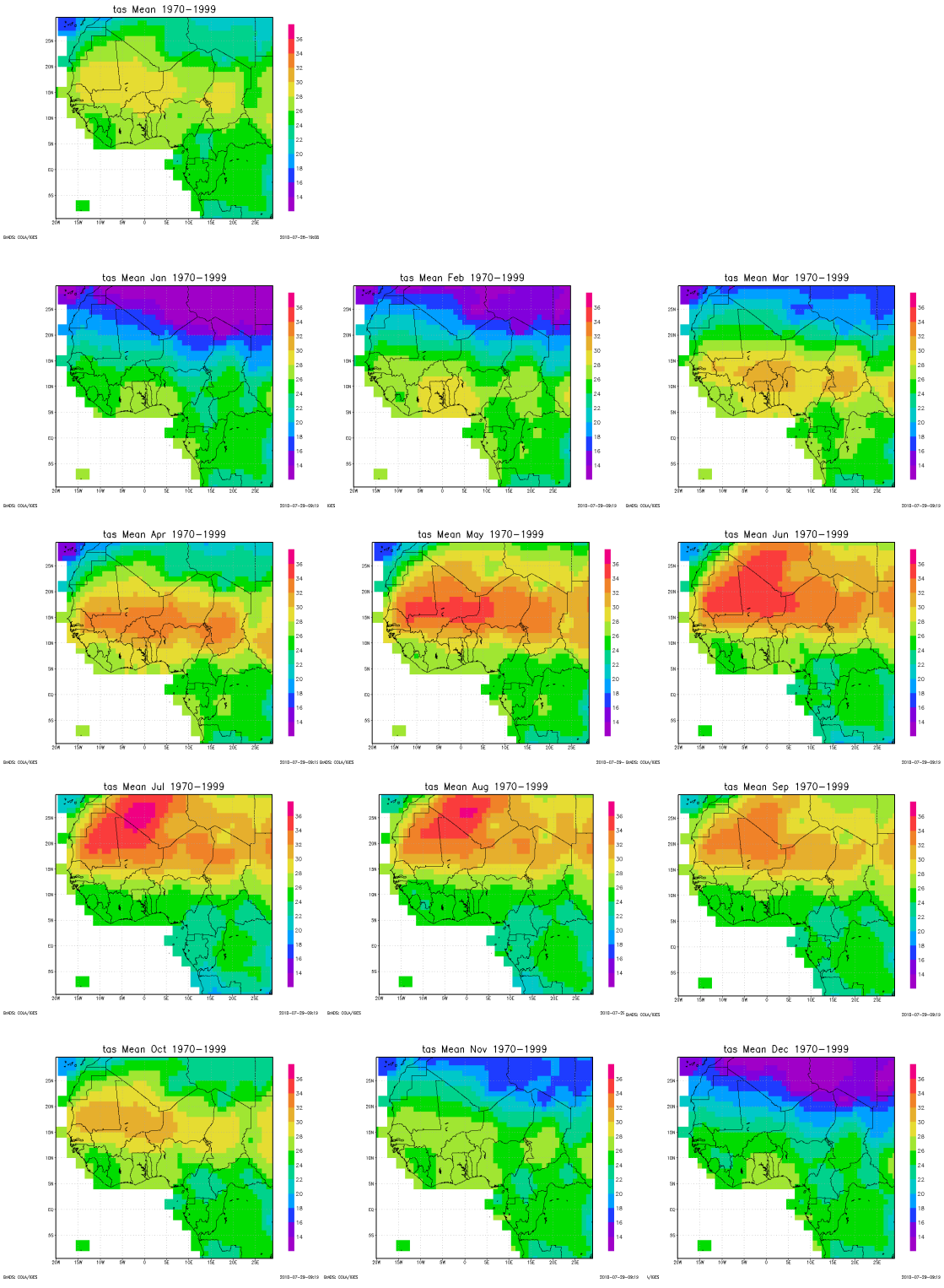

2.2.2 Precipitation

Figure 2.2 shows plots of the regional precipitation climatology for the period 1970–99. The data in Figure 2.2(a) is taken from the NCEP reanalysis and Figure 2.2(b) from the JapRe dataset. The higher intensity precipitation produced in the JapRe dataset is clearly visible in the peak precipitation locations at the coast. Furthermore, the climatological monsoon rains push further north through the Sahel in the JapRe data compared to the NCEP data. The ERA dataset (not shown) produced the most intense local precipitation peaks of the three datasets in the Guinea/Cameroon areas, but produces an intensity in the climatological cycle between the NCEP and JapRe datasets in the Sahel and other regions away from the coast.

It is evident that the monsoon cycle dominates the annual pattern of precipitation in the region. In the tropical coastal regions, the most intense precipitation is observed to shift inland in the summer, though precipitation remains relatively consistent across the year as the boundaries of the band of most intense precipitation do not stray far from the coast. Advancing northwards, the annual cycle becomes more focussed on the key summer monsoon months, with little rain observed outside this period north of 10°N. The precipitation gradient also shelves rapidly through the Sahel (10–15°N) with little precipitation even in the summer north of 20°N (<1 mm/year in many locations) compared to over 4000mm/annum in the coastal areas with most intense precipitation.

A Sahel domain is created across the region between 10°N and 15°N (Figure 2.3). Figure 2.4 shows the climatological annual cycle of precipitation in the reanalysis datasets over this domain. It can be seen that the JapRe dataset produces heavier monsoon precipitation in this region (peaking at 8 mm/day compared to 5.5 mm/day in NCEP). Analysis of individual years (not shown) shows that the pattern of precipitation in the JapRe dataset is more variable at a daily-weekly timescale during the season and the NCEP reanalysis produces more consistent intraseasonal precipitation during the monsoon. The apparently more gradual monsoon onset in the JapRe climatology is a function of greater intensity and greater interannual variability in the precipitation prior to the monsoon onset, an observation which is smoothed in the climatology.

Figure 2.2a: Annual and monthly precipitation climatology (in mm/day) for the region taken from the NCEP reanalysis dataset

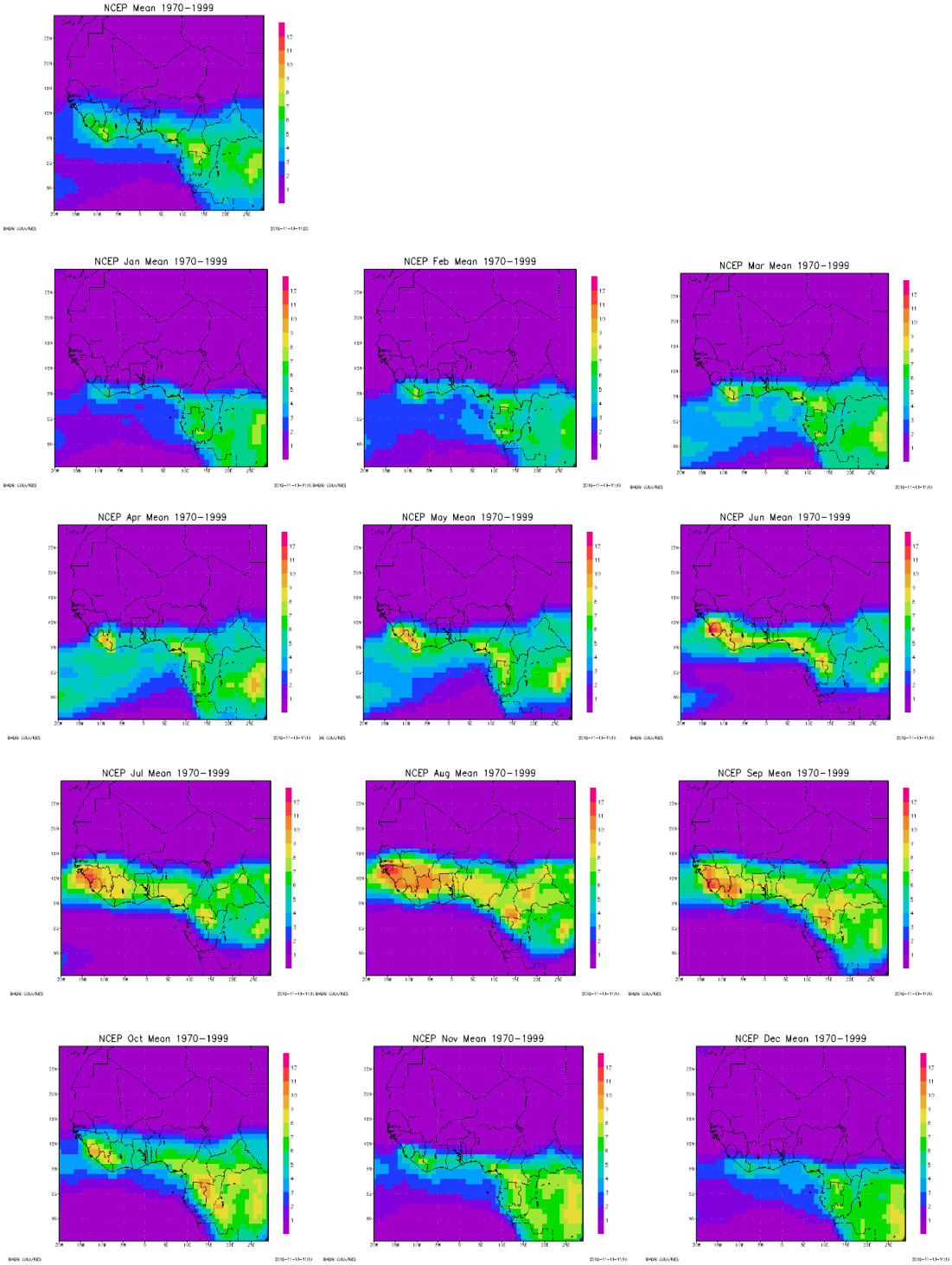

Figure 2.2b: Annual and monthly precipitation climatology (in mm/day) for the region taken from the JapRe reanalysis dataset

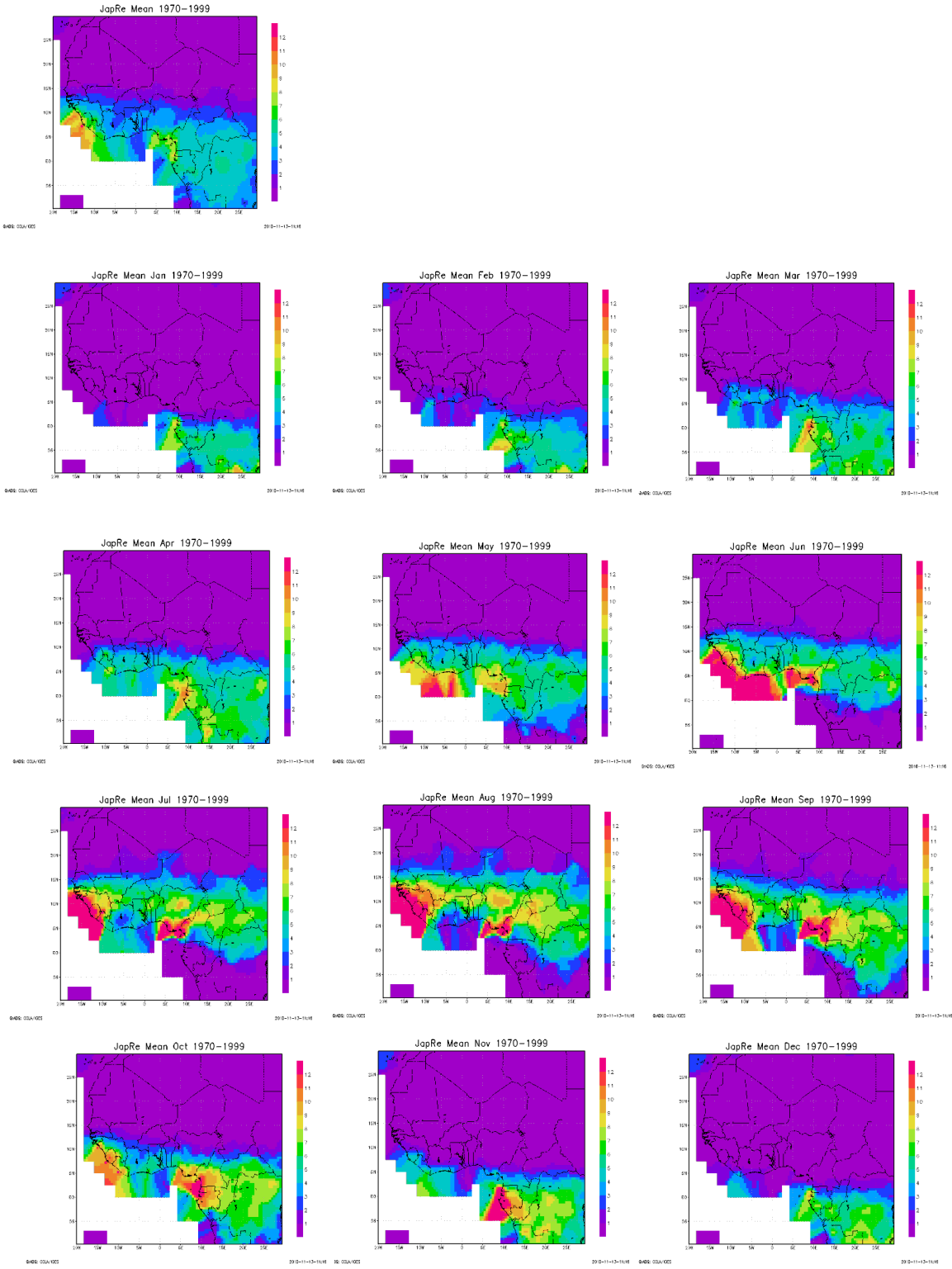

Figure 2.3: The Sahel domain, shown as pink within the white lines, used in this report

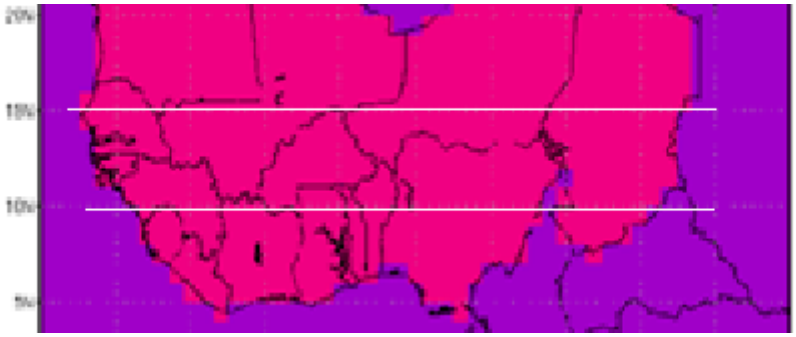

Figure 2.4: Climatological annual precipitation cycles for NCEP and JapRe, averaged across the Sahel region

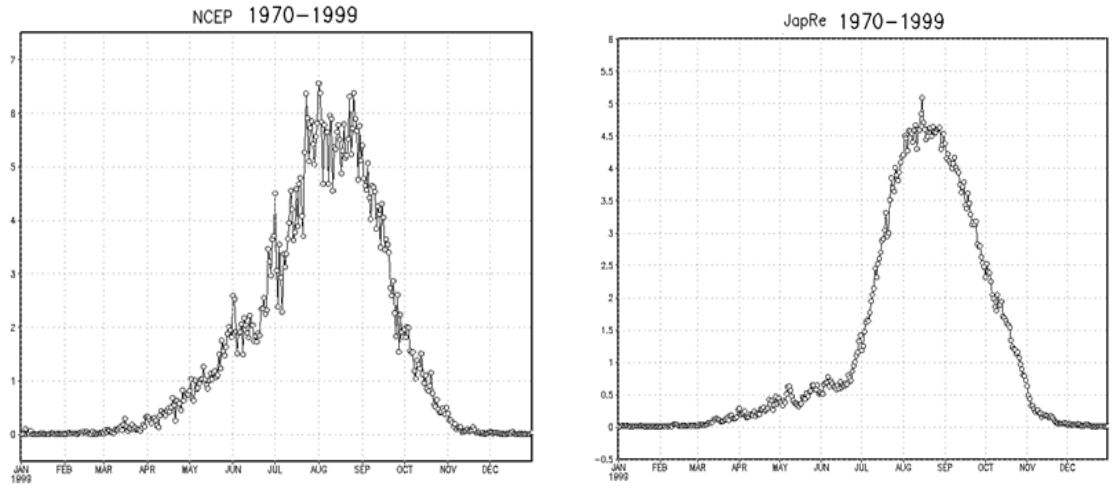

2.3 Observed variability and trends

2.3.1 Short term variability

The previous sections illustrate the complex relationship between temperature and precipitation, with both variables influencing the other both locally and regionally. From an agricultural perspective, the precipitation cycle dominates the seasonal cycle and variability in the cycle has potentially deleterious impacts on productivity (Sultan et al. 2005). Precipitation in the region exhibits high spatial and temporal variability, both interannually and intraseasonally.

Intraseasonally, mesoscale convective systems bring the greatest percentage of the precipitation in the Sahel and surrounding regions (Mathon et al. 2002) during the monsoon, with the season characterised by spells of precipitation interspersed by dry periods.

The monsoon is highly variable interannually. One mechanism responsible for variance has been identified as a "dipole" precipitation pattern which connects Sahelian precipitation with SST anomalies in the Gulf of Guinea (Nicholson 1980; Janowiak 1988; Janicot 1992; Ward 1998; Nicholson et al. 2000) resulting from meridional circulation patterns which locate anomalous subsidence over the southern Sahel when the Gulf of Guinea is warmer and leads to greater precipitation along the coast (Vizy and Cook 2001, 2002). Figure 2.5 shows Sahel precipitation since 1950 in both NCEP and JapRe. Even accounting for the drying at the end of the 1960s, annual precipitation totals since 1970 have been highly variable. Severe droughts in individual years have the capacity to impact agricultural productivity for several years in the Sahel, as such, the extent to which interseasonal variability may change in the future is an important consideration for the management of agriculture in the region. NCEP has a climatological precipitation of 1.20 mm/day and a standard deviation of 0.25 mm/day, with 1.57 mm/day and 0.15 mm/day for JapRe.

Figure 2.5: Annual average precipitation and temperature, averaged over the Sahel region since 1950 for (a) temperature, (b) precipitation (NCEP) and (c) precipitation (JapRe)

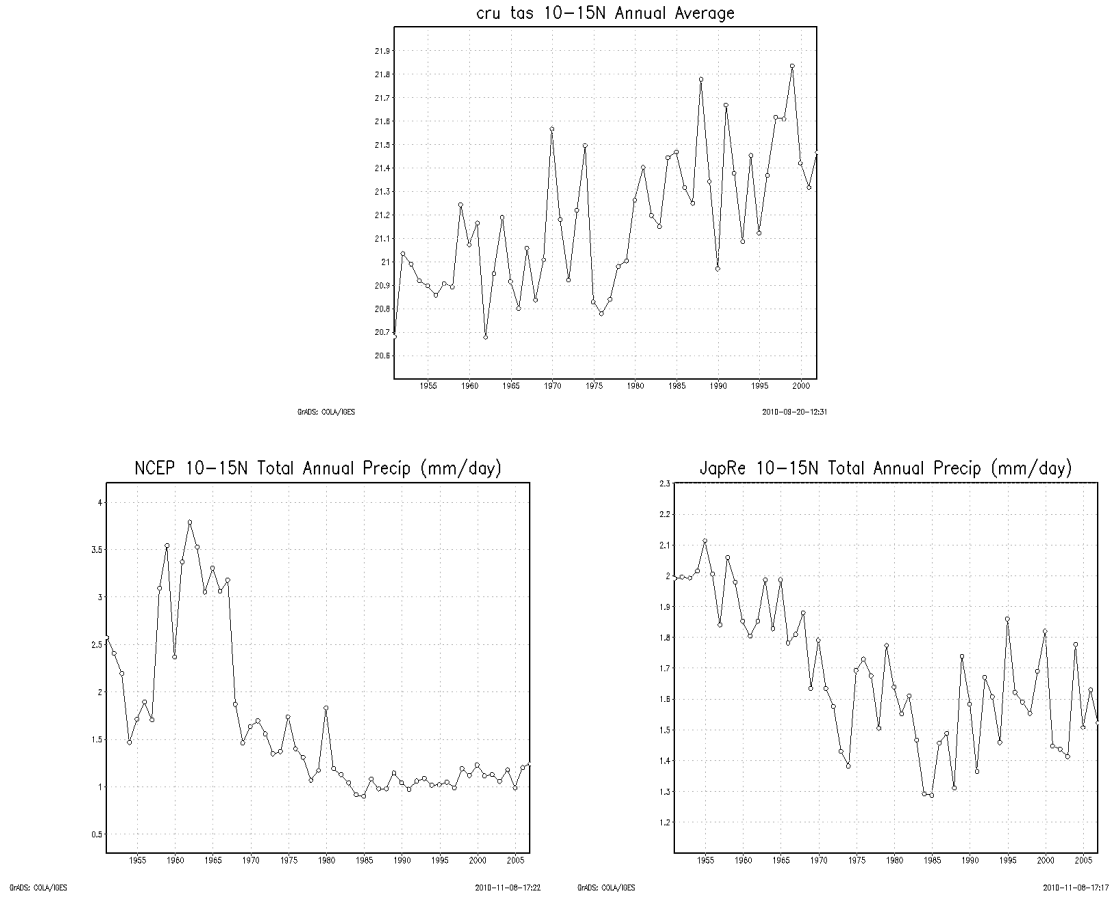

2.3.2 Decadal variability and observed trends

The literature on climatic variability in the region has recently had particular focus on the Sahel, largely driven by the significant climate changes which have been observed over the last 50 years. The climate of the Sahel shifted into a dry phase around 1968, as shown in Figure 2.5, with the annual total precipitation significantly lower after this transition. This drying trend is associated with a general decrease in precipitation in the whole West African monsoon (Zhou et al. 2008), though the anthropogenic impact has been particularly dramatic in the water stressed Sahel and the negative trend in monsoonal precipitation in the Sahel has also been outstanding. Trends and decadal variability in temperature have been more linear over the same period (Figure 2.5). Annual average surface temperatures have steadily increased, with little change in linear trends from 1950–2002 and 1970–2002 (that is, before and after the transition). These trends are slightly more significant in surface temperatures in the north of the region.

From 1970 into the mid 1990s, little trend in annually averaged precipitation was observed across the region, with a slight increase over the Gulf of Guinea coast and decrease further north. The droughts of the 1970s and 1980s were relatively uniform over the Sahel and driven by a decrease in wet events during the monsoon season (Le Barbe et al. 2002), but the recovery has been more complex, with the increase in precipitation being more significant in the eastern Sahel, though remaining below 1950–1970 levels, and dry conditions still prevailing in the western Sahel (Lebel and Ali 2009; Lebel et al. 2009).

Attribution of the causes of these trends is reliant on the ability of climate models to adequately replicate the background state of the climate and then respond appropriately to idealised forcing scenarios which enable the influence of various components of the climate system to be decomposed. Their ability to cope with this challenge is further discussed in Section 4. The recently observed increase in Sahelian precipitation has been attributed to a reorganisation of circulation in the region, including a northwesterly migration of the Saharan heat low with a more intense centre at the peak of the monsoon season, associated reinforcements of the low level winds and Tropical Easterly Jet and a northward shift of the African Easterly Jet (Fontaine et al. 2010). However, Fontaine et al. caution against interpreting these changes as a linear trend, as such; whether they represent a phase shift in the Sahelian climate regime remains an open question which lends uncertainty to future

projections of Sahelian precipitation trends (IPCC 2007). It has been noted (Coleman, personal communication) that the linear regression prediction models used for regional forecasts of the monsoon have been less successful in recent years, indicating that the observed changes may be part of a wider reorganisation of the regional climate regime. The question of whether the rains have recovered and to what extent the droughts of the 1980s were an aberration lends uncertainty to future projections if these variations cannot be adequately explained.

The monsoon is characterised by an increase in the number of rain events (Le Barbe et al. 2002) and the drought period of the late 1960s onwards has been primarily attributed to the number of rainy days in the late summer decreasing, with a 33% decrease in rainy days from 10th August to 10th September (Lebel and Ali 2010). Such changes in the timing of the most intense precipitation and drought periods during the monsoon have the potential to have negative impacts on crop production, even if climatological precipitation totals do not change significantly (Le Barbe and Lebel 1997).

Since the overall pattern of precipitation in the key Sahel region is dominated by the climate shift in the late 1960s, Figure 2.6 shows the linear trends in precipitation for both NCEP and JapRe, in absolute terms and as a percentage of 1970–1999 climatology, across the region for both 1950–2006 and 1970–2006 (the last year JapRe is available). Absolute monthly trend figures are also shown for both the 1950–2006 and 1970–2006 periods. Figure 2.7 shows the temperature trend from 1950–2002 and 1970–2002 (the last year CRU data is available). Monthly figures are also shown for both periods.

During the 1950–2002 period, annual mean temperatures have shown a trend of 0.1–0.4˚C/decade across much of the region, ahead of the rate of global average surface temperature increase (IPCC 2007), with an acceleration in trends after the late 1960s. The spatial patterns of the annual cycle of warming, and cooling, remain relatively stationary across both periods.

The two precipitation reanalyses show some divergence. The NCEP data shows more significant trends and a less homogenous temporal and spatial pattern, with trends since 1950 of over -0.4 mm per day/decade across the Sahel in the summer. As expected, these trends are most pronounced in the key monsoon period of July-September. In the 1970–2002 period, the most noticeable difference is again in the Sahel where the direction of the trend reverses,

particularly in the August–October period, consistent with the analysis of Lebel and Ali (2010). Across the year, in much of the region of interest, trends switch from negative in the 1950–2006 period, to weakly positive in the 1970–2006 period.

Comparatively, the JapRe dataset shows less significant trends across much of the region, both in absolute and percentage terms over the period. For the majority of the region, the annual precipitation trend is between -0.1 and +0.1 mm per day/decade, according to less than a ±0.5%/annum trend. In the 1950–2006 data, a slight negative trend is observed over much of the region in most months, which is more pronounced in the Sahel during August and September, though less so than in NCEP.

These trends switch to being positive after 1970, though show high spatial variability in their magnitude. The biggest change between the two epochs is in August across the Sahel, where strong negative anomalies become positive and along the coast in the south west of the region, indicating a southward migration of the rains.

Figure 2.6: Precipitation trend for NCEP (a,b) and JapRe (c,d) in absolute (a,c) and percentage (b,d) with respect at 1970-1999 climatology. Absolute monthly trends also shown for 1950-2006 (e,f) and 1970-2006 periods (g,h).

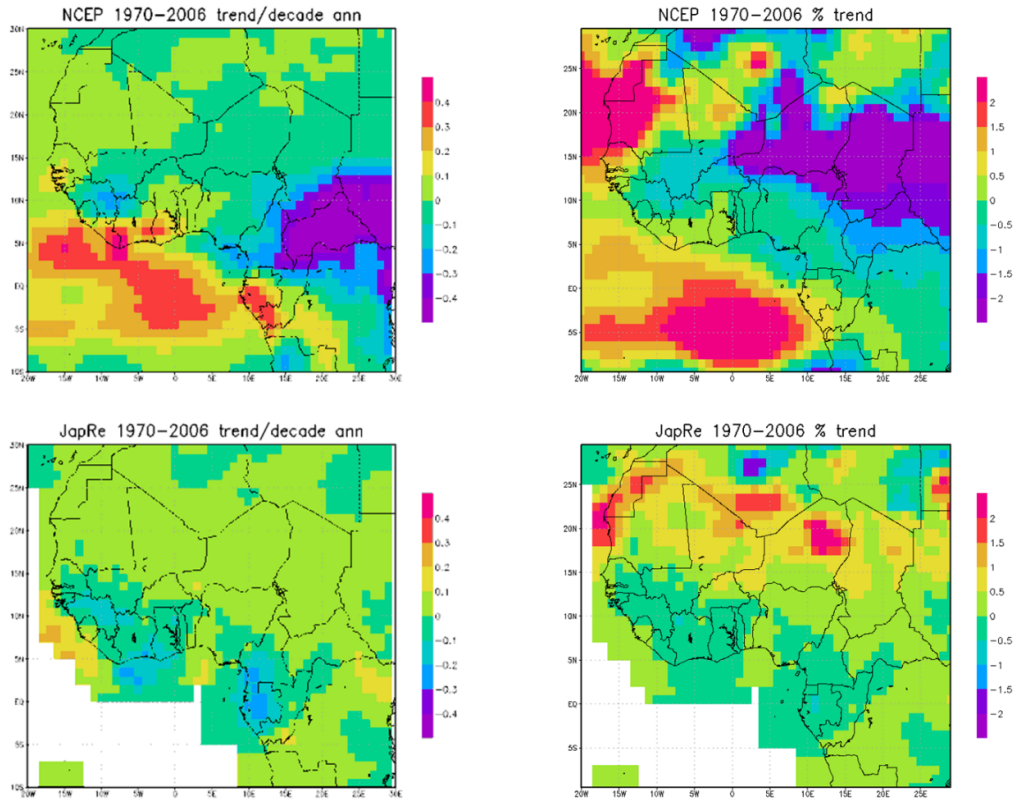

(Figure 2.6 continued)

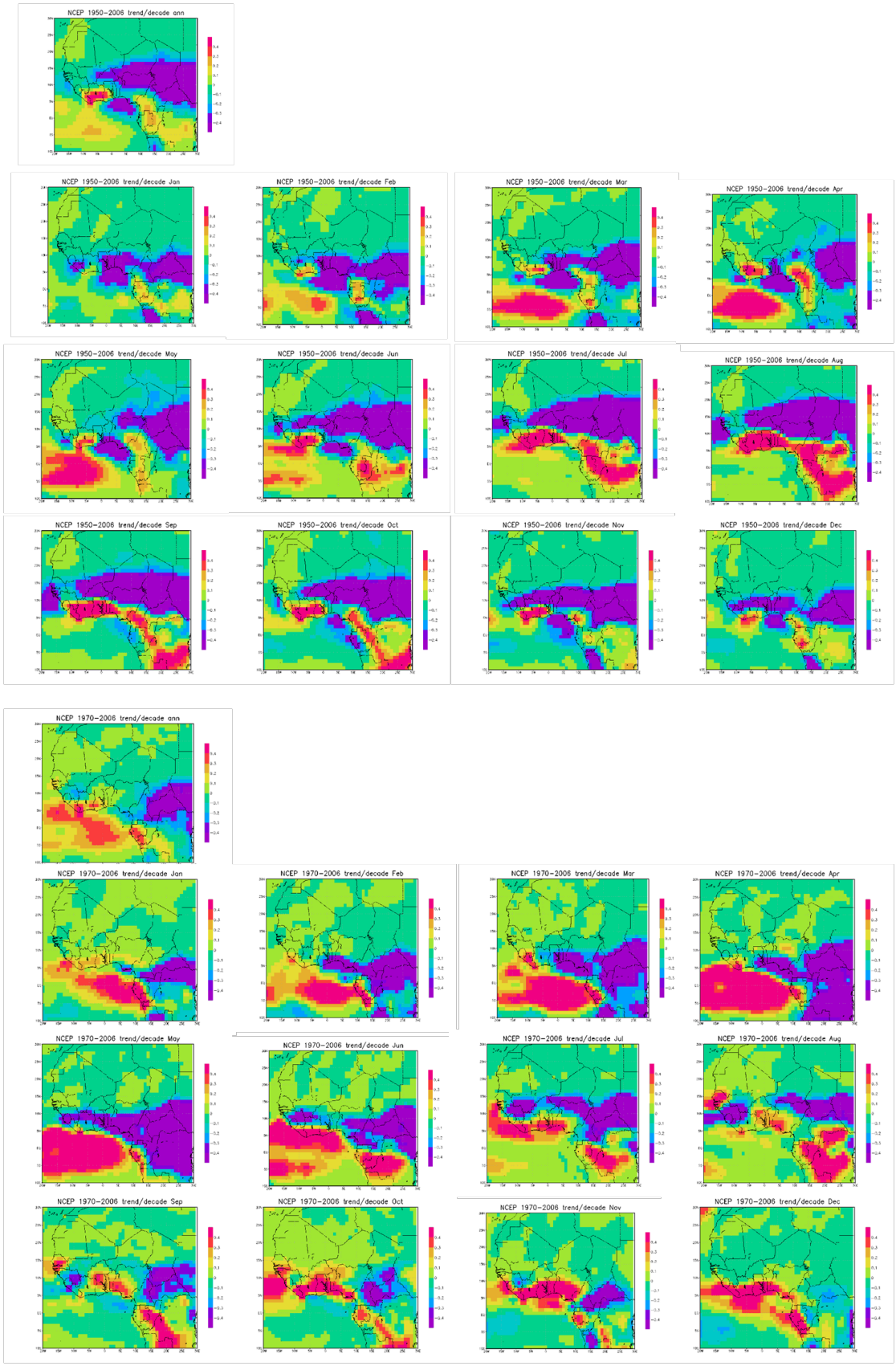

(Figure 2.6 continued)

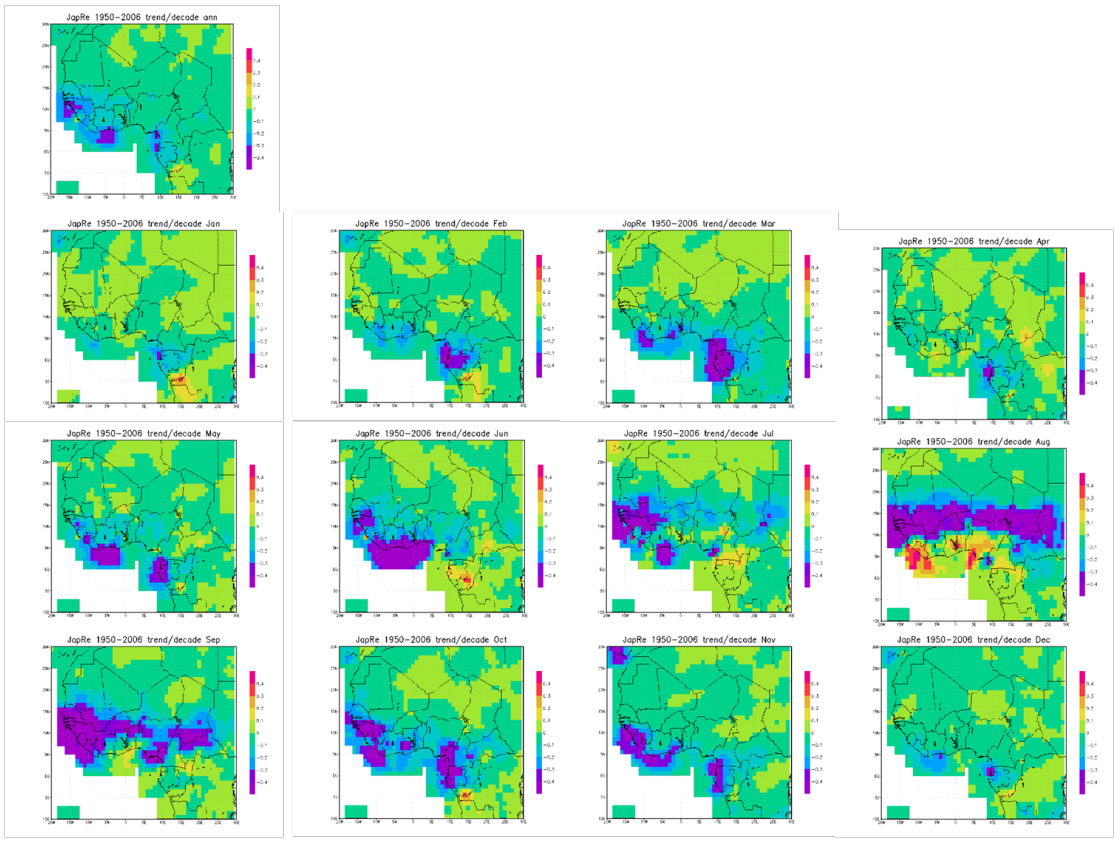

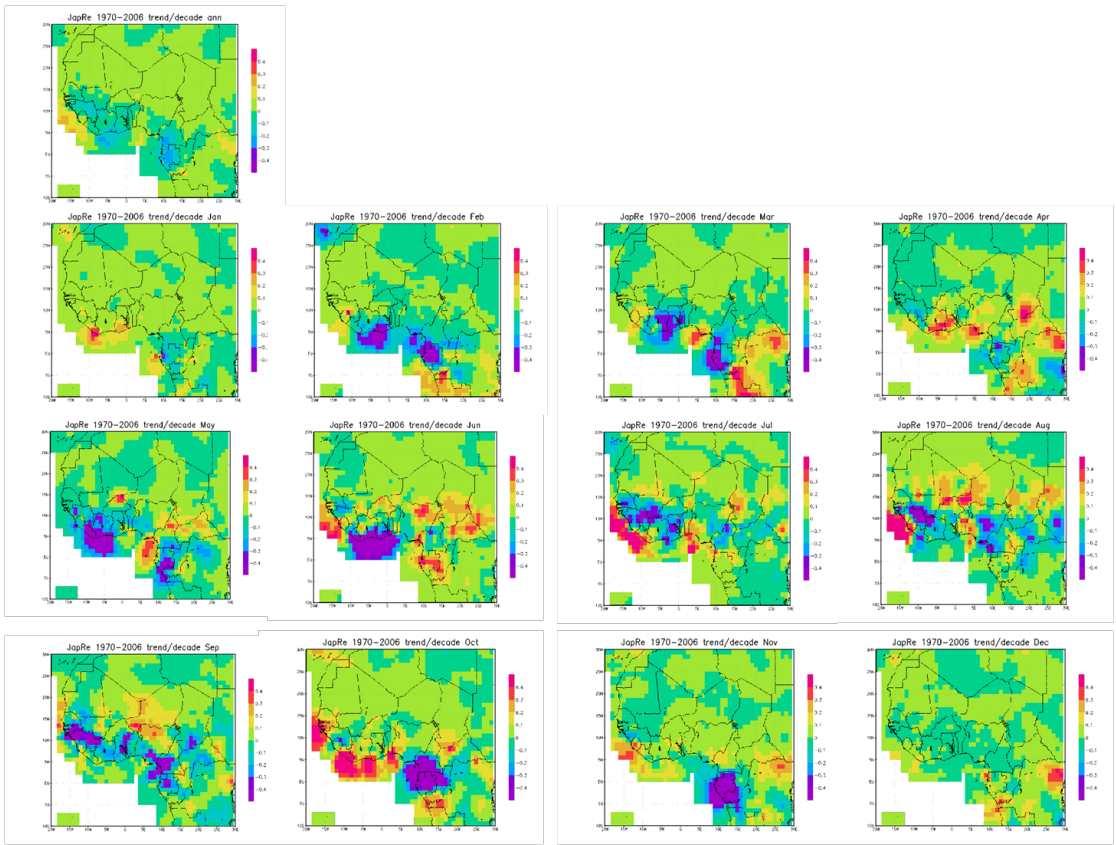

Figure 2.7: Annual average temperature trend and monthly trends for 1950-2002 and 1970-2002

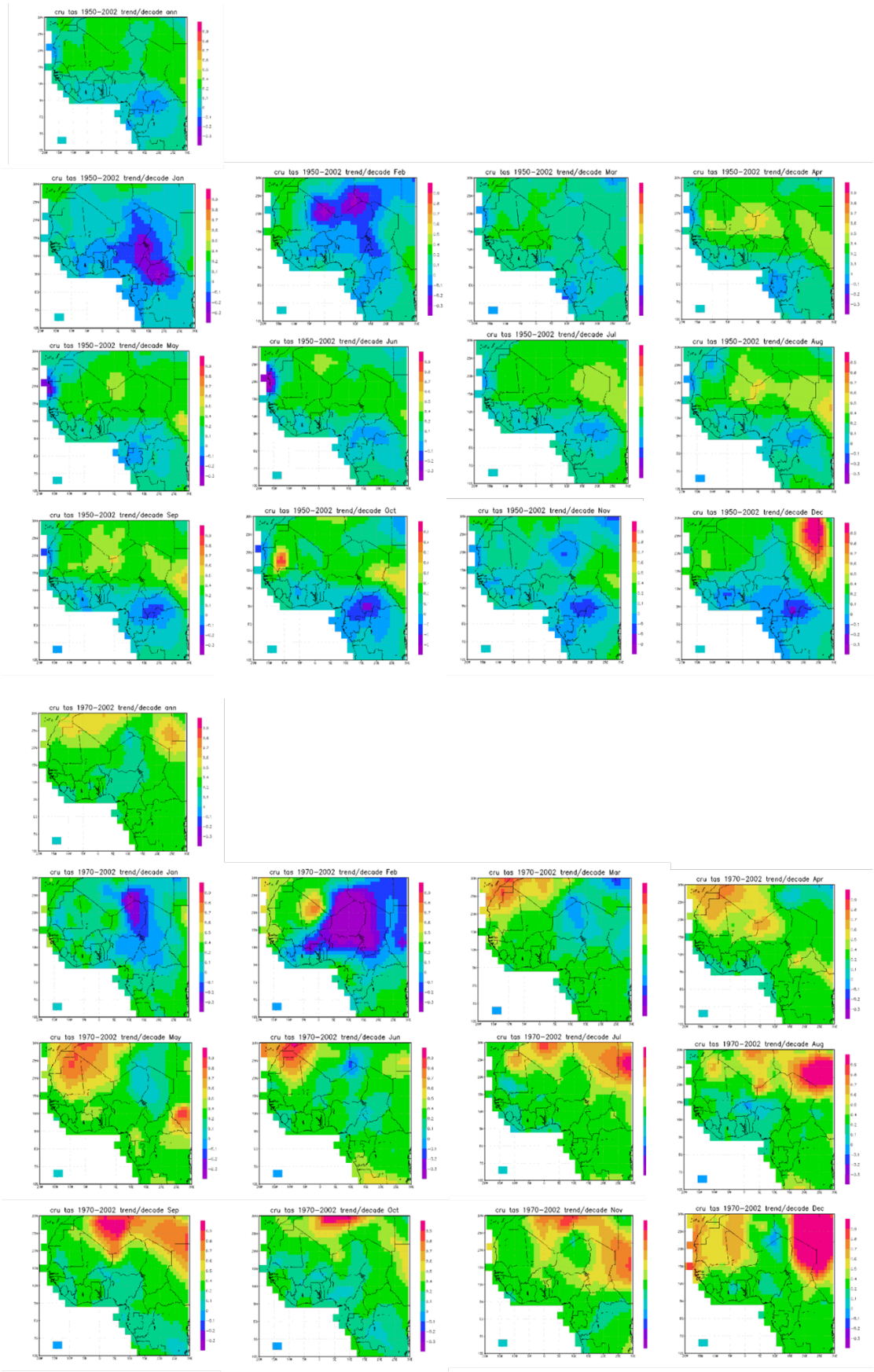

2.3.3 The Monsoon Cycle

It is challenging to capture the monsoon rains for three reasons. Firstly because the annual cycle of precipitation is not consistent across the region. The coastal regions exhibit a bi-modal seasonal pattern and in those inland regions where the uni-modal regime predominates, the summer monsoon provides a much greater contribution to the annual total precipitation further north (Lebel et al. 2003). Resultantly, its advance and departure may be captured more readily in these locations, such as in the Sahel. Secondly, the steep northward precipitation gradient means any absolute precipitation thresholds which might be used as indicia of the wet season cannot be readily applied across the domain to the same effect. Finally, attempting to determine the start of the monsoon based on data at a given grid point is not possible due to the random distribution of local convection events which characterise the onset of the monsoon. As such, and following much of the literature, defining the onset and length of the monsoon will focus on the Sahel region where the monsoon "jump" provides a potentially more homogeneous barometer of the monsoon than might be found by using other regions and indices.

Interannually, the timing of the start of the monsoon strongly correlates with the length of the rainy season. From the perspective of agriculture, particularly in areas where production is strongly reliant on precipitation, predicting and verifying the onset date is critical (Ati et al. 2002; Laux et al. 2008)—planting after a "false start", where rain is followed by a dry spell before the monsoon itself commences, can be disastrous for productivity (Sultan and Janicot 2003).

The monsoon itself can be measured through a variety of variables including surface pressure, temperature and relative humidity (Omotosho 1990, 1992). Most metrics use precipitation itself (Walter 1967; Ati et al. 2002; Laux et al. 2008), since precipitation rather than temperature is seen as the critical factor in much tropical agriculture (Stern et al. 1981), and that is the approach followed here. The purpose of this exercise is primarily to identify whether any trend has emerged in the onset date or length of the monsoon, since if such a trend is observed and is connected to global warming it might be expected to continue through the 21st century, potentially impacting on agricultural productivity in the region.

Using the Sahel domain in Figure 2.3 a threshold-based index is created which follows the onset date definitions used elsewhere (Stern et al. 1981; Sivakumar 1988; Omotosho 1990;

1992; Dodd and Jolliffe 2001; Marteau et al. 2009). The onset date is defined here as the first day of (1) 5 days where a total of 25 mm of rain falls; (2) where it rains on at least 3 of those 5 days and (3) there are no more than 7 consecutive dry days in the following 30 days. This index provides an indication of the onset date at each individual gridpoint. To create an index for the domain, two other criteria were also included: (4) all gridpoints at a given latitude must satisfy the condition (the nature of the synoptic systems which characterise the monsoon and the "jump" mean the precipitation rapidly advances northward at any given location; Hagos and Cook 2007) and (5) 40% of all gridpoints zonally satisfy condition (4). This latter condition indicates that onset has occurred at sufficient locations to represent the monsoon itself, rather than an anomalous synoptic system passing into the region prior to the monsoon. The 40% threshold was tuned using the NCEP and JapRe reanalysis data to ensure the threshold represented the observed onset of the monsoon. Other studies suggest the Sahel monsoon onset is at the end of June (Ramel et al. 2006; Fontaine and Louvet 2006) with Sultan and Janicot (2003) giving a date of 24th June ±8 days for the 1968–1990 period and Lavaysse et al. (2009) 25th June ±9 days for 1984–2001. The 40% threshold produces climatological dates (1970–2006) of 28th June and 6th July for NCEP and JapRe respectively, which are a little later than this. However, a visual inspection of individual year outputs (not shown) indicates that the point selected each year is relatively consistent and accords to a point near to the start of the monsoon rains in each dataset. The point captured in the JapRe data is slightly further from the actual onset date, though generally consistent, explaining the delay compared to both NCEP and the dates produced in other studies. Given the differences in the precipitation regimes in the two datasets, it was not possible to create an index which worked with greater capability than that used here.

As noted above, the timing and length of the monsoon are critical for agriculture. A second index was therefore derived over the Sahel domain to capture the end of the monsoon. Stern et al. (1981), Sivukamar (1988) and Sultan et al. (2010), undertaking studies in various West African locations, use a simple index of the first day after 1st September when 20 consecutive subsequent days are dry. A more sophisticated index is used here of (1) less than 25 mm in 5 days, (2) with less than 3 of those 5 days having rain and (3) less than 15 mm/day on average over the following 14 days to capture the end of the last substantive rains. Applying this to the NCEP and JapRe data produces climatological end dates of 28th October and 21st September, respectively. This significant disjuncture in the end date is due to the tendency of the point

captured in the JapRe output to be slightly earlier in the monsoon withdrawal and is related to differences in intra-seasonal precipitation patterns in the two reanalyses. The JapRe monsoon end date is also less consistent than the more robust output when the threshold is applied to the NCEP data.

Figure 2.8: Trends from 1970-2006 of the start date, end date and length of the monsoon from the NCEP and JapRe reanalyses

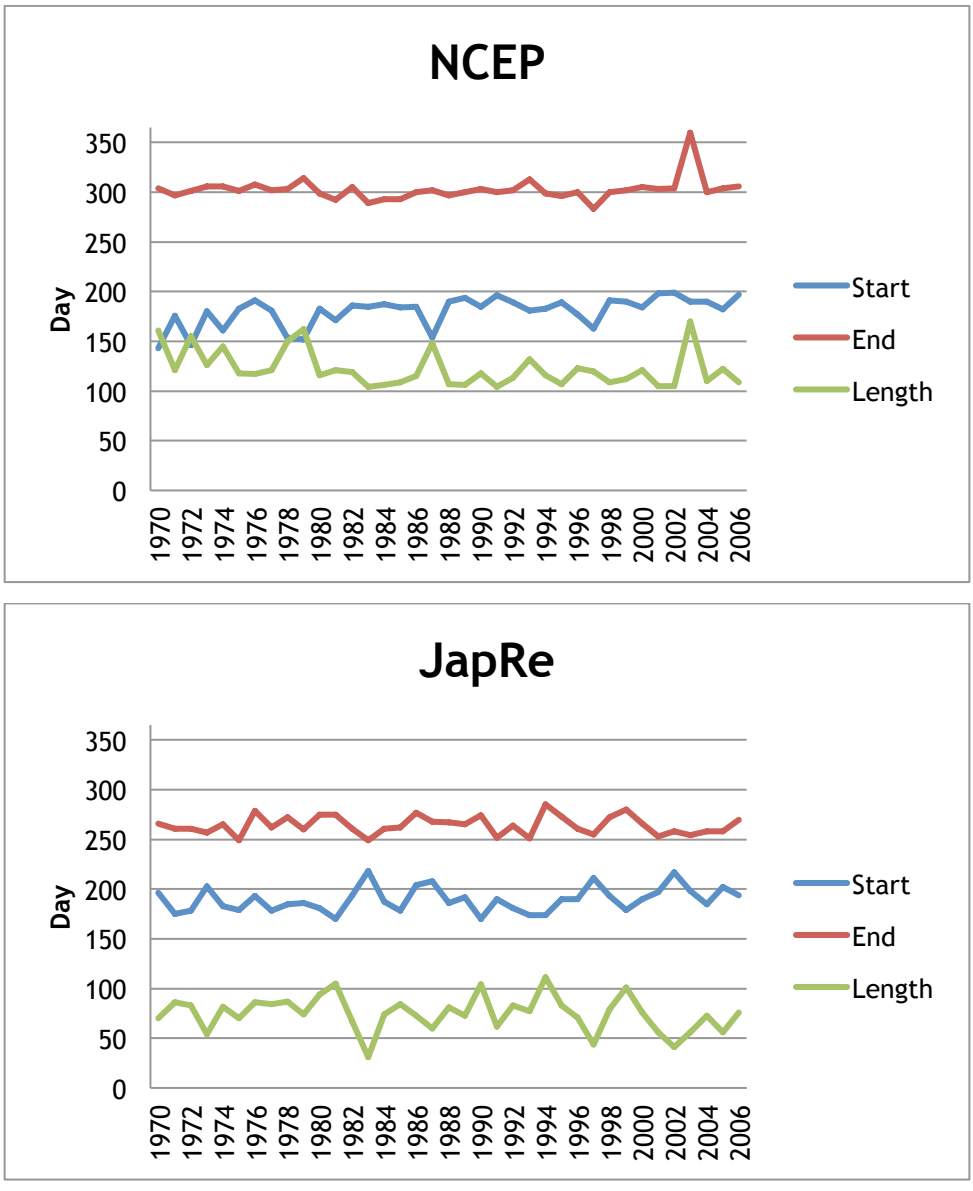

The purpose of this analysis was to investigate the possibility of trends having emerged in the monsoon seasonal cycle since 1970 when the climatological annual precipitation total has been more consistent, so in spite of the differences in end date capture and season length produced by the thresholds, the two outputs remain usefully comparable. In Figure 2.8, the dates of the start, end and length of season are plotted for the two datasets. In the 1970–2006

period, the two datasets produce negative linear trends in season length against high interannual variability of -0.59 days/year in NCEP (SD 18 days) and -0.32 days/year in JapRe (SD 17 days). Only the NCEP trend is statistically significant at 90% due to the high variability of the datasets, though both suggest a material shortening of the season. It is evident that this shortening season is dominated in both datasets by the later start date—a trend of 0.78 days/year (SD 15 days) in NCEP and 0.30 days/year (SD 12 days) in JapRe. Neither output indicates a significant trend in the end date of the monsoon, with NCEP showing a slight positive trend and JapRe no trend. If this trend is associated with anthropogenic warming, rather than natural variability, then it should be expected to continue into the future.

2.4 Climatic extremes

Climatic variability and extreme events can be as key to agricultural productivity as the mean conditions. The indices discussed here are guided by those important to the crops grown in the region, which will be introduced in the following section. Partly due to the limited temporal and spatial coverage of high quality climate data in the region, there has been less research on trends on extremes in West Africa than on the mean conditions. Furthermore, assessment of climate change signals in extreme values is not a simple task: simply because extreme events are rare by definition and, hence, are subject to sampling errors and model deficiencies (Meehl et al. 2000). The rarer the event, the more difficult it is to identify long-term changes, simply because there are fewer cases to evaluate (Frei and Schär 2001; Klein Tank and Können 2003; IPCC 2007). In a region lacking observed station data, like much of West Africa, this challenge is even greater. The African Monsoon Multidisciplinary Analysis (AMMA) field campaigns (see Lebel et al. 2009) are beginning to produce data, but their data collection work only began 2001, with more enhanced monitoring from 2005–2007, particularly during 2006. Daily data from the national meterological services is not available for analysis.

As the climate warms under anthropogenic forcing the hydrological cycle should intensify, leading to higher intensity precipitation events occurring, even in regions which are drying (Trenberth et al. 2003; Neelin et al. 2003; Alexander et al. 2006; Meehl et al. 2007; Trenberth 2010) with an increased percentage of total precipitation occurring on extreme wet days (Alexander et al. 2006). With increased average temperatures, temperature extremes should

also rise, with fewer cold days and a greater number of warm days (Alexander et al. 2006). This trend has been observed in West Africa (Easterling et al. 2003). The rate at which "high" temperature extremes and "low" extremes vary with respect to both each other and mean temperatures is not necessarily linear (Klein Tank and Konnen 2003; Moburg and Jones 2005; Alexander et al. 2006; Caesar et al. 2006).

Many crops are unable to deal with heavy precipitation and associated waterlogging during the growing season, or at specific times within the season (particularly at planting and harvest). Mesoscale convective systems bring the largest share of the precipitation in the Sahel (Mathon and Laurent 2001; Mathon et al. 2002). Precipitation, at a local level, is therefore highly variable throughout the season. Under anthropogenic warming it is likely the intensity of the wettest events will increase. Trends in 95% daily threshold events over the wider region and annual maximum 5-day precipitation events over the Sahel region are analysed since 1970. Plots for trends in NCEP and JapRe 95% precipitation events and their climatologies are in Figure 2.9. The discrepancies between the two datasets demonstrate the significant difficulties in modelling extremes—the difference in the magnitude of the climatological extremes around the coastal region is over 20 mm/day in some locations. It has been noted elsewhere (Fontaine et al. 2002) that the NCEP reanalysis underestimates peak precipitation around the Guinea coast. Turning to the trends, in the north Sahel/Sahara the trend for the two datasets is reversed, with a strong negative trend in NCEP and a strong positive trend in JapRe. The spatial distribution of the trends correlate with the trends observed in total annual precipitation observed in each dataset (Figure 2.6). These results are indicative of the difficulties in reproducing extreme precipitation events in a region with significant observed variability and a climate regime governed by multiple complex forcings and interactions.

Turning to 5-day maximum precipitation events, the climatology figures for the NCEP and JapRe datasets are 37.3 and 74.7 mm/day, respectively. The significant difference between the two is a function of both their total annual precipitation climatologies being different and the nature of the precipitation events which are generated in each, with greater intraseasonal variability and intensity in the JapRe dataset. Both show a negative trend (-0.5 mm/year and -0.87mm/year) since 1970, indicating that these events in the Sahel appear to be decreasing in severity and contrasts with the divergence in trend seen in this region for 95% daily

precipitation events. This decrease runs contrary to the general theory of more intense events occurring in a warmer climate, but may be connected to the general recovery of the rains in the Sahel over this period with the possibility that extreme events are therefore less likely to drain the water column as more consistent rain depletes atmospheric moisture content and decreases the potential for such events. The divergence in the JapRe 95% and 5-day max trends may be a function of the specific location of the Sahel domain used in this study, the northern limit of the monsoon rains (see Figure 2.2(a)) and the highly variable nature of the JapRe output. Other studies have also found inconsistency in the trends in these two indices (Kiktev et al. 2003).

Figure 2.9: Climatologies and percentage trends during the 1970-1999 period of 95% daily precipitation events taken from NCEP and JapRe. The figures are percent per decade trends.

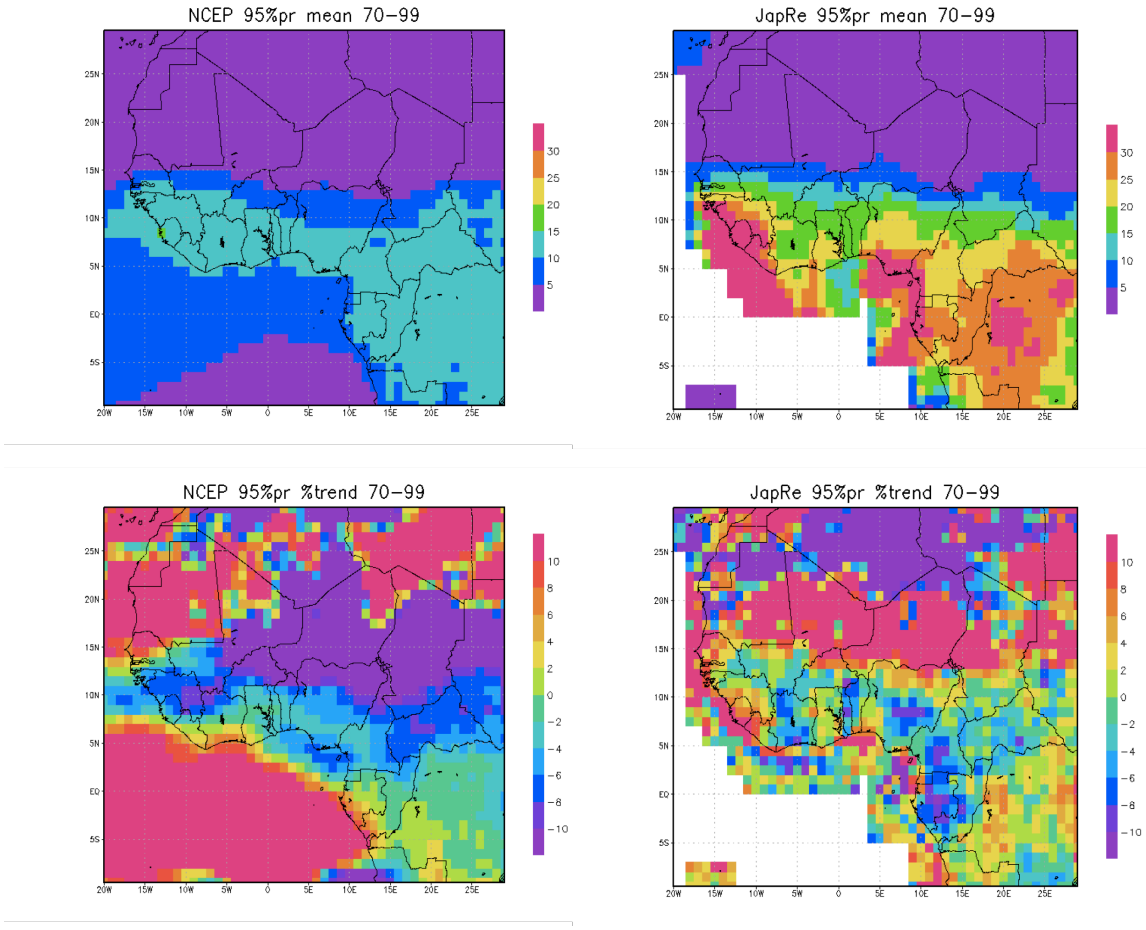

Given the importance of monsoonal precipitation for many crops and the impact that droughts within the rainy season can have, an index of the Sahel is created for the 1970–1999 period for both (1) the longest period of consecutive dry days (CDD) at each grid point during the

July-September season and (2) the number of periods of 5-or-more dry days (5DD) at each grid point. The figures for (1) are 31 and 26 days for NCEP and JapRe, respectively, and for (2) the figures are 1.3 and 0.7 events/year. These figures are indicative of the steep precipitation gradient in the region, with certain areas subject to extended dry periods (increasing the CDD index dramatically) and others to consistent precipitation throughout the period (reducing the 5DD index). Both NCEP and JapRe exhibit statistically significant trends at 90% in the CDD index, but the trends are of opposite sign, with a lengthening of the longest period in NCEP and shortening in JapRe (0.17 and -0.10 days/year, respectively). In the 5DD index the two datasets also diverge, with the number of 5DD periods increasing in NCEP and decreasing in JapRe (0.015 and 0.03 events/year, respectively. Both trends are significant at 97%).

Minimum and maximum daily temperatures are also investigated, at the 5% and 95% thresholds, respectively. Daily data was required for this analysis, and since the CRU data is monthly, the NCEP temperature reanalysis is used. Figure 2.10 shows the climatological temperatures and trends for 1970–99. The climatological cycle is most notable in the continental interior, where the greatest annual temperature cycle exists. The trends are dominated by the seasonal cycle—5% minimum temperatures have got colder in the interior, concurring with the cooling trend seen in the January and February monthly average temperatures (Figure 2.7), and 95% maximum temperatures increasing most noticeably along the coast, connected to the recovery of the Sahelian rains and the migration of the most intense precipitation onto the land during the summer monsoon period (Figure 2.6 (a) and (b)).

Figure 2.10: Trends for 95% maximum temperature and 5% minimum temperature events. Trends are in degrees per decade.

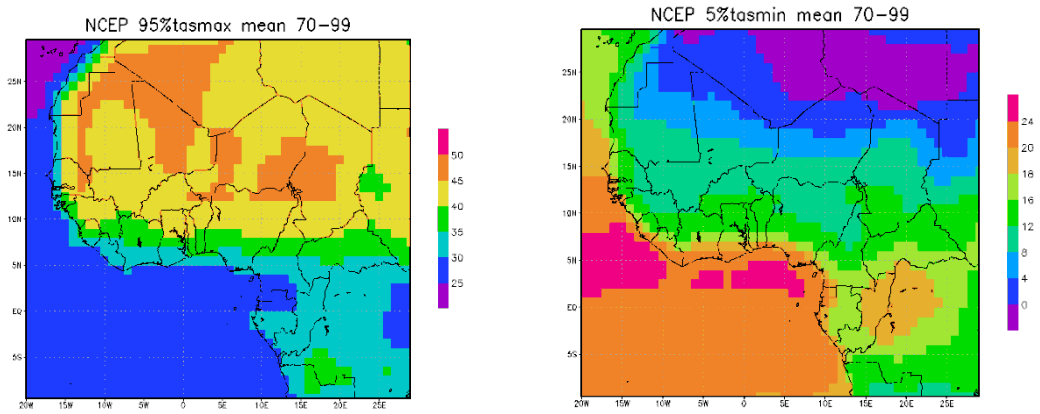

(Figure 2.10 continued)

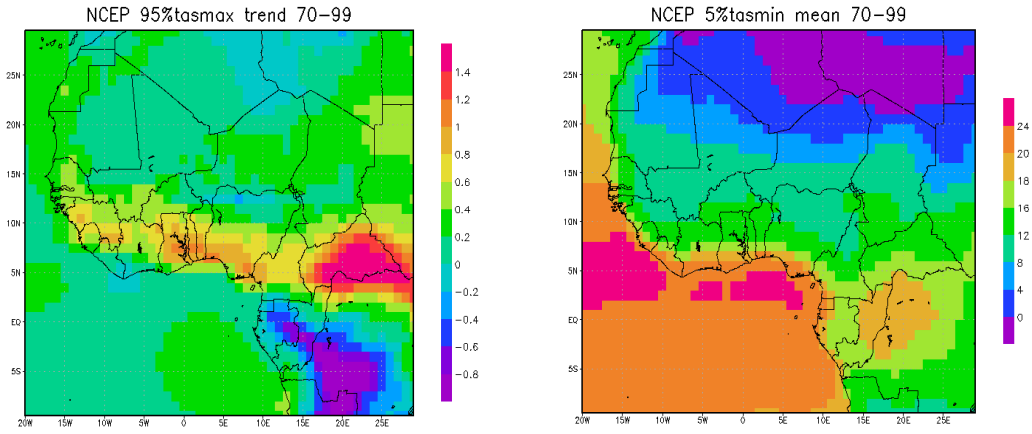

3. The Key Food Crops of West Africa

In this Section the primary food crops produced in the region are introduced. The climatic thresholds which those crops are capable of withstanding will be discussed with a view to establishing where growth of the crops is potentially limited by climate and the extent to which opportunities to expand production may exist in the current climate, to the extent they are not limited by non-climatological factors.

3.1 Crop Selection

The crops analysed in this report are selected on the basis of the importance of the crops to regional food security and in particular their importance to the countries which have been identified by CCAFS as specific targets. The selected crops and their total value to the region (based on an internationally standardised price) are shown in Table 3.1. Values are shown both including and excluding Nigeria due to the relatively high value of Nigerian agriculture in comparison to the focus countries.

Table 3.1: The crops selected for analysis in this study and their total value across the West Africa region. Figures from the United Nations Food and Agricultural Organization.

Crop	Total value ($1000s), including Nigeria	Total value ($1000s), excluding Nigeria
Cassava	3 071 029	591 445
Millet	2 085 272	926 554
Rice	1 659 813	1 007 268
Sorghum	1 435 564	514 911
Maize	957 857	422 720
Cowpea	309 181	309 181

3.2 Crop growth thresholds

A grey literature review was undertaken to establish the key growth thresholds of these crops. A summary of the findings of that review are provided in Appendix 1. These findings have been synthesised and are in Table 3.2.

The primary climatological thresholds relate to temperature and precipitation. These thresholds have been used to create maps which display the geographical limits of growth of these crops. The established limits of growth found in the literature for each crop are applied to the observed and reanalysis data to create a series of "masks" which represent, for example, the current extent of the area for which the optimum average temperature conditions for the cultivation of millet exist (20–28˚C). The masks for each climatic variable in Table 3.2 for each crop are then combined in order to provide an indication of the degree of suitability of a particular location—within the absolute limits of growth, those areas which also fall within the optimum thresholds of all variables appear as the highest order, with the numbers decreasing as less of these optimum thresholds are satisfied. The absolute limits of growth are used as a delimiting criterion, indicating where the climate is not suitable for cultivation according to the conditions relevant to each crop.

The plots are produced with respect to a 1970–1999 climatology using the thresholds in Table 3.2:

- Optimum temperature range;
- Absolute precipitation range;
- Optimum precipitation range;
- Optimum minimum temperature (single lowest instance of daily minimum temperature during relevant months);
- Optimum average minimum temperature (only applicable to rice and maize and combined with optimum minimum temperature in one mask where both conditions are satisfied); and
- Absolute/optimum maximum temperature (only applied to cassava, cowpea and rice).

Table 3.2: The crops investigated in this study and the limits of their growing conditions. Opt – optimum; abs- absolute.

CROP	Optimum Average Temp	Max Temp	Min Temp (single instance)	Optimum Average Precip	Absolute Max Avg Precip	Absolute Min Avg Precip	Capacity to deal with waterlogging/ saturation?	Capacity to deal with drought?	Growing period	Altitude	Photo-sensitivity	Harvest
Millet (Pearl)	20-28		12 - JJAS (opt)	250-600 (500+ for forage)	1200	125	No	Yes, but needs rain late in devt and cannot tolerate extreme drought	70-80	<1500m		Late summer
Cassava	22-28	30av for 8 mon	10 (opt)	1000-4000	5000	500	No	Yes, up to 2-3 months	365	<1500m	<13h light	All year
Sorghum (lowland)	28-31		15 – MJJAS (opt)	450-750		300	Yes	Yes, but not in 60 days after planting	90-120	<1500m	>12h light	Late summer
Cowpea	25-35 (Day)	35 av	15 – MJJASON (opt)	500-1500	2000	300	Unclear; not at planting and harvest	Yes	90-120 – though depends on type	<2000m	Depends on type; mostly no	Shortday – Nov/Dec
Rice (African)	30-35	35 av	0 (abs), 20 (av, opt)	760-		700	Yes	Needs 15mm/5-days and 4mth rainy season	100-120		Most varieties are not	Late summer (first crop)
Maize (lowland)	25-30	40 av	10 (abs),20 (av, opt) - MJJAS	700-1100		500	No	Not in pollenation or later growth	100-120	<1500m		Late summer

3.3 Results

The plots are shown in Appendix 2. Separate plots are produced using precipitation figures from the NCEP and JapRe datasets. The JapRe dataset only covers land, so these plots do not extend beyond the continental boundary.

Cassava: As for all crops, the primary limitation is the absolute precipitation range which cassava is capable of withstanding. The precipitation thresholds produced by JapRe push further into the Sahel since this dataset produces a more northerly monsoon cycle, as discussed in Section 2. Optimum growing conditions are found along the Gulf of Guinea coast, with the higher average and lower minimum continental temperatures limiting the range of optimum growth within the absolute domain.

Cowpea: The precipitation thresholds exhibit greater spatial variability for cowpea in comparison to cassava because the lower order precipitation thresholds are more variably produced by the two datasets. Notably, at the Gulf of Guinea coast, the wetter climatology of NCEP exceeds both the optimum and absolute limits of growth and at the northern limits of growth, the wetter Sahel climatology of JapRe extends the domain northwards. Through the Sahel, both maps suggest cowpea can be grown under relatively optimal conditions, though the northward boundary of the domain varies by up to 3˚. The comparatively high minimum temperature threshold of cowpea is a secondary limiting factor across the region with lower minimum continental temperatures making cultivation more difficult.

Rice: The absence of a maximum precipitation boundary for rice growth dictates that the absolute growth boundary is delineated by the decreasing northward precipitation gradient alone. As seen for cassava, the high threshold is more closely matched in the two reanalyses with discrepancies generally less than 2˚. With a high maximum temperature threshold and low minimum temperature threshold, rice is otherwise not climatically limited in much of the region.

Sorghum: The relatively narrow, and lower, optimum precipitation range for sorghum leads to some discrepancy in the latitudinal position of the mask in the two reanalyses. Similarly, the northern boundary of the absolute precipitation threshold exhibits a difference of 2˚ at many locations. The high, and narrow, optimum temperature thresholds provide a secondary limit to growth with minimum temperatures also influencing optimum growth locations in the

continental interior. Optimum growth conditions are found in a band across the southern Sahel, with adequate conditions further south.

Millet: The discrepancies in the absolute precipitation boundary are most apparent for this crop. With a low minimum and maximum precipitation threshold the variability in the two reanalyses is more pronounced than for the other crops. Like sorghum, the narrow optimum precipitation conditions lead to a latitudinal discrepancy in the location of the optimum growth area. The much more northerly threshold of growth suggested by the JapRe analysis is likely excessive, though the band of peak conditions through the Sahel is comparable in the two outputs. The relatively low threshold for maximum optimum average temperature provides a secondary threshold for growth.

Maize: The optimum precipitation conditions for maize are relatively narrowly constrained, but with a higher minimum optimum precipitation threshold the two datasets remain closely comparable. Similarly, with a minimum absolute precipitation of 500 mm/annum, the northern boundary of growth is reasonably well constrained. Optimum growth conditions are again in the southern Sahel, though most locations south of this also provide adequate climate for maize cultivation.

These crop ranges are compared to maps of recent crop cultivation taken from the FAO Agro-MAPS database, Figure 3.1. The most recent year available is used for each crop. For most of the crops, the locations of most widespread cultivation match the regions the climate data indicates is optimal for growth. The data for cowpea is taken from a year which is anomalous compared to the more restricted extent of crop cultivation in most other recent years. The UN/IIASA GAEZ project has also produced maps of crop cultivation range (not shown) which are comparable in spatial extent to the maps produced here.

One limitation of this approach is that it only uses a climatological value for either the whole year or the selected season, as such it is insensitive to the timing of the monsoon cycle or the annual range of temperature/precipitation, the variability of which has a significant impact on agricultural productivity (Sivakumar et al. 2000; Sultan et al., 2005). The use of irrigation and water management systems to extend regions of absolute or optimum crop growth conditions is also not considered in this report, but may have a significant impact on the extent of cultivatable land in the region.

Figure 3.1: FAO Agro-MAPS crop ranges for the most recent year available

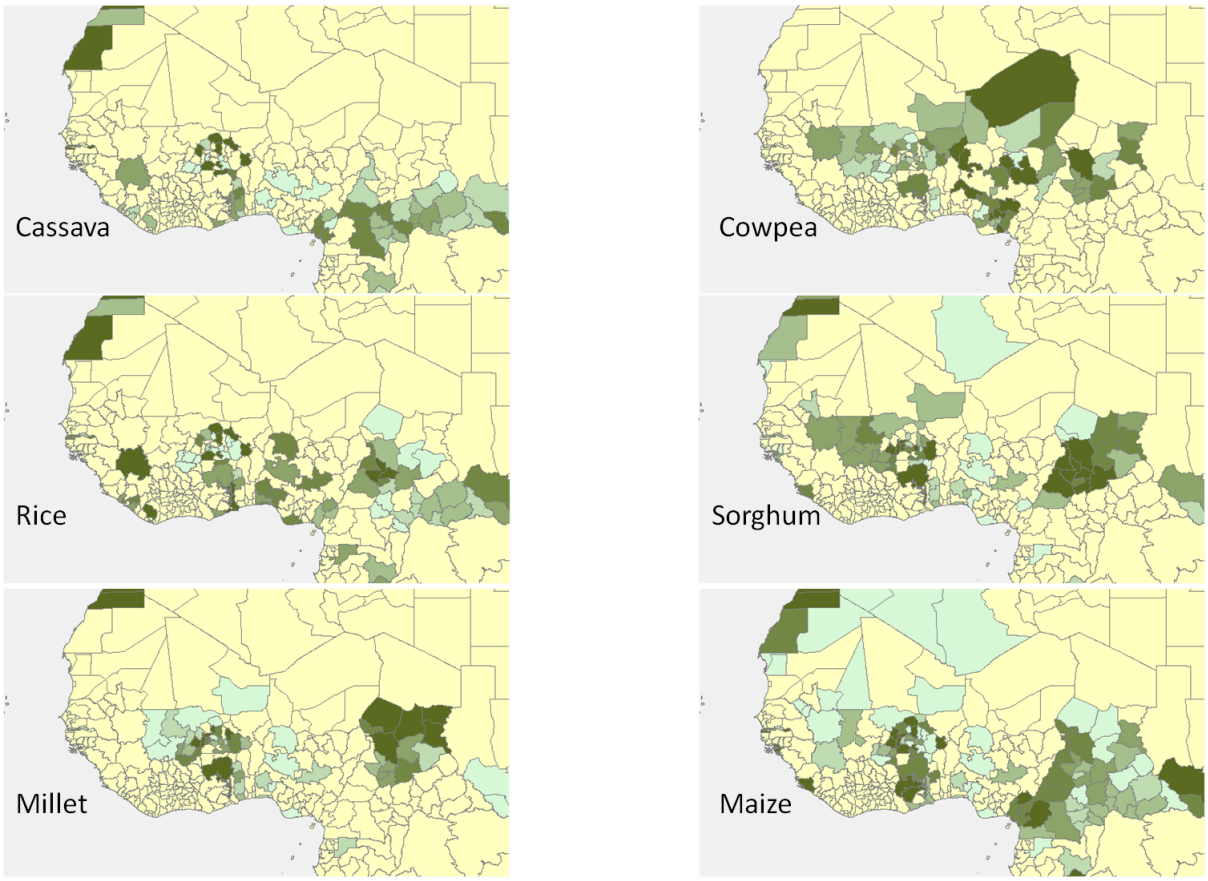

Source: http://www.fao.org/landandwater/agll/agromaps/interactive/page.jspx

In addition to the climatological data, the trends in climatic extremes investigated in Section 2 are relevant to the crops. All crops are affected by minimum temperatures, though few of the crops grow far enough inland to be where the negative minimum temperature trends are observed in Figure 2.10. These minimum temperatures are also a function of lower winter minimums, rather than indicative of a seasonal pattern, so would not affect the growth domains of the crops. The maximum temperature trends are most pronounced along the coast, where many of the crop domains are found. The relevant crops are, however, affected by increases in average maximum temperatures during the growing season, so trends in this specific index should not impact directly on crop growth. The uncertain direction of trends in, and high interannual variability of, high intensity precipitation—with a decrease in 95% events but a less certain trajectory of 5-day maximum events in the Sahel—leaves the impact on those crops which are affected by waterlogging and ground saturation as a question requiring further investigation. Finally, the lack of a robust trend in intra-seasonal drought

periods leaves another unresolved issue since all of the crops are (to varying degrees) sensitive to drought during their growing season.

4. Climate Models and the West African climate

The West African monsoon, like other global monsoon regimes, remains a significant challenge to the modelling community (Turner et al. 2009). Particular problems arise from the complex array of competing and interacting influences on the monsoon, as discussed in Section 2 above, and the challenge of accurately reproducing the spatial distribution of the observed precipitation gradient and cycle (Cook and Vizy 2006). The ability to robustly simulate observed climate conditions and trends is a necessary, but not sufficient, condition for gaining confidence in future projections (Caminade and Terray 2010). If models are unable to reproduce the climate for the period which they are tuned, confidence in their projections of future climate scenarios is decreased. The use of models is also key to attribution studies. In order to more adequately understand the mechanisms and influences through which observed patterns are formed, models must be able to reproduce the background climate state from which idealised forcing experiments can be compared. If the key variables and driving mechanisms of change cannot be identified through such studies, the ability to verify the plausibility of future projections is decreased (Giannini et al. 2008a).

One additional challenge in West Africa is the paucity of reliable, long term observational data over much of the region. In addition, given the sensitivity of Sahelian precipitation to the spatial pattern of SSTs, the lack of detailed long term sea surface temperature and circulation observations further hampers this work (Giannini et al. 2008b). Without reliable observational data to force and verify model simulations, the ability of the models cannot be accurately tested.

Given the research community's focus on the Sahelian droughts of the 1980s and 1990s, a body of literature has been produced investigating general circulation model (GCM) performance in the region. Recently, the West African Monsoon Modelling and Evaluation (WAMME) project (Druyan et al. 2010; Xue et al. 2010) and other studies have analysed regional climate model (RCM) performance in the West Africa domain.

4.1 Model selection

In this study, an evaluation of the Intergovernmental Panel on Climate Change's Fourth Assessment Report (IPCC AR4) models is undertaken. A cross-section of 8 of the models for which the necessary data is available were initially selected and they are shown in Table 4.1. For all models, the 20c3m experiments, forced using historical emissions, were analysed. The selection includes several models which other studies have shown to have performed well in the West Africa domain (Cook and Vizy 2006; Giannini 2010; Caminade and Terray 2010). Cook and Vizy (2006) investigate the climatology and ability to reproduce the prominent mode of variability (the "dipole" between low/high Sahel precipitation/Guinean coastal precipitation and warm/cold Gulf of Guinea SSTs) in 18 GCMs, finding the models' 20th century simulations to be of variable quality. Of the ensemble, 8 fail to adequately capture the monsoon cycle. They go on to analyse the 21st century output of certain better performing models (including GFDL), concluding that MRI has the most plausible output, though noting significant divergence in the models' future climates in spite of their more robust performance against the observed climate. In MRI, they find warming in the Gulf of Guinea leads to modest drying in the Sahel due to a doubling of the number of anomalously dry years by the end of the century. GFDL also projects a drier future and is at the dry end of the whole AR4 ensemble (Biasutti et al. 2009). The mean or median of the CMIP3 models has been shown to be more accurate than any single model (Gleckler et al. 2008) and is also included in the analysis. The ensemble output is based on the entire CMIP3 model archive, rather than the cross-section otherwise analysed here.

Table 4.1: The models used in this study

Modelling Group	Model designation	AGCM horizontal/ vertical resolution	OGCM horizontal/ vertical resolution	Key papers
Canadian Centre for Climate Modelling and Analysis	cccma_cgcm3_1 "CCCMA"	T63 L31	1.4 x 0..94 L29	Flato and Boer (2001); McFarlane et al. (2005)
Center National Weather Research	cnrm_cm3 "CNRM"	T63 L45	182 x 152 L31	Salas-Melia et al. (2005)
Commonwealth Scientific and Research Organisation	csiro_mk3_0 "CSIRO"	T63 L18	1.875 x 0.84 L31	Gordon et al. (2002)

U.S. Dept. Of Commerce/NOAAb/ Geophysical Fluid Dynamics Laboratory	gfdl_cm2_0 "GFDL"	T45 L24	1 x 0.33-1 L50	Delworth et al. (2006), Gnanadesikan et al. (2006), Wittenberg et al. (2006), Stouffer et al. (2006)
Goddard Institute for Space Studies, NASA	giss_model_e_r "GISS"	4 x 5	4 x 5	Schmidt et al. (2005)
Meteorological Institute, University of Bonn, Meteorological Research Institute of KMA, Model and Data Groupe at MPI-M	miub_echo_g "MIUB"	T30 L19	T42 L20	Legukte and Voss (1999)
Max Planck Institute for Meteorology	Mpi_echam5 "ECHAM"	T63 L32	1 x 1 L42	Roeckner et al. (2006)
Meteorological Research Institute	mri_cgcm2_3_2_a "MRI"	T42 L30	2.0 x 0.5-2.0 L23	Yukimoto et al. (2001)

4.2 Model ability to reproduce the observed climate

Most GCMs produce a drier Sahel (here defined as the region 10–15°N across the West Africa region) at the end of the 20th century in comparison to preindustrial climates, though tend to overestimate precipitation in comparison to the observed climate (Biasutti and Giannini 2006). Biasutti et al. (2008), however, defining the Sahel as being the region of West Africa between 10–20°N, review the CMIP3 models concluding that, climatologically, most models do not produce sufficient precipitation across the Sahel in the summer. Correlations between Sahel and oceanic precipitation (the "dipole") vary widely across the models with increased Sahel rainfall being associated with the northern edge of the ITCZ in some and a dipole pattern with Gulf of Guinea precipitation predominating in other models.

In addition to reproducing the climatological state, the models need to be able to adequately reproduce climatic variability on short and long timescales and the key teleconnections which influence this variability.

The relationship between SSTs and West African precipitation, particularly Sahelian precipitation given the recent research focus, is well established (Lamb 1978; Hastenrath 1984; Folland et al. 1986; Rowell et al. 1995) with oceanic forcing identified as the dominant driver of decadal precipitation variability in the region (Biasutti et al. 2008). Recent efforts

have sought to quantify this influence more robustly and in doing so have investigated the ability of climate models to replicate these key teleconnections. Mohino et al. (2010) decomposed the influence of SSTs on Sahelian precipitation on the multi-decadal timescale by forcing a model with SST patterns associated with an overall warming trend (an external forcing), the Atlantic Multidecadal Oscillation (AMO) and the Inter-decadal Pacific Oscillation (IPO) (forcings they argue are internal to the climate system). They found that only 10% the SST influence on the drought of the 1980s was attributable to global warming and that the AMO and IPO patterns were significantly more influential. They argue that the recent recovery in the Sahel was mainly driven by the (positive) phase of the AMO, perhaps unsurprising given the land-sea temperature contrast which is a key component of regional circulation and therefore whether precipitation is located in the Sahel (Haarsma et al. 2005), with the global warming SST pattern counteracting this increase. These results contrast with certain earlier studies (Held et al. 2005; Biasutti and Giannini 2006) and are supported by others (Lu and Delworth 2005; Hoerling et al. 2006; Caminade and Terray 2009; Ting et al. 2009), indicative of the current difficulty in robustly attributing and quantifying the role of competing influences on the region's climate.

Interannually, the relationship between Sahelian precipitation and tropical SST anomalies is reproduced by most models (Biasutti et al. 2008) though the strength of the relationship is highly variable. Philippon et al. (2010) examined intra-seasonal variation in a multi-model experiment using GCM simulations started on 1st May each year. They observed that the Sahelian mode of precipitation variability was not well captured by the models, even though other parameters relative to the atmospheric dynamics of the monsoon were more adequately reproduced, indicating the difficulty the models have capturing the monsoon precipitation on shorter timescales.

The observed relationship between the Saharan heat low and Sahelian precipitation is also variably produced by the CMIP3 models (Biasutti et al. 2009), with "wet" and "dry" models tending to produce particular signatures in their biases, though interannual variations in the heat low (and its impact on Sahelian precipitation) are generally consistent with observations.

The CMIP3 models tend to overestimate the length of the Sahelian rainy season, a result primarily attributable to the monsoon starting too early (though it also ends too late) associated with a gradual increase precipitation in the region, rather than the observed "jump".

Variability in the mean start date, end date and length of the season are also all underestimated but with a large ensemble spread and some models producing excessive variability in these metrics (Biasutti and Sobel 2009).

RCMs have begun to be applied to the West Africa domain, an activity which will increase in preparation for the IPCC's AR5, driven by observed and reanalysis datasets or GCM derived boundary conditions. Generally, the performance of RCMs is better than GCMs, a fact explicable by the spatial resolution of many fundamental features of the West African Monsoon and the feedbacks between the major processes. Comparison of experiments driven by GCM and observed/reanalysis boundary conditions also indicate downscaling GCM output in future scenarios is likely to improve the robustness of projections (Sylla et al. 2009, 2010). However, even with higher resolution, most RCMs fail to produce features such as the African Easterly Jet and Tropical Easterly Jet and, as a result, the basic evolution of the monsoon is generally adequately resolved, but variability due to the major modes is less well produced (Xue et al. 2010). Druyan et al. (2010) analysed four RCMs in the West Africa domain, finding the monsoon onset in the Sahel to be 2–5 weeks earlier than observed, indicating that even with enhanced spatial and temporal resolution, models still have difficulty resolving the complex climate of the region, and generally exhibit positive precipitation biases over much of the wider region. They found, however, that lateral boundary location could impact on the performance of the RCMs, with "edge effects" leading to defects in the simulated climate – an issue of experimental design rather than model error. In light of the possibility of relationships in the regional climate being non-stationary (see Section 2 above, and the discussion of climate projections in Section 6, below), using statistical models to adjust model output of future scenarios which have been trained on the observed period (Philippon et al. 2010; Paeth, in press) may not be appropriate.

It is clear that the West African monsoon remains a fundamental challenge to climate modelling groups. In recent years, significant improvement in the ability of models to capture the monsoon and its variability has occurred, with the CMIP3 dataset representing a marked improvement on CMIP2 (IPCC 2007) and with increased use of regional modelling, this trajectory should continue.

4.3 Model climatologies 1970-1999

The climatologies of the models selected for analysis are now reviewed. As previously noted, generally, the CMIP3 dataset produces the large scale, zonally oriented precipitation distribution, but the models do not replicate the seasonal precipitation cycle and location of the most intense precipitation as robustly (Cook and Vizy 2006).

4.3.1 Temperature

The climatological ensemble mean temperature and annual cycle is shown in Figure 4.1. The observed climatology is in Figure 2.1. Individual model monthly climatologies are in Appendix 3 and their output broadly summarised in Table 4.2. Several of the models produce robust temperature climatologies, both in terms of the timing of the seasonal cycle and the location of the regions of greatest intensity. Several are too cold, in particular in the Sahel. The ensemble output is close to the observed pattern.

Figure 4.1: Annual and monthly ensemble temperature climatology for the region

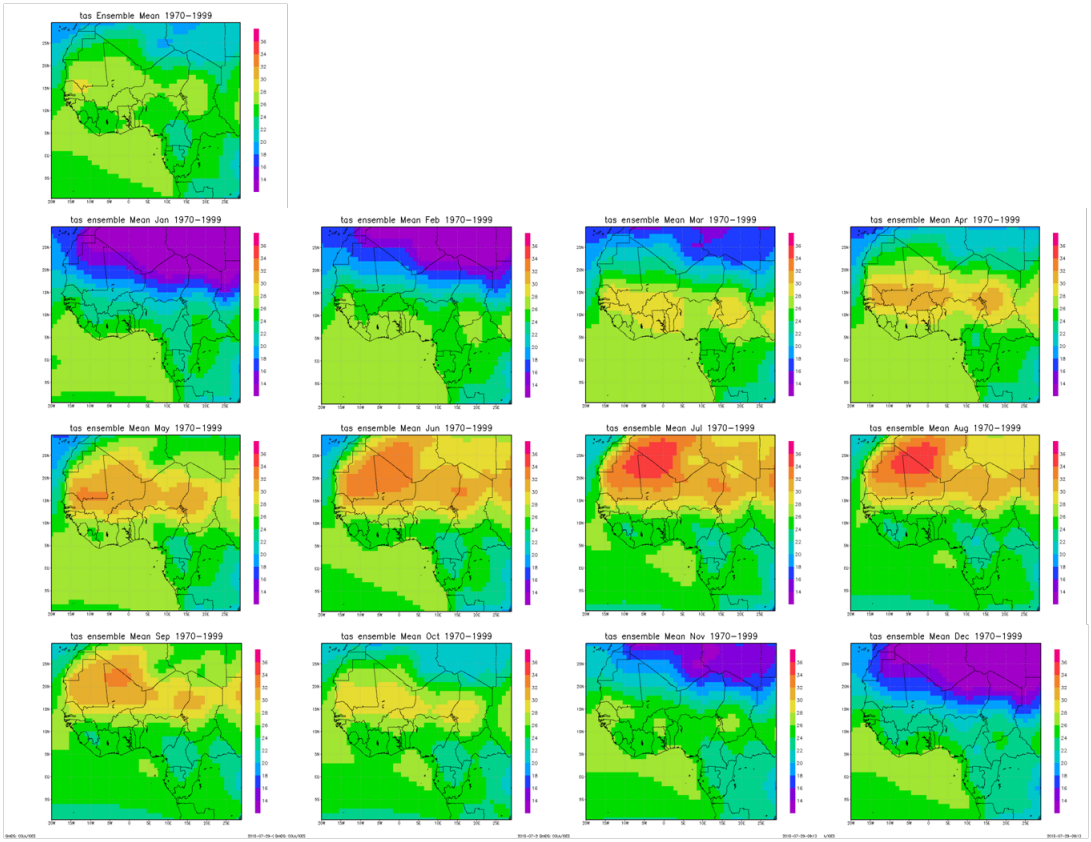

Table 4.2: Summary of the model produced climatologies

Model	Temperature	Precipitation
CCCMA	Generally too cold across the region	Monsoon precipitation reaches too far north in summer, precipitation under-resolved at coast in summer. Timing of annual cycle adequate.
CNRM	Good spatial pattern and temporal evolution. Saharan heat low too hot in summer and Sahel too cold.	Monsoon precipitation reaches too far north in summer, precipitation under-resolved at coast in summer. Timing of annual cycle adequate.
CSIRO	Good spatial pattern and temporal evolution. Saharan heat low too cold in summer and Sahel too cold.	Annual cycle starts prematurely, and reaches too far north, with excessive intensity, in summer. Monsoon retreats too soon.
GFDL	Generally too cold across the region	Adequate temporal evolution and spatial distribution of precipitation. Precipitation over-resolved in summer near southern and eastern coast.
GISS	Good spatial pattern and temporal evolution. Saharan heat low too hot in summer and Sahel too cold.	Excessive precipitation in most of the region. Annual cycle starts prematurely.
MIUB	Good spatial pattern and temporal evolution, but too cold.	Annual cycle starts prematurely. Timing and pattern of precipitation is otherwise adequate.
ECHAM	Good spatial pattern and temporal evolution, but too cold.	Good pattern and timing of precipitation, but under-resolves summer precipitation at coast.
MRI	Good spatial pattern and temporal evolution. Saharan heat low too hot in summer. Sahelian warming too late.	Good timing, but too little rain. Rainy season too short.

4.3.2 Precipitation

The climatological ensemble mean precipitation and annual cycle is shown in Figure 4.2. The two reanalysis climatologies are in Figure 2.2. Individual model climatologies are in Appendix 3 and their output is also summarised in Table 4.2. The seasonal cycle and the intensity of precipitation is generally less well resolved in comparison to the models' ability to simulate the temperature climatology. Several produce excessive summer precipitation in the northern Sahel and Sahara, these anomalies generally coincident with deficiencies in the seasonal temperature cycle/intensity of temperature, with relatively more rain in this region where the models simulate cooler conditions than observed. GISS stands out as performing significantly less adequately than the other models, with excessive precipitation all year over most regions and the summer monsoonal rains pushing too far north into the Sahara. On further analysis it appeared this error was a function of the daily model output (further evidenced in Figure 4.3) and is not replicated in the monthly precipitation dataset. GISS was not considered for further analysis as a result. The ensemble output is close to observed, though does not capture the most intense precipitation around the Gulf of Guinea coast.

The climatological cycle of precipitation across the region is shown in Figure 4.3. The NCEP and JapRe datasets diverge slightly in terms of the intensity and period of the annual cycle. However, even with this observational uncertainty it is clear that the majority of models produce excessive precipitation across the domain, with only MRI producing a climatological cycle in this region close to the reanalysis datasets.

Figure 4.2: Annual and monthly ensemble precipitation climatology for the region

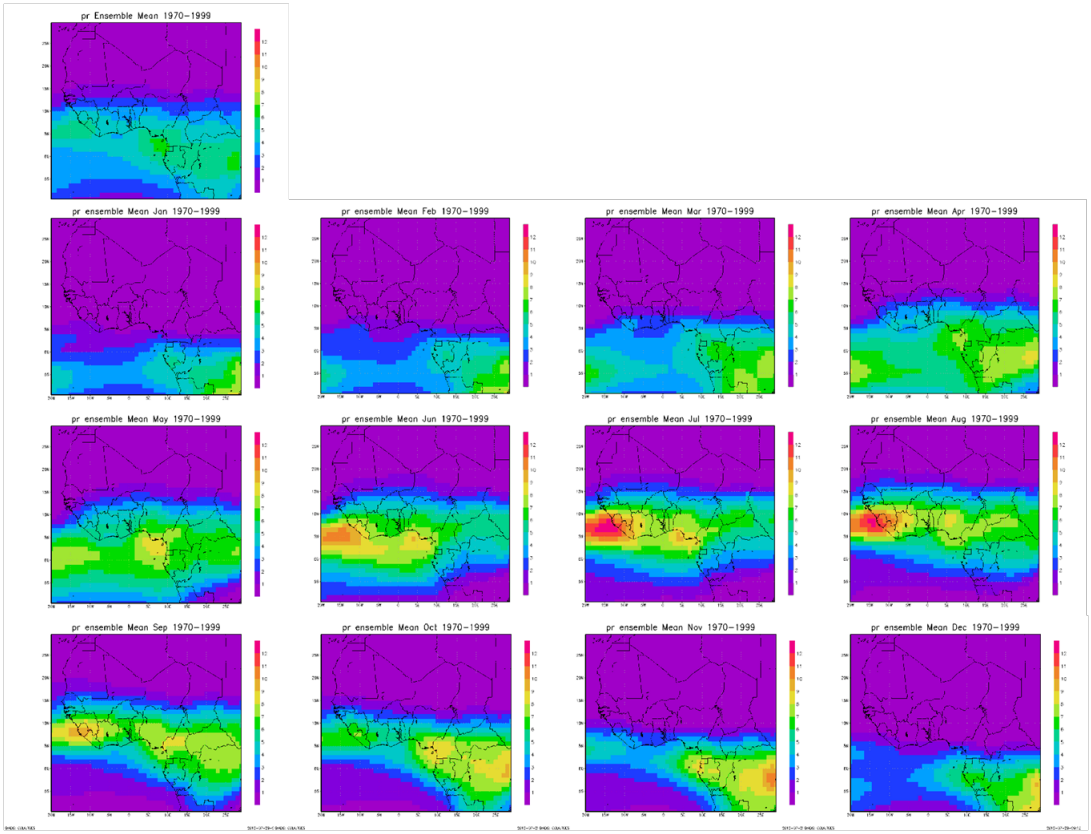

4.4 Model produced variability and trends

4.4.1 Short term variability

Phillippon et al. (2010) investigated intraseasonal variability of the West African monsoon in several GCMs, finding intra-seasonal precipitation variability to be under-resolved at the local scale. Turning to the interannual performance of the models, Table 4.3 shows the standard deviation of model produced annual Sahelian precipitation totals, in absolute and percentage terms relative to their climatological totals, compared to the two reanalysis datasets. In absolute terms, the mean figure is towards the lower end of the two reanalysis datasets but well within the boundary of uncertainty derived from the reanalysis datasets. Given the climatological precipitation produced by many models, the percentage figure shows that many

of the models under-resolve interannual variability, an important metric for agricultural purposes.

Figure 4.3: The annual precipitation cycle averaged zonally across the West Africa domain for the 1970-99 period

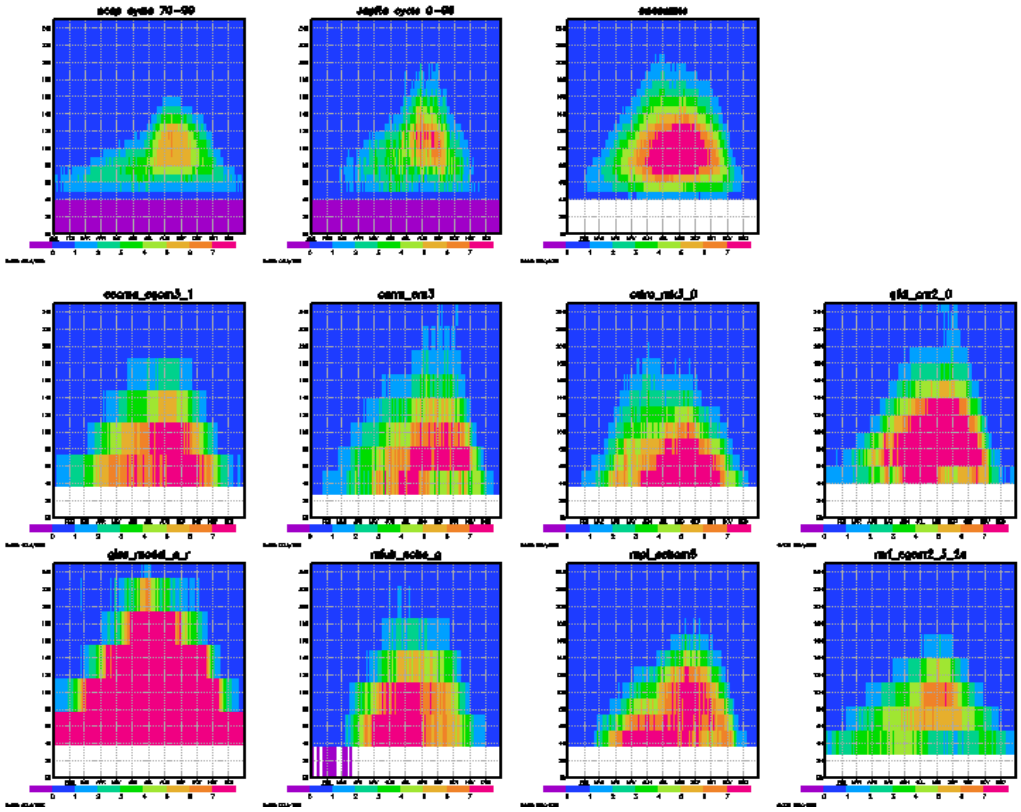

Table 4.3: The model derived Sahel precipitation climatologies (1970-99) with the standard deviation of total annual precipitation in both absolute and percentage terms.

Dataset/Model	Climatology (mm/day)	Absolute SD (mm/day)	SD as a percentage of total precipitation
NCEP	1.20	0.25	20.7
JapRe	1.57	0.15	9.7
CCCMA	1.96	0.13	6.7
CNRM	1.97	0.21	10.9
CSIRO	1.80	0.15	8.3
GFDL	3.03	0.31	10.3
MIUB	2.06	0.14	6.9
MPI	2.02	0.16	7.9
MRI	1.28	0.14	10.6
Model average	2.02	0.18	8.8

4.4.2 Decadal variability and observed trends

One difficulty in seeking to analyse trends in this region since 1950 is the late 1960s climatic shift which has already been discussed. If this inter-decadal variability is attributable to natural, internal climatic variance, for models forced by anthropogenic emissions during this period it may be that this variability is not adequately captured, even though the models may still be resolving the climate adequately within the boundaries of potential variability proscribed by the external (anthropogenic) forcing. Simulations forced by observed SSTs help increase confidence in model ability where regional and local trends and variability are not as well replicated through external forcing alone.

Hoerling et al. (2006), investigating the relationship between SSTs and trends in Sahelian precipitation, concluding that the observed patterns in the 1950–99 period cannot be explained simply through greenhouse gas forcing. Instead, the natural variability of the AMO is suggested as the key SST derived influence. Mohino et al. (2010) quantify this as a 10% greenhouse gas (GHG)/overall warming signal with the remainder largely attributable to the AMO and IPO (internal) patterns of variability. Such a conclusion makes future projections less readily verifiable, particularly in light of the current recovery in the eastern/central Sahel monsoon and the ongoing efforts to decompose the driving influences behind this (Fontaine et al. 2010). It also means that the failure of models to produce the significant inter-decadal variability observed since 1950 does not necessarily mean that they are fundamentally inadequate, nor that their future projections are inadequate, but makes verifying their competence across the domain difficult.

Figure 4.4 shows the ensemble annual and monthly temperature trends from 1950–1999, along with the observed data for comparison. The observed 1970–1999 trends are also included so the influence of the late-1960s climate shift is removed (though it is less significant for temperature than precipitation). For all months the ensemble temperature trends are generally 0–0.2°C/decade. The model annual trends are also shown, with the monthly trends in Appendix 4. Though the annual model trends are generally similar to the observed data and the ensemble average, the monthly model trends are more divergent across the domain. For most models, in most months, the majority of the region exhibits trends of 0.1–0.4°C/decade. No model faithfully replicates the observed trends in the annual cycle, though many reproduce the strongest warming trend in the Sahel/Saharan region. Errors are

not consistent in terms of direction or magnitude in any individual model or across the ensemble. Given the discrepancies between the spatial pattern of warming in the 1950–1999 and 1970–1999 observed trends, the difficulty the models encounter in resolving the spatial trends in magnitude are perhaps not surprising, given the influence of internal variability on the regions climate.

Figure 4.4 (continued on next page): Annual and monthly temperature trends in CMIP3 ensemble output. The cru trends for both 1950-99 and 1970-99 are provided for comparison.

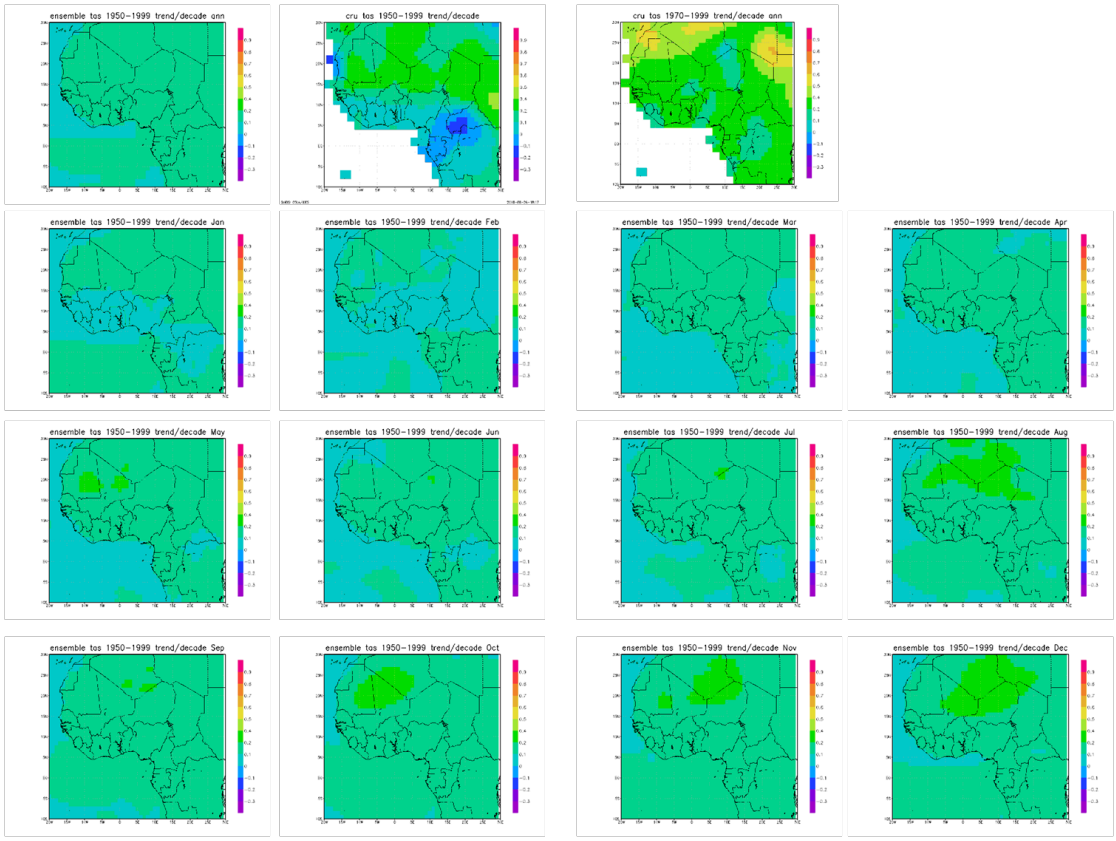

(Figure 4.4 continued)

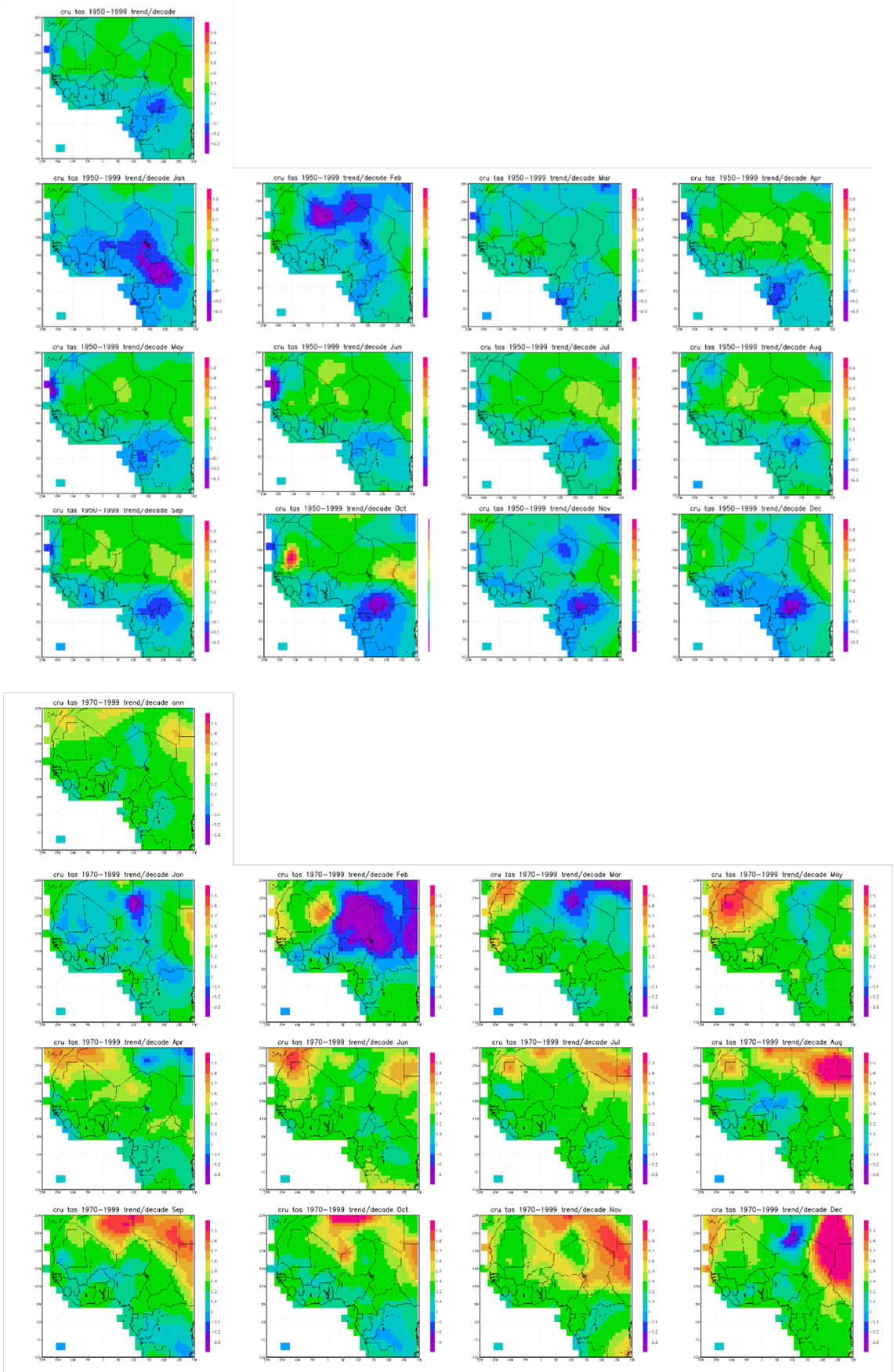

Figure 4.5: Annual temperature trends for the models and the CMIP3 ensemble output. The cru trends for both 1950-99 and 1970-99 are provided for comparison.

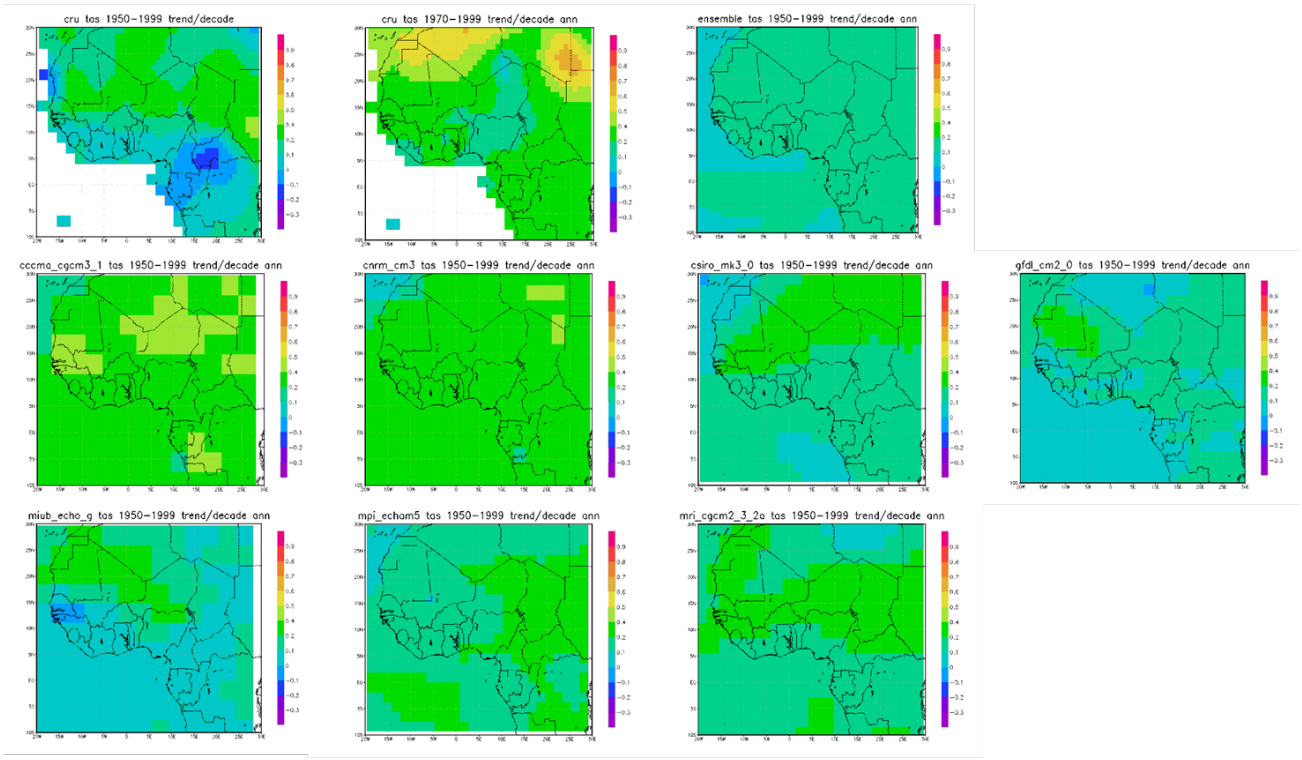

Figure 4.6 and Figure 4.7 show the same figures for precipitation, with 1950–1999 and 1970–1999 reanalysis data for comparison. The scale used (due to the size of some of the model trends) masks much of the JapRe precipitation trends, though the reversal of trend seen in Figure 2.6 is still visible, particularly in August. The JapRe data does not produce such a pronounced drying trend from 1950–99, with 0.4 mm/decade only exceeded in August in the Sahel. The NCEP data in the region is more clearly dominated by the shift in summer precipitation in the late 1960s. In the 1970–99 data, this pattern is at least dampened and in much of the Sahel/Gulf of Guinea coastal region reversed as the recovery of the monsoon becomes imprinted on the record.

It is not surprising that the models do not pick up the key spatial trends in the observed record which correspond to these localised patterns of change given their difficulty in robustly reproducing the climatological pattern of precipitation. The annual precipitation trend in many models (Figure 4.7) is relatively neutral, failing to reproduce the drying trend of the Sahel and surrounding regions, but otherwise broadly corresponding to the observed climate in the remainder of the region. Upon investigating the annual cycle in the models (Appendix 5), it is clear that these deficiencies are largely attributable in most models to a failure to reproduce

the sharp decrease in July-September precipitation which was observed in the late 1960s and is seen in both reanalysis datasets. The ensemble output is also characterised by the failure to replicate the southward shift in precipitation associated with the Sahelian drying of the late 1960s.

Figure 4.6 (this and next two pages): Annual and monthly precipitation trends in the CMIP3 ensemble output. The NCEP and JapRe trends for both 1950-99 and 1970-99 are provided for comparison.

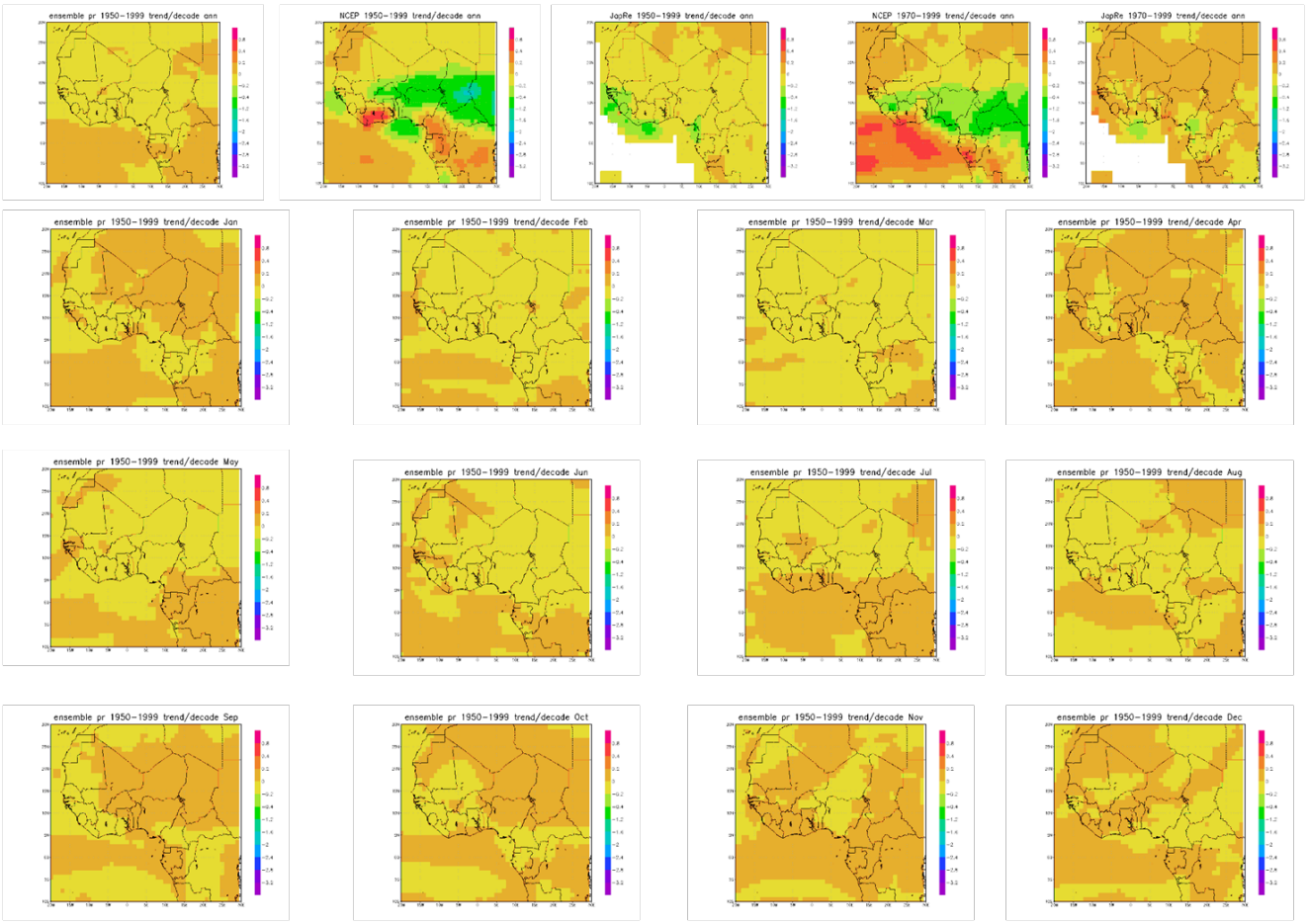

Figure 4.6 continued

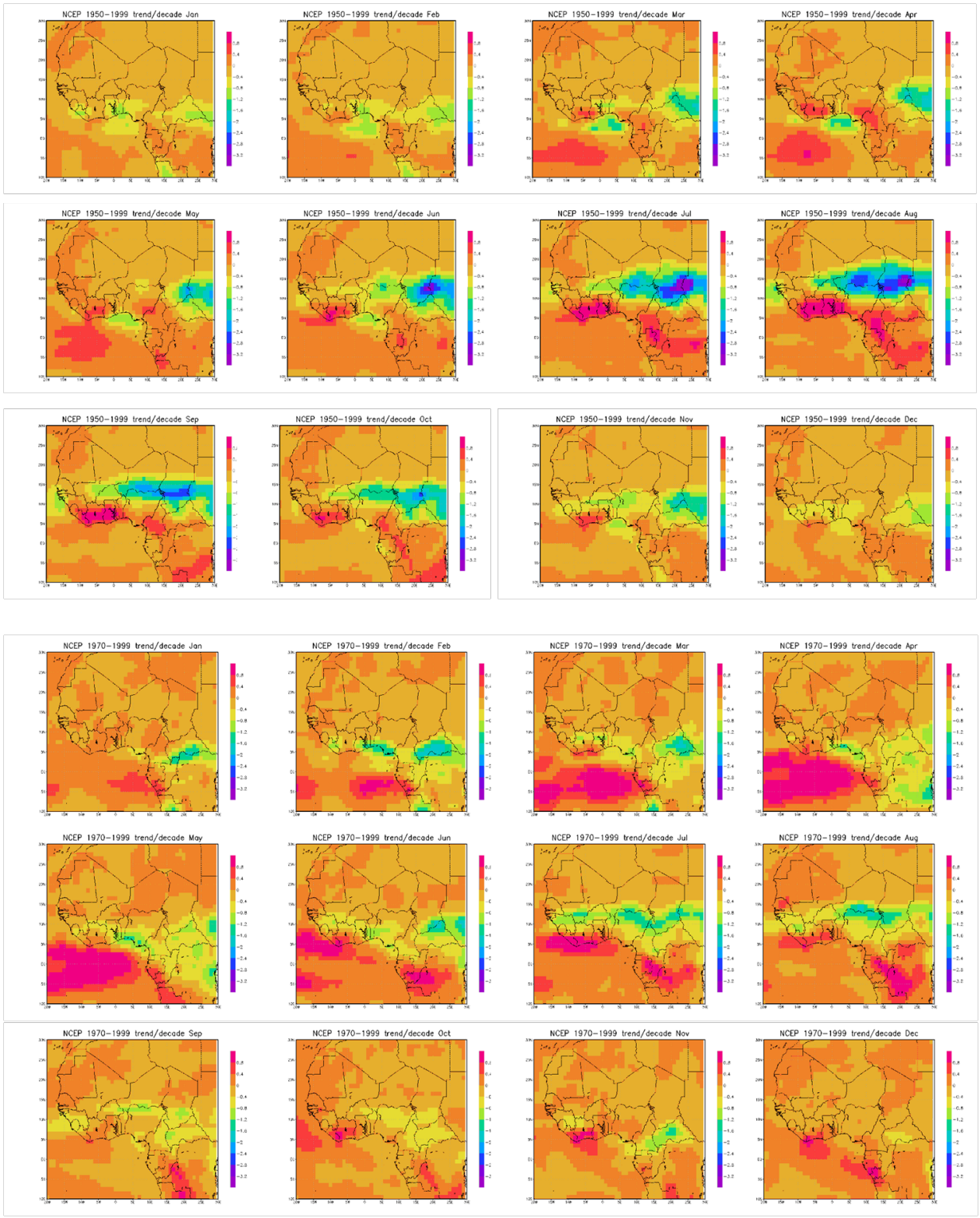

Figure 4.6 continued

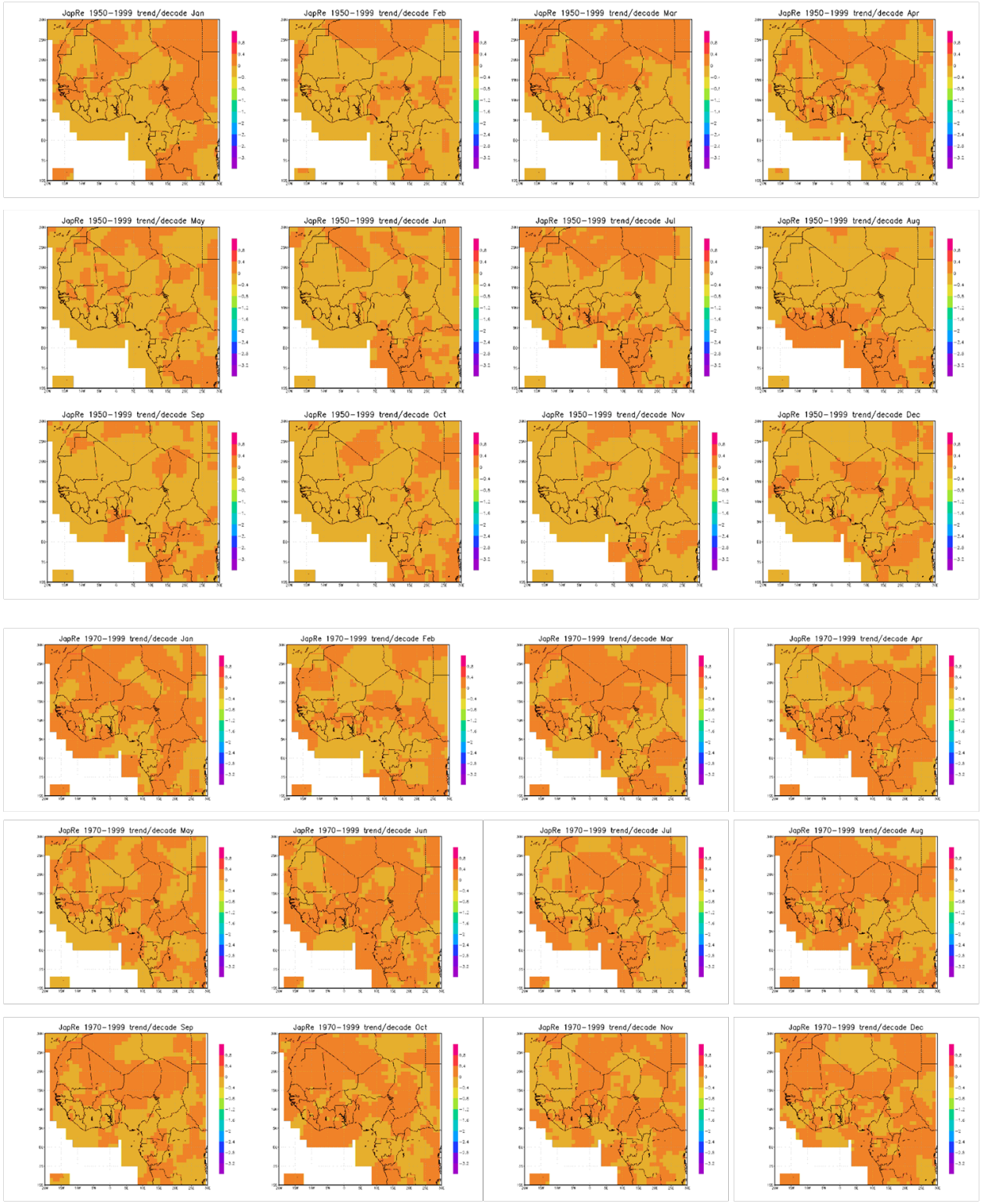

Figure 4.7: Annual precipitation trends for the models and the CMIP3 ensemble output. The NCEP and JapRe trends for both 1950-99 and 1970-99 are provided for comparison.

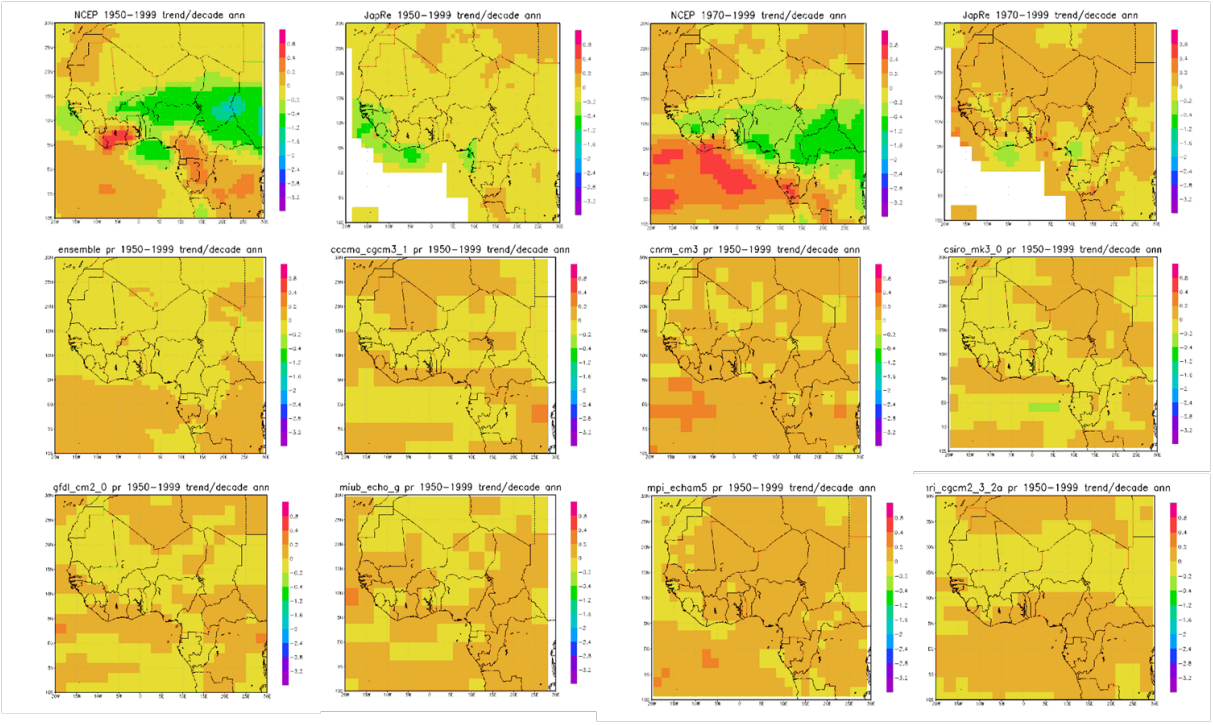

4.5 Models and the Monsoon Cycle

Biasutti et al. (2008) observed that most models do not produce sufficient precipitation across the Sahel in the summer, a result which is reconcilable with the current results by the fact that they define the Sahel as being 10–20°N, rather than 10–15°N, as used in this study. Biasutti and Sobel (2009) found the CMIP3 models tend to overestimate the length of the Sahelian rainy season primarily due to the monsoon starting too early (though it also ends too late) with mean variability in the start date, end date and length of the season underestimated but with a large inter-model spread and many models producing excessive variability. Here, the threshold based indices which were applied to the reanalysis data in Section 2.3.3 are applied to daily data from the models. The ability to capture the start and end of the monsoon accurately was more difficult given the inaccuracy with which the models produce the seasonal cycle. Individual years were analysed, with several models capturing "false starts" in certain years. Given these issues, these results must be considered provisional. Table 4.4 shows the model and reanalysis produced climatological dates. The results correlate with those of Biasutti and Sobel, with the monsoon period being too long and this discrepancy being produced in most models primarily due to the early commencement of the rains. The majority of the models also produce the negative trend in the season length, though generally

underestimate this and given the high variability in the data relative to the trend and period, only one of these trends is significant at 90%. The variability in season length is well produced and slightly higher than the reanalysis data, a function (when compared to Biasutti and Sobel's results) of the particular model selection used in this study.

Table 4.4: Monsoon start and end dates, monsoon length, trends in the length of the monsoon (for the 1970-99 period, figures in days/year) and the standard deviation of the length of the monsoon. Figures are provided for the NCEP and JapRe reanalyses for comparison, and the average of the 7 models is also included. Significant at 90% is shown in red.

Dataset/Model	Start	End	Length	Trend 1970-1999 (days/year)	Standard Deviation (days)
NCEP	28th June	28th Oct	122	-0.59	18
JapRe	6th July	1st Sept	75	-0.32	17
CCCMA	20th May	3rd Nov	168	-0.44	23
CNRM	17th Jun	11th Nov	149	-0.32	26
CSIRO	19th Apr	17th Oct	180	-0.36	16
GFDL	2nd May	15th Oct	165	0.28	14
MIUB	18th Jun	20th Oct	134	-0.74	20
MPI	5th Jun	15th Oct	132	-0.21	22
MRI	11th Jul	10th Nov	121	-0.01	15
Model average	29th May	26th Oct	150	-0.26	19

4.6 Model simulation of climatic extremes

Modelling of climate extremes is challenging. Extreme events are rare by definition and, hence, are subject to sampling errors (Meehl et al. 2000), meaning that the background climate events and trends the models are attempting to reproduce are not necessarily well constrained (Kharin et al. 2007). In the current context, the divergence in the 95% precipitation trends over the northern Sahel/Sahara in the two reanalysis datasets is particularly notable (Figure 2.5). With such a high level of uncertainty, it is difficult to assess model ability to reproduce such extremes. The spatial and temporal resolution of GCMs also means that they are unable to adequately resolve many of the most intense and short lived events (Kiktev et al. 2003; Chen and Knutson 2008). Furthermore, finding an anthropogenic "fingerprint" in patterns of change is more challenging at both a regional level and for climate extremes. To identify regional patterns in extremes and attribute them to global warming—a necessary process if reliable projections of changes in regional extremes are to be produced—

requires both of these challenges to be overcome (Min et al. 2009). Intermodel discrepancies in extremes are far larger for individual events than climatological values (Kharin et al. 2007), indicating simulation of variability in extreme events and the return period for the most extreme events is not consistently reproduced.

Kharin et al. (2005) examined GCM ability to simulate temperature and precipitation extremes, finding that models simulate the temperature extremes, especially the warm extremes, reasonably adequately. Models have more serious deficiencies in simulating precipitation extremes, particularly in the tropics. Sun et al. (2006), investigating daily precipitation intensity, found that most of the 18 GCMs in their study produced light precipitation more often than observed, too few heavy precipitation events and too little precipitation in heavy events (>10 mm day^{-1}). The errors tend to cancel, such that the seasonal mean precipitation statistics are realistic, but for the purposes of agricultural production, these extremes can be as, or more, important that the mean conditions. Models generally produce lower intensity precipitation too regularly at the expense of heavier events and resultantly produce too many rain days (Dai 2006).

Vavrus et al. (2006) used daily values of 20th century integrations from seven models to look at cold air events, finding that the climate models in their study reproduced the location and magnitude of cold air outbreaks in the current climate. Greater success has been had in downscaling studies, several of which have looked at European climate (Murphy 1999; Frei et al. 2006; Tapiador et al. 2008), as the increased spatial and temporal resolution of RCMs and the ability of statistical downscaling techniques often overcomes some of the limitations of the coarse resolution of GCMs, though these studies have generally focussed on regions with better observational networks. Model simulations of the trends in global indices is also relatively robust, but when these indices are examined at a regional level, the direction and consensus of the trends which emerges is less significant (Tebaldi et al. 2006).

Following the investigation undertaken for the observed and reanalysis data, the results from the GCMs in this study are presented. As previously noted, the discrepancies in precipitation trends in the reanalysis data are significantly greater than for temperature and this makes the verification of the model outputs difficult, since in some regions trends in the reanalyses diverge appreciably, both in magnitude and direction.

Figure 4.8: Model derived climatologies and percentage trends during the 1970-1999 period of 95% precipitation events. The NCEP and JapRe outputs are shown for comparison. The climatologies are mm/day and the trend figures are percent/decade.

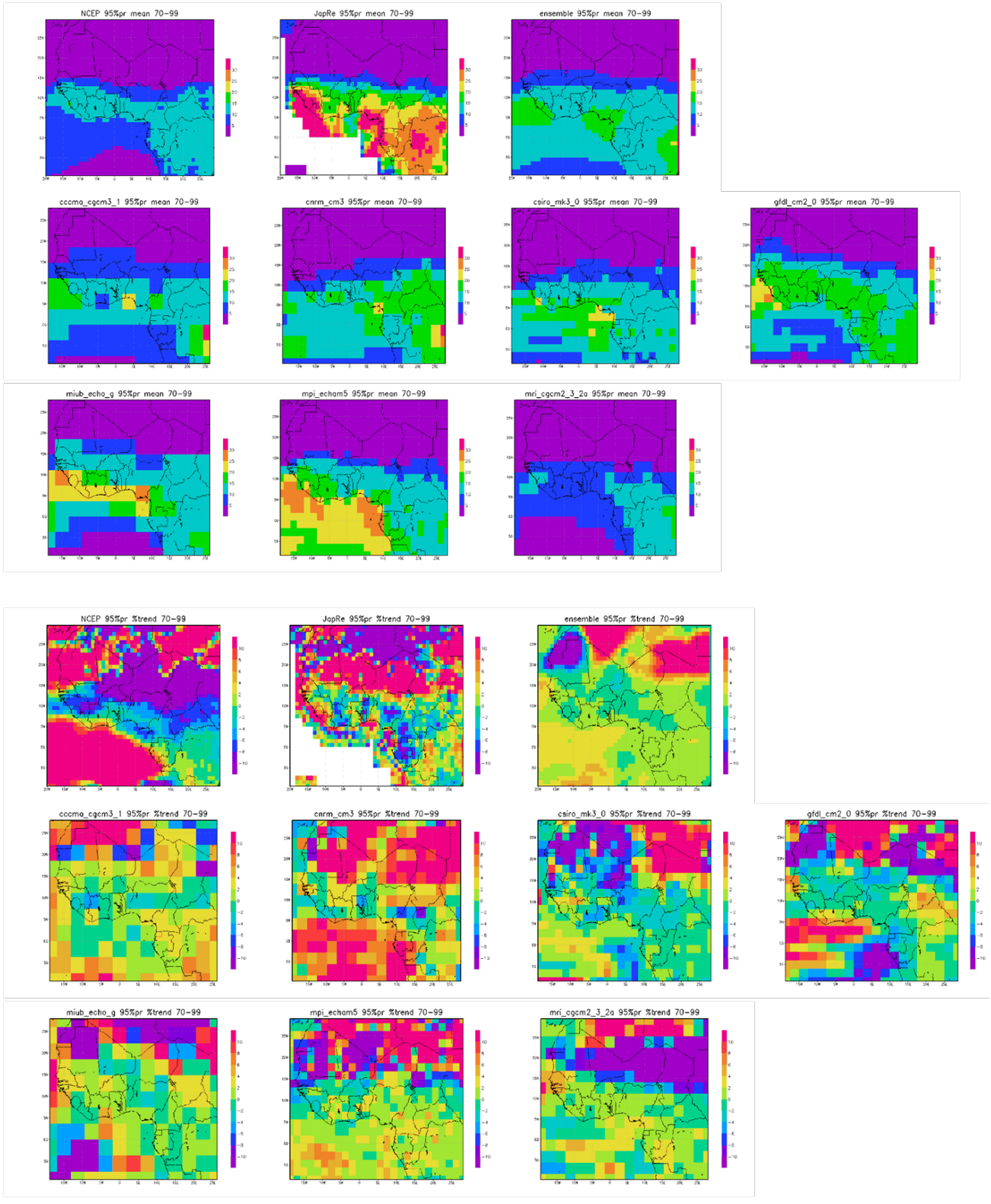

Plots for model produced trends in 95% precipitation events and their climatologies are in Figure 4.8, with the NCEP and JapRe data presented for comparison. The model produced climatologies are significantly lower than the JapRe climatology in most areas and many are close to the NCEP reanalysis, which is lower than observed (Fontaine et al. 2002). This is not surprising, given the resolution of the models. The spatial pattern of the most extreme precipitation follows the model biases in climatological mean precipitation. The model trends are, as might be expected, highly variable both spatially and in the direction and magnitude of the produced trends. Given the variability in the reanalysis data, it is not possible to comment on the reliability of these trends.

Turning to 5-day maximum precipitation events, the climatology figures for the models are in Table 4.5. Given the models' tendency to over-resolve precipitation over the Sahel domain, the maximum precipitation values are relatively high. They remain below the value for JapRe—even though the model derived climatological precipitation values (Table 4.3) are significantly higher, indicative of the inability of the models to reproduce extreme precipitation events. The trends produced by the models are also highly variable, and mostly positive, in contrast to trends in the reanalyses over the same period, decreasing confidence in model projections of change in these indices. Furthermore, none of the model produced trends are statistically significant at 90% suggesting any trends may be a function of internal variability and the short period of analysis used here. The reanalysis trends may be related to (internal) decadal variability which is not reproduced by the models, but any verification of this hypothesis would require significant further investigation.

Table 4.5: Figures, in mm/day, for 5-day maximum precipitation events in the Sahel domain. Annual maximum figures are derived for each grid point and these totals are averaged across the region. Significant at 90% is shown in red.

	NCEP	JapRe	MRI	MPI	MIUB	GFDL	CSIRO	CNRM	CCCMA
Clim	37.3	74.7	33.6	68.8	56.5	91.4	62.1	78.1	50.3
Trend	-0.5	-0.87	0.02	-0.07	0.03	0.18	-0.1	0.63	0.13

The indices of seasonal maximum dry period and the number of 5-or-greater dry days are in Table 4.6. The resolution of the models is clearly evident in these indices, with the lower variability and greater consistency in monsoon precipitation across the Sahel in the model outputs depressing the figures, particularly the length of the longest dry period. For the

periods of consecutive dry days and 5-day periods the two reanalysis datasets produce trends which are significant at 90%, but with a positive trend in NCEP and negative in JapRe in both indices. No model produces a significant trend in either index.

Table 4.6: Figures for the longest period of consecutive dry days and total number of 5-or-greater day dry periods during the July-September monsoon season. The figures are derived for each grid point and these totals are averaged across the region.

	NCEP	JapRe	MRI	MPI	MIUB	GFDL	CSIRO	CNRM	CCCMA
CDD	30.9	25.8	5.9	4.5	4.5	5.8	8.3	7.5	3.7
5+ days	1.2	0.7	0.5	0.4	0.4	0.5	1.1	1.0	0.3

The spatial variability and magnitude of the climatological 5% minimum temperatures (Figure 4.9) are reproduced relatively robustly in comparison, with the gradient and spatial distribution of the minimums following the NCEP data. The primary errors are due to an inadequacy to reproduce the lowest temperature minimums in the Sahara, even though the model average temperature climatologies produce lower temperatures than observed over this region (see Appendix 3) in the winter, again demonstrative of the difficulty models have in producing extremes. The maximum temperatures are less well resolved (Figure 4.10), with different models under and over estimating the highest temperatures in the region. Relative to the average temperatures, the ensemble position is of lower estimates in comparison to the observed/reanalysis—ensemble produced average temperatures are generally relatively higher than the comparative temperature of the extremes, once again indicative of the models' failure to adequately resolve climatic extremes. The trends in both 95% maximum and 5% minimum temperatures are generally weakly positive and spatially homogenous, failing to reproduce the decreases in minimums in the Sahel and increases in maximums at the Guinea coast. The extent to which these discrepancies might be due to decadal variability in the reanalysis data is, again, an open question.

It is clear that the models do not simulate climatic extremes as adequately as mean conditions. However, the ability to accurately verify the model output in this region is particularly hampered by the lack of observational data currently available and the variable quality of the reanalysis data. The most notable divergences in both model and reanalysis output are for trends in extreme precipitation indices, which models are well known to have difficulty in reproducing, particularly in the tropics (Tebaldi et al. 2006; Kharin et al. 2007).

Figure 4.9: Model derived maximum temperature climatologies and trends during the 1970-1999 period. The NCEP output is shown for comparison. The trend figures are °C/decade.

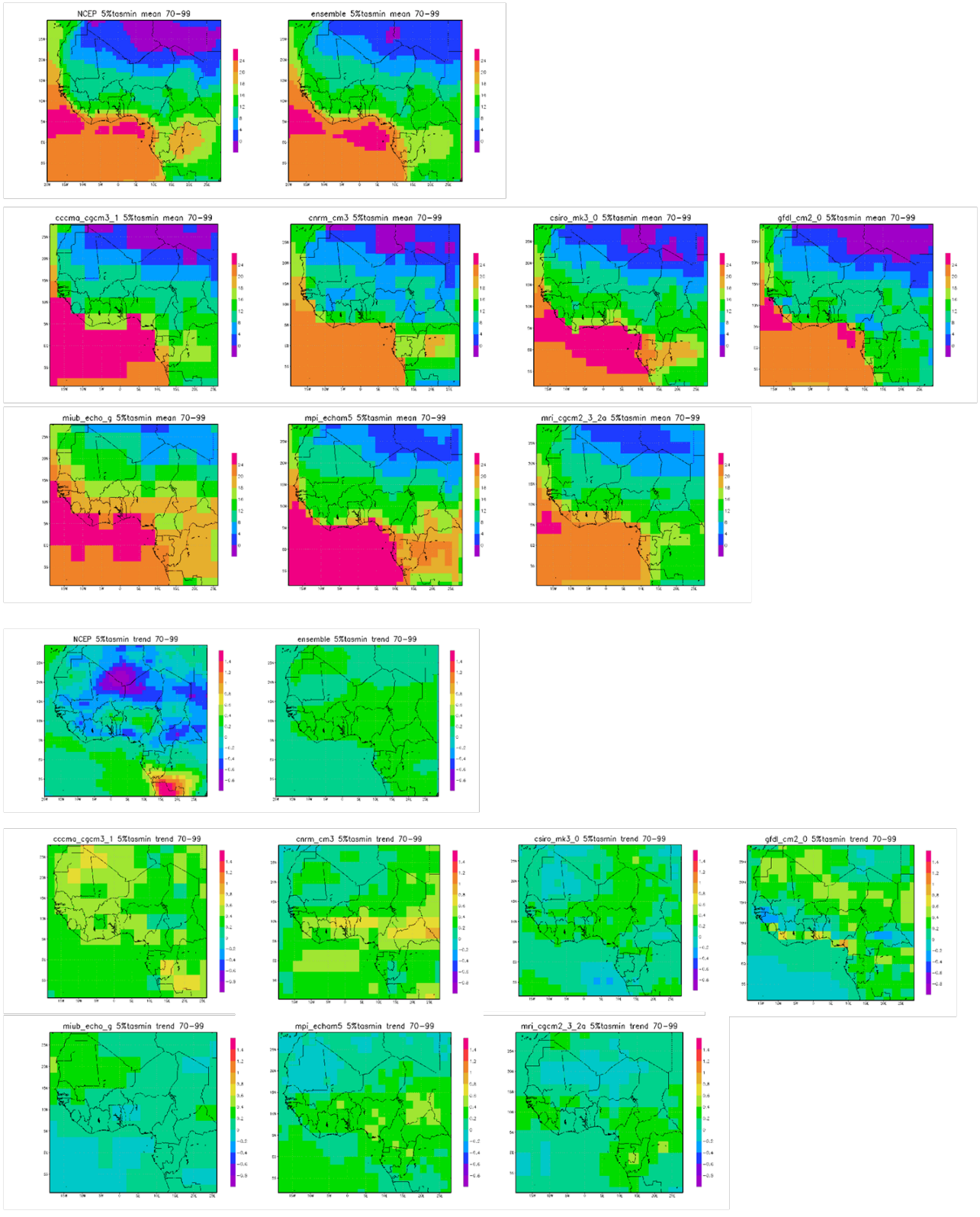

Figure 4.10: Model derived trends during the 1970-1999 period of 95% precipitation events. The NCEP output is shown for comparison. The trend figures are °C/decade.

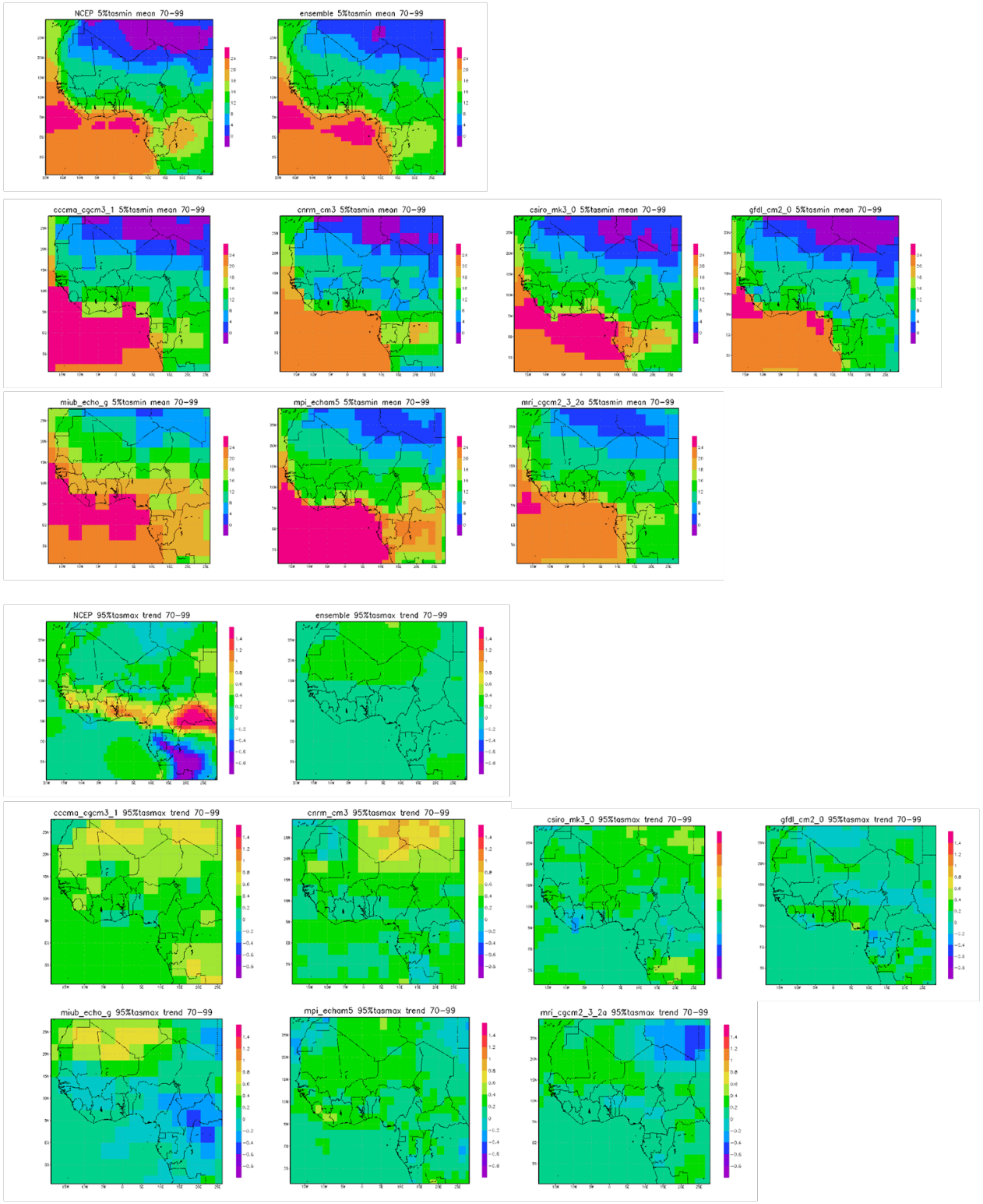

5. Model derived crop growth thresholds

Using the approach applied to the observed data in Section 3 the same exercise is repeated for the 7 remaining models and the ensemble output. This allows an analysis of the extent to which model climatology errors impact upon their projections for crop growth domains under current conditions. The ensemble output is generally computed by using the average of all CMIP3 models. For the daily indices (minimum temperature and maximum temperature) this was not practical since daily data was used. As such the relevant index was first created for each of the selected models and the thresholds applied to the individual model outputs. The results were averaged to create the ensemble mask.

The model derived crop domains are shown in Appendix 6. In Appendix 7 the domains are broken down by variable.

Cassava: The ensemble pattern follows the observed data well, with a slightly more northerly boundary of both the absolute and optimum growth thresholds. This is a function of the wet precipitation climatologies produced in the majority of the models. The secondary threshold is from minimum temperature, with model derived minimums not low enough and the threshold therefore further north than observed. In the individual model outputs, greater variability is observed, with highly variable minimum temperature thresholds and the influence of excessive optimum maximum temperatures affecting the northern reaches of certain model ranges.

Cowpea: The ensemble domain is too extensive, with both the northern and southern boundaries of growth exceeding the two observed/reanalysis domains. Model performance is more variable than for cassava, due to the lower precipitation threshold and greater spatial variability in model precipitation climatologies in drier areas. For the ensemble domain, the secondary threshold is again minimum temperature, which accounts for much variability across the model outputs. Optimum average temperature thresholds are also highly variable across the models.

Rice: The ensemble domain correlates well with both observed/reanalysis domains. The thresholds produced by all variables are similar to observed, with the exception of minimum temperature where the model domain is too extensive. The models are more variable, though

with a high precipitation threshold providing a baseline, and the domains are well constrained on the northern boundary. In several models, lower than observed average temperatures around the Gulf of Guinea coast provide the secondary growth threshold.

Sorghum: The ensemble domain is again closely matched with the observed domains, with the most optimum growing areas not captured due to the models failure to adequately resolve the narrow optimum temperature boundaries required for sorghum growth. Model performance primarily varies as a result of precipitation, with the narrow optimum precipitation boundaries being inhomogeneously replicated across the models. Minimum temperatures are variably replicated and most models also indicate that the majority of the region is outside the optimum average temperature conditions for the crop.

Millet: The narrow band of optimum precipitation and the relatively low absolute precipitation thresholds for millet affect the performance of some of the models. The ensemble domain and those produced by many models are, however, close to the observed pattern. In a small number of models, excessive average temperatures provide a secondary threshold, but the majority reproduce the observed/reanalysis thresholds adequately.

Maize: The well resolved ensemble domain disguises the variability across the models. Observed optimum and minimum temperature thresholds largely reside outside the domain of interest. In several models, both variables combine to influence the crop domain as cooler than observed temperatures along the Gulf of Guinea coast impact upon the model domains.

As previously noted, these maps are derived from climatological averages. The seasonal cycle of the monsoon (which for most models would extend the growing season) and the nature of climatic extremes other than minimum temperatures, such as heavy precipitation events or intra-seasonal droughts which could impact on crop productivity. As discussed in Section 4, the models reproduce mean conditions more adequately than climatic extremes. The model reproductions of these indices, if they could be included in the maps, would generally make the domains less comparable to those produced using observed and reanalysis data.

6. Model climate projections

6.1 Previous studies

The overall assessment of the future is of global warming intensifying the hydrological cycle – wet regions become wetter; dry regions become drier and the intensity of precipitation events in both locations increasing (Trenberth et al. 2003; Neelin et al. 2003; Meehl et al. 2007; Trenberth 2010). Logically, given the Sahel is relatively dry and the Guinean coast is relatively wet, drying of the interior and wetting at the coast might be expected to occur. However, model projections for the Sahel, the focus of much research in the region, are highly divergent. As such, it has been argued that the ensemble average projections may have limited meaning, since the mean position is often substantially different to any individual model (Caminade and Terray 2010), and the ensemble mean is not constrained by any of the physical mechanisms which constrain the models.

Two physically consistent scenarios for the Sahel have been put forward; one drying and one wetting (Giannini et al. 2008b; Giannini 2010). Simplistically, the drying interpretation centres on overall warming of the oceans and associated oceanic convection leading to decreased convection at the continental margins and resultant drying of the interior. A positive feedback from the land would lock this system in place (Neelin et al. 2003; Chou and Neelin 2004; Held et al. 2005). Alternatively, a wetter Sahel could be caused by an enhanced land-sea temperature gradient, either due to greater warming of the land and a stronger monsoon flow (Haarsma et al. 2005) or due to a reversal in the north-south Atlantic SST gradient due to internal oceanic variability (Knight et al. 2006), aerosol forcing (Rotstayn and Lohmann 2002) or a combination of internal oceanic variability and the long term background anthropogenic forcing (Ting et al. 2009). Giannini (2010) has further argued that the wet/dry divergence can be explained in terms of whether the Sahel climate is being forced remotely, by the influence of SSTs, leading to a decrease in precipitation, or locally due to terrestrial changes in evaporation associated with net surface radiation changes connected to greenhouse gas forcing, leading to an increase in precipitation. The former scenario is similar to the mechanism responsible for the recent observed Sahel droughts, though the source of the SST variability has not necessarily been attributed to global warming (Mohino et al. 2010; Ting et al. 2009).

The projections of precipitation in the Sahel are very uncertain across the CMIP3 dataset (Caminade and Terray 2010), with the models unable to agree on even the sign of the trends. Our current understanding of the mechanisms governing regional precipitation patterns increases the difficulty of assessing the plausibility of divergent projections (Biasutti et al. 2008; Giannini et al. 2008b; Giannini, 2010). Even for models which offer a more accurate replication of certain key observed relationships in the 20th century, such as the relationships between the Atlantic SST gradient and Sahelian precipitation, the pattern of these relationships in the future is divergent (Caminade and Terray 2010). No consensus emerges regarding the impact of anthropogenic warming on the Sahel's hydrology in the latter part of the 21st century (Druyan 2010).

Analysing the vertical structure of the monsoon circulation, Biasutti et al. (2009) note that a strengthening of the Saharan heat low during summertime emerges, consistent with an enhanced land-sea temperature gradient. However, the impact this has on the monsoon varies across the models they examine and appears to be dictated by the structure and location of the heat low itself, amongst other influences. Models without a strong low project drying; models with a stronger heat low project wetting. The path the low takes (stronger versus weaker) is not fully determined by the land-sea contrast and is therefore partly independent of SSTs. They also find that the SST gradient in the Atlantic does not correspond to the anomalies in Sahel precipitation produced in the 21st century scenarios they investigate, with Indo-Pacific warming potentially becoming more important to Sahelian precipitation, indicating the relationship Ting et al. (2009) and Mohino et al. (2010) suggest has been dominant over the last few decades may not continue. Given the recent Sahelian wetting and observed breakdown in linear regression models' ability to predict the monsoon rains (Coleman, personal communication), this further complicates analysis and verification of future projections. It has been argued elsewhere (Hagos and Cook 2008) that the recent recovery is consistent with an increased influence of the Indian Ocean.

In the near term, internal variability forced from other components in the climate system, such as the AMO may have a more dramatic effect than the overall trend associated with global warming (Ting et al. 2009). Local forcing, such as land degradation, may also have a significant impact (Paeth et al. 2009). Given the influence of feedback from surface conditions on the monsoon (Paeth et al. 2009), it is possible that even if the models are able to

produce accurate projections of the future based on idealised atmospheric and SST conditions, the sub-regional climate trajectories could be affected by vegetation, land use change and changes in soil moisture which are not included in many of these studies.

The evidence therefore remains inconclusive as to whether a climatological increase or decrease in precipitation is the more plausible projection of change for the Sahel. Given the impact variations in precipitation in the recent past have had on West African, particularly Sahelian, agriculture (Nicholson 2001; Le Barbe et al. 2002; Paeth et al. 2008) and the largely dominant impact of precipitation on the maps of crop growth produced in Section 3, confidence in future projections is currently limited.

Model projections are more consistent around the beginning and end of the rainy season in the Sahel, with precipitation anomalies predominantly negative at the beginning of the season (May–June) and positive at the end (October), indicating a delay in the monsoon (Biasutti and Sobel 2009). For photosensitive crops in particular, such a delay could reduce the growing season and reduce yields (Dingkuhn et al. 2006). Biasutti and Sobel, using 21st century minus 20th century anomalies, find that the beginning of the season becomes progressively later through the more aggressive forcing scenarios, with a less significant delay at the end of the season suggesting the season will shorten, though they emphasis the high inter-model variability in this trend. They identify a delay in the seasonal cycle of global SST evolution, particularly noting the possible influence of the delay in the Atlantic cycle given the well documented influence of Atlantic SSTs on Sahelian precipitation, suggesting the phase shift in the Sahel cycle may well be part of a wider global trend in the seasonal cycle.

Patricola and Cook (2010a) compare GCM and RCM projections for the end of the 21st century under an SRESA2 scenario. The RCM, forced with reanalysis boundary conditions, produced a simulation of the observed climate that was comparable or better than the 9 GCMs (4 of which are used in this study). The RCM projections were created with boundary conditions that are derived by applying monthly anomalies derived from the 9 GCMs to reanalysis climatologies from the 20th century. The RCM projections showed greater consensus than the wide divergence seen in the GCM ensemble and though the sign of precipitation anomalies remained variable, the magnitude of the variance was not as significant (Patricola and Cook 2010b). Given these anomalies are found to be largely a function of SST and lateral boundary forcing and the study only includes 1 RCM, it would be

useful to decompose the extent to which the anomalies are simply a dampened function of the driving GCM anomalies. The RCMs indicate that the early monsoon season (June/July) precipitation will decrease, with an increase in precipitation during August, September and October concurring with the results of Biasutti and Sobel (2009). They note an increase in the intensity of events and attribute the wetter late summer conditions over West Africa to the higher frequency of more intense events, increasing flood risk, a result which parallels with Lebel and Ali's (2010) explanation for the droughts of the 1980s and 1990s, which they attributed to fewer precipitation events during this period. Patricola and Cook (2010a) also note that temperature distributions exhibit positive trends, with extremes of minima and maxima both increasing, with maximum temperatures in the domain rising by 1.8–7.1°C by the end of the 21st century.

Table 6.1: Summaries of the conclusions drawn from selected studies discussed above and elsewhere

Study	Number of models analysed in study	Projection for early 21st century	Projection for late 21st century
Hulme et al. (2001)	7 GCMs	Small impacts	No consensus; ensemble drying
Held et al. (2005)	2GCMs (2 versions of GFDL CM2)	Slight wetting	Progressive drying
Haarsma et al. (2005)	1 GCM	-	Mixed – drier NW &E Sahel, wetter S Sahel
Kamga et al. (2005)	1 GCM	Progressive wetting	Progressive wetting
Hoerling et al. (2006)	18 GCMs	Progressive wetting	-
Cook and Vizy (2006)	18 GCMs	No impact	Drying in last 20 years
Biasutti et al. (2008)	19 GCMs	Uncertain	Uncertain
Paeth et al. (2009)	1 RCM forced by 1 GCM	Drying, but the trend is significantly influenced by land degradation	-
Biasutti and Sobel (2009)	24 GCMs	Projections are 21C minus 20C. Drier May-June; wetter October; no consensus July – September	
Patricola and Cook (2010a, 2010b)	1 RCM forced by 9 GCMs	-	Drier June-July, wetter August-October

Source: Adapted from Druyan (2010)

6.2 Model Projections

To provide a broad scope of projections three of the SRES forcing scenarios are used in this study. B1, A1B and A2 which represent low, medium and high emissions trajectories,

respectively, are used, thereby providing an indication of the influence of forcing uncertainty on the region's climate. Three 10-year periods will be examined—the 2030s, the 2050s and the 2090s. If the models are robust, it should be expected that any trends in the data which are the result of anthropogenic forcing will increase in magnitude over time and through the forcing scenarios. The smallest impact should be observed in the B1 2030s output and the greatest impact in the A2 2090s output. The response may not be linear across the ensemble of scenarios and periods, but should be sequential. The spread of the model projections for each forcing scenario provides the model uncertainty associated with the projections.

6.2.1 Temperature

Figure 6.1 shows climatological temperature anomalies for the ensemble output for the three periods and three forcing scenarios relative to a 1970–99 climatology. The model climatologies are in Appendix 8(a). The ensemble temperature anomalies show a generally steady increase over the period, with anomalies of 2–3°C across the region by the 2090s under the stronger forcing scenarios. The models all exhibit similar trends, but with high variability in the magnitude and spatial distribution of the increases. Several indicate anomalies of in excess of 5°C across the Sahara by the 2090s in the sresa2 scenario, which in several models shows significantly greater warming in comparison to either the sresa2 2050s or sresa1b 2090s scenarios, indicating a strong non-linearity in response to forcing. The ensemble output is clearly lower than the majority of the models analysed here. Given the short climatology period, this could partly be a function of internal variability within the particular models used here, but is more likely a function of the spread of the CMIP3 model projections.

6.2.2 Precipitation

As for temperature, precipitation climatologies are in Figure 6.2 for the ensemble and Appendix 8(b) for the individual models. The ensemble climatologies show a spatially and temporally coherent trend, responding with increased precipitation around the Nigerian coast which increases steadily over time/forcing and a general trend towards increasing precipitation across the eastern and central Sahel. The response in the western Sahel is more mixed. The individual model projections are highly divergent, ranging from a significant drying across much of the region (GFDL, CSIRO) to a significant increase in precipitation (CNRM, MIUB) with other models providing a spatially variable outlook. The MRI model, which Cook and Vizy (2006) argued provided the most plausible projections, shows the least

coherence in the temporal evolution of anomalies. In all other models, a trend towards positive/negative anomalies evolves as the forcing increases, indicating a clear response to anthropogenic forcing. The projections of the MRI model do not evolve with the same coherence – the pattern and strength of anomalies is present in the sresb1 2030s climatology and they do not increase coherently under continued forcing, suggesting (at least) a less direct relationship between the projections and external climate forcing. It is evident that the evolution of precipitation and temperature are connected, with trends in temperature dampened in the regions of greatest precipitation increase (e.g. the Sahel in MIUB) and more significant temperature increases where precipitation decreases (e.g. the Sahel in GFDL).

Figure 6.1: Temperature anomalies (in °C) from the model ensemble for the 2030s, 2050s and 2090s under sresb1, sresa1b and sresa2 scenarios relative to a 1970-99 climatology.

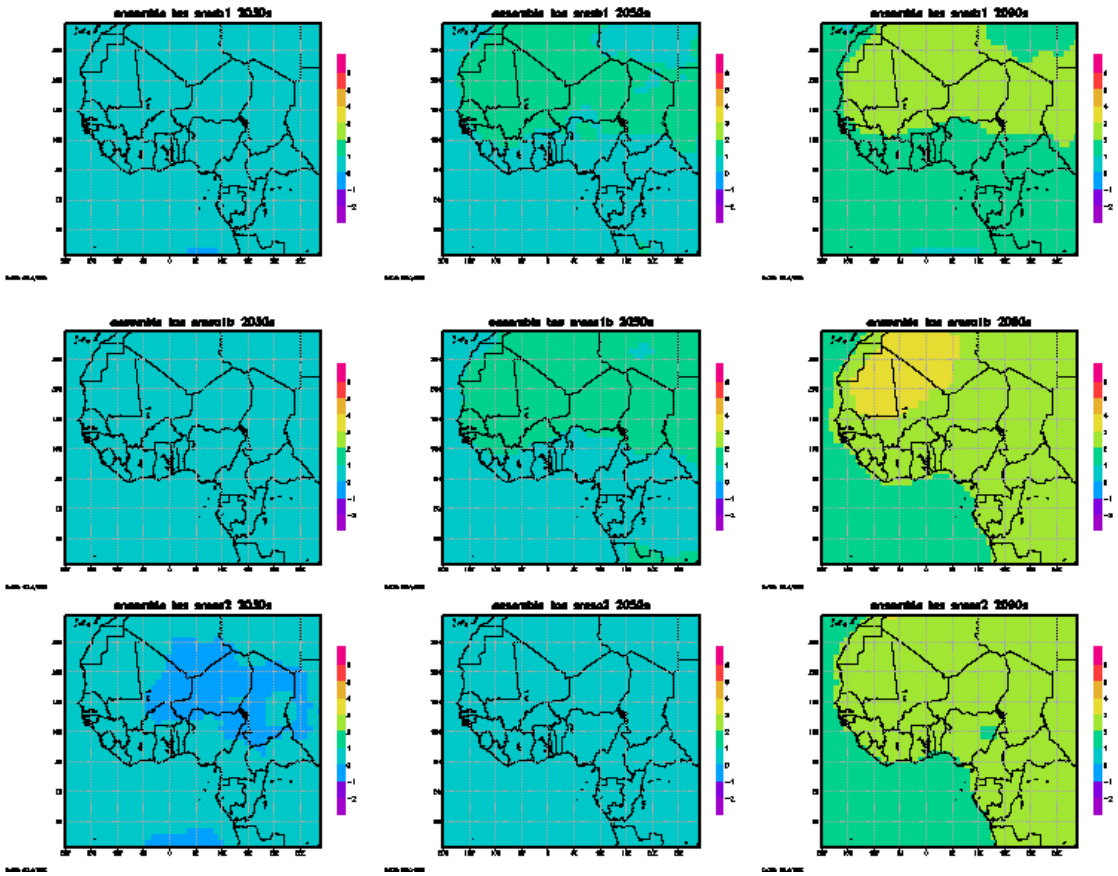

Over the Sahel, the climatological precipitation projections of the models are shown in Table 6.2. It can be clearly seen that though several of the models have trends towards drying or wetting, none has a linear trend across the scenarios/periods analysed. GFDL has the most robust drying trend, with climatological precipitation falling by almost 30% by the 2090s in

the strongest forcing scenario, but shows little response in the sresb1 scenario. MIUB has the strongest wetting trend, with an increase of 40% from the climatology. The ensemble projections indicate a relatively insignificant trend in the climatology and are of variable sign across the forcing scenarios.

Figure 6.2: Precipitation anomalies (in mm/day) from the model ensemble for the 2030s, 2050s and 2090s under sresb1, sresa1b and sresa2 scenarios relative to a 1970-99 climatology.

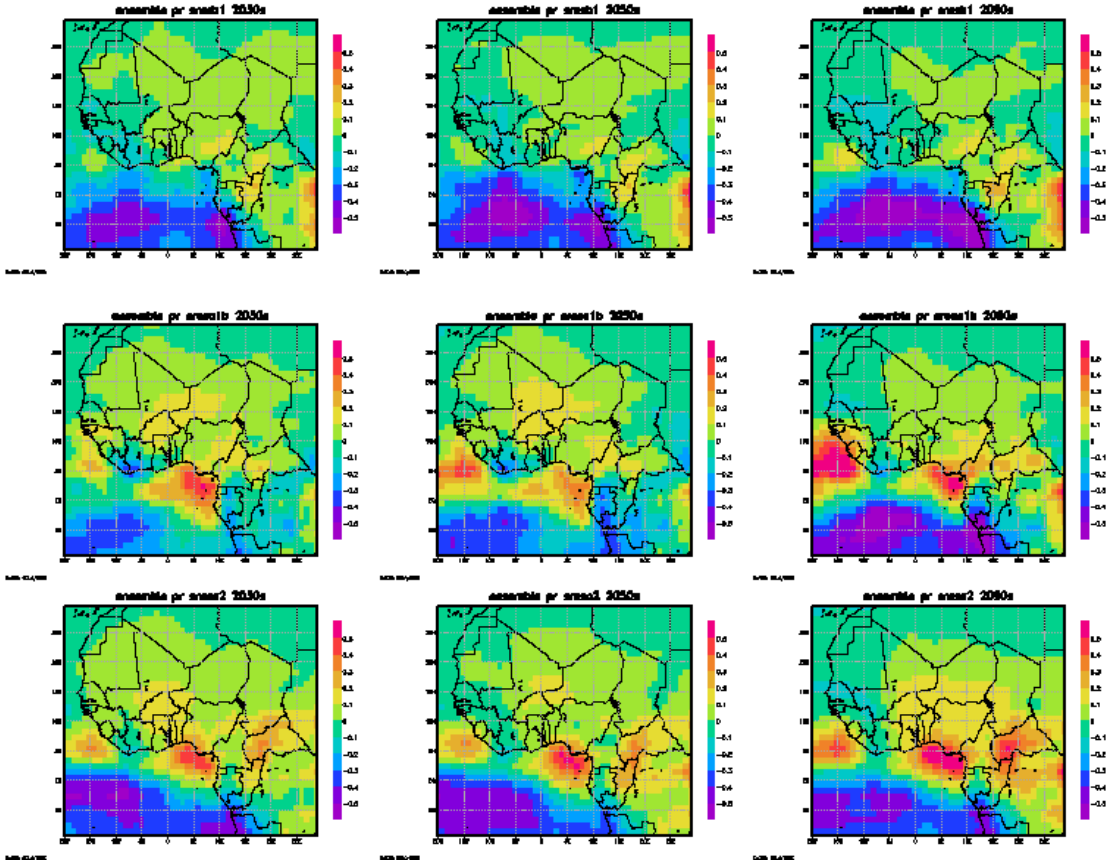

With an intensified hydrological cycle and more intense precipitation events, intraseasonal precipitation variability should increase in both areas which are drying and wetting (Trenberth et al. 2003; Neelin et al. 2003; Meehl et al. 2007). Interannually, an increase in the variability of the monsoon precipitation would make productivity less predictable and may increase the likelihood of desertification in water-stressed areas (Nicholson 2001). Due to the short periods analysed here, statistical analysis of prospective changes in interannual total precipitation variability is not included.

Table 6.2: Projections of precipitation climatologies produced by the models for the 21st-century (mm/day).

Model	Climatology	Period	sresb1	sresa1b	sresa2
CCCMA	1.96	30-39	1.61	1.81	1.69
		50-59	1.65	1.71	1.70
		90-99	1.66	1.64	1.57
CNRM	1.97	30-39	2.20	2.15	2.17
		50-59	2.09	2.19	2.06
		90-99	2.19	2.17	2.23
CSIRO	1.80	30-39	1.70	1.64	1.76
		50-59	1.71	1.75	1.70
		90-99	1.87	1.66	1.67
GFDL	3.03	30-39	3.14	2.90	3.03
		50-59	2.83	2.71	2.79
		90-99	2.65	2.23	2.15
MIUB	2.06	30-39	2.62	2.82	2.55
		50-59	2.61	2.71	2.60
		90-99	2.60	2.89	2.87
MPI	2.03	30-39	2.08	1.96	1.95
		50-59	1.98	2.02	2.10
		90-99	2.15	1.98	1.96
MRI	1.28	30-39	1.28	1.29	1.11
		50-59	1.28	1.09	1.16
		90-99	1.34	1.28	1.13
Ensemble	2.11	30-39	2.11	2.19	2.19
		50-59	2.0	2.17	2.14
		90-99	2.07	2.16	2.18

The analysis performed on the monsoon length for the observed period is repeated for the scenarios. However, daily data is unavailable from the CMIP3 archive for the 2030s, so only the two later periods are considered. The results are shown in Table 6.3. All models produce a longer monsoon, in spite of the fact some project lower annual precipitation totals, with the

additional period ranging from 10–40 days. The primary cause of this is a delay in the end of the season, with trends observed in the start date being more variable. During the observed 1970–99 period, the majority of the models produced a trend towards a shortened monsoon, as was observed in the NCEP and JapRe data. Given the consistent response across the models for the late 21st century, this suggests the currently observed trend may be a function of decadal variation. The periods analysed here are short, so the results are initial, particularly since the trends across the two periods and across the forcing scenarios do not show a sequential trend with increased forcing. To further investigate these trends, anomalies of ensemble monthly precipitation across the Sahel domain are shown in Figure 6.3. Individual model outputs are in Appendix 9. The GDFL model shows a robust drying trend across the whole monsoon season. The majority of the other models produce projections of lower early season precipitation and increased late season precipitation, supporting the results in Table 6.3 and indicating that the season as a whole may be delayed, with the peak monsoon rains arriving later than currently observed. The magnitude of the trends with respect to anthropogenic forcing is not linear and given the decadal timeslice presented in these results, they are provisional. They concur with the results of Biasutti and Sobel (2009), whose study used anomalies for the entire 20th and 21st centuries, lending further support to the conclusion that a projections of a seasonal shift in the timing of the monsoon as a whole are robust—a result which contrasts with the wide model spread for projections of annual precipitation totals in the Sahel.

6.2.3 Projections of extremes

Studies of model projections of extremes have often looked at global or hemispheric averages of indices (Kharin et al. 2007; Sillman and Roechner 2008; Brown et al. 2008), since model resolution makes studying regional indices less viable. Few RCM studies have looked at West Africa (Sylla et al. 2009). These global projections suggest that extremes of temperature will increase, though not necessarily at the same rate as mean temperatures, and in most regions precipitation extremes become more intense and have shorter return periods (Kharin et al. 2007). Given the high variability in model projections of mean climate for the region, particularly for precipitation, using global projections to assess probable changes in precipitation extremes may not be beneficial. In the downscaling results of Hewitson and Crane (2006) and Tadross et al. (2005a), both investigating Southern Africa, changes in local

median precipitation event magnitude were found to sometimes diverge from the projected changes in seasonal totals, highlighting this issue.

Table 6.3: Model derived projections of start and end date of the monsoon and season length for the 21st-century. In the CCCMA model, the end date was not captured for most years in the sres scenarios due to the nature of the precipitation regime and is thus excluded.

				46-65				80-99		
		Climatology		sresb1	sresa1b	sresa2		sresb1	sresa1b	sresa2
MRI	start	12th Jul		12th Jul	20th Jul	20th Jul		15th Jul	16th Jul	22nd Jul
	end	10th Nov		29th Nov	29th Nov	28th Nov		27th Nov	23rd Nov	27th Nov
	length	121		139	132	131		135	130	127
MPI	start	5th Jun		1st Jun	6th Jun	2nd Jun		2nd Jun	10th Jun	17th Jun
	end	15th Oct		31st Oct	30th Oct	1st Nov		2nd Nov	2nd Nov	31st Oct
	length	132		153	146	153		154	145	136
MIUB	start	18th Jun		17th May	18th May	18th May		13th May	16th May	17th May
	end	20th Oct		7th Nov	5th Nov	7th Nov		6th Nov	6th Nov	4th Nov
	length	134		174	172	172		177	174	171
GFDL	start	2nd May		23rd Apr	20th Apr	24th Apr		2nd May	29th Apr	30th Apr
	end	15th Oct		1st Nov	1st Nov	3rd Nov		31st Oct	31st Oct	3rd Nov
	length	165		192	195	193		182	185	187
CSIRO	start	19th Apr		27th Apr	25th Apr	25th Apr		28th Apr	20th Apr	20th Apr
	end	17th Oct		22nd Nov	19th Nov	24th Nov		21st Nov	19th Nov	23rd Nov
	length	180		209	209	213		208	203	207
CNRM	start	17th Jun		19th Jun	12th Jun	18th Jun		10th Jun	14th Jun	19th Jun
	end	11th Nov		23rd Nov	23rd Nov	20th Nov		22nd Nov	20th Nov	23rd Nov
	length	149		156	164	155		165	159	157
Average	start	29th May		27th May	27th May	28th May		27th May	30th May	2nd Jun
	end	26th Oct		13th Nov	13th Nov	14th Nov		13th Nov	12th Nov	13th Nov
	length	150		171	170	170		170	166	164

Figure 6.3: Precipitation anomalies in the Sahel region, relative to a 1970-99 baseline. Figures for the 2050s are black and the 2090s are green.

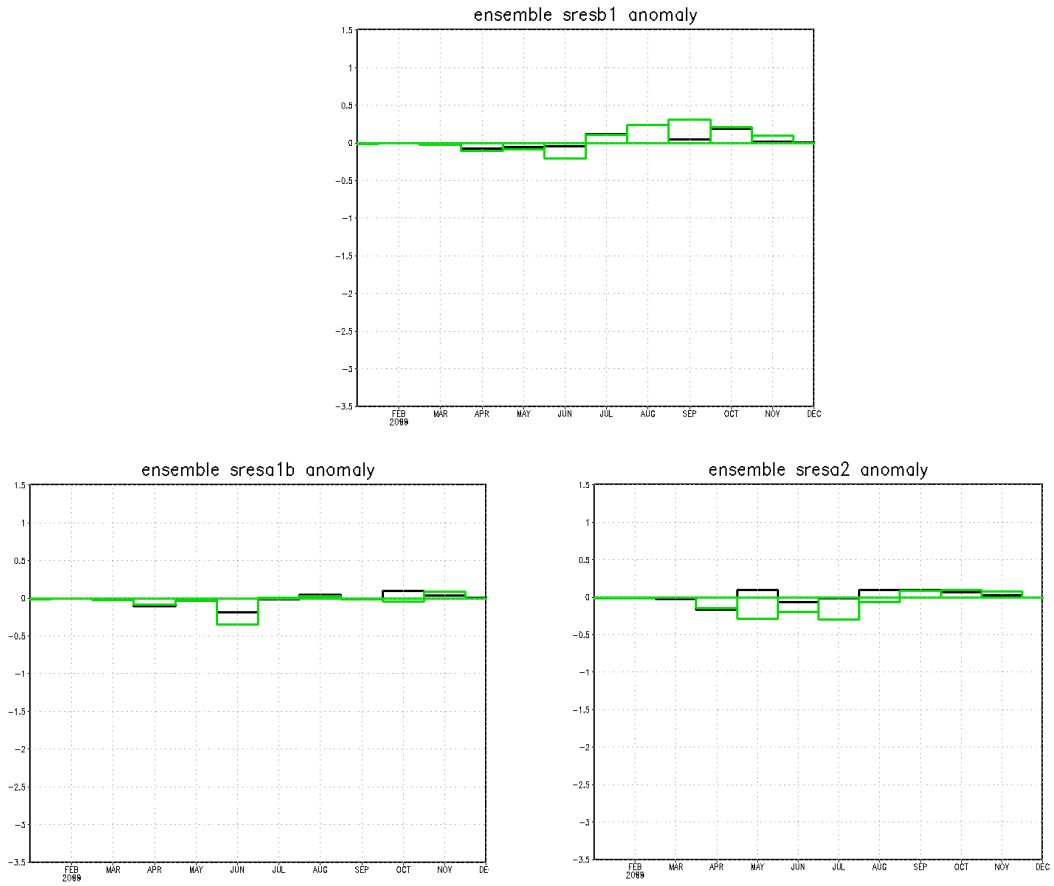

Projections for temperature extremes in the region are more coherent than for precipitation (Paeth and Thamm 2007; Paeth et al. 2009). Sylla et al. (2009), using an RCM forced with sresa1b boundary conditions in the ECHAM model, found that across the region by the end of the 21st century there was a general trend towards longer dry periods during the monsoon and in most locations a decrease in maximum 5-day precipitation, indicating both less intense precipitation and longer dry spells. Less consistent precipitation may impact on many of the crops in this study, since they are all sensitive to precipitation frequency at various stages in their cultivation. Paeth et al. (2009) found, using three forcing scenarios in an RCM, that patterns of change in dry spells were more coherent in space across West Africa than changes in positive precipitation extremes, with dry spells becoming longer of most of the region and increasing in length as the forcing increases, indicating a weakening of the hydrological cycle over the region.

The regional projections that are produced here are displayed as anomalies with respect to the model produced climatologies, providing an indication of the direction and magnitude of the projected trends. Given the model climatology biases, providing absolute values would be less useful.

In Figure 6.4 the ensemble 95% precipitation anomalies are displayed. Across the whole region, the projections are of an increase in maximums (1-2mm/day) relative to a climatological value of 5-10mm/day across much of the region. The trend does not increase sequentially across the forcing scenarios, which may partly be a function of the short periods used and the high interannual variability of the index. Comparing the output of the models (Appendix 10), it can be seen that the ensemble output masks high inter-model variance. The two models with the greatest divergence, MIUB and GFDL, are also the models with the greatest divergence in climatological precipitation in the Sahel (Table 6.2). The trends in each model are non-linear and are approximately sequential across the forcing scenarios. Where the model indicates a drying Sahel (GFDL) it also projects a decrease in the magnitude of these 95% precipitation events; if it projects a wetting Sahel (MIUB) the 95% events are projected to increase.

The projections for 5-day precipitation maximum events across the Sahel domain are shown in Table 6.4. Given the short time periods in the 21st century and the highly variable nature of this index, these results can only be considered provisional. Only one model indicates a negative trend in the magnitude of these events, with the majority of the models indicating a positive trend in the most intense precipitation across the region—a result which concurs with the wider literature on such events (Trenberth et al. 2003; Neelin et al. 2003; Meehl et al. 2007; Trenberth 2010). Notably, both MIUB (as expected) and GFDL indicate increases in the intensity of the 5-day events. The trends are not sequential, which given the short periods being analysed is not surprising. The divergence between the robust trends in 95% precipitation events (negative) and 5-day events (positive) across the Sahel in GFDL is less expected, though may be explicable through the overall drying in the region in this model and the fact that only the most extreme events may propagate far enough north to register in the Sahel area in the future, leading to a decrease in magnitude of all but the most intense events.

Figure 6.4: Anomalies in the 95% precipitation event threshold, averaged across the model ensemble. Figures are in mm/day.

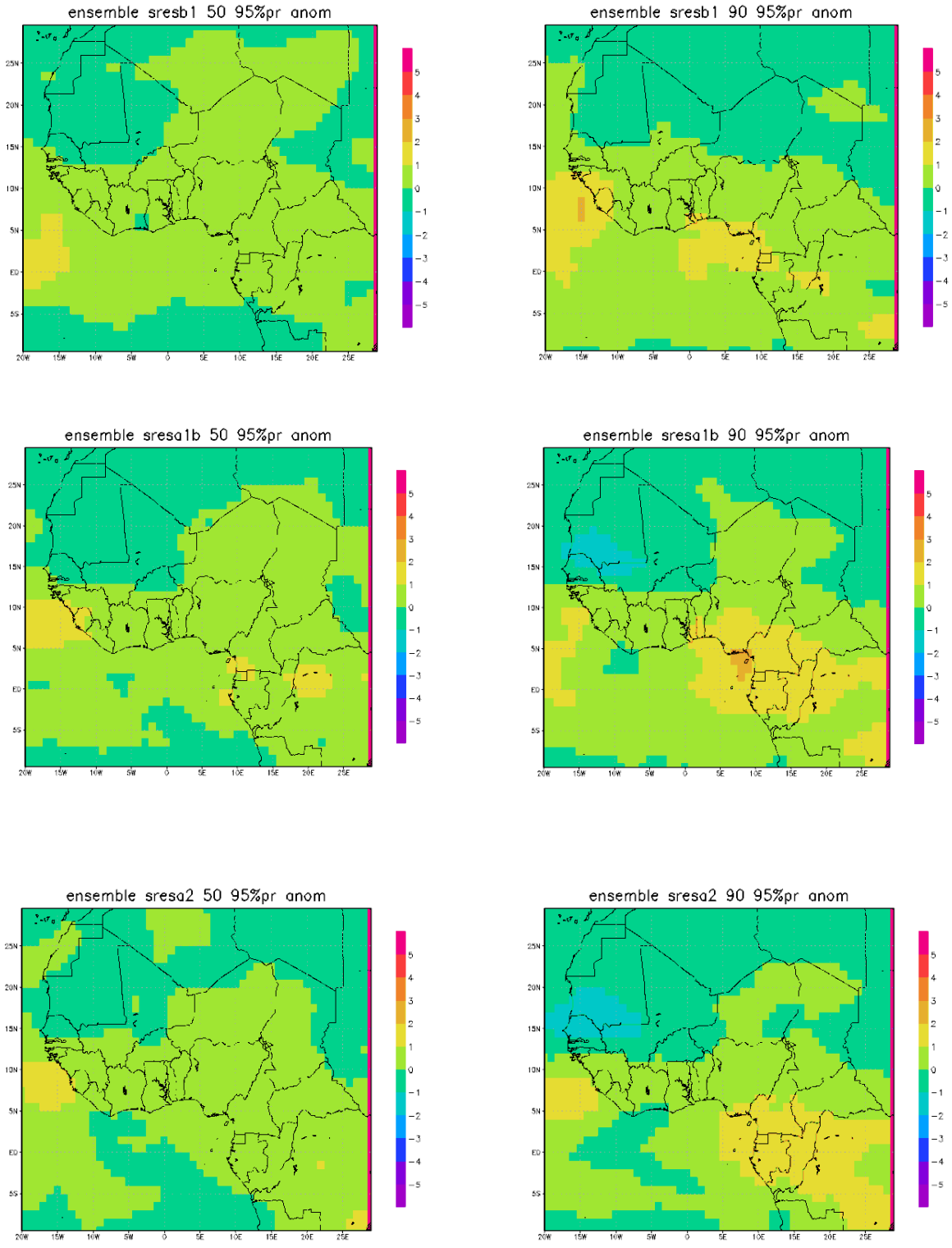

Table 6.4: Model derived projections for 5-day precipitation maximum events across the Sahel domain.

	MRI				MPI		
	sresb1	sresa1b	sresa2		sresb1	sresa1b	sresa2
clim	33.59				68.78		
50s	33.32	31.61	34.24		77.75	83.13	78.01
90s	34.42	35.19	31.41		85.44	79.41	91.78
	MIUB				GFDL		
	sresb1	sresa1b	sresa2		sresb1	sresa1b	sresa2
clim	56.54				91.36		
50s	64.65	62.81	63.38		90.19	96.14	101.58
90s	65.19	73.16	70.44		99.10	104.15	98.62
	CSIRO				CNRM		
	sresb1	sresa1b	sresa2		sresb1	sresa1b	sresa2
clim	62.13				78.12		
50s	64.83	65.23	65.49		79.11	88.95	88.49
90s	66.84	62.25	66.39		87.34	92.93	93.49
	CCCMA						
	sresb1	sresa1b	sresa2				
clim	50.27						
50s	47.74	47.71	52.52				
90s	45.67	48.59	44.65				

The indices of seasonal maximum dry period and the number of 5-or-greater dry day incidents are in Table 6.5. The majority of the models fail to show a significant positive or negative trend in either index. Turning to the wettest (MIUB) and driest (GFDL) models, they exhibit trends which indicate a *shortening* of the longest dry periods and a *decrease* in the number of 5-or-greater day events under a wetter future and a *lengthening* of these periods and an *increase* in the number of 5-or-greater day events in a drier future, respectively. Combining these results with those seen above, this suggests that in a drier Sahel the precipitation will be more sporadic with lower total precipitation and less precipitation in the majority of precipitation events but that the very heaviest precipitation events might increase in magnitude—a scenario that would have a negative impact on crop production, particularly if the heaviest events lead to flooding/short-term waterlogging. In the wetting scenario, the precipitation increases in frequency, with precipitation events intensifying. Even with heavier

extreme precipitation, with a more consistent pattern of precipitation across the season, this may be more manageable from an agricultural perspective in many areas.

The ensemble 5% minimum and 95% maximum temperature projections are provided in Figure 6.5 as anomalies relative to the ensemble 1970–99 climatologies. The increases are sequential and non-linear, with the greatest increases in maximum temperatures occurring in the Sahara (>5°C) as the heat low intensifies and minimum temperatures inland of Guinea (>5°C) increasing in connection with higher summer precipitation and the overall trend to warming. The models (Appendix 11) all indicate warming across the entire region in both indices. The magnitude of those changes is variable, however, from less than 1°C in 2050 in some sresb1 projections, to over 7°C in sresa2 projections. All models indicate a sequential and non-linear increase over time in these indices through the 21st century under all forcing scenarios, providing high confidence in the nature of the trends. The models are also, individually, spatially consistent in the location of the greatest increases in both indices, but between models the spatial variability in the magnitude of change is notable. The MIUB and GFDL models are not the end members of the ensemble with respect to these indices, across both the Sahel and the whole domain, indicating that the rate of change in extreme temperatures may not be closely connected to changes in extreme precipitation events, a relationship that appears more robust in the projected changes in mean conditions.

The trends for extremes into the 21st century are taken from models which were found in many instances to perform an inadequate simulation of the region's 20th century climate. Given this, and the short periods being analysed in this study, conclusions as to the possible direction and magnitude of trends in extreme events must be considered provisional. The high uncertainty in future mean conditions, particularly in the Sahel, compounds this uncertainty. However, where the models show strong agreement in the direction of extreme events and the change in these events is consistent under forcing or correlates with trends in the mean conditions, some confidence in the projections can be taken. In areas which experience a drier climate, precipitation is likely to become less consistent during the rainy season with relatively greater increases in minimum and maximum temperatures. The most intense precipitation events may increase, though this is less clear. In areas which become wetter, precipitation is likely to become more consistent, with heavier precipitation events and an increase in the magnitude of extreme events. The increased precipitation is likely to have an

ameliorating effect on the increase in minimum and maximum temperatures, though these events will nevertheless become warmer.

Table 6.5: Model derived projections of seasonal maximum dry period and the number of 5-or-greater dry days across the Sahel domain.

	MRI					MPI		
	sresb1	sresa1b	sresa2			sresb1	sresa1b	sresa2
clim	5.88				clim	4.50		
50s	4.83	5.70	5.49		50s	5.22	5.21	4.62
90s	4.61	4.27	4.88		90s	4.92	5.63	6.33
clim	0.47				clim	0.42		
50s	0.35	0.51	0.48		50s	0.56	0.65	0.44
90s	0.44	0.27	0.37		90s	0.49	0.71	0.84
	MIUB					GFDL		
	sresb1	sresa1b	sresa2			sresb1	sresa1b	sresa2
clim	4.53				clim	5.78		
50s	3.81	4.31	3.56		50s	6.92	6.03	6.09
90s	3.45	3.60	3.19		90s	7.21	8.13	8.12
clim	0.41				clim	0.53		
50s	0.29	0.38	0.23		50s	0.70	0.62	0.64
90s	0.18	0.23	0.18		90s	0.60	0.83	0.96
	CSIRO					CNRM		
	sresb1	sresa1b	sresa2			sresb1	sresa1b	sresa2
clim	8.30				clim	7.50		
50s	7.64	8.11	8.09		50s	6.46	5.42	7.04
90s	6.30	7.27	8.23		90s	8.45	6.50	8.19
clim	1.11				clim	1.01		
50s	1.09	1.02	1.04		50s	0.82	0.95	0.61
90s	0.78	0.98	1.11		90s	0.87	0.78	0.77
	CCCMA							
	sresb1	sresa1b	sresa2					
clim	3.65							
50s	4.08	3.23	5.21					
90s	4.29	3.49	3.47					
clim	0.33							
50s	0.33	0.30	0.38					
90s	0.31	0.22	0.31					

Figure 6.5: Projections of 5% minimum and 95% maximum temperatures, averaged across the model ensemble and displayed as anomalies relative to a 1970-99 baseline. Figures in °C.

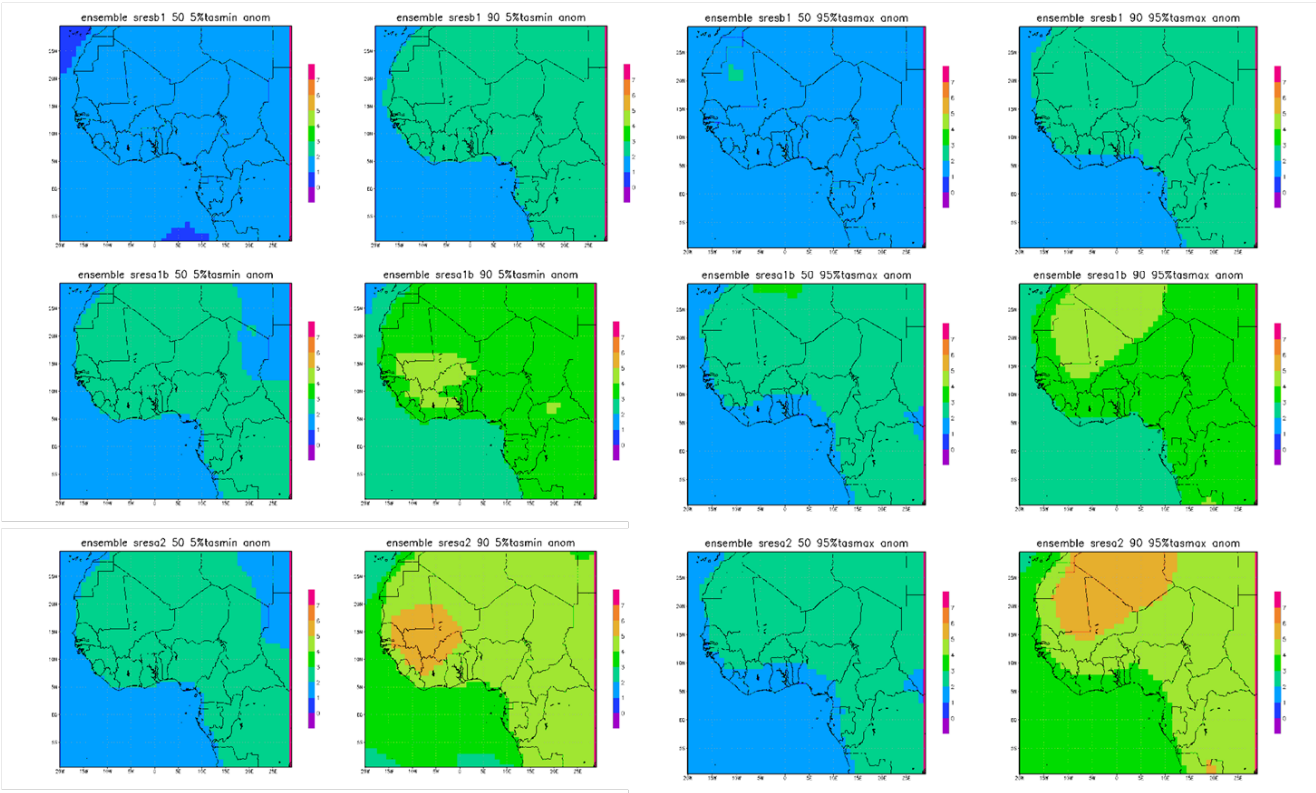

7. Future Climate Scenarios and Impact on Food Crops in West Africa

Using the same approach as applied to the observed data and models previously, the output from the models and the CMIP3 ensemble is used to analyse prospective change in crop growth domains. Given the errors in the climatological model growth domains seen in Section 5, the approach taken is that anomalies are derived from the model 2030/2050/2090s climatologies with respect to their 1970–1999 climatologies. These anomalies are then applied to the observed and reanalysis climatologies. The crop growth thresholds are then applied to this data to create the crop domains. The projections produced are not affected by the bias in the model 20c3m experiments and provide a more robust assessment of the impact of climate change on the crop domains than simply applying the thresholds to the sres

experiment outputs. Daily data was not available for the 2030s, so the minimum temperature threshold could not be applied to this period. Two datasets have therefore been produced—one including this data for the 2050s and 2090s and one without it for all periods. Extremes of low temperature are expected to become less frequent with overall climate warming (Kharin et al. 2007), so this threshold should become less important as anthropogenic forcing takes greater effect.

In Appendix 12 the ensemble crop domains are shown, compared to the observed/reanalysis climatologies. The individual model domains are provided in Appendix 13. It should be noted that these domains do not include the influence of climatic extremes, which are further discussed below.

Cassava: The absolute extent of the ensemble domains do not change significantly. The ensemble, however, represents the average of a wide divergence in precipitation projections across the CMIP3 dataset. A small amount of additional uncertainty is created by the differences between the two precipitation reanalyses, but these are generally less than 1˚ at the northern boundary of growth across the models. Comparing the change in domain of two of the model outputs with strong wetting (MIUB) and drying (GFDL), the projections vary over the Sahel, with a maximum southward migration of around 2˚ in the driest scenario. No scenarios indicate a significant northward expansion of cultivatable land. The relatively high precipitation threshold for cassava explains the broad consensus across the models, with greater variability in projections occurring in the driest areas. Due to the small change in the absolute spatial extent of the domains in the models, it is difficult to establish whether the precipitation driven trends are non-linear. The more spatially significant changes in the domain, which are non-linear across the century and the forcing scenarios, are due to the increase in temperatures across the region, with much of the observed optimum growth domain becoming less suitable for cultivation due to increased temperature, with both the 28°C and 30°C thresholds being crossed in much of the region of currently observed potential growth. Differences between models are significantly greater than differences between forcing scenarios in individual models (that is, model uncertainty is greater than forcing uncertainty).

Based on these results, the outlook for growth of cassava in the region appears to be predominantly one of an uncertain change in the northern limits of growth, with that

uncertainty lying within the Sahel itself, and that the conditions within the currently cultivatable area will become more challenging due to increased temperatures. The impact of this change in climate is likely to occur non-linearly over time, with a more rapid deterioration of growing conditions as anthropogenic forcing increases.

Cowpea: In the ensemble output, the absolute extent of the current growth domain across southern West Africa does not change significantly. The extent of optimum growth conditions within this domain increases over time as the areas which are below the current optimum average temperature or experience lower minimum temperature steadily recede. The impact of the discrepancies between the NCEP and JapRe datasets, which provide the baseline for the projections, has a much greater impact on the spread of model projections for cowpea. Across the models, with a lower precipitation threshold, the response in terms of growing domain is more variable than for cassava with the northern boundary of growth diverging by upwards of 5˚ between models from the same reanalysis baseline and up to 10˚ when taken from the two reanalysis datasets (MIUB sresa2 anomalies from a JapRe baseline v GFDL sresa2 anomalies from an NCEP baseline). The drier scenarios indicate the northern boundary of cultivation could move up to 2˚ south to a position around 11˚N. The regions where growth is currently optimal change significantly less in spatial extent across the models. In addition to changes in the spatial extent of optimum precipitation, the optimum growth domains generally expand as the growth limiting influence of minimum temperatures decreases. Given the influence of minimum temperatures, it is difficult to comment on the linearity of the trends (with no 2030s output to compare). In the ensemble output, the trends appear relatively uniform in the absence of the influence of minimum temperature (since the wide model divergence in precipitation projections cancels out), but in individual model outputs the trends are non-linear, both as a result of the changes in precipitation distribution (both positive and negative) and minimum temperature (uniformly positive). Again, model uncertainty is greater than forcing uncertainty.

The outlook for cowpea is therefore of an uncertain change in the northern limits of the climatically limited growth domain, and a more significant divergence in the possible extent of the domain than seen for cassava, with inter-model variance layered onto observational/reanalysis uncertainty creating a highly variable prognosis for the end of the

century. Within the precipitation limited domain, the conditions appear to improve, with the current limiting impact of minimum temperatures abating over time.

Rice: Due to the higher minimum precipitation requirements of rice, the limit of cultivation lies further south than the other crops. As a result, the models show less divergence in their projections for future growth domains. The reanalysis datasets are also better constrained than for the crops which can be cultivated in lower precipitation areas, with discrepancies of generally 1˚ or less in the observed period. These discrepancies do not amplify divergence in the model projections and in some models the differences between the two outputs decrease over time as the overall trend in precipitation become significantly more dominant.

The ensemble absolute growth domain changes very little, with an expansion of optimal conditions driven by the increase in average temperatures passing the 25˚C threshold in the few areas within the existing growth domain where it is not already satisfied. The greatest inter-model divergence is of 2-3˚ (including uncertainty derived from the reanalysis discrepancies) in the projections for the northern limit of cultivation by the 2090s under an sresa2 scenario. Within the precipitation prescribed limits of growth, the optimum growth domains expand as the constraining influence of low average temperatures abates. For both precipitation and temperature, the models indicate a non-linear response to forcing over the period.

The outlook for rice appears better constrained than cowpea or cassava, with the higher precipitation thresholds more consistently produced across the models. The primary uncertainty is, again, the northern boundary of cultivation with a projected change of less than 2˚ either north or south under the most extreme forcing scenario. Where changes in precipitation do not adversely impact on growth, increasing temperatures should improve growth conditions.

Sorghum: The ensemble projections for sorghum are of very little change in the absolute boundaries of the growth domain. Within the domain, the narrow boundaries of optimum average temperature expand where they were previously below the lower threshold of 28˚C but are also constrained by a greater area within the region exceeding 31˚C. The area of most optimum growth changes very little across the century, even under the strongest forcing scenario. The uncertainty derived from differences in the reanalysis data is greater than the changes the ensemble output suggests by the end of the century.

Uncertainty derived from the reanalysis data is generally less than 2˚ for individual models at the northern boundary of the domain, slightly greater in the wettest model. When uncertainty derived from the two most divergent model projections is included, the difference becomes in excess of 8˚ in the central Sahel when model and reanalysis uncertainties are combined. The wettest scenario of any of the models suggests that the northern boundary of growth is likely to migrate northwards by around 2˚, with this occurring non-linearly through the century. In the driest scenario, a southward withdrawal of the limits of growth of up to 2˚ is projected in the central Sahel, again non-linearly with most change occurring between the 2050s and 2090s. In addition to changes in precipitation, the area which is too warm for optimum growth conditions increases in all models, with the most notable decline in optimum temperature in the drier models, likely due to feedbacks from reduced precipitation acting to enhance local warming. This change in temperature threshold is also non-linear.

The outlook for sorghum is of high uncertainty in the absolute northern limit of growth when different forcing scenarios are combined with observational/reanalysis uncertainty, and is further amplified by model uncertainty, this effect becomes pronounced under increased forcing with the region of divergence in projections covering much of the northern Sahel. In addition, the narrow optimum temperature conditions of the crop lead to a significant change of which areas, within the precipitation governed absolute growth domain, are most suitable for cultivation by the end of the century.

Millet: The ensemble projections for millet are dominated by the high variability in the precipitation reanalyses. Given the narrow, and low, precipitation thresholds for the crop, the optimum growth area diverges at both the northern and southern boundary by up to 5˚ in some locations. The future projections diverge relatively little, with the primary changes in domain resulting from the non-linear expansion in the areas which are too warm for optimum growth.

As a result of this significant variation in the reanalysis data, the growth domains of the wettest and driest projections, when combined with the reanalysis uncertainty, have very little overlap, with the southern limit of growth by the end of the century around the same latitude (10-12˚N) as the northerly limit in the driest scenario. Discounting the influence of the reanalysis data, the band of suitable conditions migrates northward and expands under the wettest scenario, with the southern boundary moving around 1˚ and the northern boundary up to 3˚ in the central Sahel. The driest scenario, by contrast, contracts the domain at both the

northern and southern boundaries, becoming centred on the southern Sahel. Optimum temperatures also cross the upper threshold of 28˚C across almost all of the projected growth domains in all models and in all forcing scenarios. The change in absolute growth domain changes non-linearly in both the wetter and drier models, though the impact is more apparent in the wetter projections as the domain expands. Optimum temperature thresholds are exceeded early in the century, so response thereafter (though likely to be non-linear) is already above the thresholds analysed here. Further temperature increases would make millet cultivation even more challenging.

The outlook for millet is highly uncertain, largely as a result of the comparatively narrow precipitation thresholds which growth is constrained by. In addition to the uncertainty derived from observations/reanalysis, divergence in the model projections is such that by the end of the century, the most extreme scenarios have very little overlap in terms of the areas they project the crop can be grown at all. In either scenario, within these regions, the increase in average temperatures will provide an additional challenge to cultivation.

Maize: The ensemble projections for maize are well constrained. The differences between the reanalysis datasets is less than 1˚ at the northern boundary of the domain across much of the region, with the primary difference being the southern extent of optimum precipitation. Little change in the northern boundary of the domain occurs across the forcing scenarios, with a slight decrease in the area of optimum growth partly attributable to changes in precipitation. Within the domain, the more significant influence is that increased temperatures reduce the optimum limits of growth non-linearly throughout the century as more of the region passes the 30˚C upper temperature threshold.

The wettest model (MIUB) accentuates the discrepancies between the reanalysis data, though these differences remain generally less than 2˚ at the northern boundaries of the domain. The greatest model/reanalysis differences lead to a 5˚ difference in the northern boundary of cultivation by the end of the century. In the wettest scenario, there is a small northward expansion of the domain, but the more significant changes are the decrease in extent of the most optimum areas, a change driven by increased average temperatures and one which occurs non-linearly over the century. The same trajectory is seen in the driest scenario, with the most notable changes in the growth domain also driven by temperature increases leading to average temperatures over 30˚C across almost the entire area by the end of the century.

The outlook for millet therefore appears relatively well constrained in comparison to several of the other crops, a function of the higher precipitation threshold of the crop and the fact that the models (and reanalyses) are more consistent in the wetter areas. The maximum extent of the domain is projected to migrate north or south, likely by less than 2˚, with the conditions within this domain becoming more challenging as the region exceeds the maximum optimum temperature conditions by the end of the century.

7.1 The impact of changes in extremes

Against these projections, which are based on climatological mean conditions, the (uncertain) projections for extreme climate events must be considered. With the models generally indicating an increase in the most intense annual precipitation, even in areas which become drier, cultivation of those crops sensitive to waterlogging (millet, maize, cassava, and cowpea) may become even more difficult. With a delay in the rainy season, if harvest of sorghum is delayed, due to its photosensitivity this may provide an additional challenge to cultivation.

Millet, maize, sorghum and rice are all to some extent affected by drought during their growing periods. The projections for changes in dry periods during the rainy season are highly variable and correlate with overall projections for precipitation. If total precipitation decreases, which will already stress these crops, the increase in intra-seasonal variability of precipitation will provide a further challenge to their cultivation. In the event that total precipitation increases, it appears likely that the impact of droughts during the monsoon will become less pronounced as precipitation events become more temporally consistent.

Increases in maximum temperature extremes should not have a significant impact on the crops since even those crops which are affected by maximum temperatures are impacted by the average conditions, rather than individual events. The increase in minimum temperatures is already included in the analysis above, but the additional increase in the very lowest minimums relative to the mean increase further suggests that minimum temperature extremes are likely to have a diminishing impact on West African crop production in the future.

8. Discussion and Conclusions

This report has investigated the climate and primary food crops of West Africa, investigating current climate and crop growth domains and the implications of global warming for agriculture in the region, with a particular focus on those aspects of climate change which will have greatest impact on the crops which are currently grown in West Africa. In undertaking this analysis, the ability of several GCMs in reproducing the observed climate has been investigated, with a view to establishing how reliable future climate (and associated crop growth) projections which are produced by these models are.

The climate of West Africa is dominated by the monsoonal cycle and high spatial and temporal variability in precipitation. The high annual precipitation and bi-modal precipitation regime at the Guinea coast gives way to a uni-modal summer precipitation peak towards the continental interior associated with the monsoon. The steep precipitation gradient of the region and high precipitation variability (on daily to decadal timescales) is one of the primary features of the climate, particularly in the drier regions. Much focus of recent research has been on the Sahel and this report has also paid particular attention to this region. The lack of reliable observed data in the region provides a significant additional challenge, since gridded data, reanalysis and model data are less readily verified and/or forced.

The influences and interactions which control the climate of the region are complex and climate models have difficulty in simulating the observed climate. Temperature climatologies, variability and trends are generally robustly reproduced. GCMs do not perform as adequately in their simulation of regional precipitation patterns, with biases in the model climatologies and further uncertainty in the reproduction of variability and trends. The spatial and temporal resolution of the models makes resolving the complex climate of the region particularly challenging. The models' ability to reproduce climatic extremes, which can have a significant impact on agriculture, are particularly variable for precipitation based extremes. The models perform more adequately for temperature derived indices, but generally underestimate climatic variability.

The current climatic limits of growth for the primary crops of the region were investigated, with particular uncertainty derived from divergence in the climatological precipitation in the reanalysis datasets. This uncertainty means accurate verification of the model climatologies is

not possible and leads to a decreased ability to assess model ability to simulate the observed climate—a necessary but not sufficient condition for establishing confidence in model derived projections of the future climate and, in this study, crop growth domains.

Model projections of the future in the region are highly uncertain. Temperature trends, including extreme indices, are all positive, though the models vary in the magnitude of the projected increases under the various forcing scenarios. Precipitation projections vary from significant decreases in precipitation and extended droughts in certain models in some regions, particularly the Sahel, most notably in the GFDL model, to increases in precipitation and decreased frequency and length of droughts, most notably in the MIUB model. Given the wide spread of model projections, the ensemble precipitation projections (which are generally neutral) are not particularly useful, since they represent the average of a wide spread and are not constrained by the physical mechanisms which control the model scenarios. The temperature and precipitation trends produced in the models are mostly non-linear, in either direction, indicating that the response of the climate system to external forcing will become more pronounced as the 21st century continues.

The uncertainty in the projections, particularly precipitation since it has a significant controlling influence over agriculture in West Africa, are such that the projections for change in crop cultivation limits are highly variable over space and time. The individual models produce spatially consistent changes in the crop domains under continued anthropogenic climate forcing, but the inter-model spread is wide. For crops with lower precipitation growth thresholds, this impact is particularly pronounced, with the growth domain projections produced by the end members of the ensemble having little overlap for some of the crops. Temperature trends increase in all models and for all temperature indices, with varying impact on the crops depending on their particular climatic limits of growth. In addition, the divergence in trends in many extreme events provides an additional layer of uncertainty.

The outlook for agriculture, based on climate change alone, in West Africa is therefore of significant uncertainty, particularly in the vulnerable Sahel region. Insufficient observational records constrain the accuracy of reanalysis and gridded data, making the verification of models and identification of local trends and mechanisms challenging. This initial uncertainty is compounded by the wide divergence in model projections for the regions climate by the end of the 21st century. Temperatures will clearly increase across the region and agriculture

may be modified in anticipation of such changes. The wide divergence in precipitation projections provides a greater challenge to adaptation strategies.

Appendix 1: Grey Literature Review of Crop Growth Thresholds

Climate Conditions for Cultivation for Cassava

Source	Details
Natural History Museum - http://www.nhm.ac.uk/jdsml/nature-online/seeds-of-trade/page.dsml?section=crops&page=agriculture&ref=cassava	Temperature: Cassava is essentially a lowland crop, which cannot withstand temperatures below 10ºC. Climate: At its distribution extremes, it can be grown up to 1,500 metres above sea level at the equator where there is an annual rainfall of 1-4 metres. It has an agronomic value in areas with violent changes in rainfall because, after three weeks in the ground, it can withstand drought.
International Institute of Tropical Agriculture - http://www.iita.org/cms/details/cassava_project_details.aspx?zoneid=63&articleid=267	Because cassava roots can be stored in the ground for up to 24 months, and some varieties for up to 36 months, harvest may be delayed until market, processing, or other conditions are favorable.
Purdue University Horticulture - http://www.hort.purdue.edu/newcrop/CropFactSheets/cassava.html#Ecology	Temperature: Cassava is a tropical root crop, requiring at least 8 months of warm weather to produce a crop. Climate: It is traditionally grown in a savanna climate, but can be grown in extremes of rainfall. In moist areas it does not tolerate flooding. In droughty areas it loses its leaves to conserve moisture, producing new leaves when rains resume. It takes 18 or more months to produce a crop under adverse conditions such as cool or dry weather. Cassava does not tolerate freezing conditions. It tolerates a wide range of soil pH 4.0 to 8.0 and is most productive in full sun.
UN FAO - http://www.fao.org/docrep/x5032e/x5032e01.htm	Temperature: Cassava is a typical tropical plant. In general, the crop requires a warm humid climate. Temperature is important, as all growth stops at about 10ºC. Typically the crop is grown in areas that are frost free the year round. The highest root production can be expected in the tropical lowlands, below 150 m altitude, where temperatures average 25-27°C, but some varieties grow at altitudes of up to 1 500 m. Climate: The plant produces best when rainfall is fairly abundant, but it can be grown where annual rainfall is as low as 500 mm or where it is as high as 5000 mm. The plant can stand prolonged periods of drought in which most other food crops would perish. This makes it valuable in regions where annual rainfall is low or where seasonal distribution is irregular. In tropical climates the dry season has about the same effect on Cassava as low temperature has on deciduous perennials in other parts of the world. The period of dormancy lasts two to three months and growth resumes when the rains begin again. As a tropical crop, cassava is a short-day plant. Experiments conducted in hothouses show that the optimum light period is about 12 hours and that longer light periods inhibit starch storage. Cassava grows best on light sandy loams or on loamy sands which are moist, fertile and deep, but it also does well on soils ranging in texture from the sands to the clays and on soils of relatively low fertility. In practice, it is grown on a wide range of soils, provided the soil texture is friable enough to allow the development of the tubers. Cassava can

Source	Details
	produce an economic crop on soils so depleted by repeated cultivation that they have become unsuitable for other crops.
UN FAO Ecocrop - http://ecocrop.fao.org/ecocrop/srv/en/cropView?id=1420	Short-lived perennial. The 'sweet' cassavas mature in 180-270 days, the 'bitter' in 12-18 months. Growing period 6-24 months, depending on cultivar and conditions. Cassava is seldom grown above 1800 m in elevation in the tropics, maximum elevation for successful cultivation is about 1000 m. Prefers moderate humidity. Tuber production is delayed and reduced in daylengths greater than 10-12 hours.
FAO GAEZ	Cassava in tropical climates: Growing season of 12 months; temperatures of 15-20C for less than 33% of the season (ideally less than 16%) and average temperature over 30C for less than 66% of the season; temperature never below 15C. Temperature sum during growing season > 6500 (ideally > 7500).

Climate Conditions for Cultivation for Cowpea

Source	Details
Lost Crops of Africa: Volume II - Vegetables - http://books.nap.edu/openbook.php?record_id=11763&page=107	**Climate: Dry Areas** Excellent. Cowpeas are more drought-tolerant than peanut or maize (but not more than millet), and are vitally important in the West African savanna, where the bulk of the crop is produced. One of the more remarkable and valuable things about this species is that certain of its cultivars mature with as little as 300 mm of rainfall. Traditional cowpea types in the Sahel and savannas are attuned to subtle differences in the length of day. As if reading a calendar, they burst into flower just as the rainy season ends and the long period of dryness begins. Depending on cultivar and climate, cowpeas may take as few as 60 or as many as 240 days to mature their seeds. Harvesting is complicated by the prolonged and uneven ripening characterizing many types. The pods must be harvested as soon as they mature because they shatter easily and after a few days wantonly scatter the seeds on the ground. Further, seeds that get damp from rain or excessive humidity before being harvested start sprouting inside the pods while yet on the plants.
UN FAO Case Study - http://www.fao.org/ag/aGp/agpc/doc/publicat/cowpea_cisse/cowpea_cisse_e.htm	Climate: The traits that distinguish cowpea from many other crops currently grown in Africa include: substantial adaptation to drought; tolerance to high temperatures during the vegetative stage. The adaptation to drought is especially important for the dry Sahelian and other Savanna zones of western Africa. Cowpea production, because of its high adaptability to drought-prone conditions, relative to other crops, is the crop of choice in these harsh environments. In 1968 the annual rainfall was only 212 mm and the cowpea and peanut crop failed to produce much food. There are two distinct groups: short-day cowpeas that are extremely sensitive to photoperiod (day length), and a group that is either insensitive or only slightly sensitive to day length with respective to the initiation of flowering. When planting date of these short-day varieties is delayed until mid-August, such as is practiced in relay intercropping, excessive vegetative growth and competition with pearl millet is avoided. In the relay intercropping system, significant cowpea grain can be produced by November to December, which is during the beginning of the dry season, providing the rainy season has provided sufficient reserves of moisture in the soil profile.

Source	Details
	Except for Ndout and Baye Ngange, the traditional cowpea varieties are relatively insensitive to day length.
UN FAO Ecocrop - http://ecocrop.fao.org/ecocrop/srv/en/cropView?id=2153	Temperature: Occurs in areas with summer temperatures between 25-35°C. Climate: Occurs in areas with annual rainfall between 400-2000mm. It does not tolerate extended flooding or salinity. Annual growing period. Some cowpea accessions may start flowering 30 days after sowing and are ready for harvest of dry seeds 25 days later; others may take more than 90 days to flower, and 210-240 days to mature. Most cowpea accessions exhibit classic short-day responses with respect to time of flowering, although a range of sensitivities occur and the effect is modulated by temperature. Cultivated at elevations between sea level and 2000 m.
Plant Resources of Tropical Africa (PROTA) Database - http://database.prota.org/dbtw-wpd/exec/dbtwpub.dll?AC=GET_RECORD&XC=/dbtw-wpd/exec/dbtwpub.dll&BU=http%3A%2F%2Fdatabase.prota.org%2Fsearch.htm&TN=Protabase&SN=AUTO7450&SE=791&RN=2&MR=20&TR=0&TX=1000&ES=0&CS=1&XP=&RF=Webreport&EF=Basic+Record+Form&DF=Webdisplay&RL=0&EL=1&DL=0&NP=3&ID=&MF=&MQ=&TI=0&DT=&ST=0&IR=711&NR=0&NB=0&SV=0&SS=0&BG=&FG=&QS=Search&OEX=ISO-8859-1&OEH=ISO-8859-1	Temperature: Cowpea grows best at day temperatures of 25–35°C; night temperatures should not be less than 15ºC and consequently cultivation is restricted to low and medium altitudes. At altitudes above 700 m growth is retarded. Cowpea does not tolerate frost, and temperatures above 35°C cause flower and pod shedding. Climate: Cowpea is generally grown as a rainfed crop in sub-Saharan Africa. Short-duration determinate types can be grown with less than 500 mm rainfall per year. Long-duration types require 600–1500 mm. Cultivation in the dry season with ample irrigation is practised, as well as cultivation during the rainy season, although sowing during the rainy season can result in damage to the emerging or young plants. Most cowpea cultivars are quantitative short-day plants, but day-neutral types also exist. Cowpea can be grown on a wide range of soil types, provided they are well drained. Wild types grow up to 1500 m altitude, occasionally up to 2500 m altitude.
FAO GAEZ	Cowpea in tropical climates: Growing season of 80 to 120 days; temperatures of 15-20ºC for less than 16% of the season (ideally never); temperature never below 15C. Temperature sum during growing season > 1800 (ideally > 2100).

Climate Conditions for Cultivation for Rice (Species: Oryza glaberrima Common Name: African rice.)

Source	Details
Lost Crops of Africa: Volume 1 - Grains http://books.nap.edu/openbook.php?record_id=2305&page=24	Temperature: Average temperatures below about 25°C retard growth and reduce yields. Below about 20°C these effects are pronounced. African rice does well at temperatures above 30°C. Above about 35°C, however, spikelet fertility drops off noticeably. Climate: For the truly arid zones African rice is not a suitable crop, but on moderately watered sites (for example, where annual rainfall is at least 760 mm) or seasonally flooded sites its prospects seem good. The fact that some varieties mature 10-20 days before their principal Asian-rice rivals is significant in drylands where precipitation is often erratic. Some upland varieties can produce adequately with precipitation as low as about 700 mm. The dryland form thrives in light soils wherever there is a rainy season of at least 4 months and minimum rainfall of 760 mm. About 40 percent of the rice production in Africa's 15 major rice-producing countries relies on rain as the only source of water. Almost all

Source	Details
	of that area employs the Asian species, but West Africa still grows a small but significant amount of dryland African rice. Indeed, in certain parts of Ghana and Togo it is the chief staple. Today's varieties mature in 90-170 days. In the River Niger's inland delta in Mali, farmers grow various forms of floating African rice. Only about one-sixth of Africa's rice is produced using irrigation and 60 percent of that is in just one country—Madagascar. Swamp rice, however, is being increasingly cultivated in former mangrove areas of the Gambia, Guinea-Bissau, Guinea, and Sierra Leone. Most dryland types now in use are sensitive to photoperiod. They flower with the advent of the dry season. On the other hand, most floating types (at least in northern Mali) show little sensitivity to daylength.
UN FAO Grassland Species Profile - http://www.fao.org/ag/AGP/agpc/doc/GBASE/data/pf000274.htm (Asian rice)	Temperature: Optimum temperature for growth is a mean temperature above 21°C. It will not stand frosts. Climate: Rain-grown rice usually requires an annual rainfall in excess of 1 500 mm. Most of the world's rice is grown under irrigation and water is supplied as required. The amount may be in the vicinity of 7-9 million litres per hectare. It has little drought tolerance. Upland varieties need fairly good drainage. Upland varieties are not adapted to flooding.
Plant Resources of Tropical Africa (PROTA) Database - http://database.prota.org/dbtw-wpd/exec/dbtwpub.dll?AC=GET_RECORD&XC=/dbtw-wpd/exec/dbtwpub.dll&BU=http%3A%2F%2Fdatabase.prota.org%2Fsearch.htm&TN=Protabase&SN=AUTO7793&SE=792&RN=0&MR=20&TR=0&TX=1000&ES=0&CS=1&XP=&RF=Webreport&EF=Basic+Record+Form&DF=Webdisplay&RL=0&EL=1&DL=0&NP=3&ID=&MF=&MQ=&TI=0&DT=&ST=0&IR=676&NR=0&NB=0&SV=0&SS=0&BG=&FG=&QS=Search&OEX=ISO-8859-1&OEH=ISO-8859-1	Temperature: African rice grows well above 30°C, but above 35°C spikelet fertility is noticeably reduced. Temperatures below 25°C reduce growth and yield; temperatures below 20°C do so markedly. Climate: African rice is grown from sea-level to 1700 m altitude. It is generally a short-day plant, but photosensitivity varies between cultivars from day-neutral to strongly sensitive.
Africa Rice Centre - http://www.warda.org/publications/nerica-comp/module%206_Low.pdf NERICA rice	Climate: In general, upland rice can grow in any environment with at least 15 to 20 mm of five-day rainfall during the growing cycle. During germination and early growth stages, 15 mm per five-day rainfall is sufficient. In environments where there are two distinct cropping seasons, it is important to establish the time to sow in each season based on the long term (15-year) daily rainfall pattern or actual trials on optimum sowing date. In the monomodal rainfall savannah zone of Côte d'Ivoire, West Africa upland rice is sown in May–June while sowing in March–April (first season) and May–June (second season) is recommended in the bimodal rainfall forest zone.
"African rice (*Oryza glaberrima*): History and future potential" Linares (2002) http://www.pnas.org/content/99/25/16360.full	In the coastal area, where rice is a dominant subsistence crop, isolated pockets of O. glaberrima cultivation remain in Guinea Bissau, Guinea, Sierra Leone, and in the Casamance region of southern Senegal. Everywhere, however, O. glaberrima types are fast being replaced by the higher yielding O. sativa varieties.

Climate Conditions for Cultivation for Sorghum

Source	Details
Lost Crops of Africa: Volume 1 - Grains http://books.nap.edu/openbook.php?record_id=2305&page=127	Temperature: The plant is killed by frost. Optimum growth occurs at about 30°C. Climate: Although many cultivars are insensitive to photoperiod, sorghum is basically a short-day species. Most traditional varieties differentiate from vegetative to reproductive growth when daylengths shorten to 12 hours. This switch to flowering often happens just when the rains diminish, and the crop matures in the dry season that follows, a feature that greatly helps the farmer. Some of these traditional forms are extremely susceptible to photoperiod and reach impossible heights if not planted as daylengths shorten. Although part of the crop is grown in rainy regions, sorghum is remarkably drought-resistant and is vitally important where the climate is just too dry for maize. Sorghum is grown from sea level to above 3,000 m. It is one of the quickest maturing food plants (certain types can mature in as little as 75 days and can provide three harvests a year).
UN FAO Ecocrop - http://ecocrop.fao.org/ecocrop/srv/en/cropView?id=1982	Temperature: Lowland tropical sorghums are adapted to warm days and night temperatures above 22°C throughout the growing season. Climate: Sweet sorghum can be found at elevations between sea level and 1500 m, most East African sorghum is grown between the altitudes of 900-1500 m, and cool-tolerant varieties are grown between 1600 and 2500 m. Annual or short-term perennial grass. Most sorghum plants take 90-120 days to mature, the boot stage is reached in 50-60 days, flowering in 60-70 days and full grain maturity in 90-120 days.
US National Sorghum Producers - http://www.sorghumgrowers.com	Temperature: Plant at 18C soil temp, 15C minimum. Climate: Key period for moisture is first 60 days after planting.
UN FAO Grassland Species Profile - http://www.fao.org/ag/agp/agpc/doc/gbase/data/pf000319.htm	Temperature: Optimum temperature for growth is 30°C. Sorghum is very susceptible to frost. Climate: Mostly grown in an annual rainfall range of 400-750 mm. It is grown in areas which are too dry for maize. Sorghum can become dormant under adverse conditions and can resume growth after relatively severe drought. Early drought stops growth before floral initiation and the plant remains vegetative; it will resume leaf production and flower when conditions again become favourable for growth. Late drought stops leaf development but not floral initiation. Good drainage is necessary. Sorghum is intolerant of sustained flooding, but will survive temporary waterlogging. Altitude range from sea-level to 1000 m.
Plant Resources of Tropical Africa (PROTA) database - http://database.prota.org/dbtw-wpd/exec/dbtwpub.dll?AC=GET_RECORD&XC=/dbtw-wpd/exec/dbtwpub.dll&BU=http%3A%2F%2Fdatabase.prota.org%2Fsearch.htm&TN=Protabase&SN=AUTO7254&SE=789&RN=0&MR=20&TR=0&TX=1000&ES=0&CS=1&XP=&RF=Webreport&EF=Basic+Re	Temperature: The optimum temperature for sorghum seed germination is 27–35°C. The optimum (seasonal) temperature is 25–31°C, but temperatures as low as 21°C will not dramatically affect growth and yield. Sterility can occur when night temperatures fall below 12–15°C during the flowering period. Sorghum is susceptible to frost, but to a lesser extent than maize and light night-frosts during ripening cause little damage. Climate: A rainfall of 500–800 mm evenly distributed over the cropping season is normally adequate for cultivars maturing in 3–4 months. Sorghum tolerates waterlogging and can also be grown in areas of high

Source	Details
cord+Form&DF=Webdisplay&RL=0&EL=1&DL=0&NP=3&ID=&MF=&MQ=&TI=0&DT=&ST=0&IR=692&NR=0&NB=0&SV=0&SS=0&BG=&FG=&QS=Search&OEX=ISO-8859-1&OEH=ISO-8859-1	rainfall. It tolerates a wide range of temperatures and is also grown widely in temperate regions and at altitudes up to 2300 m in the tropics. Sorghum is well suited to grow on heavy Vertisols commonly found in the tropics, where its tolerance of waterlogging is often required, but is equally suited to light sandy soils.
Natural History Museum - http://www.nhm.ac.uk/jdsml/nature-online/seeds-of-trade/page.dsml?section=crops&page=agriculture&ref=sorghum	Temperature: Its optimum growth temperature is 30°C, and it cannot survive frosts. Climate: Sorghum is a short-day plant, and is adapted to a wide range of ecological conditions. Because sorghum is drought-resistant, plants can remain dormant during periods of drought and resume growth when conditions improve; conversely, they cannot tolerate waterlogging. In some countries plants can be grown under irrigation.
FAO GAEZ	Climate and Temperature. Two independent sets of temperature conditions for sorghum cultivation are specified: Lowland Sorghum in tropical climates (note that this definition also covers maize): growing season of 3 to 4.5 months; temperatures of 15-20ºC for less than 16% of the season (ideally never); temperature sum during season > 2200 (ideally > 2500) Highland sorghum in tropical climates (note that this definition also covers maize): growing season lengthens with ambient temperature from 3.5 months @ 20ºC to 10 months at 15ºC; no average temperatures above 25ºC or below 10ºC; temperatures 10-15ºC for less than 50% of season (ideally < 33% of season); temperatures 20-25ºC for < 33% of season; temperature sum during growing season > 2200 (ideally > 2500)

Climate Conditions for Cultivation of Millet

Pearl Millet is over half of global millet production and is the primary millet species in the Sahel (Lost Crops of Africa: http://books.nap.edu/openbook.php?record_id=2305&page=80). Extracts are therefore based on pearl millet.

Source	Details
Wikipedia - http://en.wikipedia.org/wiki/Pearl_millet	Climate. Pearl millet is well adapted to production systems characterized by drought, low soil fertility, and high temperature. It performs well in soils with high salinity or low pH. Because of its tolerance to difficult growing conditions, it can be grown in areas where other cereal crops, such as maize or wheat, would not survive.
Lost Crops of Africa: Volume 1 - Grains http://books.nap.edu/openbook.php?record_id=2305&page=91	Temperature. The plant is generally sensitive to low temperatures at the seedling stage and at flowering. High daytime temperatures are needed for the grain to mature. In Africa's pearl millet zone, temperatures are typically above 30°C. Climate. Pearl millet is usually a short-day plant, but some varieties are daylength neutral. Although the crop is grown where rainfall ranges from 200 to 1,500 mm, most occurs in areas receiving 250-700 mm. Although very drought resistant, pearl millet requires its rainfall to be evenly distributed during the growing season. (Unlike sorghum, it cannot retreat into dormancy during droughts.) On the other hand, too much rain at flowering can also cause a crop failure. It performs poorly in clay

Source	Details
	soils and cannot tolerate waterlogging. Pearl millet is seldom found above 1,200 m in Africa.
ICRISAT - http://www.icrisat.org/vasat/learning_resources/crops/pm/pm_prod_practices/html/m2_2.3/index.html	Climate: Optimally planted between 25-30C in moist soil. 75 day total growth period.
UN FAO Ecocrop - http://ecocrop.fao.org/ecocrop/srv/en/cropView?id=8418	Summer annual growing period. Early millets, requires 60-95 days of growing period, medium duration types, about 80 days, and long duration types, 100-120 days. In the tropics, it can be grown at altitude between sea level and 1800 m. Pearl millet is the staple food in parts of tropical Africa, which are too hot, dry and sandy for sorghum production.
UN FAO Grassland Species Profile - http://www.fao.org/ag/agp/agpc/doc/gbase/DATA/PF000297.HTM	Temperature: Summer temperatures should be high. Maximum germination occurs at a day/night temperature of 20/25°C. Minimum temperature for growth of 7.0°C. Low temperatures retard germination and at 10°C, photosynthesis is negligible. Temperatures near 0°C are lethal. Climate: It is grown in areas with an average annual rainfall of 125-900 mm, the lower rainfall areas using it as a grain crop where maize and sorghum fail. Where dry matter for forage is the consideration, a minimum rainfall of 500 mm is required. Late rainfall is important for grain development in weeks 5-12. It is drought tolerant. It does not tolerate flooding, especially during the summer. It can be grown at altitude between 800-1800 m.
Plant Resources of Tropical Africa (PROTA) database - http://database.prota.org/dbtw-wpd/exec/dbtwpub.dll?AC=GET_RECORD&XC=/dbtw-wpd/exec/dbtwpub.dll&BU=http%3A%2F%2Fdatabase.prota.org%2Fsearch.htm&TN=Protabase&SN=AUTO6571&SE=788&RN=0&MR=20&TR=0&TX=1000&ES=0&CS=1&XP=&RF=Webreport&EF=Basic+Record+Form&DF=Webdisplay&RL=0&EL=1&DL=0&NP=3&ID=&MF=&MQ=&TI=0&DT=&ST=0&IR=684&NR=0&NB=0&SV=0&SS=0&BG=&FG=&QS=Search&OEX=ISO-8859-1&OEH=ISO-8859-1	Temperature: The optimum temperature for germination of pearl millet seeds is 33–35°C; no germination occurs below 12°C. The optimum temperature for tiller production and development is 21–24°C, and for spikelet initiation and development about 25°C. Extreme high temperatures before anthesis reduce pollen viability, panicle size and spikelet density, thus reducing yield. Climate: In West Africa, from the oases of the Sahara desert (under irrigation) to the northern Sahel (characterized by 250 mm annual rainfall), pearl millet cultivars are grown that are photoperiod insensitive and mature in 55–65 days. In the 250–400 mm rainfall zone, where very high temperatures are common, especially at planting time, it is the dominant cereal. Pearl millet does not tolerate waterlogging. Once established, the crop is fairly tolerant of salinity.
Natural History Museum - http://www.nhm.ac.uk/jdsml/nature-online/seeds-of-trade/page.dsml?section=crops&page=agriculture&ref=millet	Pearl millet is suited to soils with low fertility and moisture levels. In Africa, it is normally grown as a rain-fed crop but is occasionally irrigated. Although drought-resistant, pearl millet cannot go into dormancy in extreme drought conditions and thus depends on a certain amount of moisture for growth. Pearl millet thrives where sorghum would die, and performs better in sandy loams than in pure sand.
FAO GAEZ	Pearl Millet in tropical climates: Growing season of 70 to 90 days; temperatures of 15-20ºC for less than 16% of the season (ideally never); temperature never below 15C. Temperature sum during growing season > 1600 (ideally > 1800).

Climate Conditions for Cultivation for Maize

Source	Details
Wikipedia - http://en.wikipedia.org/wiki/Maize	Temperature. Maize is a facultative long-night plant and flowers in a certain number of growing degree days > 50 °F (10 °C) in the environment to which it is adapted.
Natural History Museum - http://www.nhm.ac.uk/jdsml/nature-online/seeds-of-trade/page.dsml?section=crops&ref=maize&page=agriculture	Temperature. Maize is an annual crop requiring 110-140 frost-free days
FAO GAEZ	Climate and Temperature. Four independent sets of temperature conditions for maize cultivation are specified: Lowland Maize in tropical climates (note that this definition also covers sorghum): growing season of 3 to 4.5 months; temperatures of 15-20ºC for less than 16% of the season (ideally never); temperature sum during season > 2200 (ideally > 2500) Highland maize in tropical climates (note that this definition also covers sorghum): growing season lengthens with ambient temperature from 3.5 months @ 20ºC to 10 months at 15ºC; no average temperatures above 25ºC or below 10ºC; temperatures 10-15ºC for less than 50% of season (ideally < 33% of season); temperatures 20-25ºC for < 33% of season; temperature sum during growing season > 2200 (ideally > 2500) Maize for grain in the subtropics (with both summer and winter rains) and at temperate latitudes: growing season of 3.5 to 6 months; temperatures of 10-15ºC for < 50% of season and never < 10ºC; temperature sum during growing season > 1900 (ideally > 2400) Maize for silage in temperate latitudes: growing season of 3.5 to 6 months; temperatures of 10-15ºC for < 66% of season and never < 10ºC; temperature sum during growing season > 1700 (ideally > 1900); no permafrost
UN FAO Grassland Species Profile - http://www.fao.org/ag/agp/agpc/doc/gbase/DATA/PF000342.HTM	Temperature: Minimum temperature for growth is 8.7°C for Kitale hybrids in Kenya. It is very susceptible to frosts. Climate: An annual rainfall of more than 500 mm is needed, with best yields usually in the 1200-1500 mm area; it is often an irrigated crop. Experiments show that the more rainfall after five weeks' growth, the higher the yield. It is fairly drought tolerant up to five weeks, but thereafter is very susceptible. Dry weather at pollination time seriously affects pollination and hence yields.
Plant Resources of Tropical Africa (PROTA) Database - http://database.prota.org/dbtw-wpd/exec/dbtwpub.dll?AC=GET_RECORD&XC=/dbtw-wpd/exec/dbtwpub.dll&BU=http%3A%2F%2Fdatabase.prota.org%2Fsearch.htm&TN=Protabase&SN=AUTO8021&SE=794&RN=0&MR=20&TR=0&TX=1000&ES=0&CS=1&XP=&RF=Webreport&EF=Basic+Record+Form&DF=Webdisplay&RL=0&EL=1&DL=0&NP=3&ID=&MF=&MQ=&TI=0&DT=&ST=0&IR=712&NR=0&NB=0&SV=0&SS=0&BG=&FG=&QS=Search&OEX=ISO-8859-1&OEH=ISO-8859-1	Temperature: The crop requires an average daily temperature of at least 20°C for adequate growth and development; the optimum temperature for growth and development is 25–30°C; temperatures above 35° reduce yields. Frost is not tolerated. Climate: Maize is less drought-resistant than sorghum, pearl millet and finger millet. In the tropics it does best with 600–900 mm well-distributed rainfall during the growing season. It is especially sensitive to drought and high temperatures around the time of flowering. It does not tolerate waterlogging and is sensitive to salinity.

Source	Details
Agrometeorologist – Andy Challinor (University of Leeds)	Climate. Non-climatic influences, and the range of responses to climate, mean that the particular variety grown can play a key role in determining yields. Basic requirements: 500-800 mm rain over 4-5 months; maximum temperature 30-32ºC, minimum 13-17ºC. More complex option: reaches photosynthetic peak at 30-40ºC, but negligible growth at 44-50ºC; optimal daytime leaf temperatures of 30-33ºC with cool nights (i.e. favours seasonally-arid, as opposed to humid, tropics); radiation use efficiency for photosynthetically active radiation (PAR) 5-7%; APAR 3-4g/MJ, i.e. approximately 4-6g/MJ PAR; maximum grains per plant with temperature maximum in range 27-32ºC and minimum 13-17ºC; sensitive to water stress during flowering; development slows with temperatures < 20ºC; water requirement 500-800 mm with water use efficiency 11g/kg; 2100-3200 growing degree days with threshold temperature of 10ºC or 1000-1800 with threshold of 8ºC; duration 80-100 days for early growth, total 110-140 days

Appendix 2: Thresholds of Production in West Africa

Thresholds of production across the West Africa region, as realised from mean climatic conditions, for the crops in this study. Maps are provided using both the NCEP and JapRe precipitation reanalyses, both use the CRU temperature dataset.

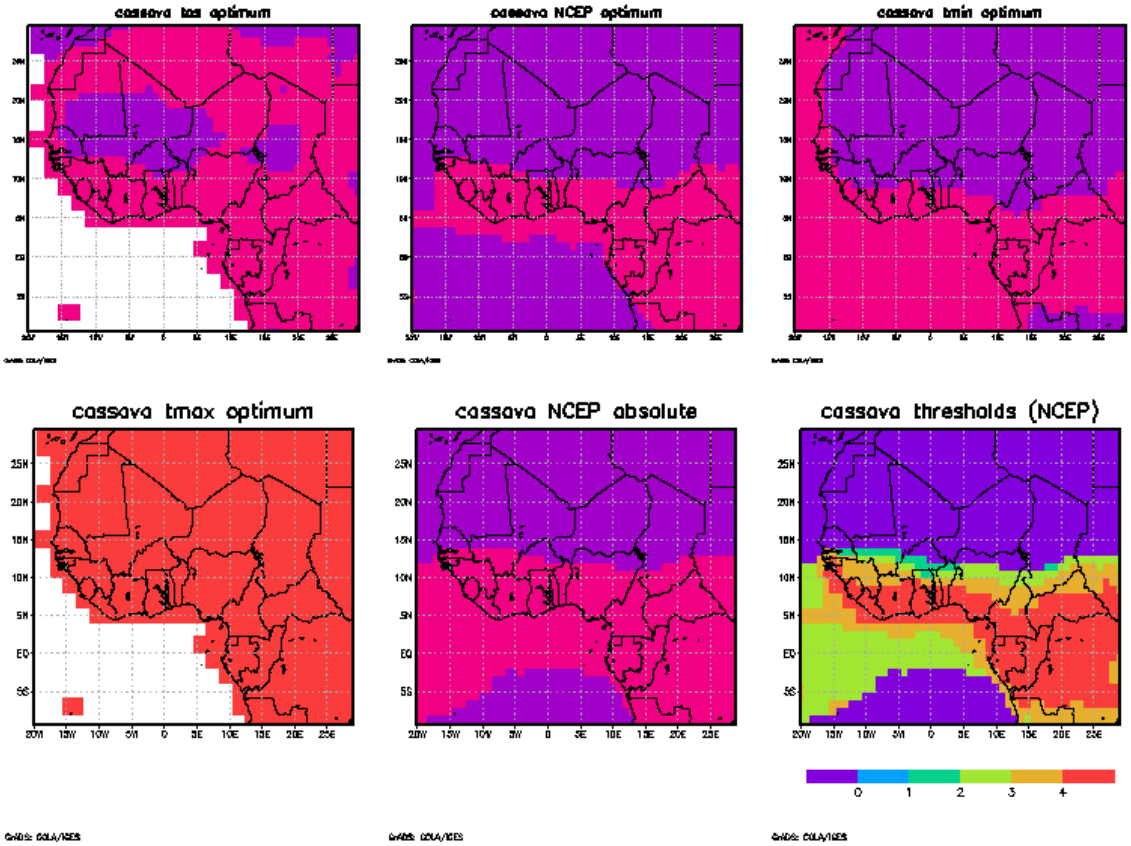

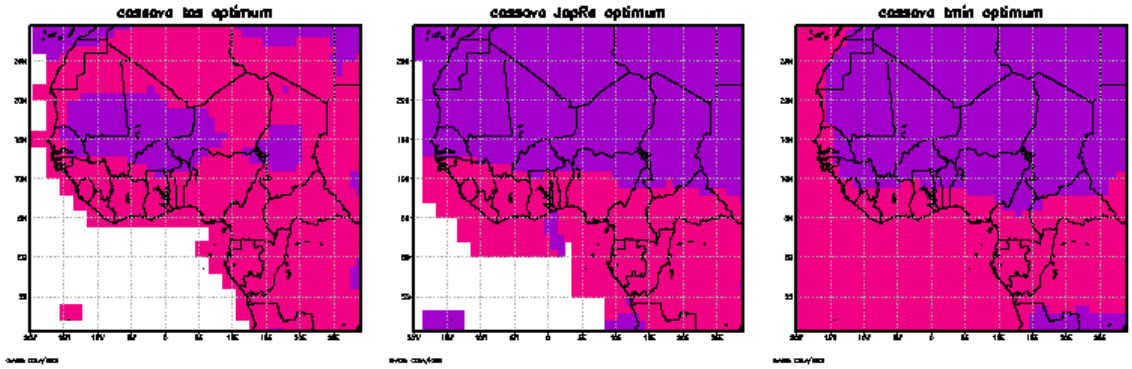
cassava tas optimum
cassava JapRe optimum
cassava tmin optimum

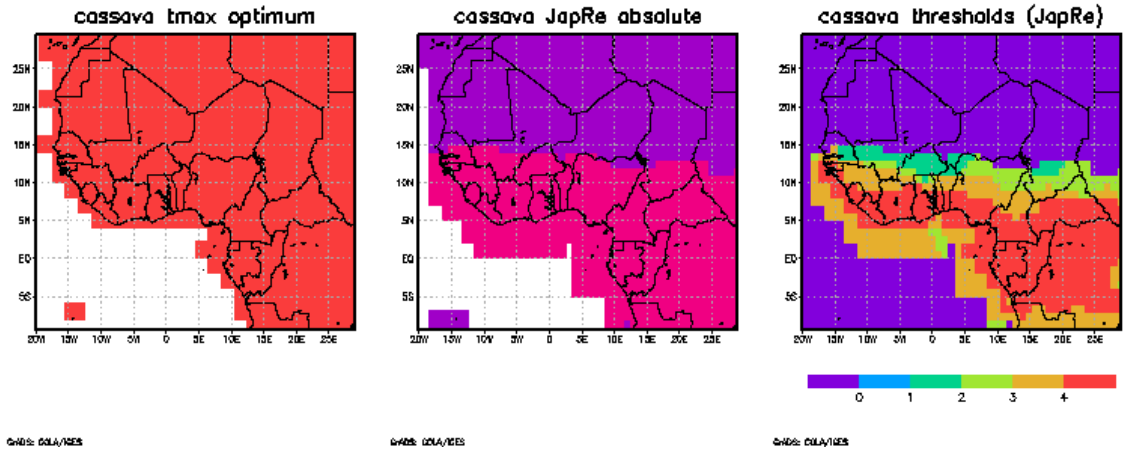
cassava tmax optimum
cassava JapRe absolute
cassava thresholds (JapRe)
0
1
2
3
4

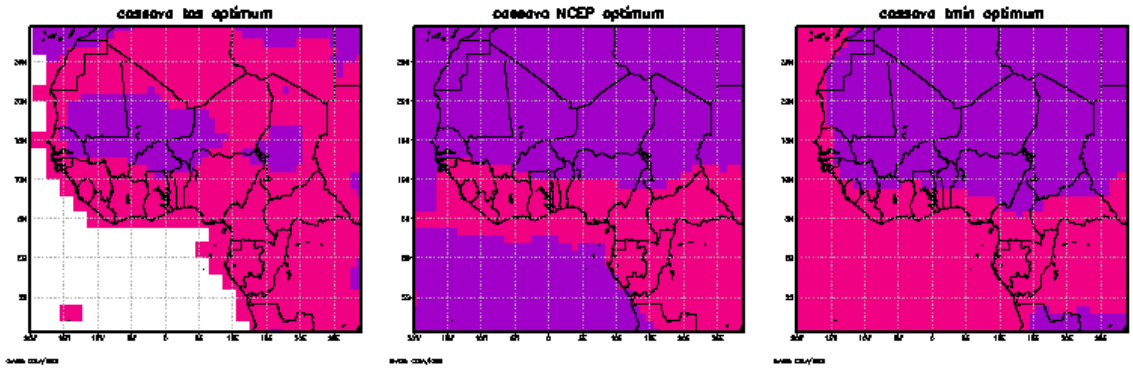
cassava tas optimum
cassava NCEP optimum
cassava tmin optimum

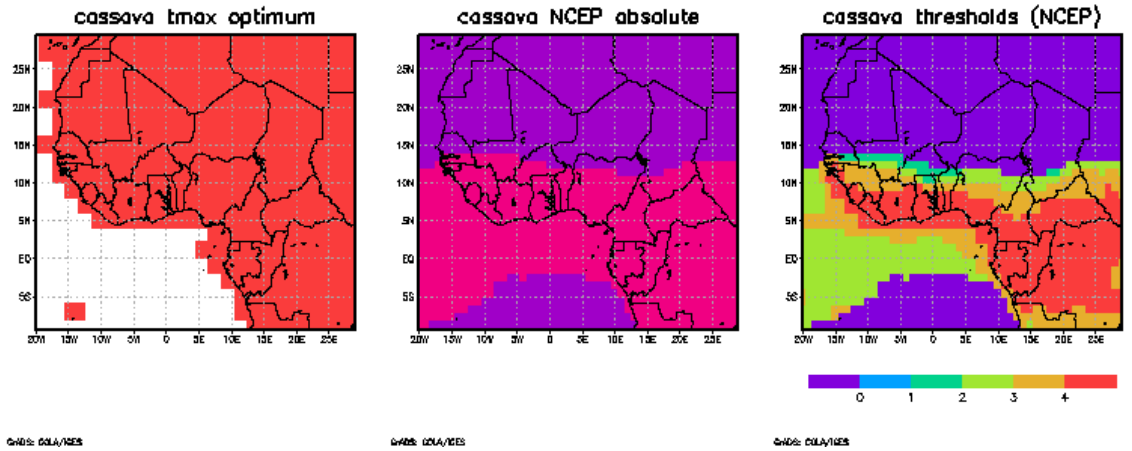
cassava tmax optimum
cassava NCEP absolute
cassava thresholds (NCEP)
0
1
2
3
4

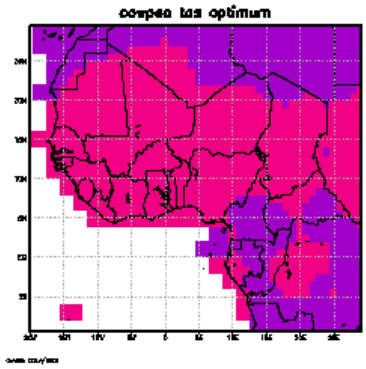
cowpea tas optimum

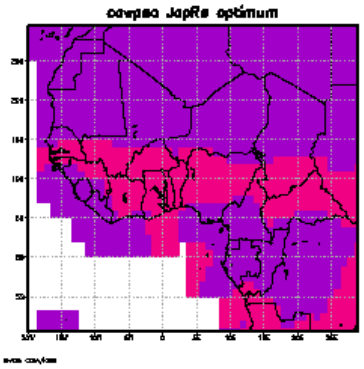
cowpea JapRe optimum

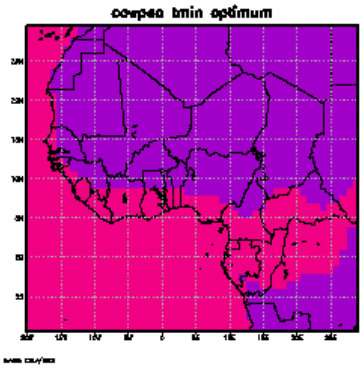
cowpea tmin optimum

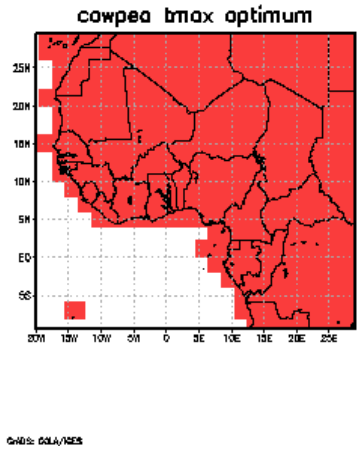
cowpea tmax optimum

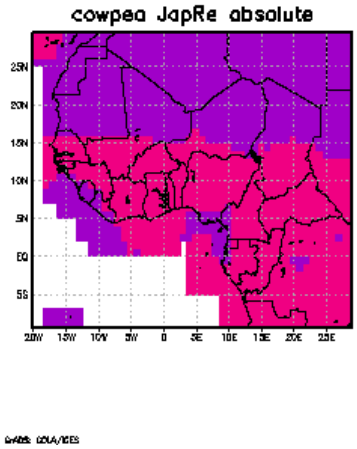
cowpea JapRe absolute

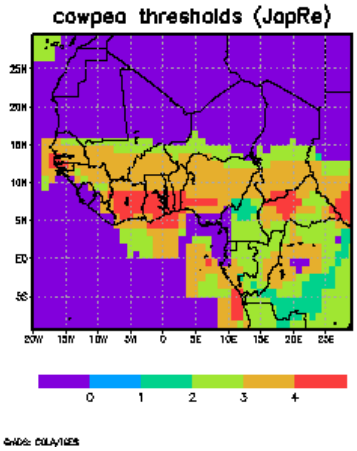
cowpea thresholds (JapRe)
0
1
2
3
4

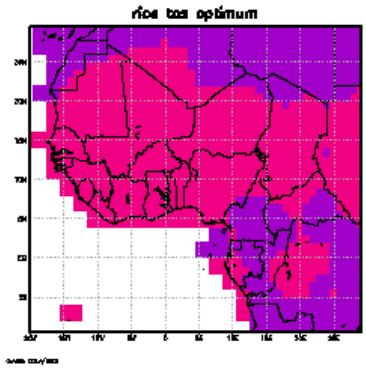
rice tas optimum

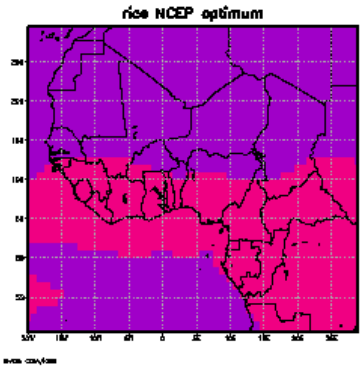
rice NCEP optimum

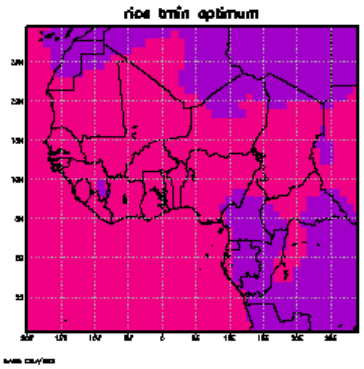
rice tmin optimum

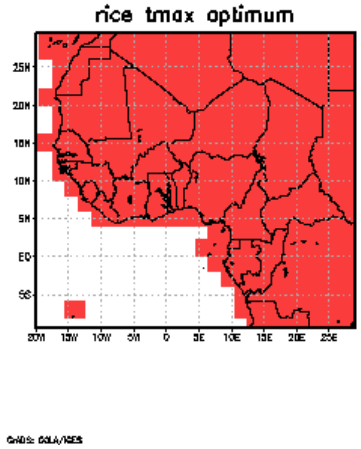
rice tmax optimum

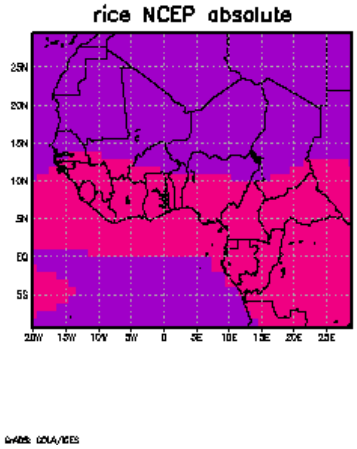
rice NCEP absolute

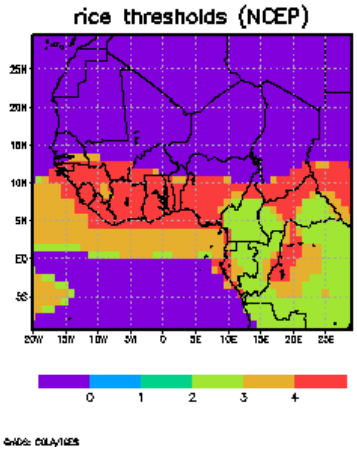
rice thresholds (NCEP)
0
1
2
3
4

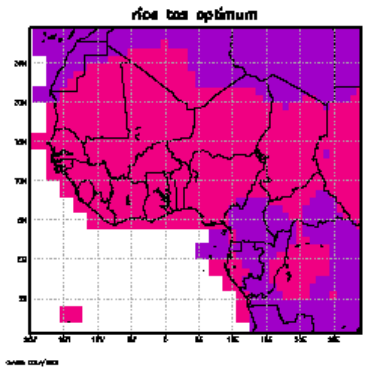
rice tas optimum

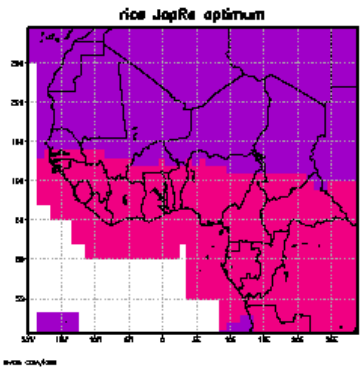
rice JapRe optimum

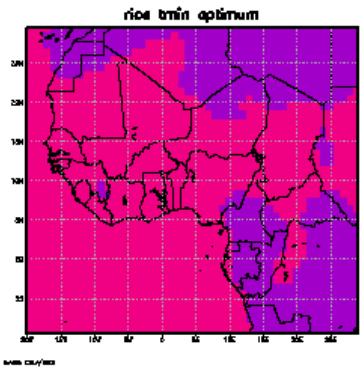
rice tmin optimum

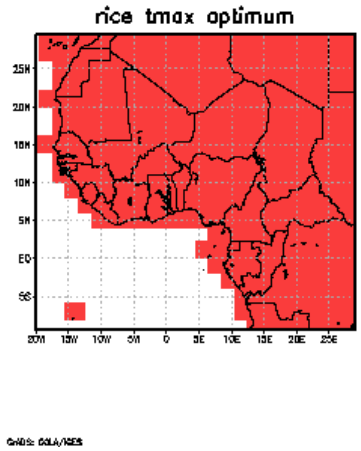
rice tmax optimum

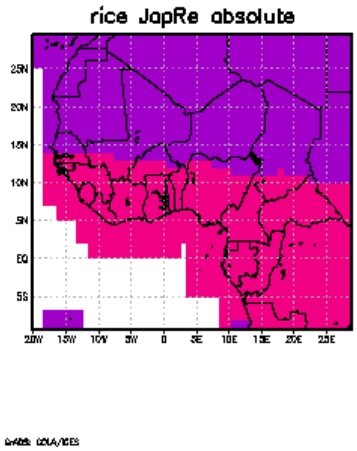
rice JapRe absolute

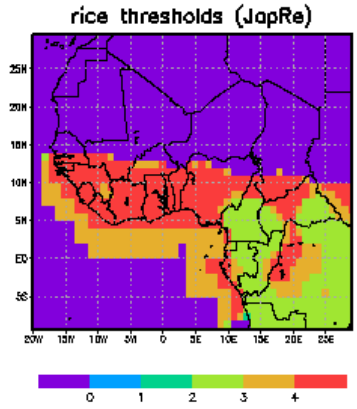
rice thresholds (JapRe)
0
1
2
3
4

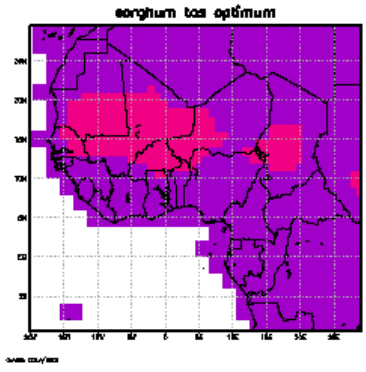
sorghum tas optimum

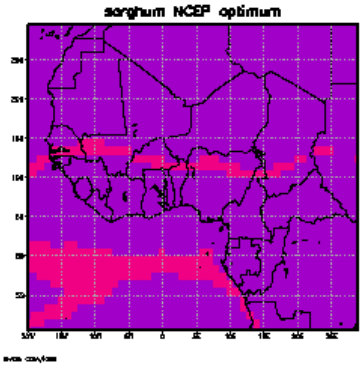
sorghum NCEP optimum

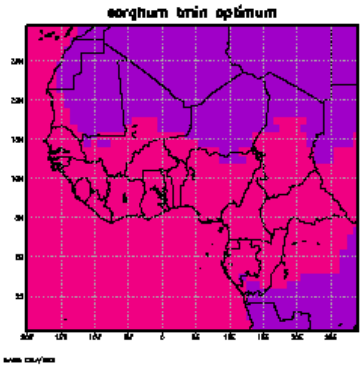
sorghum tmin optimum

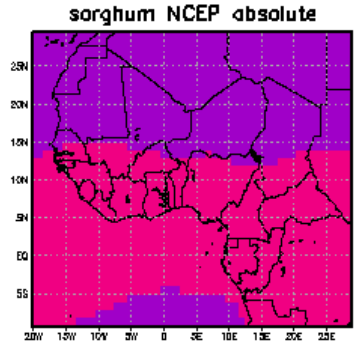
sorghum NCEP absolute

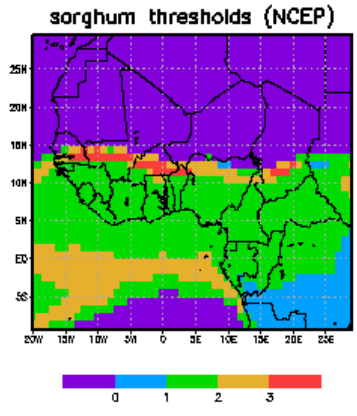
sorghum thresholds (NCEP)
0
1
2
3

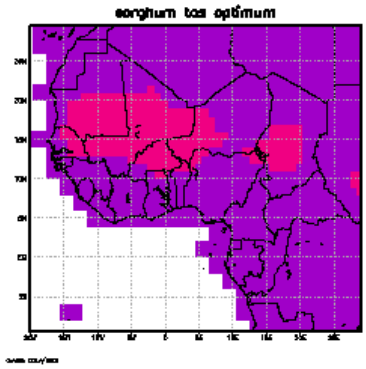
sorghum tas optimum

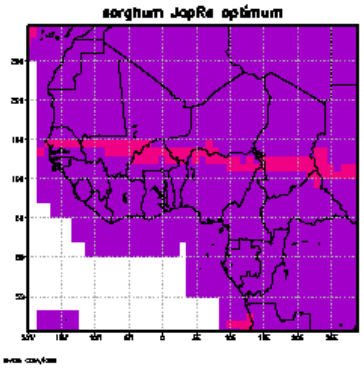
sorghum JapRe optimum

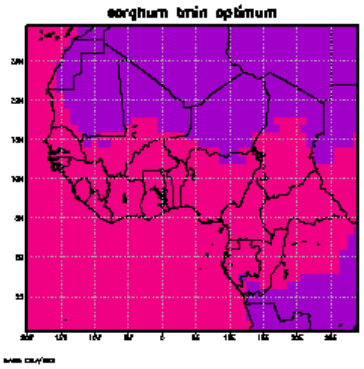
sorghum tmin optimum

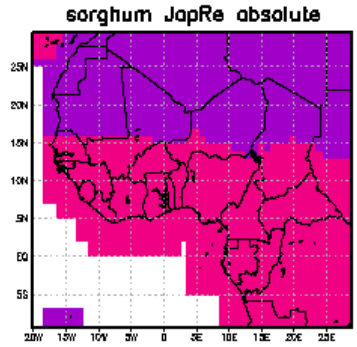
sorghum JapRe absolute

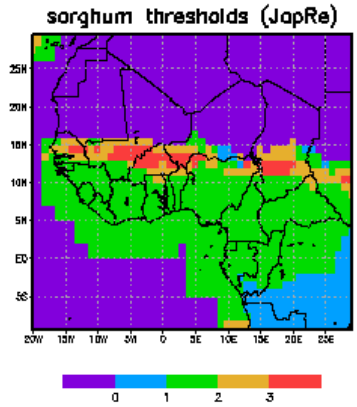
sorghum thresholds (JapRe)
0
1
2
3

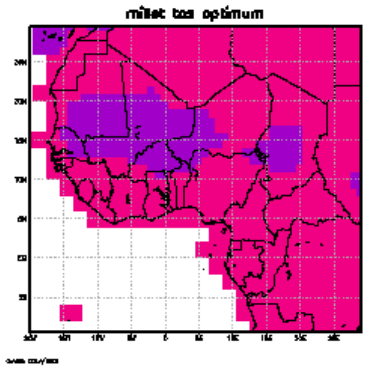
millet tas optimum

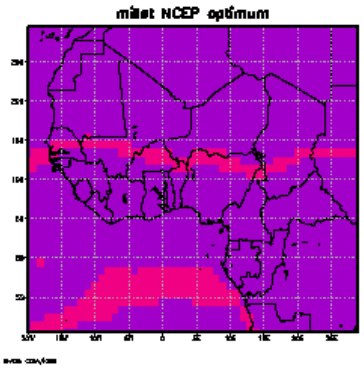
millet NCEP optimum

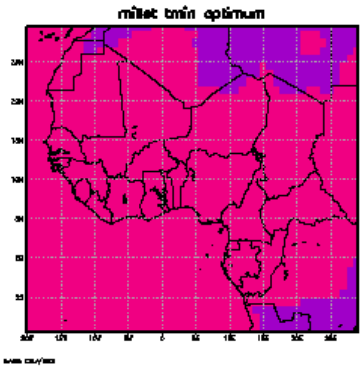
millet tmin optimum

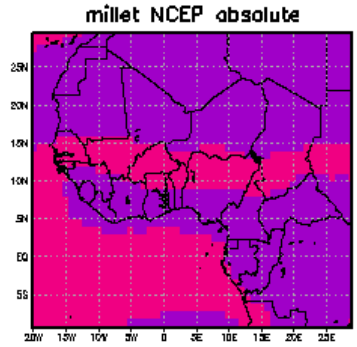
millet NCEP absolute

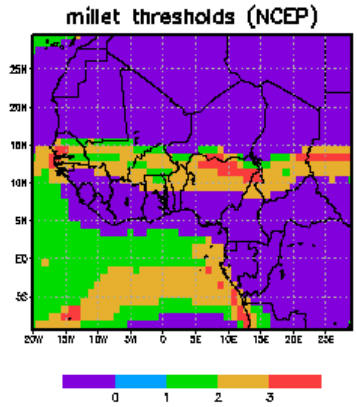
millet thresholds (NCEP)
0
1
2
3

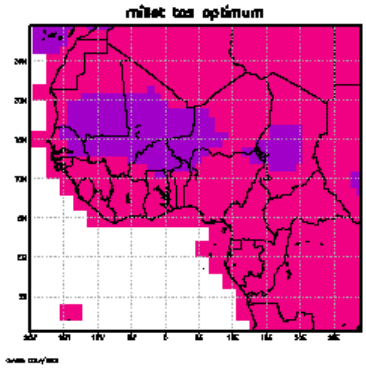
millet tas optimum

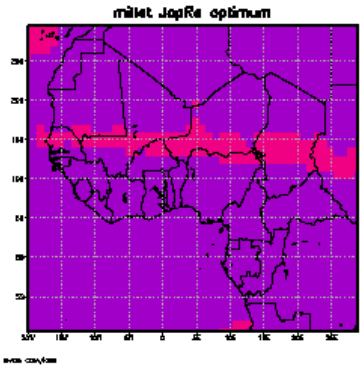
millet JapRe optimum

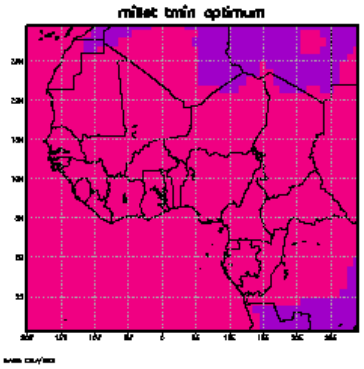
millet tmin optimum

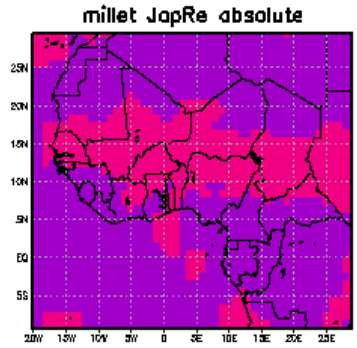
millet JapRe absolute

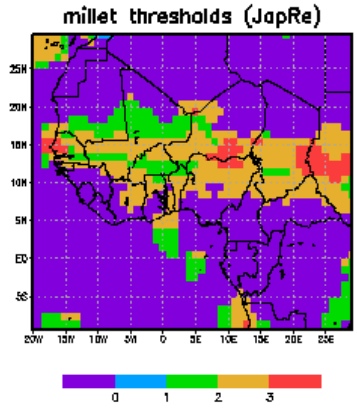
millet thresholds (JapRe)
0
1
2
3

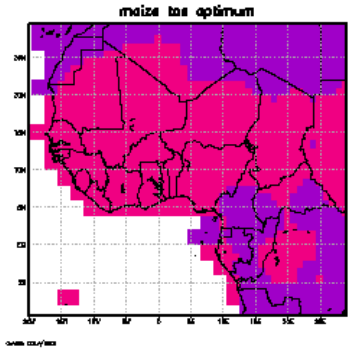
maize tas optimum

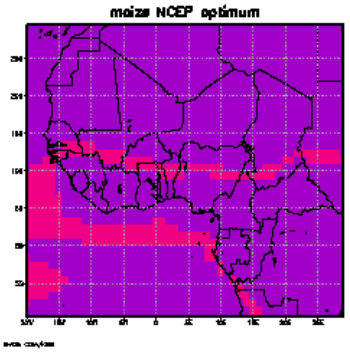
maize NCEP optimum

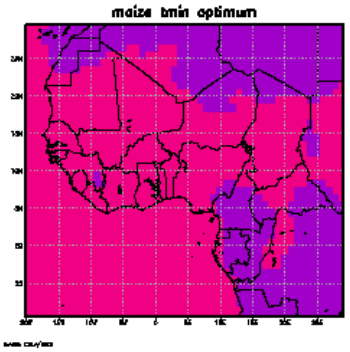
maize tmin optimum

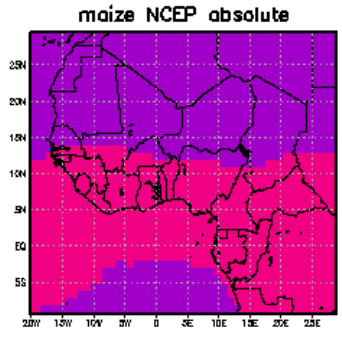
maize NCEP absolute

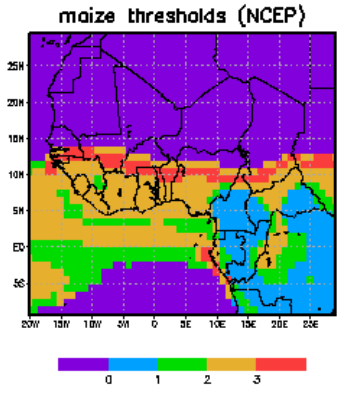
maize thresholds (NCEP)
0
1
2
3

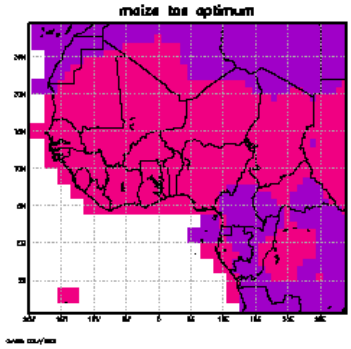
maize tas optimum

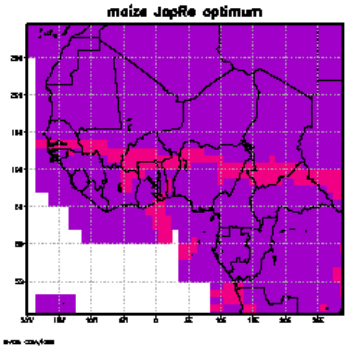
maize JapRe optimum

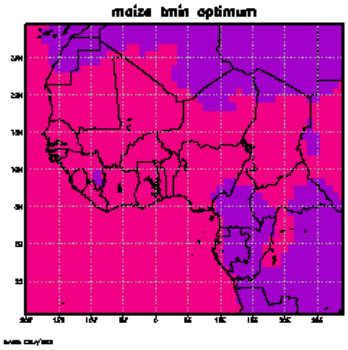
maize tmin optimum

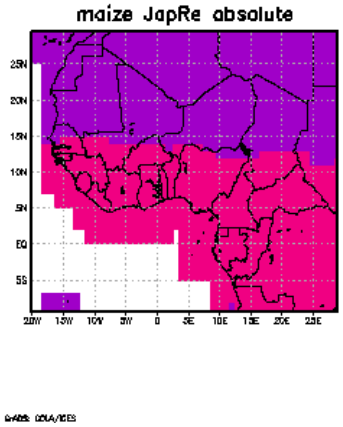
maize JapRe absolute

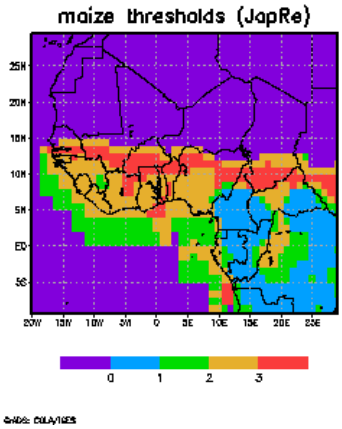
maize thresholds (JapRe)
0
1
2
3

Appendix 3: Model produced climatologies (1970-99) of temperature and precipitation

Temperature

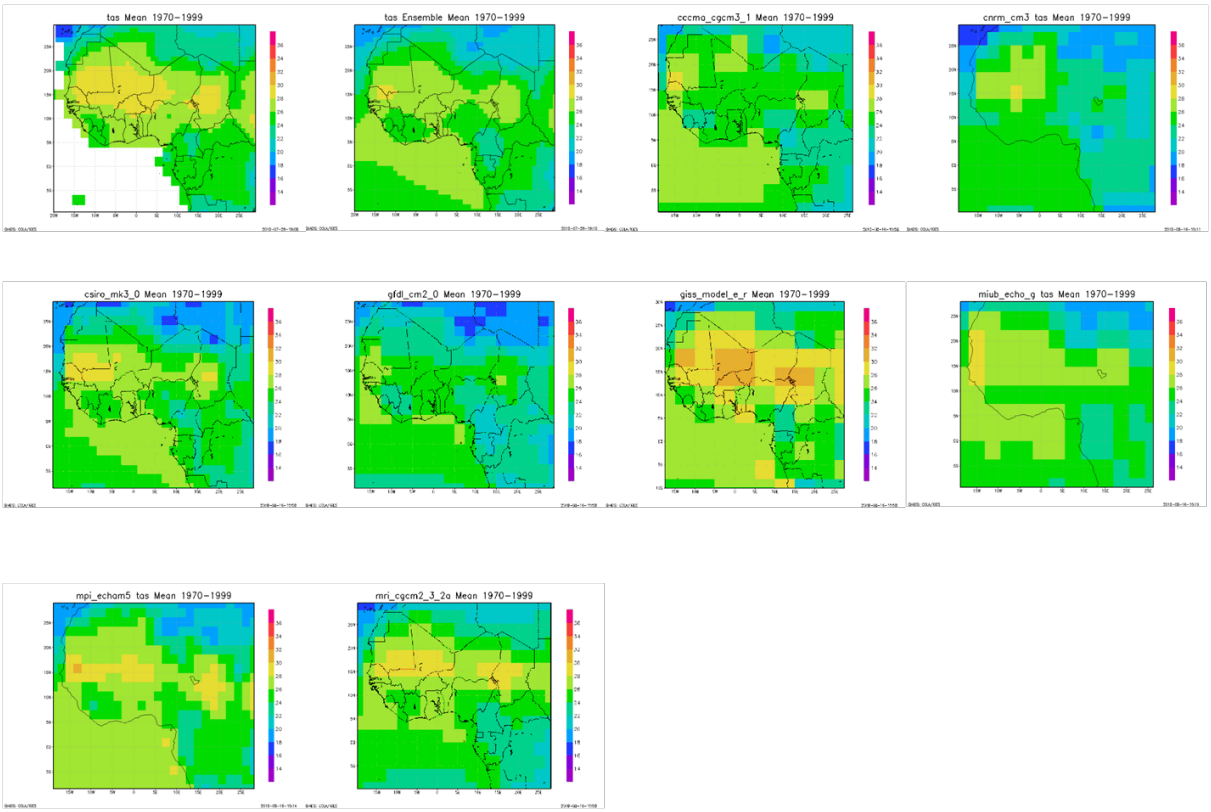

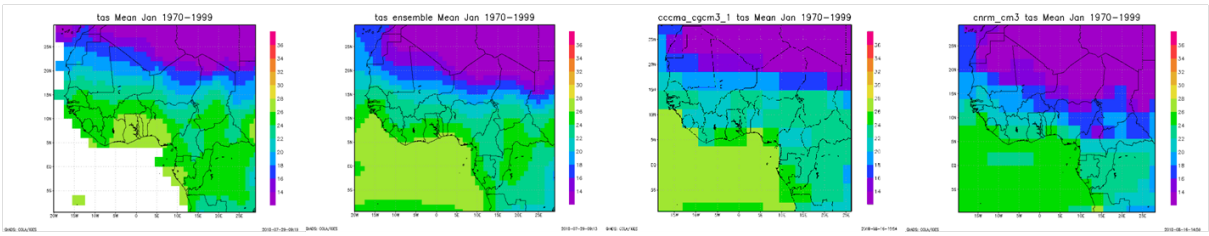
tas Mean Jan 1970-1999
tas ensemble Mean Jan 1970-1999
cccma_cgcm3_1 tas Mean Jan 1970-1999
cnrm_cm3 tas Mean Jan 1970-1999

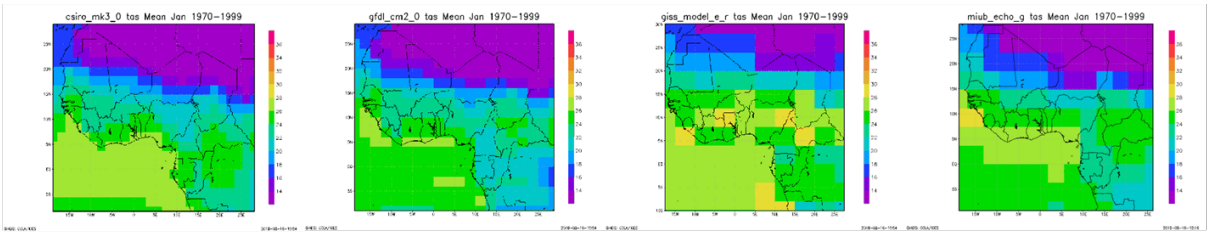
csiro_mk3_0 tas Mean Jan 1970-1999
gfdl_cm2_0 tas Mean Jan 1970-1999
giss_model_e_r tas Mean Jan 1970-1999
miub_echo_g tas Mean Jan 1970-1999

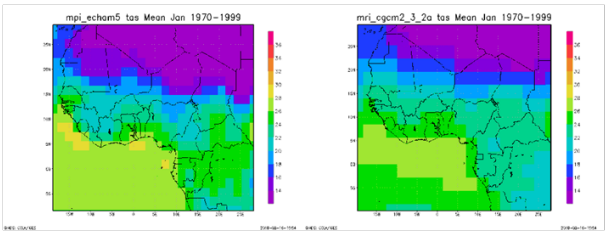
mpi_echam5 tas Mean Jan 1970-1999
mri_cgcm2_3_2a tas Mean Jan 1970-1999

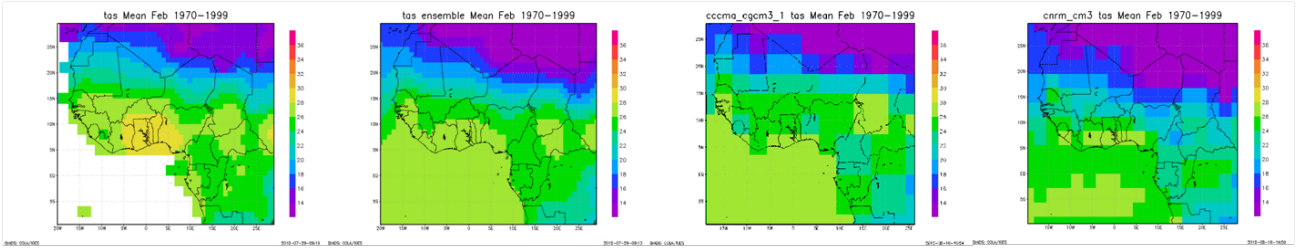
tas Mean Feb 1970-1999
tas ensemble Mean Feb 1970-1999
cccma_cgcm3_1 tas Mean Feb 1970-1999
cnrm_cm3 tas Mean Feb 1970-1999

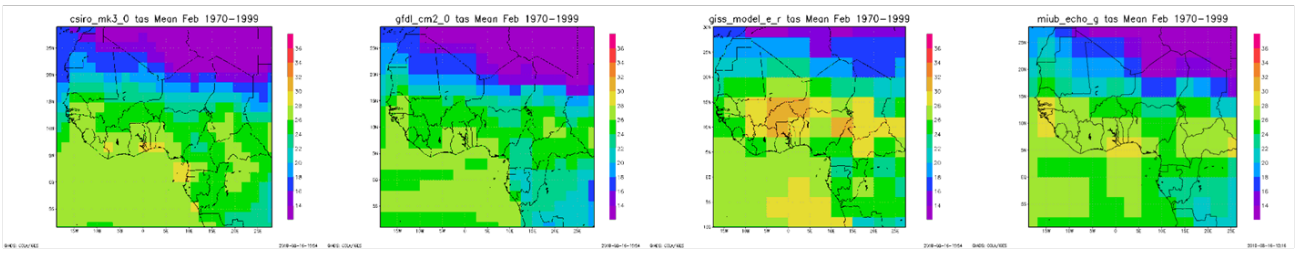
csiro_mk3_0 tas Mean Feb 1970-1999
gfdl_cm2_0 tas Mean Feb 1970-1999
giss_model_e_r tas Mean Feb 1970-1999
miub_echo_g tas Mean Feb 1970-1999

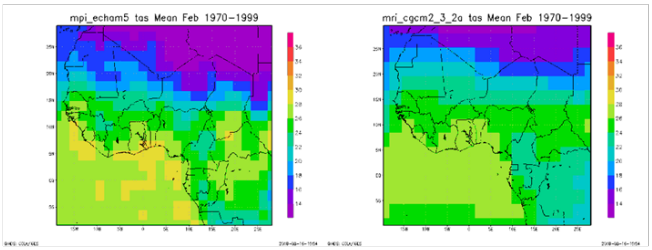
mpi_echam5 tas Mean Feb 1970-1999
mri_cgcm2_3_2a tas Mean Feb 1970-1999

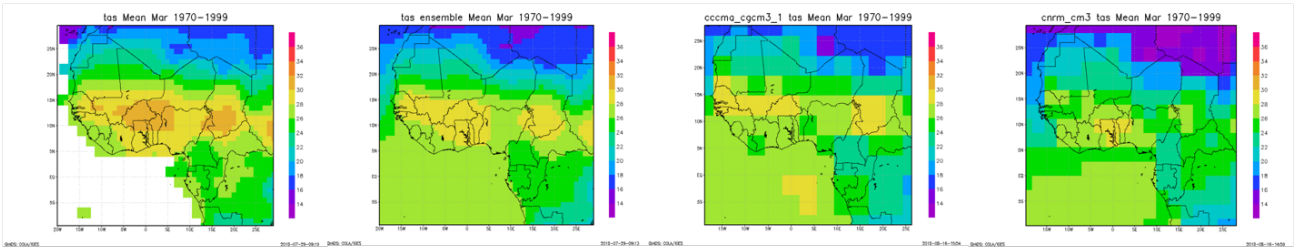
tas Mean Mar 1970-1999
tas ensemble Mean Mar 1970-1999
cccma_cgcm3_1 tas Mean Mar 1970-1999
cnrm_cm3 tas Mean Mar 1970-1999

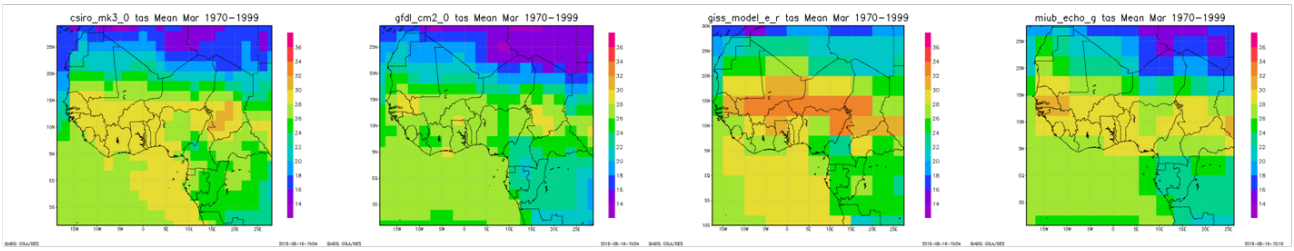
csiro_mk3_0 tas Mean Mar 1970-1999
gfdl_cm2_0 tas Mean Mar 1970-1999
giss_model_e_r tas Mean Mar 1970-1999
miub_echo_g tas Mean Mar 1970-1999

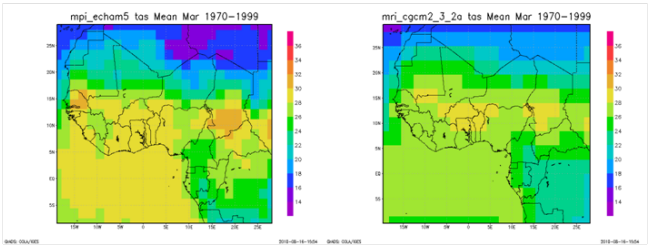
mpi_echam5 tas Mean Mar 1970-1999
mri_cgcm2_3_2a tas Mean Mar 1970-1999

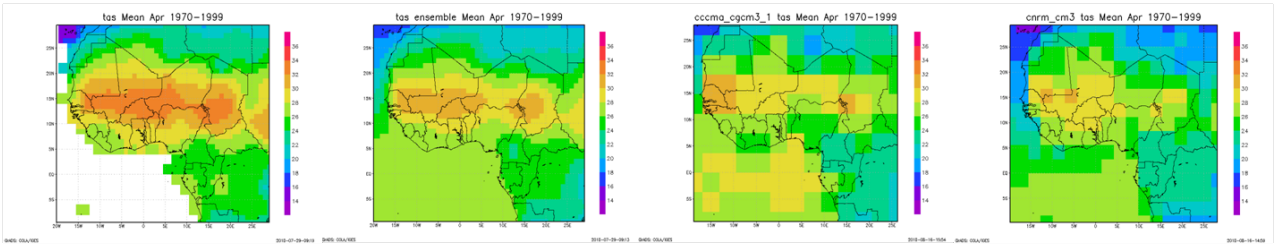
tas Mean Apr 1970-1999
tas ensemble Mean Apr 1970-1999
cccma_cgcm3_1 tas Mean Apr 1970-1999
cnrm_cm3 tas Mean Apr 1970-1999

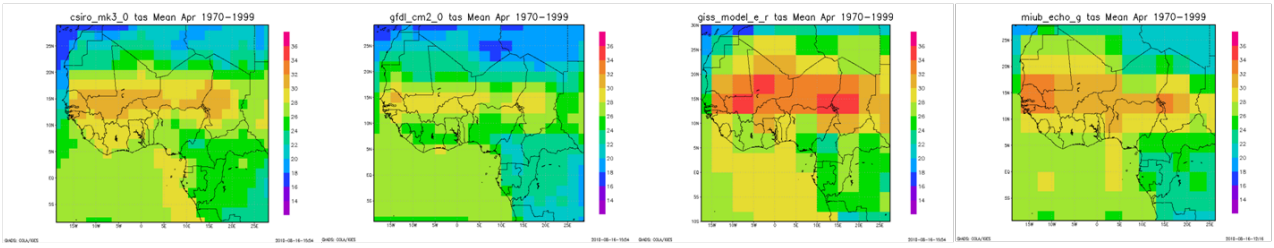
csiro_mk3_0 tas Mean Apr 1970-1999
gfdl_cm2_0 tas Mean Apr 1970-1999
giss_model_e_r tas Mean Apr 1970-1999
miub_echo_g tas Mean Apr 1970-1999

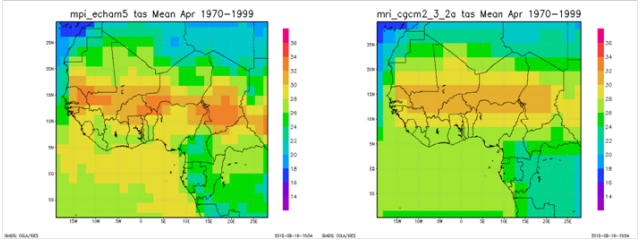
mpi_echam5 tas Mean Apr 1970-1999
mri_cgcm2_3_2a tas Mean Apr 1970-1999

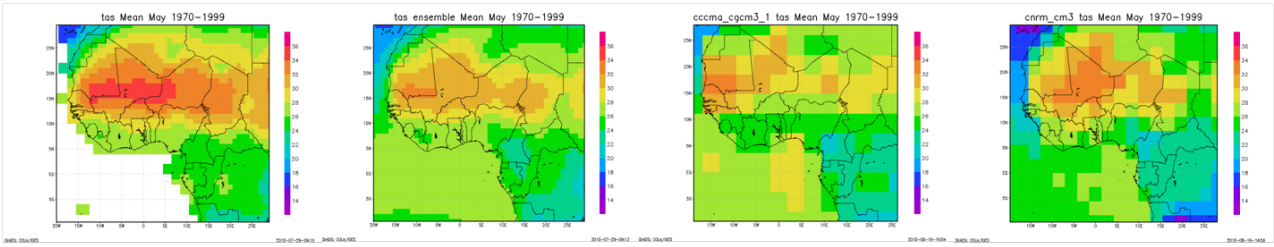
tas Mean May 1970-1999
tas ensemble Mean May 1970-1999
cccma_cgcm3_1 tas Mean May 1970-1999
cnrm_cm3 tas Mean May 1970-1999

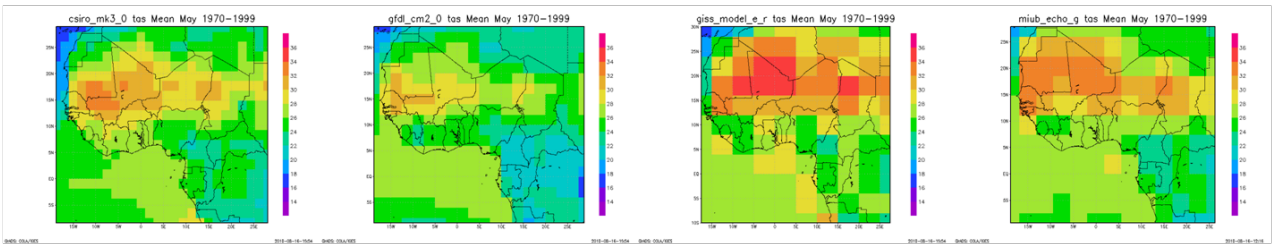
csiro_mk3_0 tas Mean May 1970-1999
gfdl_cm2_0 tas Mean May 1970-1999
giss_model_e_r tas Mean May 1970-1999
miub_echo_g tas Mean May 1970-1999

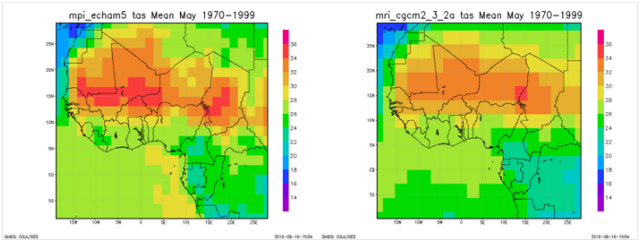
mpi_echam5 tas Mean May 1970-1999
mri_cgcm2_3_2a tas Mean May 1970-1999

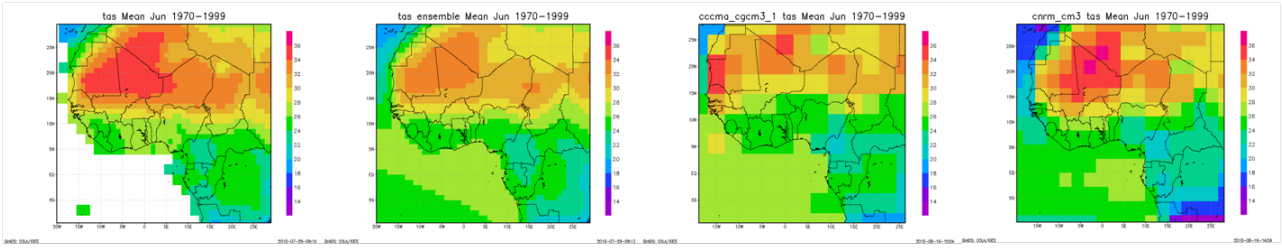
tas Mean Jun 1970-1999
tas ensemble Mean Jun 1970-1999
cccma_cgcm3_1 tas Mean Jun 1970-1999
cnrm_cm3 tas Mean Jun 1970-1999

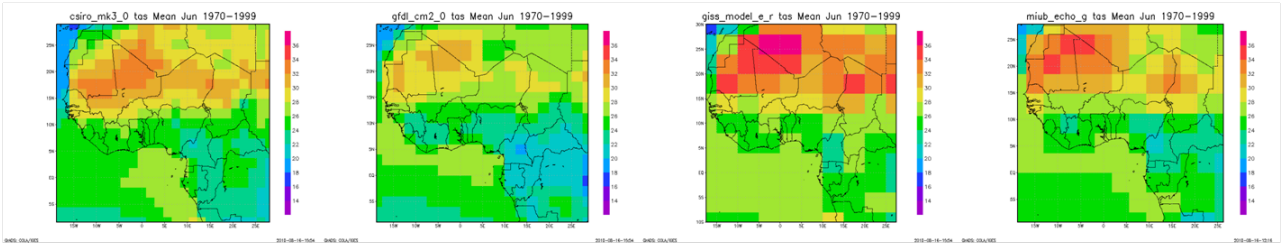
csiro_mk3_0 tas Mean Jun 1970-1999
gfdl_cm2_0 tas Mean Jun 1970-1999
giss_model_e_r tas Mean Jun 1970-1999
miub_echo_g tas Mean Jun 1970-1999

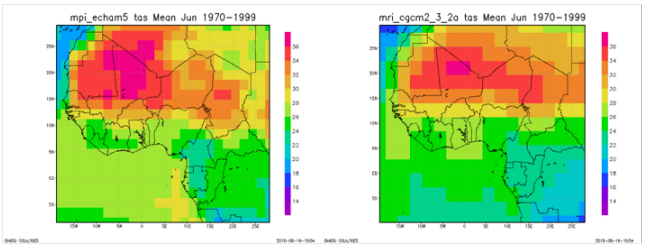
mpi_echam5 tas Mean Jun 1970-1999
mri_cgcm2_3_2a tas Mean Jun 1970-1999

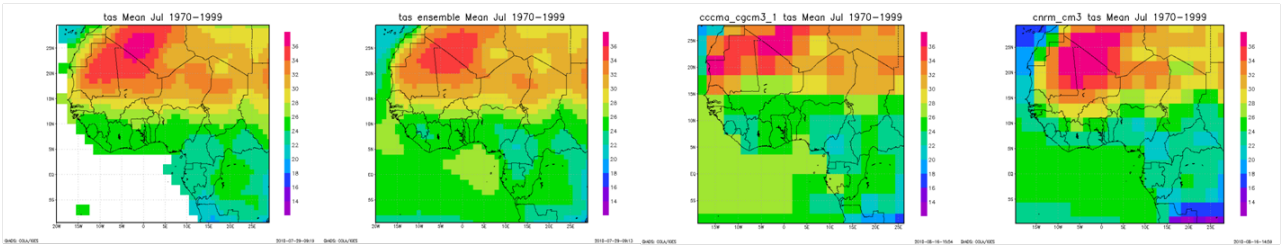
tas Mean Jul 1970-1999
tas ensemble Mean Jul 1970-1999
cccma_cgcm3_1 tas Mean Jul 1970-1999
cnrm_cm3 tas Mean Jul 1970-1999

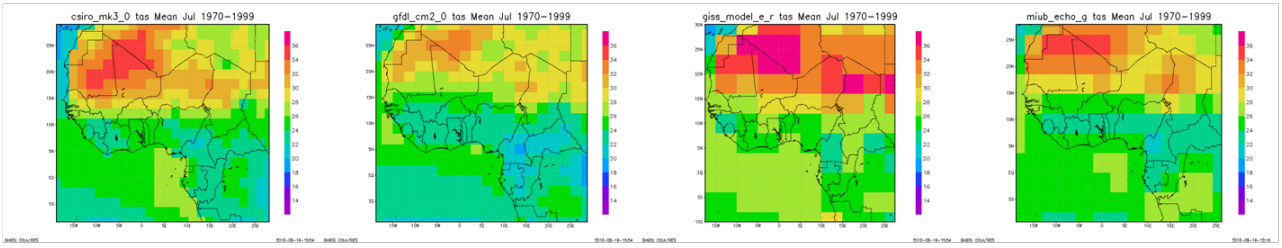
csiro_mk3_0 tas Mean Jul 1970-1999
gfdl_cm2_0 tas Mean Jul 1970-1999
giss_model_e_r tas Mean Jul 1970-1999
miub_echo_g tas Mean Jul 1970-1999

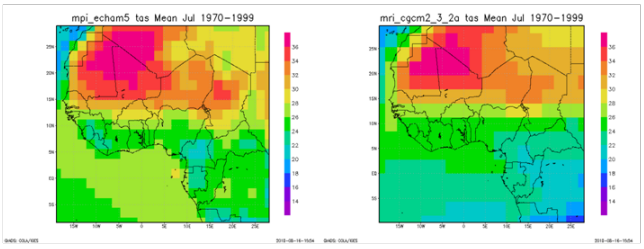
mpi_echam5 tas Mean Jul 1970-1999
mri_cgcm2_3_2a tas Mean Jul 1970-1999

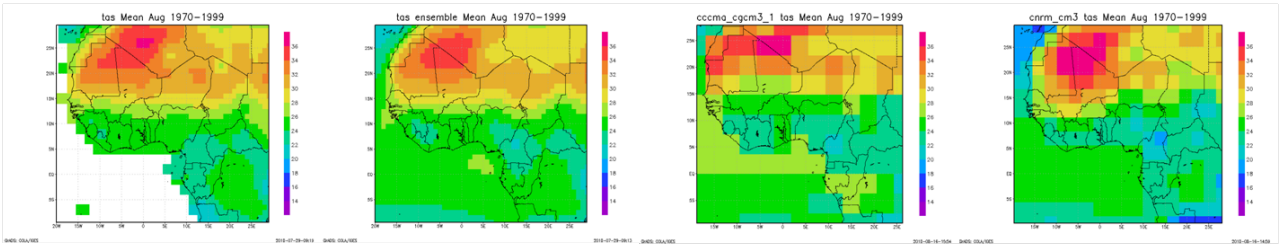
tas Mean Aug 1970-1999
tas ensemble Mean Aug 1970-1999
cccma_cgcm3_1 tas Mean Aug 1970-1999
cnrm_cm3 tas Mean Aug 1970-1999

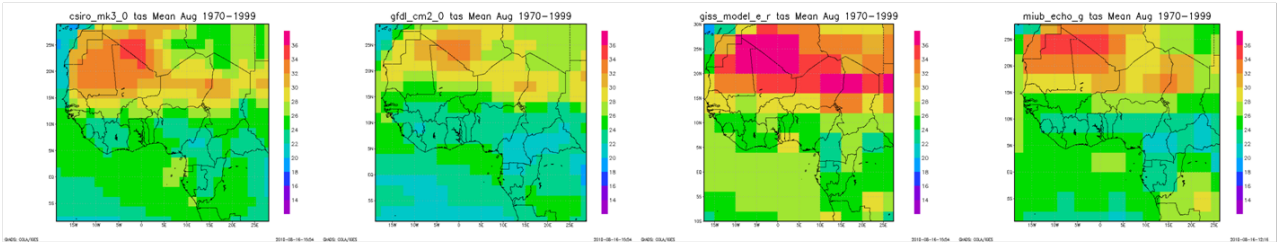
csiro_mk3_0 tas Mean Aug 1970-1999
gfdl_cm2_0 tas Mean Aug 1970-1999
giss_model_e_r tas Mean Aug 1970-1999
miub_echo_g tas Mean Aug 1970-1999

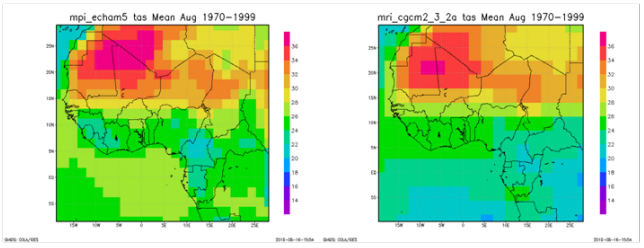
mpi_echam5 tas Mean Aug 1970-1999
mri_cgcm2_3_2a tas Mean Aug 1970-1999

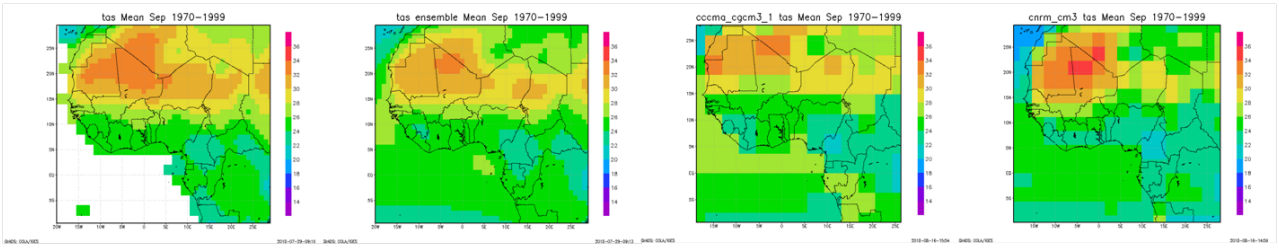
tas Mean Sep 1970–1999
tas ensemble Mean Sep 1970–1999
cccma_cgcm3_1 tas Mean Sep 1970–1999
cnrm_cm3 tas Mean Sep 1970–1999

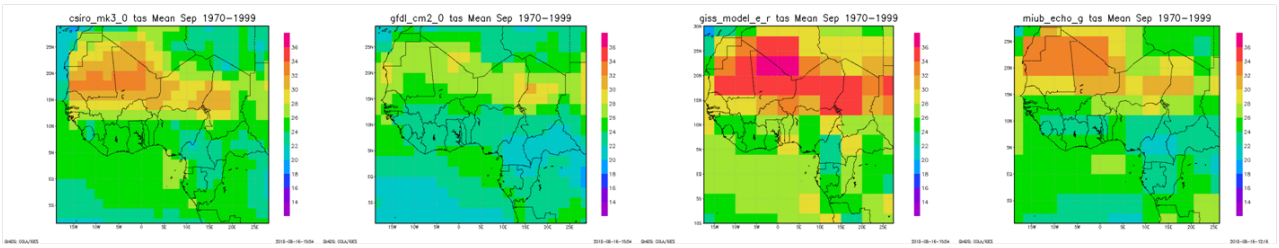
csiro_mk3_0 tas Mean Sep 1970–1999
gfdl_cm2_0 tas Mean Sep 1970–1999
giss_model_e_r tas Mean Sep 1970–1999
miub_echo_g tas Mean Sep 1970–1999

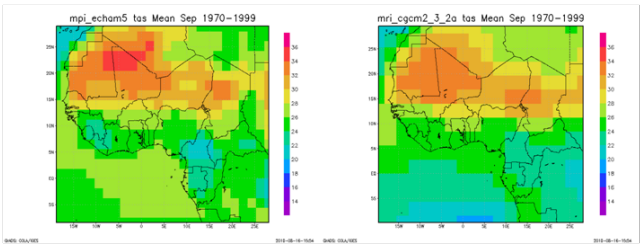
mpi_echam5 tas Mean Sep 1970–1999
mri_cgcm2_3_2a tas Mean Sep 1970–1999

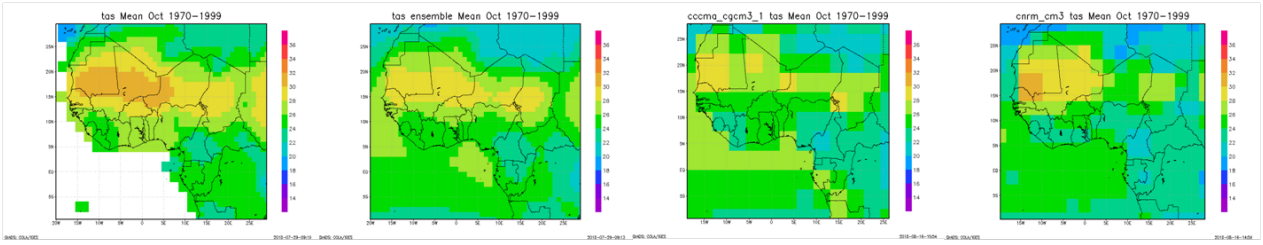
tas Mean Oct 1970–1999
tas ensemble Mean Oct 1970–1999
cccma_cgcm3_1 tas Mean Oct 1970–1999
cnrm_cm3 tas Mean Oct 1970–1999

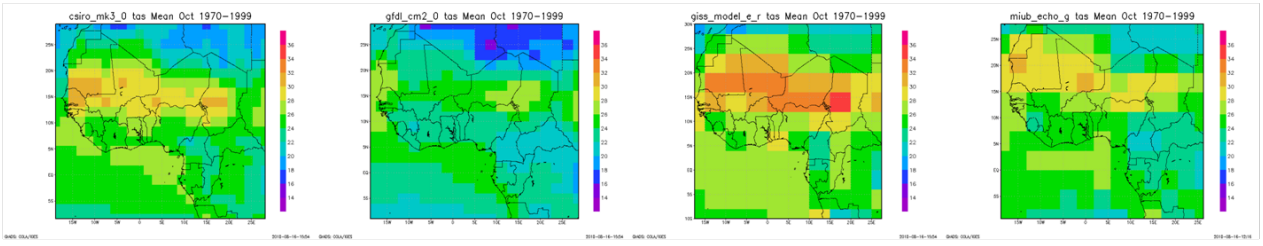
csiro_mk3_0 tas Mean Oct 1970–1999
gfdl_cm2_0 tas Mean Oct 1970–1999
giss_model_e_r tas Mean Oct 1970–1999
miub_echo_g tas Mean Oct 1970–1999

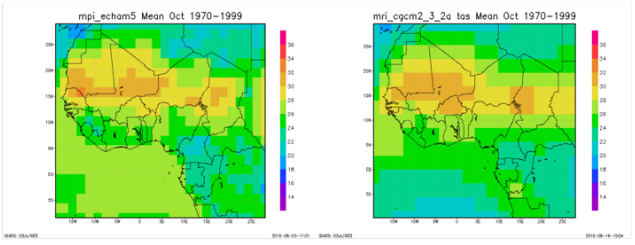
mpi_echam5 Mean Oct 1970–1999
mri_cgcm2_3_2a tas Mean Oct 1970–1999

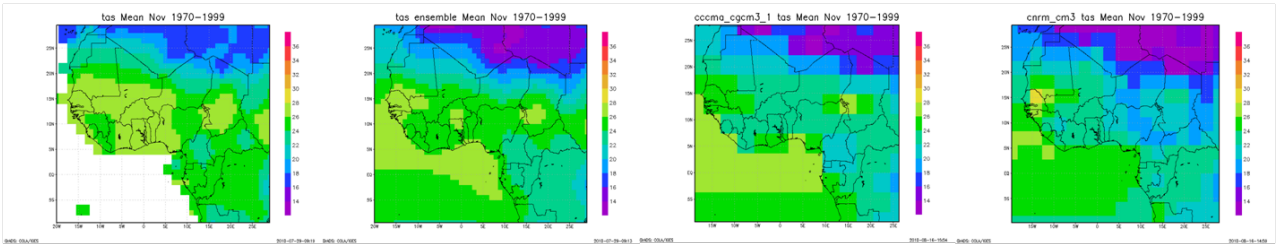
tas Mean Nov 1970-1999
tas ensemble Mean Nov 1970-1999
cccma_cgcm3_1 tas Mean Nov 1970-1999
cnrm_cm3 tas Mean Nov 1970-1999

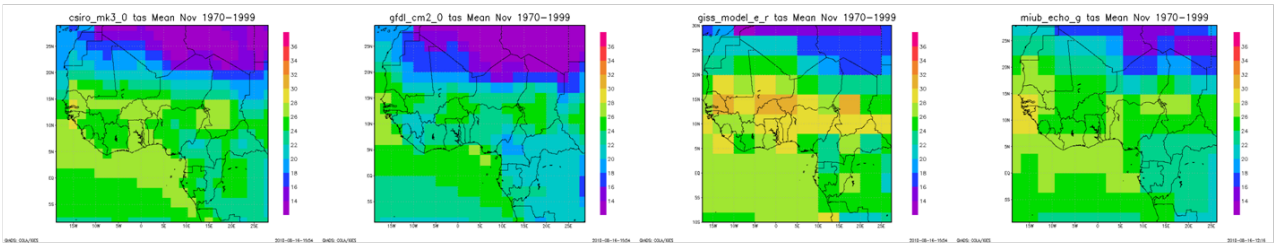
csiro_mk3_0 tas Mean Nov 1970-1999
gfdl_cm2_0 tas Mean Nov 1970-1999
giss_model_e_r tas Mean Nov 1970-1999
miub_echo_g tas Mean Nov 1970-1999

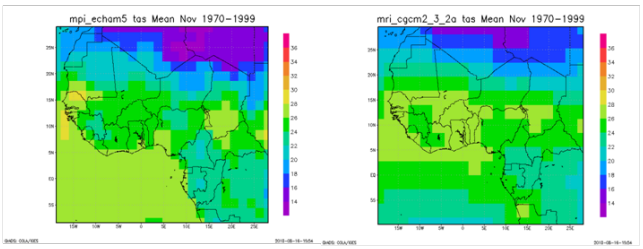
mpi_echam5 tas Mean Nov 1970-1999
mri_cgcm2_3_2a tas Mean Nov 1970-1999

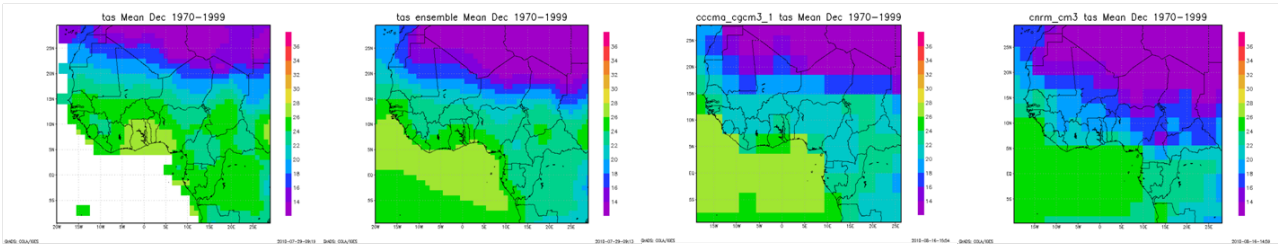
tas Mean Dec 1970-1999
tas ensemble Mean Dec 1970-1999
cccma_cgcm3_1 tas Mean Dec 1970-1999
cnrm_cm3 tas Mean Dec 1970-1999

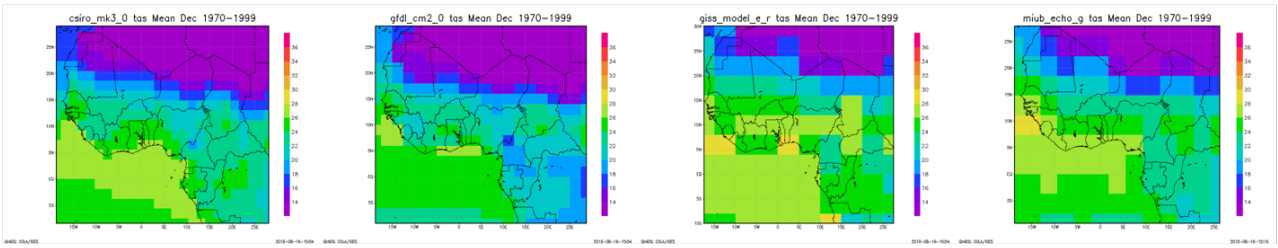
csiro_mk3_0 tas Mean Dec 1970-1999
gfdl_cm2_0 tas Mean Dec 1970-1999
giss_model_e_r tas Mean Dec 1970-1999
miub_echo_g tas Mean Dec 1970-1999

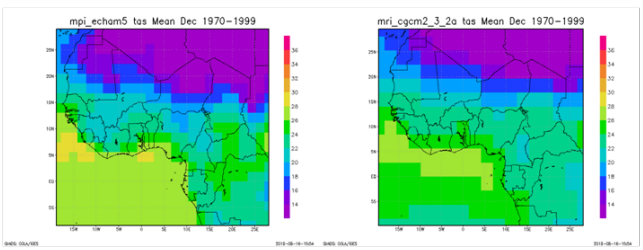
mpi_echam5 tas Mean Dec 1970-1999
mri_cgcm2_3_2a tas Mean Dec 1970-1999

Precipitation

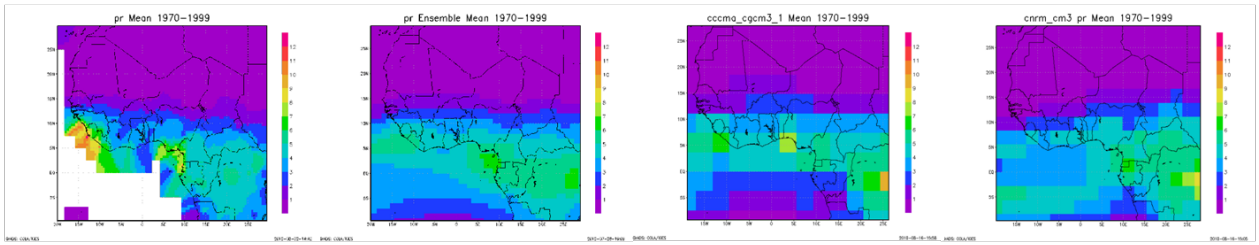

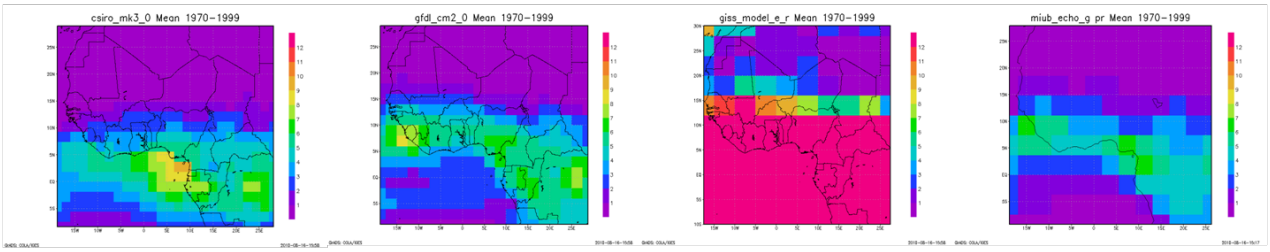

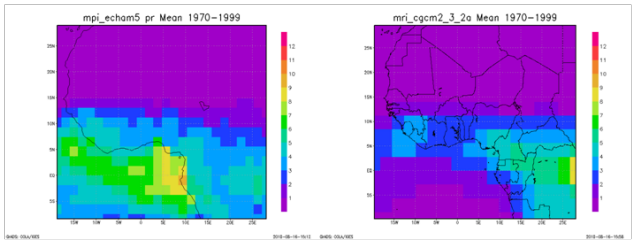

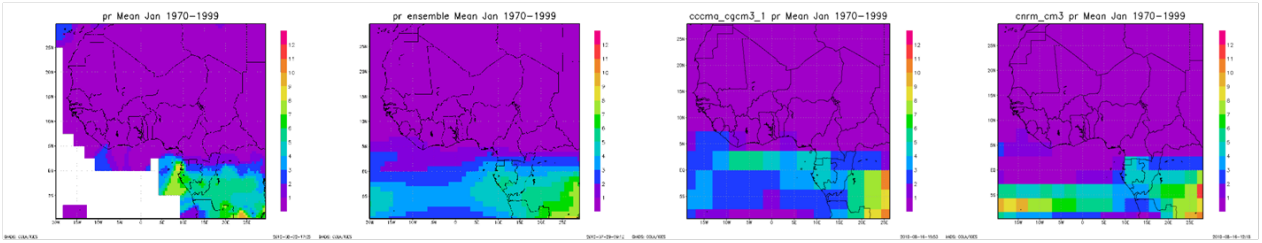

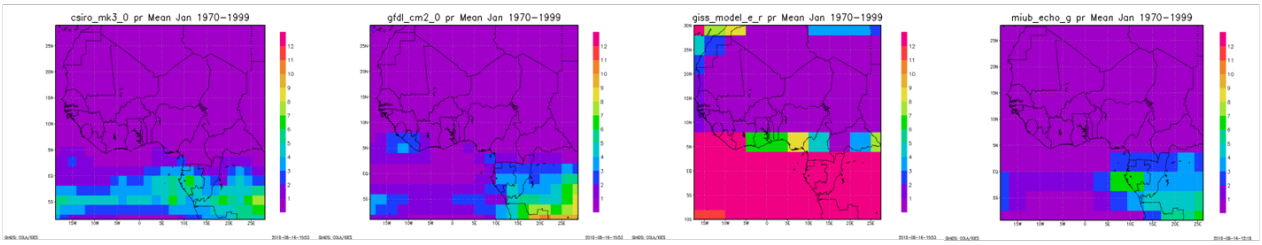

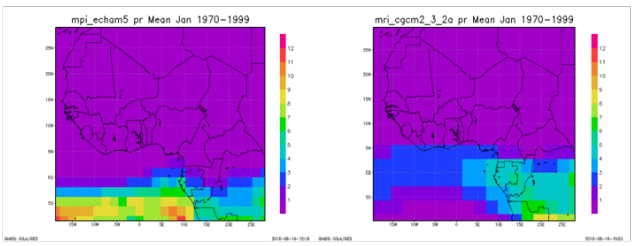

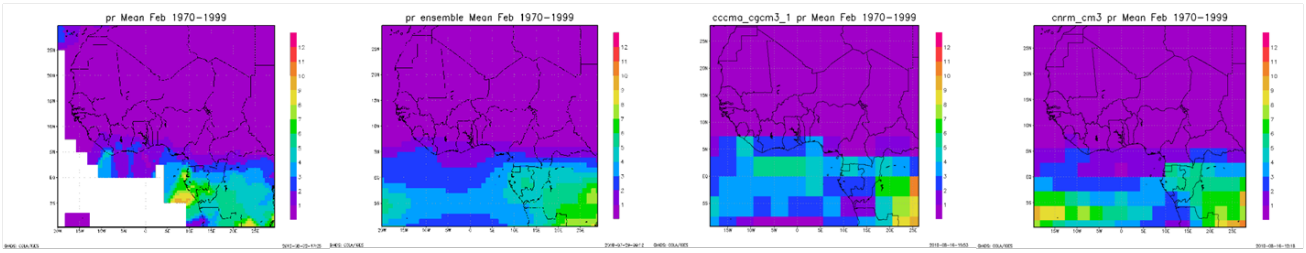
pr Mean Feb 1970-1999
pr ensemble Mean Feb 1970-1999
cccma_cgcm3_1 pr Mean Feb 1970-1999
cnrm_cm3 pr Mean Feb 1970-1999

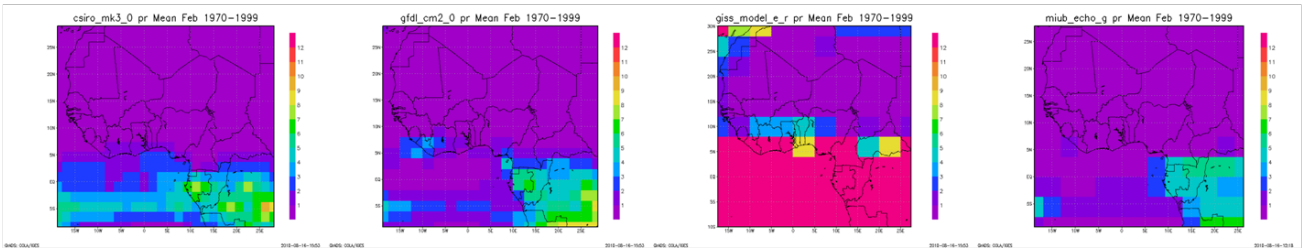
csiro_mk3_0 pr Mean Feb 1970-1999
gfdl_cm2_0 pr Mean Feb 1970-1999
giss_model_e_r pr Mean Feb 1970-1999
miub_echo_g pr Mean Feb 1970-1999

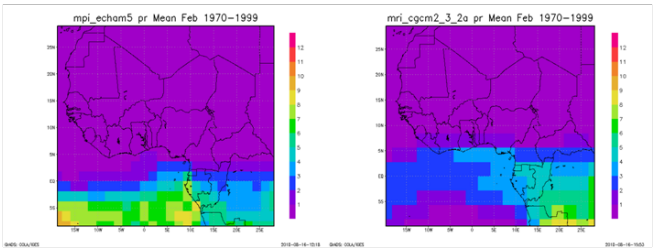
mpi_echam5 pr Mean Feb 1970-1999
mri_cgcm2_3_2a pr Mean Feb 1970-1999

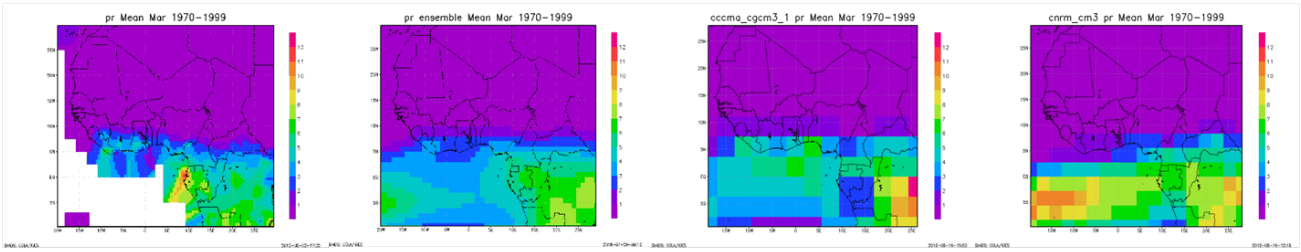
pr Mean Mar 1970-1999
pr ensemble Mean Mar 1970-1999
cccma_cgcm3_1 pr Mean Mar 1970-1999
cnrm_cm3 pr Mean Mar 1970-1999

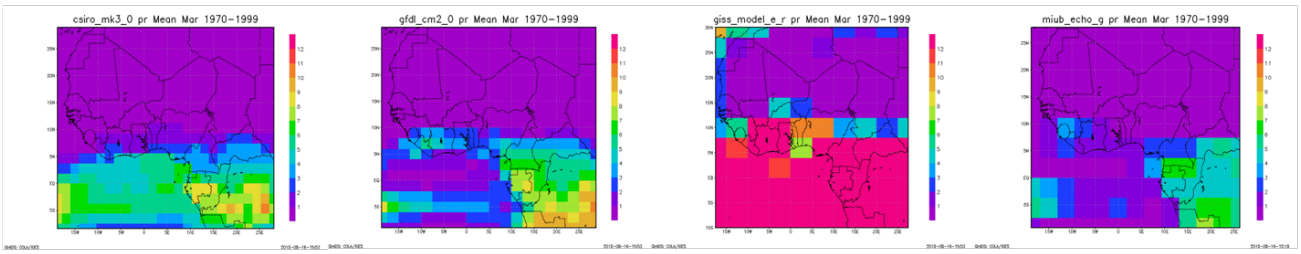
csiro_mk3_0 pr Mean Mar 1970-1999
gfdl_cm2_0 pr Mean Mar 1970-1999
giss_model_e_r pr Mean Mar 1970-1999
miub_echo_g pr Mean Mar 1970-1999

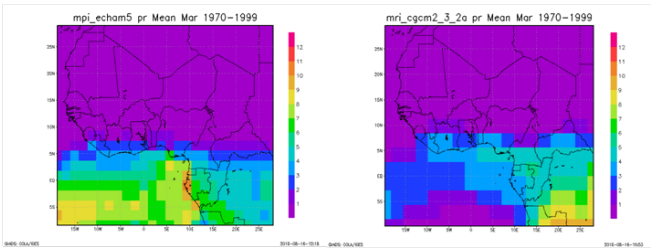
mpi_echam5 pr Mean Mar 1970-1999
mri_cgcm2_3_2a pr Mean Mar 1970-1999

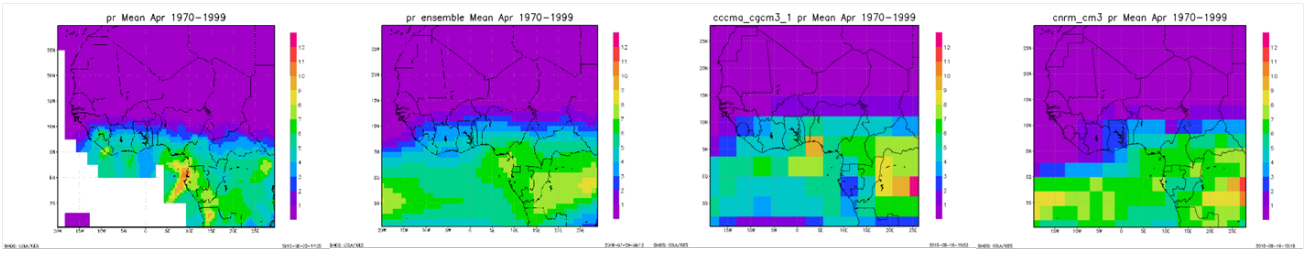
pr Mean Apr 1970-1999
pr ensemble Mean Apr 1970-1999
cccma_cgcm3_1 pr Mean Apr 1970-1999
cnrm_cm3 pr Mean Apr 1970-1999

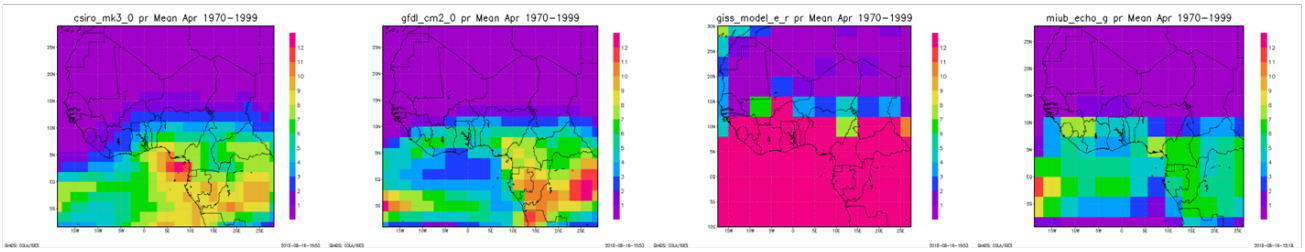
csiro_mk3_0 pr Mean Apr 1970-1999
gfdl_cm2_0 pr Mean Apr 1970-1999
giss_model_e_r pr Mean Apr 1970-1999
miub_echo_g pr Mean Apr 1970-1999

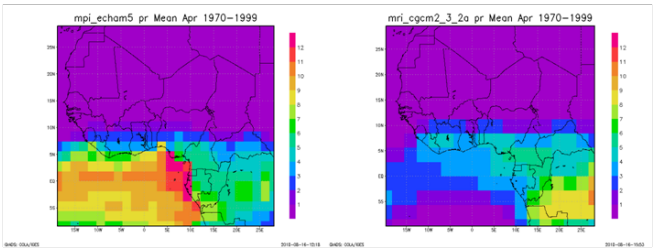
mpi_echam5 pr Mean Apr 1970-1999
mri_cgcm2_3_2a pr Mean Apr 1970-1999

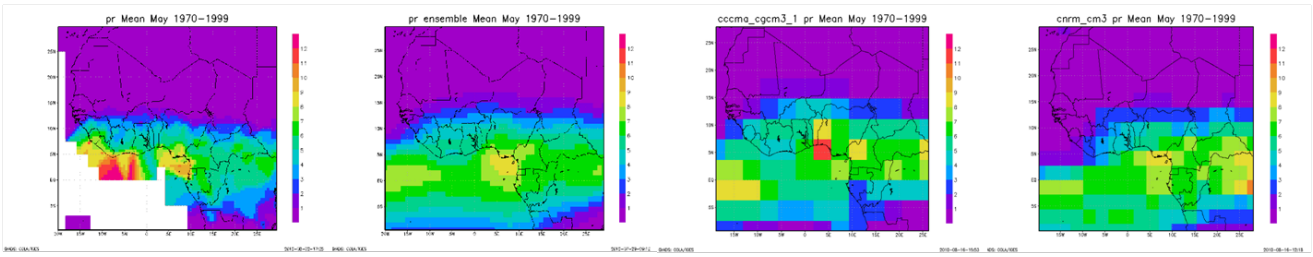
pr Mean May 1970-1999
pr ensemble Mean May 1970-1999
cccma_cgcm3_1 pr Mean May 1970-1999
cnrm_cm3 pr Mean May 1970-1999

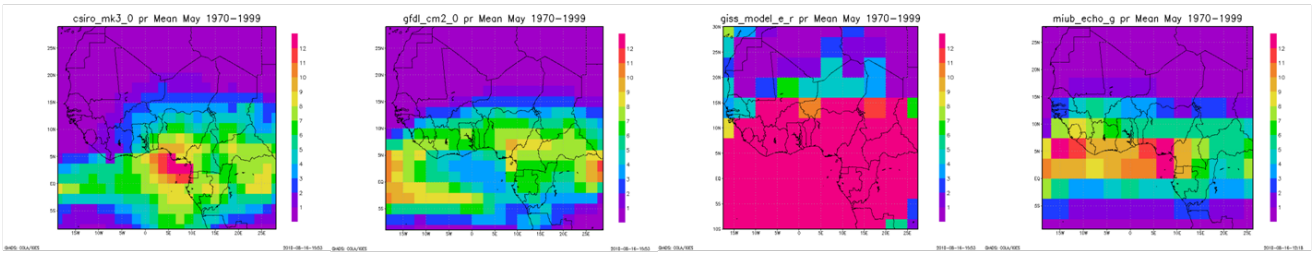
csiro_mk3_0 pr Mean May 1970-1999
gfdl_cm2_0 pr Mean May 1970-1999
giss_model_e_r pr Mean May 1970-1999
miub_echo_g pr Mean May 1970-1999

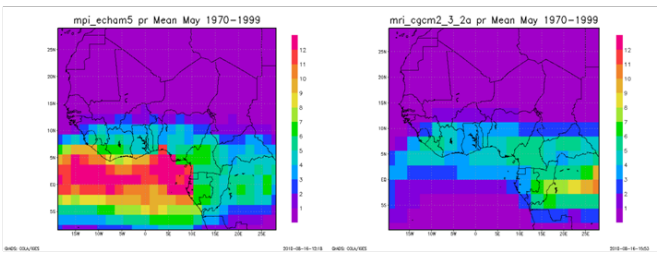
mpi_echam5 pr Mean May 1970-1999
mri_cgcm2_3_2a pr Mean May 1970-1999

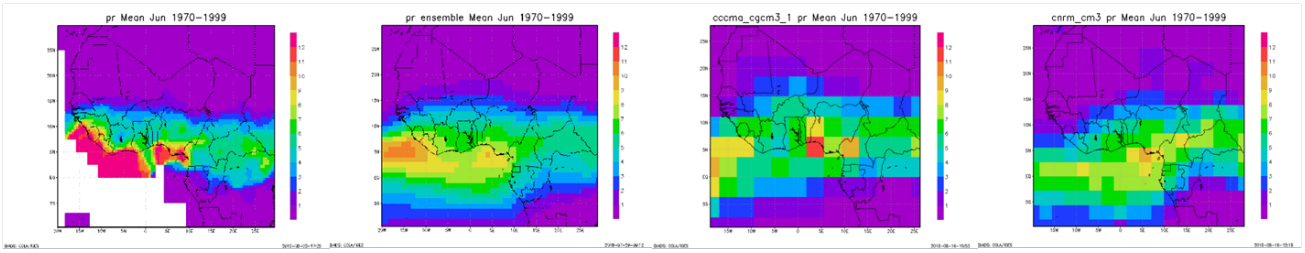
pr Mean Jun 1970-1999
pr ensemble Mean Jun 1970-1999
cccma_cgcm3_1 pr Mean Jun 1970-1999
cnrm_cm3 pr Mean Jun 1970-1999

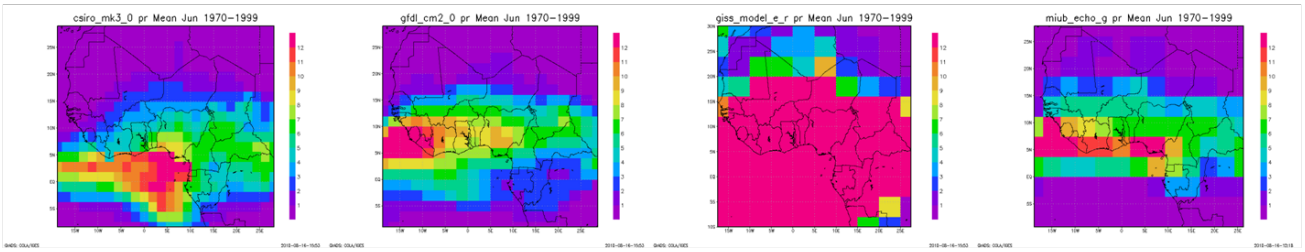
csiro_mk3_0 pr Mean Jun 1970-1999
gfdl_cm2_0 pr Mean Jun 1970-1999
giss_model_e_r pr Mean Jun 1970-1999
miub_echo_g pr Mean Jun 1970-1999

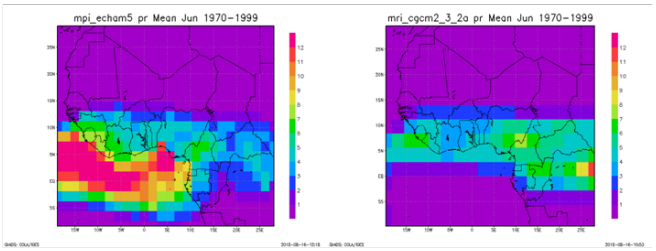
mpi_echam5 pr Mean Jun 1970-1999
mri_cgcm2_3_2a pr Mean Jun 1970-1999

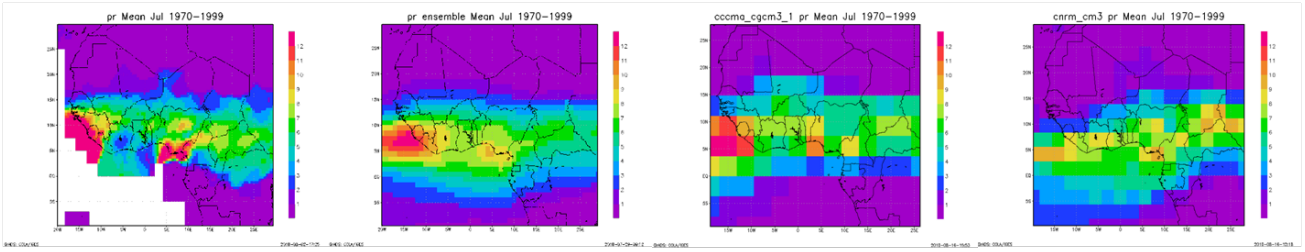
pr Mean Jul 1970-1999
pr ensemble Mean Jul 1970-1999
cccma_cgcm3_1 pr Mean Jul 1970-1999
cnrm_cm3 pr Mean Jul 1970-1999

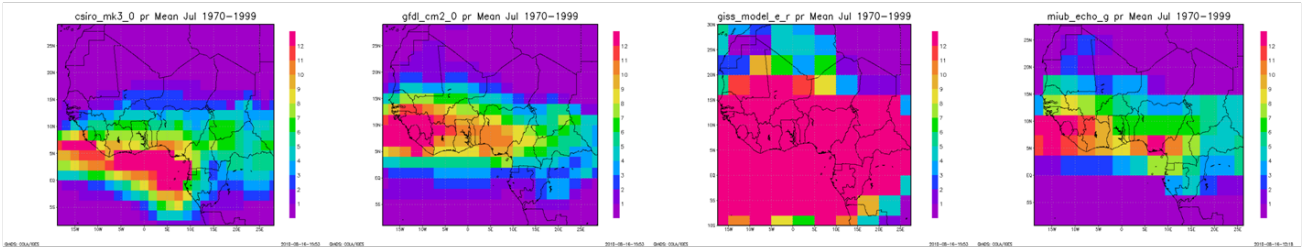
csiro_mk3_0 pr Mean Jul 1970-1999
gfdl_cm2_0 pr Mean Jul 1970-1999
giss_model_e_r pr Mean Jul 1970-1999
miub_echo_g pr Mean Jul 1970-1999

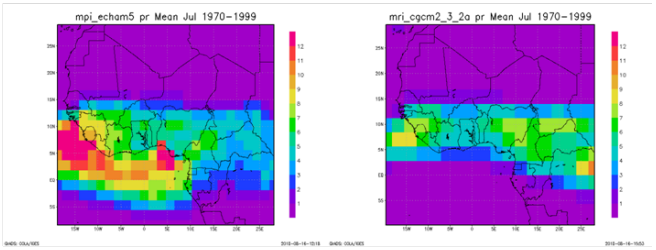
mpi_echam5 pr Mean Jul 1970-1999
mri_cgcm2_3_2a pr Mean Jul 1970-1999

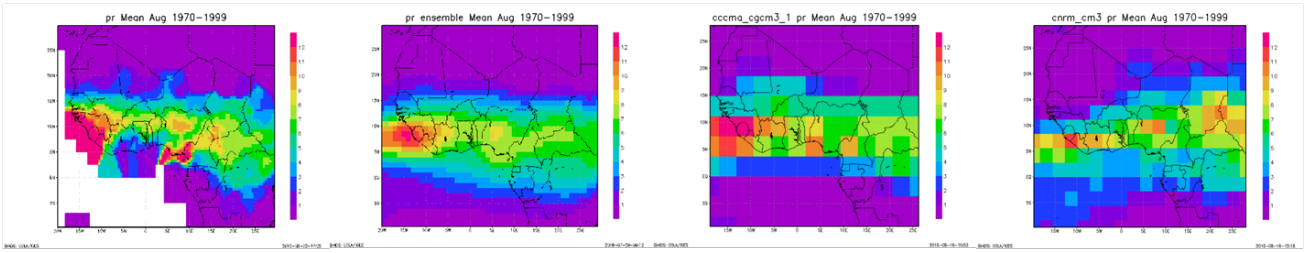
pr Mean Aug 1970-1999
pr ensemble Mean Aug 1970-1999
cccma_cgcm3_1 pr Mean Aug 1970-1999
cnrm_cm3 pr Mean Aug 1970-1999

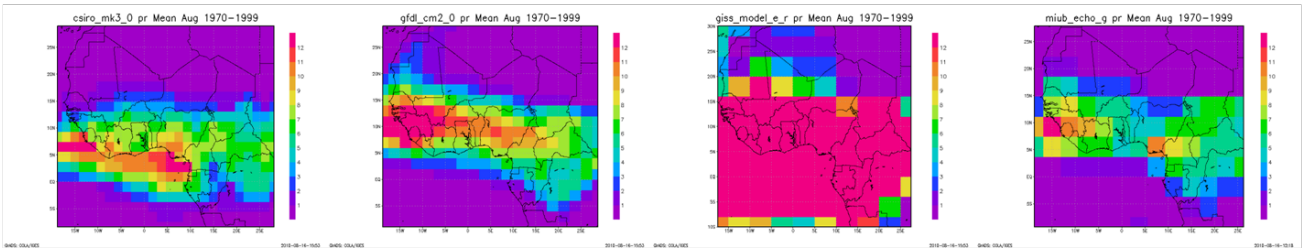
csiro_mk3_0 pr Mean Aug 1970-1999
gfdl_cm2_0 pr Mean Aug 1970-1999
giss_model_e_r pr Mean Aug 1970-1999
miub_echo_g pr Mean Aug 1970-1999

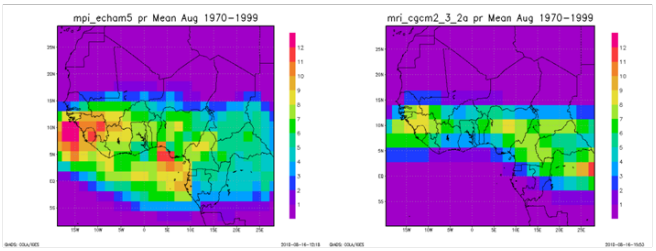
mpi_echam5 pr Mean Aug 1970-1999
mri_cgcm2_3_2a pr Mean Aug 1970-1999

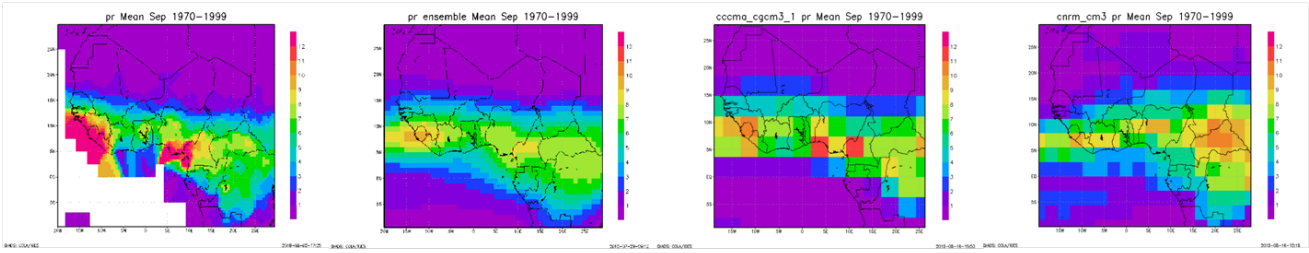
pr Mean Sep 1970-1999
pr ensemble Mean Sep 1970-1999
cccma_cgcm3_1 pr Mean Sep 1970-1999
cnrm_cm3 pr Mean Sep 1970-1999

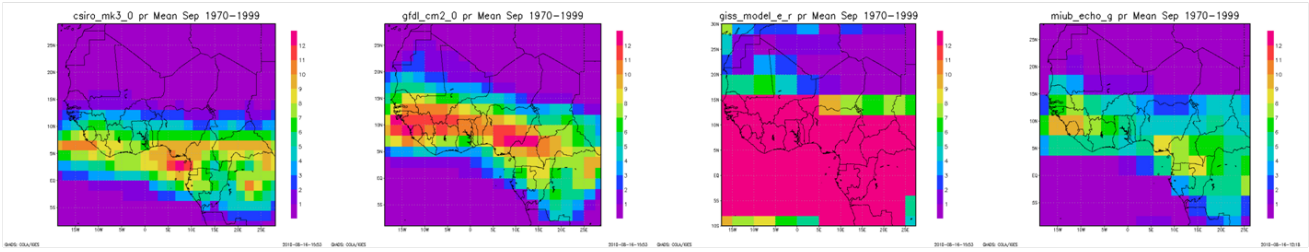
csiro_mk3_0 pr Mean Sep 1970-1999
gfdl_cm2_0 pr Mean Sep 1970-1999
giss_model_e_r pr Mean Sep 1970-1999
miub_echo_g pr Mean Sep 1970-1999

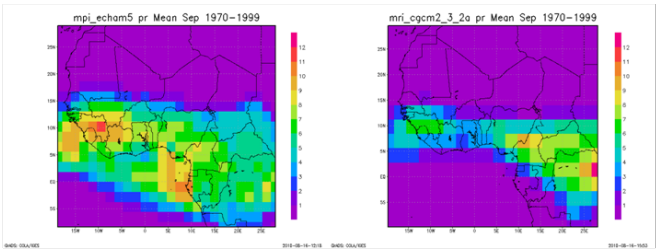
mpi_echam5 pr Mean Sep 1970-1999
mri_cgcm2_3_2a pr Mean Sep 1970-1999

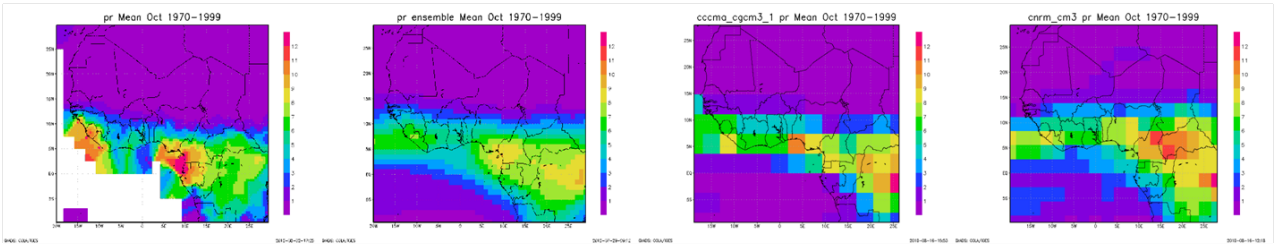
pr Mean Oct 1970-1999
pr ensemble Mean Oct 1970-1999
cccma_cgcm3_1 pr Mean Oct 1970-1999
cnrm_cm3 pr Mean Oct 1970-1999

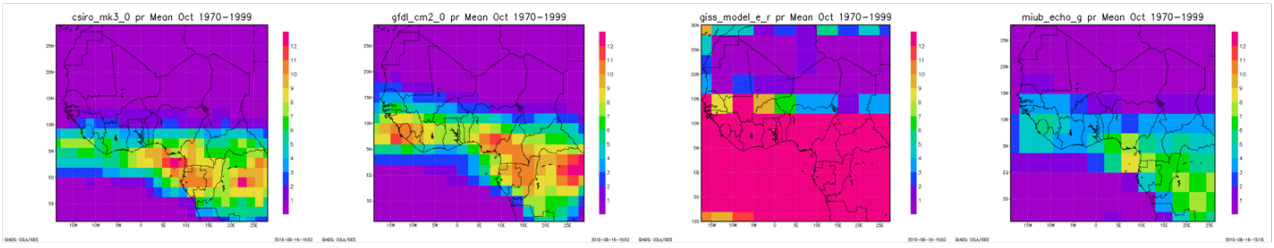
csiro_mk3_0 pr Mean Oct 1970-1999
gfdl_cm2_0 pr Mean Oct 1970-1999
giss_model_e_r pr Mean Oct 1970-1999
miub_echo_g pr Mean Oct 1970-1999

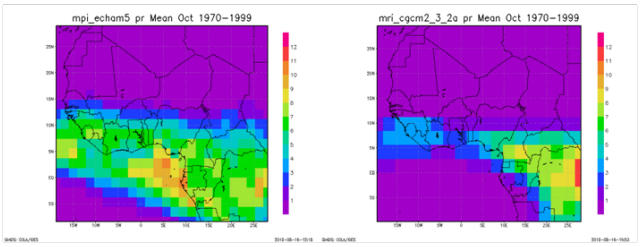
mpi_echam5 pr Mean Oct 1970-1999
mri_cgcm2_3_2a pr Mean Oct 1970-1999

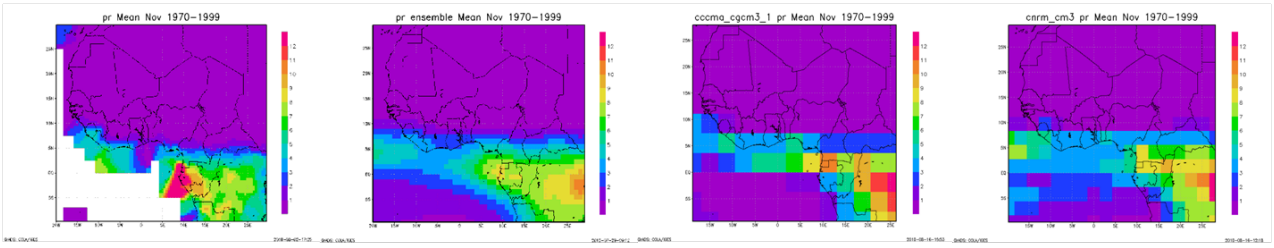
pr Mean Nov 1970-1999
pr ensemble Mean Nov 1970-1999
cccma_cgcm3_1 pr Mean Nov 1970-1999
cnrm_cm3 pr Mean Nov 1970-1999

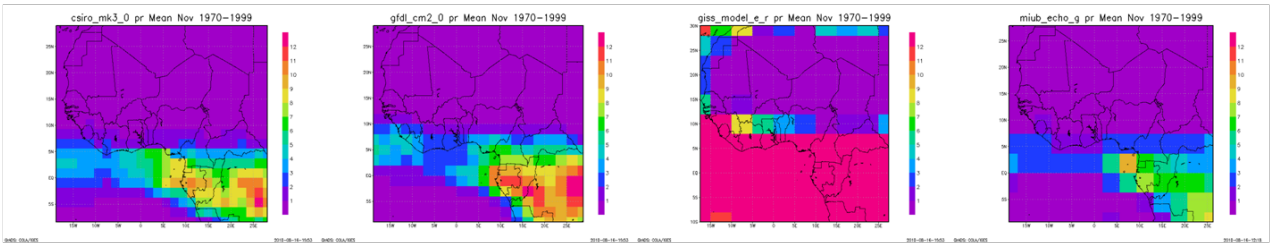
csiro_mk3_0 pr Mean Nov 1970-1999
gfdl_cm2_0 pr Mean Nov 1970-1999
giss_model_e_r pr Mean Nov 1970-1999
miub_echo_g pr Mean Nov 1970-1999

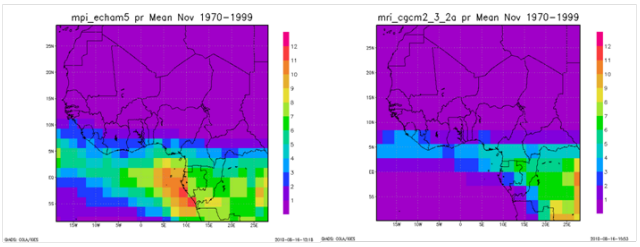
mpi_echam5 pr Mean Nov 1970-1999
mri_cgcm2_3_2a pr Mean Nov 1970-1999

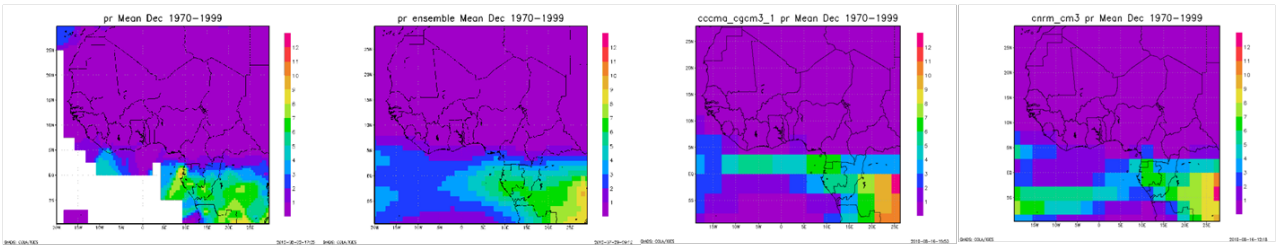
pr Mean Dec 1970-1999
pr ensemble Mean Dec 1970-1999
cccma_cgcm3_1 pr Mean Dec 1970-1999
cnrm_cm3 pr Mean Dec 1970-1999

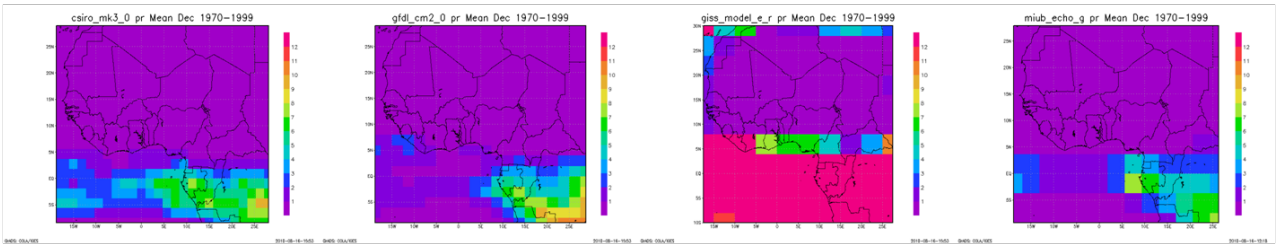
csiro_mk3_0 pr Mean Dec 1970-1999
gfdl_cm2_0 pr Mean Dec 1970-1999
giss_model_e_r pr Mean Dec 1970-1999
miub_echo_g pr Mean Dec 1970-1999

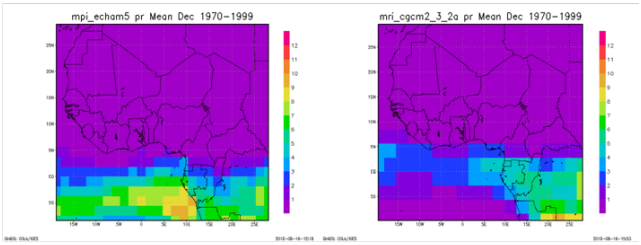
mpi_echam5 pr Mean Dec 1970-1999
mri_cgcm2_3_2a pr Mean Dec 1970-1999

Appendix 4: Model derived monthly and annual temperature trends

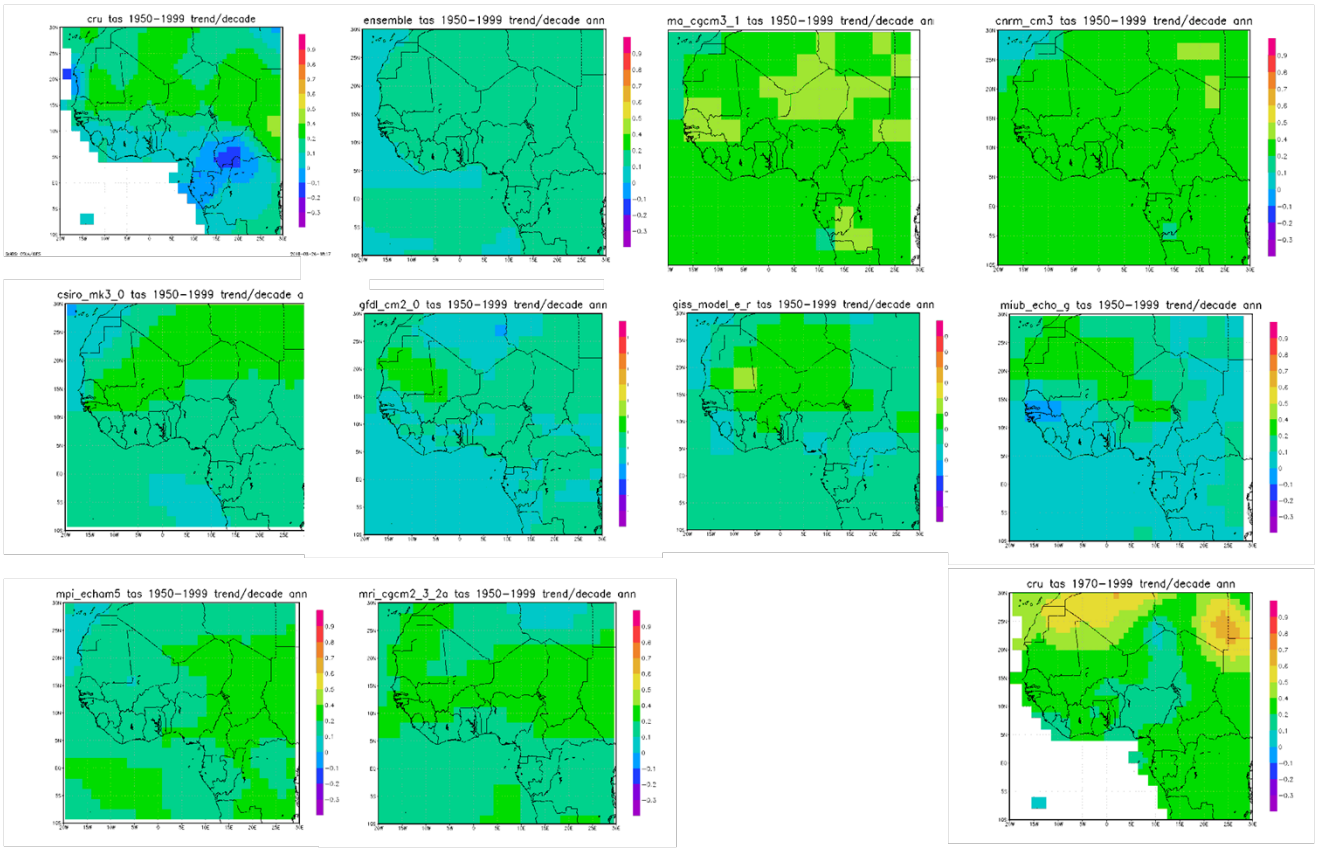

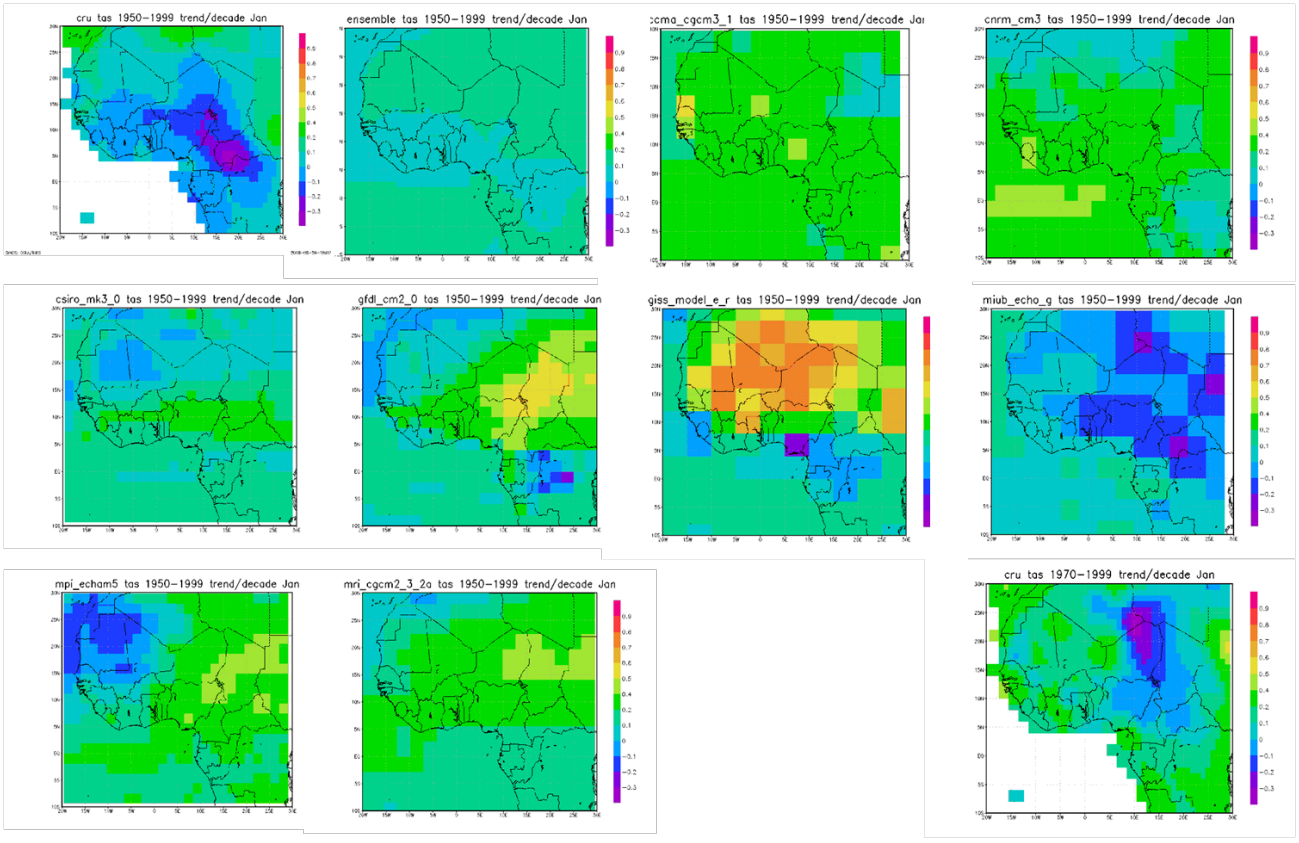
cru tas 1950-1999 trend/decade Jan
ensemble tas 1950-1999 trend/decade Jan
cccma_cgcm3_1 tas 1950-1999 trend/decade Jan
cnrm_cm3 tas 1950-1999 trend/decade Jan
csiro_mk3_0 tas 1950-1999 trend/decade Jan
gfdl_cm2_0 tas 1950-1999 trend/decade Jan
giss_model_e_r tas 1950-1999 trend/decade Jan
miub_echo_g tas 1950-1999 trend/decade Jan
mpi_echam5 tas 1950-1999 trend/decade Jan
mri_cgcm2_3_2a tas 1950-1999 trend/decade Jan
cru tas 1970-1999 trend/decade Jan

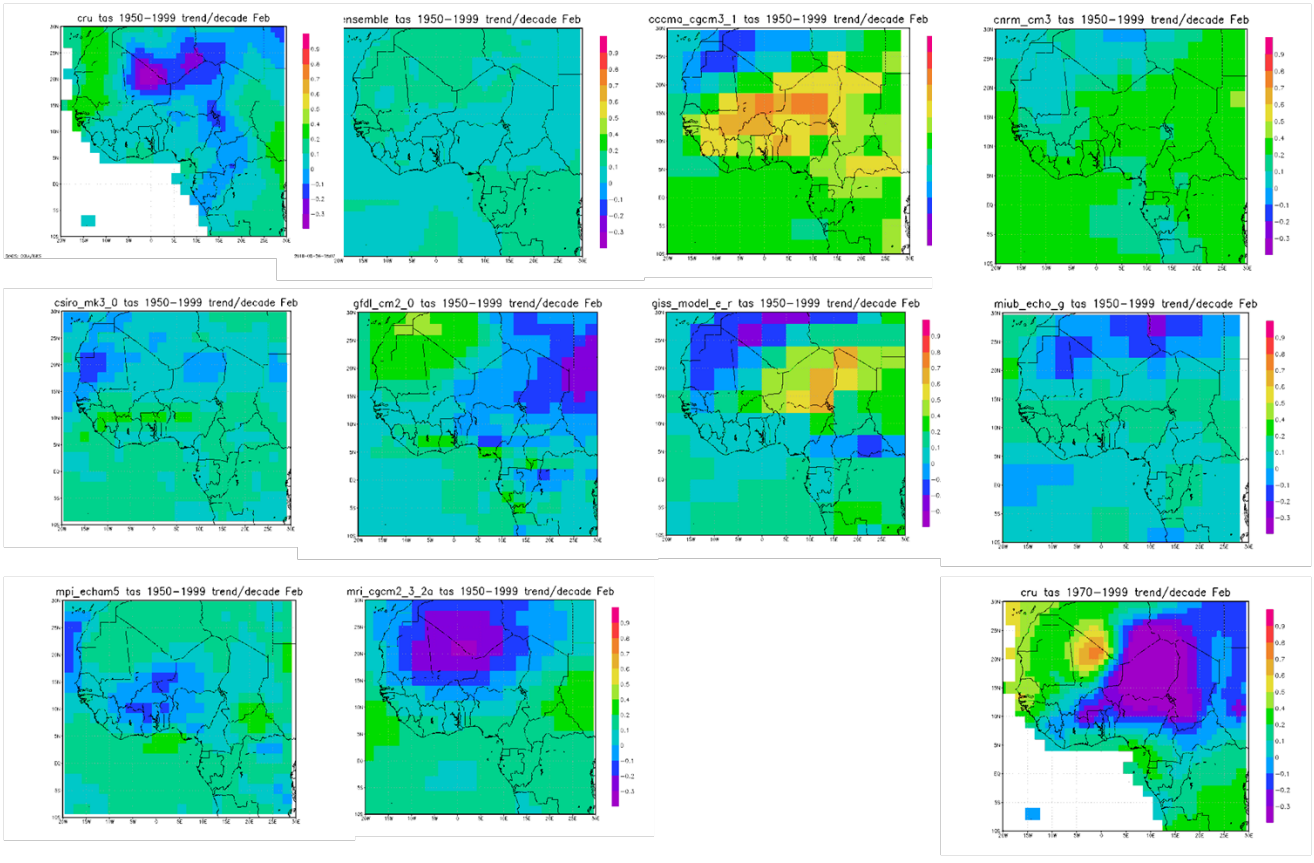
cru tas 1950-1999 trend/decade Feb
ensemble tas 1950-1999 trend/decade Feb
cccma_cgcm3_1 tas 1950-1999 trend/decade Feb
cnrm_cm3 tas 1950-1999 trend/decade Feb
csiro_mk3_0 tas 1950-1999 trend/decade Feb
gfdl_cm2_0 tas 1950-1999 trend/decade Feb
giss_model_e_r tas 1950-1999 trend/decade Feb
miub_echo_g tas 1950-1999 trend/decade Feb
mpi_echam5 tas 1950-1999 trend/decade Feb
mri_cgcm2_3_2a tas 1950-1999 trend/decade Feb
cru tas 1970-1999 trend/decade Feb

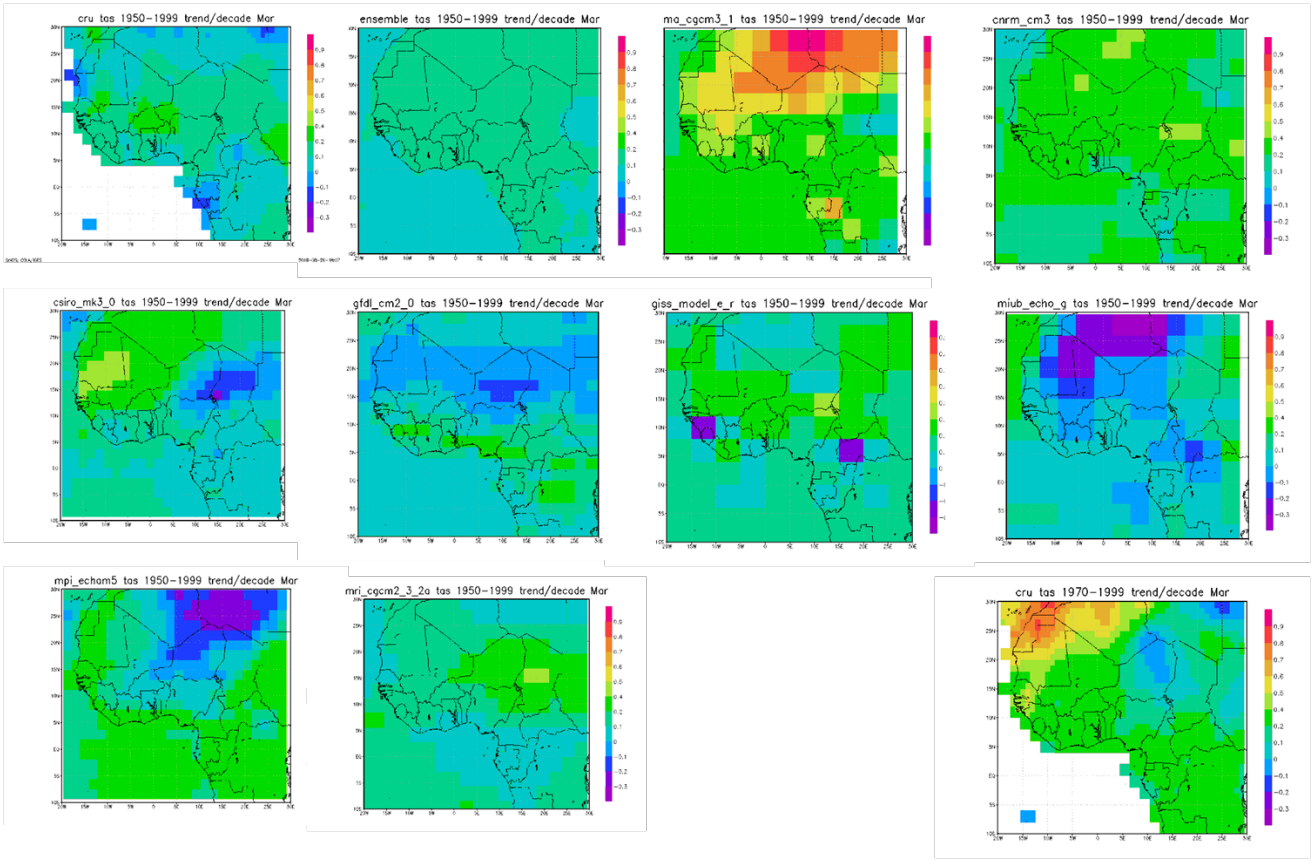
cru tas 1950-1999 trend/decade Mar
ensemble tas 1950-1999 trend/decade Mar
ma_cgcm3_1 tas 1950-1999 trend/decade Mar
cnrm_cm3 tas 1950-1999 trend/decade Mar
csiro_mk3_0 tas 1950-1999 trend/decade Mar
gfdl_cm2_0 tas 1950-1999 trend/decade Mar
giss_model_e_r tas 1950-1999 trend/decade Mar
miub_echo_g tas 1950-1999 trend/decade Mar
mpi_echam5 tas 1950-1999 trend/decade Mar
mri_cgcm2_3_2a tas 1950-1999 trend/decade Mar
cru tas 1970-1999 trend/decade Mar

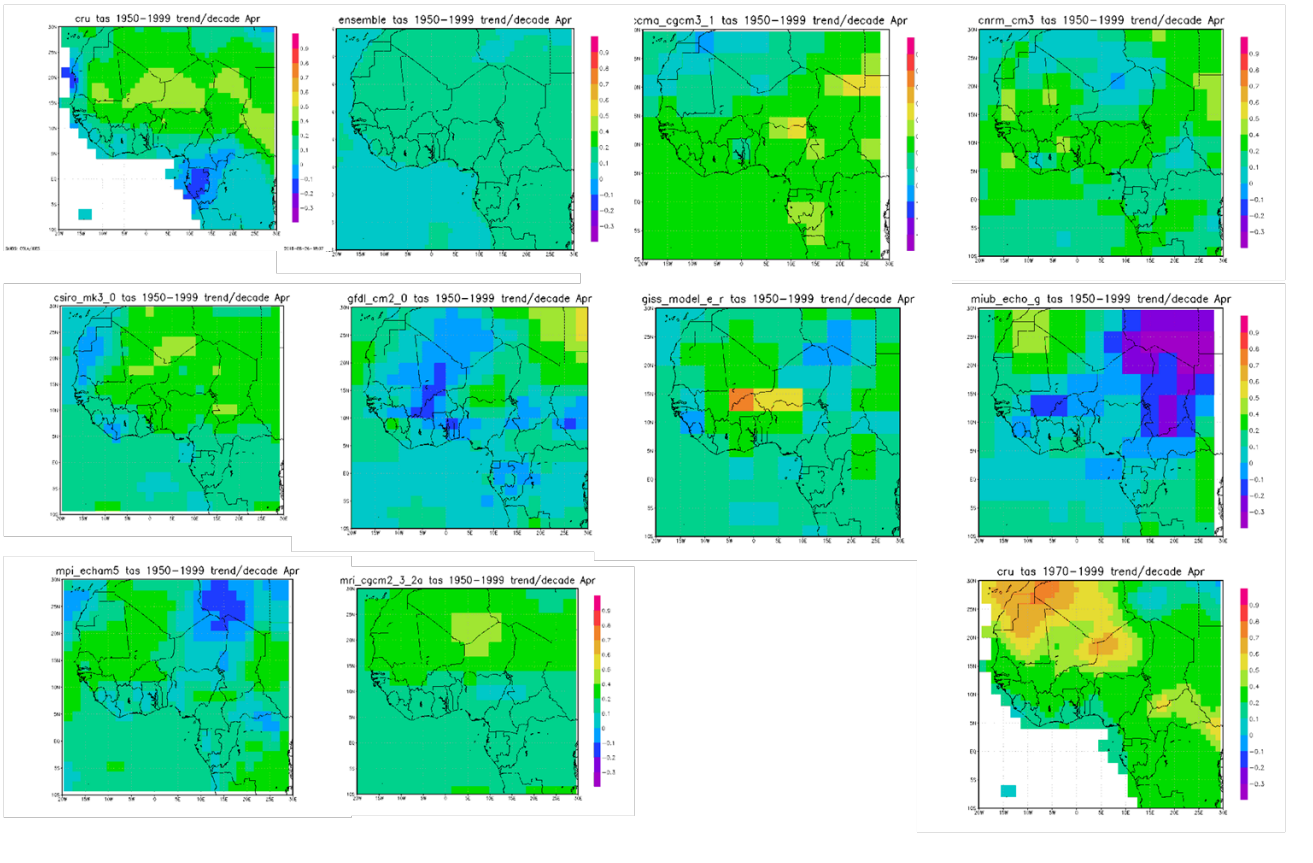
cru tas 1950-1999 trend/decade Apr
ensemble tas 1950-1999 trend/decade Apr
cnrm_cm3 tas 1950-1999 trend/decade Apr
csiro_mk3_0 tas 1950-1999 trend/decade Apr
gfdl_cm2_0 tas 1950-1999 trend/decade Apr
giss_model_e_r tas 1950-1999 trend/decade Apr
miub_echo_g tas 1950-1999 trend/decade Apr
mpi_echam5 tas 1950-1999 trend/decade Apr
mri_cgcm2_3_2a tas 1950-1999 trend/decade Apr
cru tas 1970-1999 trend/decade Apr

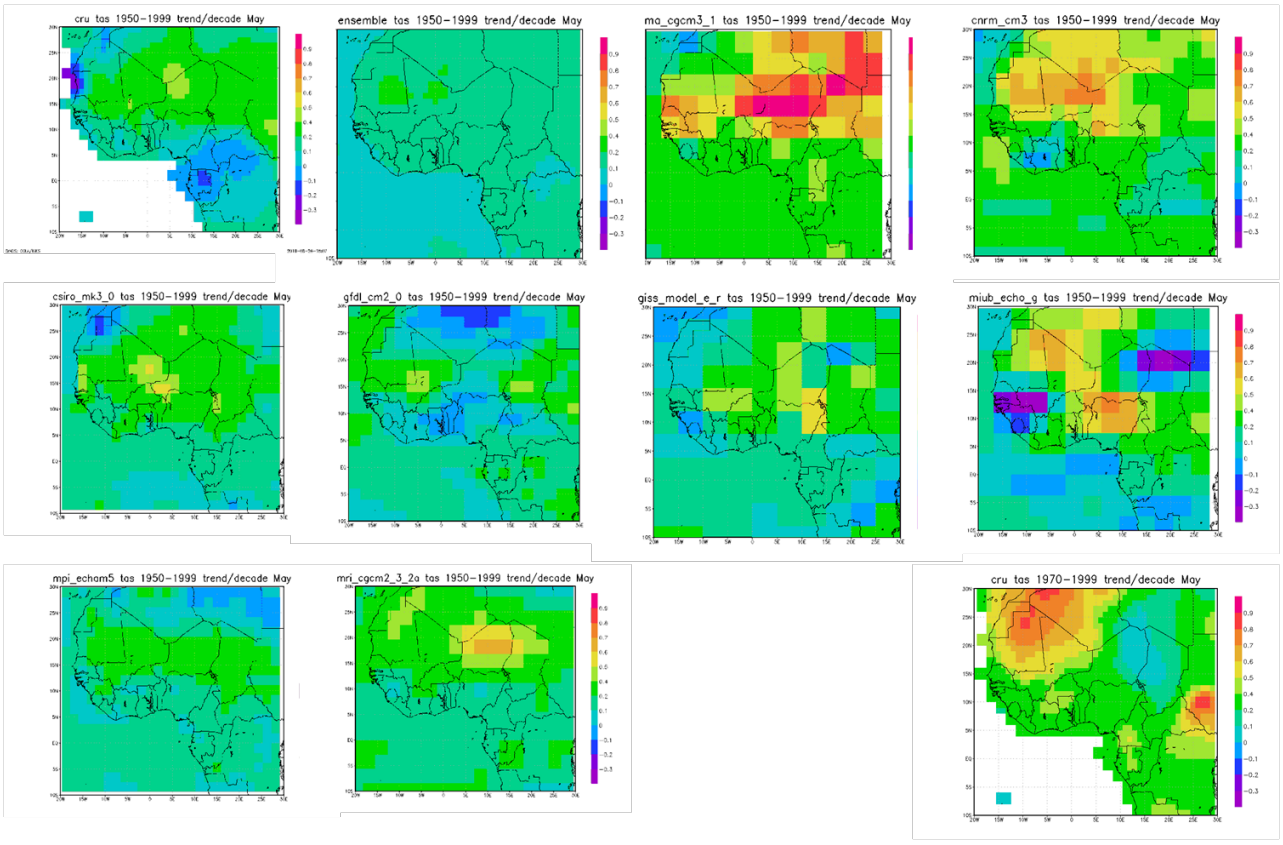
cru tas 1950-1999 trend/decade May
ensemble tas 1950-1999 trend/decade May
ma_cgcm3_1 tas 1950-1999 trend/decade May
cnrm_cm3 tas 1950-1999 trend/decade May
csiro_mk3_0 tas 1950-1999 trend/decade May
gfdl_cm2_0 tas 1950-1999 trend/decade May
giss_model_e_r tas 1950-1999 trend/decade May
miub_echo_g tas 1950-1999 trend/decade May
mpi_echam5 tas 1950-1999 trend/decade May
mri_cgcm2_3_2a tas 1950-1999 trend/decade May
cru tas 1970-1999 trend/decade May

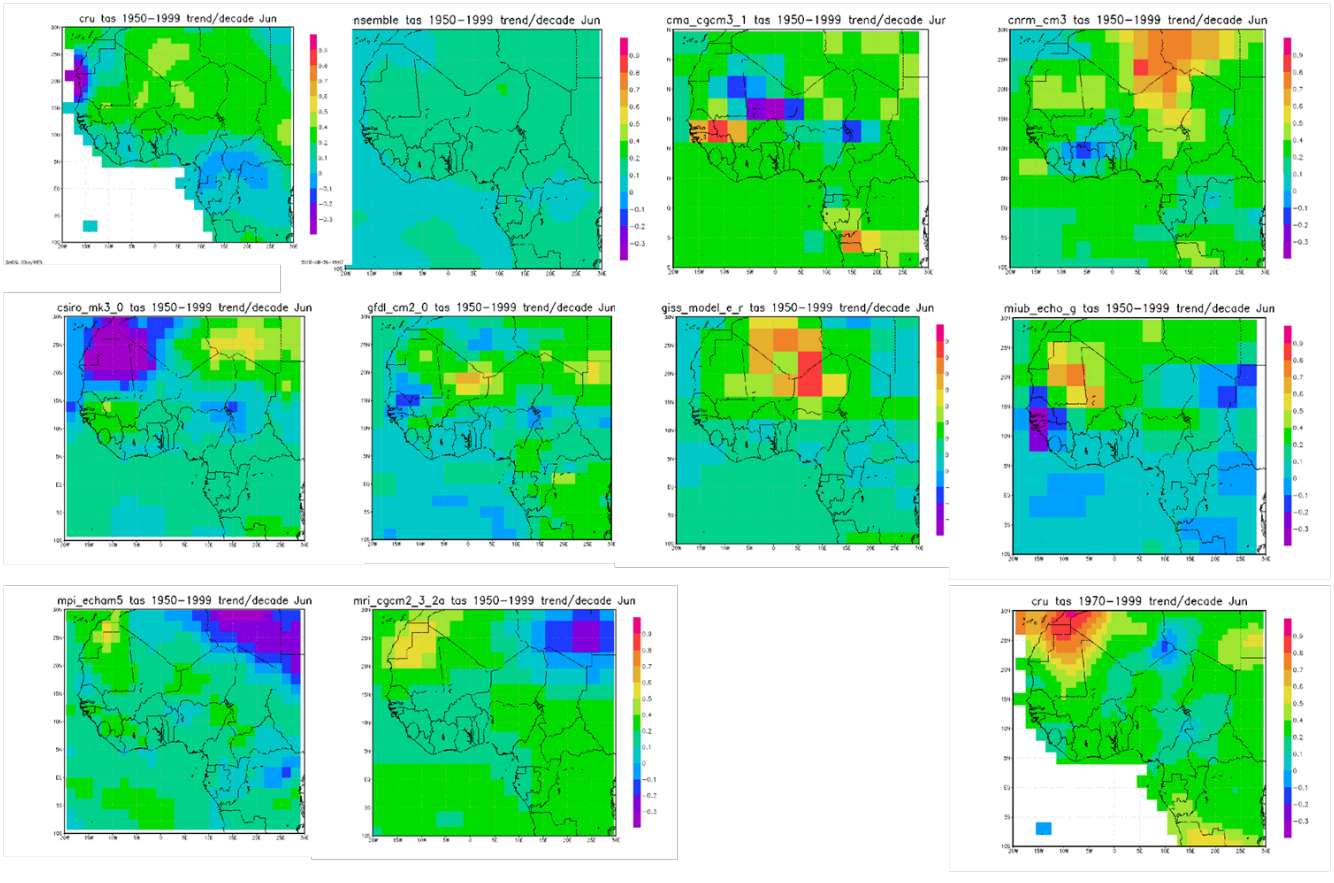
cru tas 1950-1999 trend/decade Jun
nsemble tas 1950-1999 trend/decade Jun
cma_cgcm3_1 tas 1950-1999 trend/decade Jur
cnrm_cm3 tas 1950-1999 trend/decade Jun
csiro_mk3_0 tas 1950-1999 trend/decade Jun
gfdl_cm2_0 tas 1950-1999 trend/decade Jun
giss_model_e_r tas 1950-1999 trend/decade Jun
miub_echo_g tas 1950-1999 trend/decade Jun
mpi_echam5 tas 1950-1999 trend/decade Jun
mri_cgcm2_3_2a tas 1950-1999 trend/decade Jun
cru tas 1970-1999 trend/decade Jun

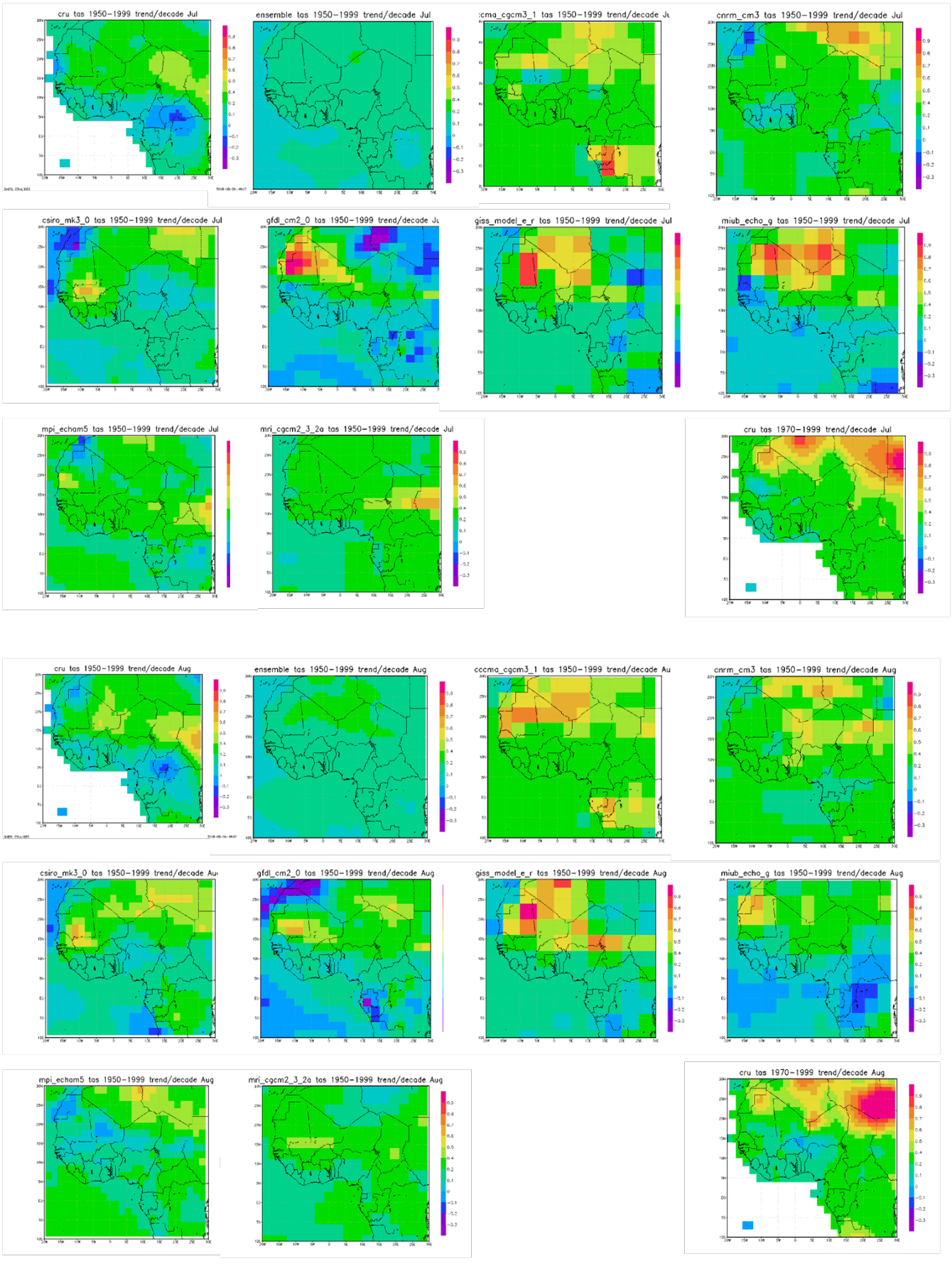
cru tas 1950-1999 trend/decade Jul
ensemble tas 1950-1999 trend/decade Jul
cnrm_cm3 tas 1950-1999 trend/decade Jul
csiro_mk3_0 tas 1950-1999 trend/decade Jul
gfdl_cm2_0 tas 1950-1999 trend/decade Ju
giss_model_e_r tas 1950-1999 trend/decade Jul
miub_echo_g tas 1950-1999 trend/decade Jul
mpi_echam5 tas 1950-1999 trend/decade Jul
mri_cgcm2_3_2a tas 1950-1999 trend/decade Jul
cru tas 1970-1999 trend/decade Jul
cru tas 1950-1999 trend/decade Aug
ensemble tas 1950-1999 trend/decade Aug
cnrm_cm3 tas 1950-1999 trend/decade Aug
csiro_mk3_0 tas 1950-1999 trend/decade Aug
gfdl_cm2_0 tas 1950-1999 trend/decade Aug
giss_model_e_r tas 1950-1999 trend/decade Aug
miub_echo_g tas 1950-1999 trend/decade Aug
mpi_echam5 tas 1950-1999 trend/decade Aug
mri_cgcm2_3_2a tas 1950-1999 trend/decade Aug
cru tas 1970-1999 trend/decade Aug

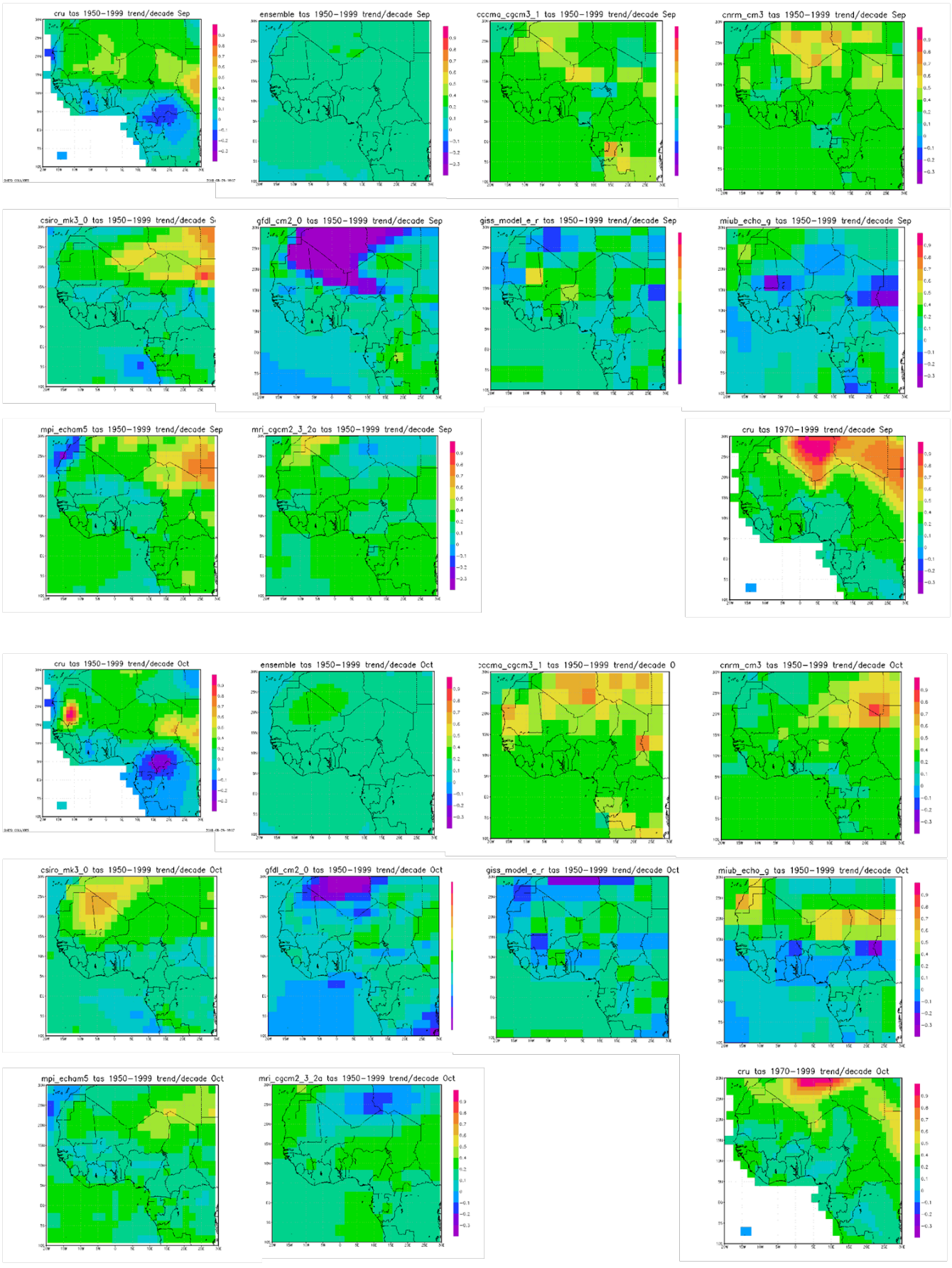
cru tas 1950-1999 trend/decade Sep
ensemble tas 1950-1999 trend/decade Sep
cccma_cgcm3_1 tas 1950-1999 trend/decade Sep
cnrm_cm3 tas 1950-1999 trend/decade Sep
csiro_mk3_0 tas 1950-1999 trend/decade S
gfdl_cm2_0 tas 1950-1999 trend/decade Sep
giss_model_e_r tas 1950-1999 trend/decade Sep
miub_echo_g tas 1950-1999 trend/decade Sep
mpi_echam5 tas 1950-1999 trend/decade Sep
mri_cgcm2_3_2a tas 1950-1999 trend/decade Sep
cru tas 1970-1999 trend/decade Sep
cru tas 1950-1999 trend/decade Oct
ensemble tas 1950-1999 trend/decade Oct
cccma_cgcm3_1 tas 1950-1999 trend/decade O
cnrm_cm3 tas 1950-1999 trend/decade Oct
csiro_mk3_0 tas 1950-1999 trend/decade Oct
gfdl_cm2_0 tas 1950-1999 trend/decade Oct
giss_model_e_r tas 1950-1999 trend/decade Oct
miub_echo_g tas 1950-1999 trend/decade Oct
mpi_echam5 tas 1950-1999 trend/decade Oct
mri_cgcm2_3_2a tas 1950-1999 trend/decade Oct
cru tas 1970-1999 trend/decade Oct

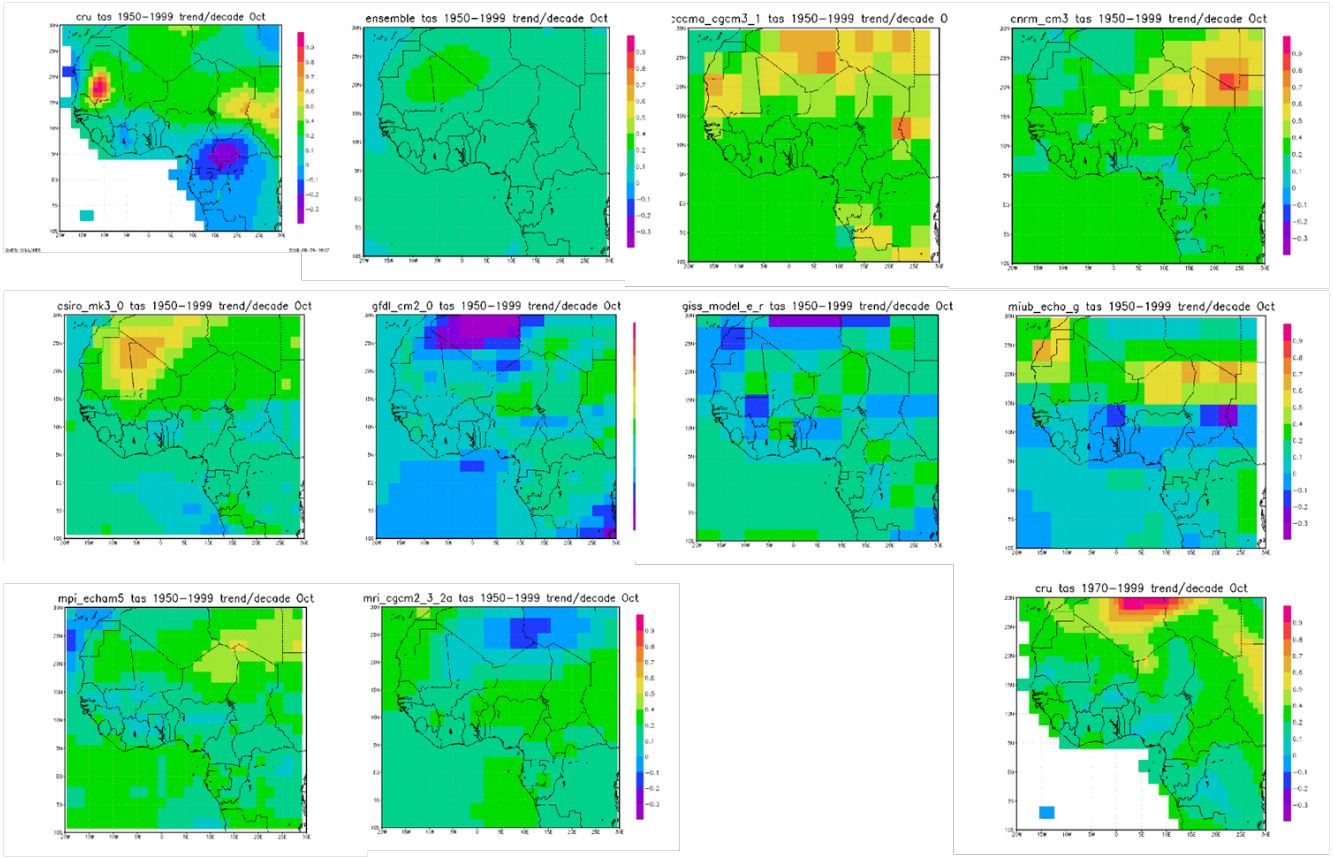
cru tas 1950-1999 trend/decade Oct
ensemble tas 1950-1999 trend/decade Oct
ccma_cgcm3_1 tas 1950-1999 trend/decade O
cnrm_cm3 tas 1950-1999 trend/decade Oct
csiro_mk3_0 tas 1950-1999 trend/decade Oct
gfdl_cm2_0 tas 1950-1999 trend/decade Oct
giss_model_e_r tas 1950-1999 trend/decade Oct
miub_echo_g tas 1950-1999 trend/decade Oct
mpi_echam5 tas 1950-1999 trend/decade Oct
mri_cgcm2_3_2a tas 1950-1999 trend/decade Oct
cru tas 1970-1999 trend/decade Oct

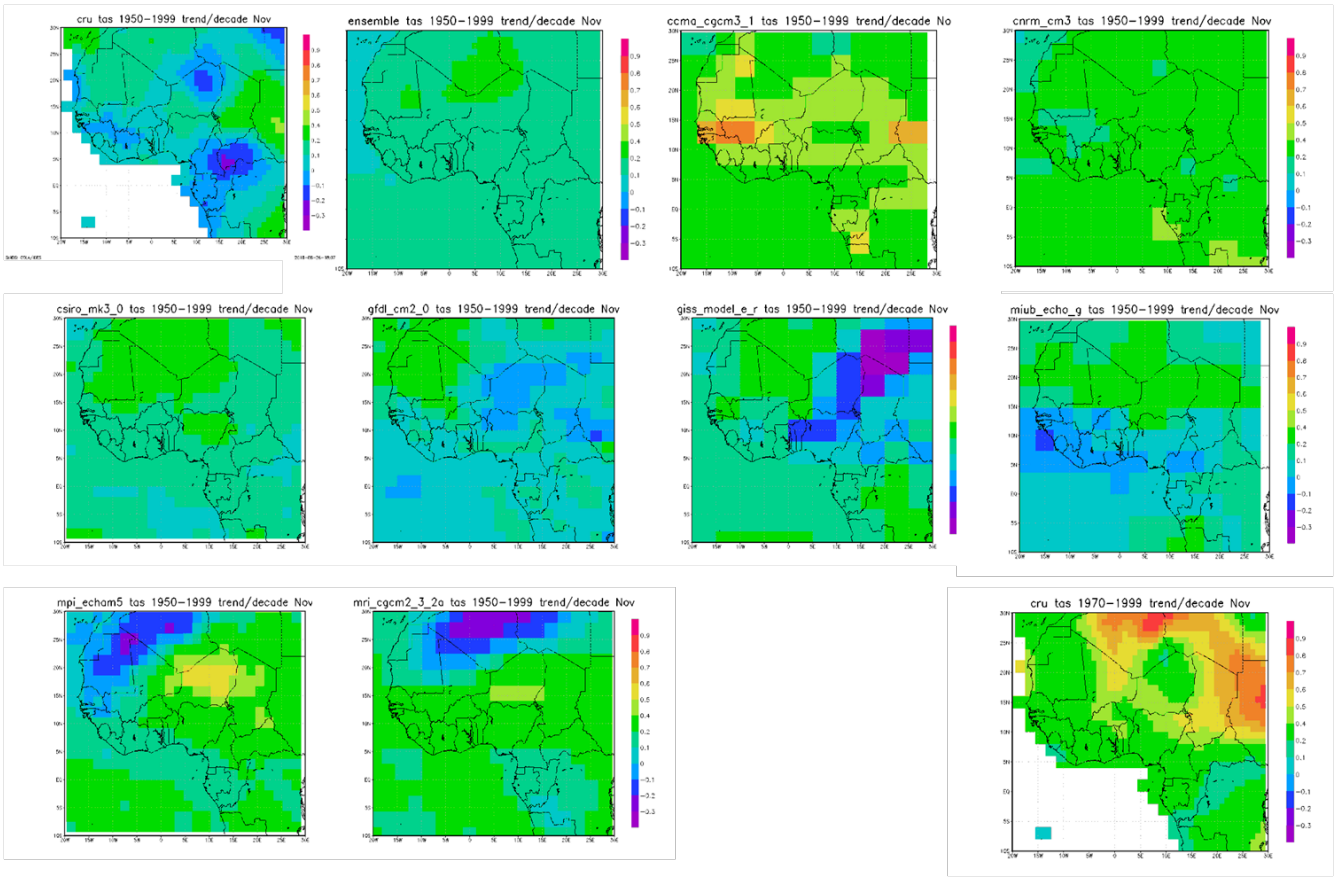
cru tas 1950-1999 trend/decade Nov
ensemble tas 1950-1999 trend/decade Nov
ccma_cgcm3_1 tas 1950-1999 trend/decade No
cnrm_cm3 tas 1950-1999 trend/decade Nov
csiro_mk3_0 tas 1950-1999 trend/decade Nov
gfdl_cm2_0 tas 1950-1999 trend/decade Nov
giss_model_e_r tas 1950-1999 trend/decade Nov
miub_echo_g tas 1950-1999 trend/decade Nov
mpi_echam5 tas 1950-1999 trend/decade Nov
mri_cgcm2_3_2a tas 1950-1999 trend/decade Nov
cru tas 1970-1999 trend/decade Nov

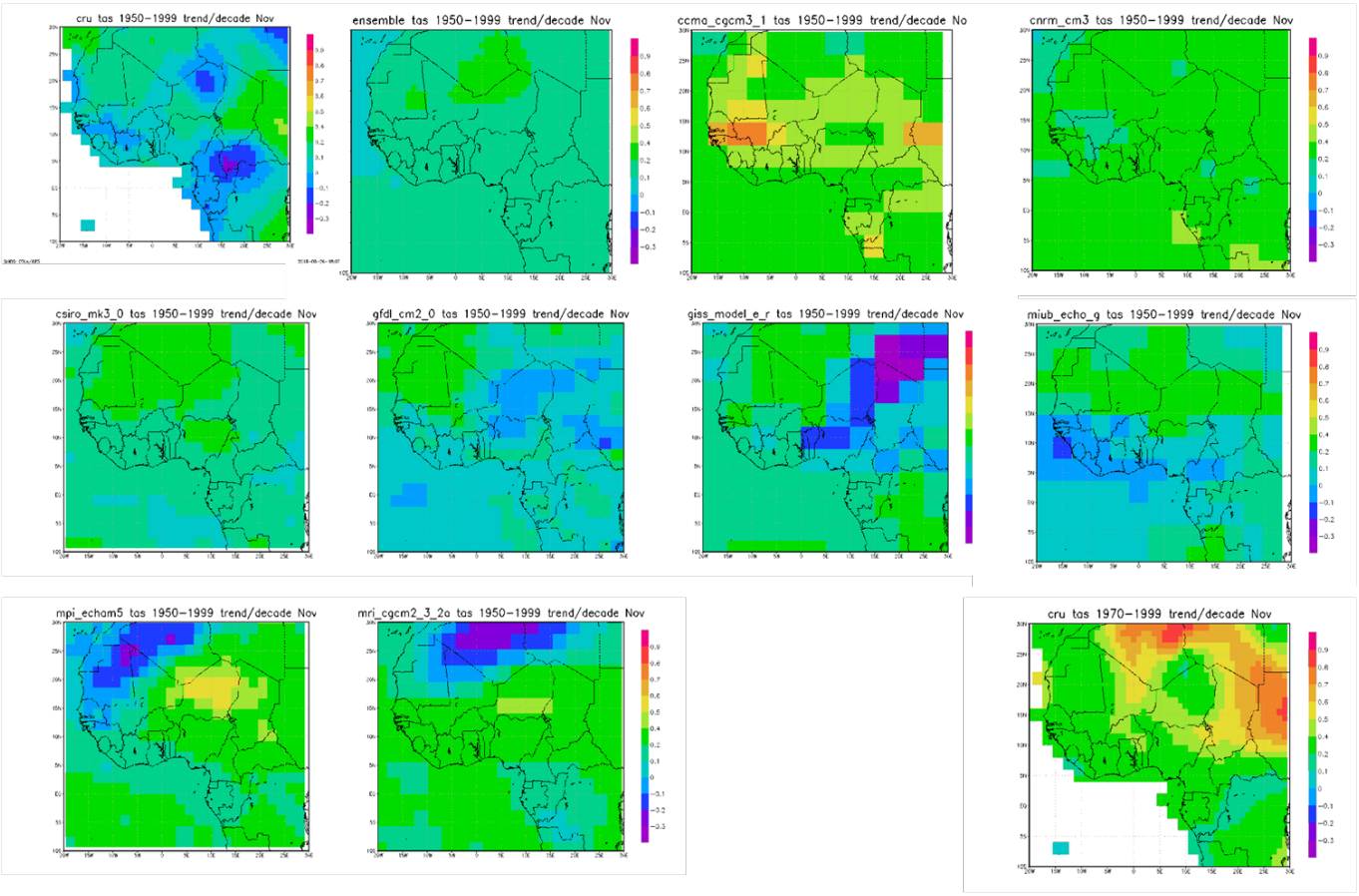
cru tas 1950–1999 trend/decade Nov
ensemble tas 1950–1999 trend/decade Nov
ccma_cgcm3_1 tas 1950–1999 trend/decade No
cnrm_cm3 tas 1950–1999 trend/decade Nov
csiro_mk3_0 tas 1950–1999 trend/decade Nov
gfdl_cm2_0 tas 1950–1999 trend/decade Nov
giss_model_e_r tas 1950–1999 trend/decade Nov
miub_echo_g tas 1950–1999 trend/decade Nov
mpi_echam5 tas 1950–1999 trend/decade Nov
mri_cgcm2_3_2a tas 1950–1999 trend/decade Nov
cru tas 1970–1999 trend/decade Nov

Appendix 5: Model derived monthly and annual precipitation trends

The individual model trends for the 1950–99 period are shown with NCEP and JapRe trends for both the 1950–99 and 1970–99 periods, which show the effect that the precipitation change in the late 1960s has on the overall trend in these datasets. The ensemble trend is also shown.

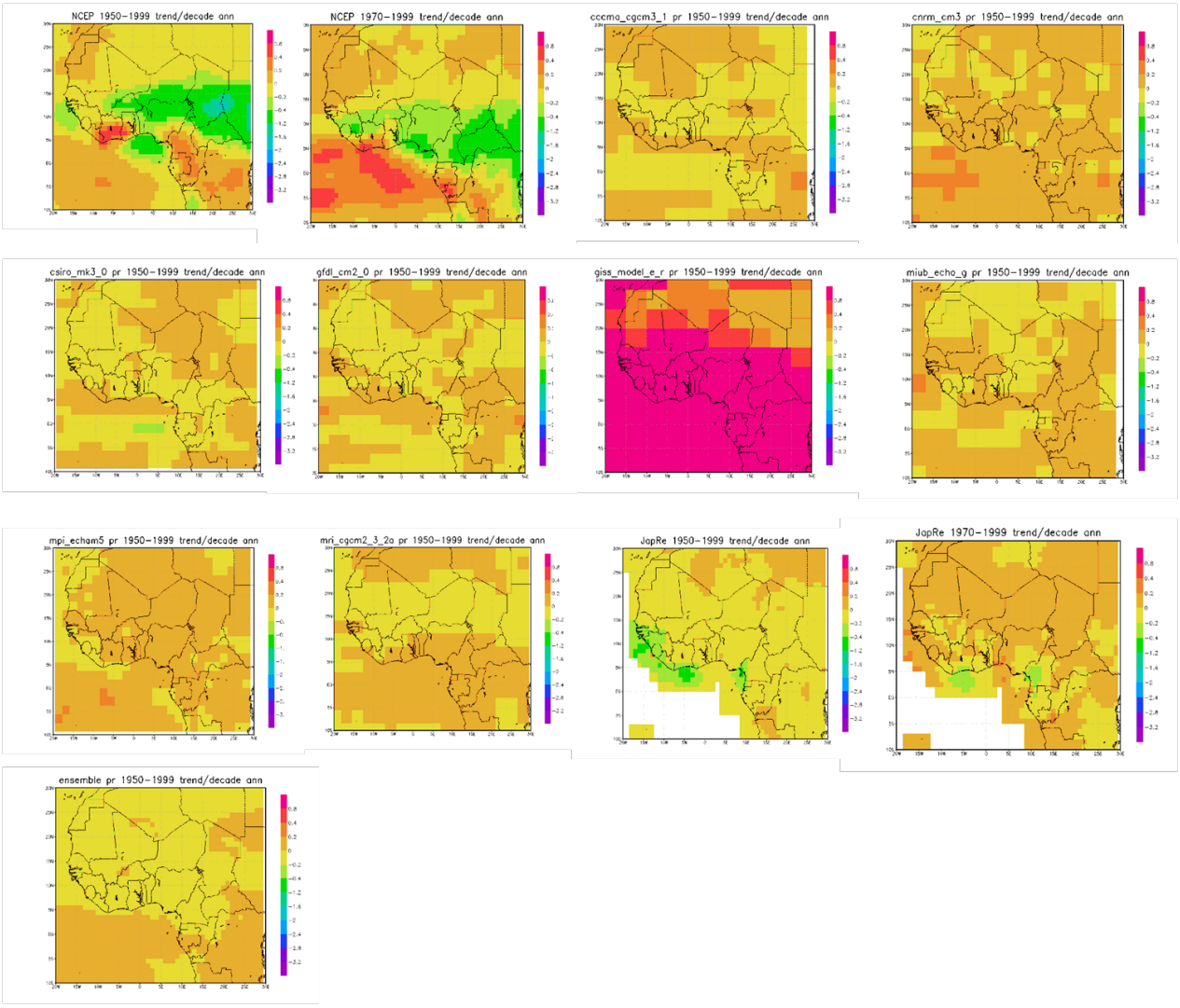

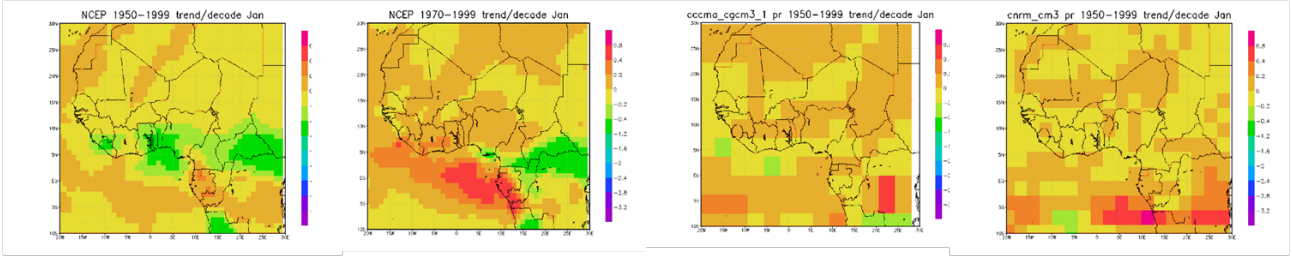
NCEP 1950–1999 trend/decade Jan
NCEP 1970–1999 trend/decade Jan
cccma_cgcm3_1 pr 1950–1999 trend/decade Jan
cnrm_cm3 pr 1950–1999 trend/decade Jan

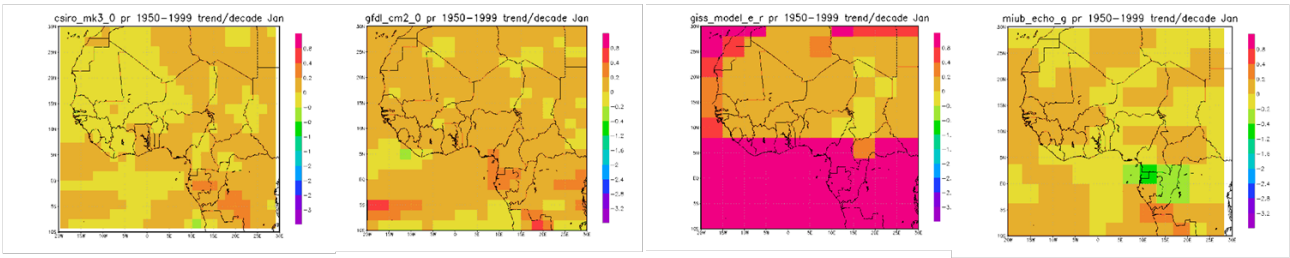
csiro_mk3_0 pr 1950–1999 trend/decade Jan
gfdl_cm2_0 pr 1950–1999 trend/decade Jan
giss_model_e_r pr 1950–1999 trend/decade Jan
miub_echo_g pr 1950–1999 trend/decade Jan

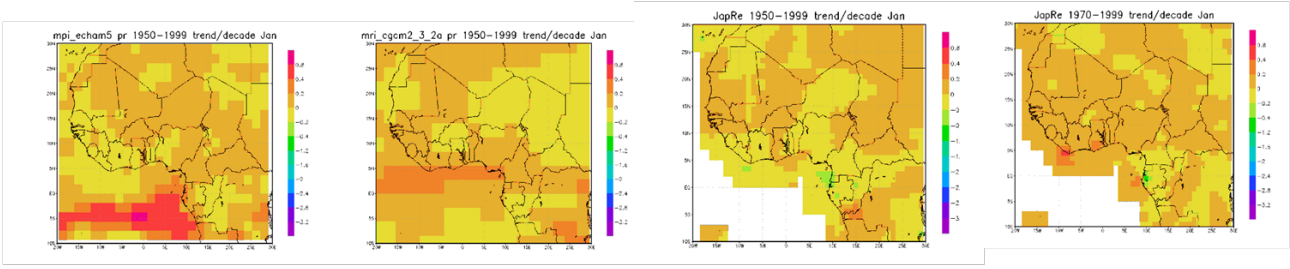
mpi_echam5 pr 1950–1999 trend/decade Jan
mri_cgcm2_3_2a pr 1950–1999 trend/decade Jan
JapRe 1950–1999 trend/decade Jan
JapRe 1970–1999 trend/decade Jan

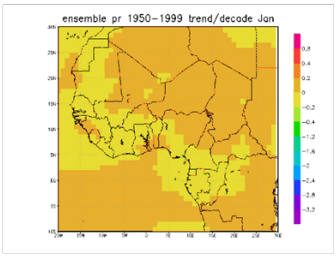
ensemble pr 1950–1999 trend/decade Jan

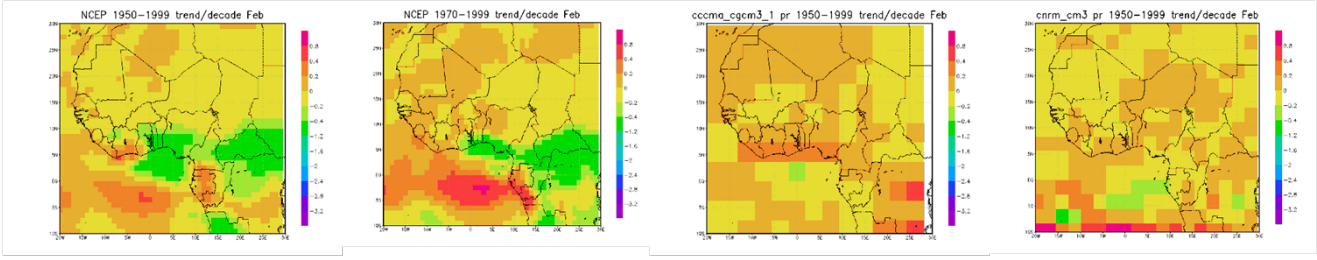
NCEP 1950–1999 trend/decade Feb
NCEP 1970–1999 trend/decade Feb
cccma_cgcm3_1 pr 1950–1999 trend/decade Feb
cnrm_cm3 pr 1950–1999 trend/decade Feb

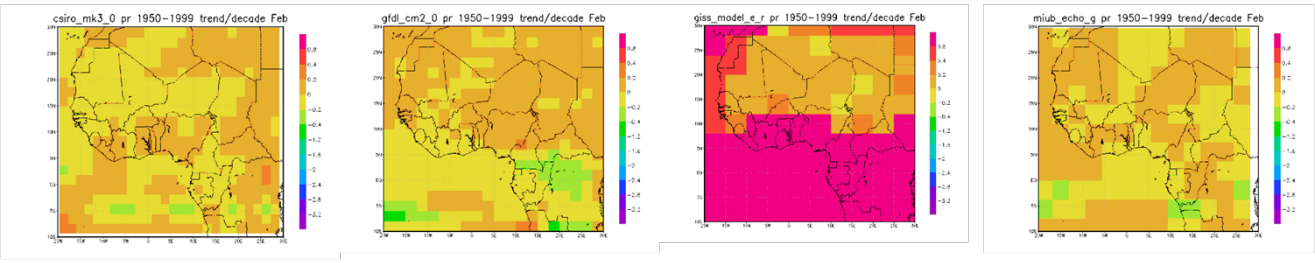
csiro_mk3_0 pr 1950–1999 trend/decade Feb
gfdl_cm2_0 pr 1950–1999 trend/decade Feb
giss_model_e_r pr 1950–1999 trend/decade Feb
miub_echo_g pr 1950–1999 trend/decade Feb

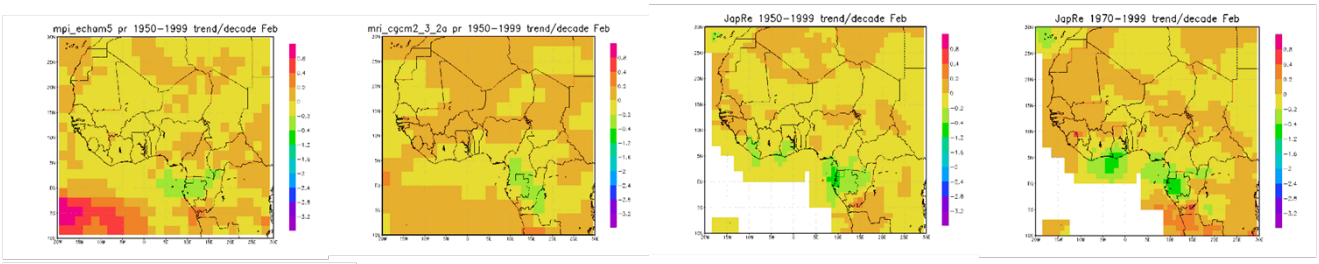
mpi_echam5 pr 1950–1999 trend/decade Feb
mri_cgcm2_3_2a pr 1950–1999 trend/decade Feb
JapRe 1950–1999 trend/decade Feb
JapRe 1970–1999 trend/decade Feb

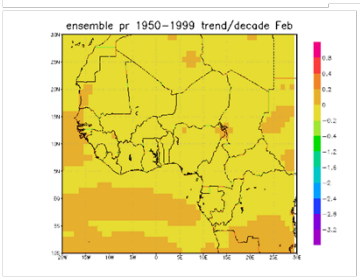
ensemble pr 1950–1999 trend/decade Feb

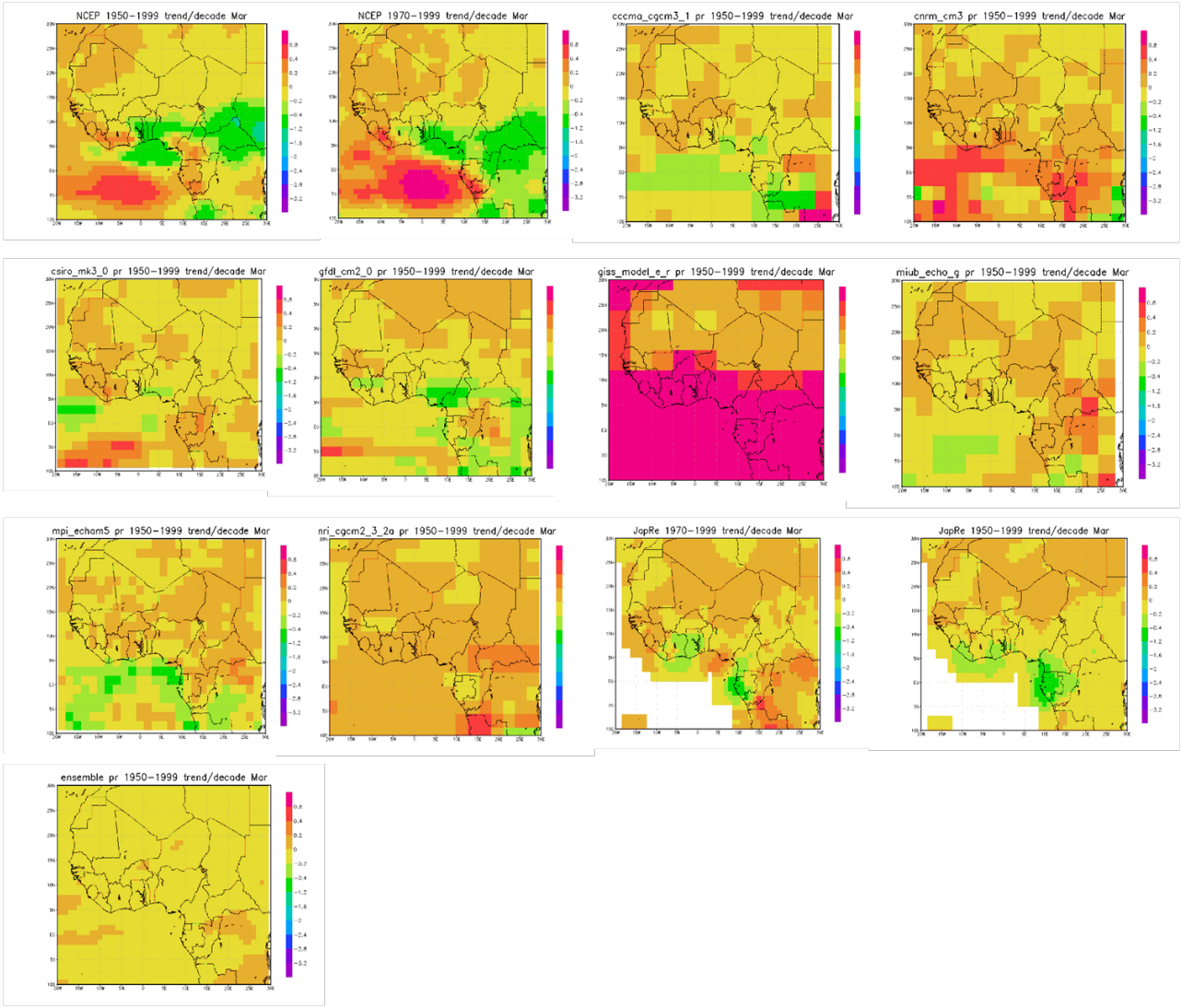
NCEP 1950–1999 trend/decade Mar
NCEP 1970–1999 trend/decade Mar
cccma_cgcm3_1 pr 1950–1999 trend/decade Mar
cnrm_cm3 pr 1950–1999 trend/decade Mar
csiro_mk3_0 pr 1950–1999 trend/decade Mar
gfdl_cm2_0 pr 1950–1999 trend/decade Mar
giss_model_e_r pr 1950–1999 trend/decade Mar
miub_echo_g pr 1950–1999 trend/decade Mar
mpi_echam5 pr 1950–1999 trend/decade Mar
nri_cgcm2_3_2a pr 1950–1999 trend/decade Mar
JapRe 1970–1999 trend/decade Mar
JapRe 1950–1999 trend/decade Mar
ensemble pr 1950–1999 trend/decade Mar

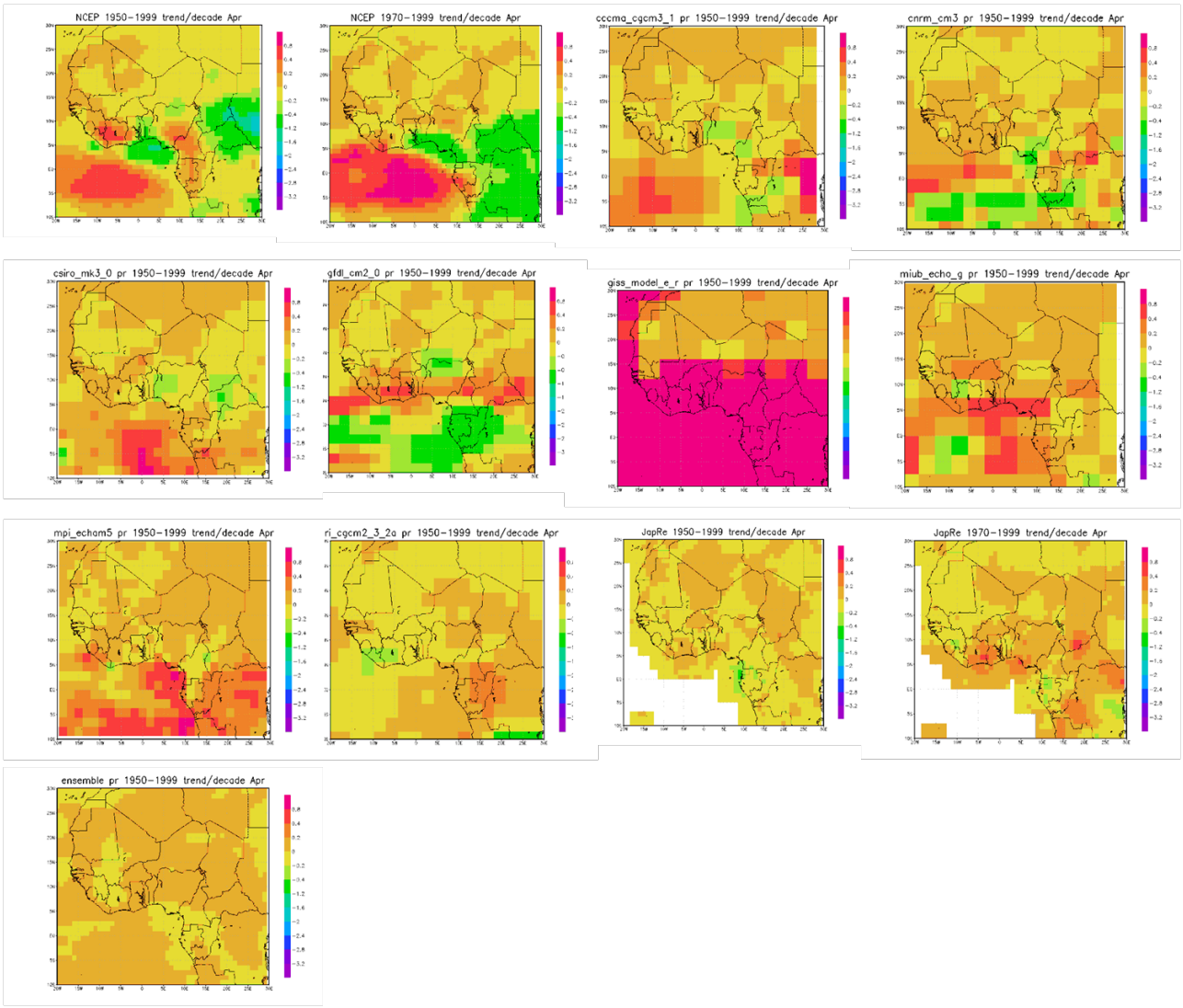
NCEP 1950–1999 trend/decade Apr
NCEP 1970–1999 trend/decade Apr
cccma_cgcm3_1 pr 1950–1999 trend/decade Apr
cnrm_cm3 pr 1950–1999 trend/decade Apr
csiro_mk3_0 pr 1950–1999 trend/decade Apr
gfdl_cm2_0 pr 1950–1999 trend/decade Apr
giss_model_e_r pr 1950–1999 trend/decade Apr
miub_echo_g pr 1950–1999 trend/decade Apr
mpi_echam5 pr 1950–1999 trend/decade Apr
ri_cgcm2_3_2a pr 1950–1999 trend/decade Apr
JapRe 1950–1999 trend/decade Apr
JapRe 1970–1999 trend/decade Apr
ensemble pr 1950–1999 trend/decade Apr

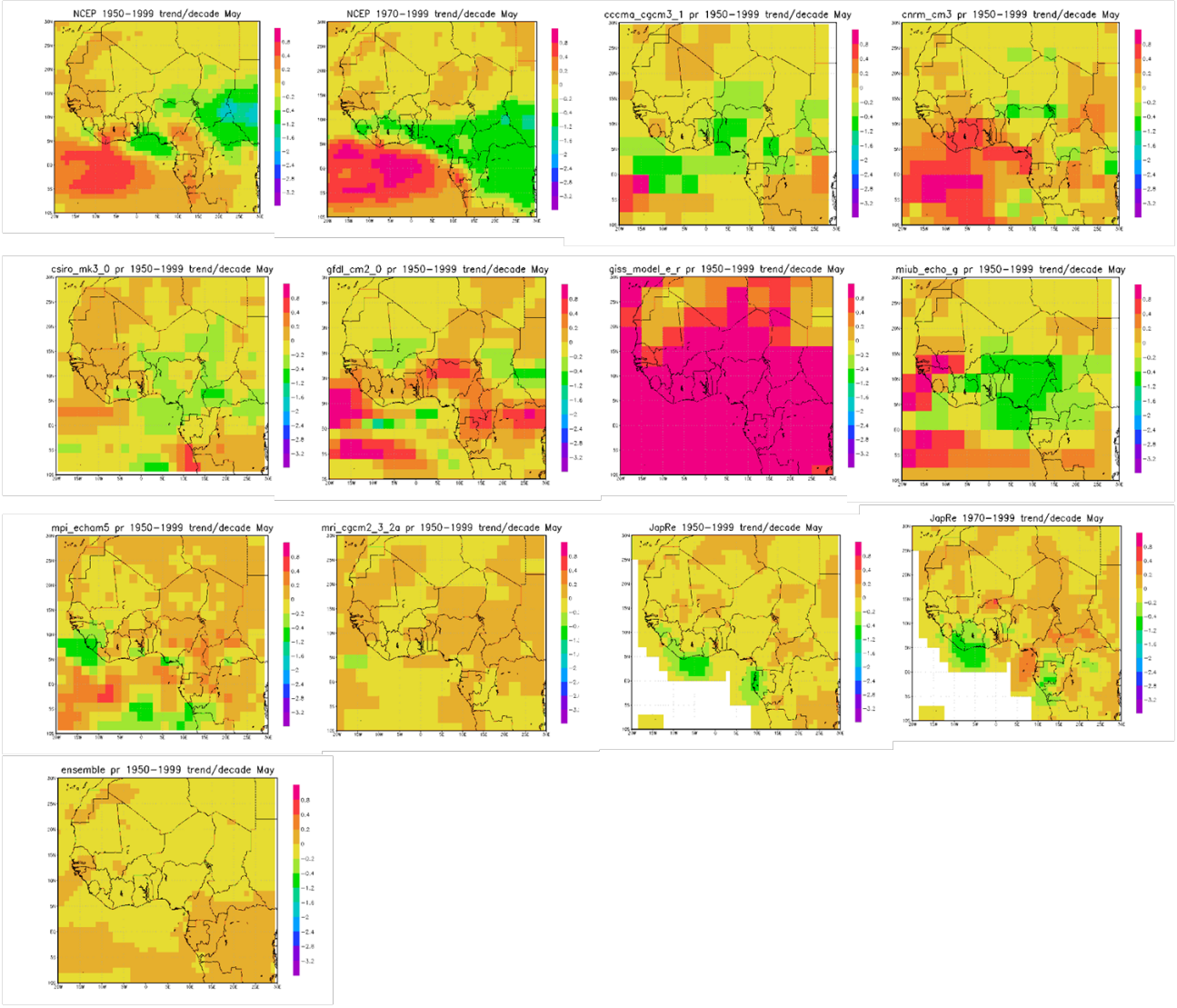
NCEP 1950–1999 trend/decade May
NCEP 1970–1999 trend/decade May
cccma_cgcm3_1 pr 1950–1999 trend/decade May
cnrm_cm3 pr 1950–1999 trend/decade May
csiro_mk3_0 pr 1950–1999 trend/decade May
gfdl_cm2_0 pr 1950–1999 trend/decade May
giss_model_e_r pr 1950–1999 trend/decade May
miub_echo_g pr 1950–1999 trend/decade May
mpi_echam5 pr 1950–1999 trend/decade May
mri_cgcm2_3_2a pr 1950–1999 trend/decade May
JapRe 1950–1999 trend/decade May
JapRe 1970–1999 trend/decade May
ensemble pr 1950–1999 trend/decade May

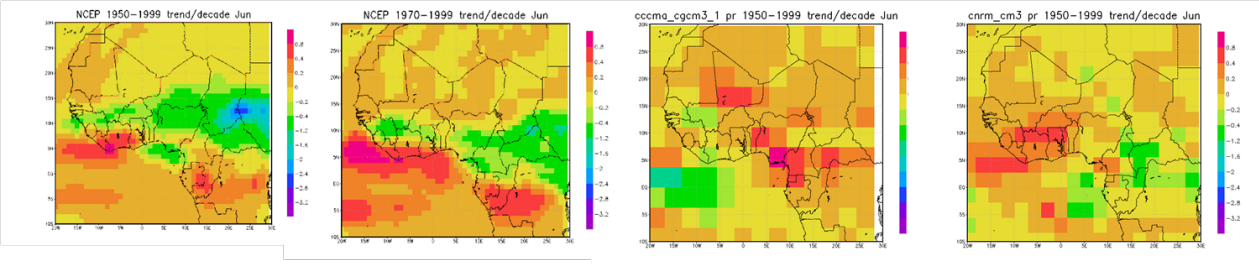
NCEP 1950–1999 trend/decade Jun
NCEP 1970–1999 trend/decade Jun
cccma_cgcm3_1 pr 1950–1999 trend/decade Jun
cnrm_cm3 pr 1950–1999 trend/decade Jun

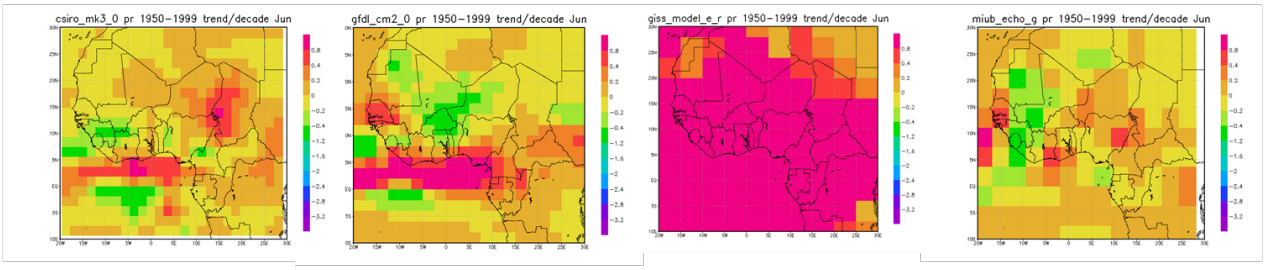
csiro_mk3_0 pr 1950–1999 trend/decade Jun
gfdl_cm2_0 pr 1950–1999 trend/decade Jun
giss_model_e_r pr 1950–1999 trend/decade Jun
miub_echo_g pr 1950–1999 trend/decade Jun

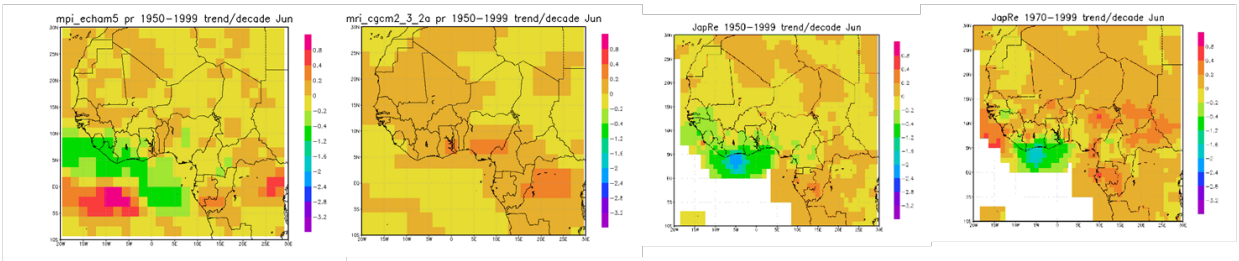
mpi_echam5 pr 1950–1999 trend/decade Jun
mri_cgcm2_3_2a pr 1950–1999 trend/decade Jun
JapRe 1950–1999 trend/decade Jun
JapRe 1970–1999 trend/decade Jun

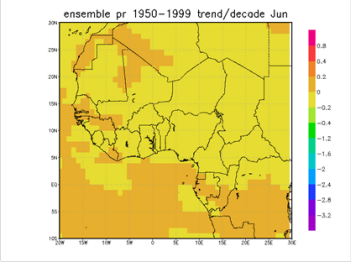
ensemble pr 1950–1999 trend/decade Jun

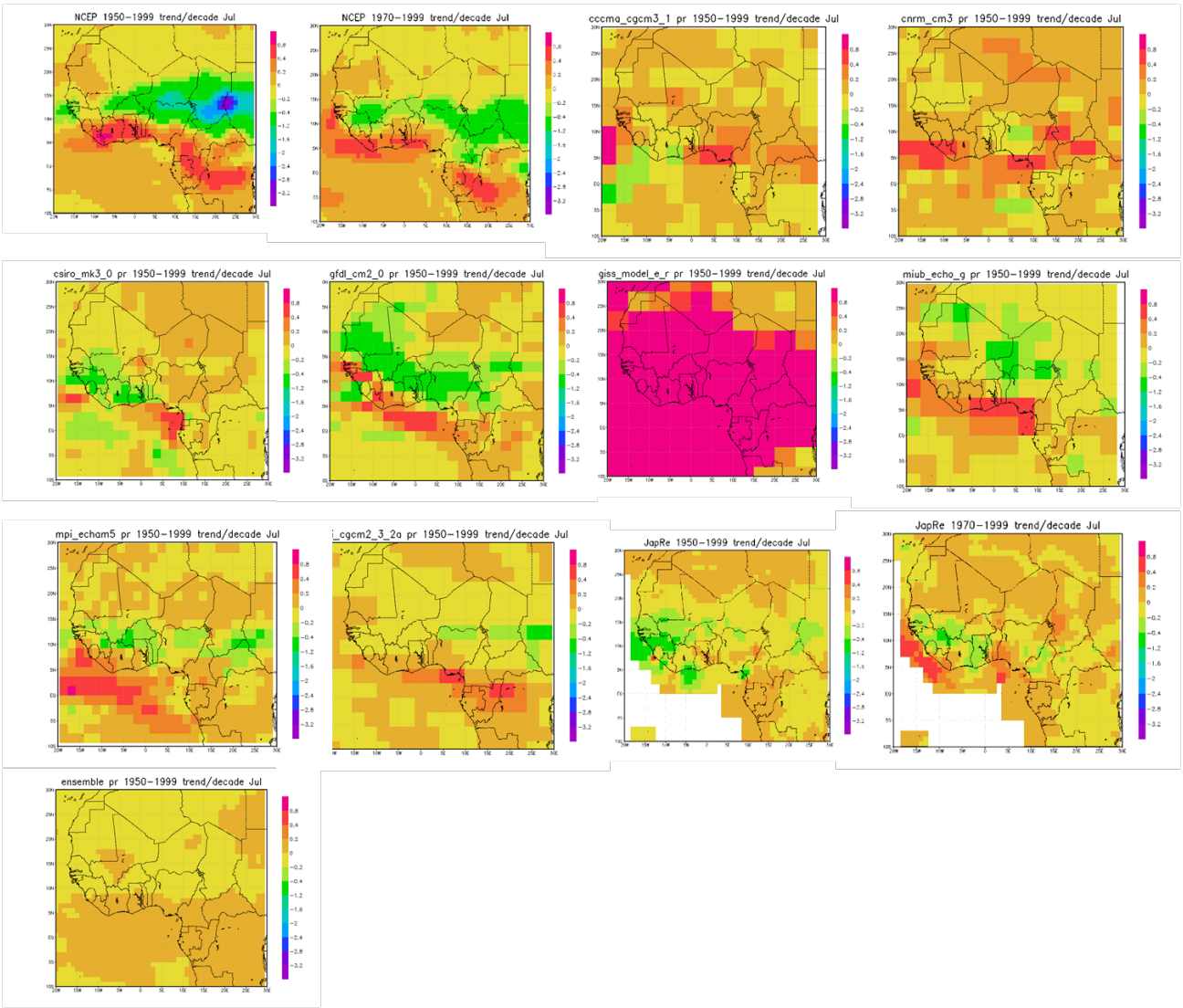
NCEP 1950–1999 trend/decade Jul
NCEP 1970–1999 trend/decade Jul
cccma_cgcm3_1 pr 1950–1999 trend/decade Jul
cnrm_cm3 pr 1950–1999 trend/decade Jul
csiro_mk3_0 pr 1950–1999 trend/decade Jul
gfdl_cm2_0 pr 1950–1999 trend/decade Jul
giss_model_e_r pr 1950–1999 trend/decade Jul
miub_echo_g pr 1950–1999 trend/decade Jul
mpi_echam5 pr 1950–1999 trend/decade Jul
_cgcm2_3_2a pr 1950–1999 trend/decade Jul
JapRe 1950–1999 trend/decade Jul
JapRe 1970–1999 trend/decade Jul
ensemble pr 1950–1999 trend/decade Jul

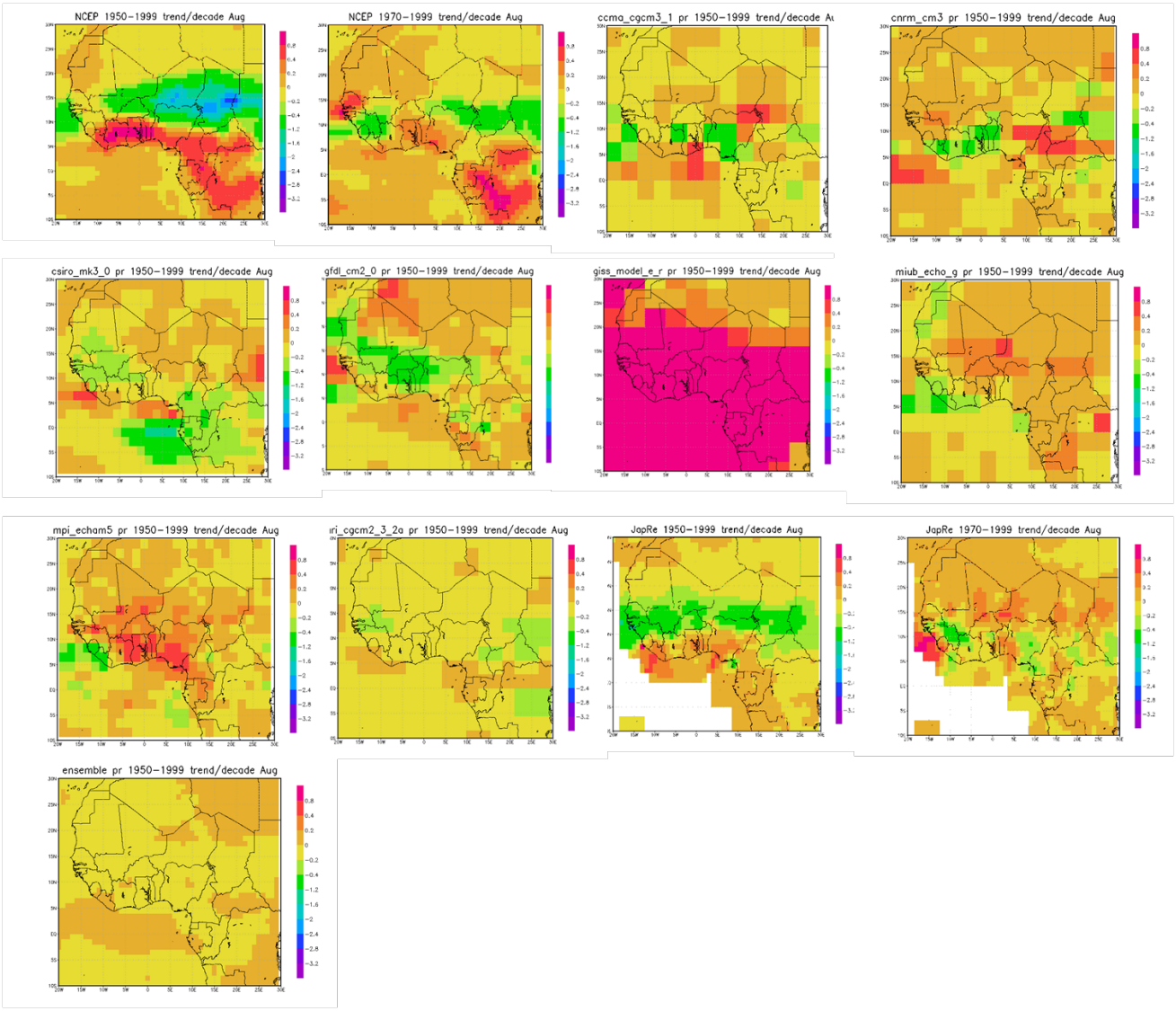
NCEP 1950–1999 trend/decade Aug
NCEP 1970–1999 trend/decade Aug
ccma_cgcm3_1 pr 1950–1999 trend/decade Au
cnrm_cm3 pr 1950–1999 trend/decade Aug
csiro_mk3_0 pr 1950–1999 trend/decade Aug
gfdl_cm2_0 pr 1950–1999 trend/decade Aug
giss_model_e_r pr 1950–1999 trend/decade Aug
miub_echo_g pr 1950–1999 trend/decade Aug
mpi_echam5 pr 1950–1999 trend/decade Aug
iri_cgcm2_3_2a pr 1950–1999 trend/decade Aug
JapRe 1950–1999 trend/decade Aug
JapRe 1970–1999 trend/decade Aug
ensemble pr 1950–1999 trend/decade Aug

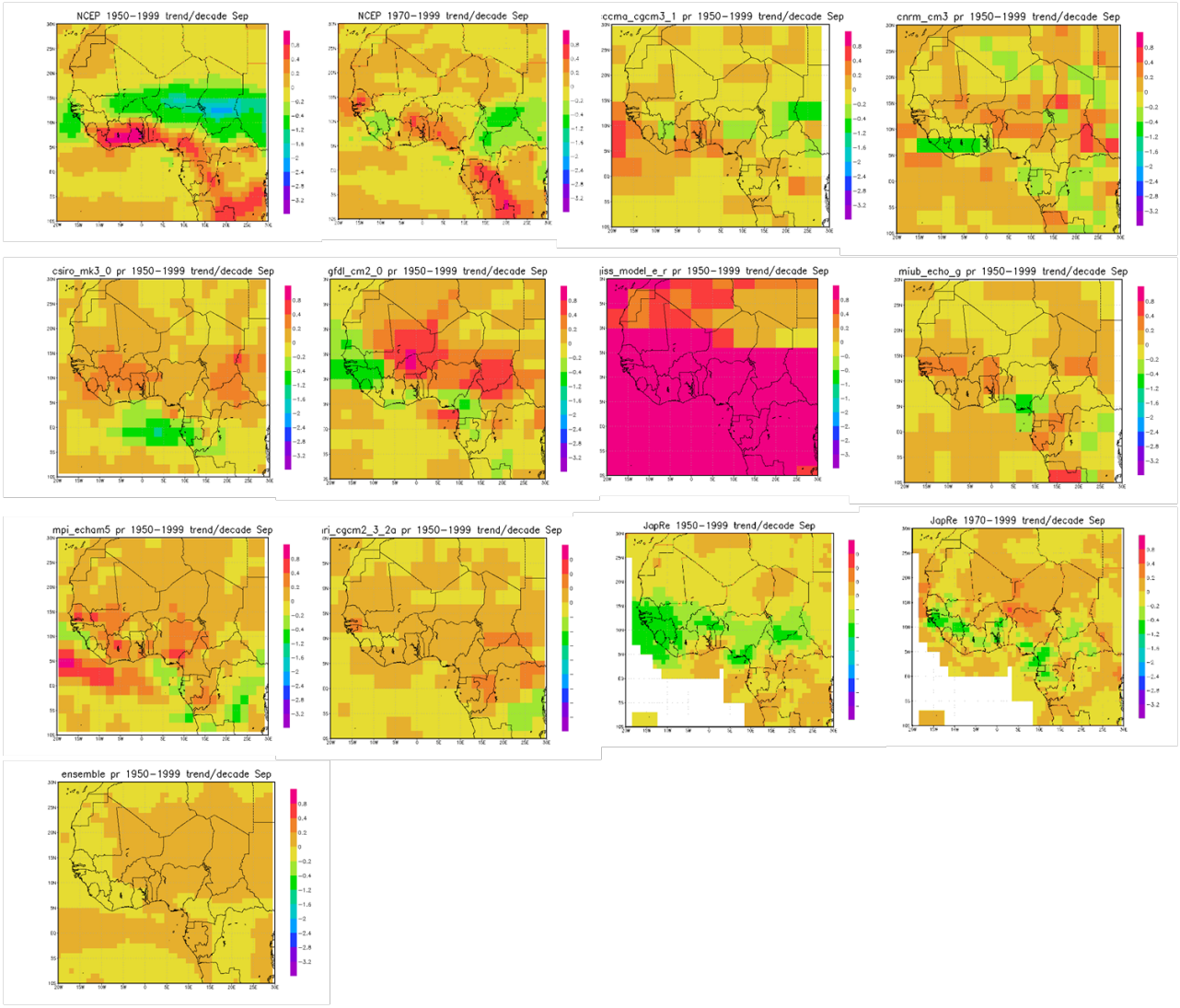
NCEP 1950–1999 trend/decade Sep
NCEP 1970–1999 trend/decade Sep
ccma_cgcm3_1 pr 1950–1999 trend/decade Sep
cnrm_cm3 pr 1950–1999 trend/decade Sep
csiro_mk3_0 pr 1950–1999 trend/decade Sep
gfdl_cm2_0 pr 1950–1999 trend/decade Sep
giss_model_e_r pr 1950–1999 trend/decade Sep
miub_echo_g pr 1950–1999 trend/decade Sep
mpi_echam5 pr 1950–1999 trend/decade Sep
iri_cgcm2_3_2a pr 1950–1999 trend/decade Sep
JapRe 1950–1999 trend/decade Sep
JapRe 1970–1999 trend/decade Sep
ensemble pr 1950–1999 trend/decade Sep

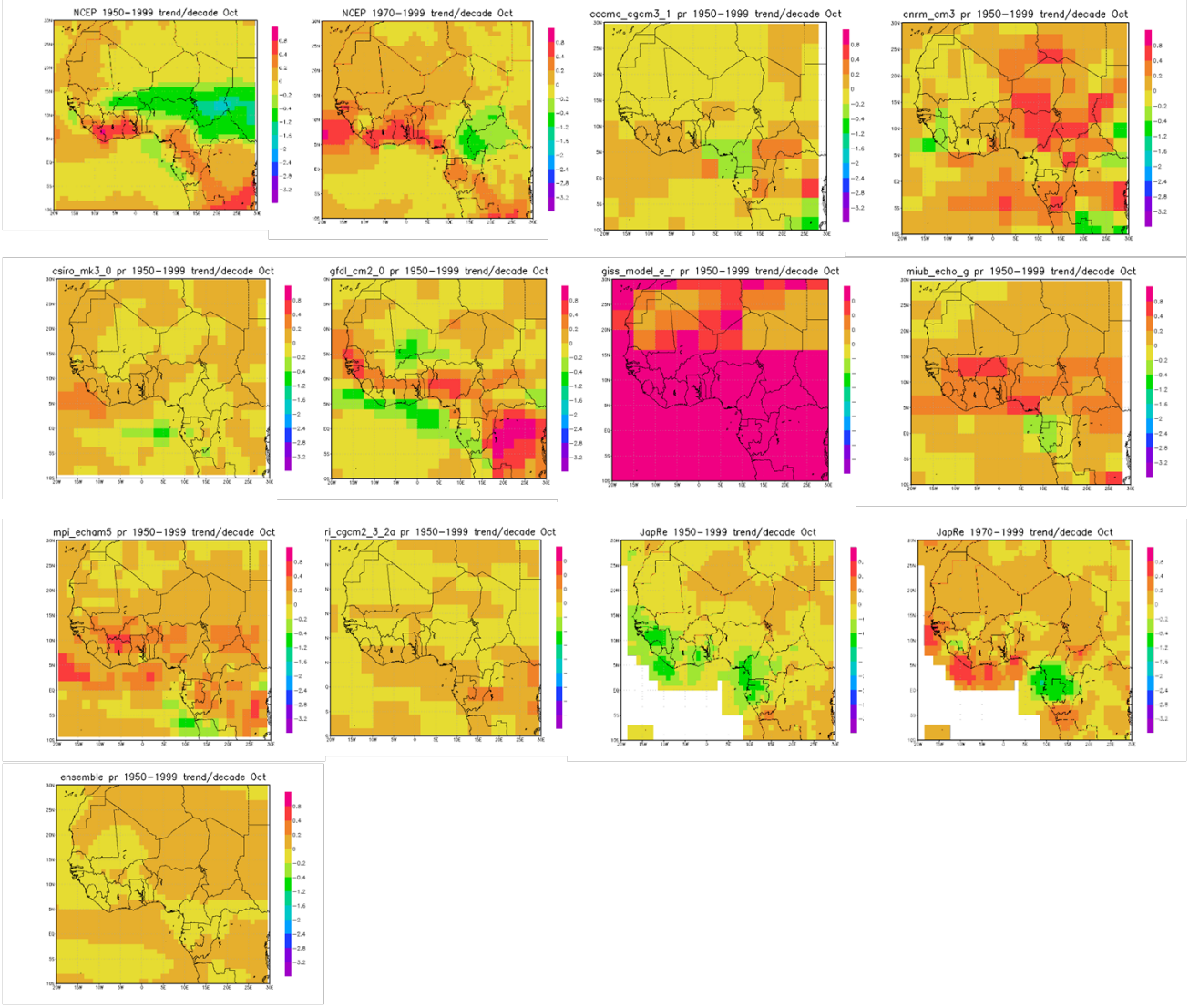
NCEP 1950–1999 trend/decade Oct
NCEP 1970–1999 trend/decade Oct
cccma_cgcm3_1 pr 1950–1999 trend/decade Oct
cnrm_cm3 pr 1950–1999 trend/decade Oct
csiro_mk3_0 pr 1950–1999 trend/decade Oct
gfdl_cm2_0 pr 1950–1999 trend/decade Oct
giss_model_e_r pr 1950–1999 trend/decade Oct
miub_echo_g pr 1950–1999 trend/decade Oct
mpi_echam5 pr 1950–1999 trend/decade Oct
ri_cgcm2_3_2a pr 1950–1999 trend/decade Oct
JapRe 1950–1999 trend/decade Oct
JapRe 1970–1999 trend/decade Oct
ensemble pr 1950–1999 trend/decade Oct

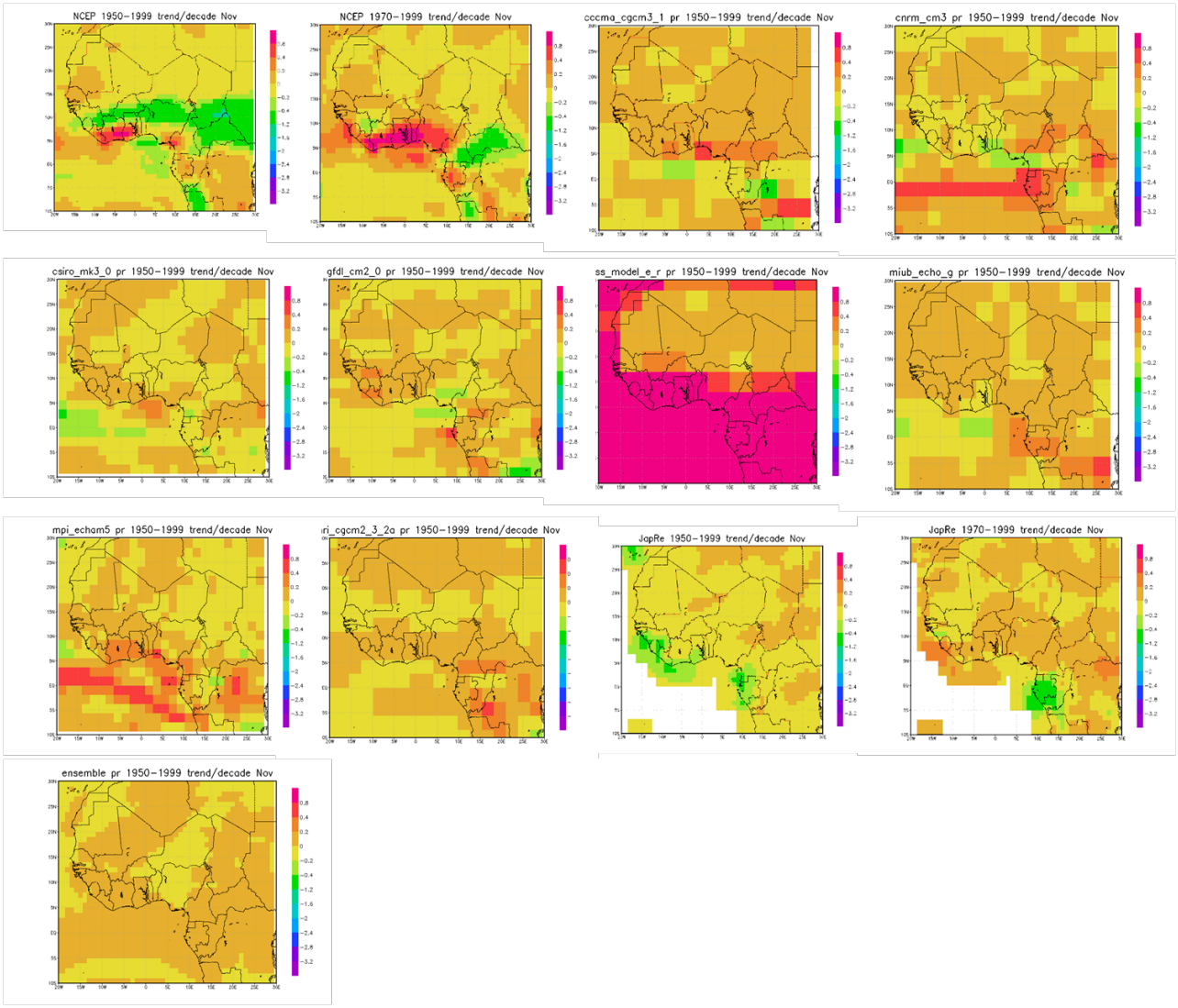
NCEP 1950–1999 trend/decade Nov
NCEP 1970–1999 trend/decade Nov
cccma_cgcm3_1 pr 1950–1999 trend/decade Nov
cnrm_cm3 pr 1950–1999 trend/decade Nov
csiro_mk3_0 pr 1950–1999 trend/decade Nov
gfdl_cm2_0 pr 1950–1999 trend/decade Nov
ss_model_e_r pr 1950–1999 trend/decade Nov
miub_echo_g pr 1950–1999 trend/decade Nov
mpi_echam5 pr 1950–1999 trend/decade Nov
iri_cgcm2_3_2a pr 1950–1999 trend/decade Nov
JapRe 1950–1999 trend/decade Nov
JapRe 1970–1999 trend/decade Nov
ensemble pr 1950–1999 trend/decade Nov

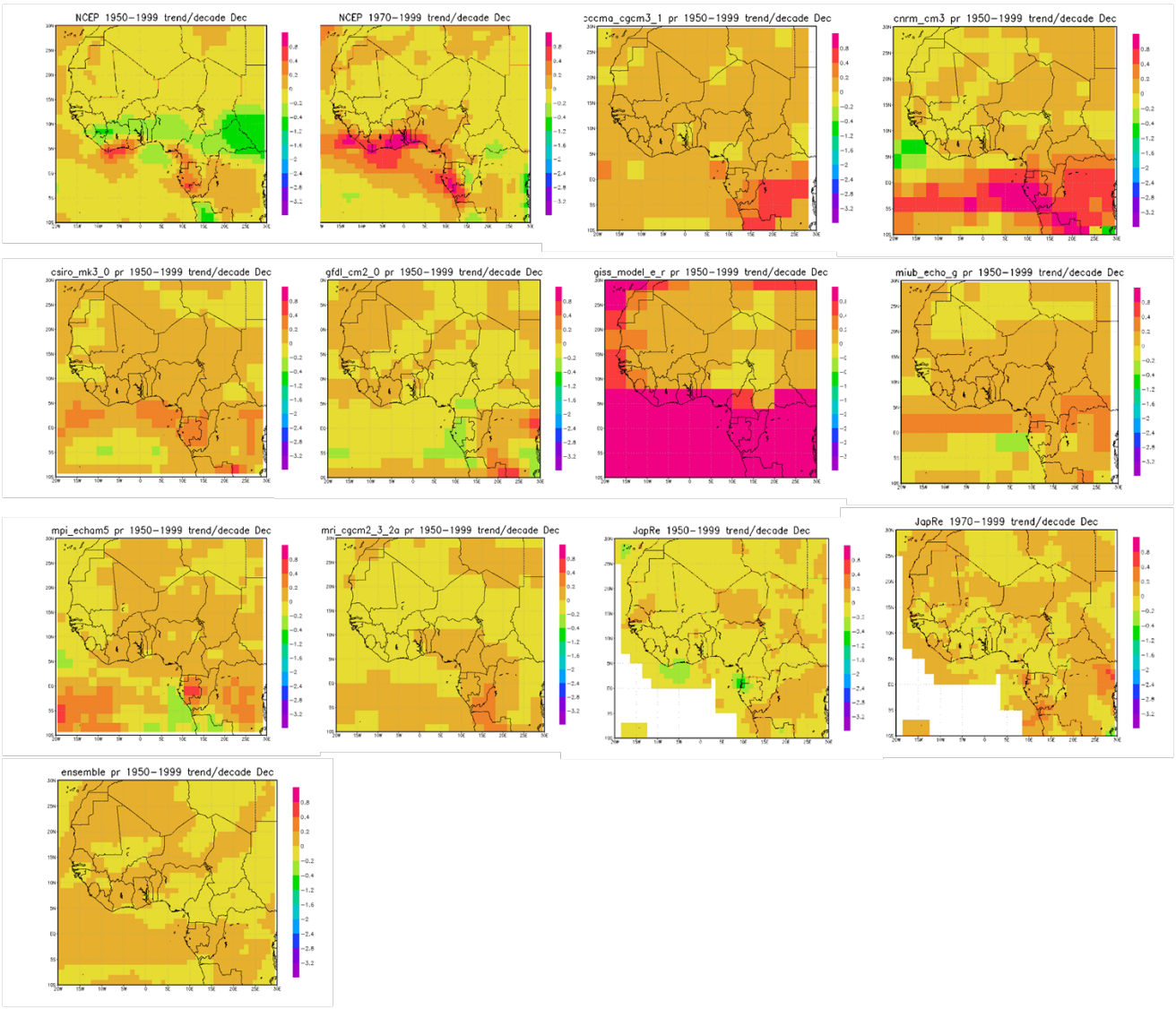
NCEP 1950–1999 trend/decade Dec
NCEP 1970–1999 trend/decade Dec
cccma_cgcm3_1 pr 1950–1999 trend/decade Dec
cnrm_cm3 pr 1950–1999 trend/decade Dec
csiro_mk3_0 pr 1950–1999 trend/decade Dec
gfdl_cm2_0 pr 1950–1999 trend/decade Dec
giss_model_e_r pr 1950–1999 trend/decade Dec
miub_echo_g pr 1950–1999 trend/decade Dec
mpi_echam5 pr 1950–1999 trend/decade Dec
mri_cgcm2_3_2a pr 1950–1999 trend/decade Dec
JapRe 1950–1999 trend/decade Dec
JapRe 1970–1999 trend/decade Dec
ensemble pr 1950–1999 trend/decade Dec

Appendix 6: Model Derived Crop Domains Created Using Climatology Data for the 1970-99 Period

The NCEP and JapRe domains are included for comparison.

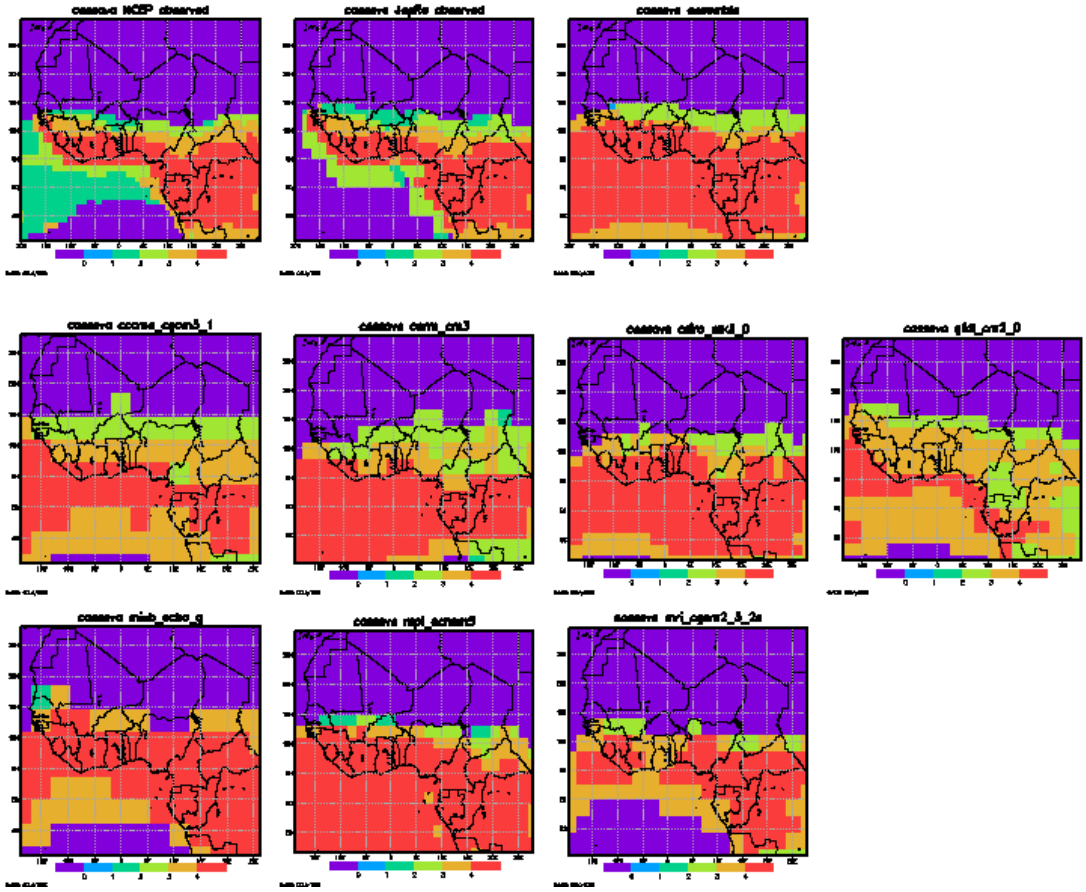

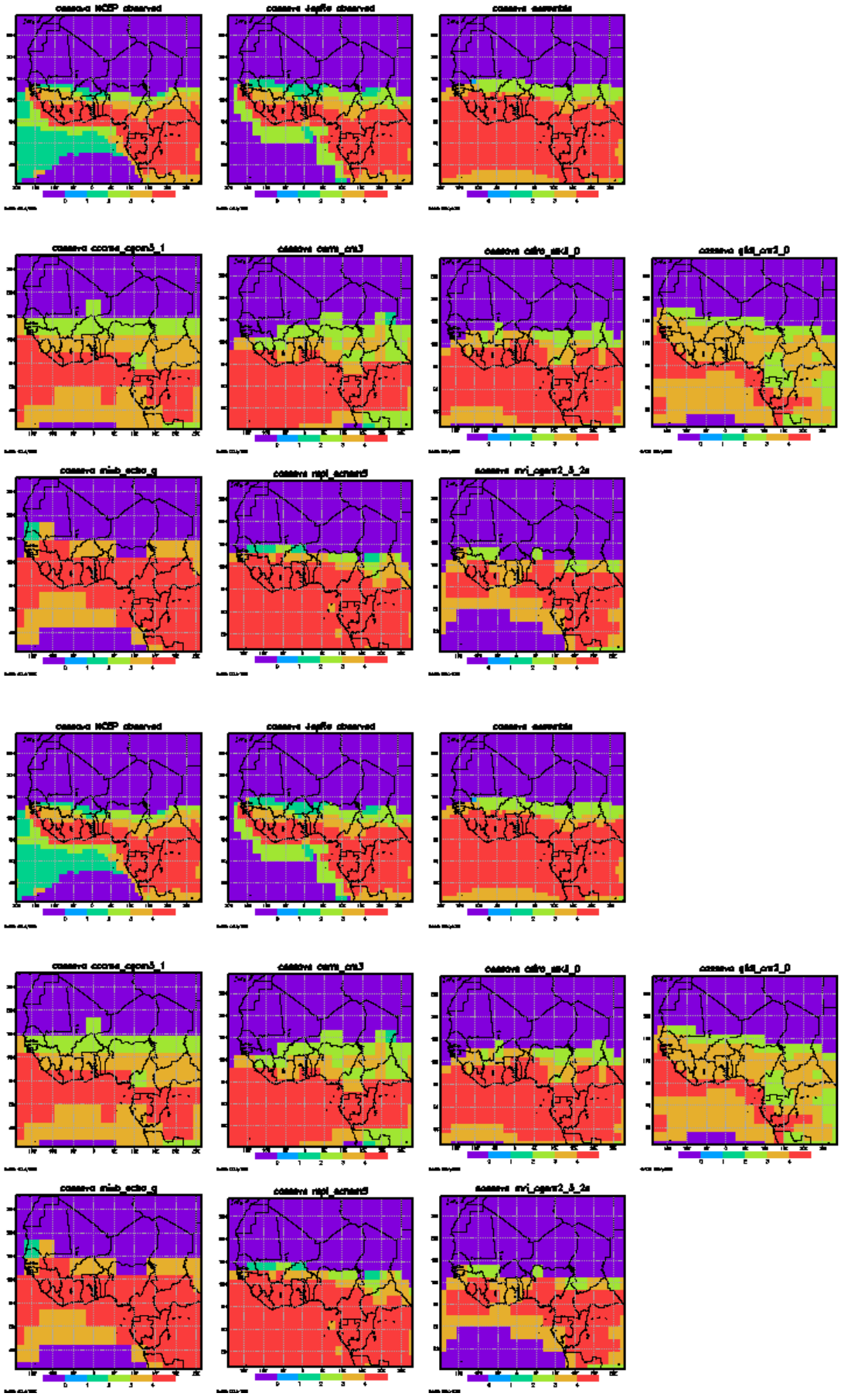
cassava NCEP observed
cassava Jaffe observed
cassava ensemble
cassava cccma_cgcm3_1
cassava csiro_mk3_0
cassava gfdl_cm2_0
cassava miub_echo_g
cassava mpi_echam5
cassava mri_cgcm2_3_2a
cassava NCEP observed
cassava Jaffe observed
cassava ensemble
cassava cccma_cgcm3_1
cassava csiro_mk3_0
cassava gfdl_cm2_0
cassava miub_echo_g
cassava mpi_echam5
cassava mri_cgcm2_3_2a

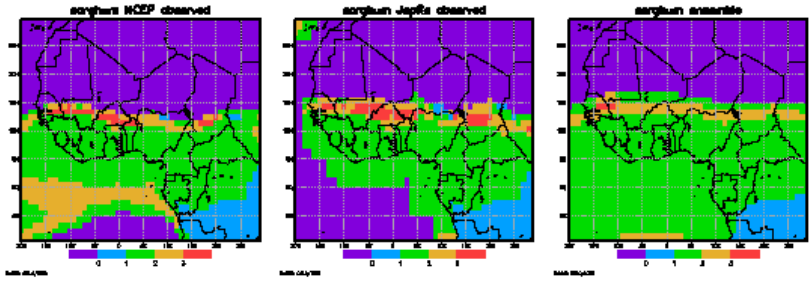
sorghum NCEP observed
sorghum Jagtap observed
sorghum ensemble

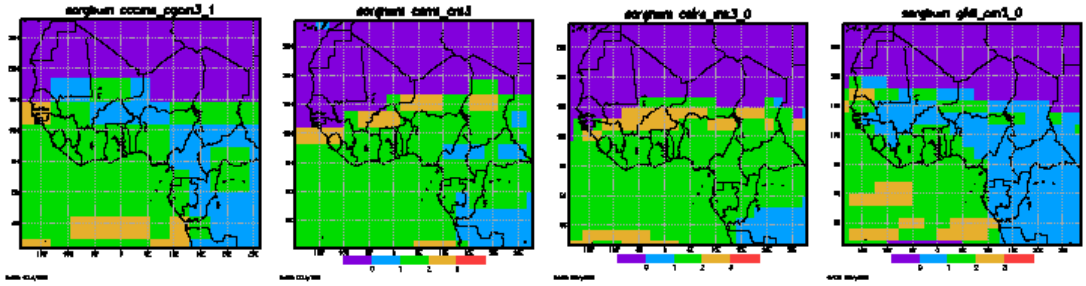
sorghum cccma_cgcm3_1
sorghum csiro_mk3_0
sorghum gfdl_cm2_0

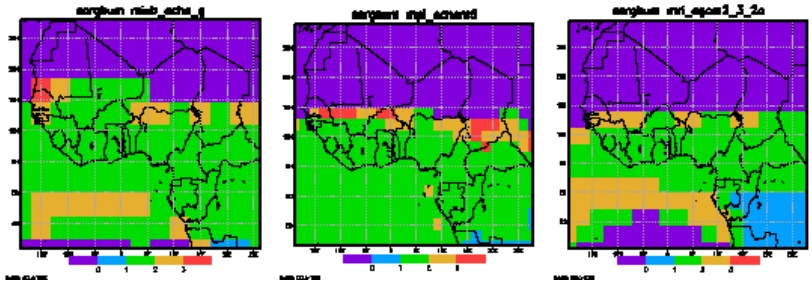
sorghum miub_echo_g
sorghum mri_cgcm2_3_2a

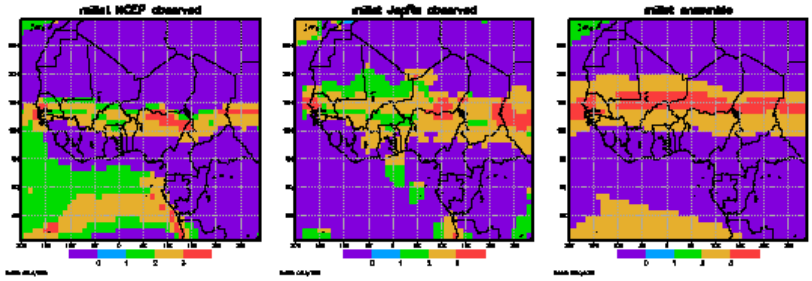
millet NCEP observed
millet Jagtap observed
millet ensemble

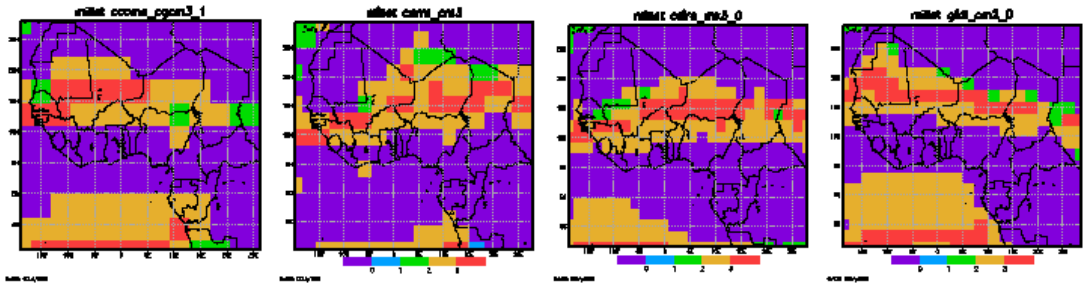
millet cccma_cgcm3_1
millet csiro_mk3_0
millet gfdl_cm2_0

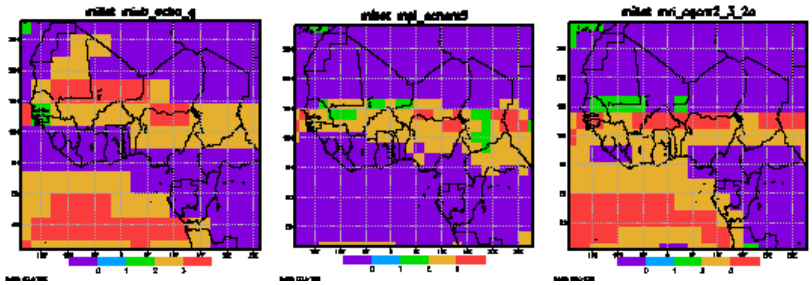
millet miub_echo_g
millet mri_cgcm2_3_2a

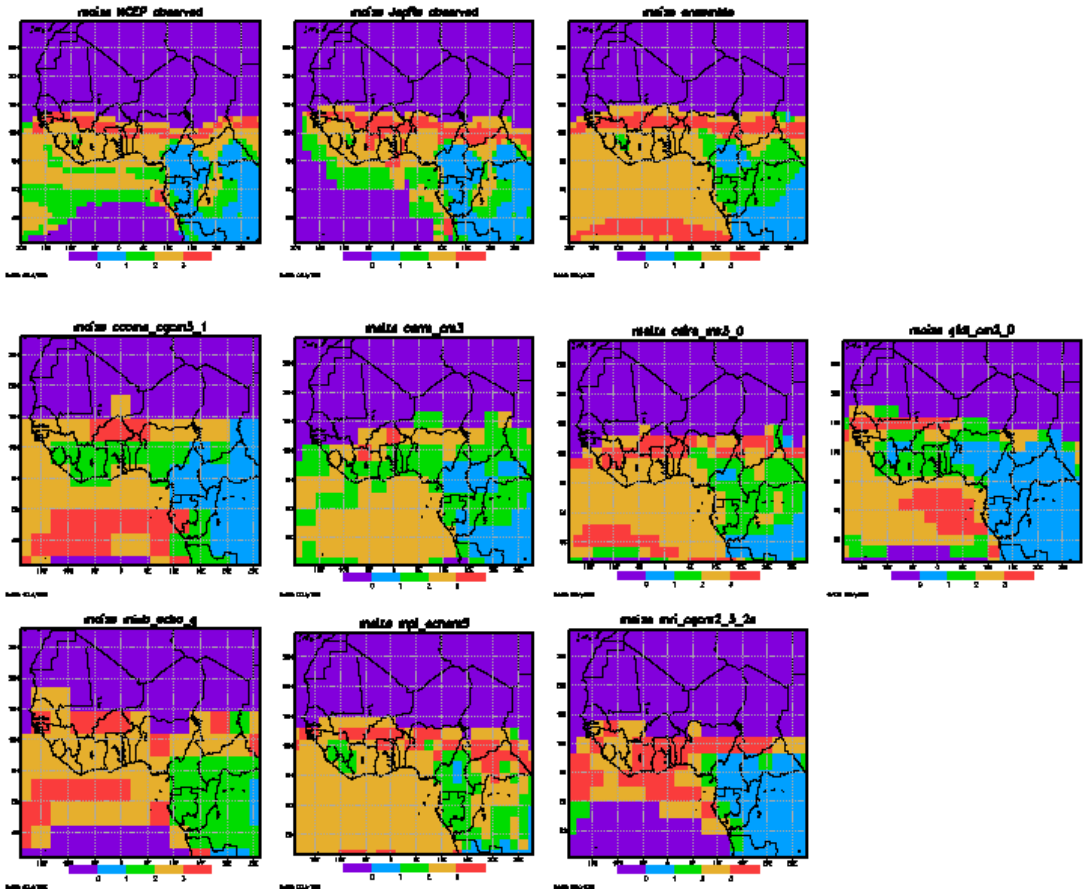
maize NCEP observed
maize Jagtap observed
maize ensemble
maize ccsm4_cgcm3_1
maize cam_cm3
maize cdfs_m3_0
maize gfdl_cm3_0
maize miub_echo_g
maize mpi_echam5
maize mri_cgcm2_3_2a

Appendix 7: Model derived growth domains from 20c3m experiments (1970-1999)

Cassava

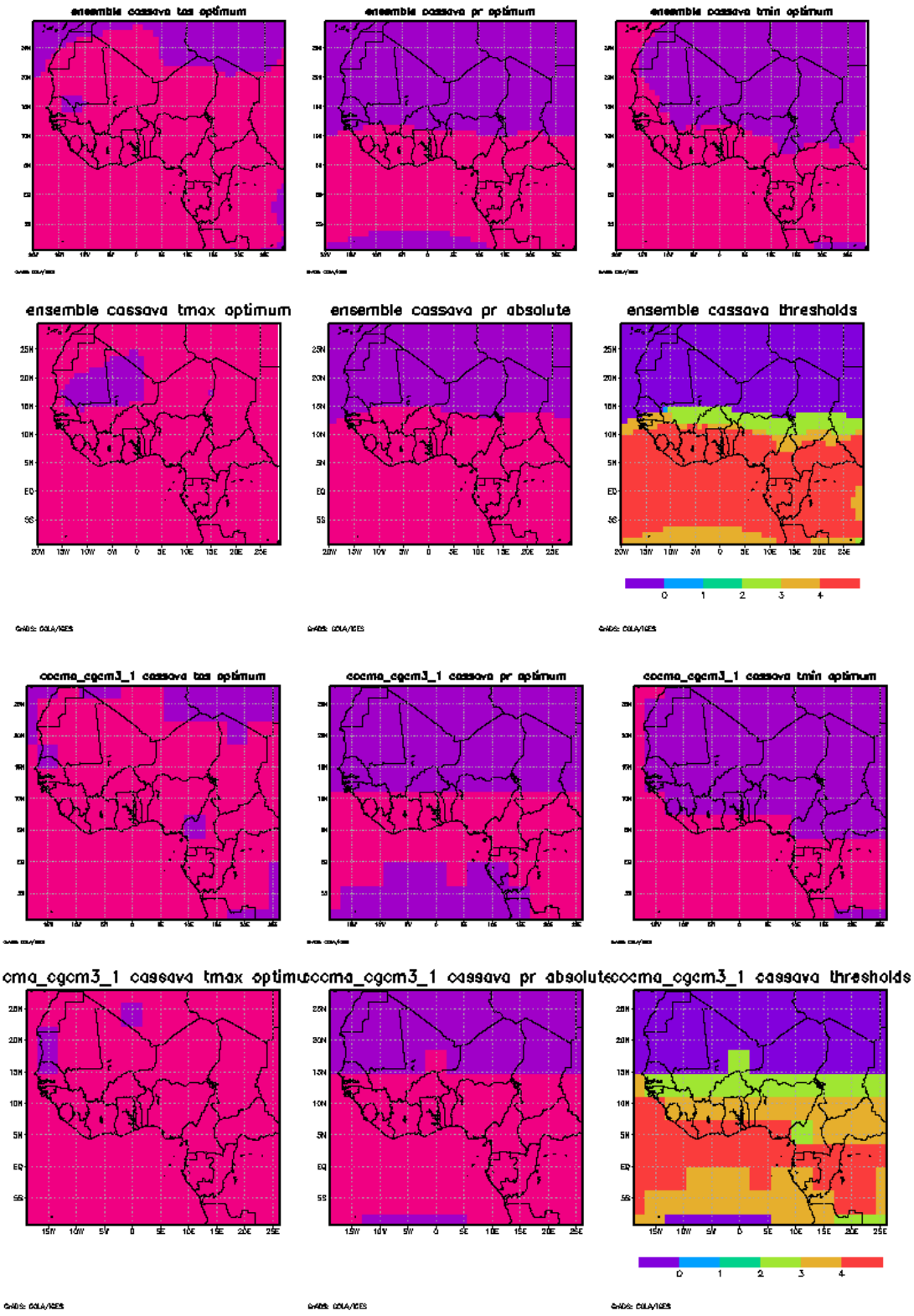

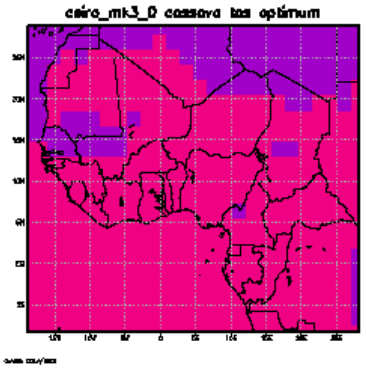
csiro_mk3_0 cassava tas optimum

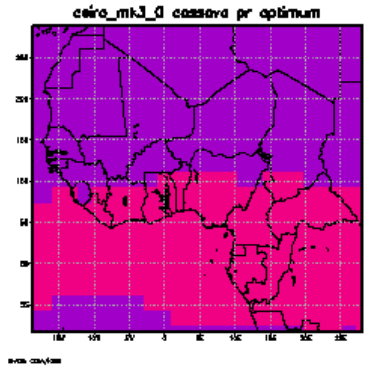
csiro_mk3_0 cassava pr optimum

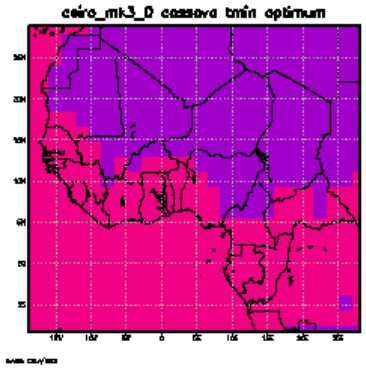
csiro_mk3_0 cassava tmin optimum

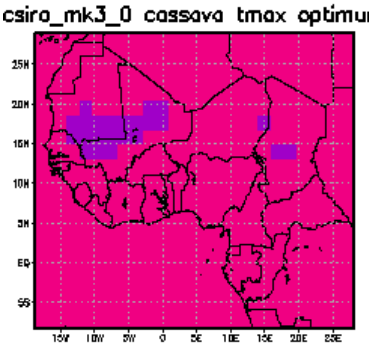
csiro_mk3_0 cassava tmax optimum

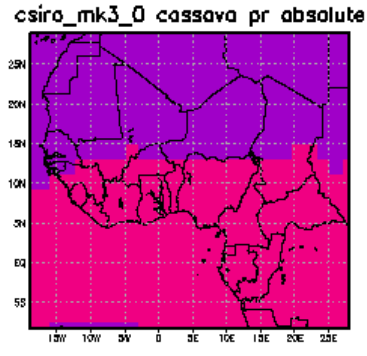
csiro_mk3_0 cassava pr absolute

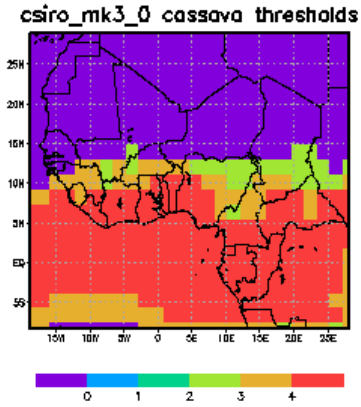
csiro_mk3_0 cassava thresholds
0
1
2
3
4

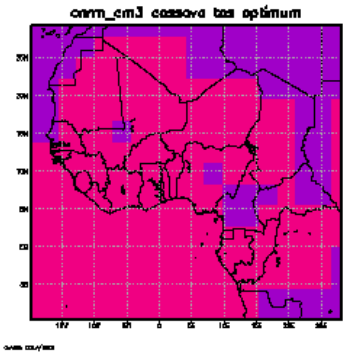
cnrm_cm3 cassava tas optimum

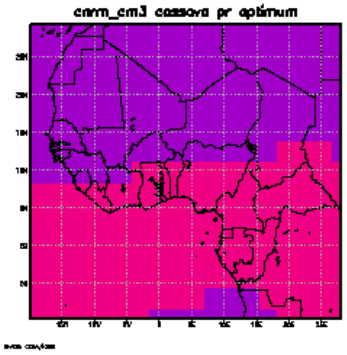
cnrm_cm3 cassava pr optimum

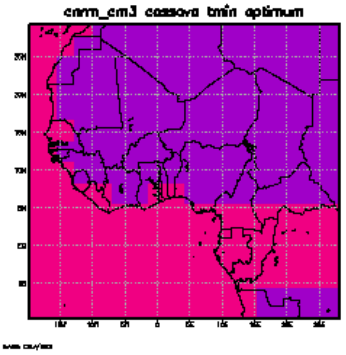
cnrm_cm3 cassava tmin optimum

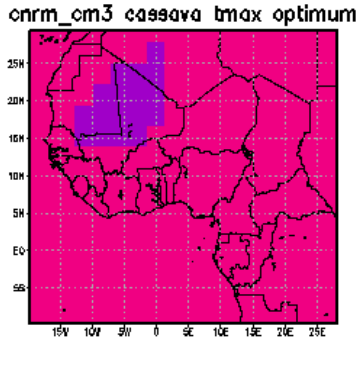
cnrm_cm3 cassava tmax optimum

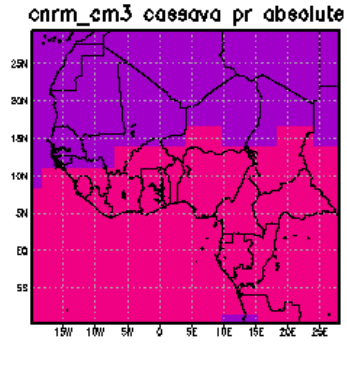
cnrm_cm3 cassava pr absolute

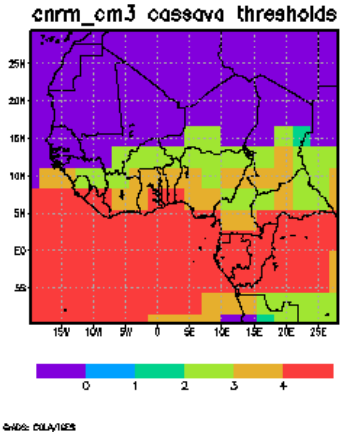
cnrm_cm3 cassava thresholds
0
1
2
3
4

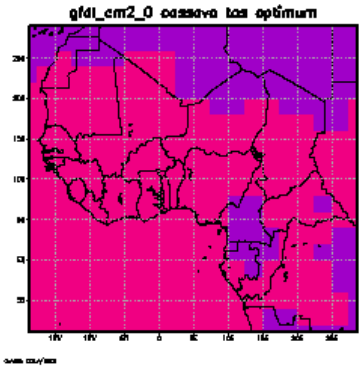
gfdl_cm2_0 cassava tas optimum

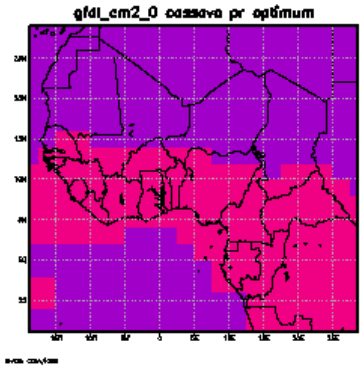
gfdl_cm2_0 cassava pr optimum

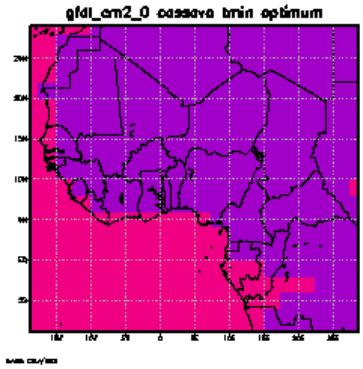
gfdl_cm2_0 cassava tmin optimum

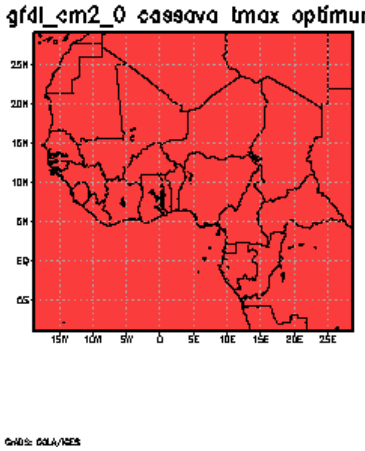
gfdl_cm2_0 cassava tmax optimum

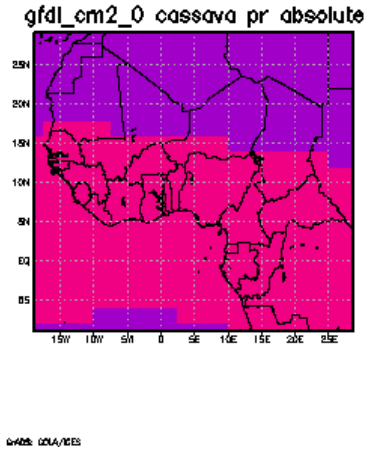
gfdl_cm2_0 cassava pr absolute

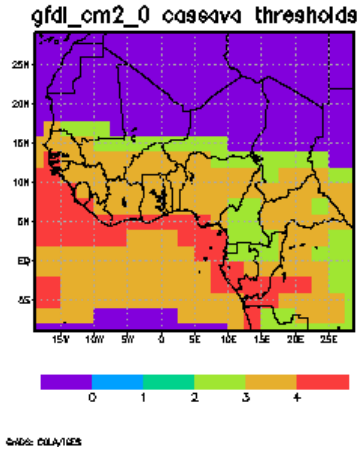
gfdl_cm2_0 cassava thresholds
0
1
2
3
4

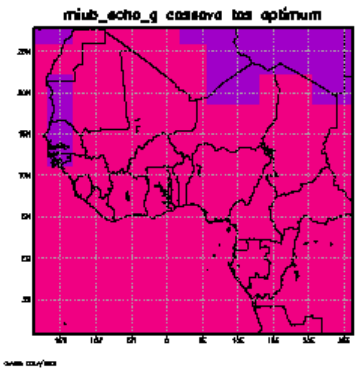
miub_echo_g cassava tas optimum

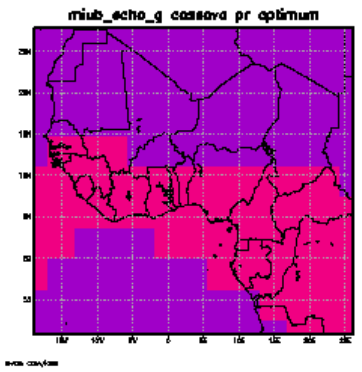
miub_echo_g cassava pr optimum

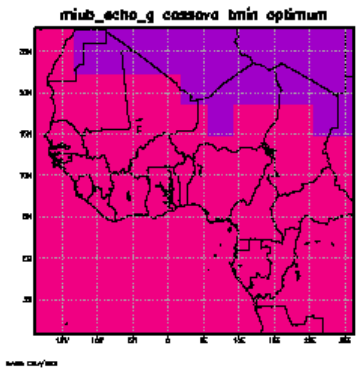
miub_echo_g cassava tmin optimum

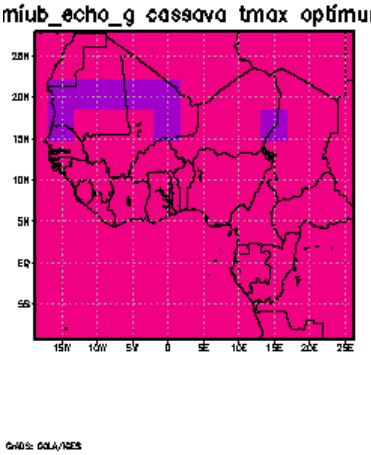
miub_echo_g cassava tmax optimum

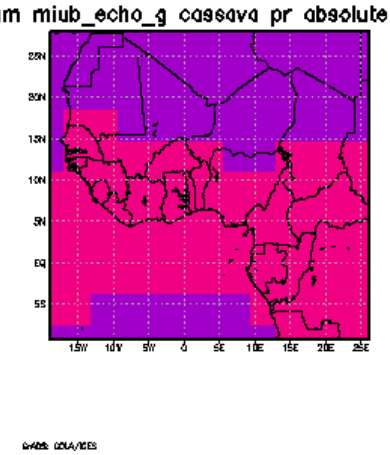
miub_echo_g cassava pr absolute

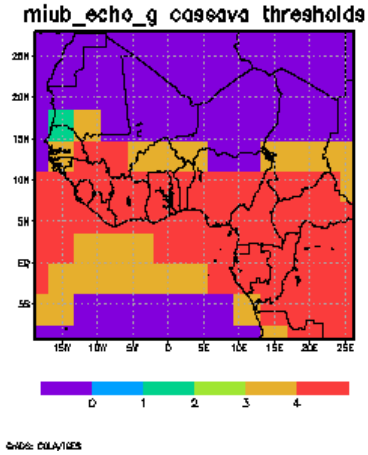
miub_echo_g cassava thresholds
0
1
2
3
4

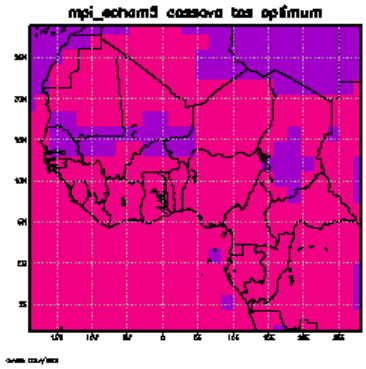
mpi_echam5 cassava tas optimum

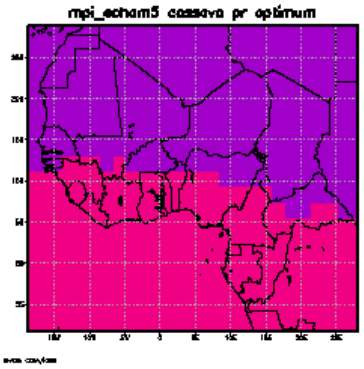
mpi_echam5 cassava pr optimum

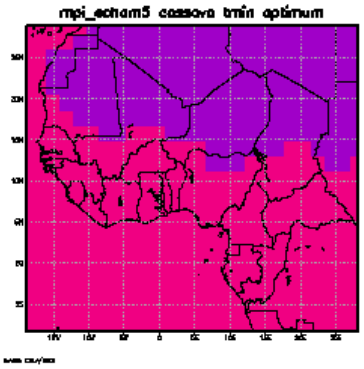
mpi_echam5 cassava tmin optimum

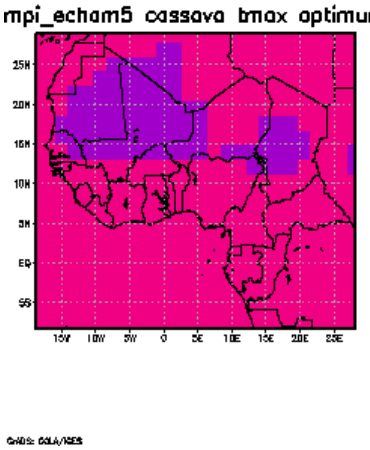
mpi_echam5 cassava tmax optimum

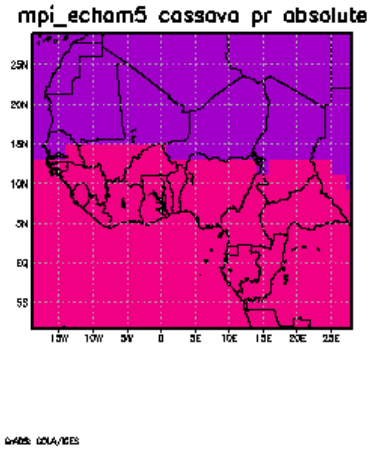
mpi_echam5 cassava pr absolute

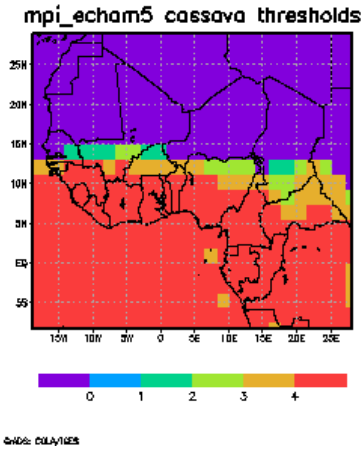
mpi_echam5 cassava thresholds

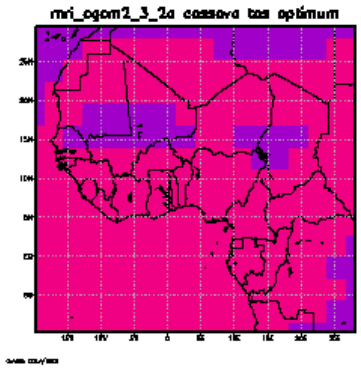
mri_cgcm2_3_2a cassava tas optimum

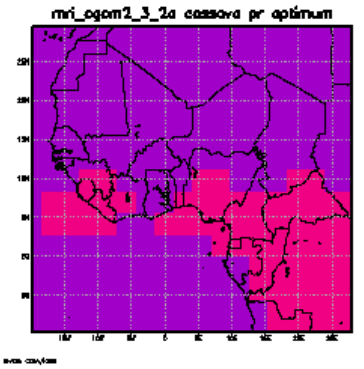
mri_cgcm2_3_2a cassava pr optimum

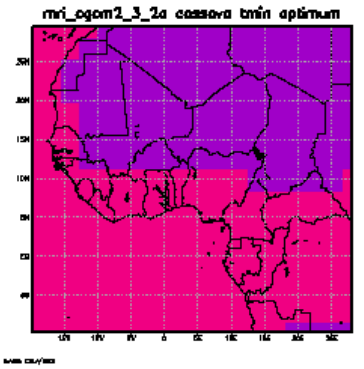
mri_cgcm2_3_2a cassava tmin optimum

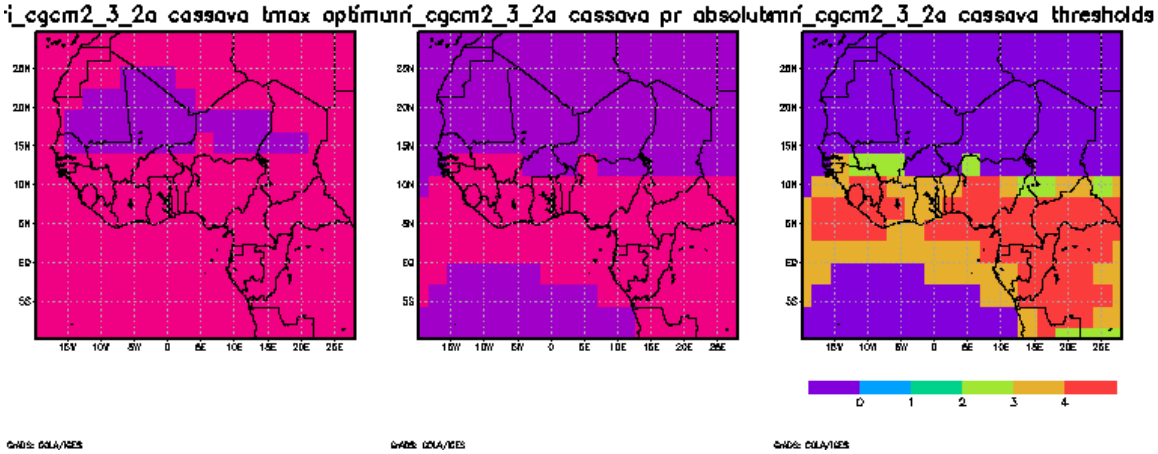
i_cgcm2_3_2a cassava tmax optimumri_cgcm2_3_2a cassava pr absolutemri_cgcm2_3_2a cassava thresholds

Cowpea

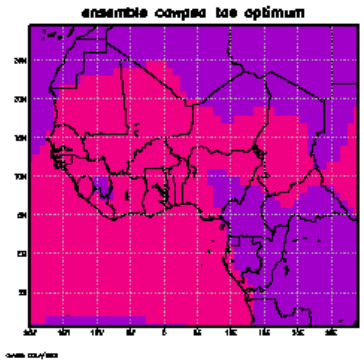
ensemble cowpea tas optimum

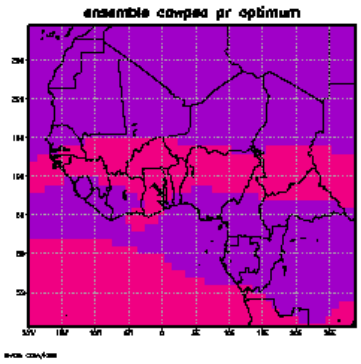
ensemble cowpea pr optimum

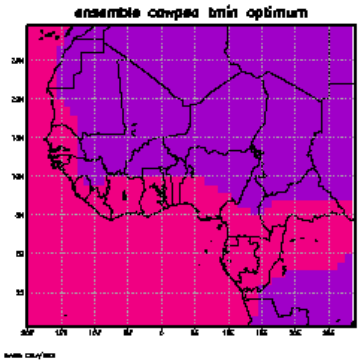
ensemble cowpea tmin optimum

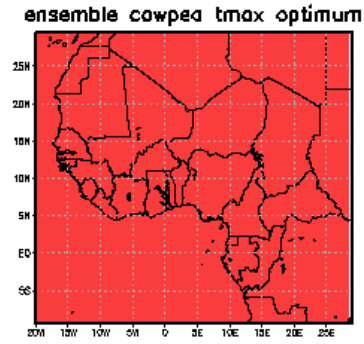
ensemble cowpea tmax optimum

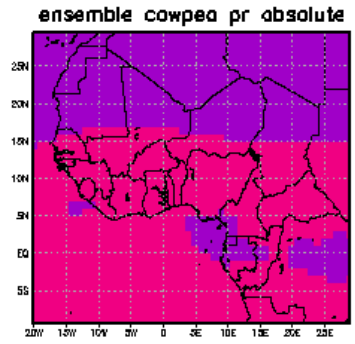
ensemble cowpea pr absolute

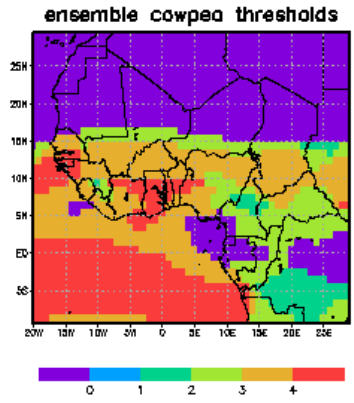
ensemble cowpea thresholds
0
1
2
3
4

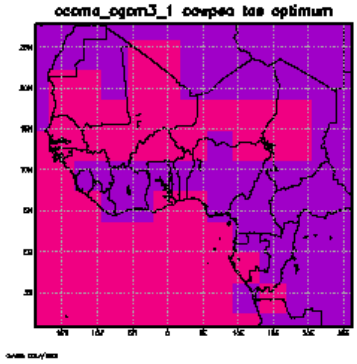
ccsm4_cgcm3_1 cowpea tas optimum

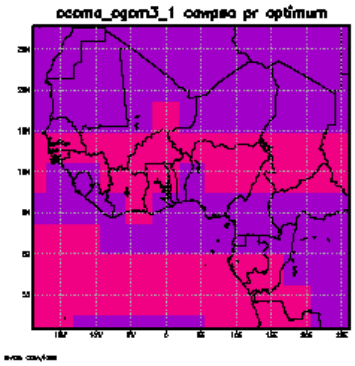
ccsm4_cgcm3_1 cowpea pr optimum

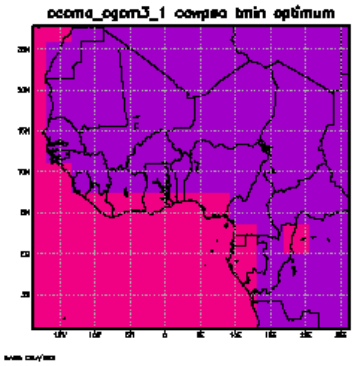
ccsm4_cgcm3_1 cowpea tmin optimum

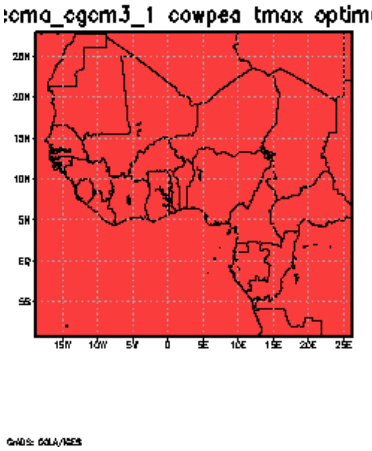
ccsm4_cgcm3_1 cowpea tmax optimum

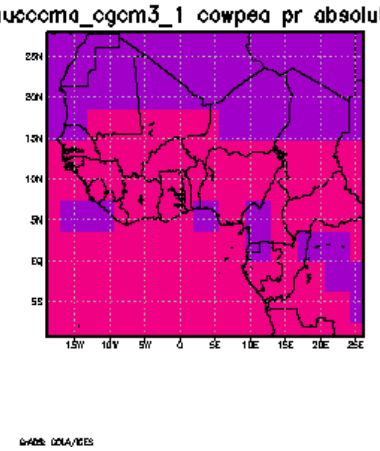
ccsm4_cgcm3_1 cowpea pr absolute

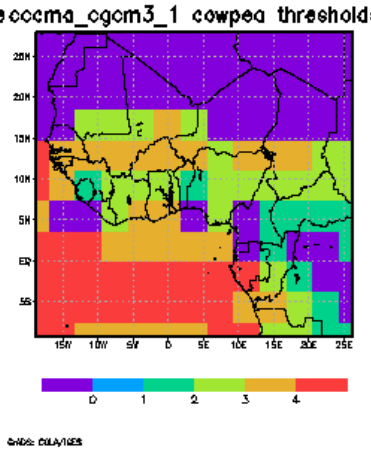
ccsm4_cgcm3_1 cowpea thresholds
0
1
2
3
4

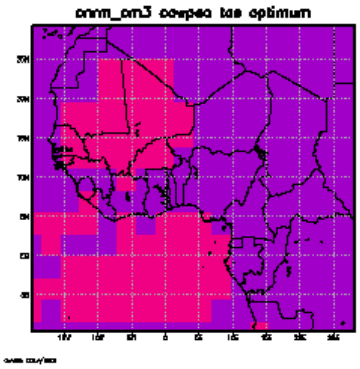
cnrm_cm3 cowpea tas optimum

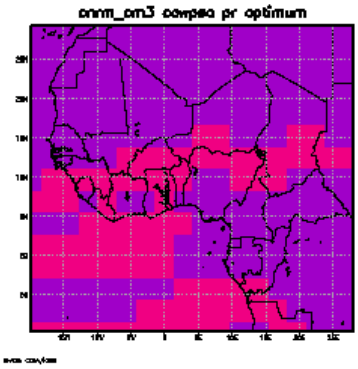
cnrm_cm3 cowpea pr optimum

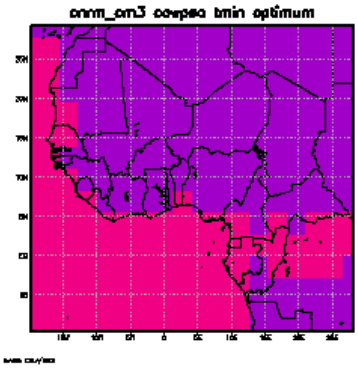
cnrm_cm3 cowpea tmin optimum

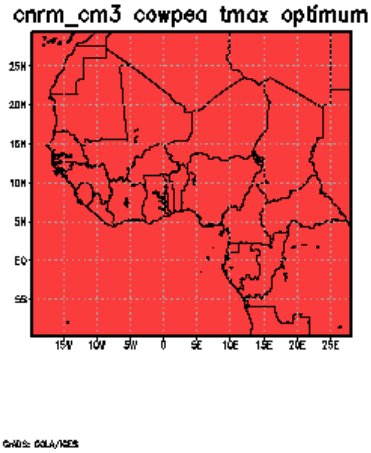
cnrm_cm3 cowpea tmax optimum

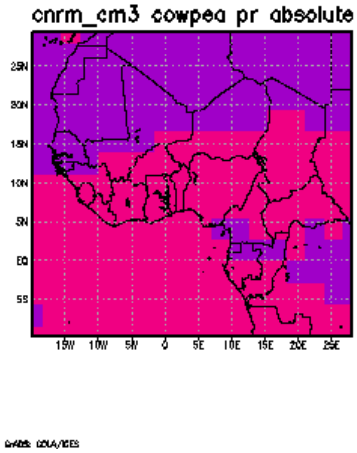
cnrm_cm3 cowpea pr absolute

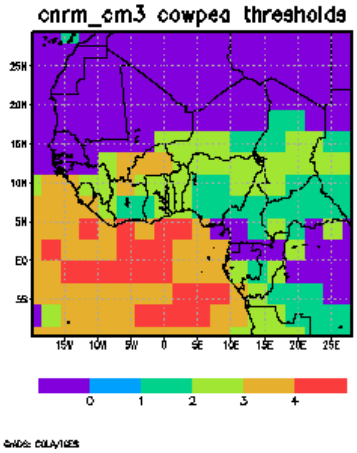
cnrm_cm3 cowpea thresholds
0
1
2
3
4

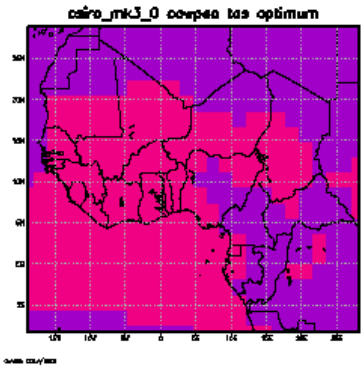
csiro_mk3_0 cowpea tas optimum

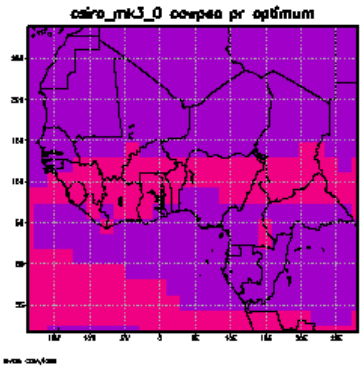
csiro_mk3_0 cowpea pr optimum

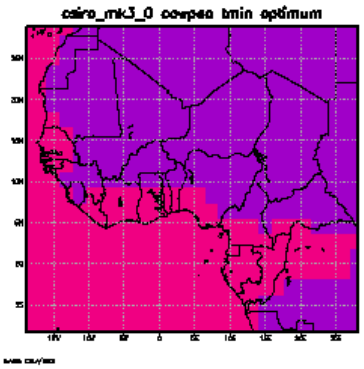
csiro_mk3_0 cowpea tmin optimum

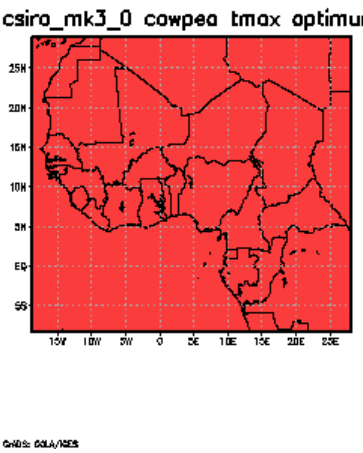
csiro_mk3_0 cowpea tmax optimum

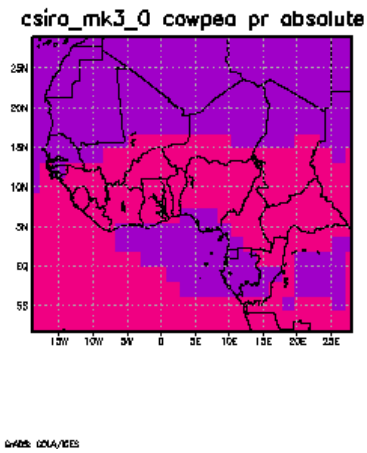
csiro_mk3_0 cowpea pr absolute

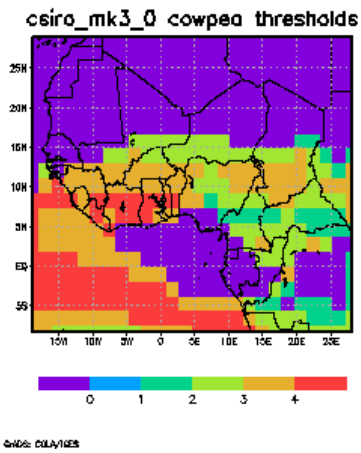
csiro_mk3_0 cowpea thresholds
0
1
2
3
4

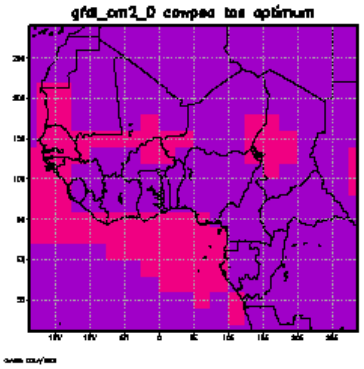
gfdl_cm2_0 cowpea tas optimum

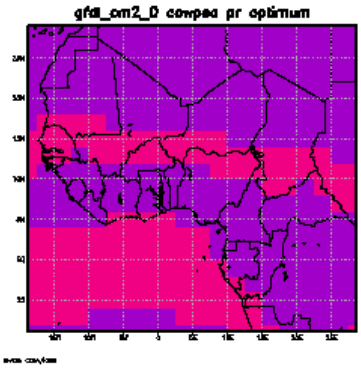
gfdl_cm2_0 cowpea pr optimum

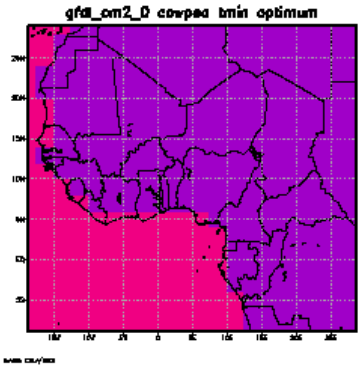
gfdl_cm2_0 cowpea tmin optimum

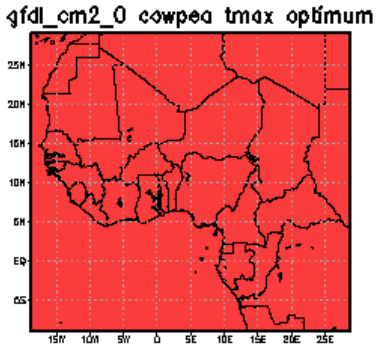
gfdl_cm2_0 cowpea tmax optimum

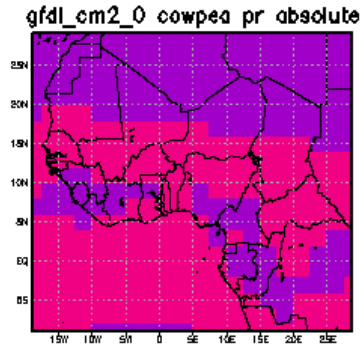
gfdl_cm2_0 cowpea pr absolute

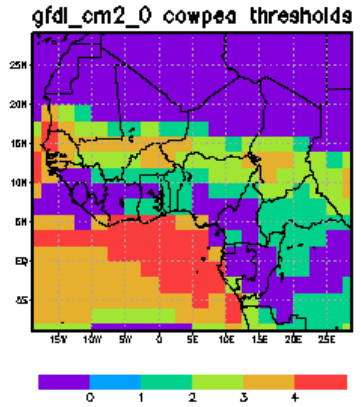
gfdl_cm2_0 cowpea thresholds
0
1
2
3
4

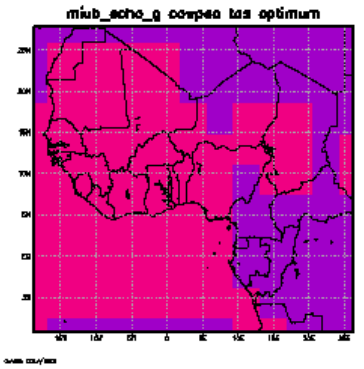
miub_echo_g cowpea tas optimum

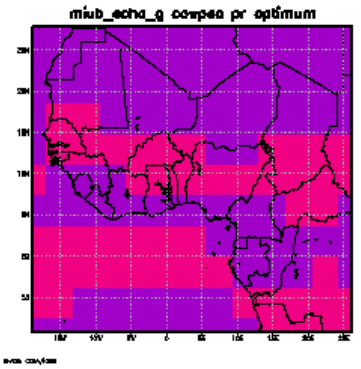
miub_echo_g cowpea pr optimum

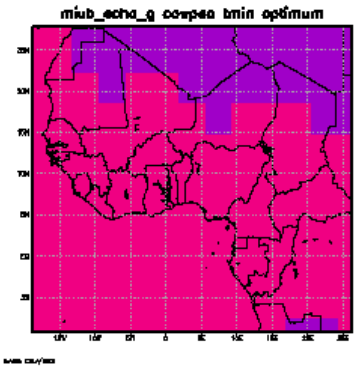
miub_echo_g cowpea tmin optimum

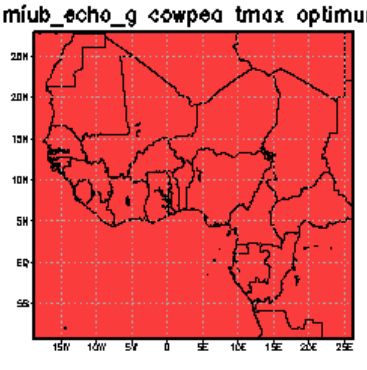
miub_echo_g cowpea tmax optimum

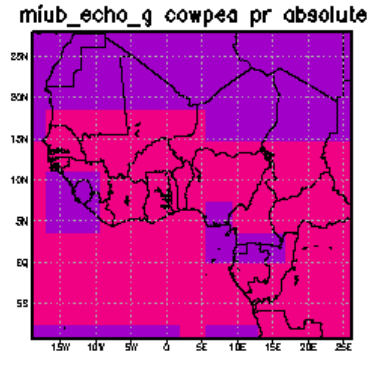
miub_echo_g cowpea pr absolute

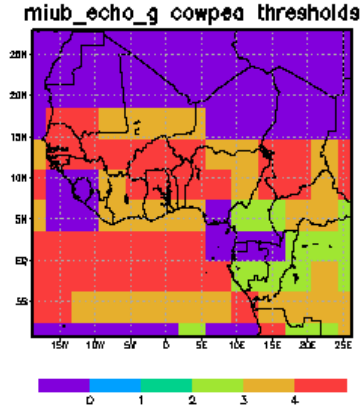
miub_echo_g cowpea thresholds
0
1
2
3
4

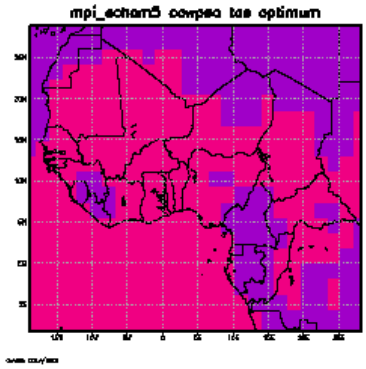
mpi_echam5 cowpea tas optimum

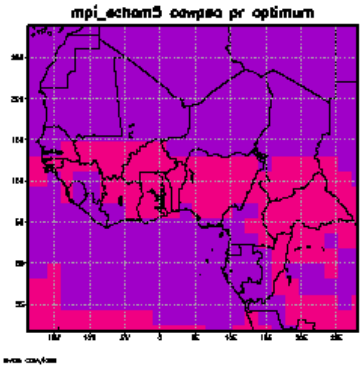
mpi_echam5 cowpea pr optimum

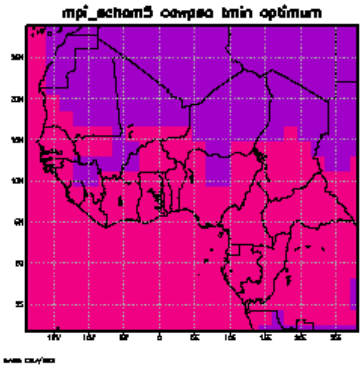
mpi_echam5 cowpea tmin optimum

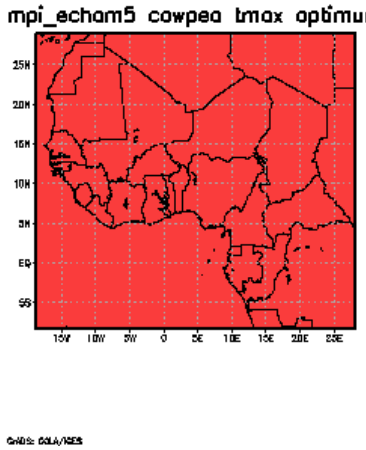
mpi_echam5 cowpea tmax optimum

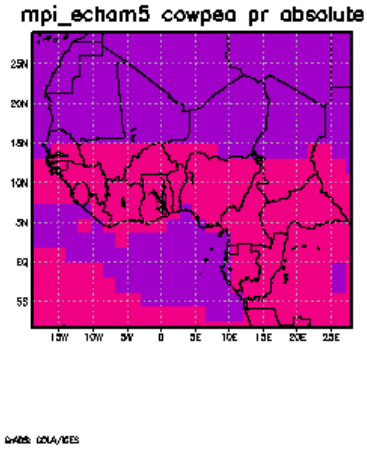
mpi_echam5 cowpea pr absolute

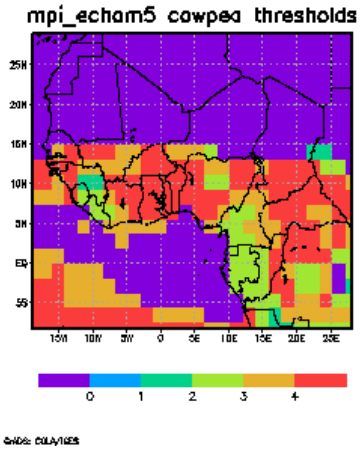
mpi_echam5 cowpea thresholds
0
1
2
3
4

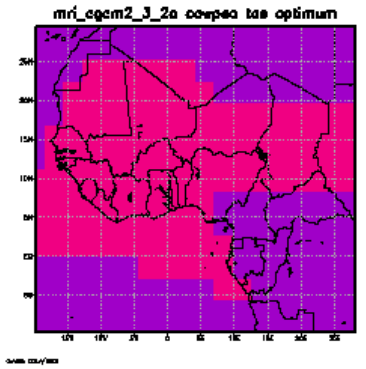
mri_cgcm2_3_2a cowpea tas optimum

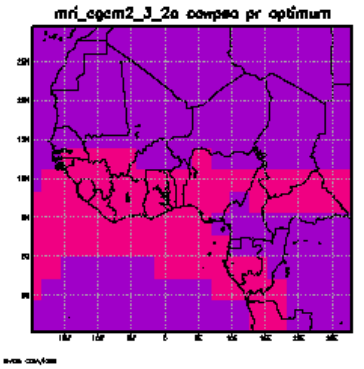
mri_cgcm2_3_2a cowpea pr optimum

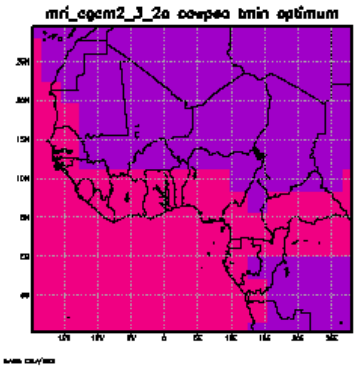
mri_cgcm2_3_2a cowpea tmin optimum

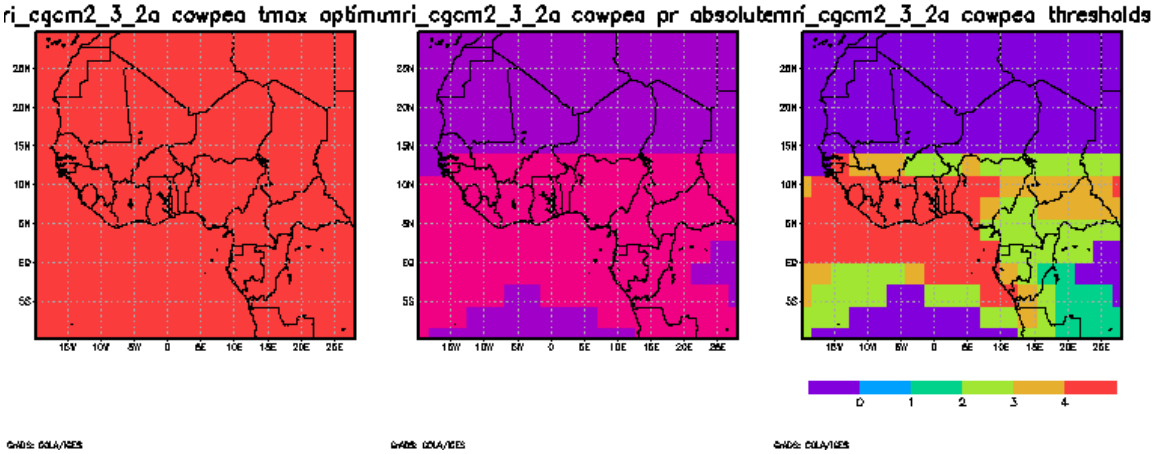
ri_cgcm2_3_2a cowpea tmax optimum
ri_cgcm2_3_2a cowpea pr absolute
mri_cgcm2_3_2a cowpea thresholds
0
1
2
3
4

Rice

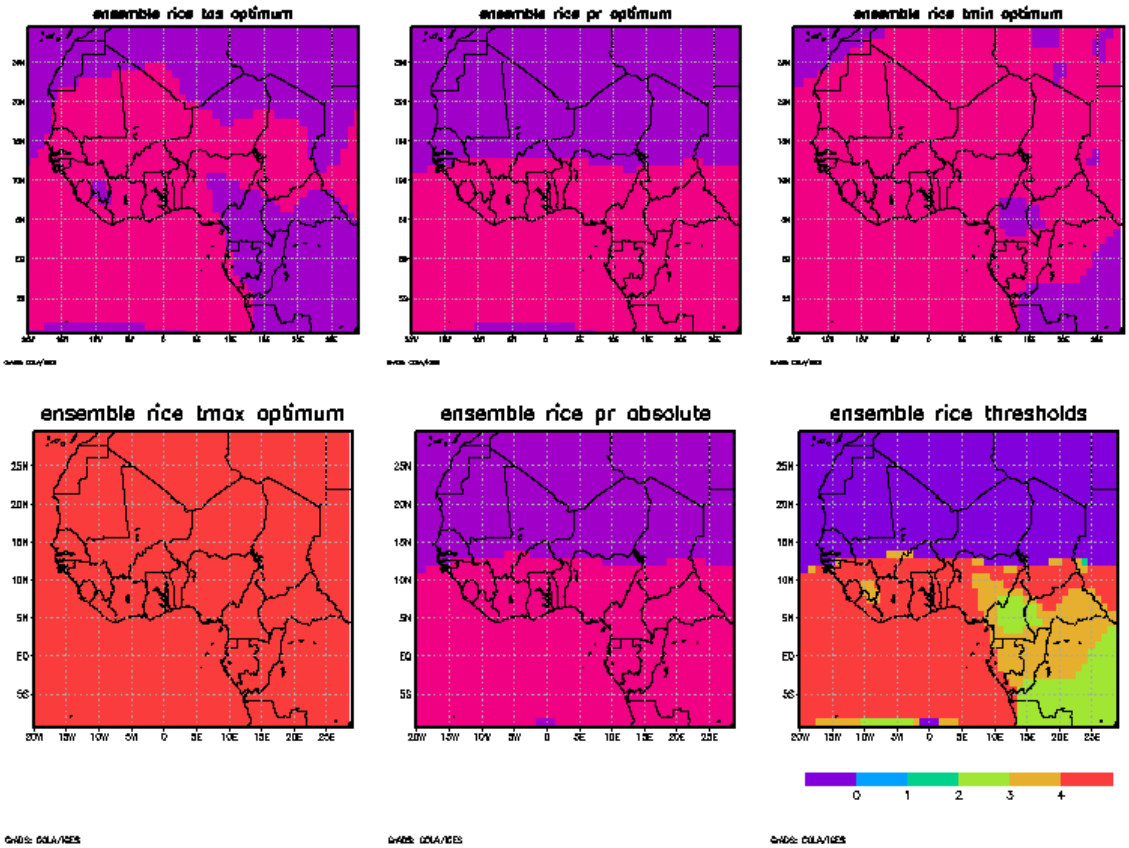
ensemble rice tas optimum
ensemble rice pr optimum
ensemble rice tmin optimum
ensemble rice tmax optimum
ensemble rice pr absolute
ensemble rice thresholds
0
1
2
3
4

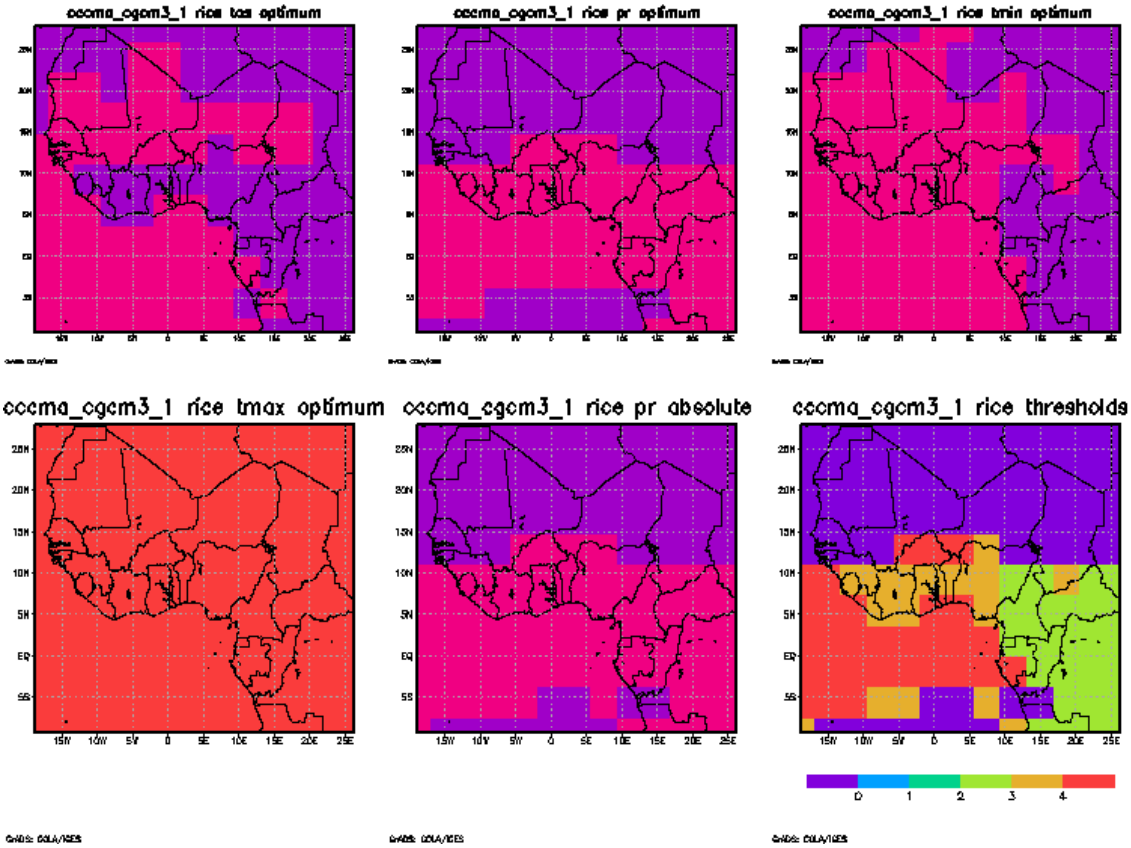
cccma_cgcm3_1 rice tas optimum
cccma_cgcm3_1 rice pr optimum
cccma_cgcm3_1 rice tmin optimum
cccma_cgcm3_1 rice tmax optimum
cccma_cgcm3_1 rice pr absolute
cccma_cgcm3_1 rice thresholds
0
1
2
3
4

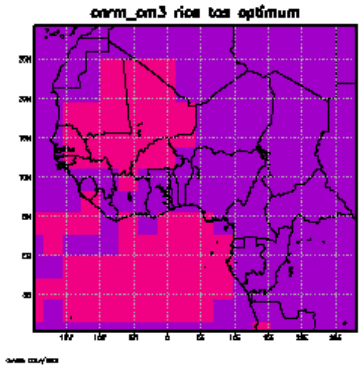
cnrm_cm3 rice tas optimum

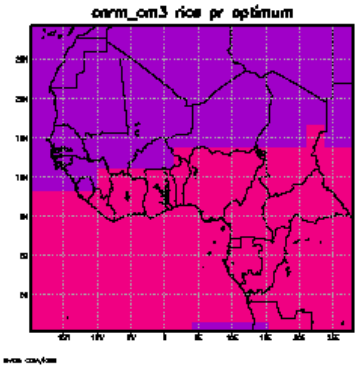
cnrm_cm3 rice pr optimum

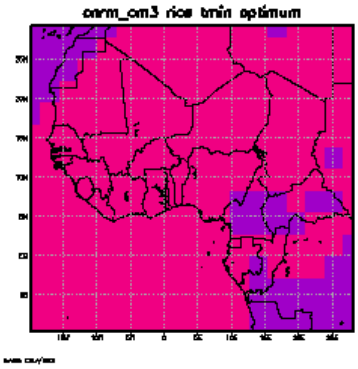
cnrm_cm3 rice tmin optimum

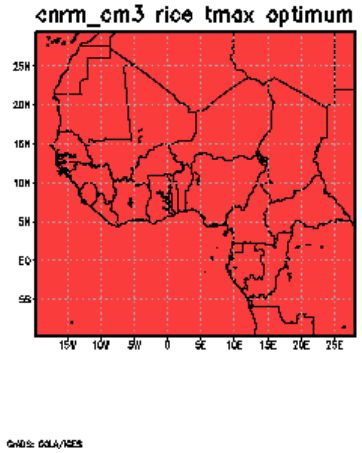
cnrm_cm3 rice tmax optimum

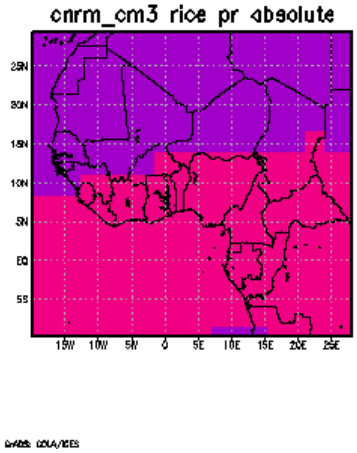
cnrm_cm3 rice pr absolute

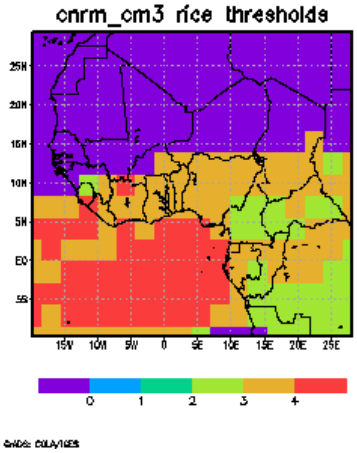
cnrm_cm3 rice thresholds

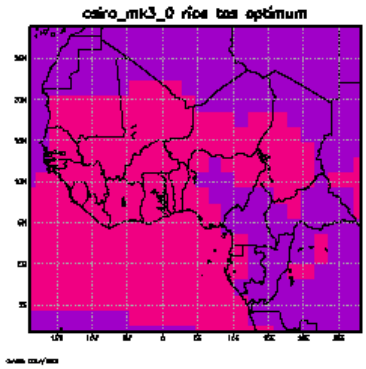
csiro_mk3_0 rice tas optimum

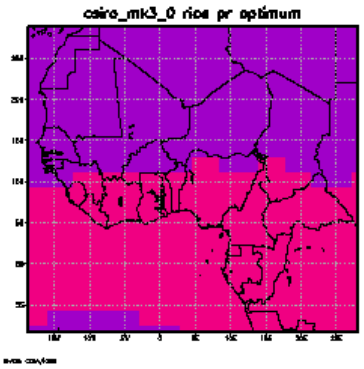
csiro_mk3_0 rice pr optimum

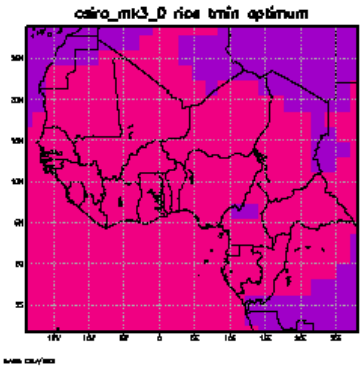
csiro_mk3_0 rice tmin optimum

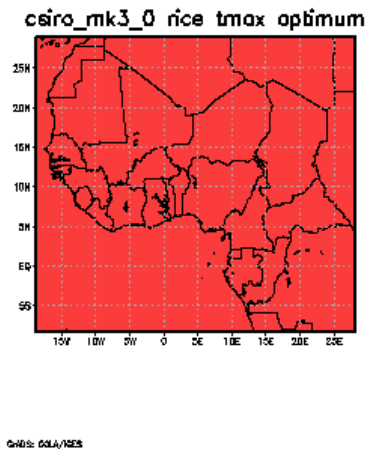
csiro_mk3_0 rice tmax optimum

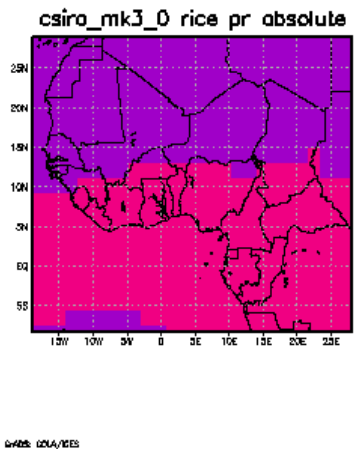
csiro_mk3_0 rice pr absolute

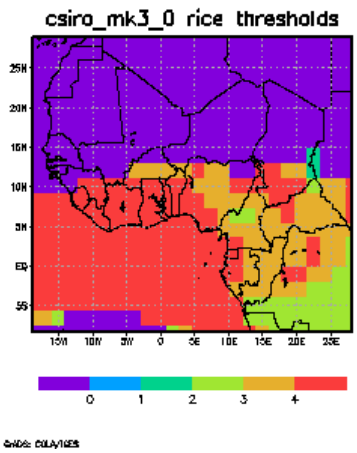
csiro_mk3_0 rice thresholds

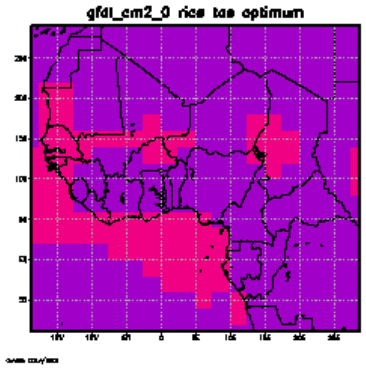
gfdl_cm2_0 rice tas optimum

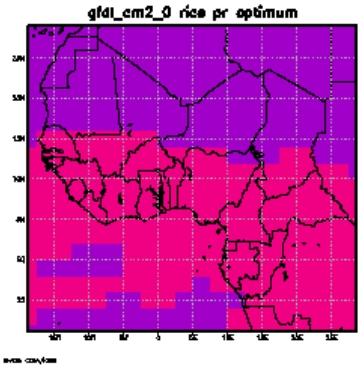
gfdl_cm2_0 rice pr optimum

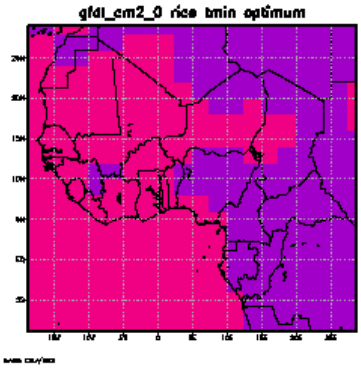
gfdl_cm2_0 rice tmin optimum

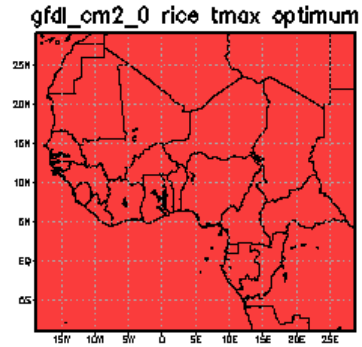
gfdl_cm2_0 rice tmax optimum

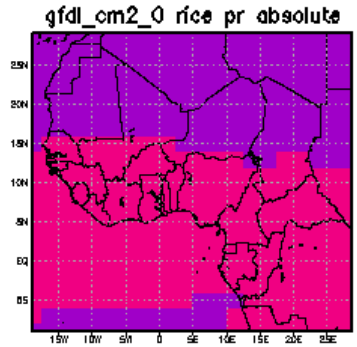
gfdl_cm2_0 rice pr absolute

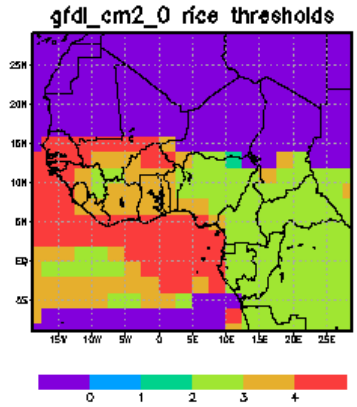
gfdl_cm2_0 rice thresholds
0
1
2
3
4

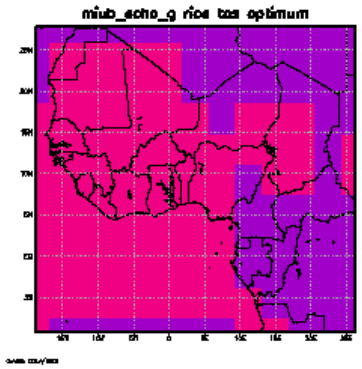
miub_echo_g rice tas optimum

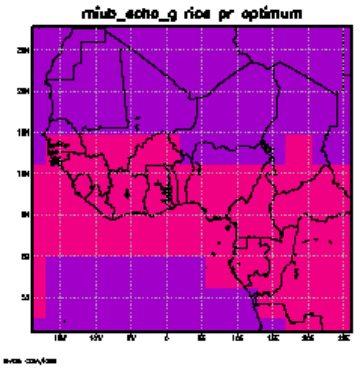
miub_echo_g rice pr optimum

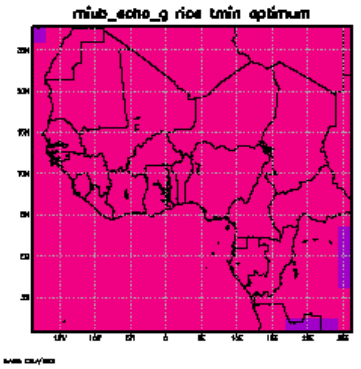
miub_echo_g rice tmin optimum

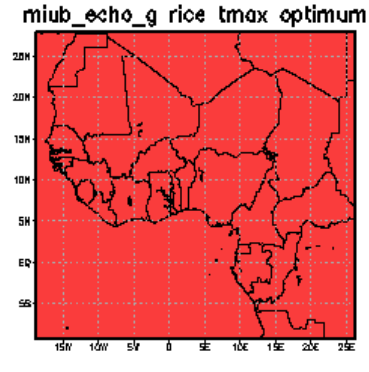
miub_echo_g rice tmax optimum

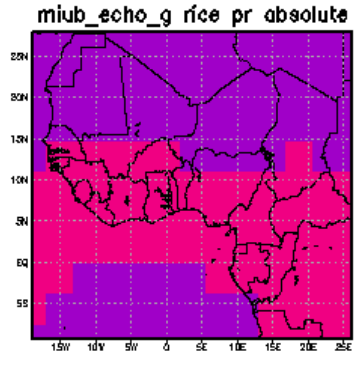
miub_echo_g rice pr absolute

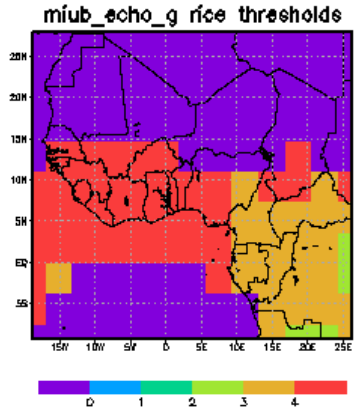
miub_echo_g rice thresholds
0
1
2
3
4

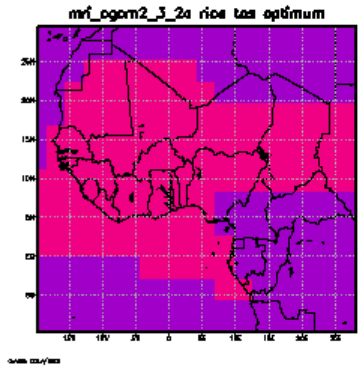
mri_cgcm2_3_2a rice tas optimum

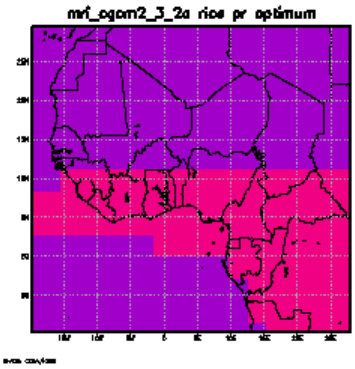
mri_cgcm2_3_2a rice pr optimum

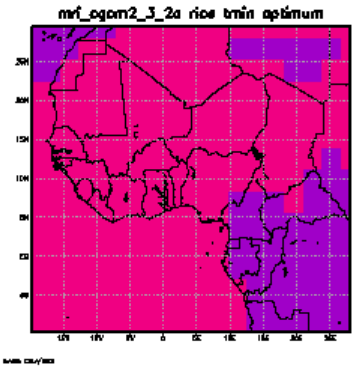
mri_cgcm2_3_2a rice tmin optimum

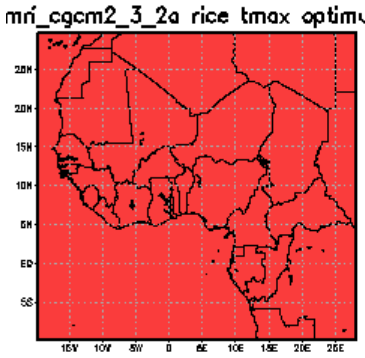
mri_cgcm2_3_2a rice tmax optimum

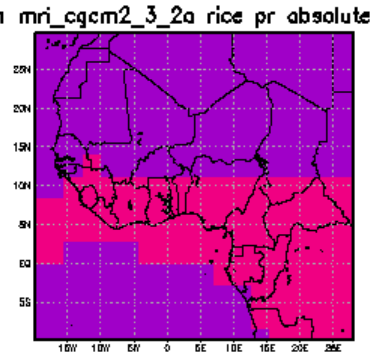
mri_cgcm2_3_2a rice pr absolute

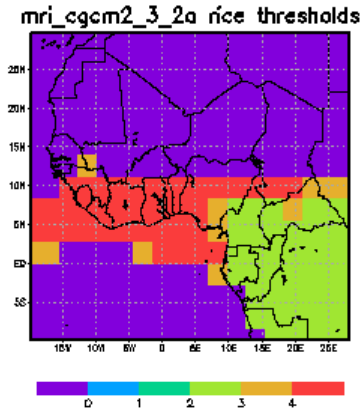
mri_cgcm2_3_2a rice thresholds
0
1
2
3
4

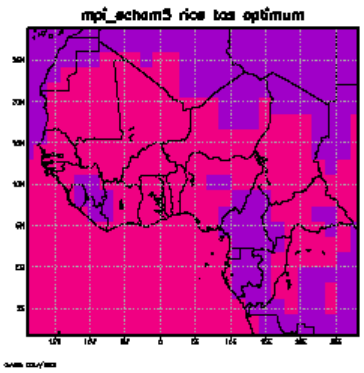
mpi_echam5 rice tas optimum

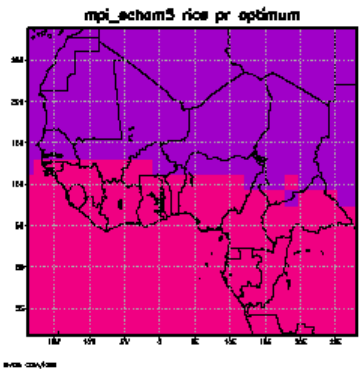
mpi_echam5 rice pr optimum

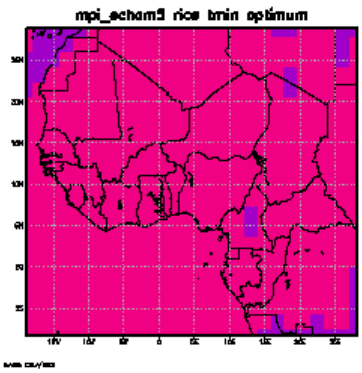
mpi_echam5 rice tmin optimum

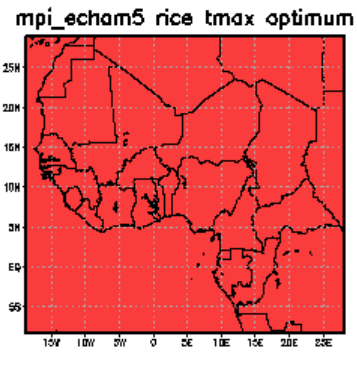
mpi_echam5 rice tmax optimum

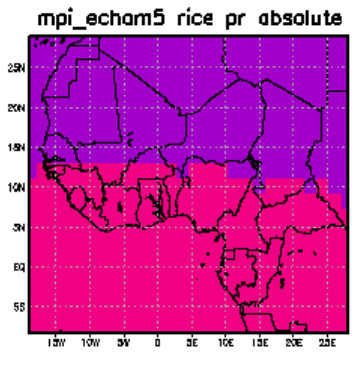
mpi_echam5 rice pr absolute

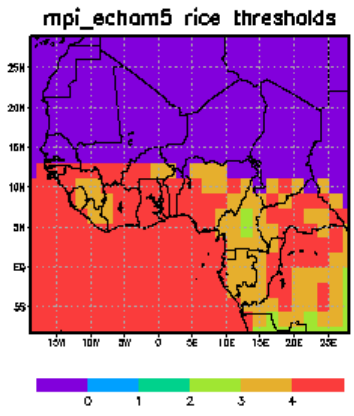
mpi_echam5 rice thresholds
0
1
2
3
4

Sorghum

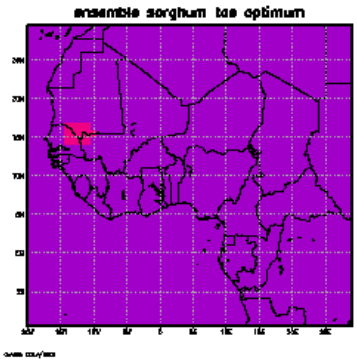
ensemble sorghum tas optimum

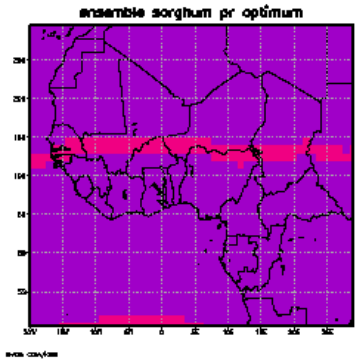
ensemble sorghum pr optimum

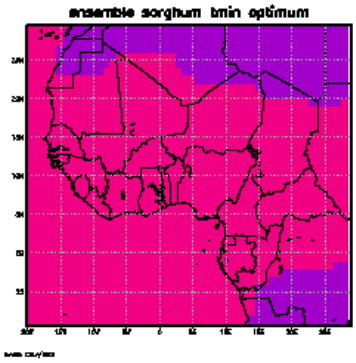
ensemble sorghum tmin optimum

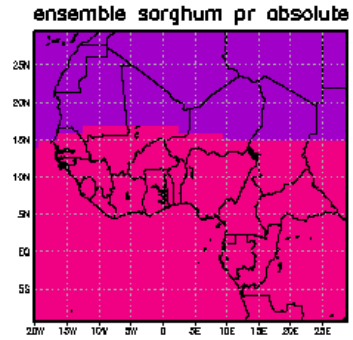
ensemble sorghum pr absolute

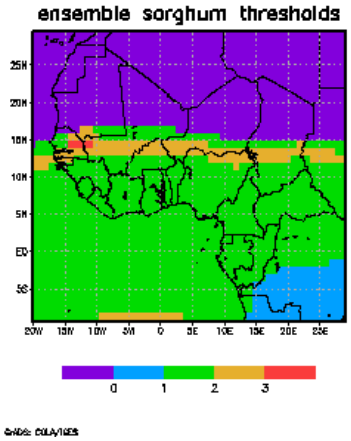
ensemble sorghum thresholds
0
1
2
3

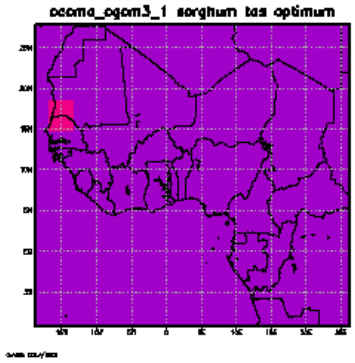
ccsm4_cgcm3_1 sorghum tas optimum

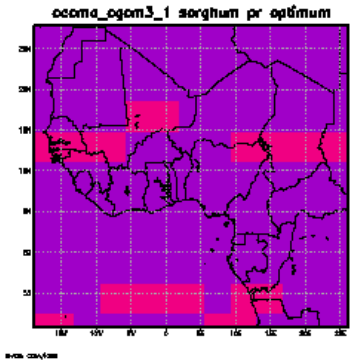
ccsm4_cgcm3_1 sorghum pr optimum

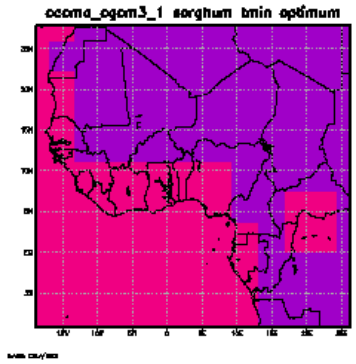
ccsm4_cgcm3_1 sorghum tmin optimum

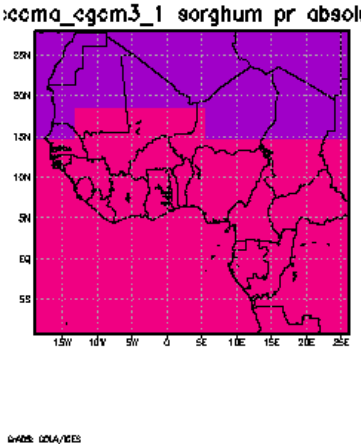
ccsm4_cgcm3_1 sorghum pr absolute

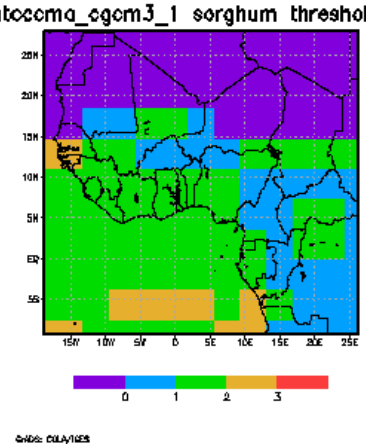
ccsm4_cgcm3_1 sorghum thresholds
0
1
2
3

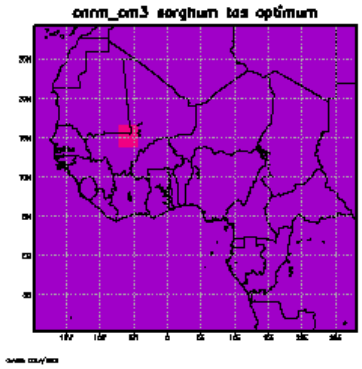
cnrm_cm3 sorghum tas optimum

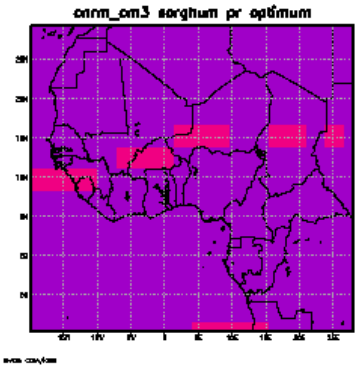
cnrm_cm3 sorghum pr optimum

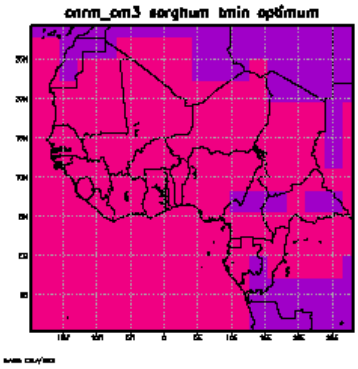
cnrm_cm3 sorghum tmin optimum

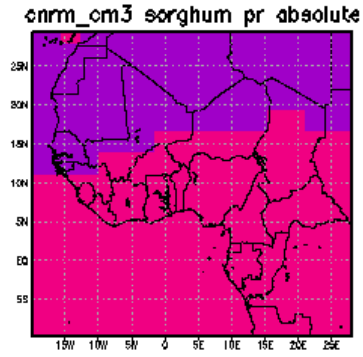
cnrm_cm3 sorghum pr absolute

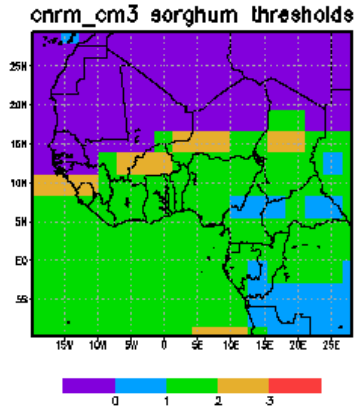
cnrm_cm3 sorghum thresholds
0
1
2
3

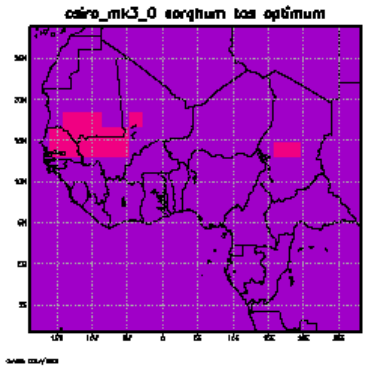
csiro_mk3_0 sorghum tas optimum

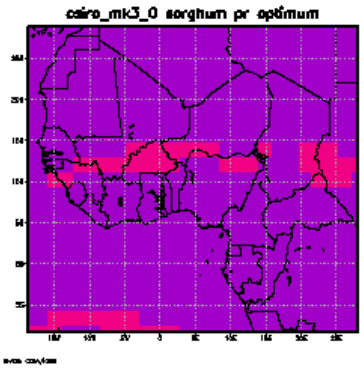
csiro_mk3_0 sorghum pr optimum

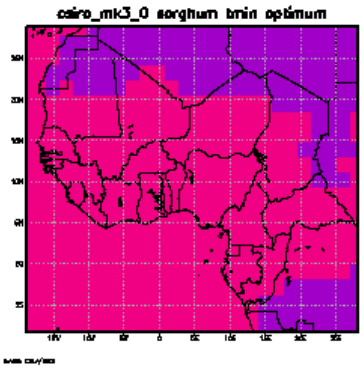
csiro_mk3_0 sorghum tmin optimum

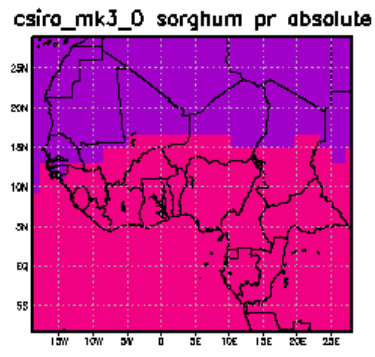
csiro_mk3_0 sorghum pr absolute

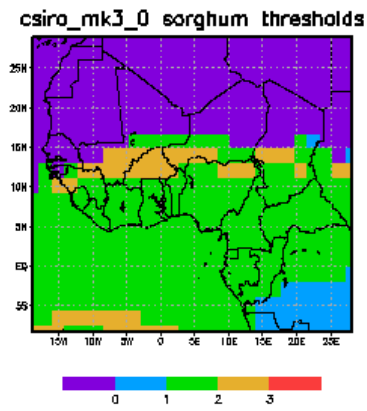
csiro_mk3_0 sorghum thresholds
0
1
2
3

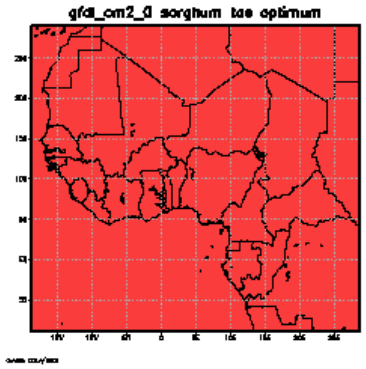
gfdl_cm2_0 sorghum tas optimum

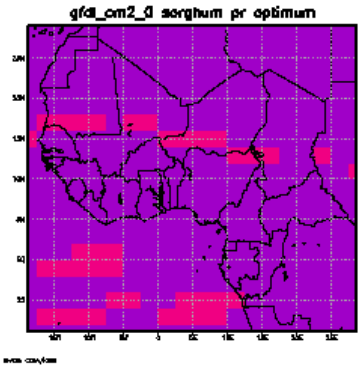
gfdl_cm2_0 sorghum pr optimum

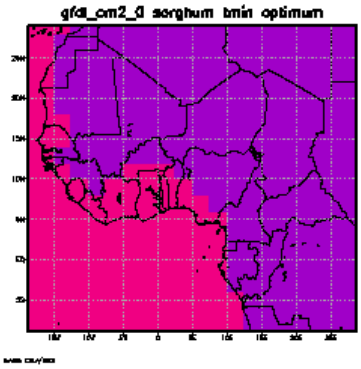
gfdl_cm2_0 sorghum tmin optimum

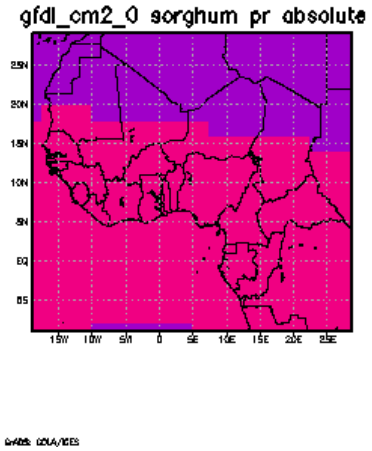
gfdl_cm2_0 sorghum pr absolute

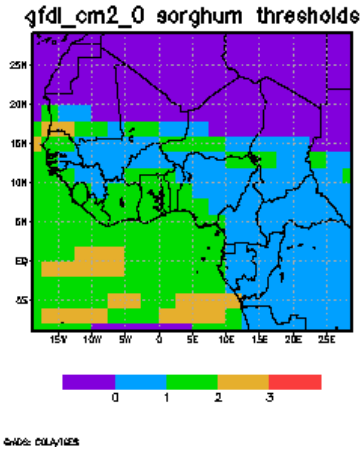
gfdl_cm2_0 sorghum thresholds
0
1
2
3

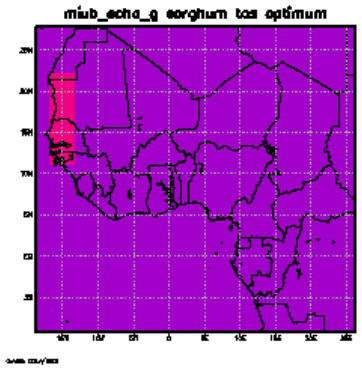
miub_echo_g sorghum tas optimum

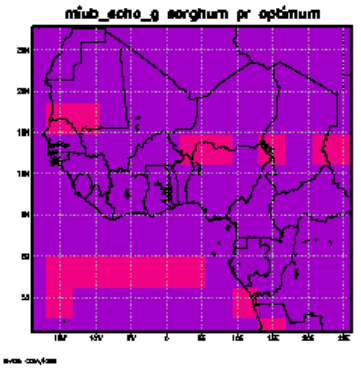
miub_echo_g sorghum pr optimum

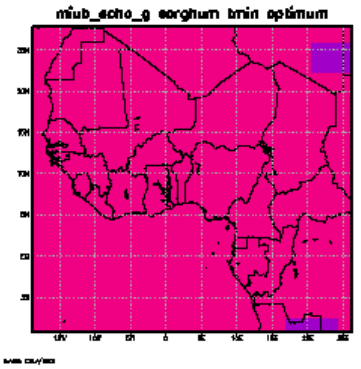
miub_echo_g sorghum tmin optimum

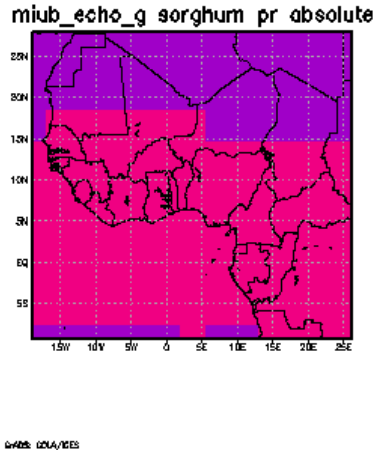
miub_echo_g sorghum pr absolute

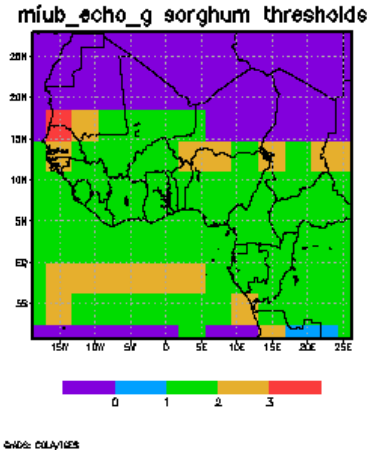
miub_echo_g sorghum thresholds
0
1
2
3

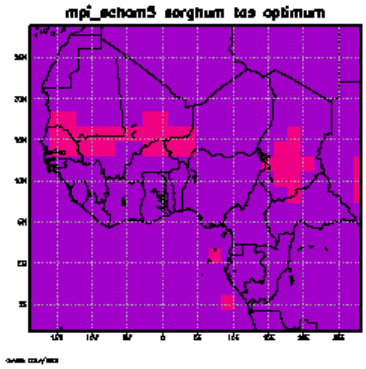
mpi_echam5 sorghum tas optimum

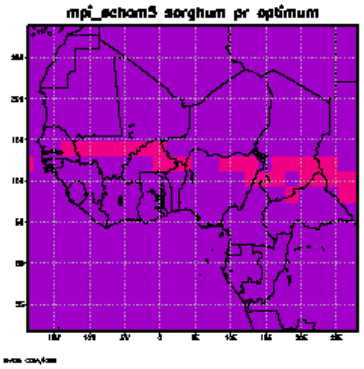
mpi_echam5 sorghum pr optimum

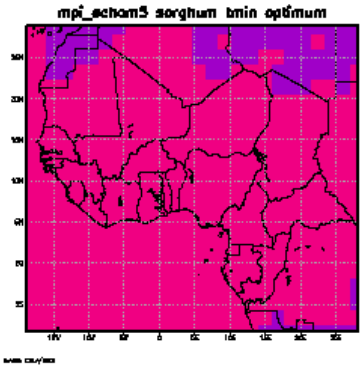
mpi_echam5 sorghum tmin optimum

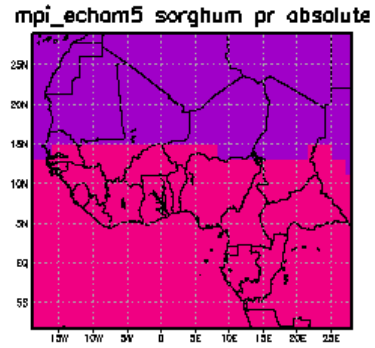
mpi_echam5 sorghum pr absolute

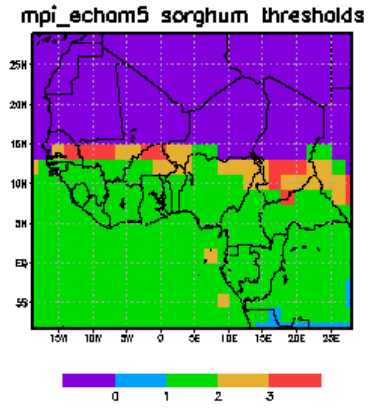
mpi_echam5 sorghum thresholds
0
1
2
3

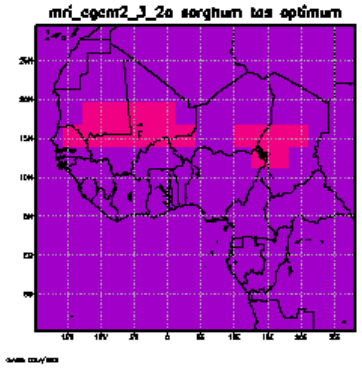
mri_cgcm2_3_2a sorghum tas optimum

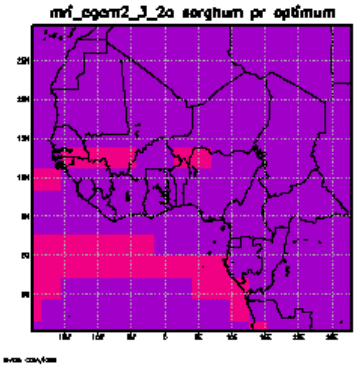
mri_cgcm2_3_2a sorghum pr optimum

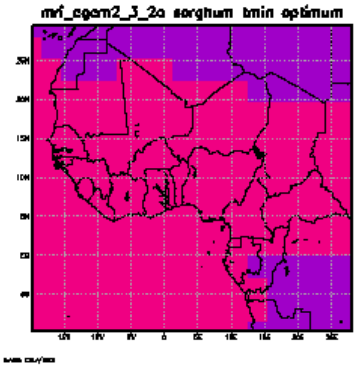
mri_cgcm2_3_2a sorghum tmin optimum

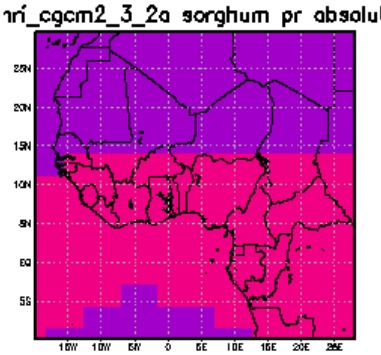
mri_cgcm2_3_2a sorghum pr absolut

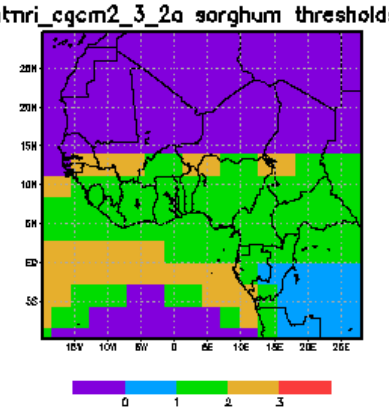
mri_cgcm2_3_2a sorghum thresholds
0
1
2
3

Millet

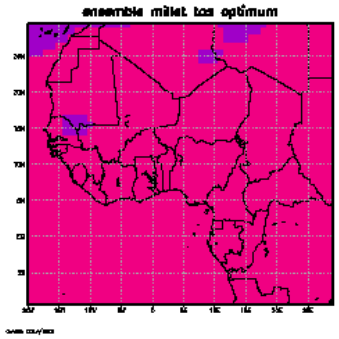
ensemble millet tas optimum

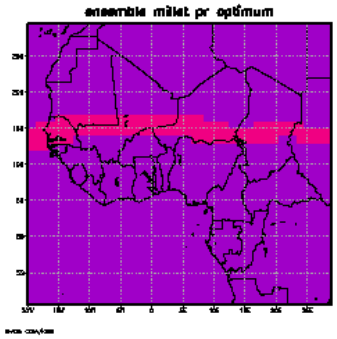
ensemble millet pr optimum

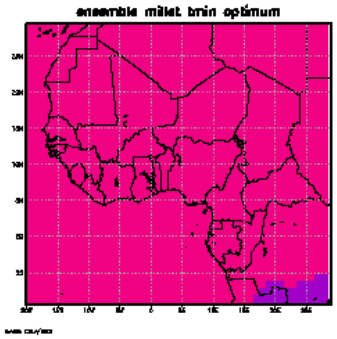
ensemble millet tmin optimum

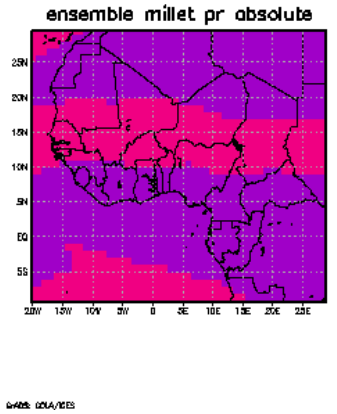
ensemble millet pr absolute

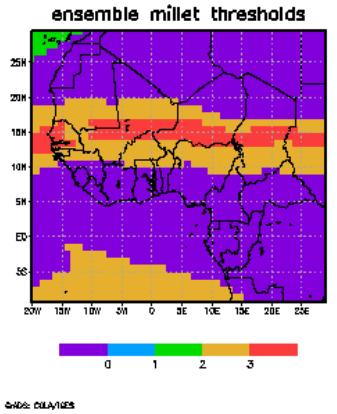
ensemble millet thresholds
0
1
2
3

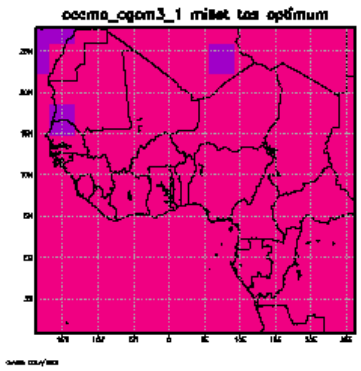
cccma_cgcm3_1 millet tas optimum

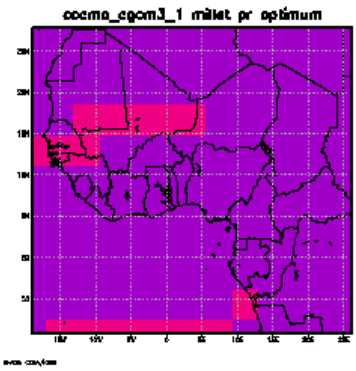
cccma_cgcm3_1 millet pr optimum

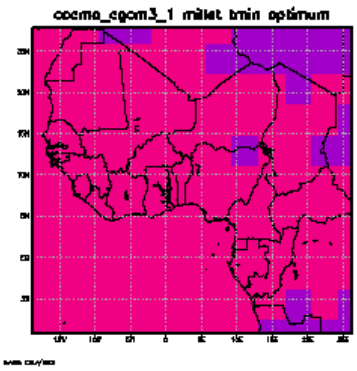
cccma_cgcm3_1 millet tmin optimum

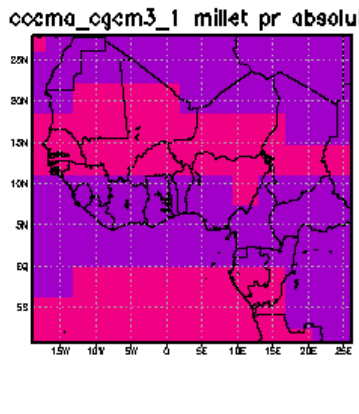
cccma_cgcm3_1 millet pr absolute

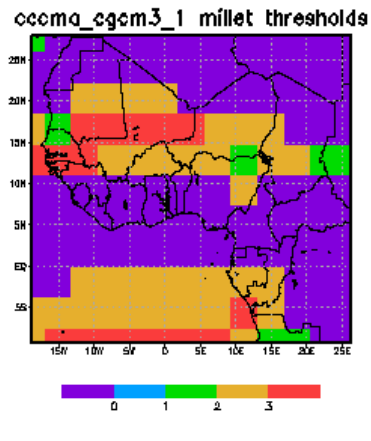
cccma_cgcm3_1 millet thresholds
0
1
2
3

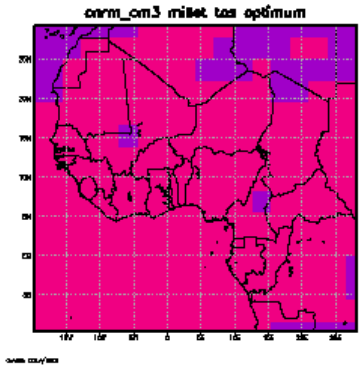
cnrm_cm3 millet tas optimum

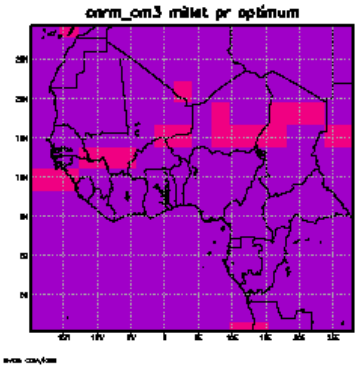
cnrm_cm3 millet pr optimum

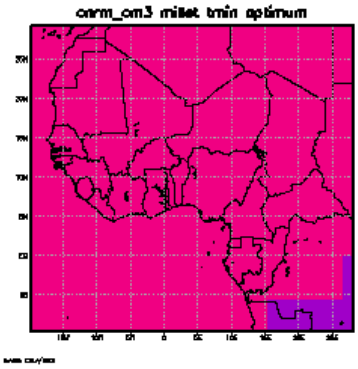
cnrm_cm3 millet tmin optimum

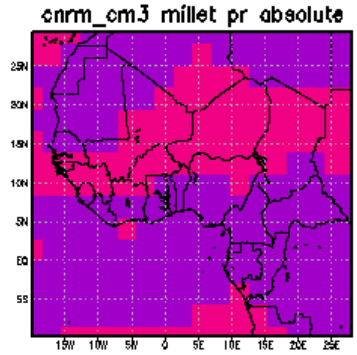
cnrm_cm3 millet pr absolute

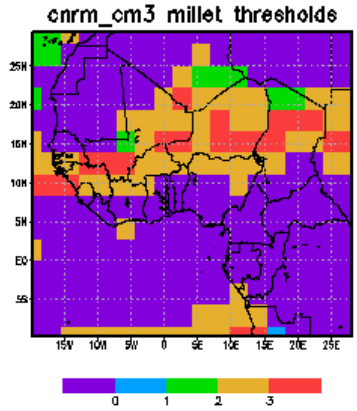
cnrm_cm3 millet thresholds
0
1
2
3

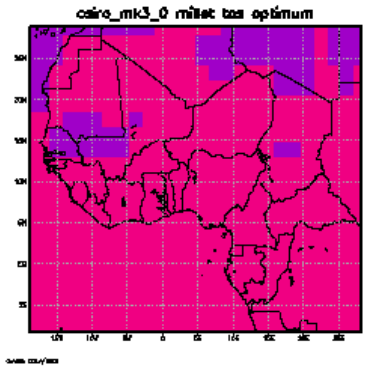
csiro_mk3_0 millet tas optimum

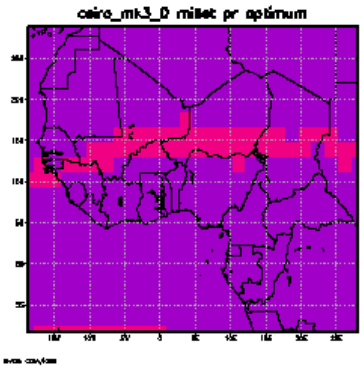
csiro_mk3_0 millet pr optimum

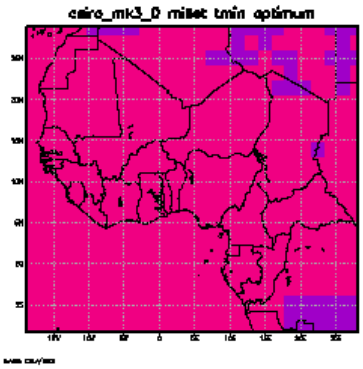
csiro_mk3_0 millet tmin optimum

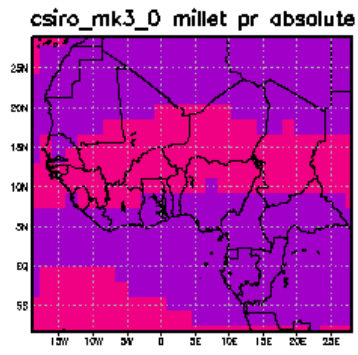
csiro_mk3_0 millet pr absolute

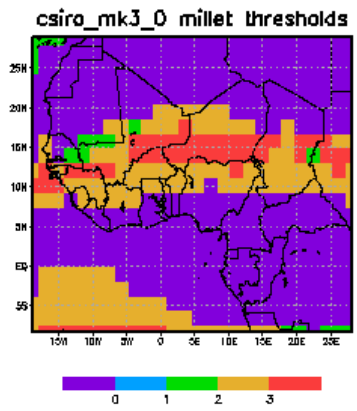
csiro_mk3_0 millet thresholds
0
1
2
3

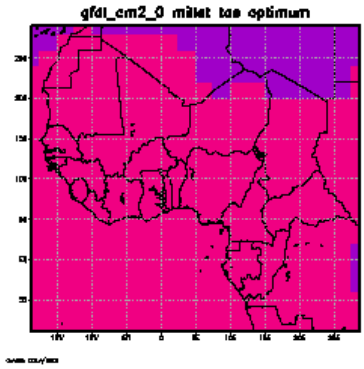
gfdl_cm2_0 millet tas optimum

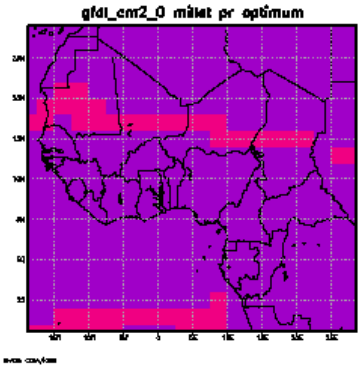
gfdl_cm2_0 millet pr optimum

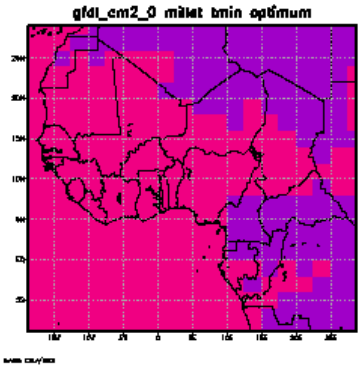
gfdl_cm2_0 millet tmin optimum

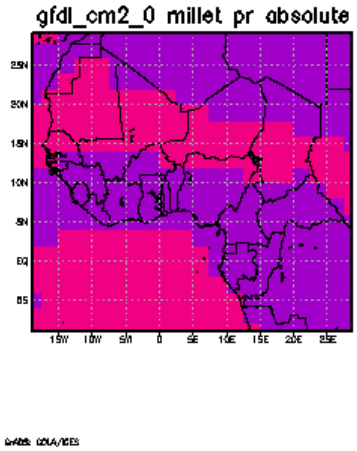
gfdl_cm2_0 millet pr absolute

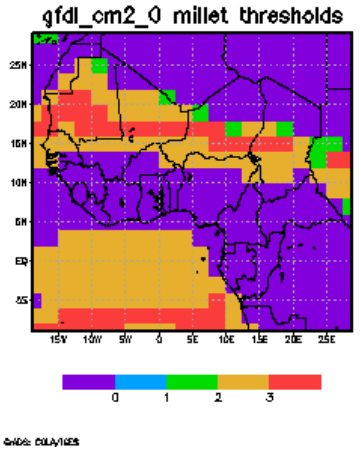
gfdl_cm2_0 millet thresholds
0
1
2
3

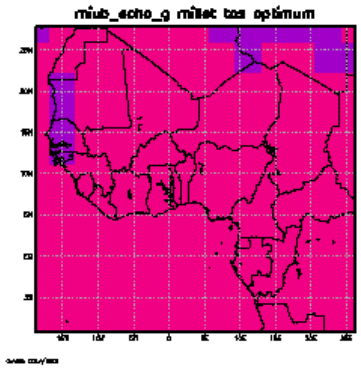
miub_echo_g millet tas optimum

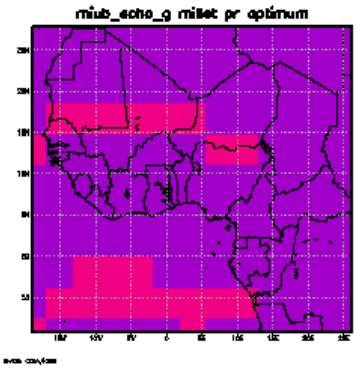
miub_echo_g millet pr optimum

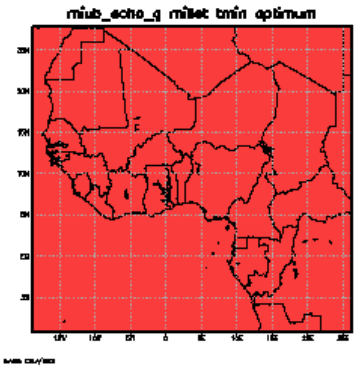
miub_echo_g millet tmin optimum

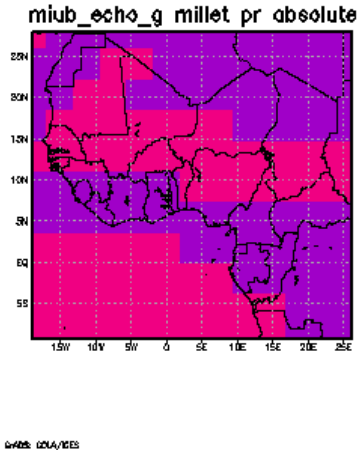
miub_echo_g millet pr absolute

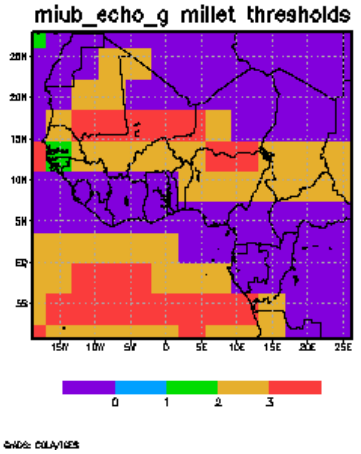
miub_echo_g millet thresholds
0
1
2
3

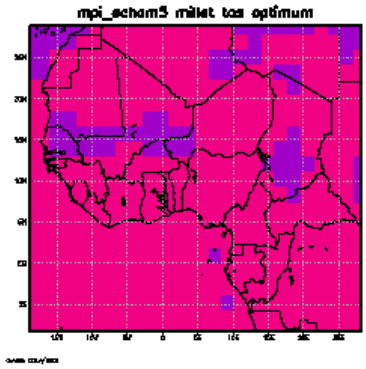
mpi_echam5 millet tas optimum

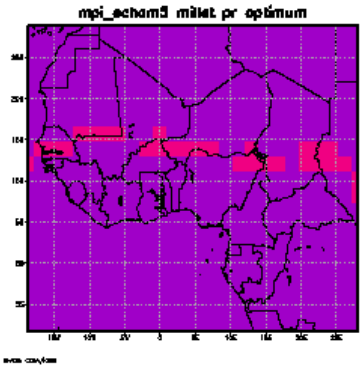
mpi_echam5 millet pr optimum

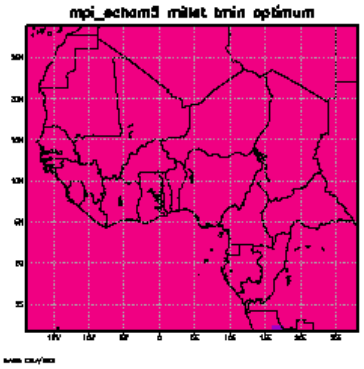
mpi_echam5 millet tmin optimum

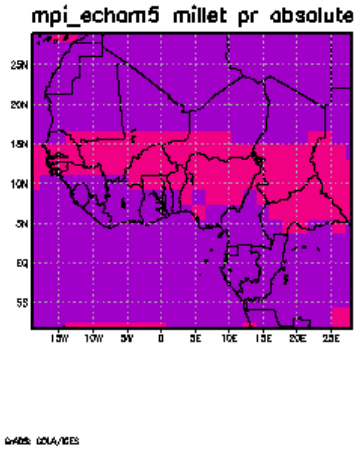
mpi_echam5 millet pr absolute

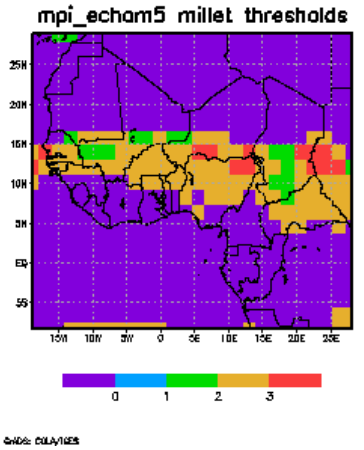
mpi_echam5 millet thresholds
0
1
2
3

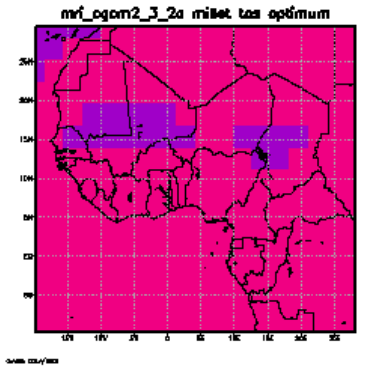
mri_cgcm2_3_2a millet tas optimum

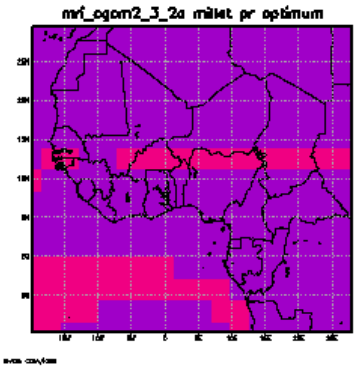
mri_cgcm2_3_2a millet pr optimum

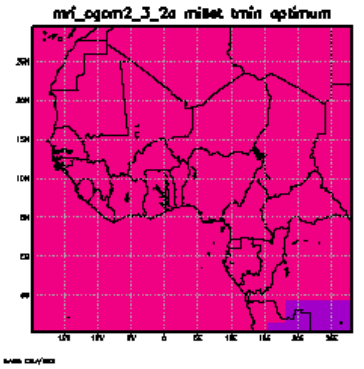
mri_cgcm2_3_2a millet tmin optimum

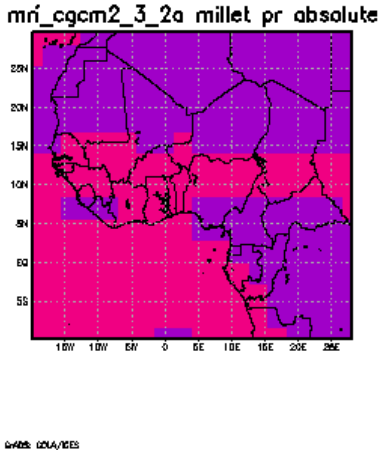
mri_cgcm2_3_2a millet pr absolute

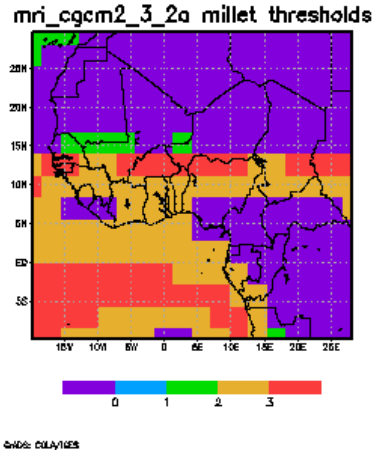
mri_cgcm2_3_2a millet thresholds
0
1
2
3

Maize

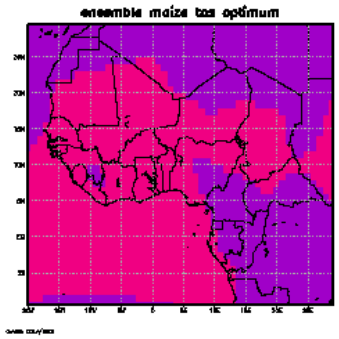
ensemble maize tas optimum

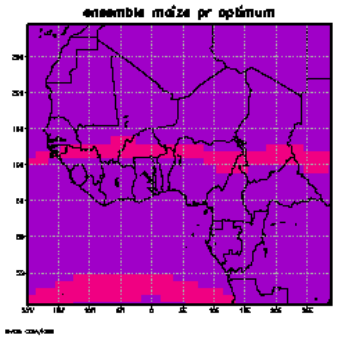
ensemble maize pr optimum

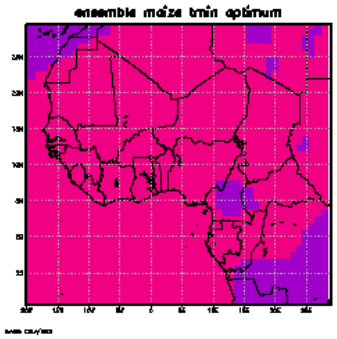
ensemble maize tmin optimum

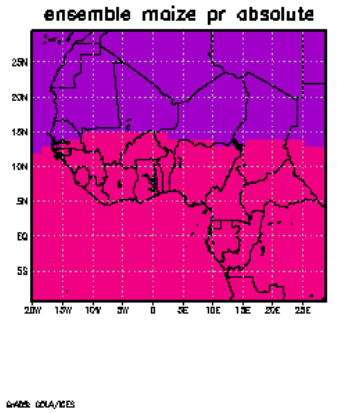
ensemble maize pr absolute

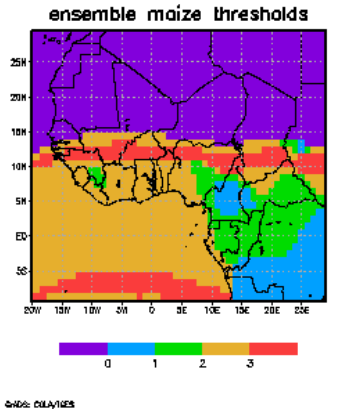
ensemble maize thresholds
0
1
2
3

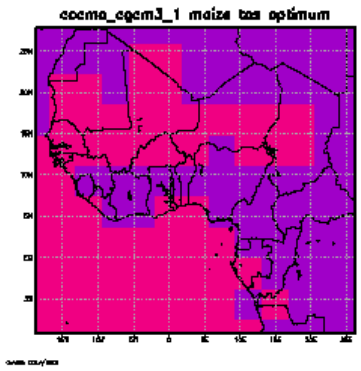
cccma_cgcm3_1 maize tas optimum

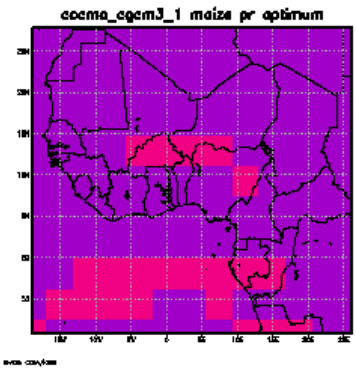
cccma_cgcm3_1 maize pr optimum

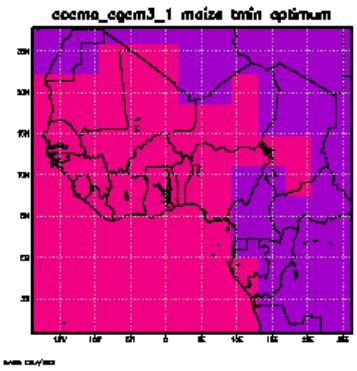
cccma_cgcm3_1 maize tmin optimum

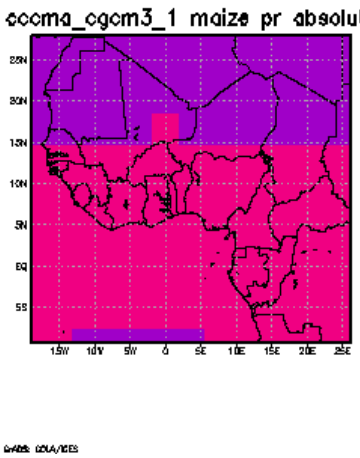
cccma_cgcm3_1 maize pr absolute

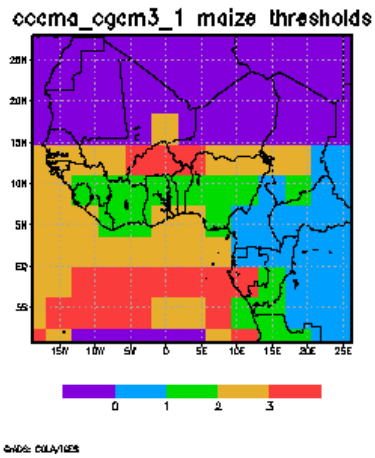
cccma_cgcm3_1 maize thresholds
0
1
2
3

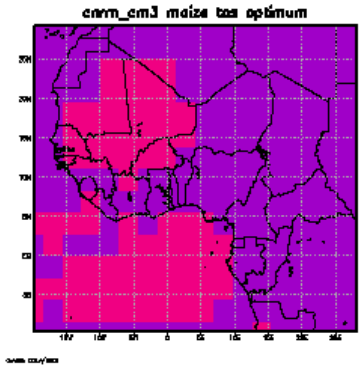
cnrm_cm3 maize tas optimum

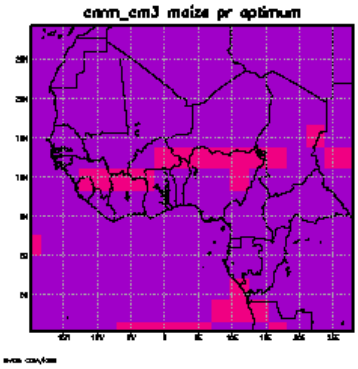
cnrm_cm3 maize pr optimum

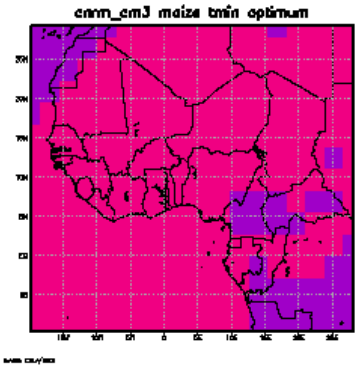
cnrm_cm3 maize tmin optimum

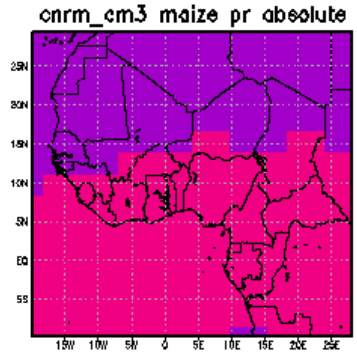
cnrm_cm3 maize pr absolute

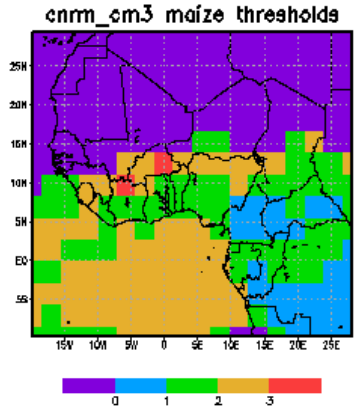
cnrm_cm3 maize thresholds
0
1
2
3

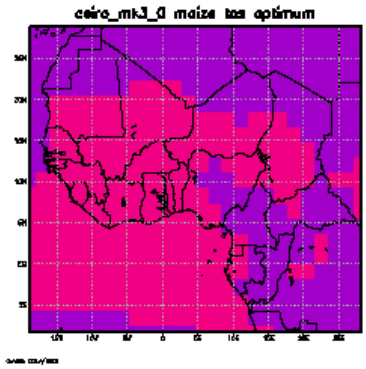
csiro_mk3_0 maize tas optimum

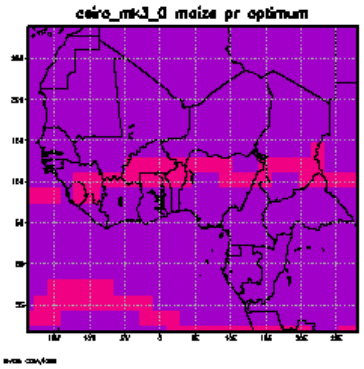
csiro_mk3_0 maize pr optimum

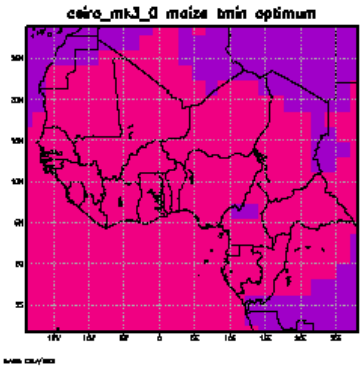
csiro_mk3_0 maize tmin optimum

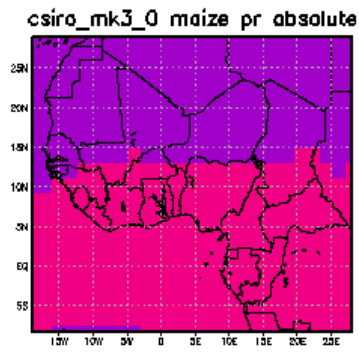
csiro_mk3_0 maize pr absolute

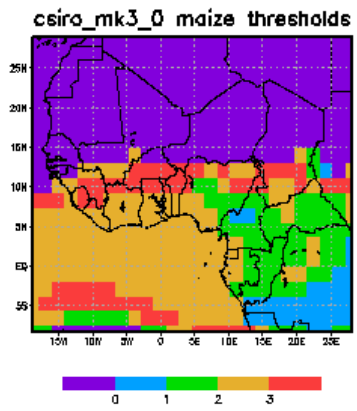
csiro_mk3_0 maize thresholds
0
1
2
3

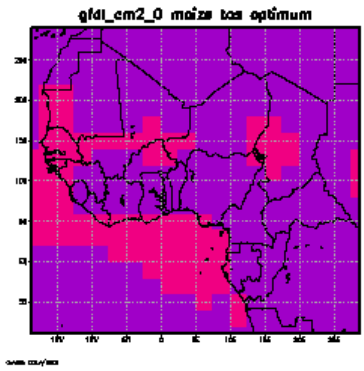
gfdl_cm2_0 maize tas optimum

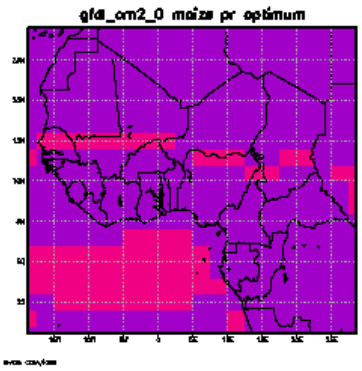
gfdl_cm2_0 maize pr optimum

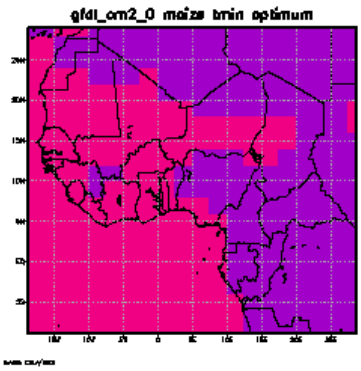
gfdl_cm2_0 maize tmin optimum

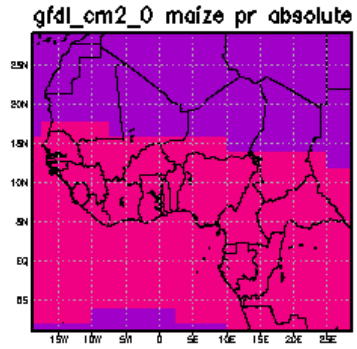
gfdl_cm2_0 maize pr absolute

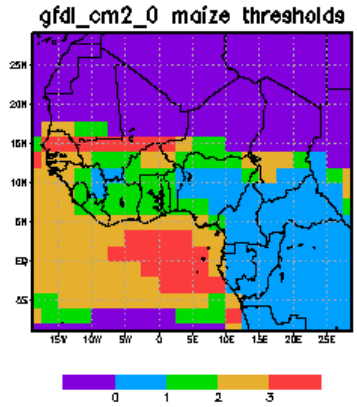
gfdl_cm2_0 maize thresholds
0
1
2
3

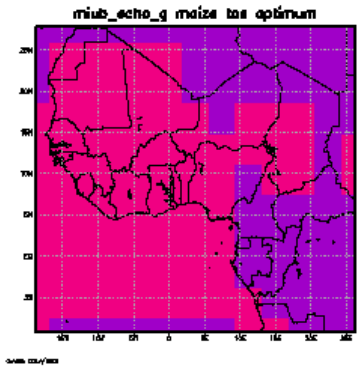
miub_echo_g maize tas optimum

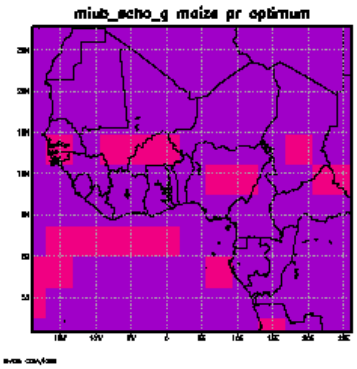
miub_echo_g maize pr optimum

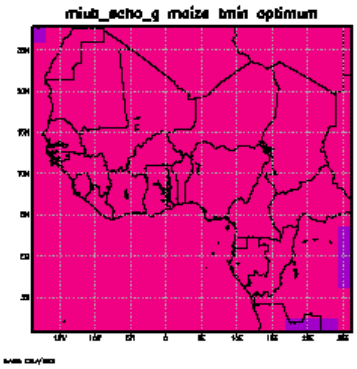
miub_echo_g maize tmin optimum

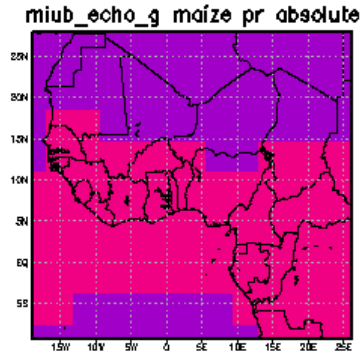
miub_echo_g maize pr absolute

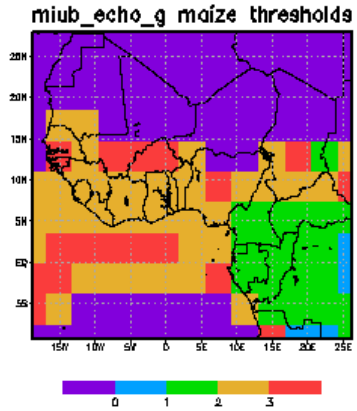
miub_echo_g maize thresholds
0
1
2
3

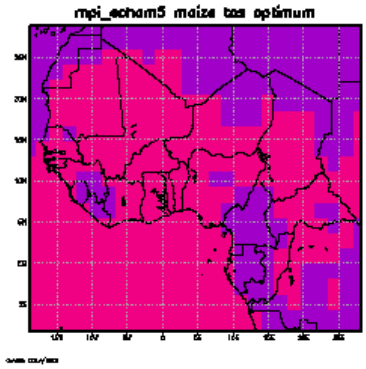
mpi_echam5 maize tas optimum

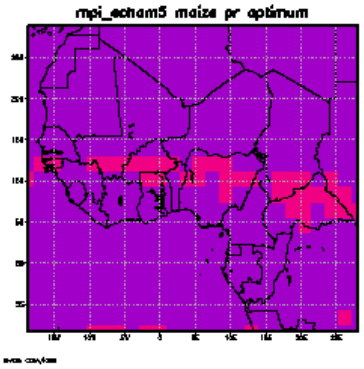
mpi_echam5 maize pr optimum

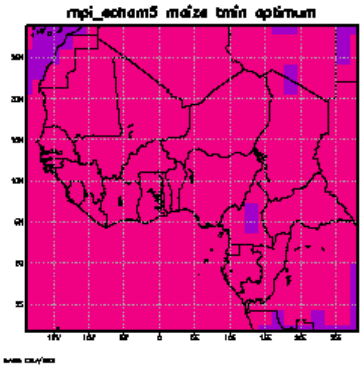
mpi_echam5 maize tmin optimum

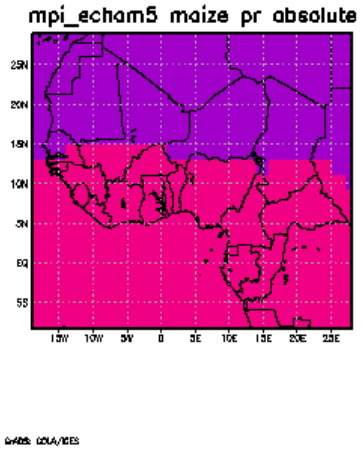
mpi_echam5 maize pr absolute

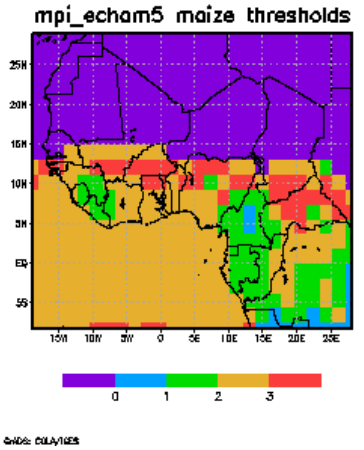
mpi_echam5 maize thresholds
0
1
2
3

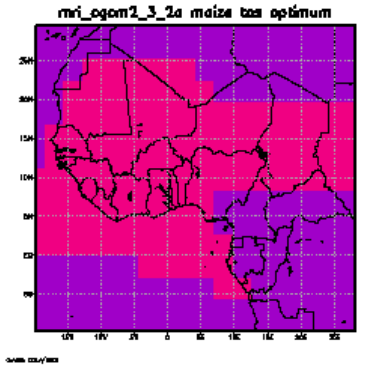
mri_cgcm2_3_2a maize tas optimum

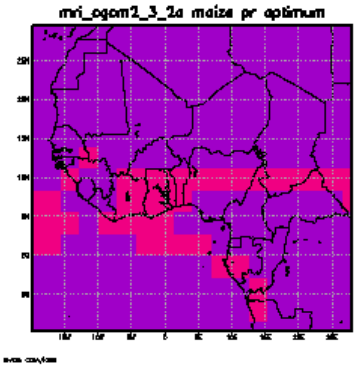
mri_cgcm2_3_2a maize pr optimum

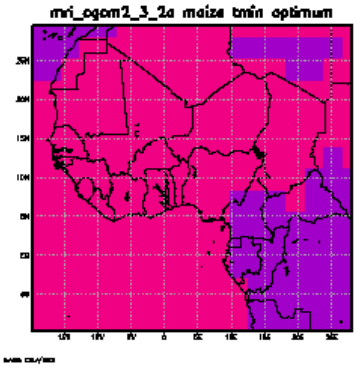
mri_cgcm2_3_2a maize tmin optimum

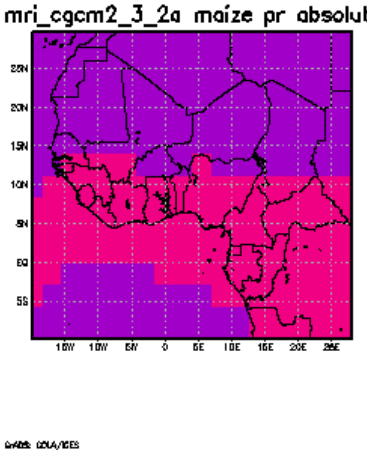
mri_cgcm2_3_2a maize pr absolute

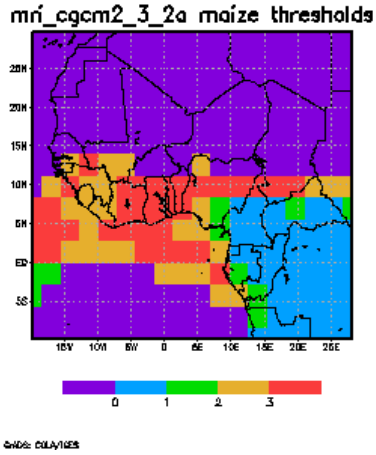
mri_cgcm2_3_2a maize thresholds
0
1
2
3

Appendix 8: Temperature and Precipitation Anomalies Relative to 20c3m Climatologies for sres Experiments

a. Temperature

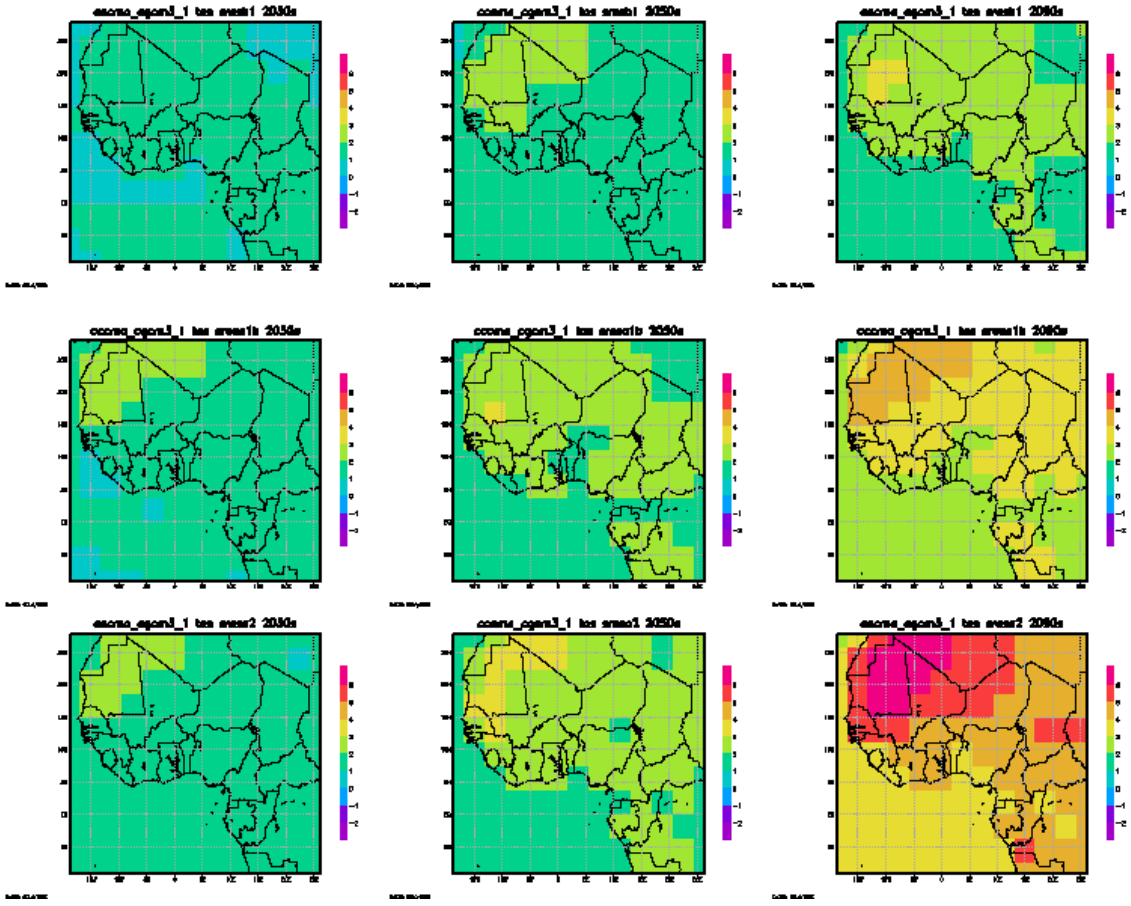

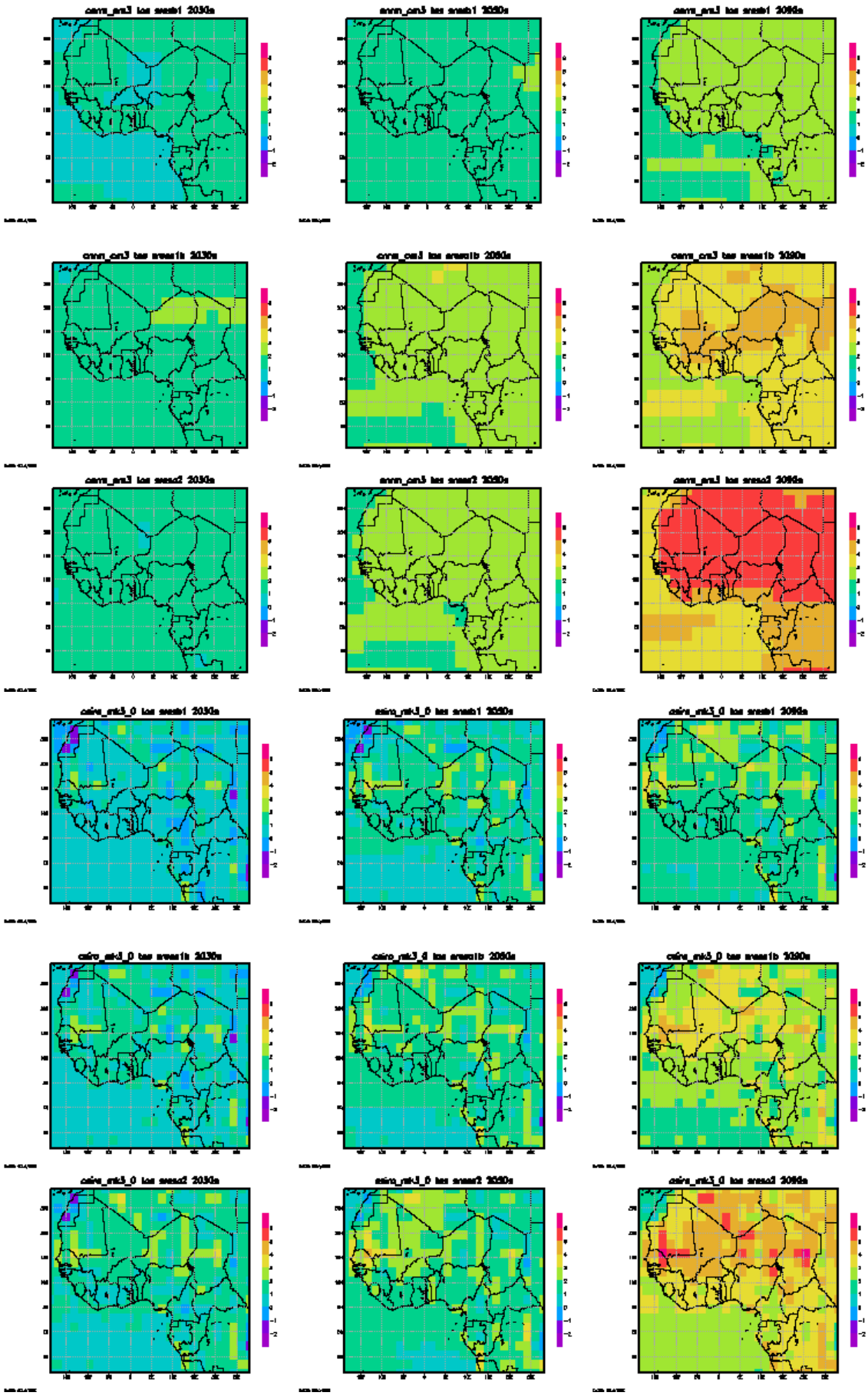

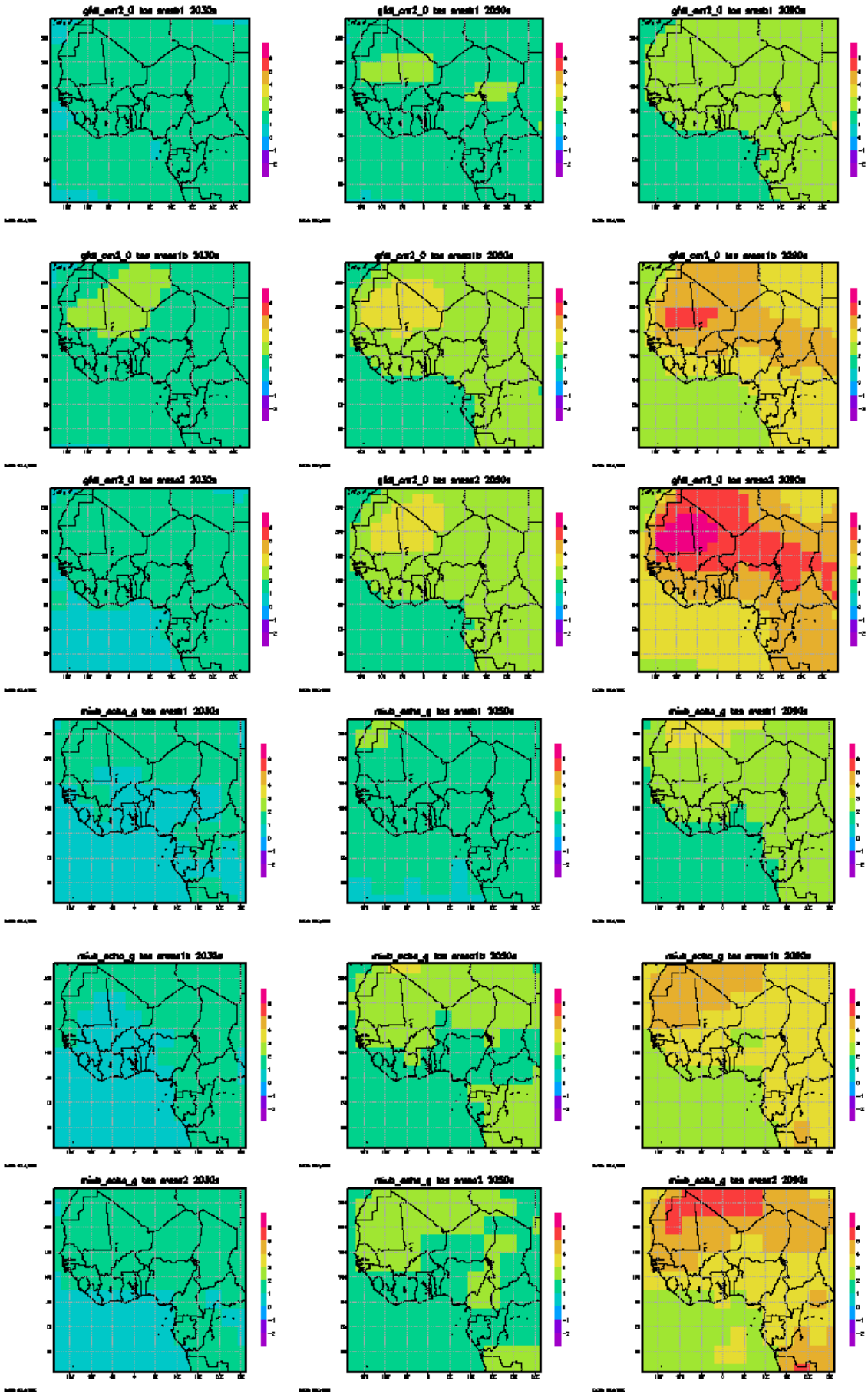

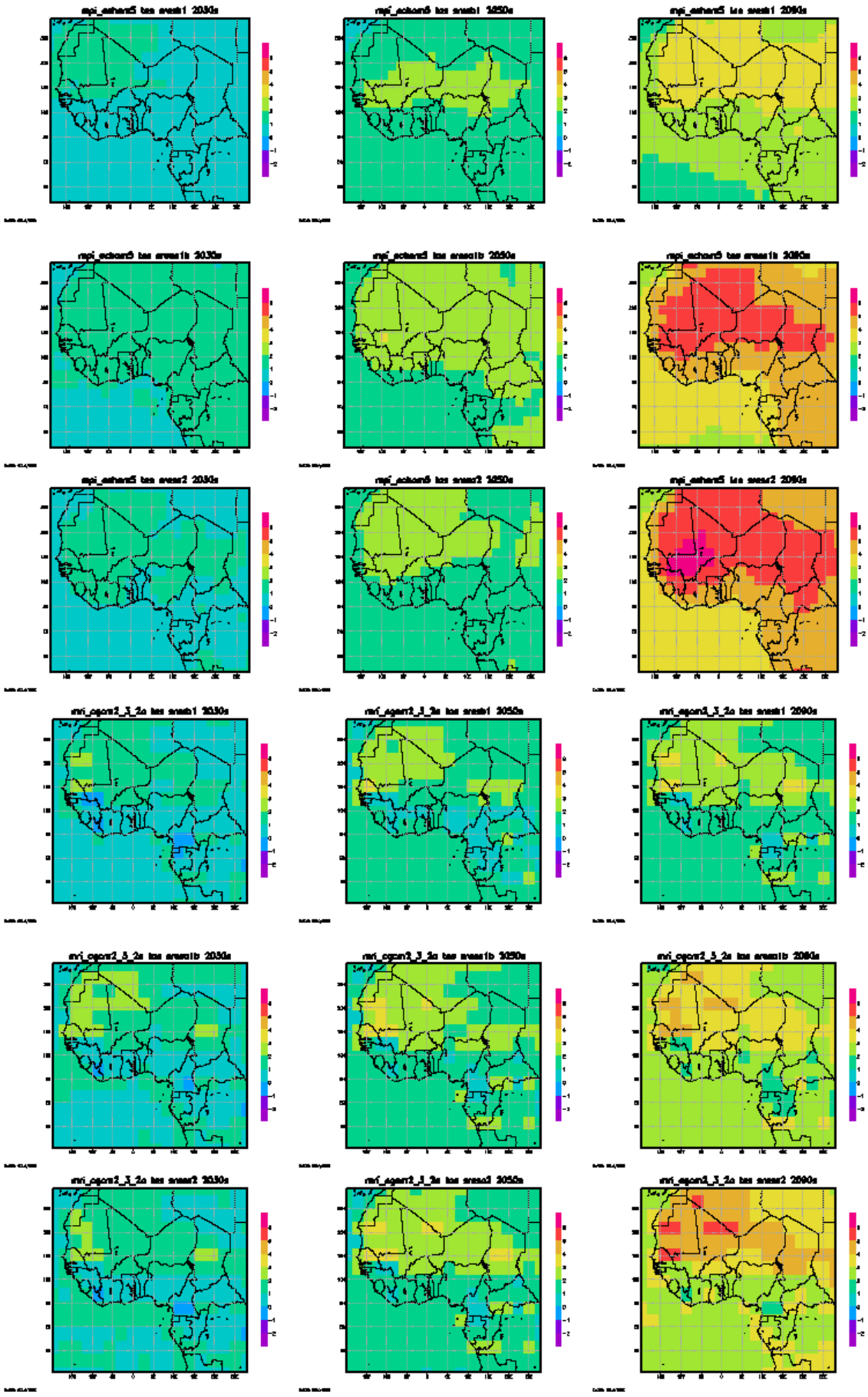

b. Precipitation

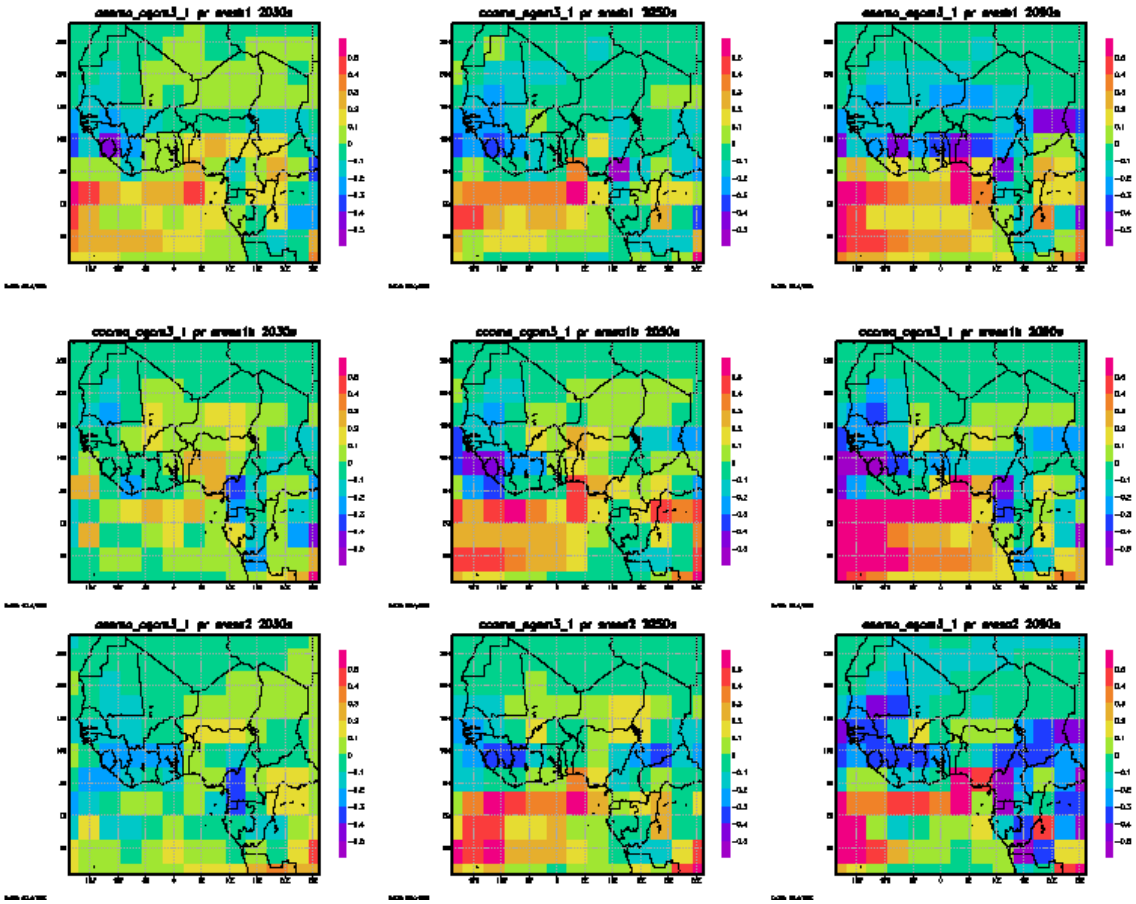

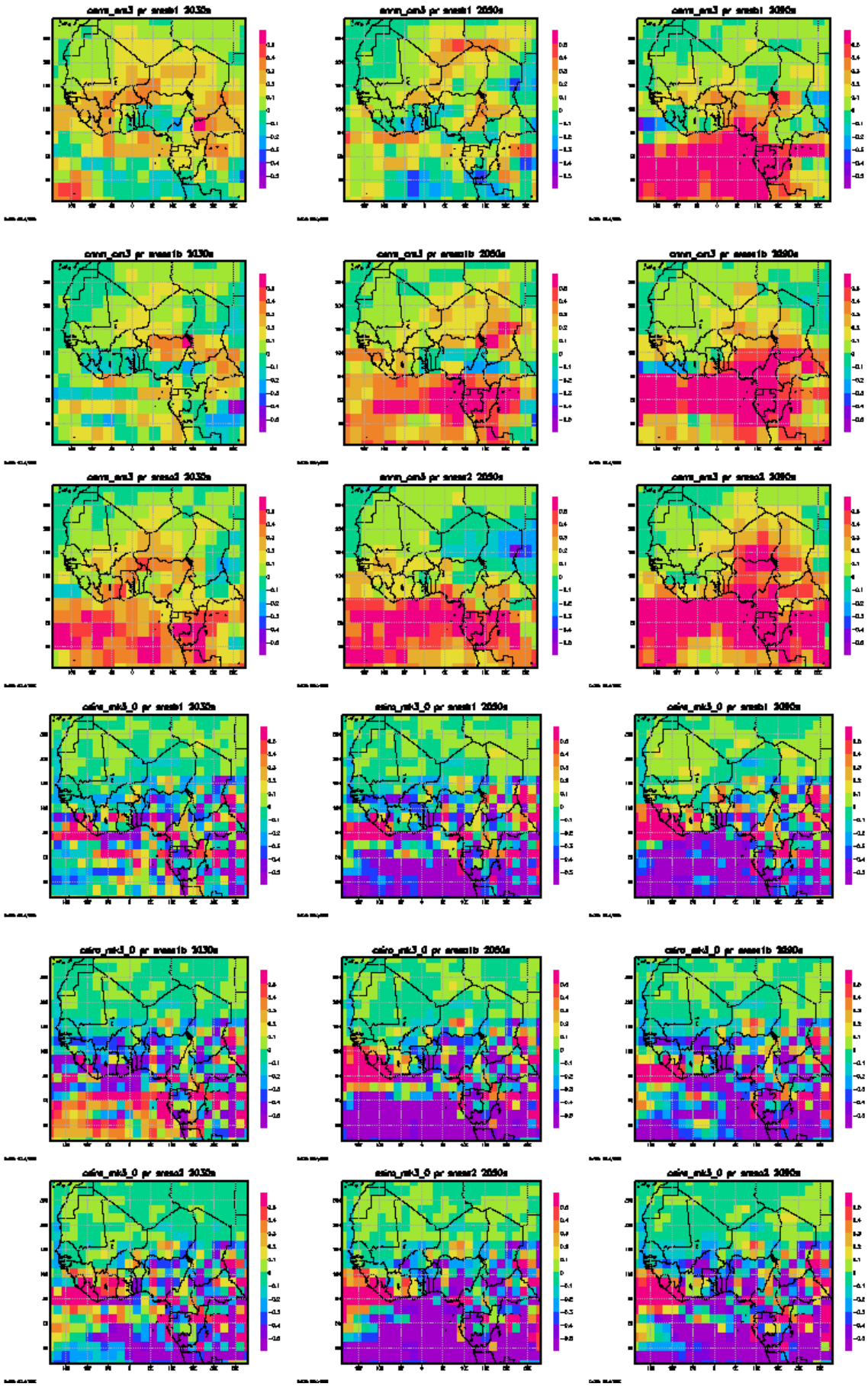

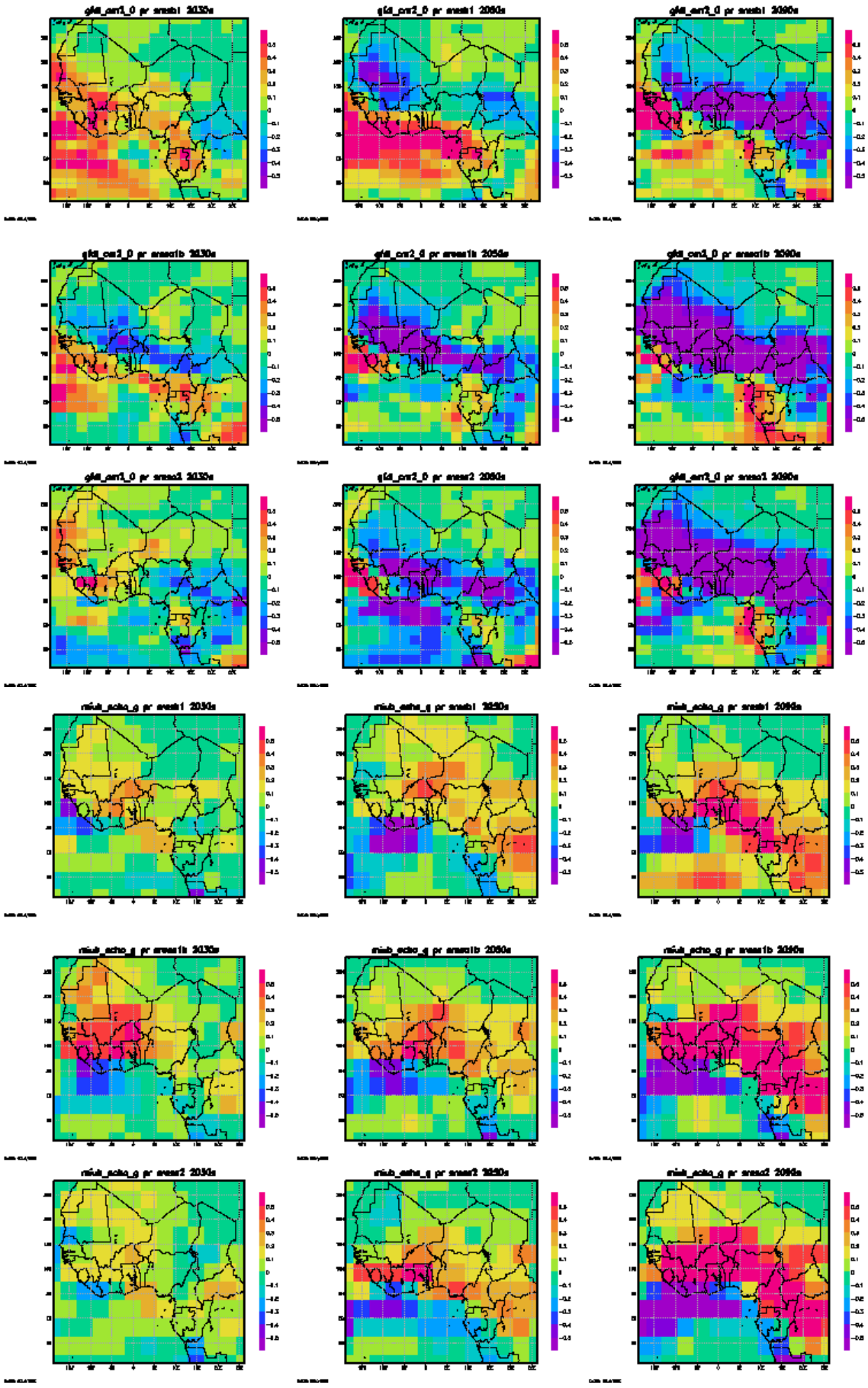

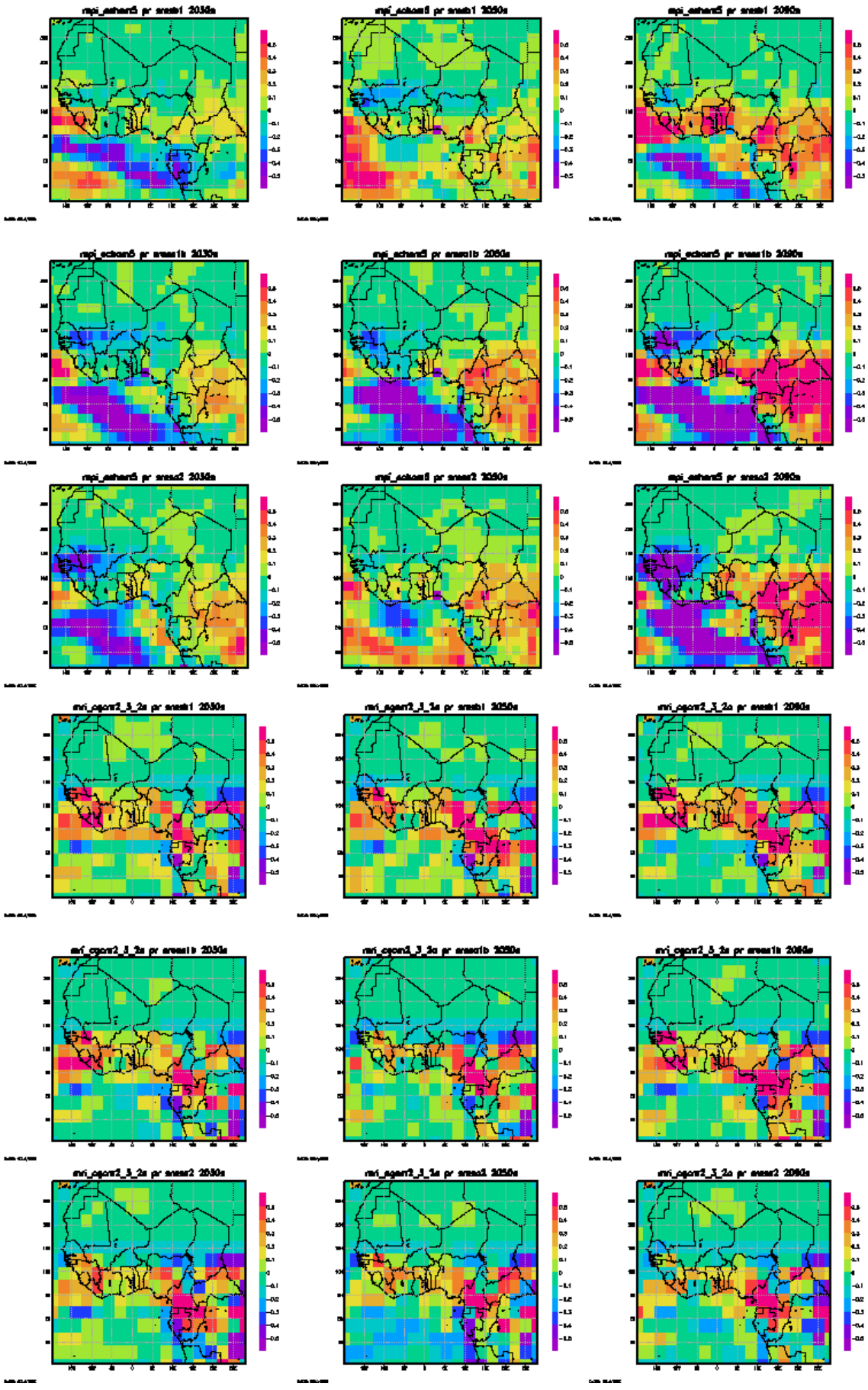

Appendix 9: Model derived monthly precipitation anomalies, relative to 20c3m climatologies

Black denotes the anomaly for the 2050s relative to the 1970-1999 baseline. Green denotes the anomaly for the 2090s relative to the 1970-1999 baseline.

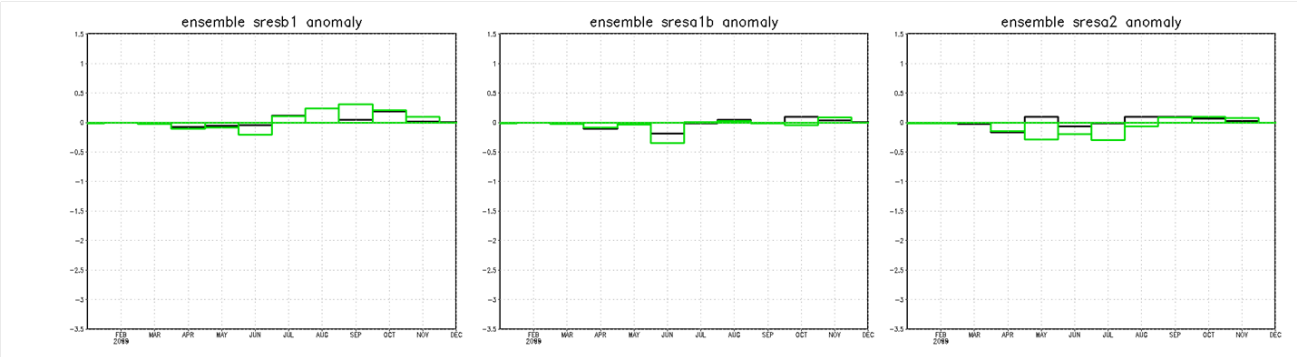

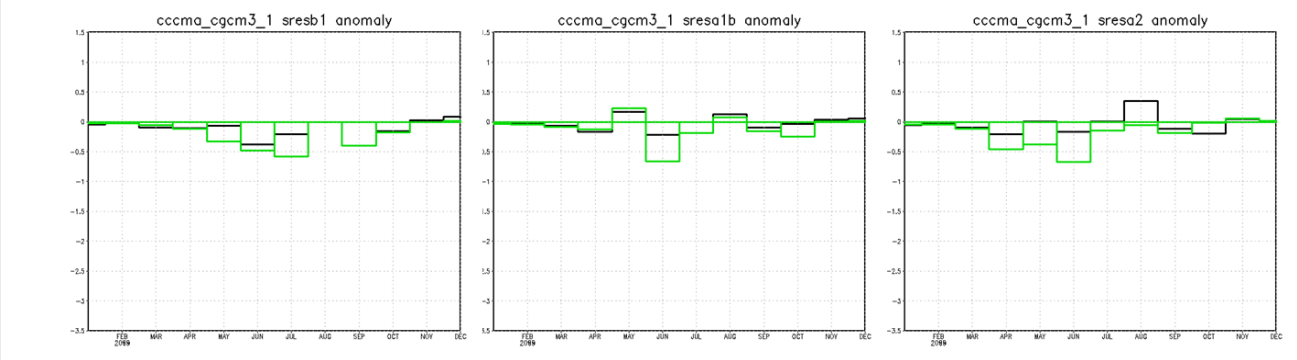

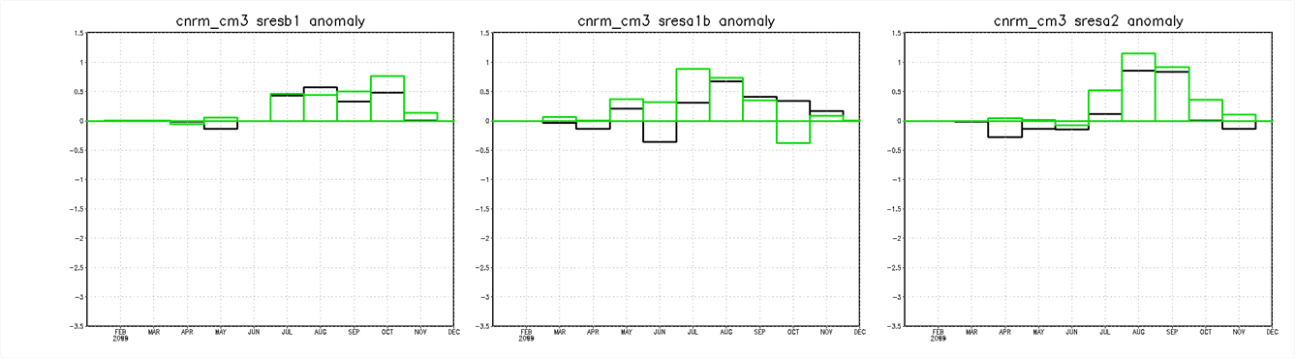

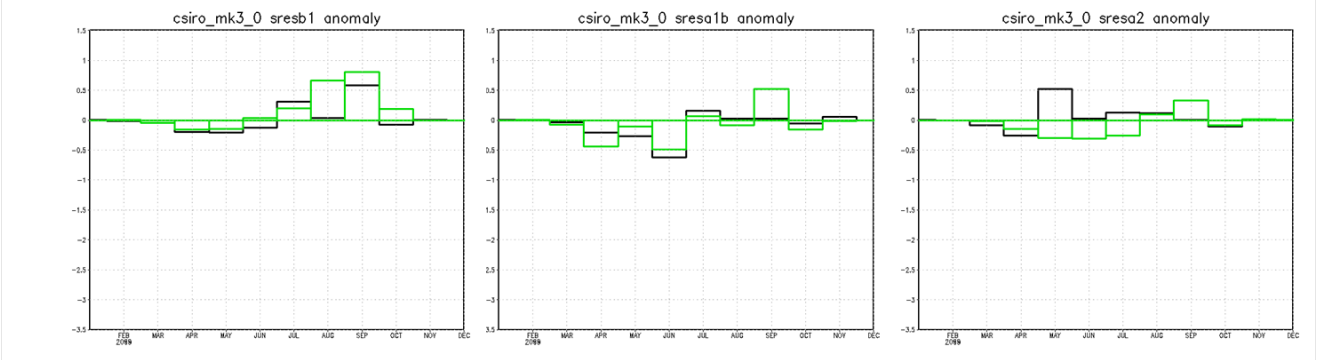

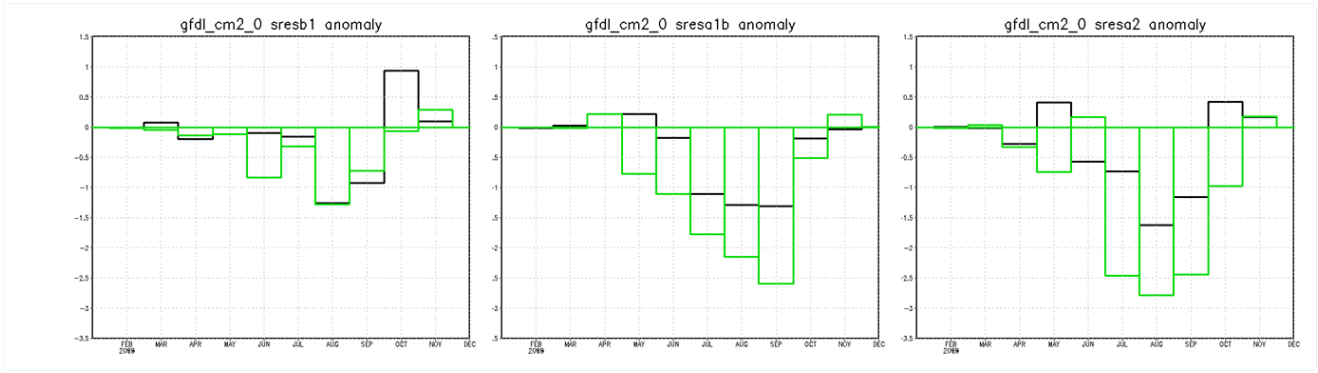
gfdl_cm2_0 sresb1 anomaly
gfdl_cm2_0 sresa1b anomaly
gfdl_cm2_0 sresa2 anomaly

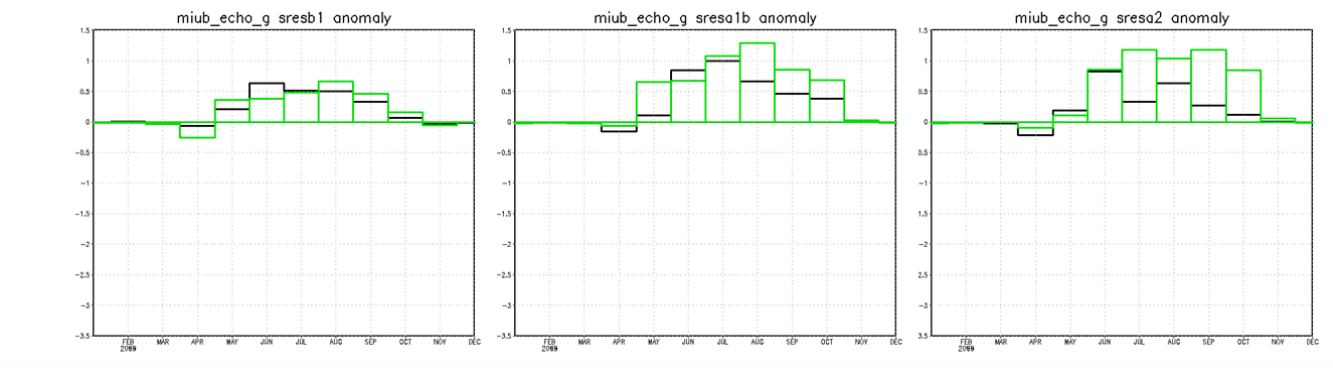
miub_echo_g sresb1 anomaly
miub_echo_g sresa1b anomaly
miub_echo_g sresa2 anomaly

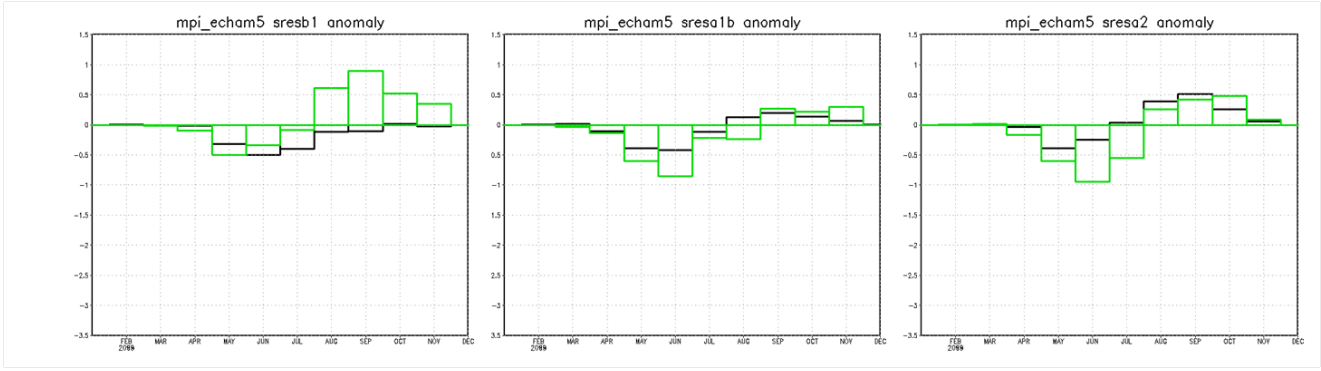
mpi_echam5 sresb1 anomaly
mpi_echam5 sresa1b anomaly
mpi_echam5 sresa2 anomaly

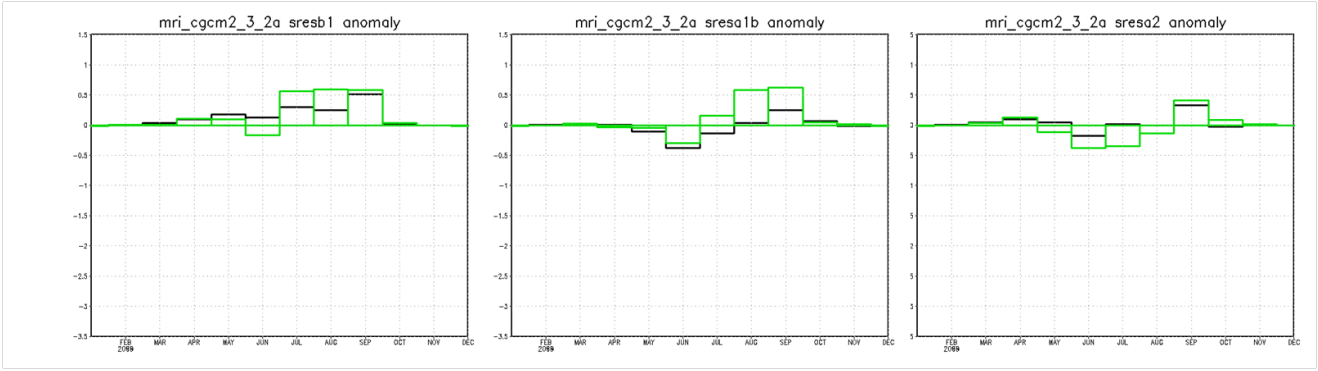
mri_cgcm2_3_2a sresb1 anomaly
mri_cgcm2_3_2a sresa1b anomaly
mri_cgcm2_3_2a sresa2 anomaly

Appendix 10: Model Derived 95% Maximum Precipitation Anomalies, Relative to 20c3m Climatologies

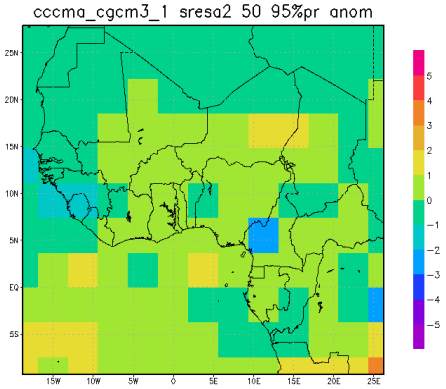

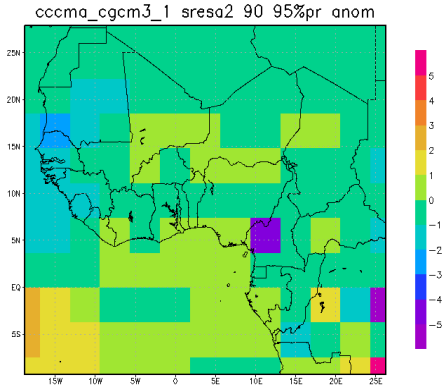

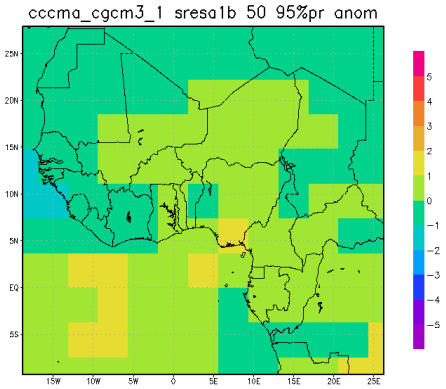

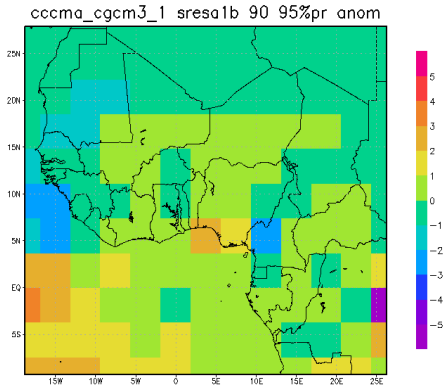

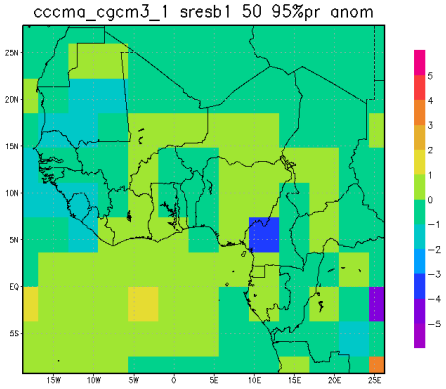

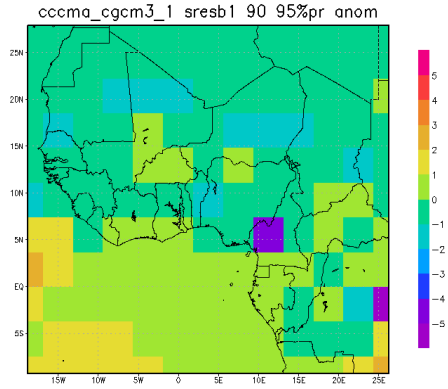

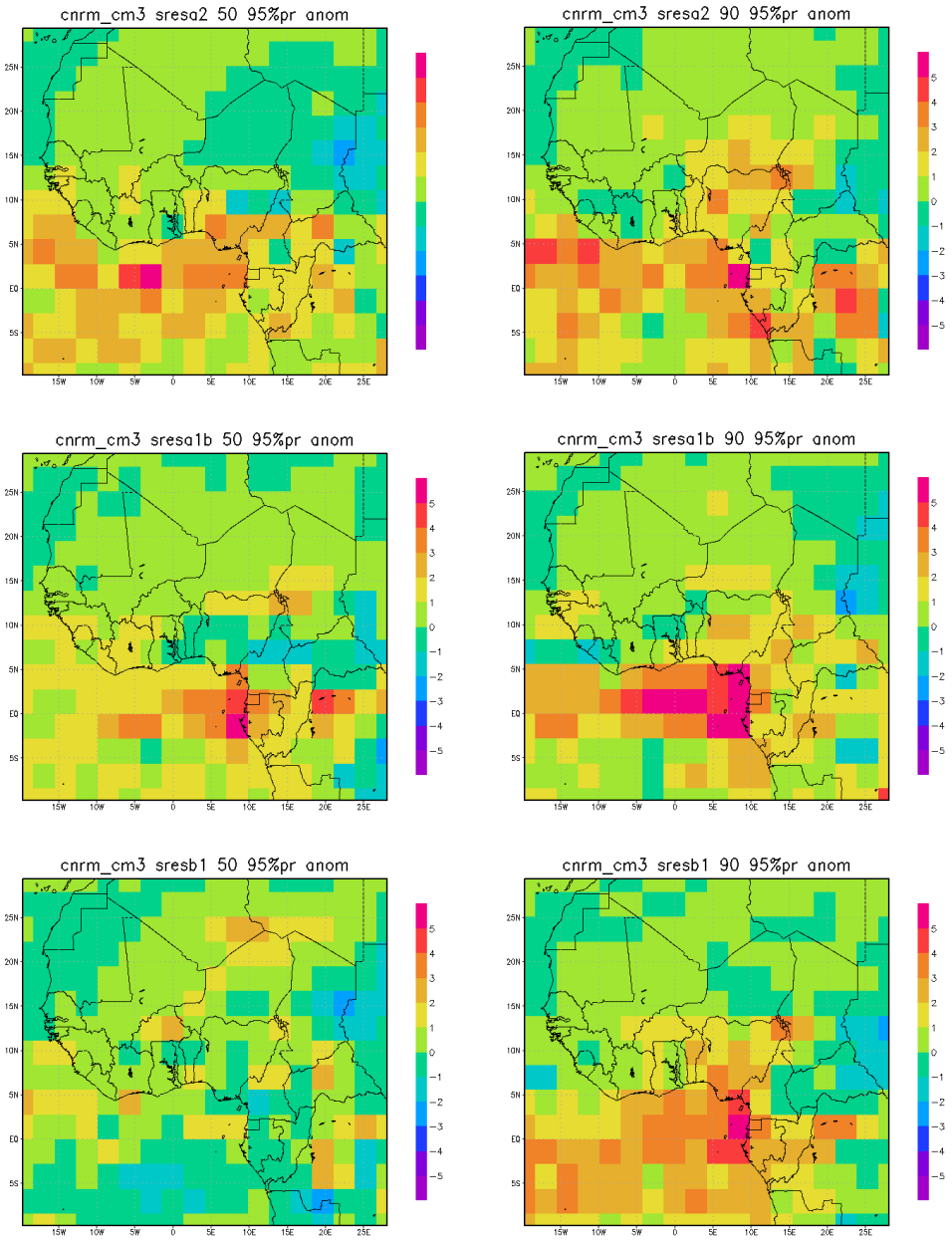
cnrm_cm3 sresa2 50 95%pr anom
cnrm_cm3 sresa2 90 95%pr anom
cnrm_cm3 sresa1b 50 95%pr anom
cnrm_cm3 sresa1b 90 95%pr anom
cnrm_cm3 sresb1 50 95%pr anom
cnrm_cm3 sresb1 90 95%pr anom

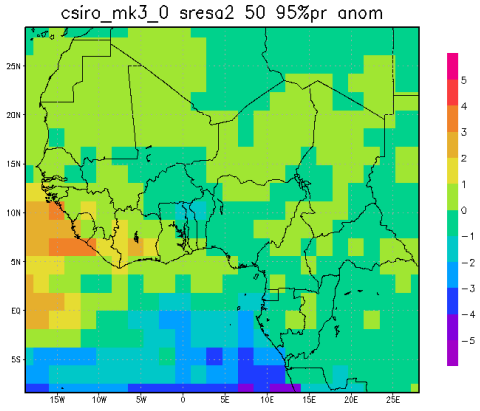
csiro_mk3_0 sresa2 50 95%pr anom

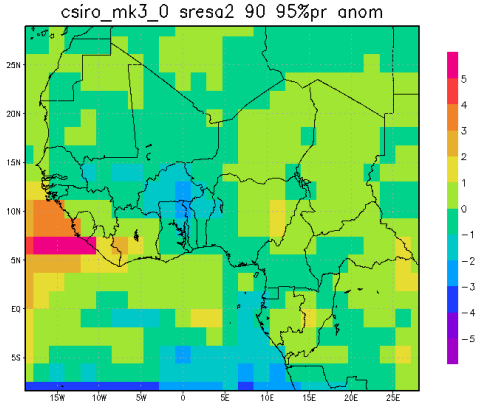
csiro_mk3_0 sresa2 90 95%pr anom

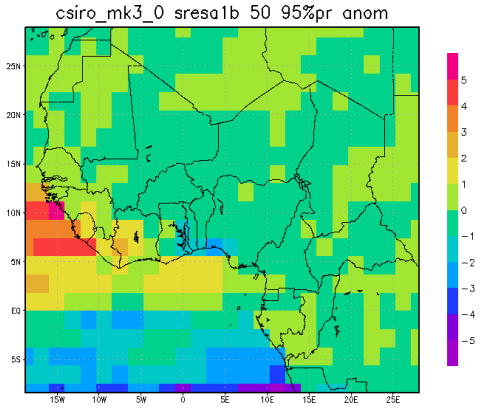
csiro_mk3_0 sresa1b 50 95%pr anom

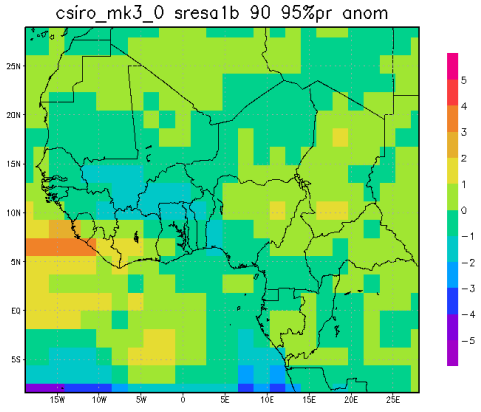
csiro_mk3_0 sresa1b 90 95%pr anom

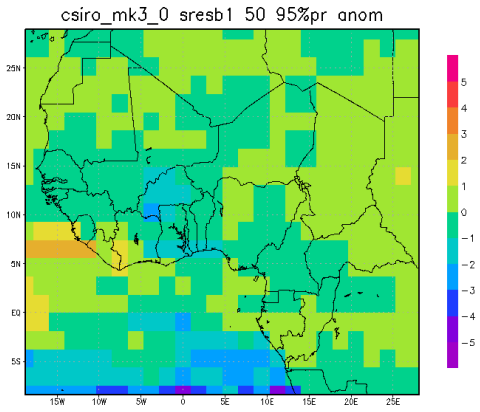
csiro_mk3_0 sresb1 50 95%pr anom

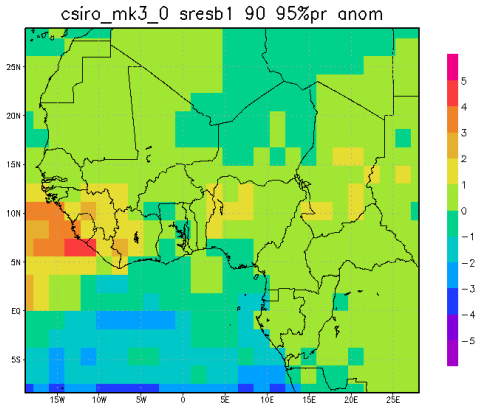
csiro_mk3_0 sresb1 90 95%pr anom

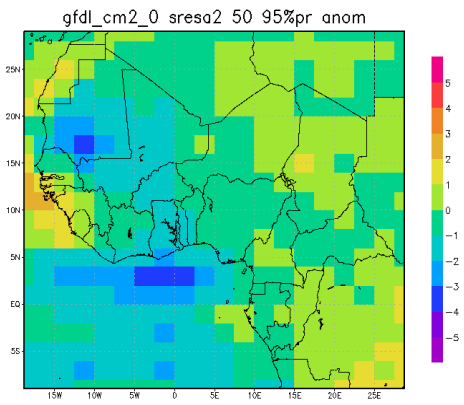
gfdl_cm2_0 sresa2 50 95%pr anom

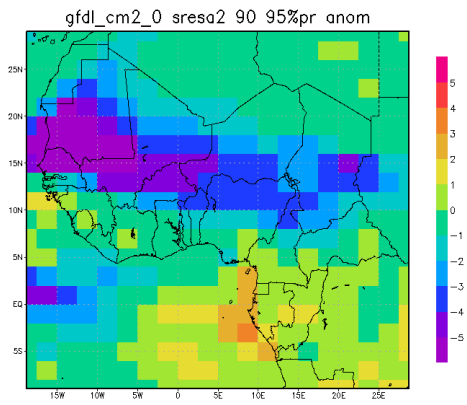
gfdl_cm2_0 sresa2 90 95%pr anom

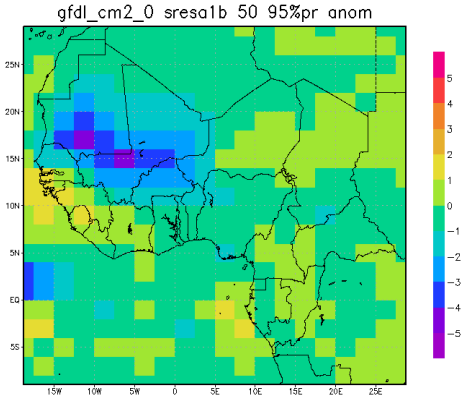
gfdl_cm2_0 sresa1b 50 95%pr anom

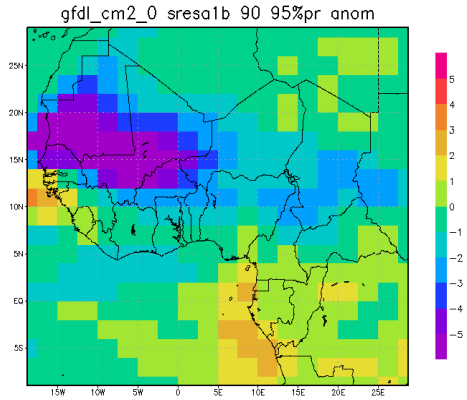
gfdl_cm2_0 sresa1b 90 95%pr anom

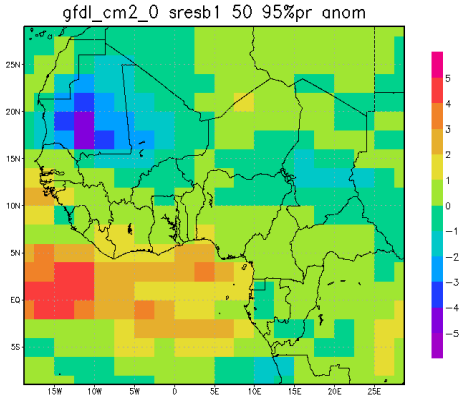
gfdl_cm2_0 sresb1 50 95%pr anom

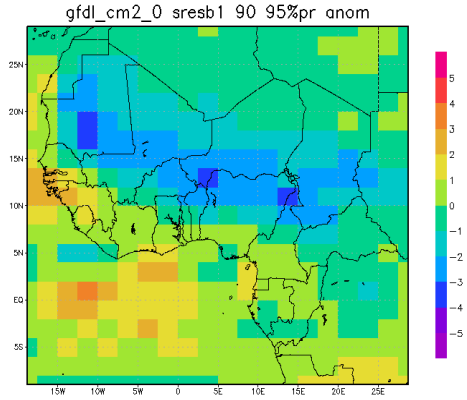
gfdl_cm2_0 sresb1 90 95%pr anom

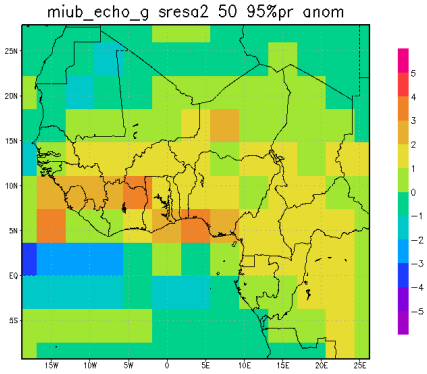
miub_echo_g sresa2 50 95%pr anom

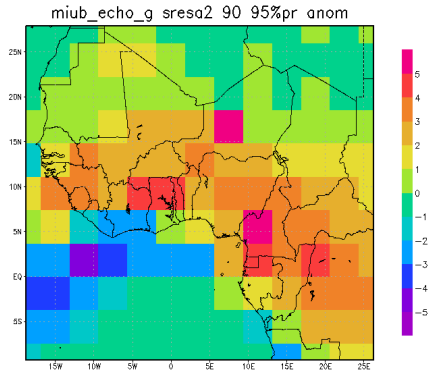
miub_echo_g sresa2 90 95%pr anom

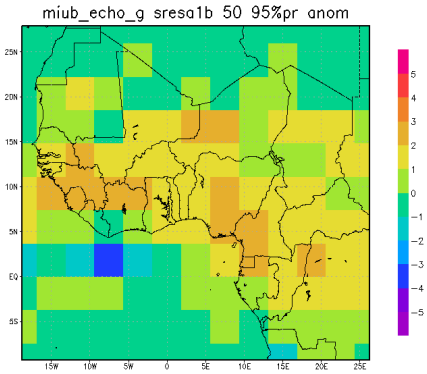
miub_echo_g sresa1b 50 95%pr anom

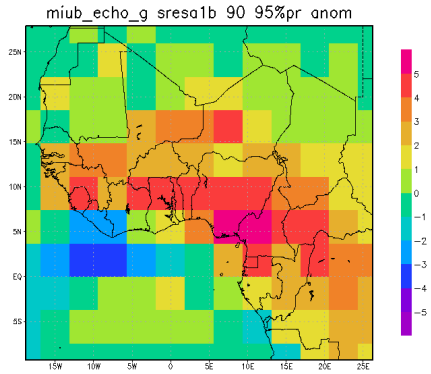
miub_echo_g sresa1b 90 95%pr anom

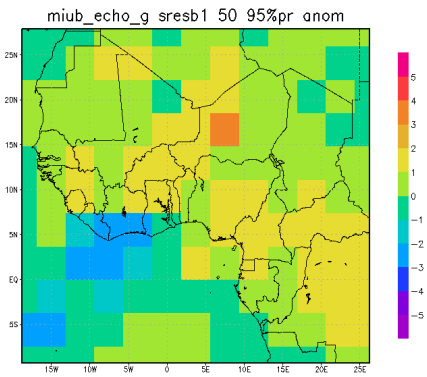
miub_echo_g sresb1 50 95%pr anom

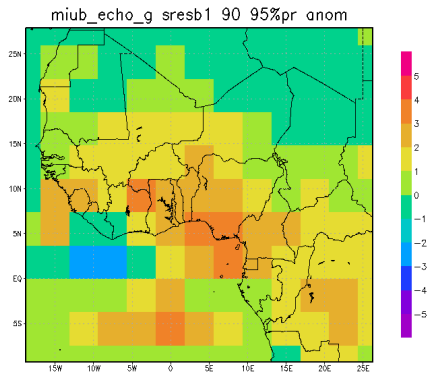
miub_echo_g sresb1 90 95%pr anom

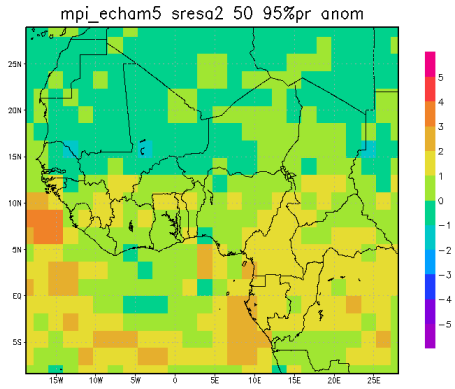
mpi_echam5 sresa2 50 95%pr anom

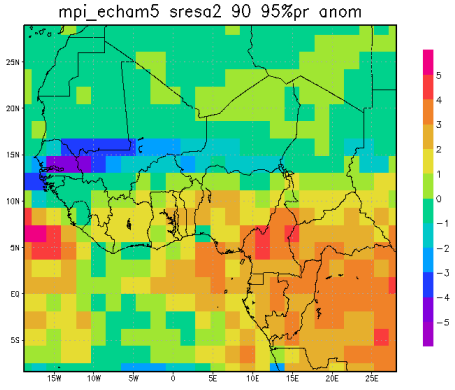
mpi_echam5 sresa2 90 95%pr anom

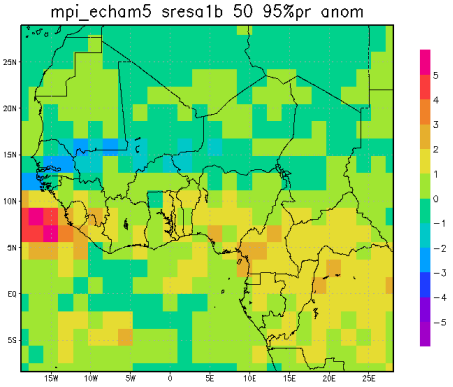
mpi_echam5 sresa1b 50 95%pr anom

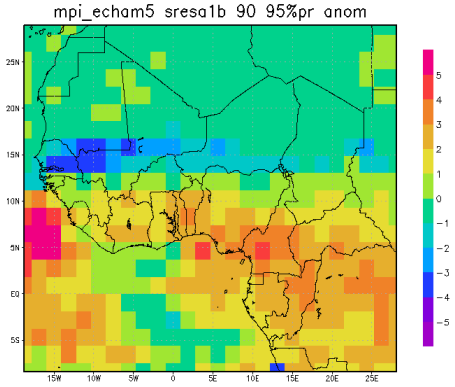
mpi_echam5 sresa1b 90 95%pr anom

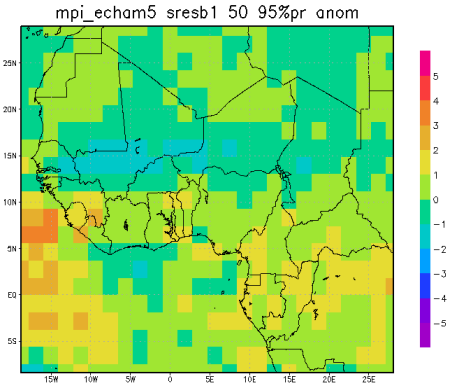
mpi_echam5 sresb1 50 95%pr anom

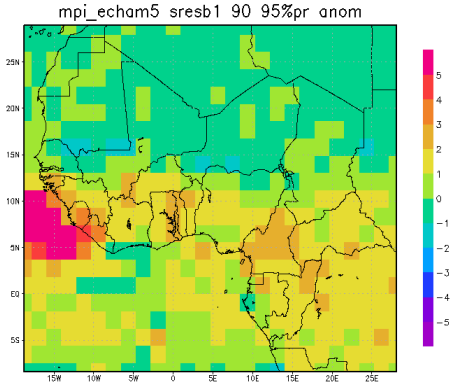
mpi_echam5 sresb1 90 95%pr anom

mri_cgcm2_3_2a sresa2 50 95%pr anom

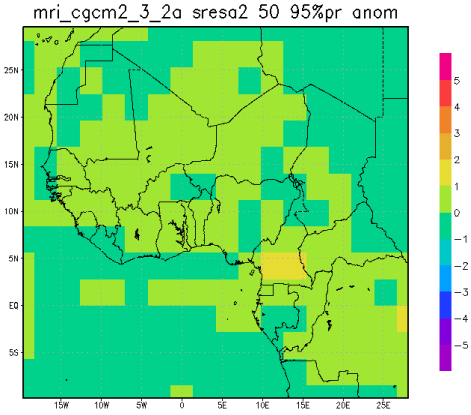

mri_cgcm2_3_2a sresa2 90 95%pr anom

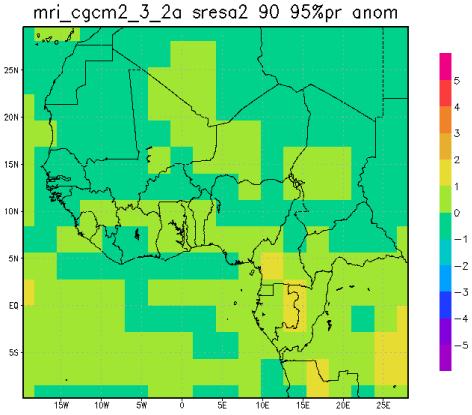

mri_cgcm2_3_2a sresa1b 50 95%pr anom

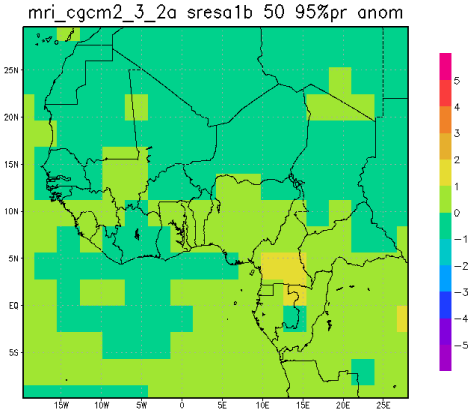

mri_cgcm2_3_2a sresa1b 90 95%pr anom

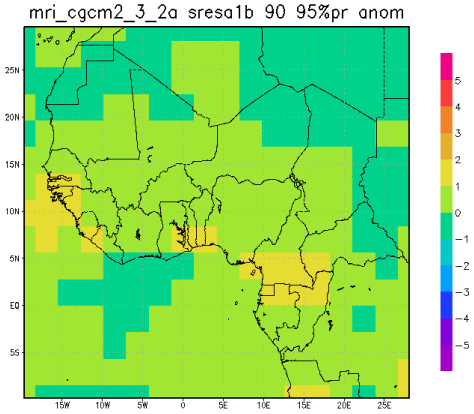

mri_cgcm2_3_2a sresb1 50 95%pr anom

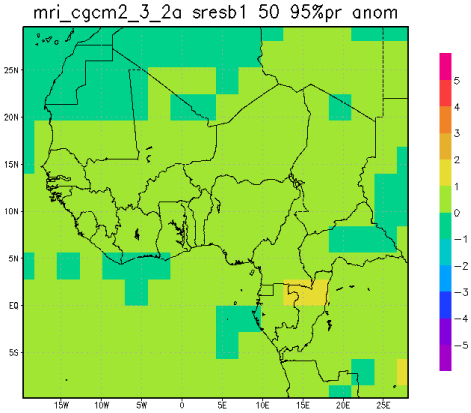

mri_cgcm2_3_2a sresb1 90 95%pr anom

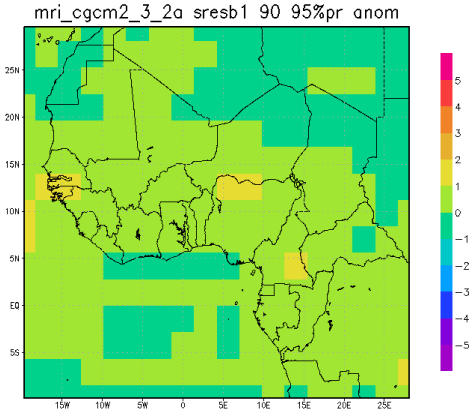

Appendix 11: Model derived 95% maximum and 5% minimum temperature anomalies, relative to 20c3m climatologies

a. 95% maximum anomalies

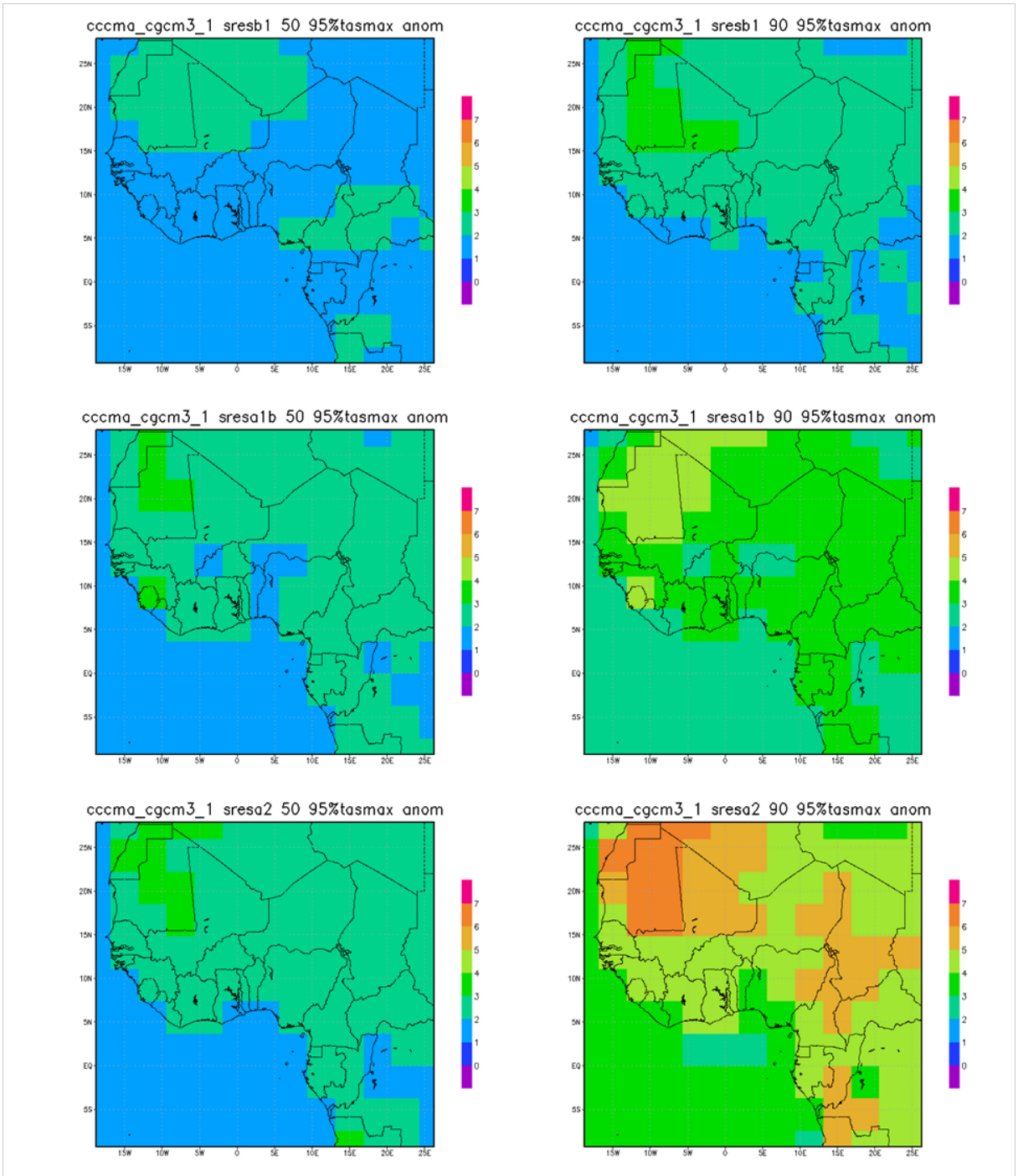

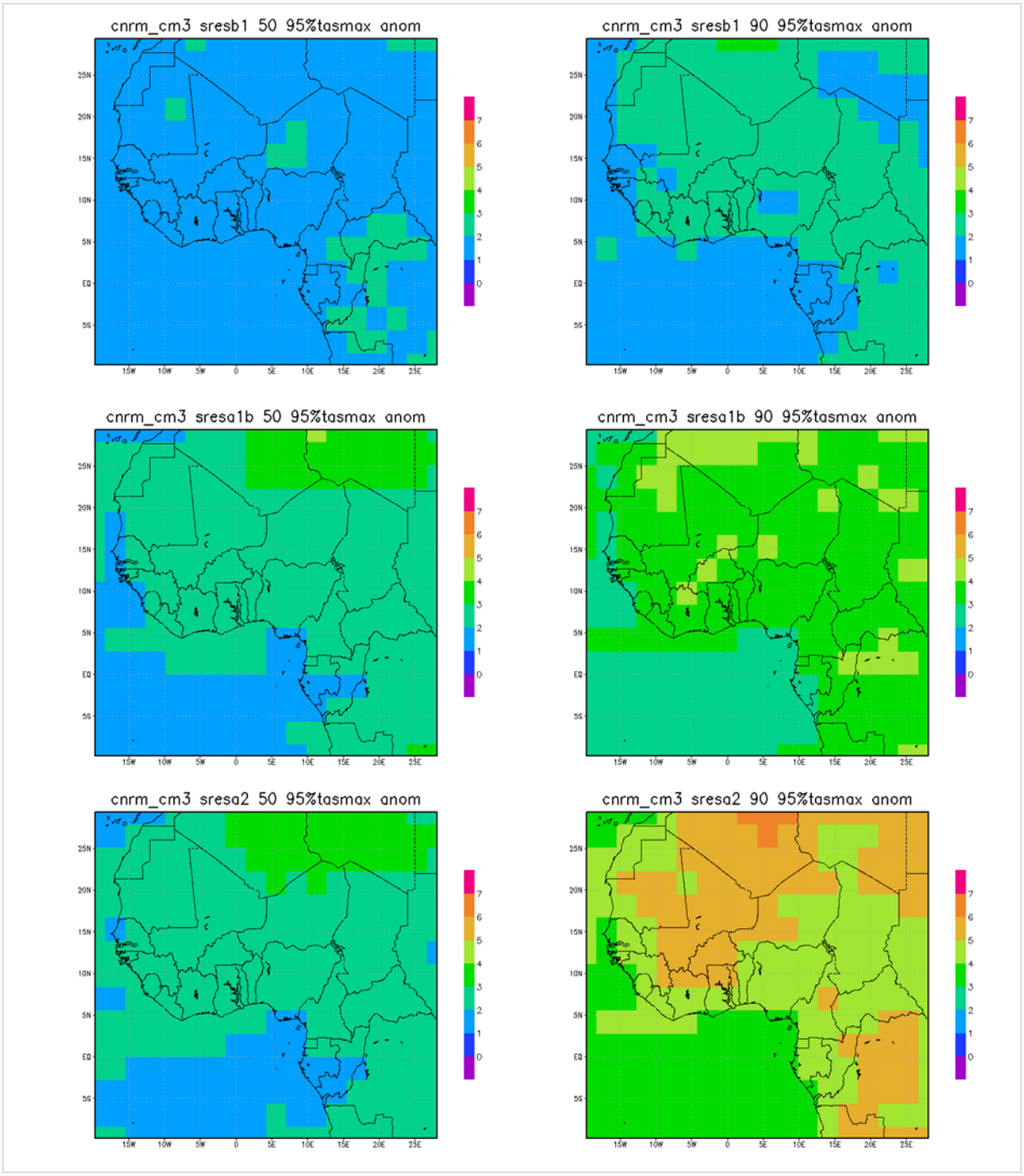
cnrm_cm3 sresb1 50 95%tasmax anom
cnrm_cm3 sresb1 90 95%tasmax anom
cnrm_cm3 sresa1b 50 95%tasmax anom
cnrm_cm3 sresa1b 90 95%tasmax anom
cnrm_cm3 sresa2 50 95%tasmax anom
cnrm_cm3 sresa2 90 95%tasmax anom

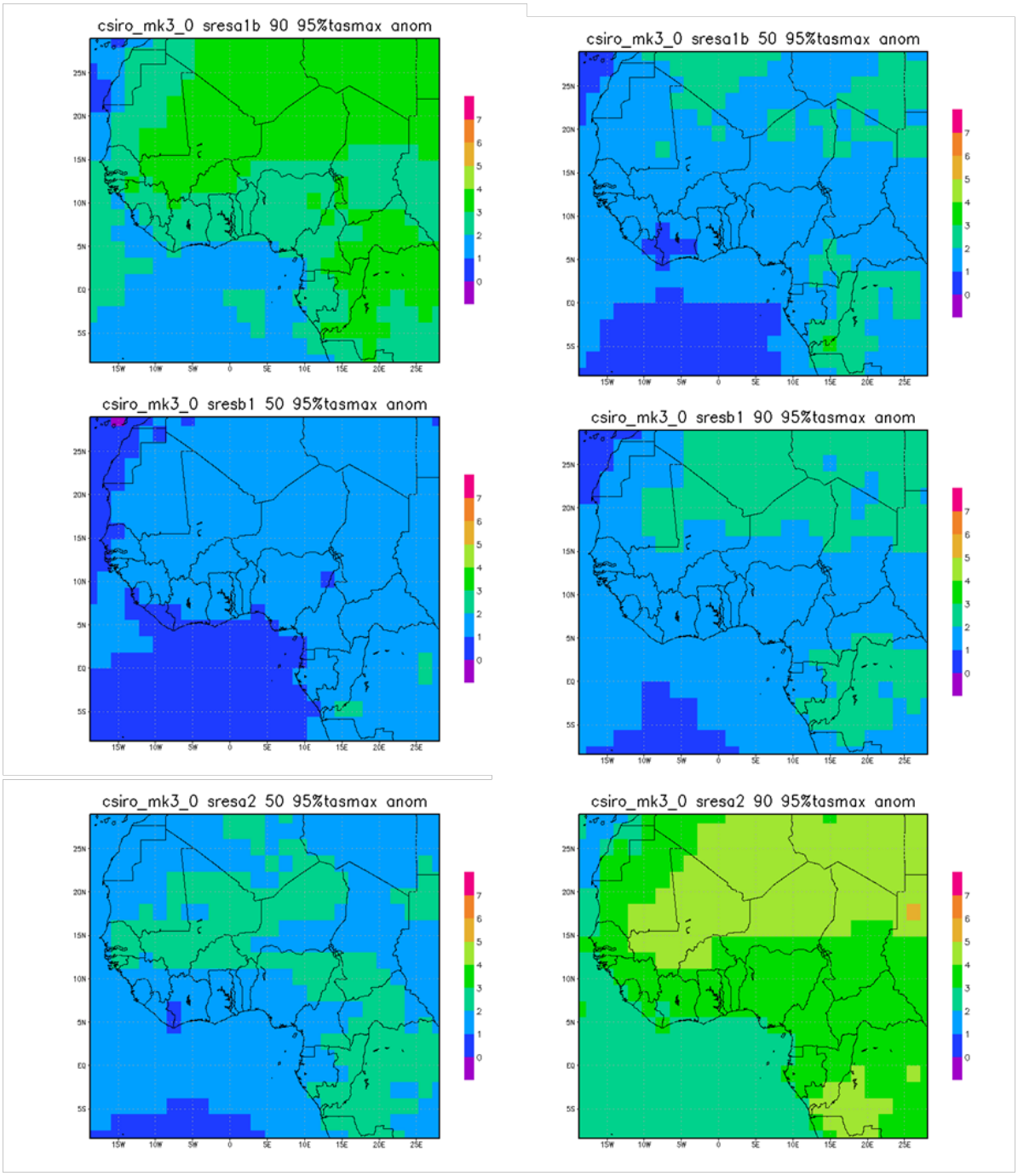
csiro_mk3_0 sresa1b 90 95%tasmax anom
csiro_mk3_0 sresa1b 50 95%tasmax anom
csiro_mk3_0 sresb1 50 95%tasmax anom
csiro_mk3_0 sresb1 90 95%tasmax anom
csiro_mk3_0 sresa2 50 95%tasmax anom
csiro_mk3_0 sresa2 90 95%tasmax anom

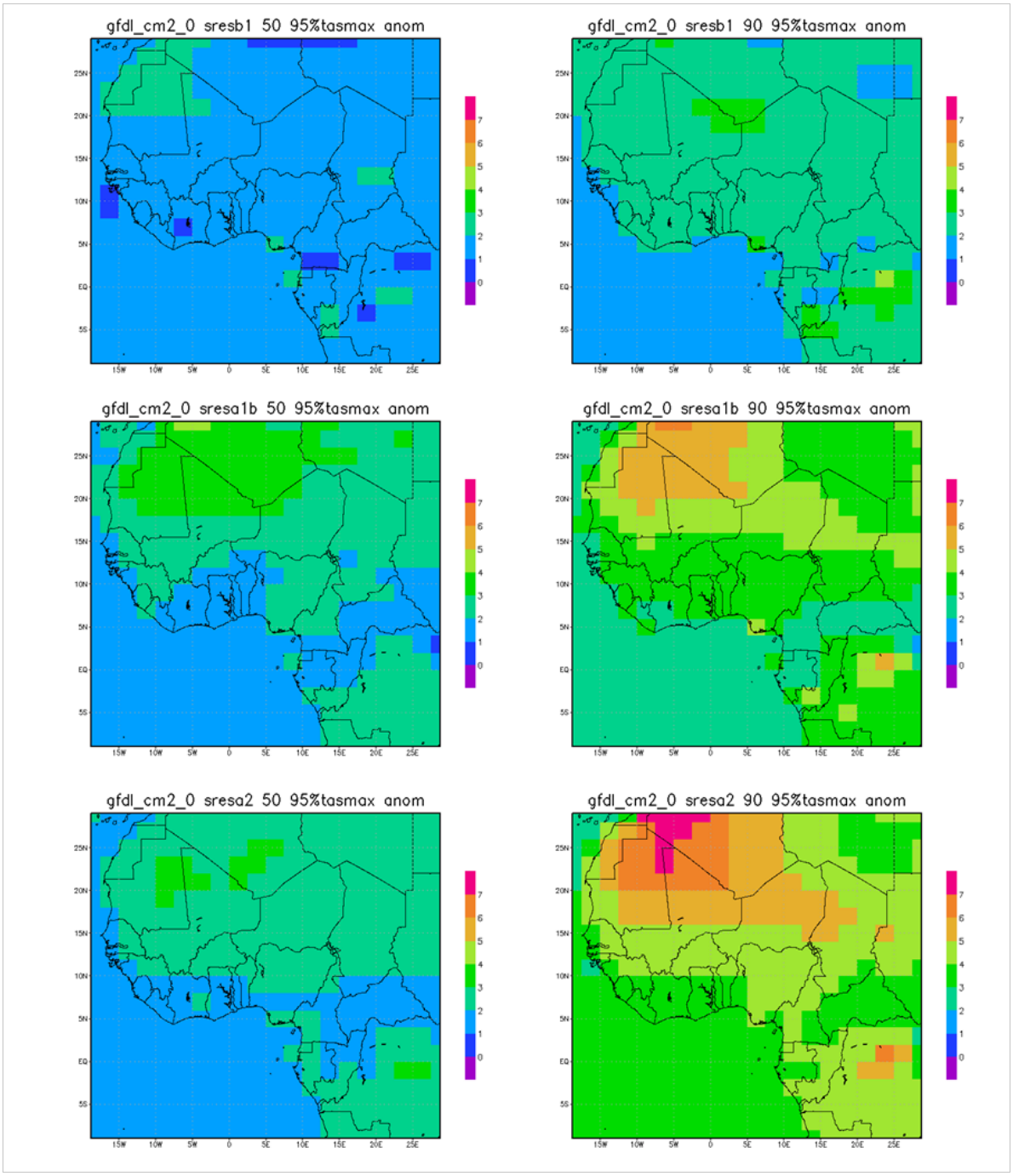
gfdl_cm2_0 sresb1 50 95%tasmax anom
gfdl_cm2_0 sresb1 90 95%tasmax anom
gfdl_cm2_0 sresa1b 50 95%tasmax anom
gfdl_cm2_0 sresa1b 90 95%tasmax anom
gfdl_cm2_0 sresa2 50 95%tasmax anom
gfdl_cm2_0 sresa2 90 95%tasmax anom

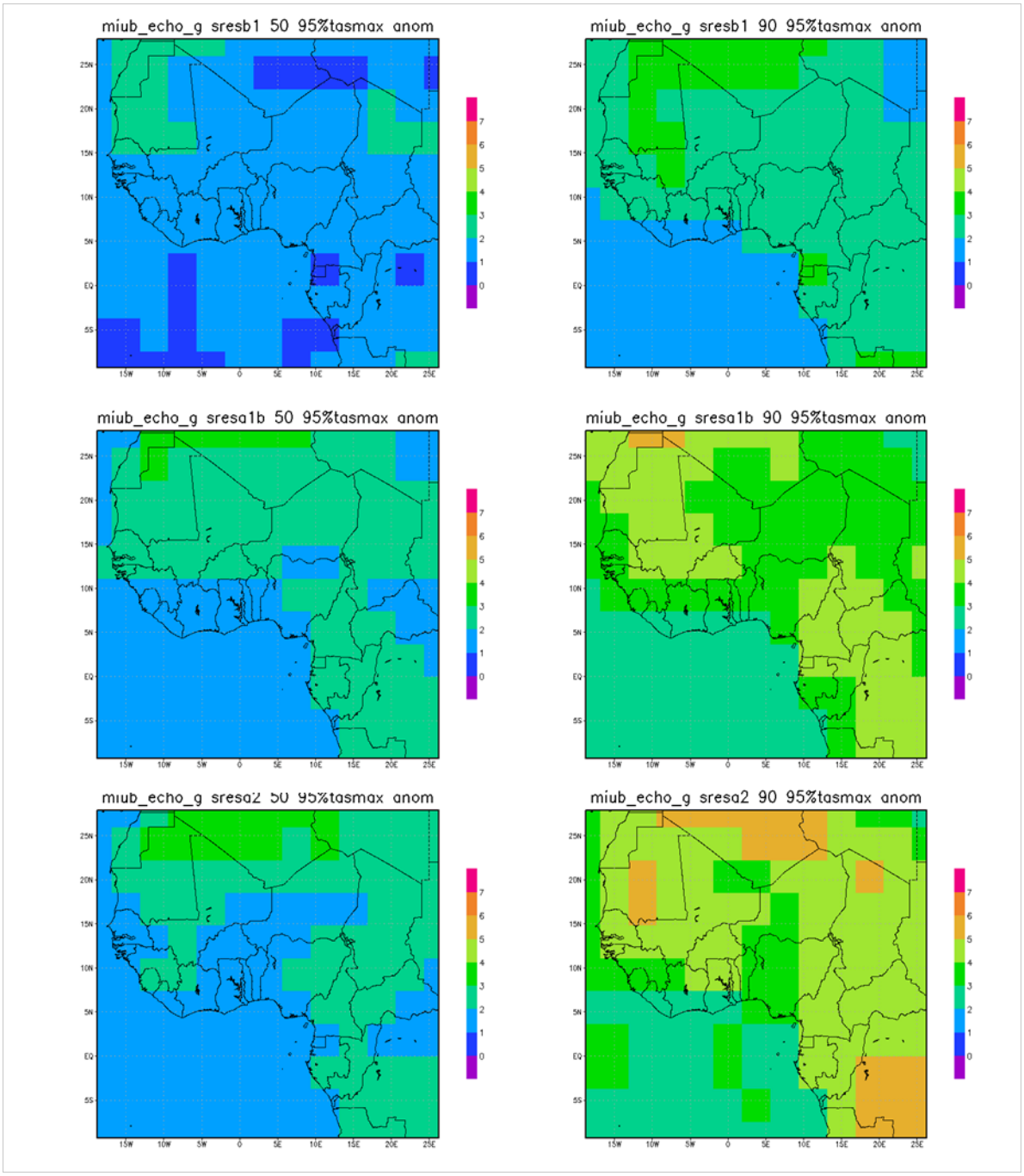
miub_echo_g sresb1 50 95%tasmax anom
miub_echo_g sresb1 90 95%tasmax anom
miub_echo_g sresa1b 50 95%tasmax anom
miub_echo_g sresa1b 90 95%tasmax anom
miub_echo_g sresa2 50 95%tasmax anom
miub_echo_g sresa2 90 95%tasmax anom

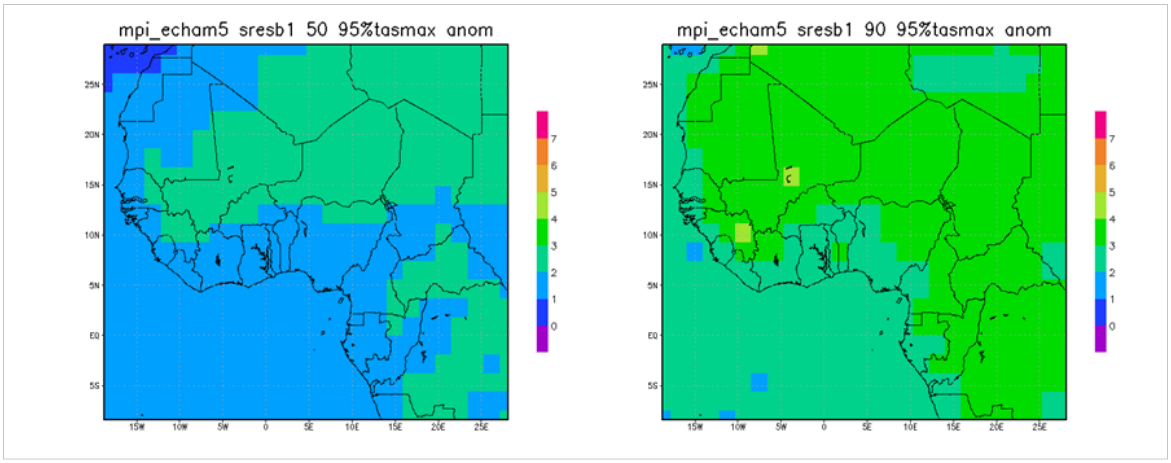
mpi_echam5 sresb1 50 95%tasmax anom
mpi_echam5 sresb1 90 95%tasmax anom

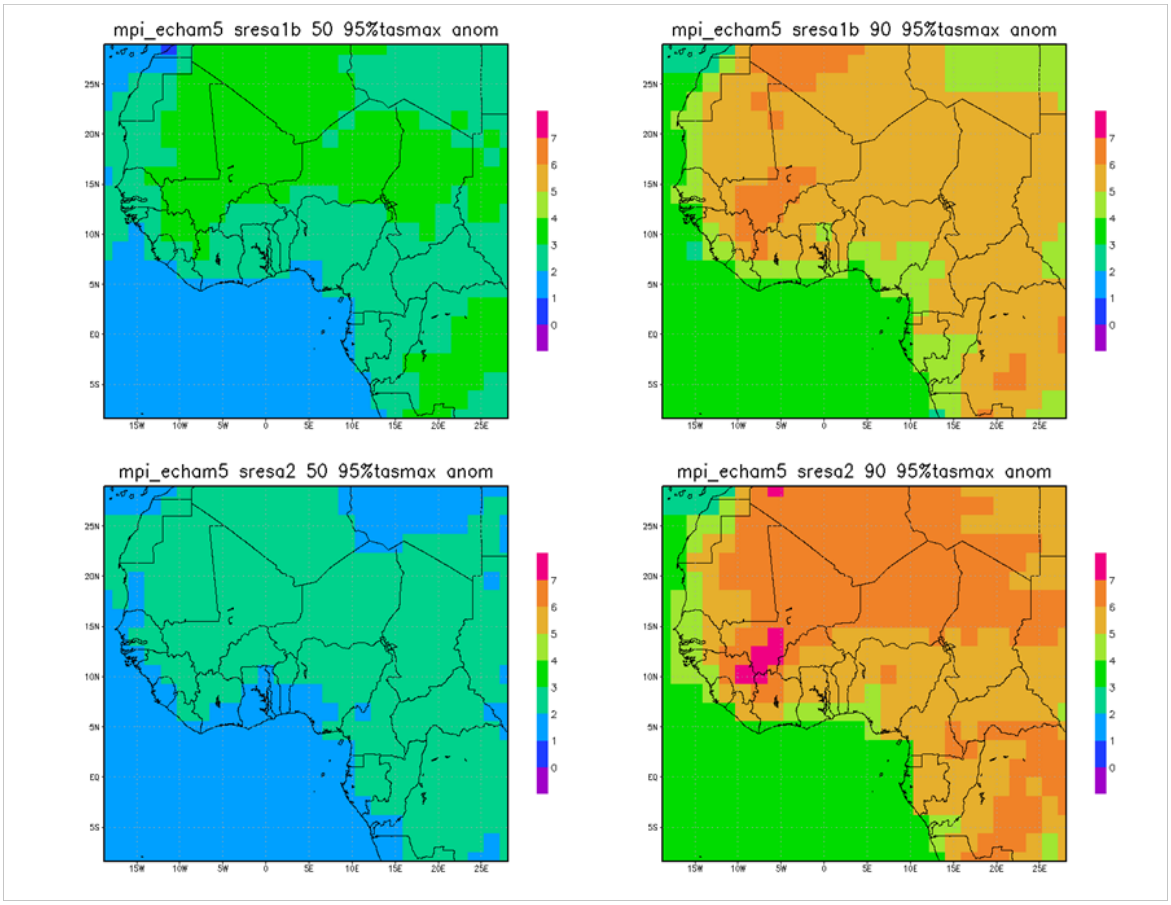
mpi_echam5 sresa1b 50 95%tasmax anom
mpi_echam5 sresa1b 90 95%tasmax anom
mpi_echam5 sresa2 50 95%tasmax anom
mpi_echam5 sresa2 90 95%tasmax anom

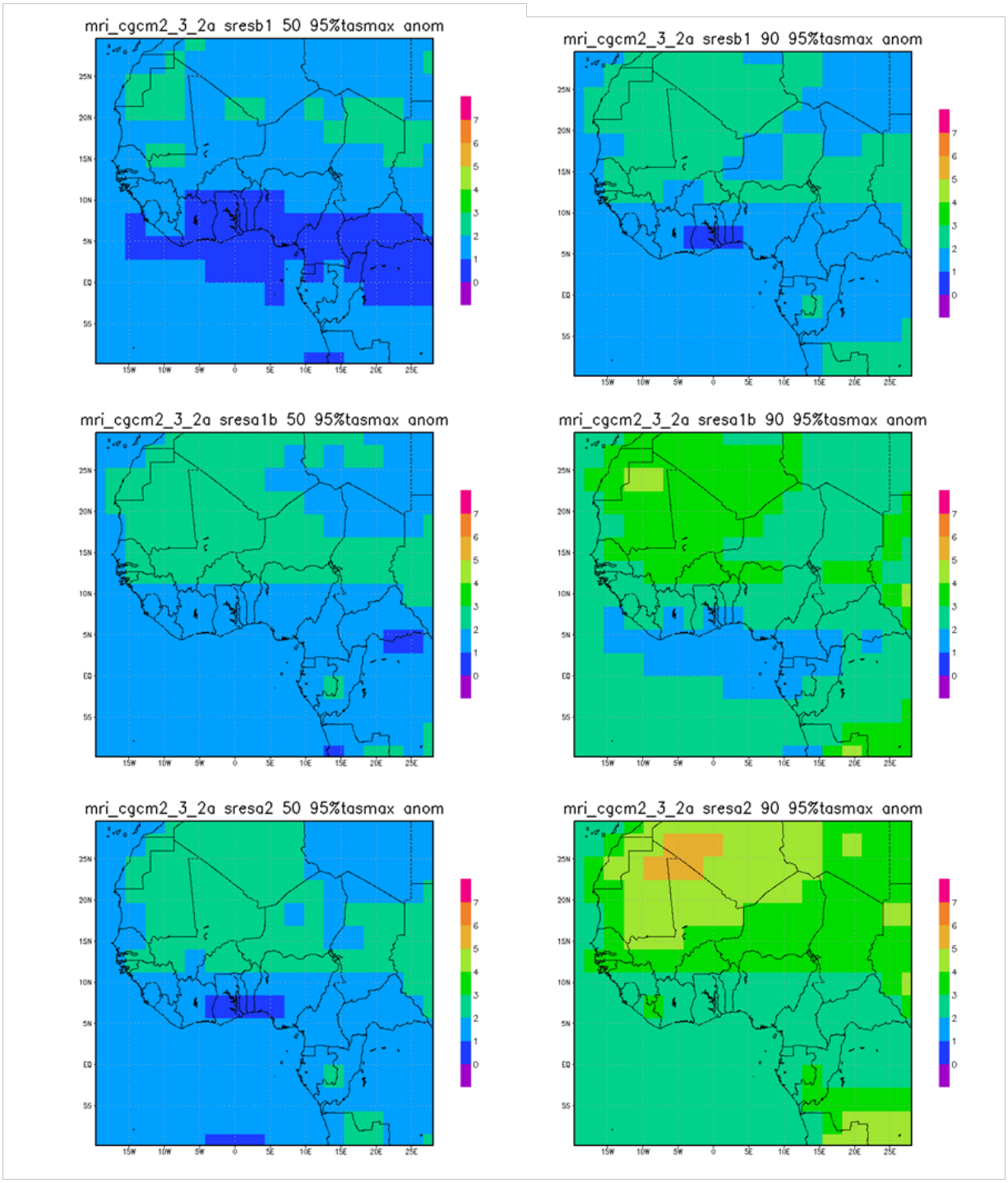
mri_cgcm2_3_2a sresb1 50 95%tasmax anom
mri_cgcm2_3_2a sresb1 90 95%tasmax anom
mri_cgcm2_3_2a sresa1b 50 95%tasmax anom
mri_cgcm2_3_2a sresa1b 90 95%tasmax anom
mri_cgcm2_3_2a sresa2 50 95%tasmax anom
mri_cgcm2_3_2a sresa2 90 95%tasmax anom

b. 5% minimum anomalies

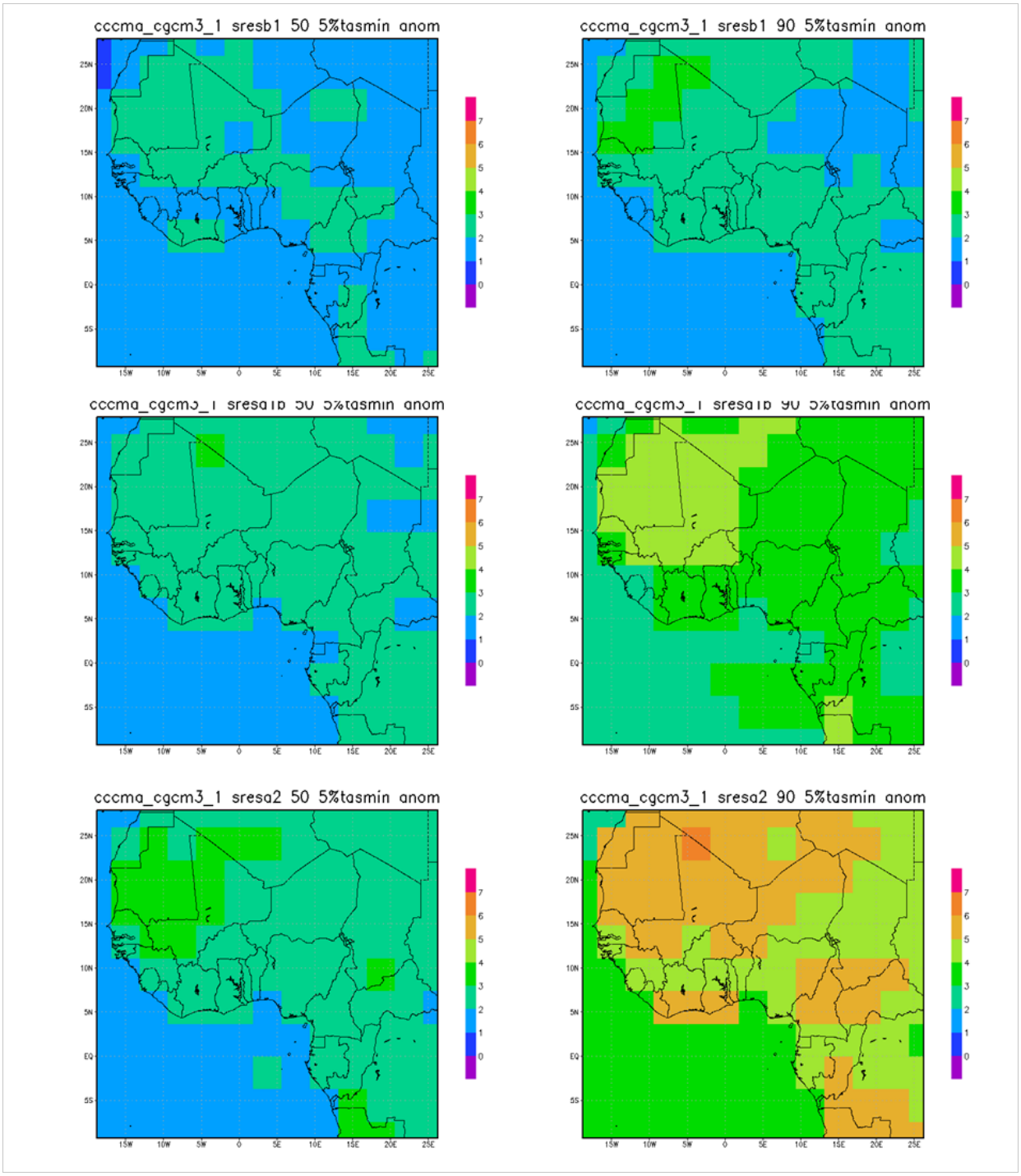

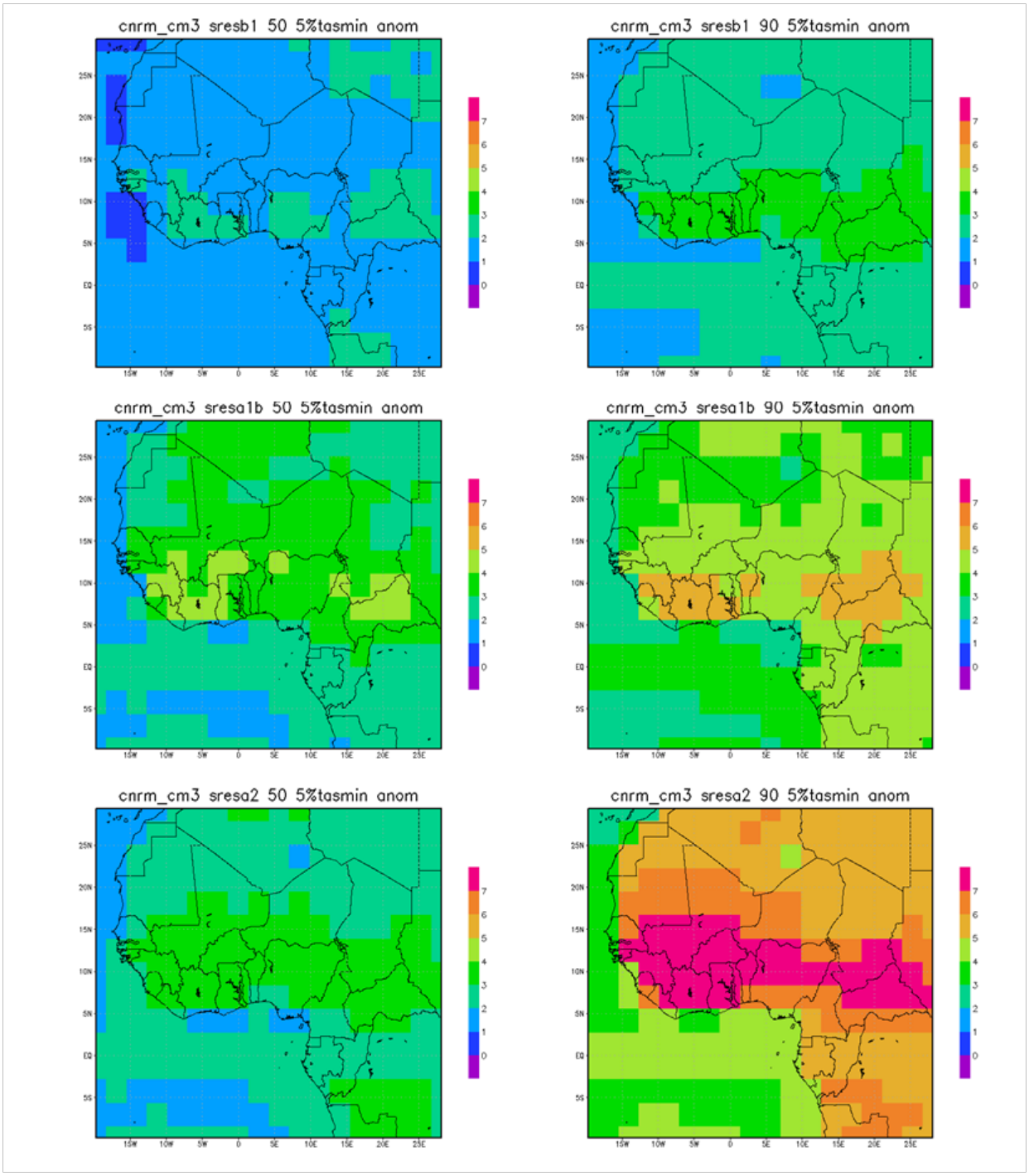
cnrm_cm3 sresb1 50 5%tasmin anom
cnrm_cm3 sresb1 90 5%tasmin anom
cnrm_cm3 sresa1b 50 5%tasmin anom
cnrm_cm3 sresa1b 90 5%tasmin anom
cnrm_cm3 sresa2 50 5%tasmin anom
cnrm_cm3 sresa2 90 5%tasmin anom

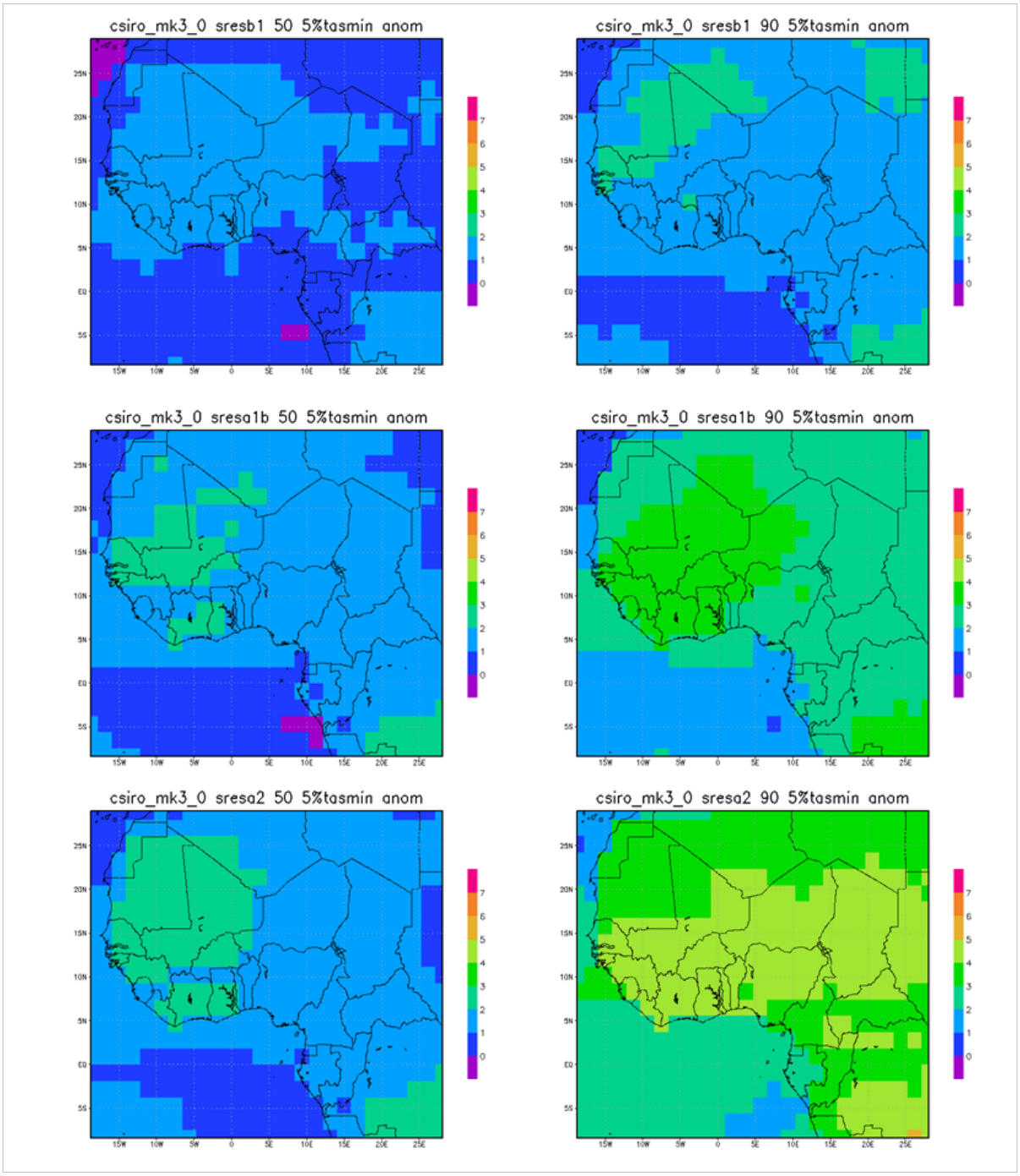
csiro_mk3_0 sresb1 50 5%tasmin anom
csiro_mk3_0 sresb1 90 5%tasmin anom
csiro_mk3_0 sresa1b 50 5%tasmin anom
csiro_mk3_0 sresa1b 90 5%tasmin anom
csiro_mk3_0 sresa2 50 5%tasmin anom
csiro_mk3_0 sresa2 90 5%tasmin anom

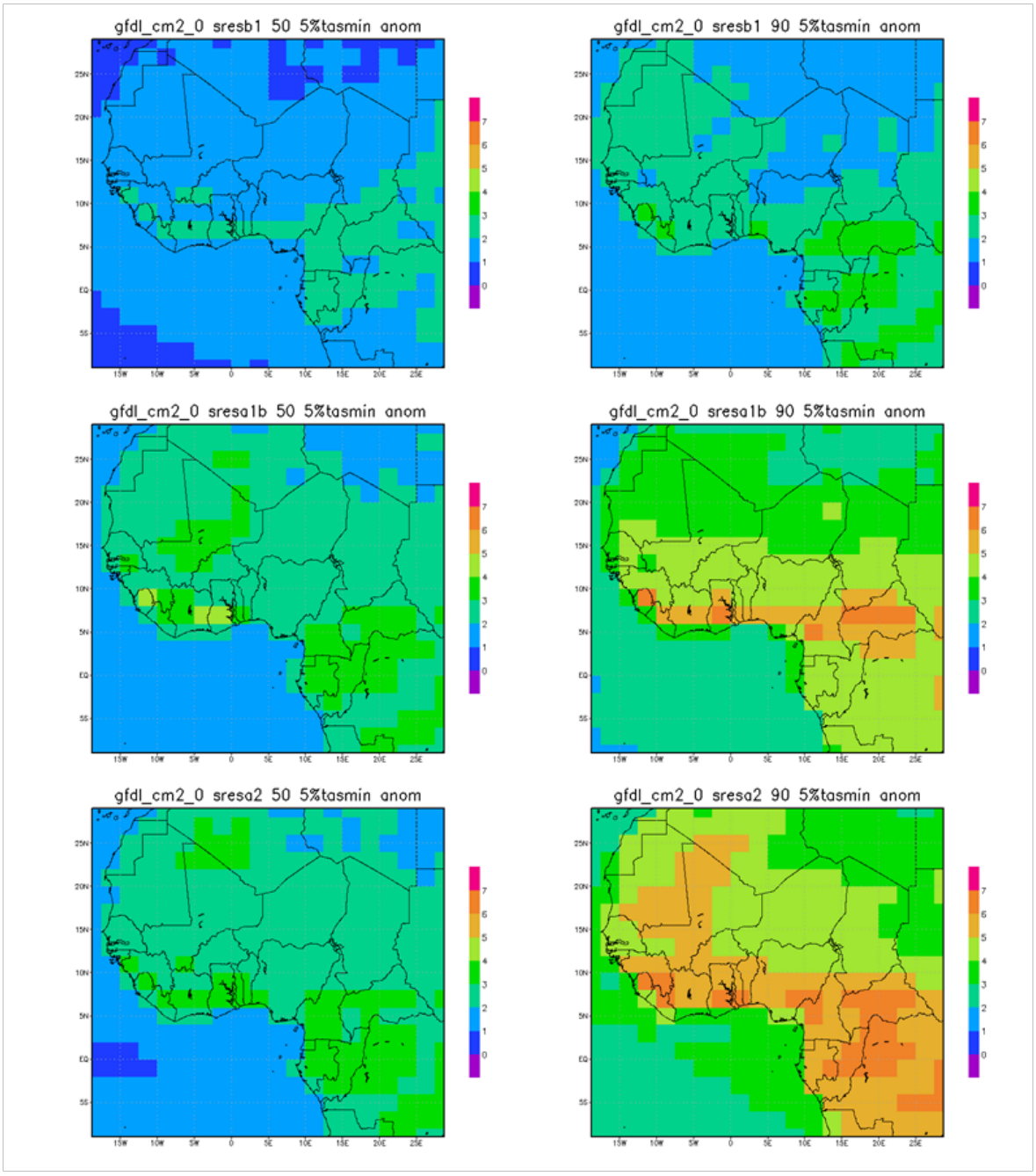
gfdl_cm2_0 sresb1 50 5%tasmin anom
gfdl_cm2_0 sresb1 90 5%tasmin anom
gfdl_cm2_0 sresa1b 50 5%tasmin anom
gfdl_cm2_0 sresa1b 90 5%tasmin anom
gfdl_cm2_0 sresa2 50 5%tasmin anom
gfdl_cm2_0 sresa2 90 5%tasmin anom

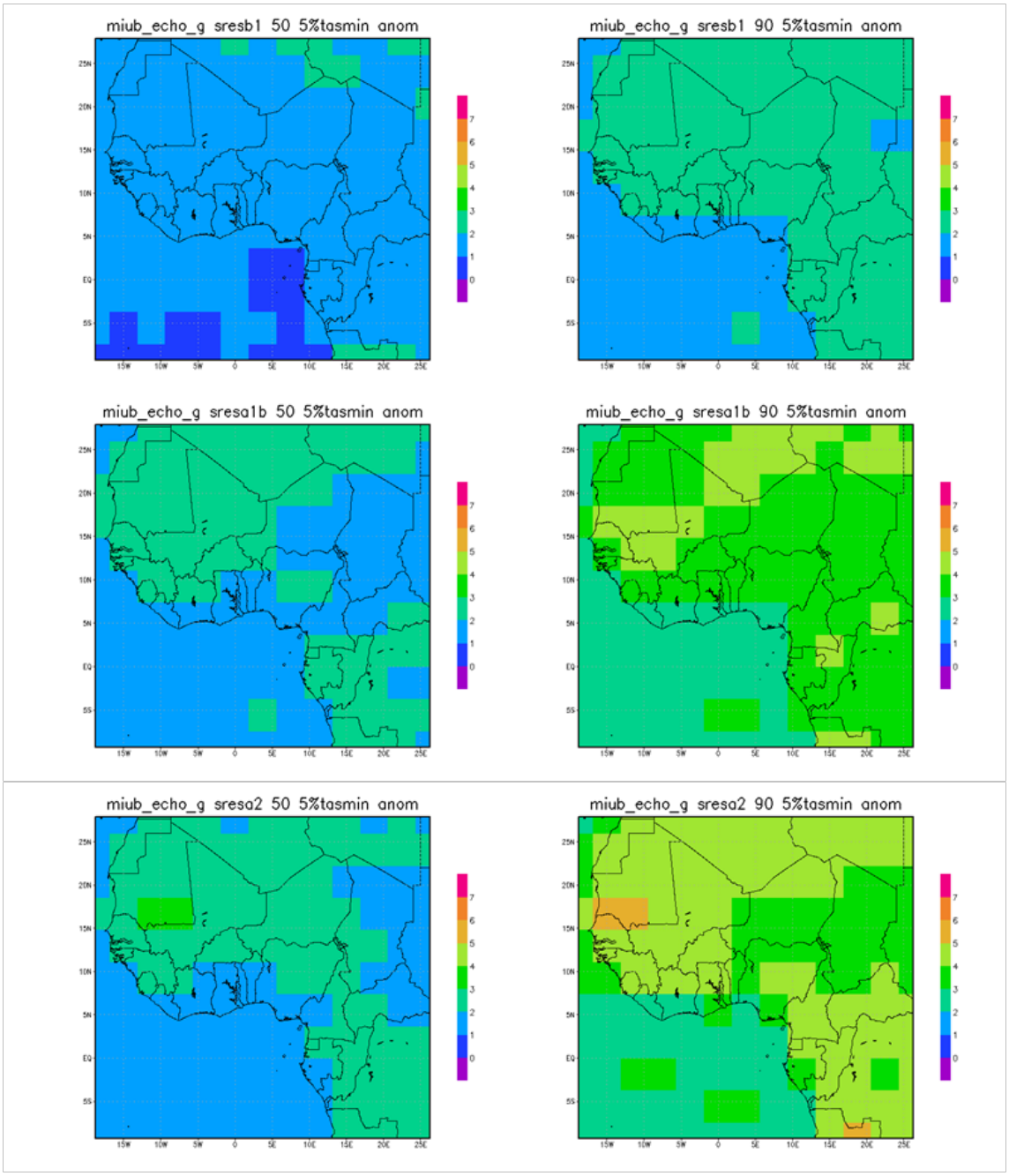
miub_echo_g sresb1 50 5%tasmin anom
miub_echo_g sresb1 90 5%tasmin anom
miub_echo_g sresa1b 50 5%tasmin anom
miub_echo_g sresa1b 90 5%tasmin anom
miub_echo_g sresa2 50 5%tasmin anom
miub_echo_g sresa2 90 5%tasmin anom

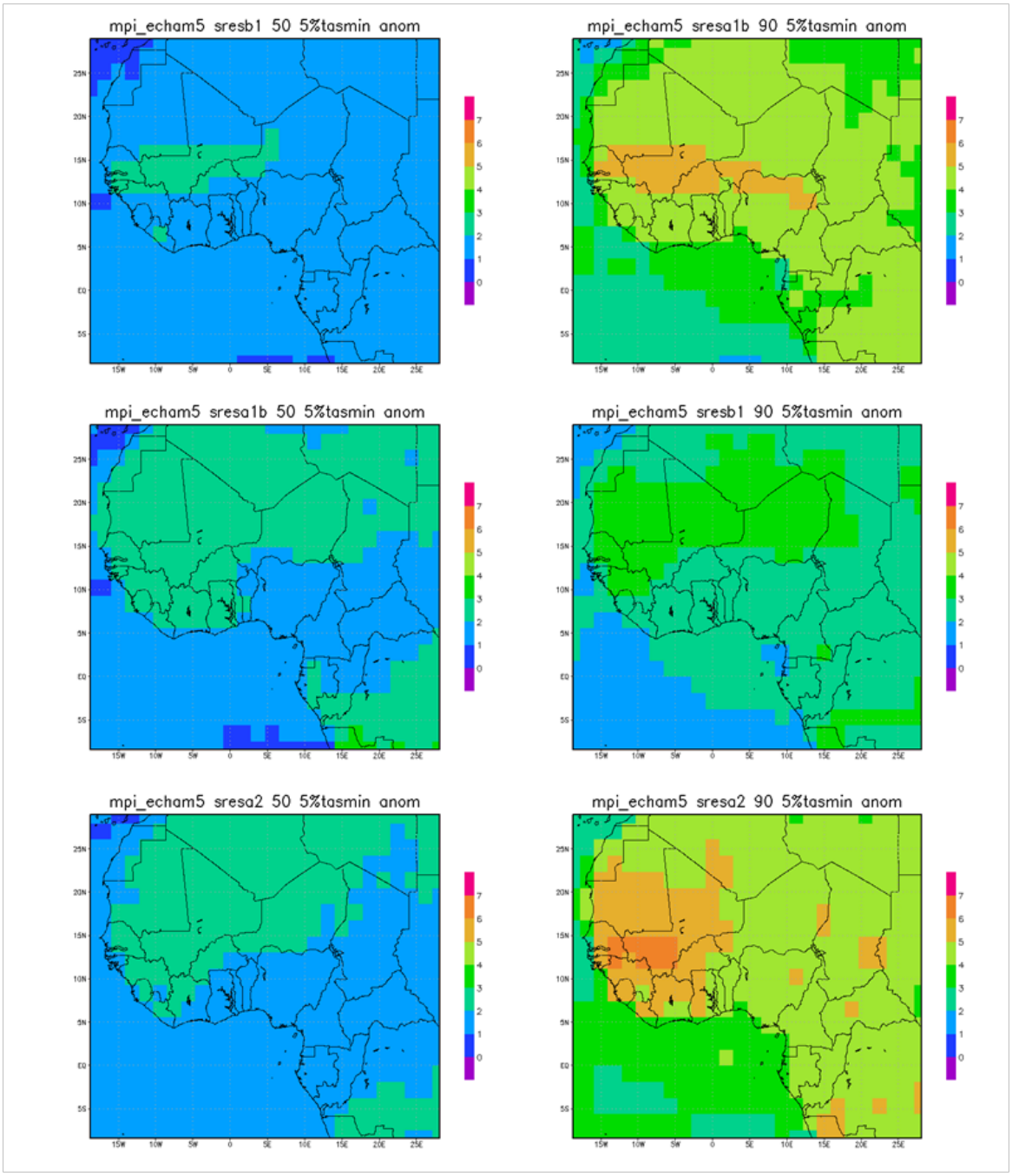
mpi_echam5 sresb1 50 5%tasmin anom
mpi_echam5 sresa1b 90 5%tasmin anom
mpi_echam5 sresa1b 50 5%tasmin anom
mpi_echam5 sresb1 90 5%tasmin anom
mpi_echam5 sresa2 50 5%tasmin anom
mpi_echam5 sresa2 90 5%tasmin anom

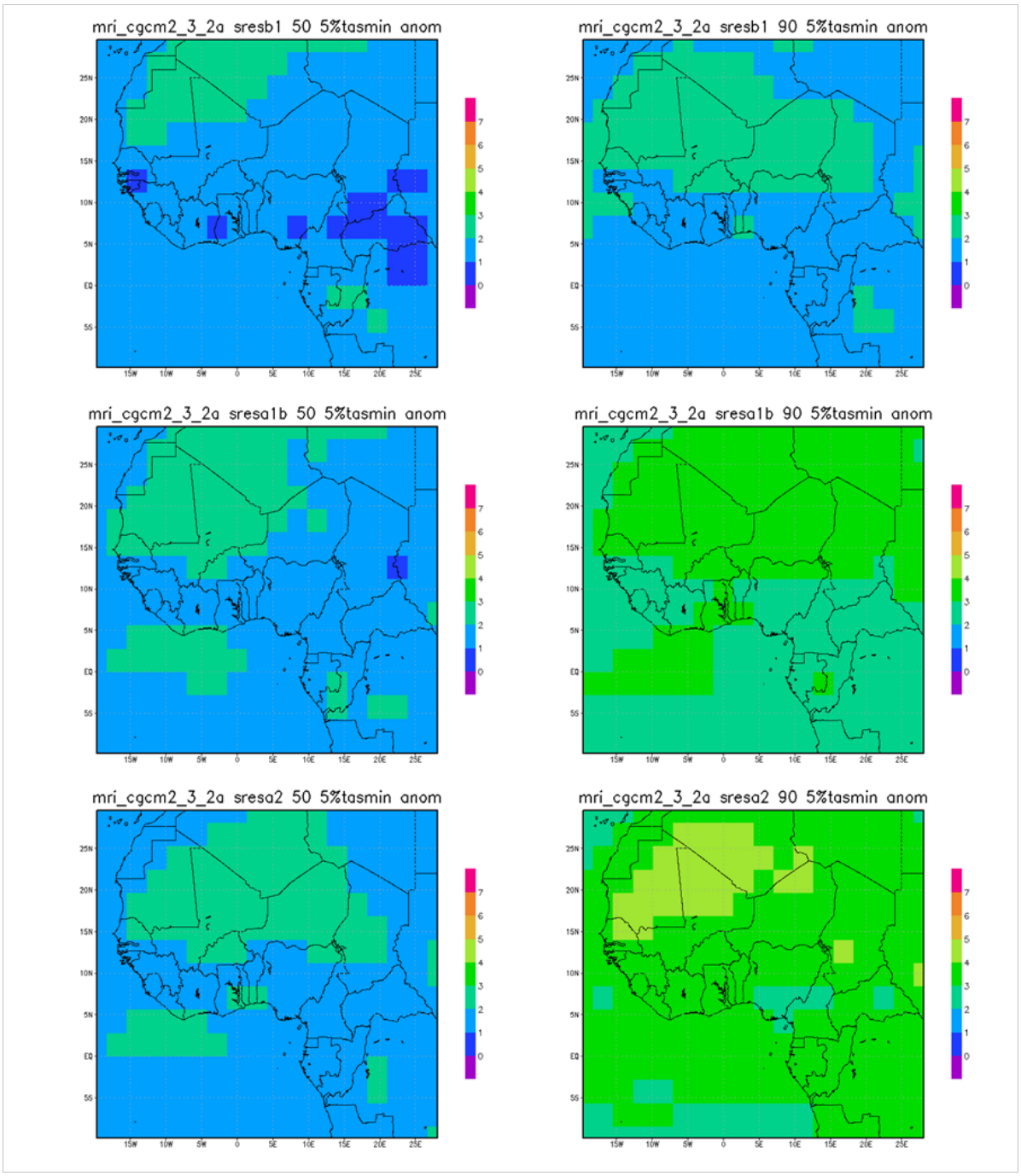
mri_cgcm2_3_2a sresb1 50 5%tasmin anom
mri_cgcm2_3_2a sresb1 90 5%tasmin anom
mri_cgcm2_3_2a sresa1b 50 5%tasmin anom
mri_cgcm2_3_2a sresa1b 90 5%tasmin anom
mri_cgcm2_3_2a sresa2 50 5%tasmin anom
mri_cgcm2_3_2a sresa2 90 5%tasmin anom

Appendix 12: Model Ensemble Derived Crop Domains

Model ensemble derived crop domains for the three periods and three forcing scenarios used in this study. Two sets of projections are provided - one based on anomalies relative to the NCEP data and other relative to the JapRe data, providing a form of initial condition uncertainty. Projections are provided for 2030s, 2050s and 2090s without minimum temperature data, and for the 2050s and 2090s including this data.

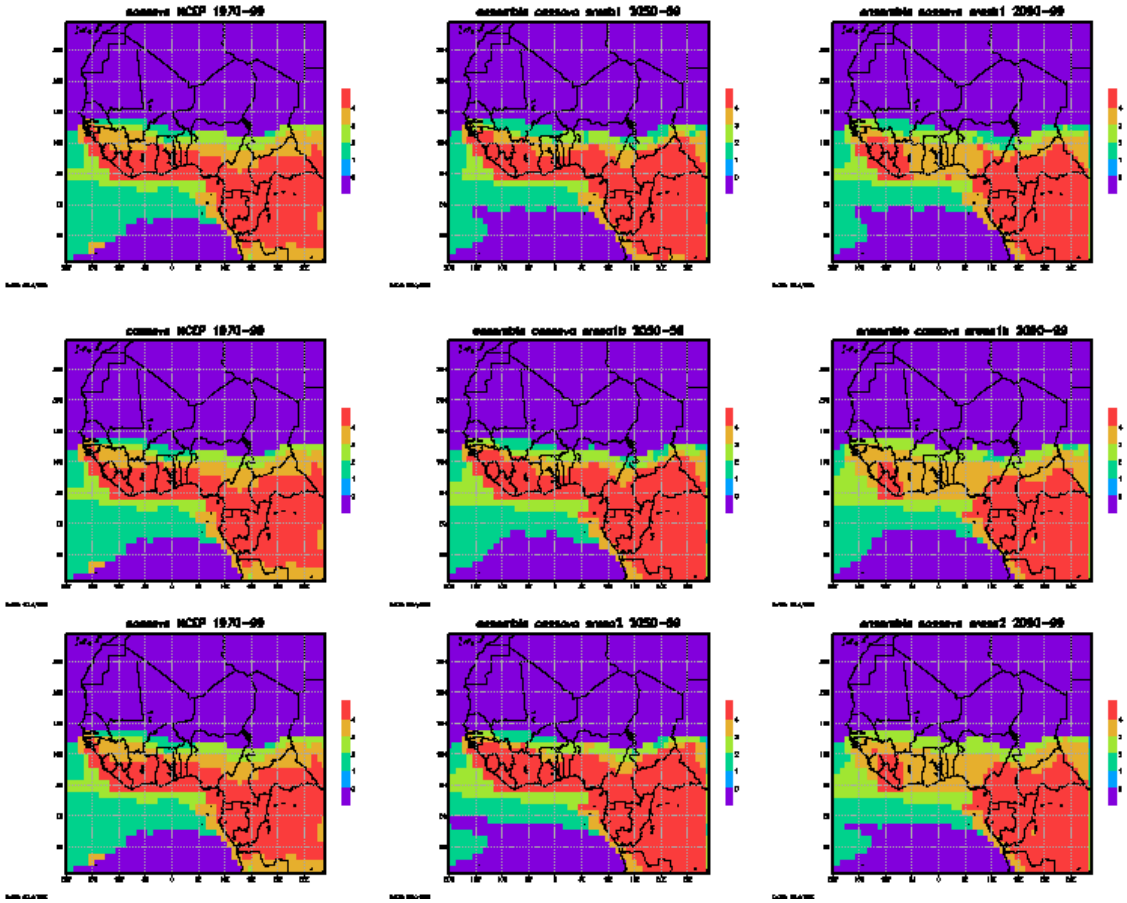

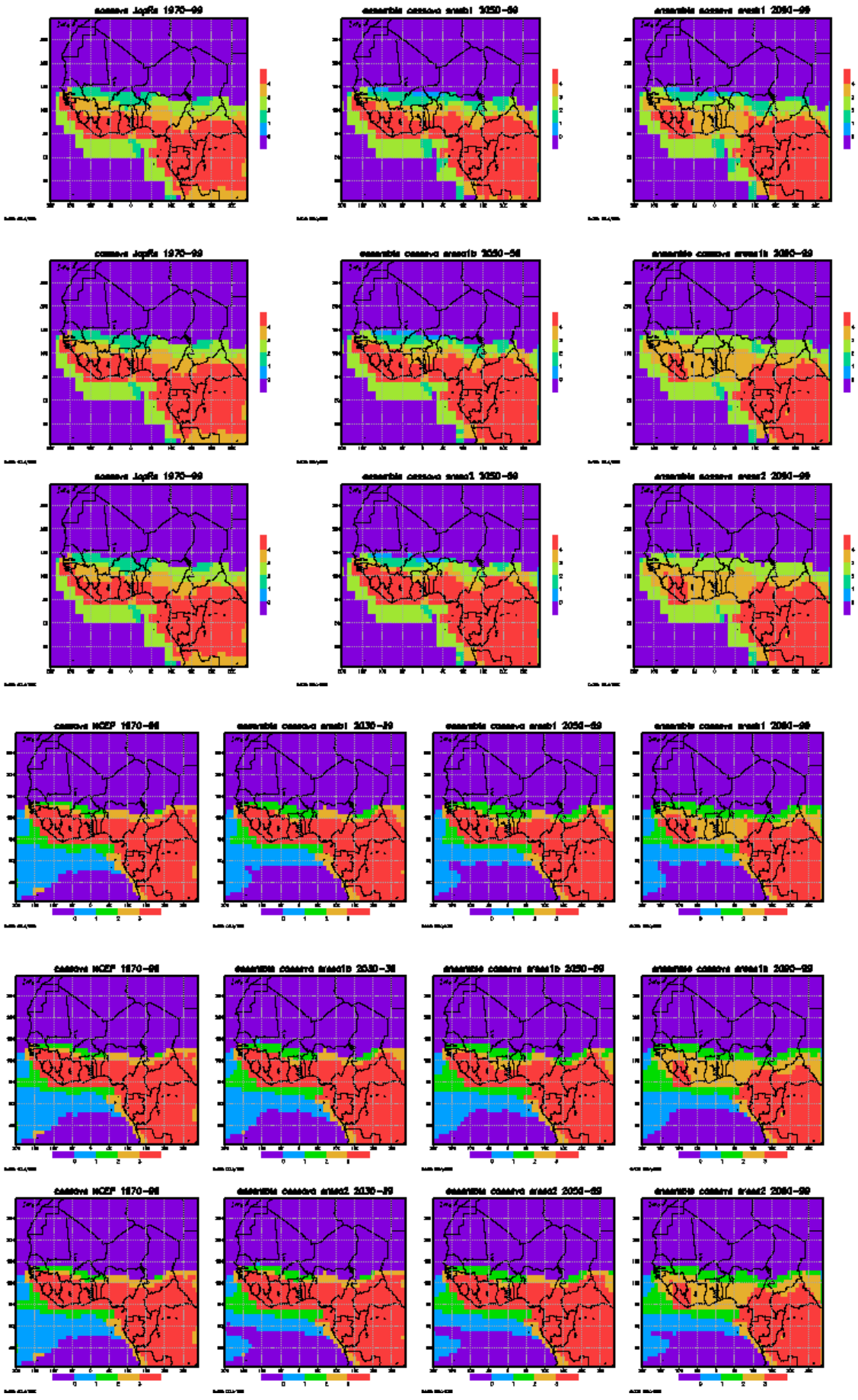

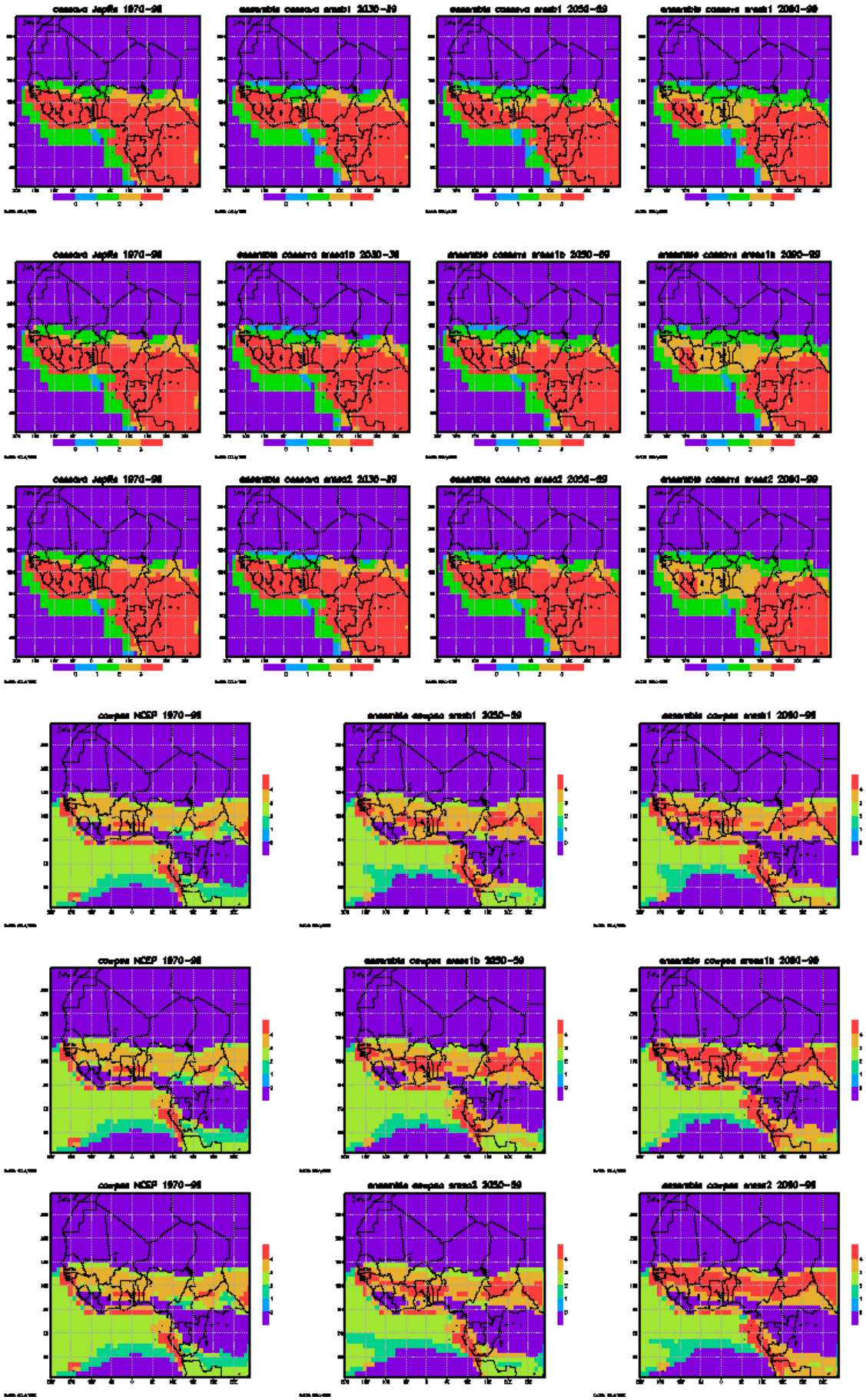

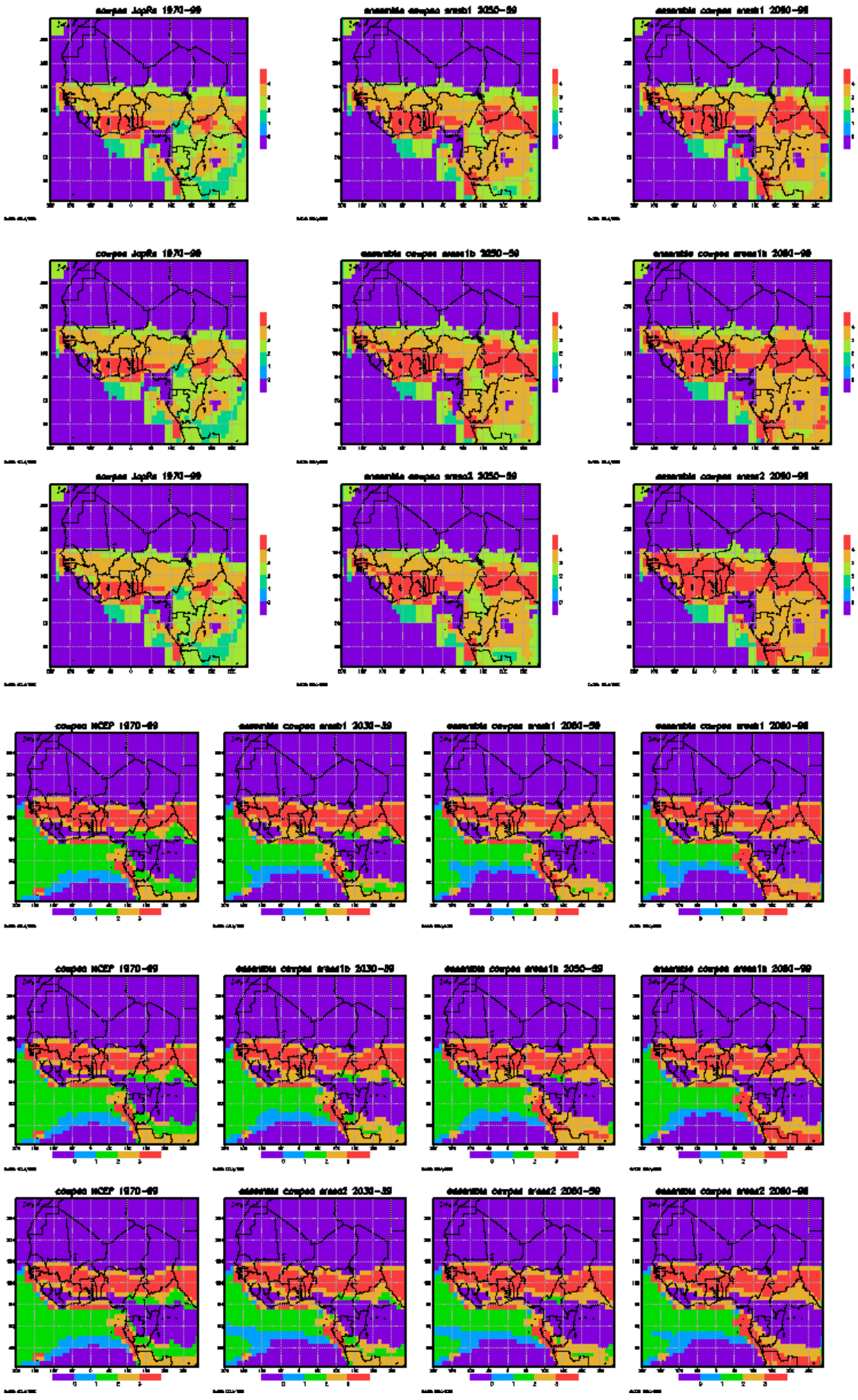

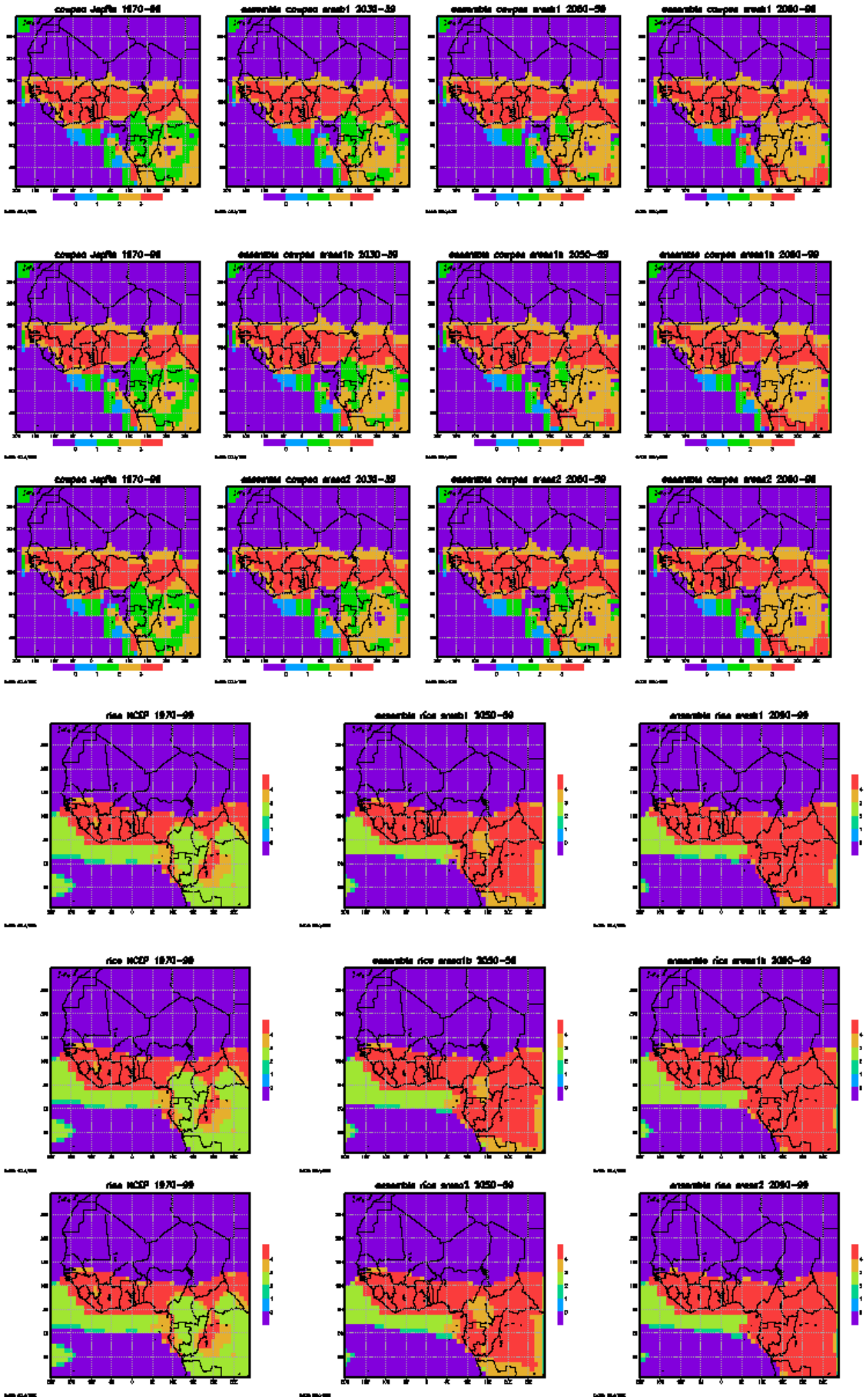

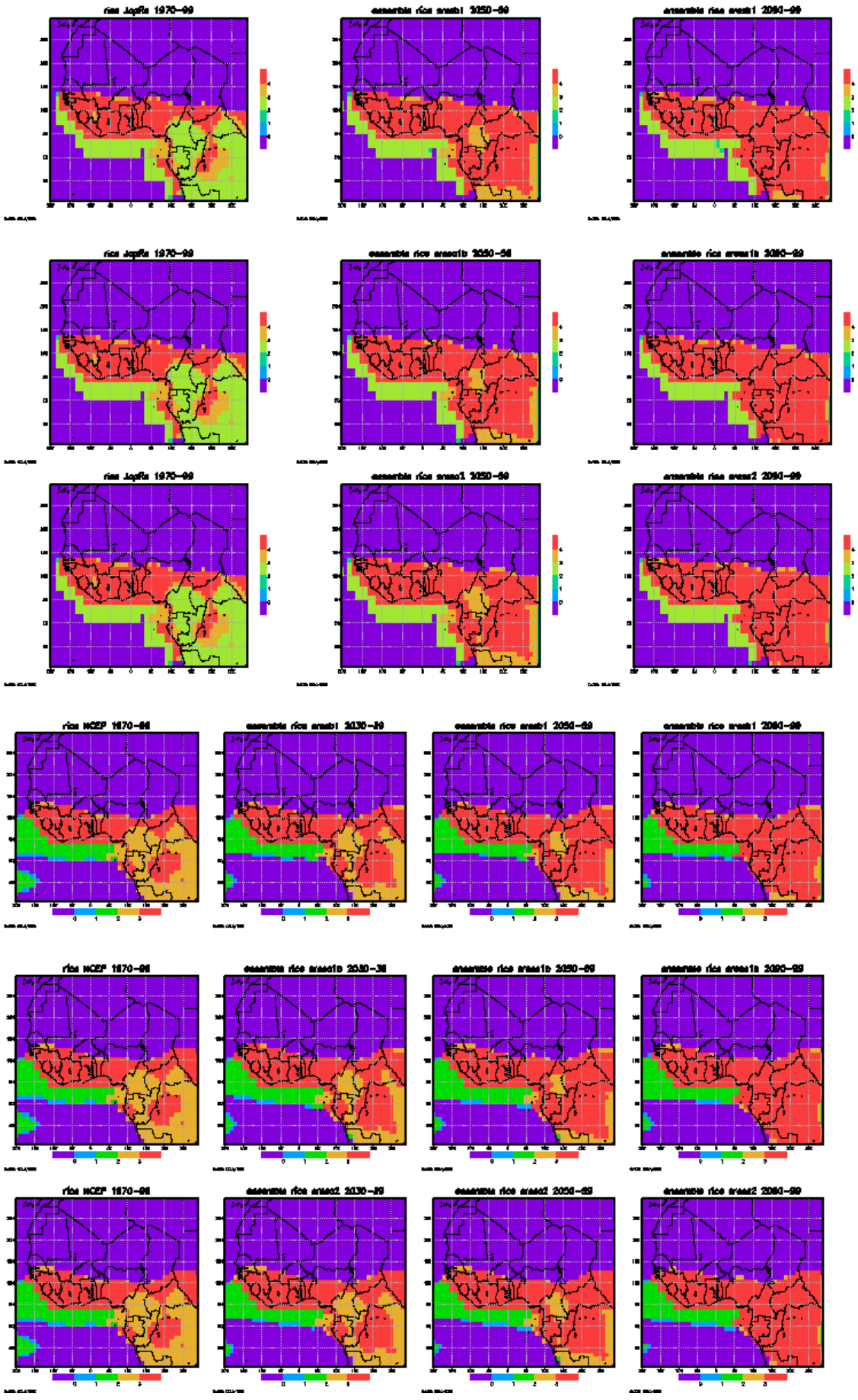

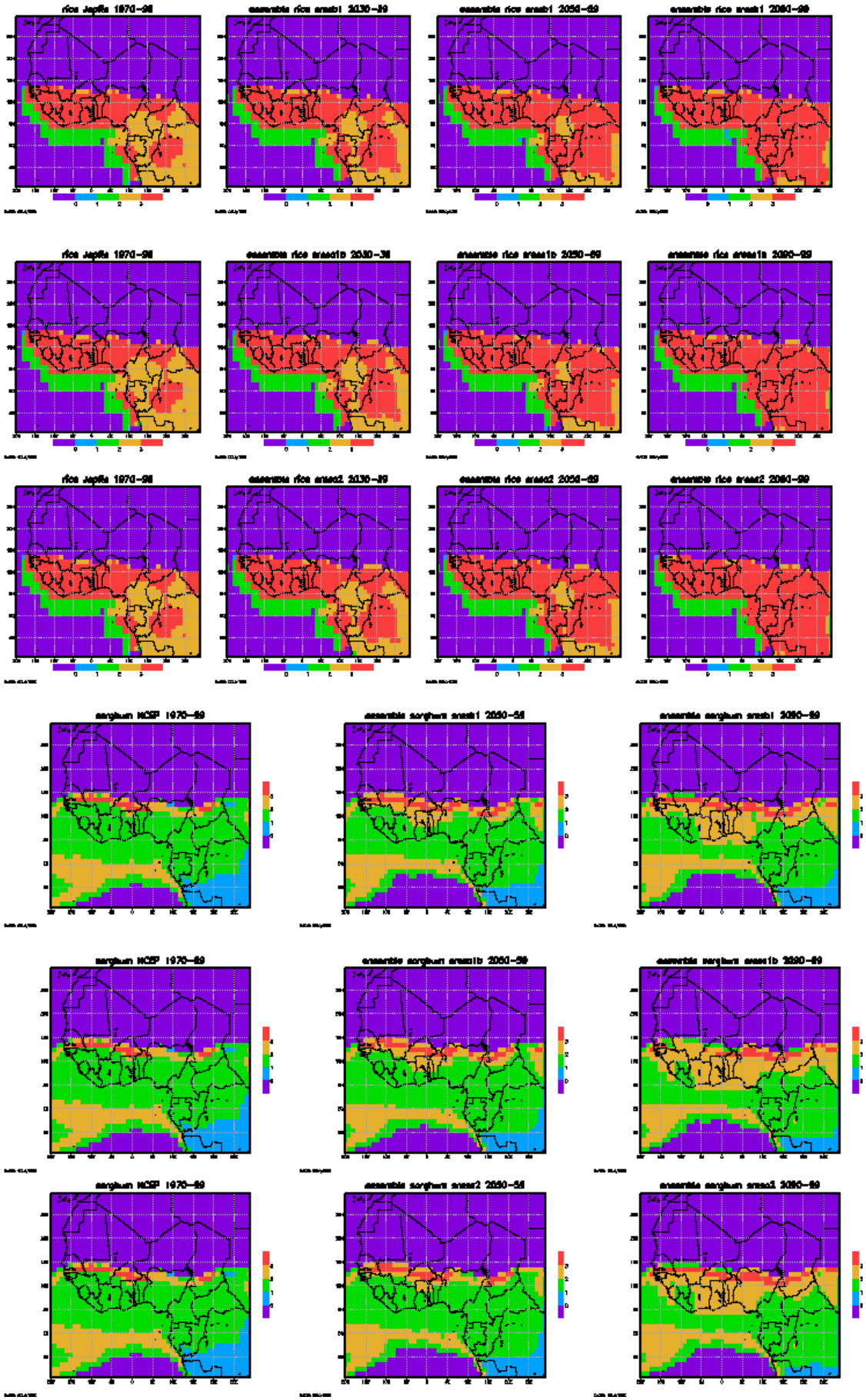

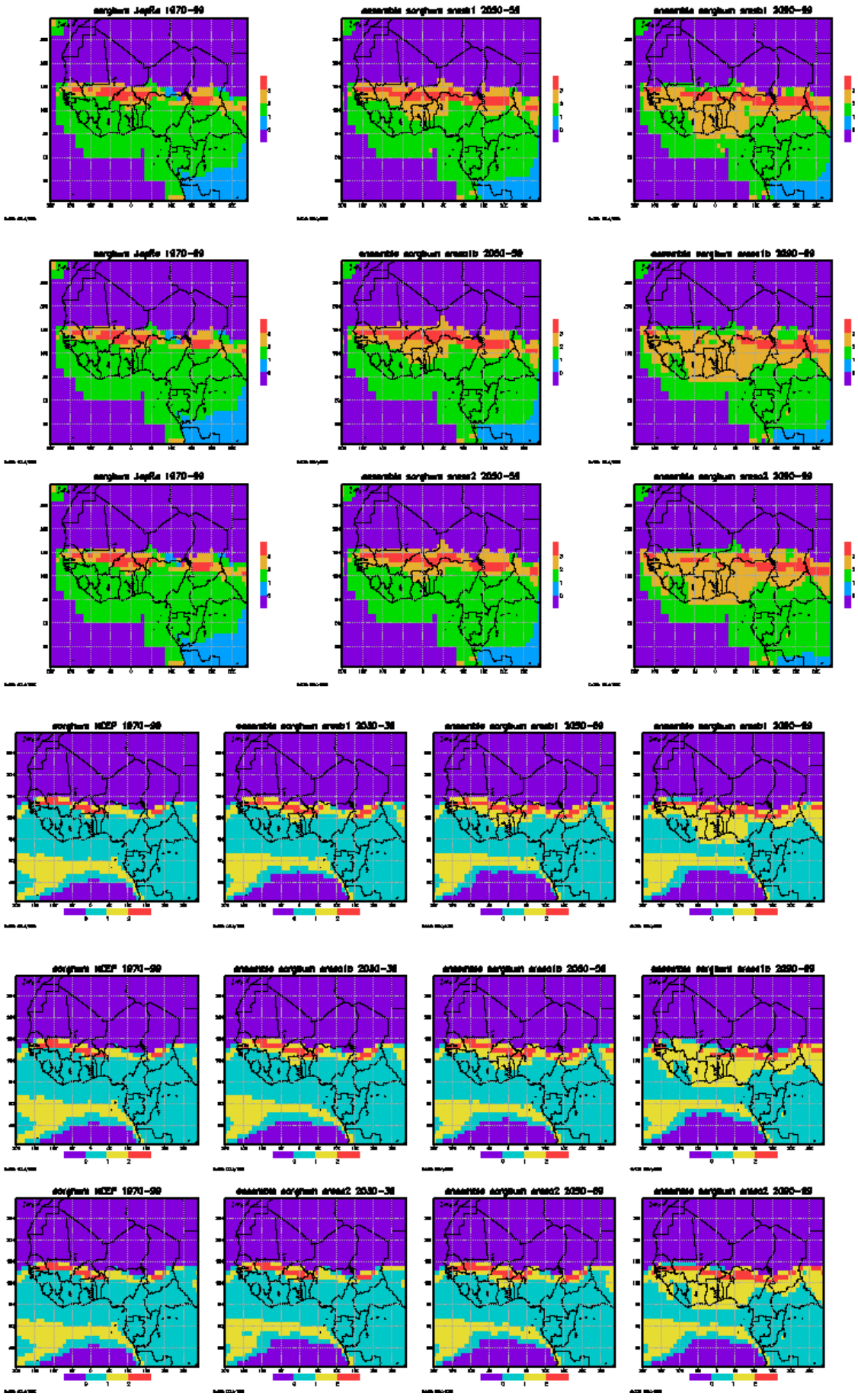

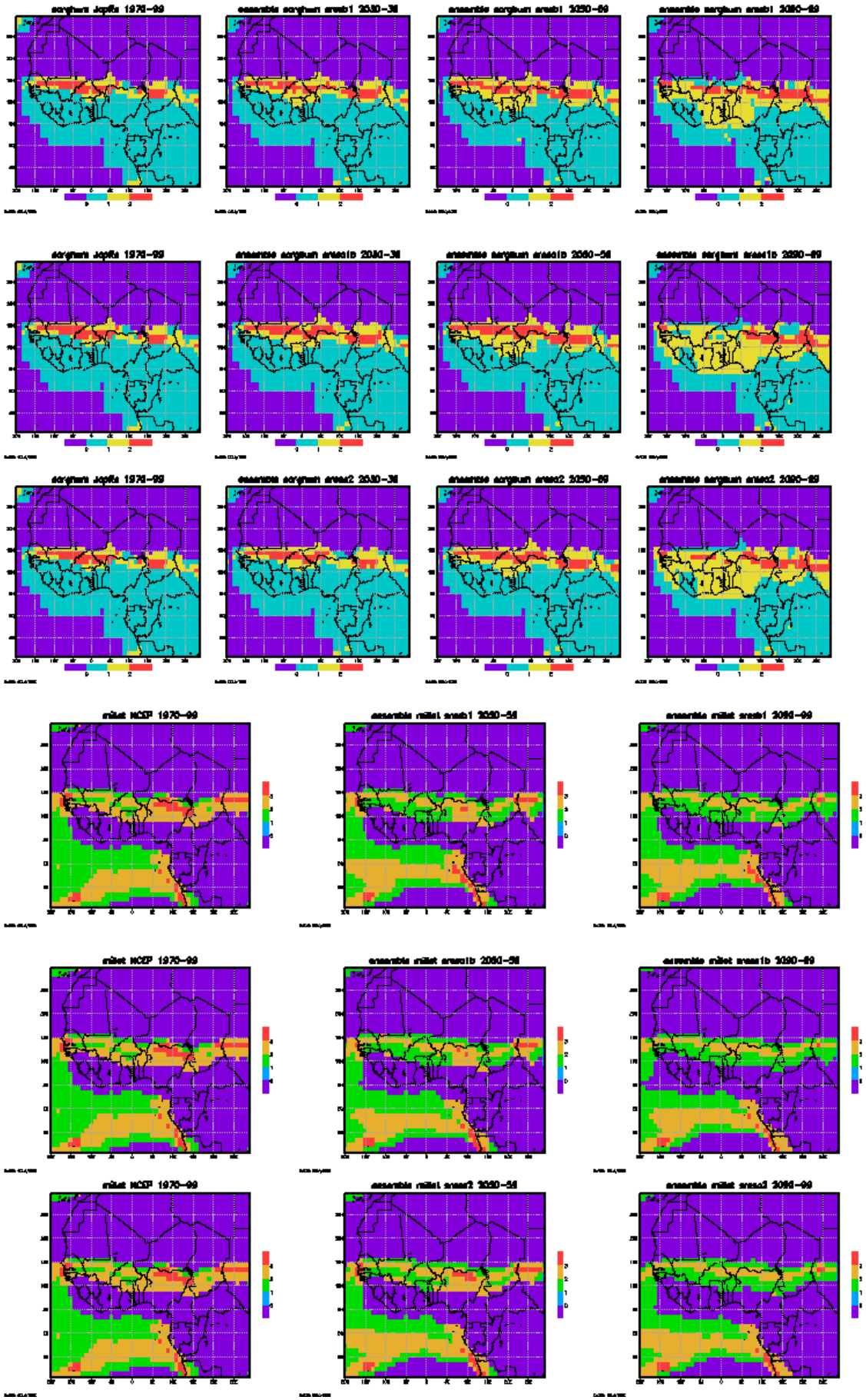

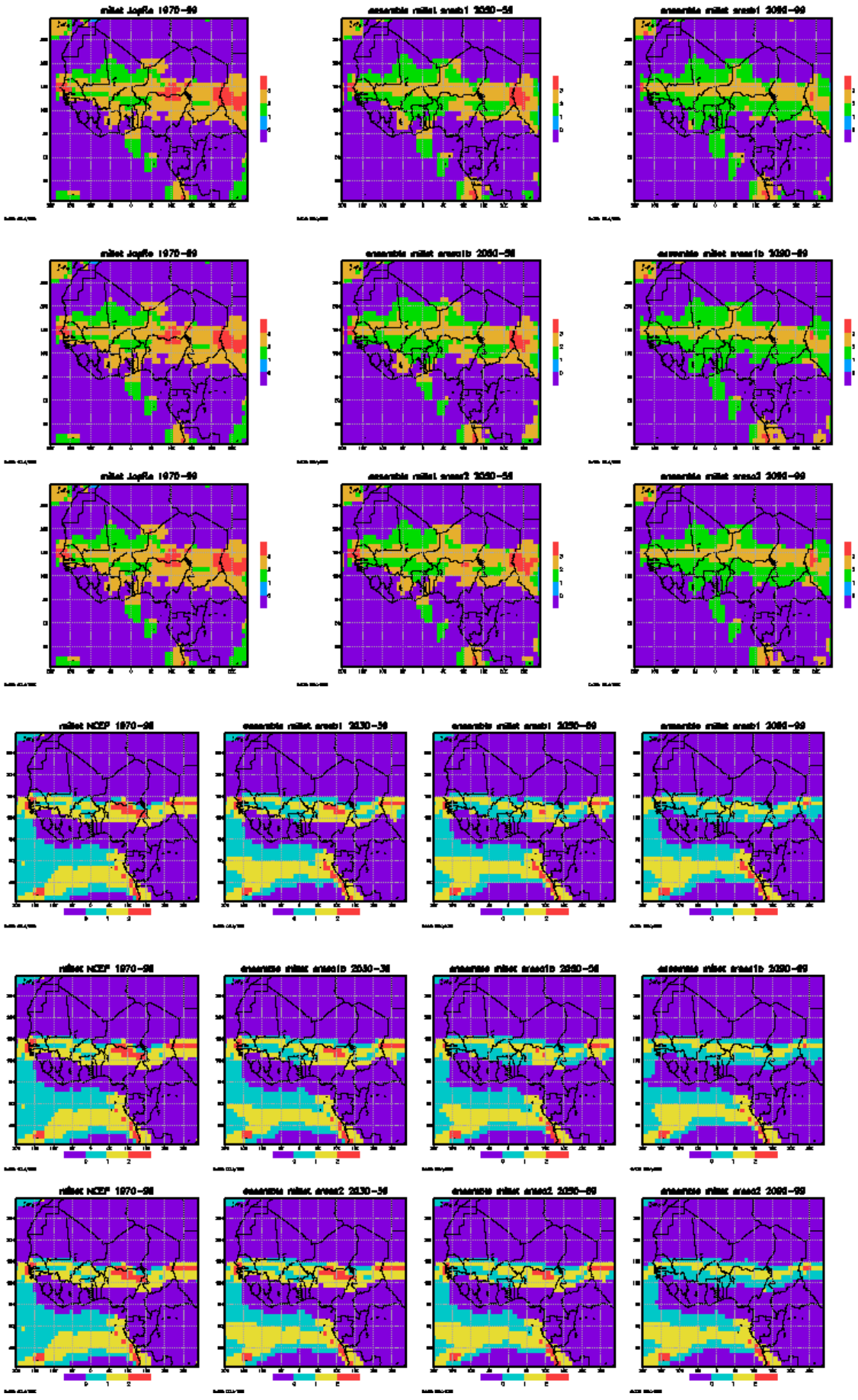

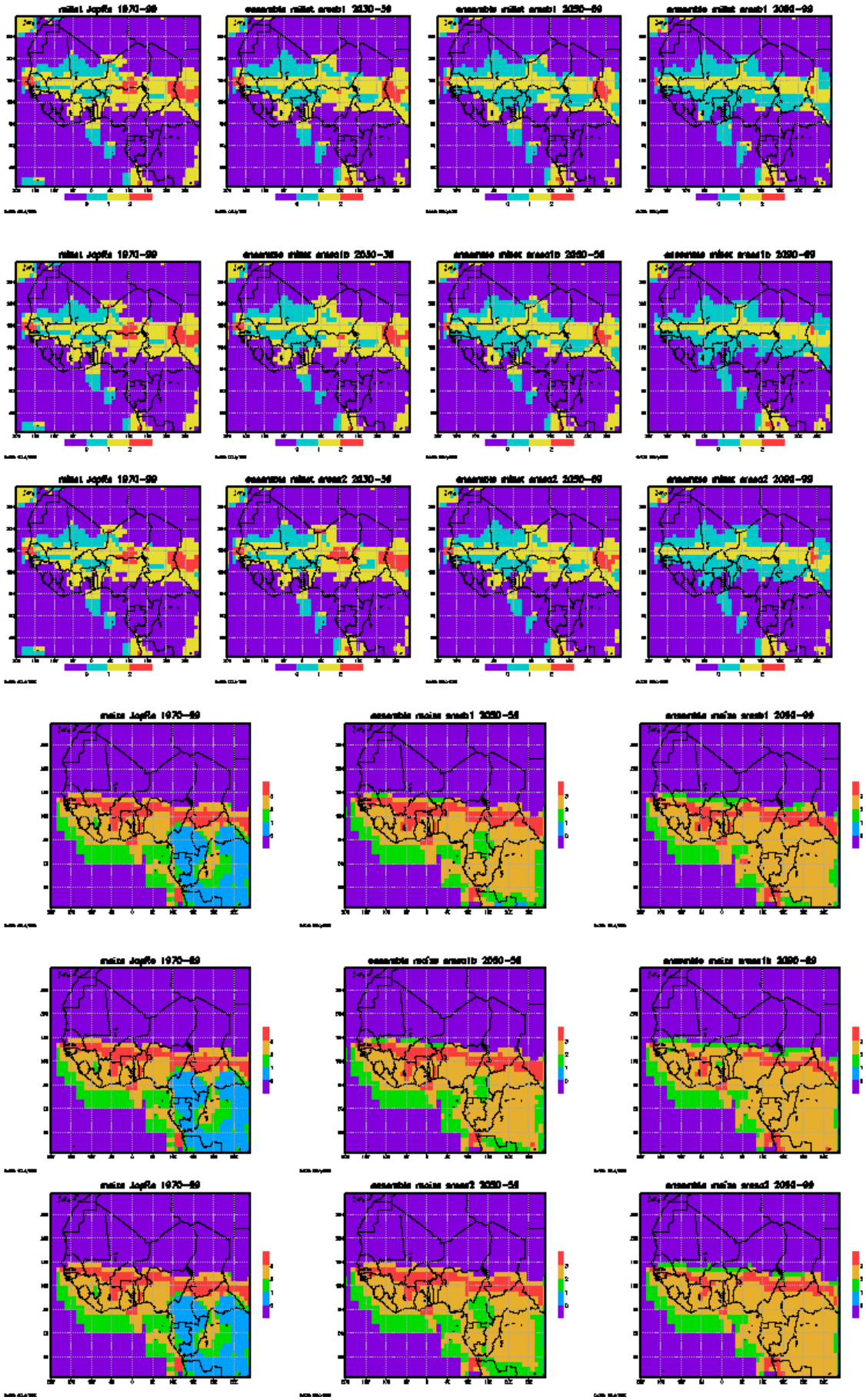

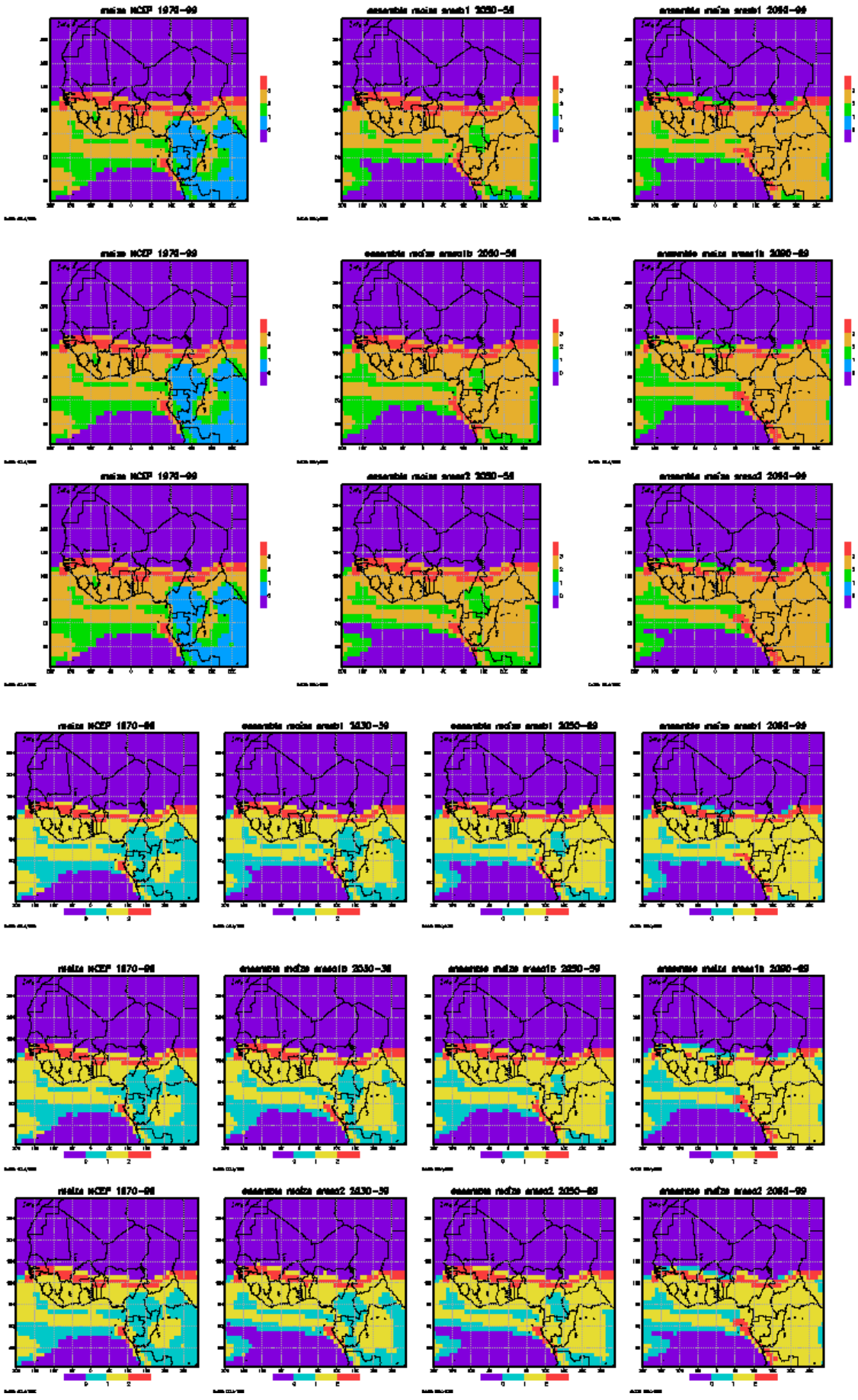

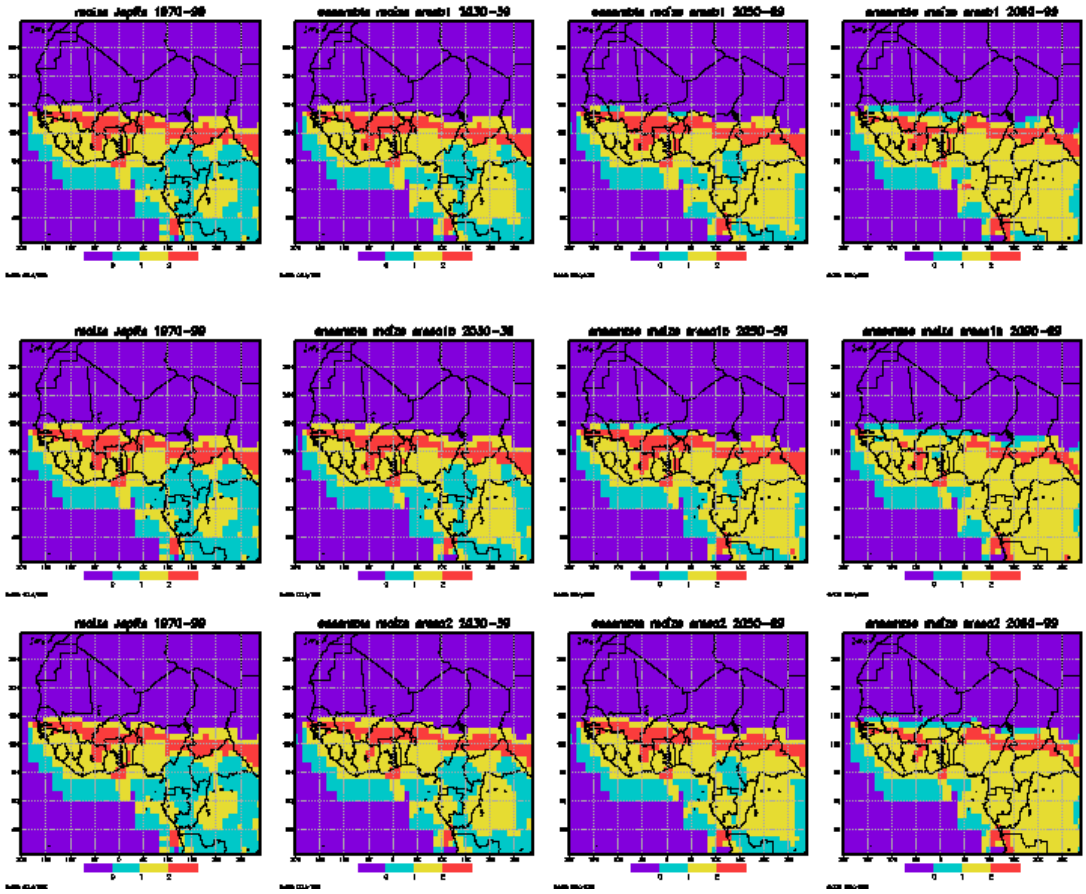

Appendix 13: Model Derived Crop Growth Domain Projections for the 21st Century

The domains are shown for each crop for each model in the following order:

- NCEP baseline—including minimum temperatures for 2050s and 2090s
- NCEP baseline—excluding minimum temperatures for the 2030s, 2050s and 2090s
- JapRe baseline—including minimum temperatures for 2050s and 2090s
- JapRe baseline—excluding minimum temperatures for 2030s, 2050s and 2090s.

The models are listed in alphabetical order with the crop projections grouped by model. The crops are in the order cassava, cowpea, rice, sorghum, millet and maize.

a. CCCMA

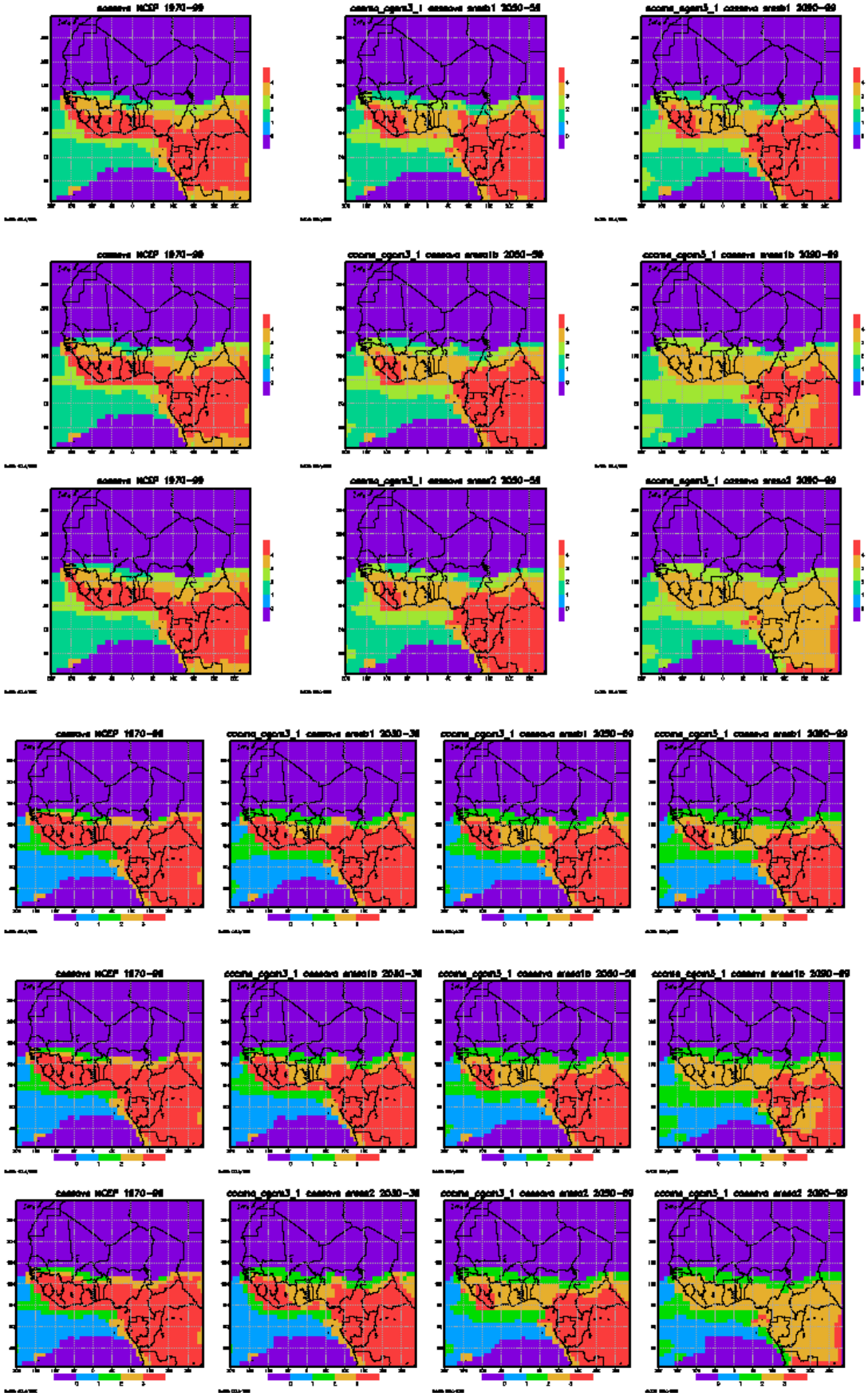

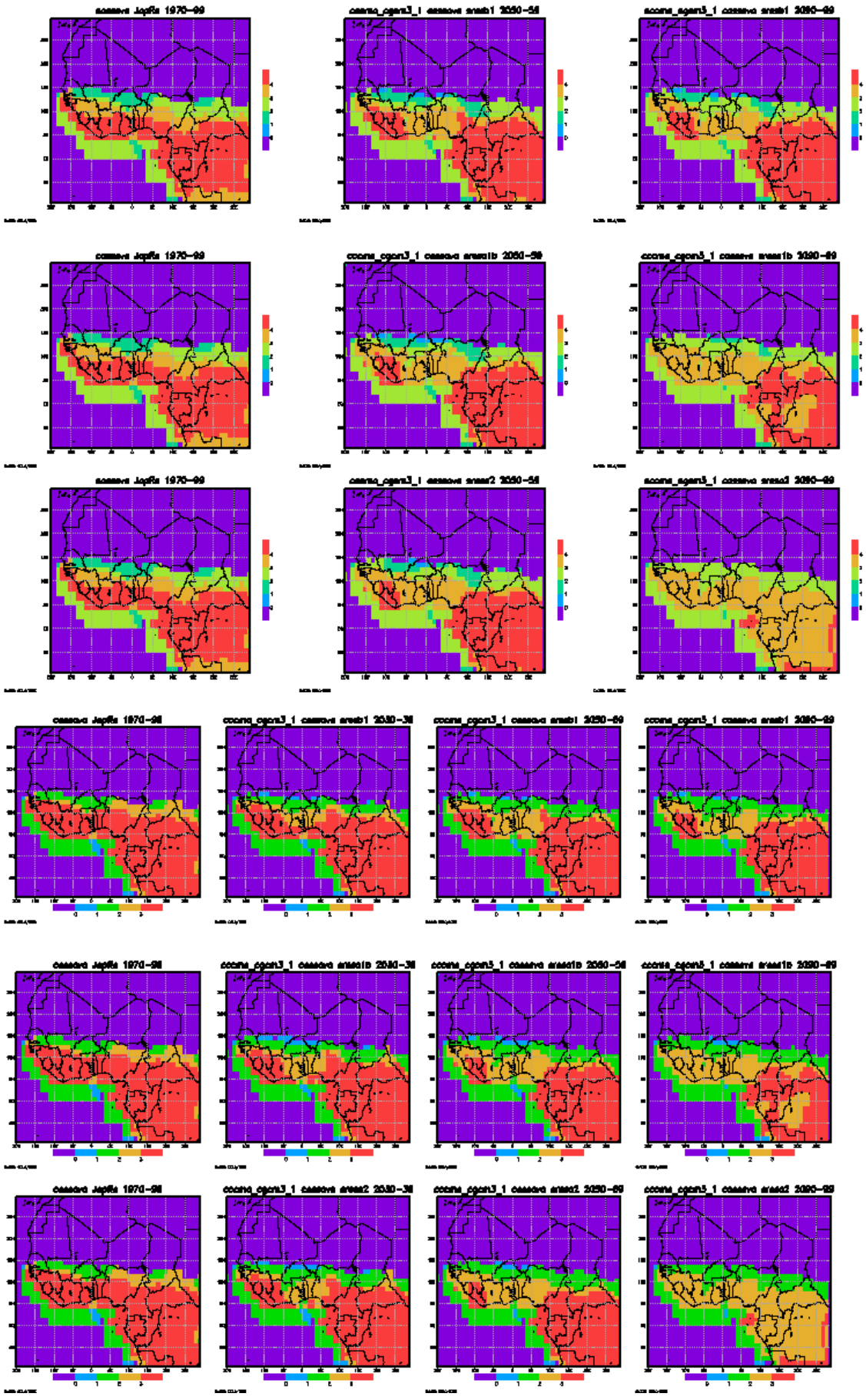

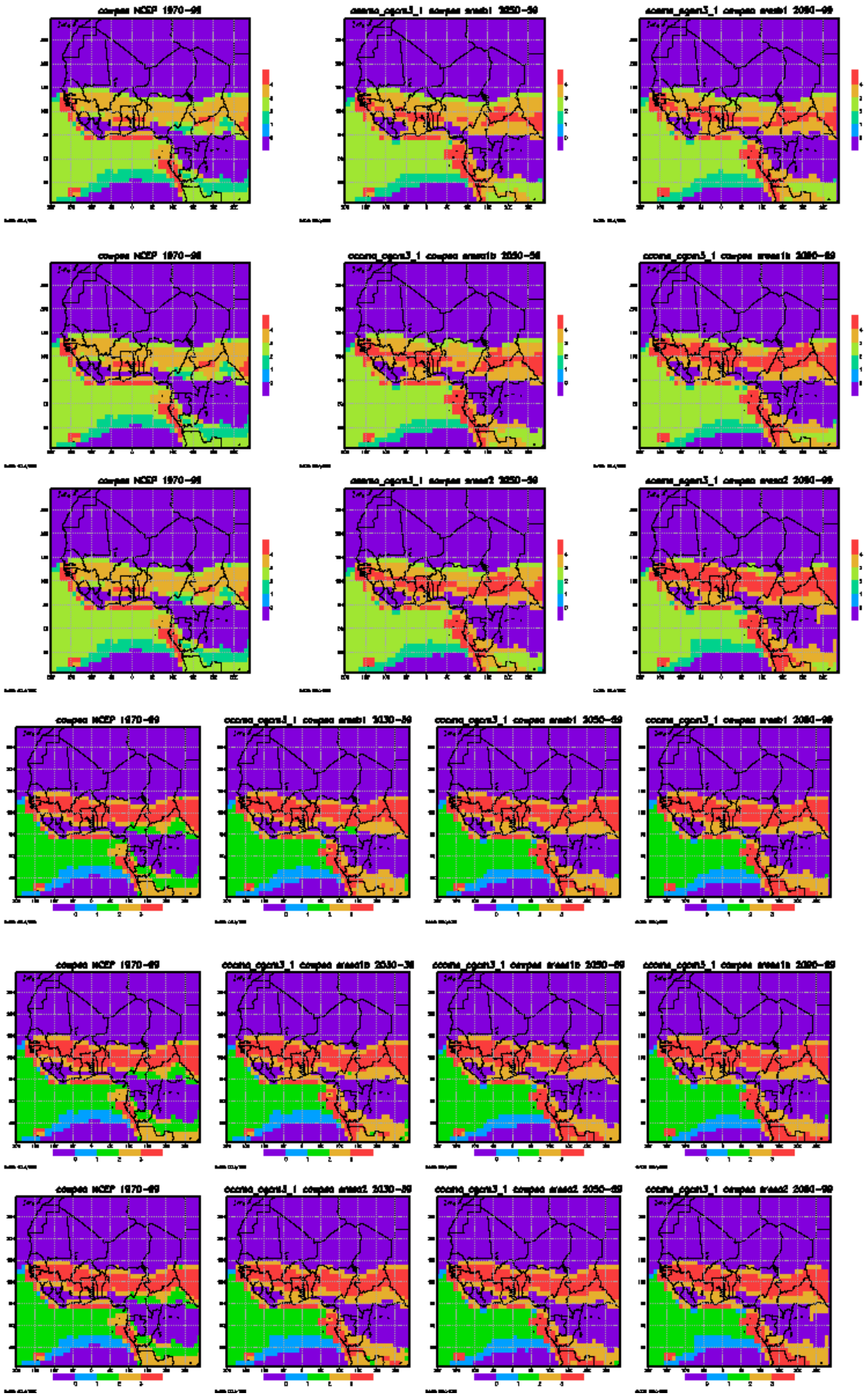

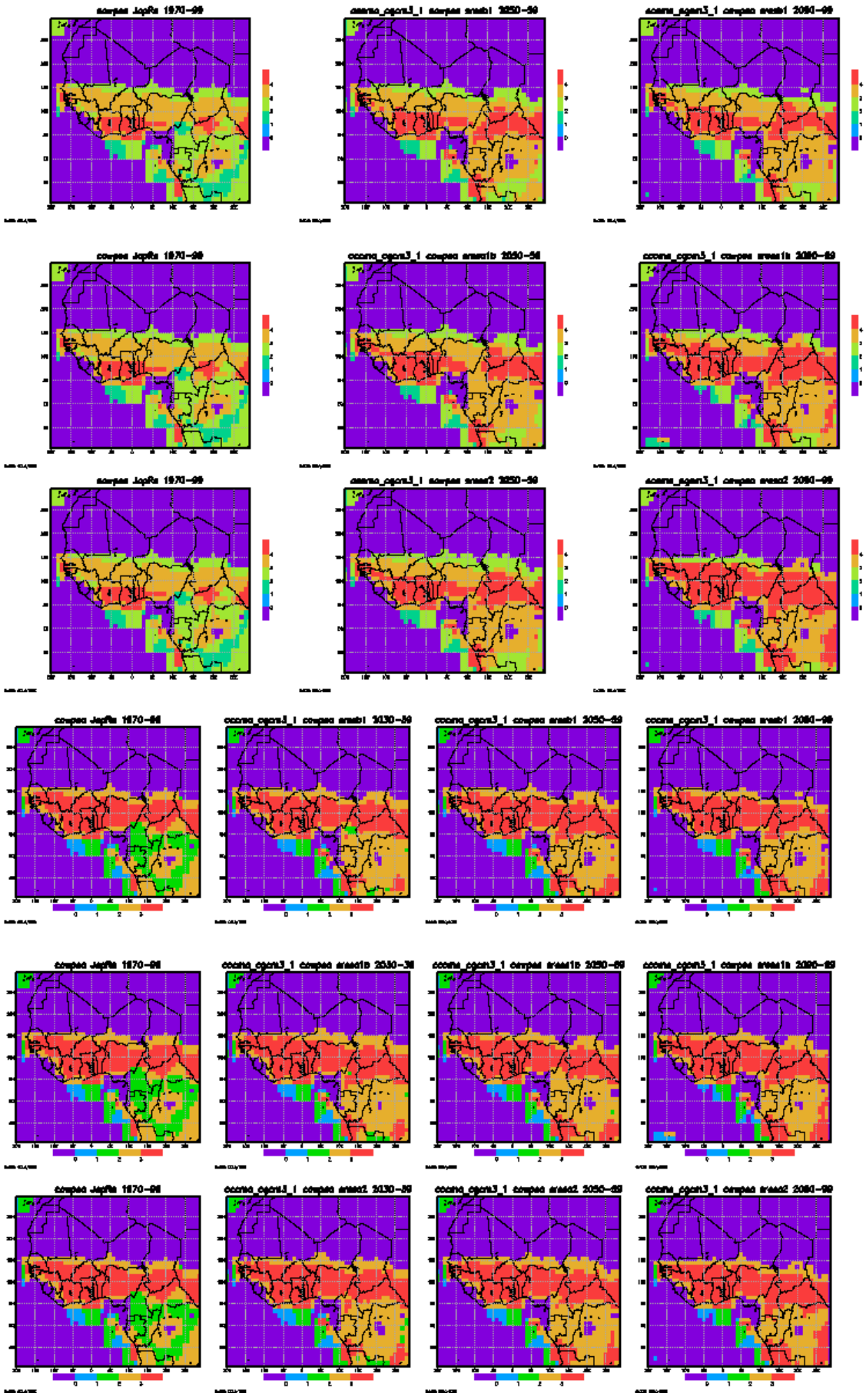

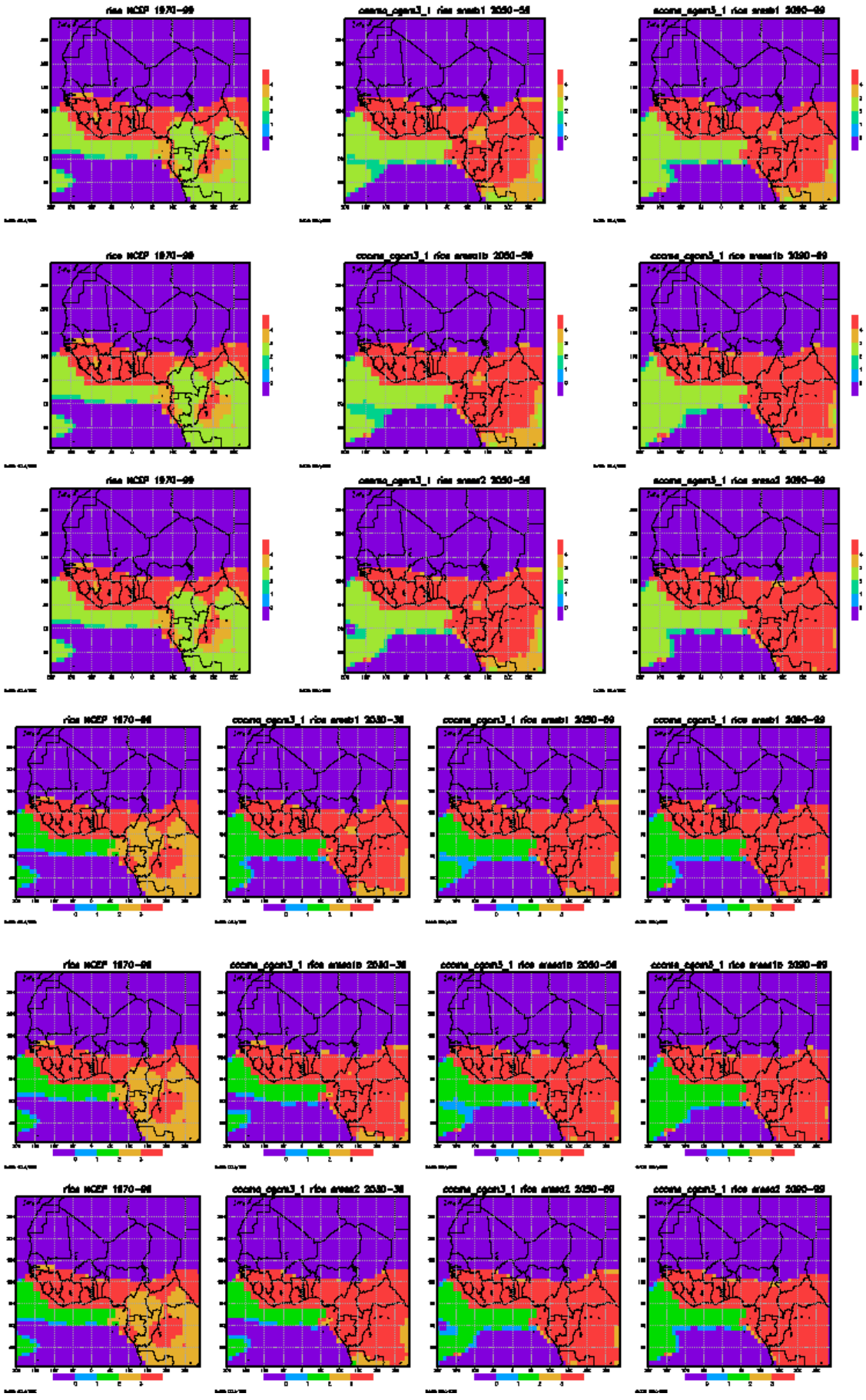
rice NCEP 1971–99
ccsm3_cgcm3_1 rice sresb1 2030–58
ccsm3_cgcm3_1 rice sresb1 2070–99
rice NCEP 1971–99
ccsm3_cgcm3_1 rice sresb1b 2030–58
ccsm3_cgcm3_1 rice sresb1b 2070–99
rice NCEP 1971–99
ccsm3_cgcm3_1 rice sresa2 2030–58
ccsm3_cgcm3_1 rice sresa2 2070–99
rice NCEP 1970–99
ccsm3_cgcm3_1 rice sresb1 2030–38
ccsm3_cgcm3_1 rice sresb1 2070–99
ccsm3_cgcm3_1 rice sresb1 2070–99
rice NCEP 1970–99
ccsm3_cgcm3_1 rice sresb1b 2030–38
ccsm3_cgcm3_1 rice sresb1b 2070–58
ccsm3_cgcm3_1 rice sresb1b 2070–99
rice NCEP 1970–99
ccsm3_cgcm3_1 rice sresa2 2030–38
ccsm3_cgcm3_1 rice sresa2 2070–99
ccsm3_cgcm3_1 rice sresa2 2070–99

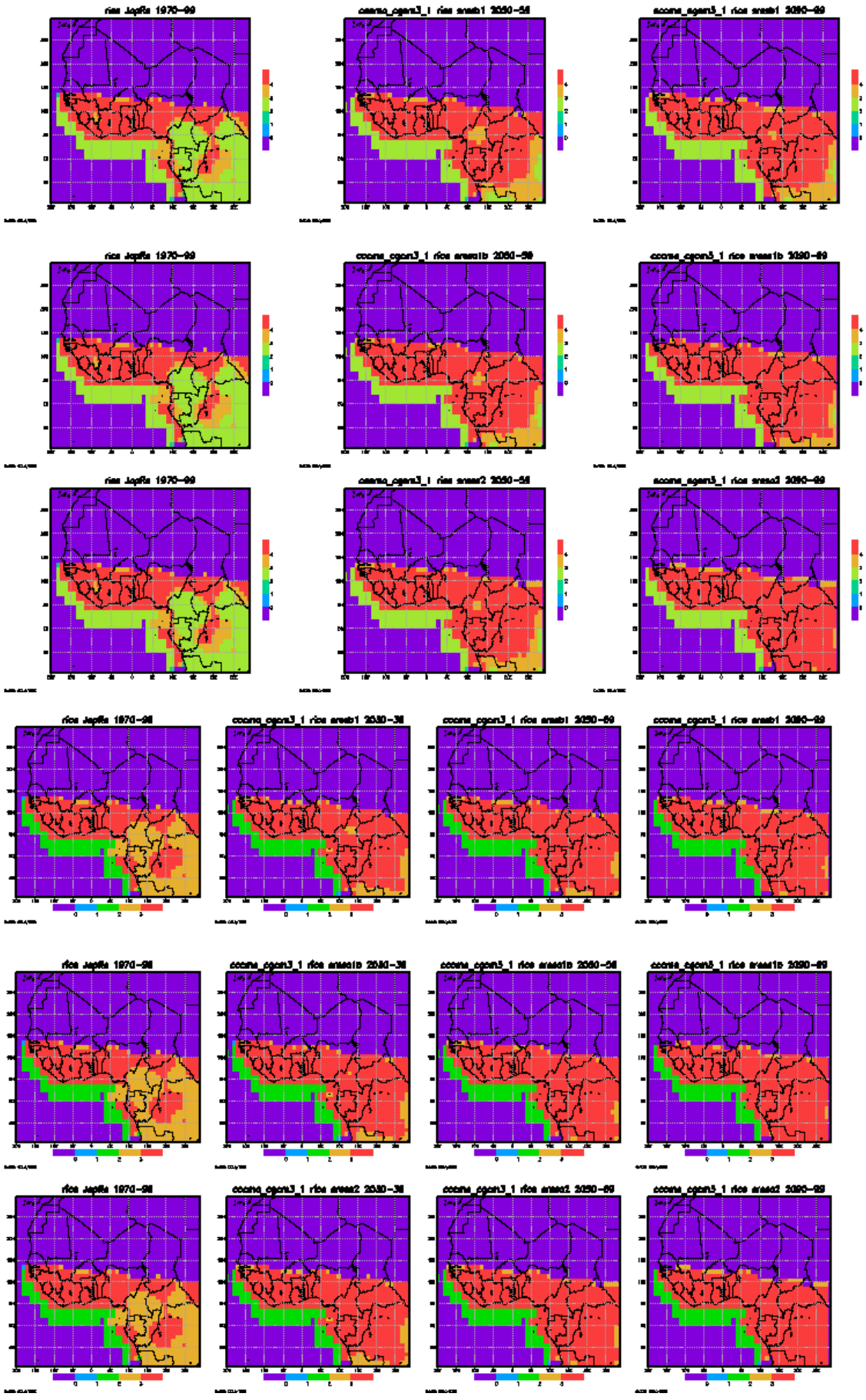

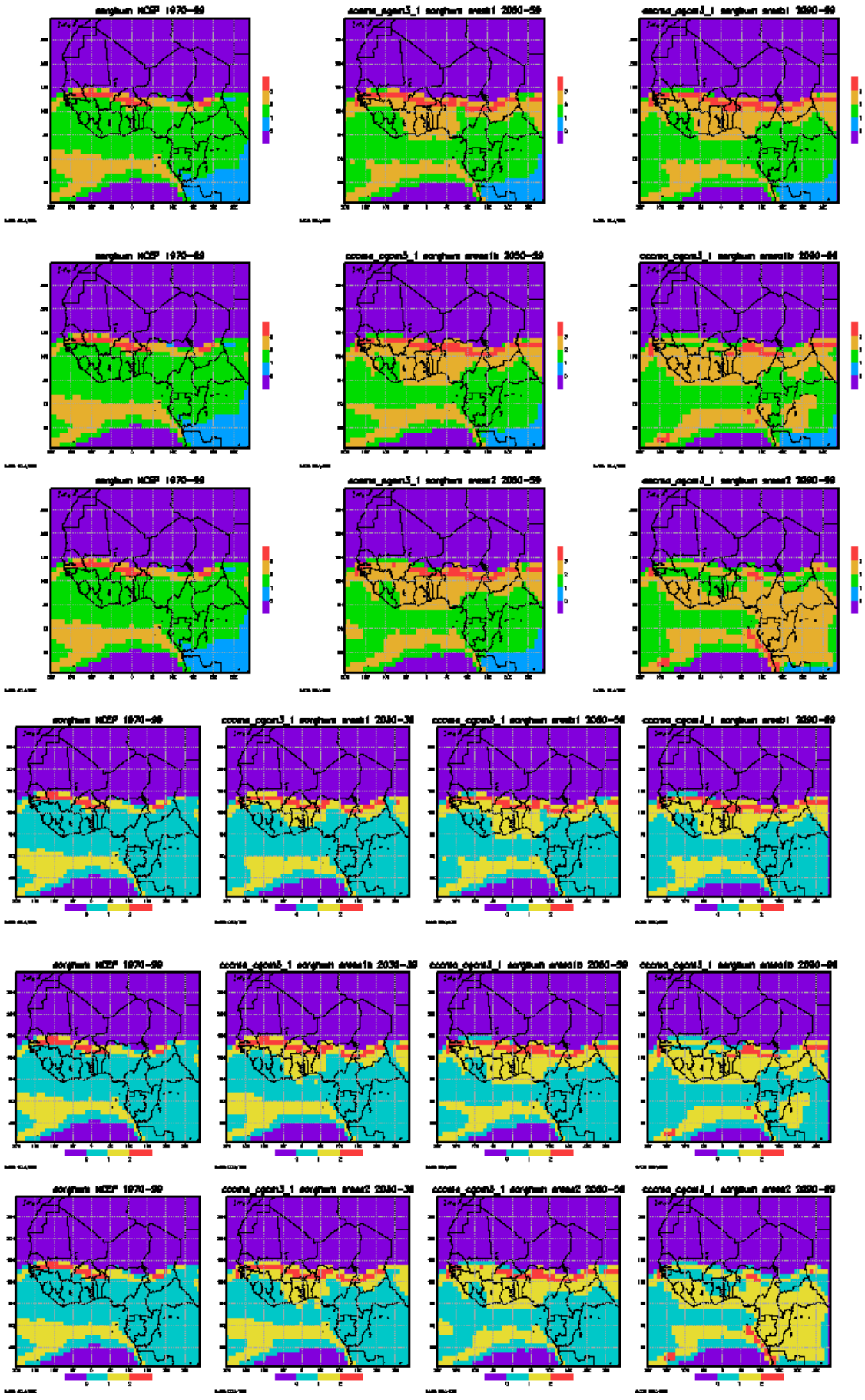

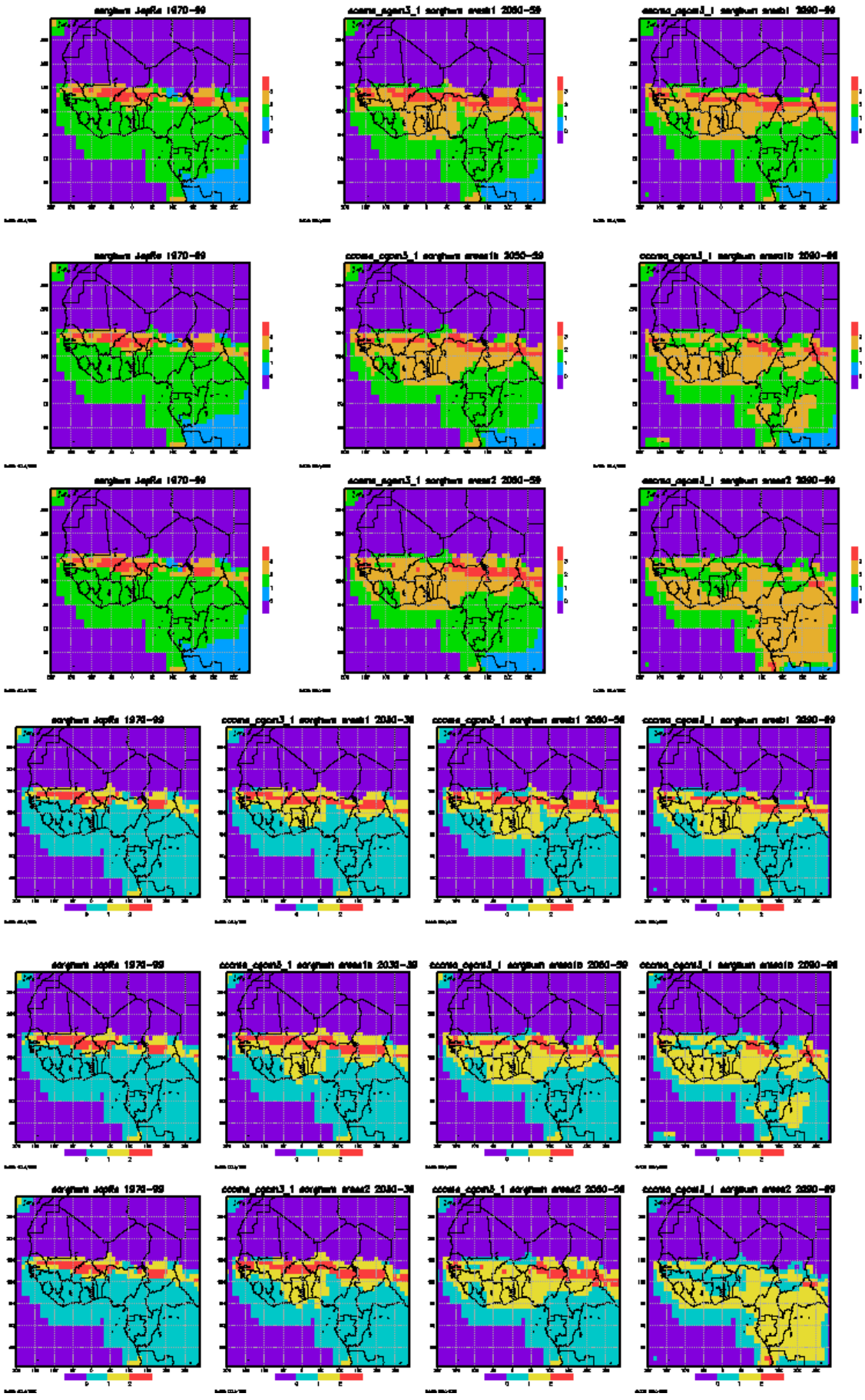

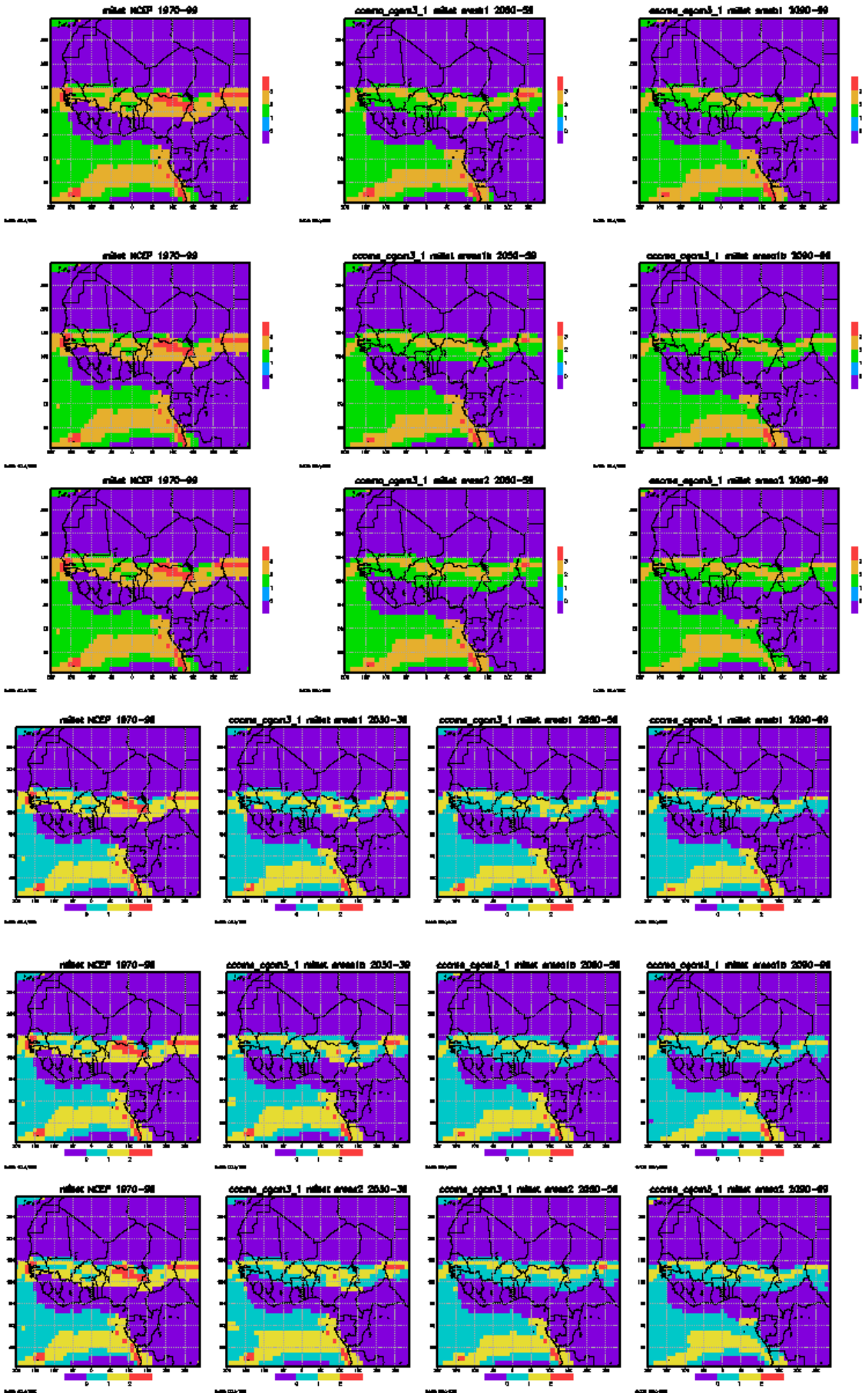

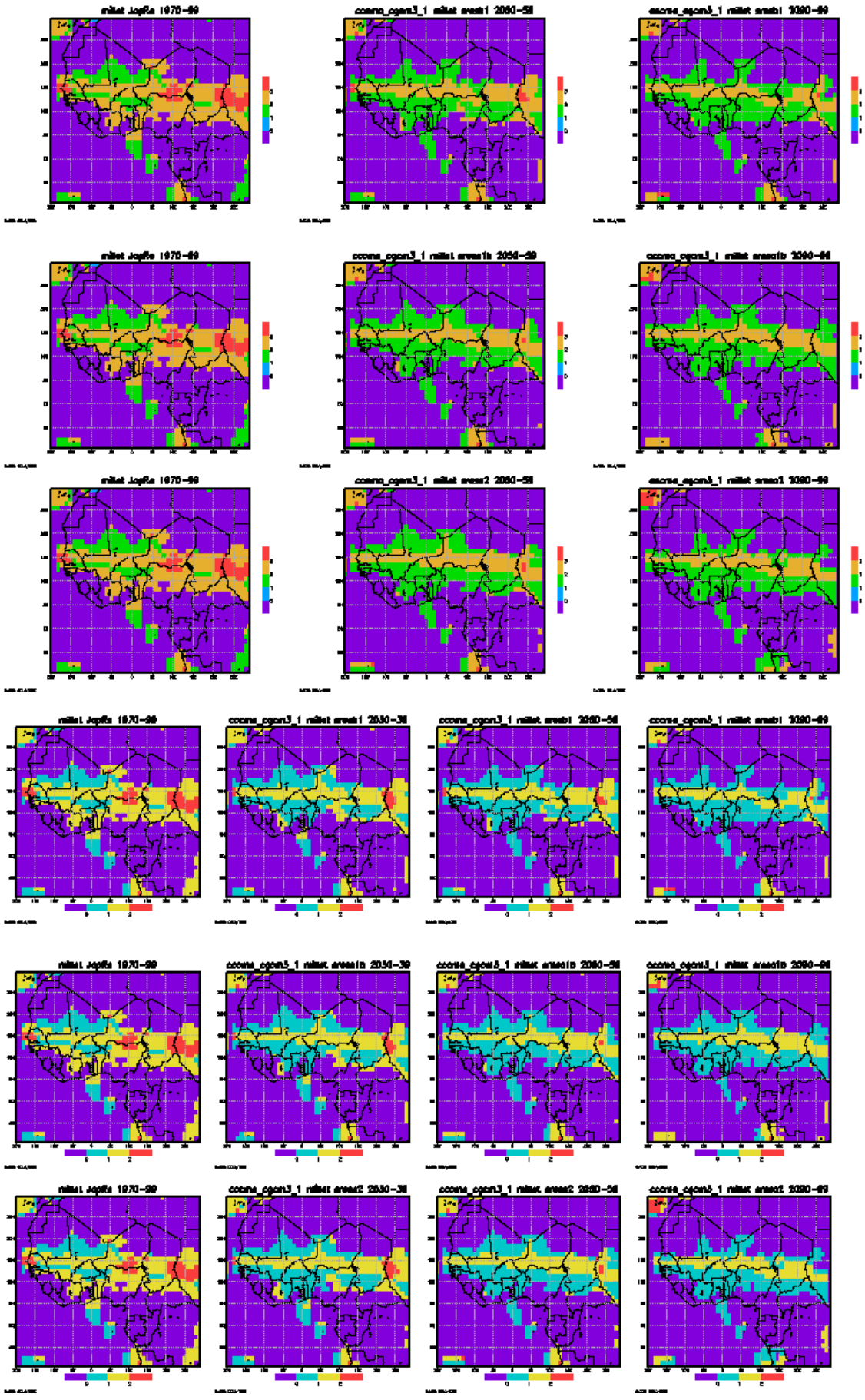

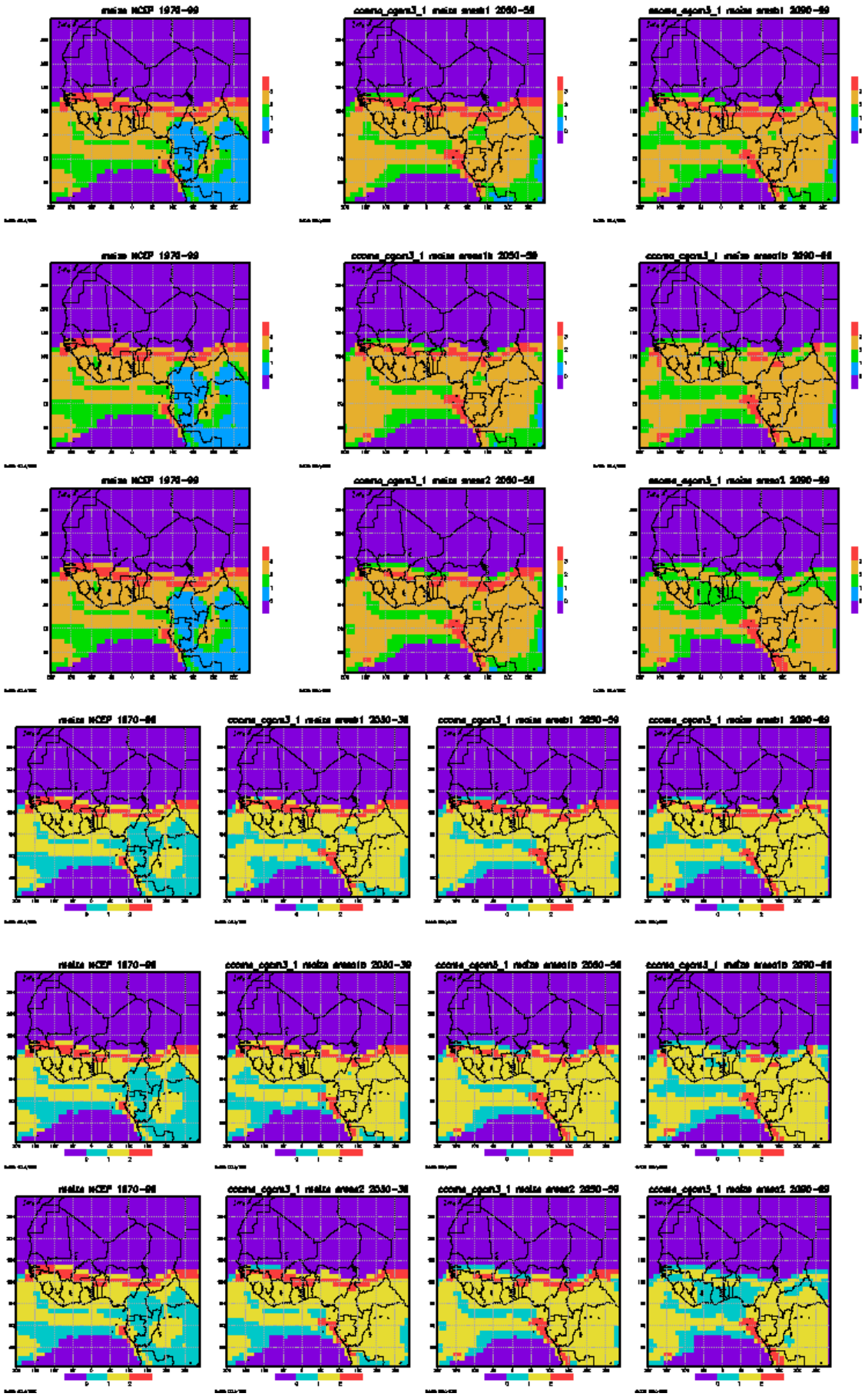
maize NCEP 1970-99
cccma_cgcm3_1 maize sresa1 2030-59
cccma_cgcm3_1 maize sresa1 2070-99
maize NCEP 1970-99
cccma_cgcm3_1 maize sresa1b 2030-59
cccma_cgcm3_1 maize sresa1b 2070-99
maize NCEP 1970-99
cccma_cgcm3_1 maize sresa2 2030-59
cccma_cgcm3_1 maize sresa2 2070-99
maize NCEP 1970-99
cccma_cgcm3_1 maize sresa1 2030-59
cccma_cgcm3_1 maize sresa1 2050-59
cccma_cgcm3_1 maize sresa1 2070-99
maize NCEP 1970-99
cccma_cgcm3_1 maize sresa1b 2030-59
cccma_cgcm3_1 maize sresa1b 2050-59
cccma_cgcm3_1 maize sresa1b 2070-99
maize NCEP 1970-99
cccma_cgcm3_1 maize sresa2 2030-59
cccma_cgcm3_1 maize sresa2 2050-59
cccma_cgcm3_1 maize sresa2 2070-99

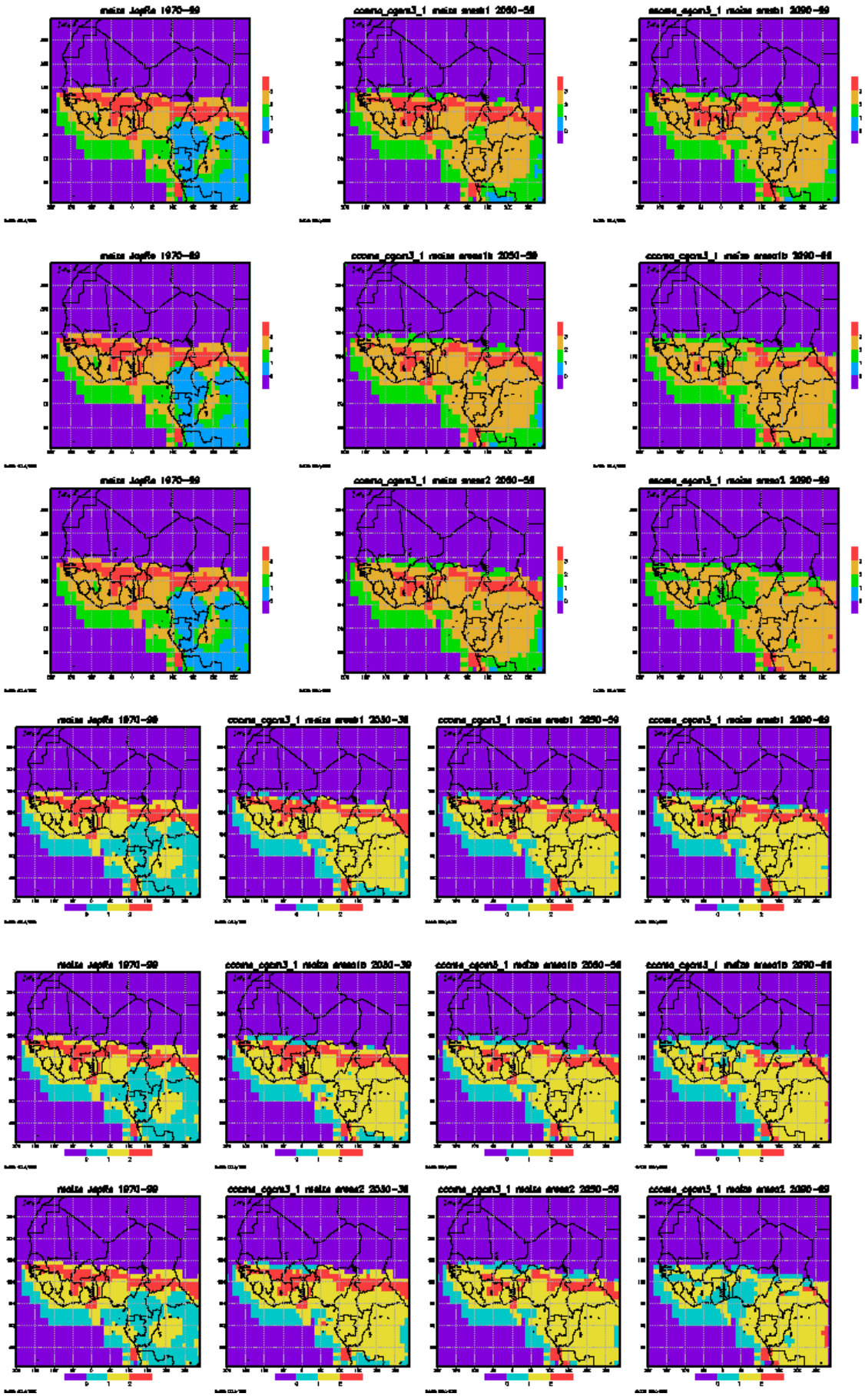

b. CNRM

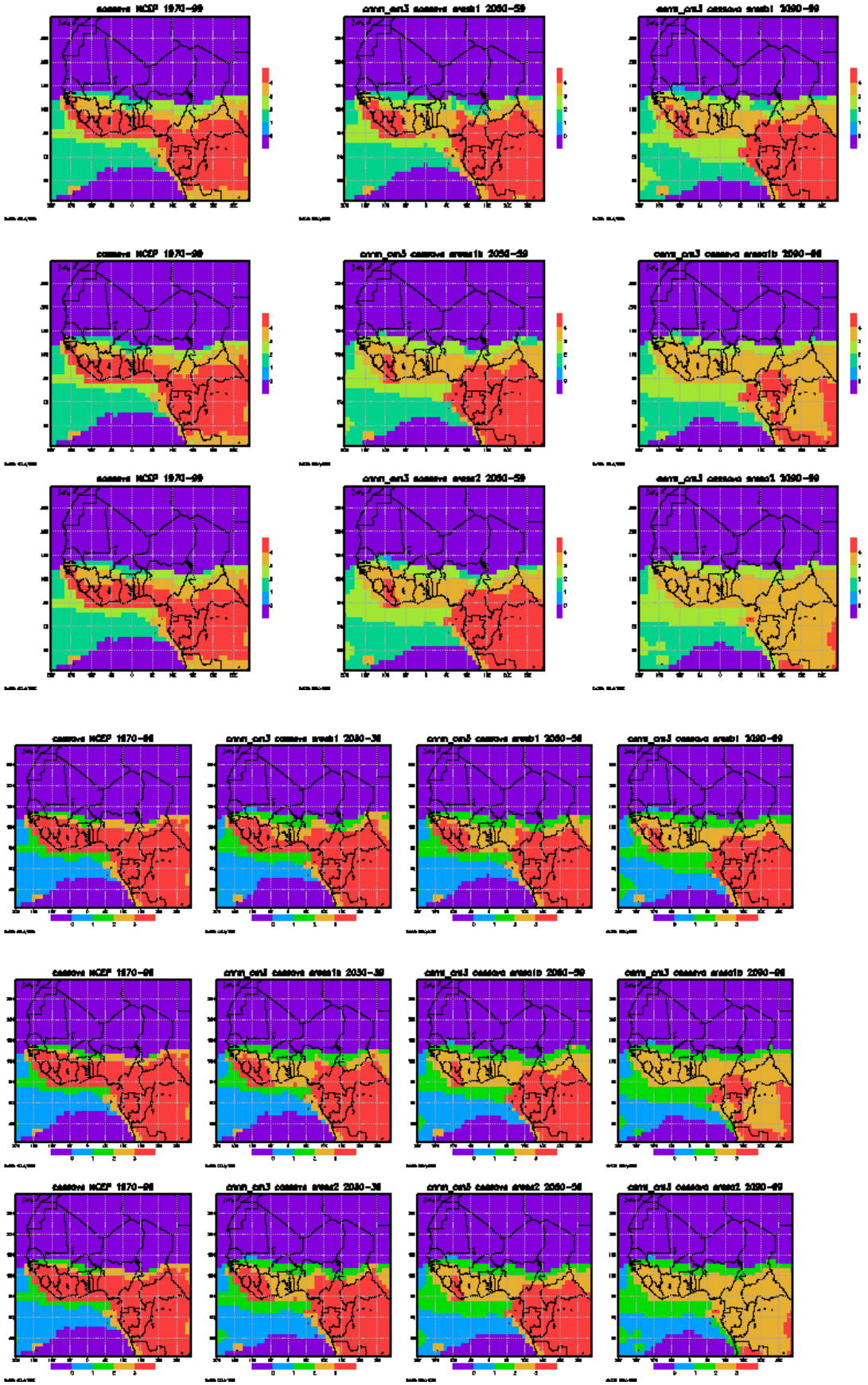

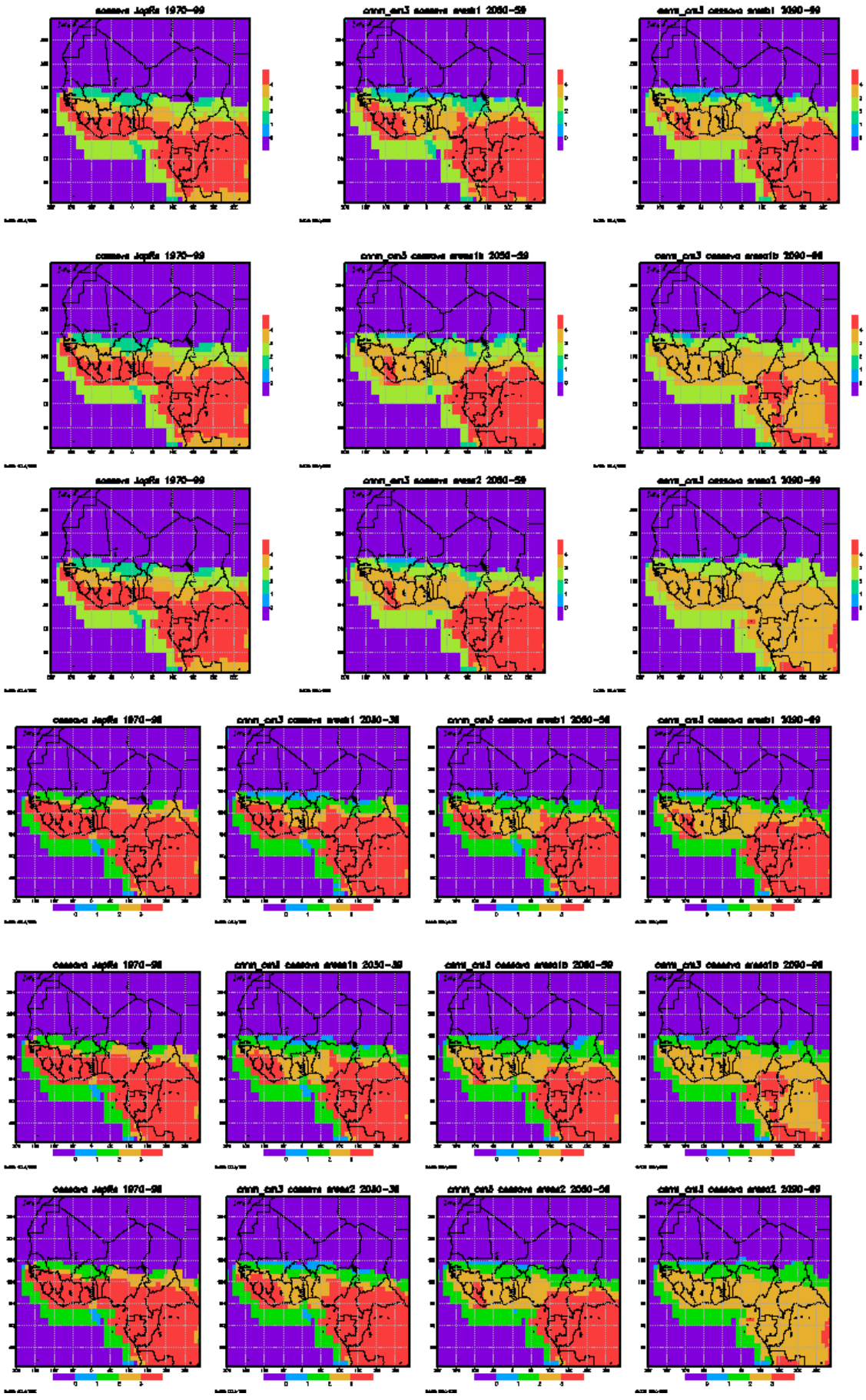

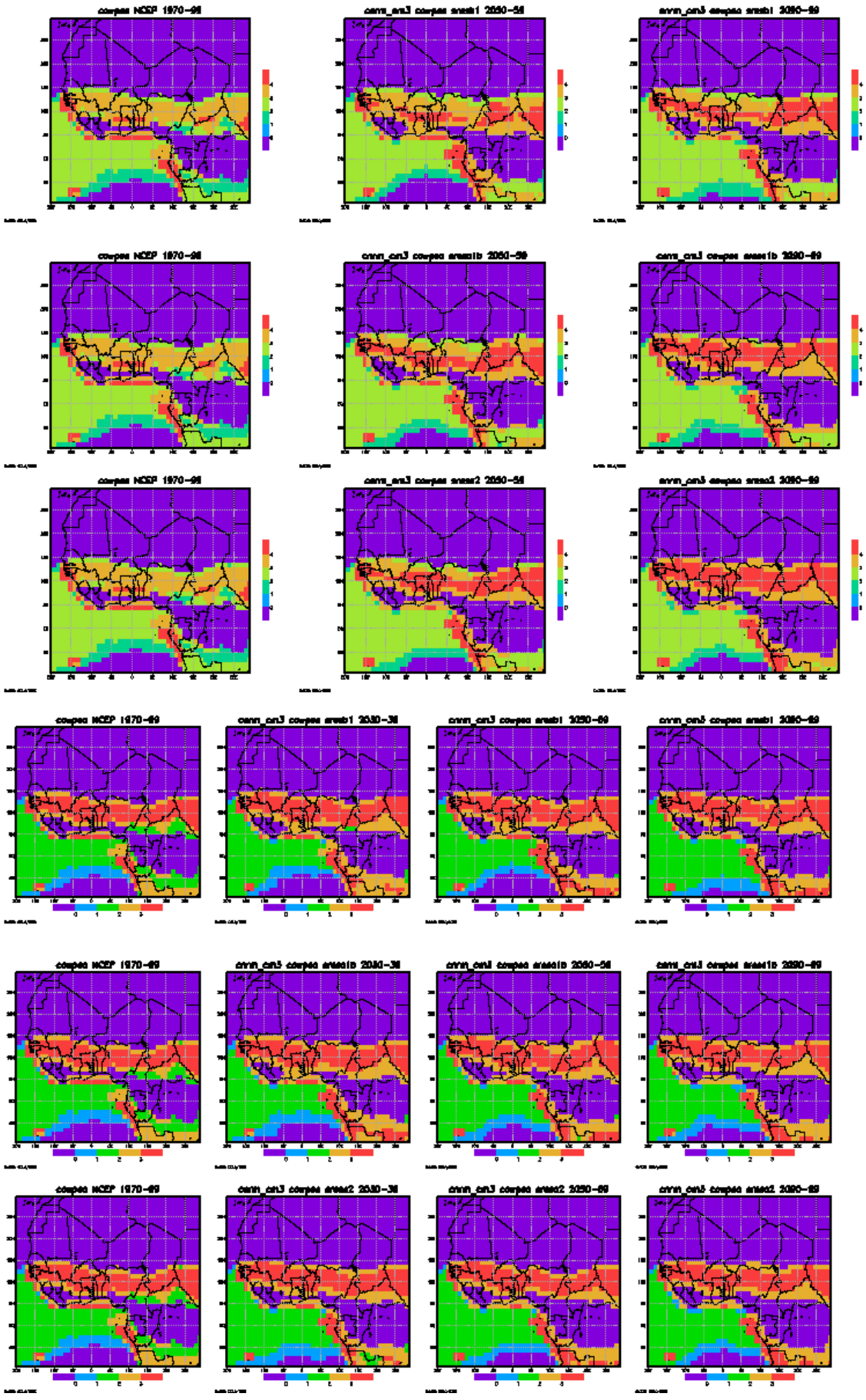

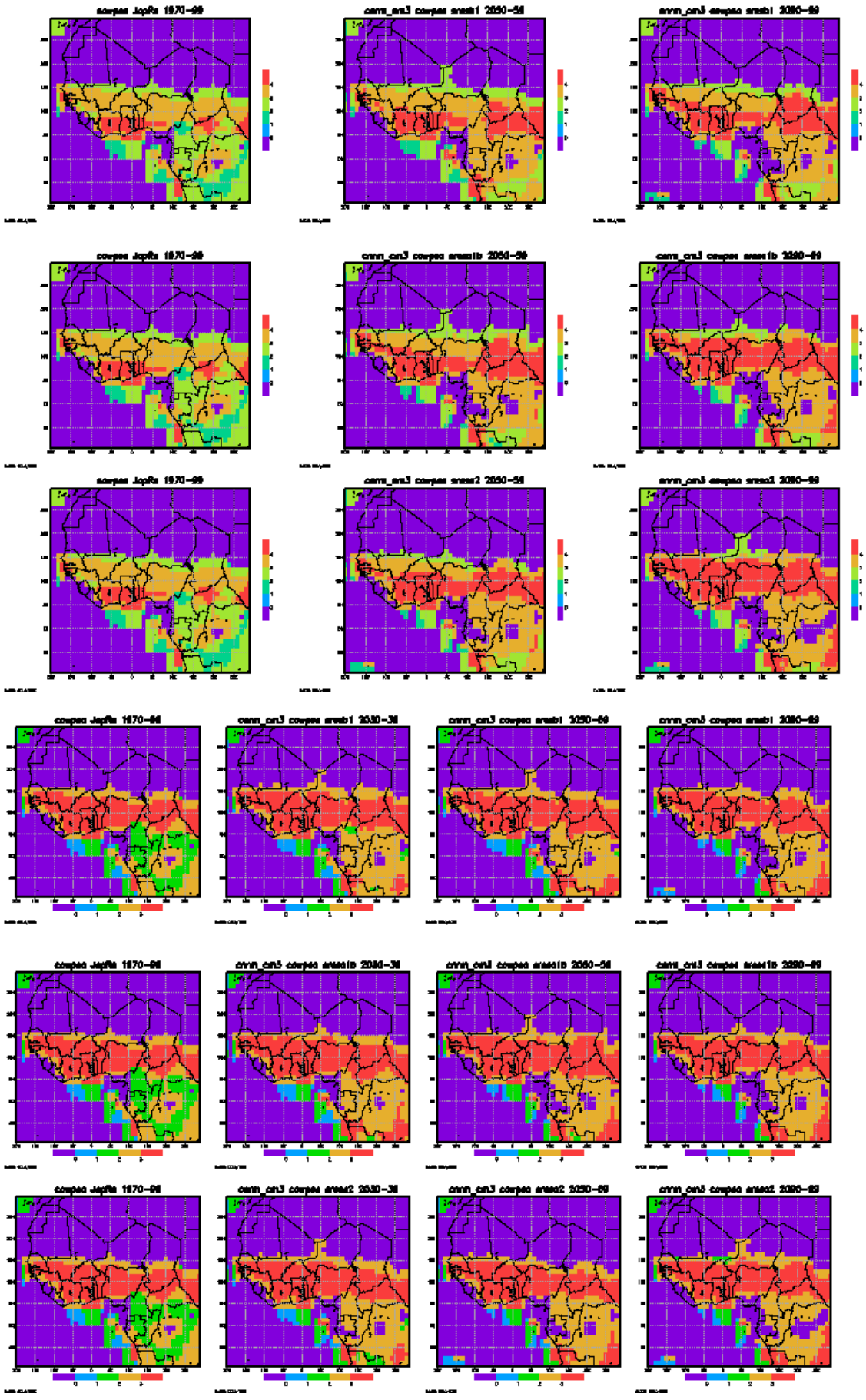

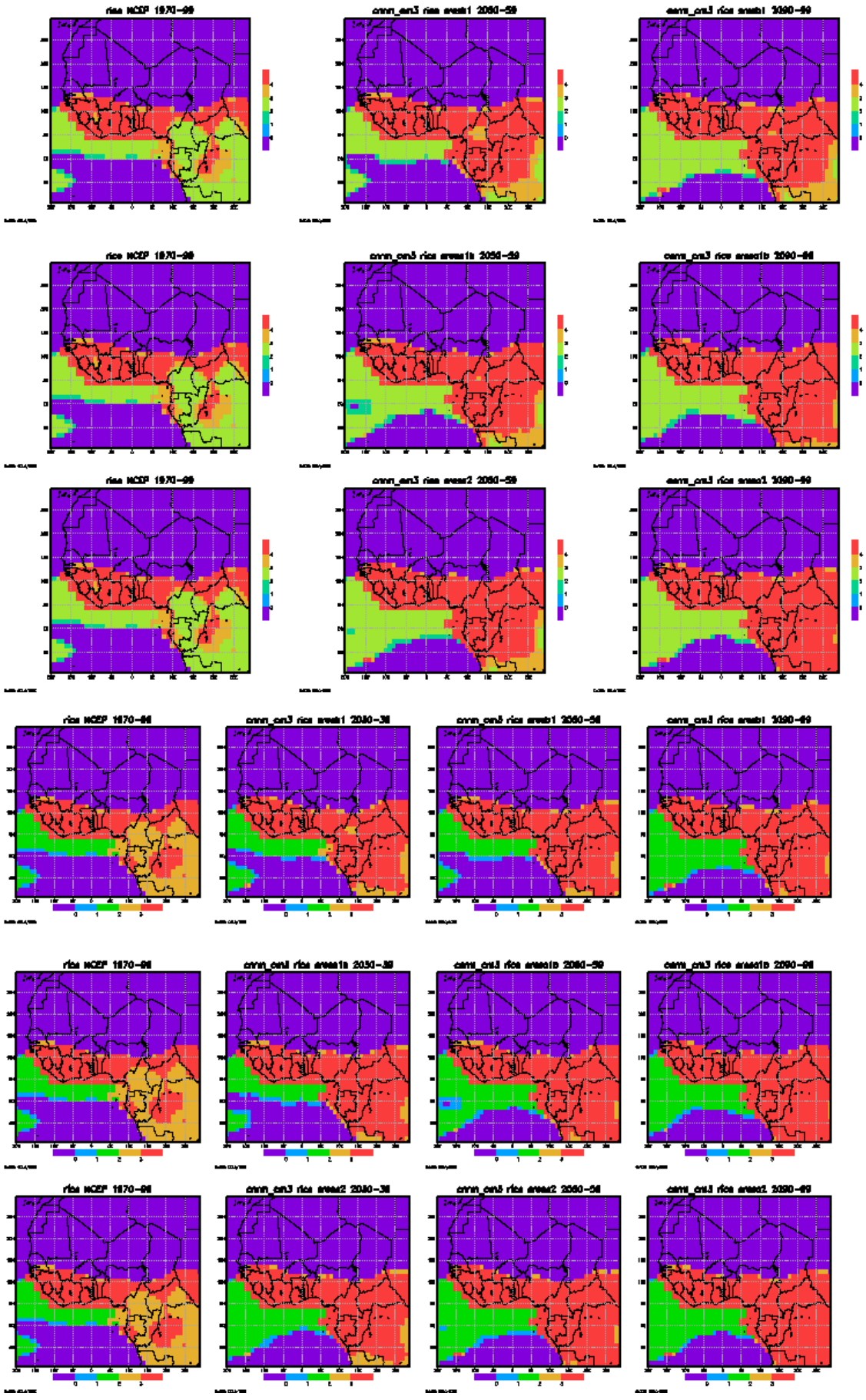

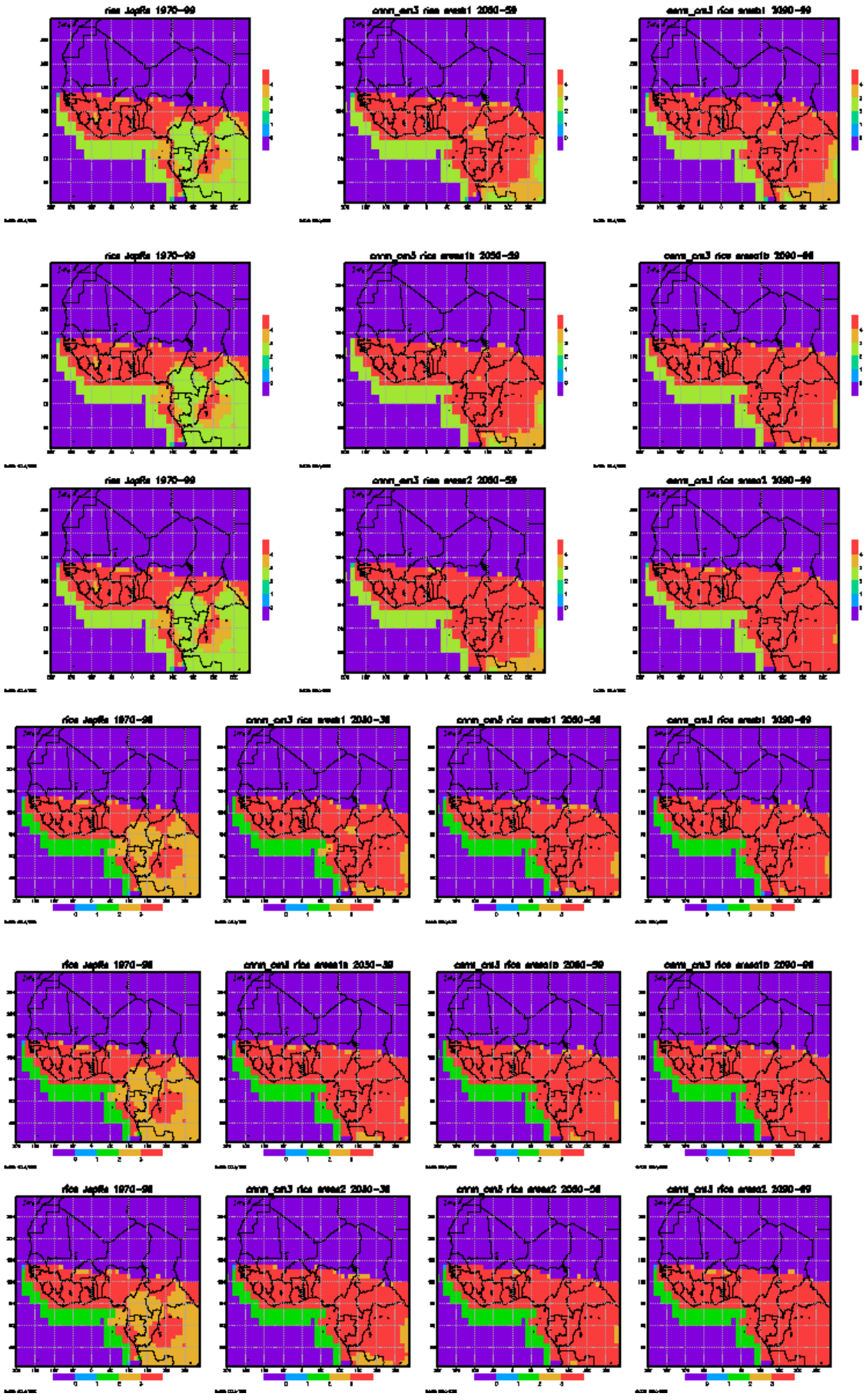

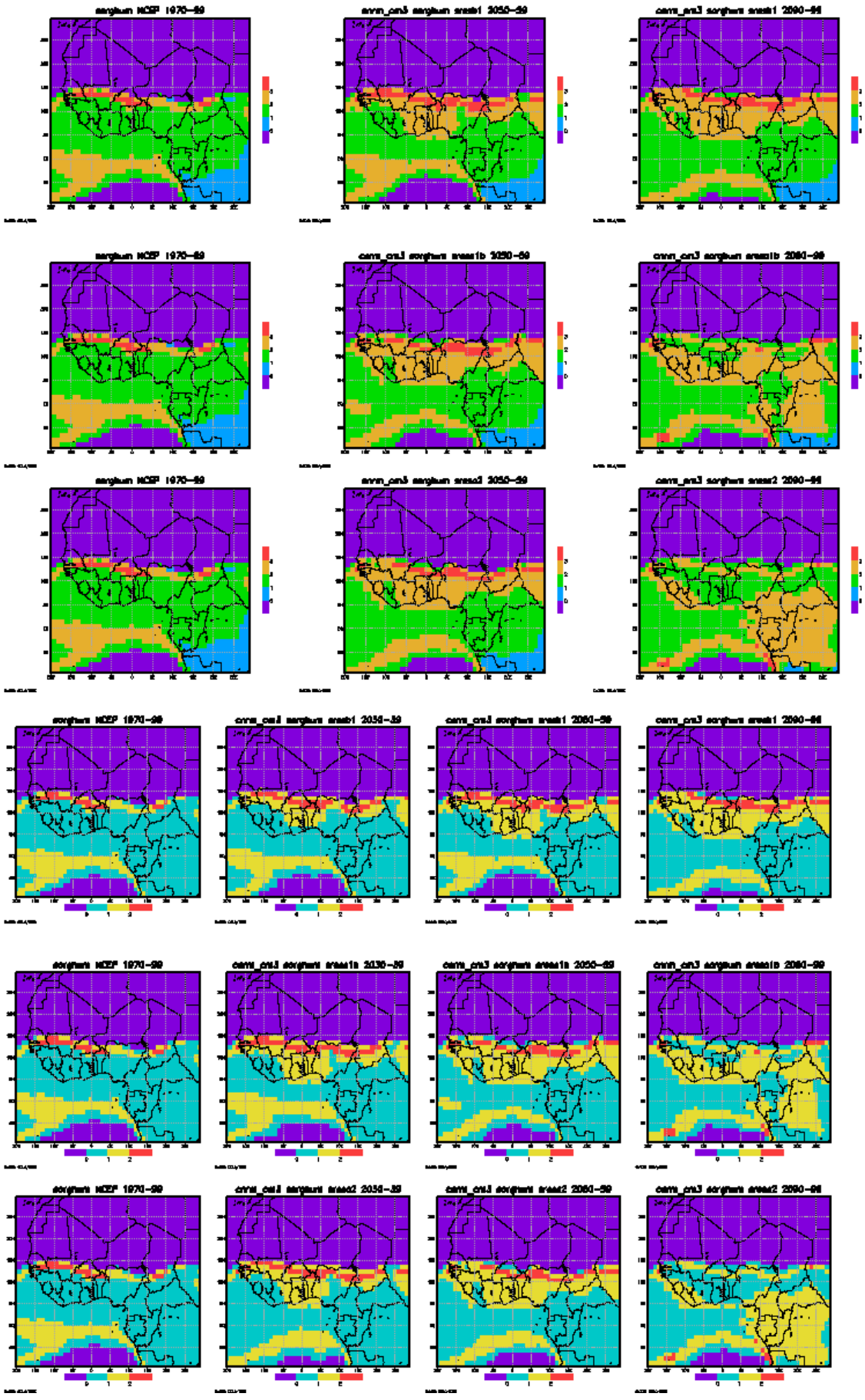

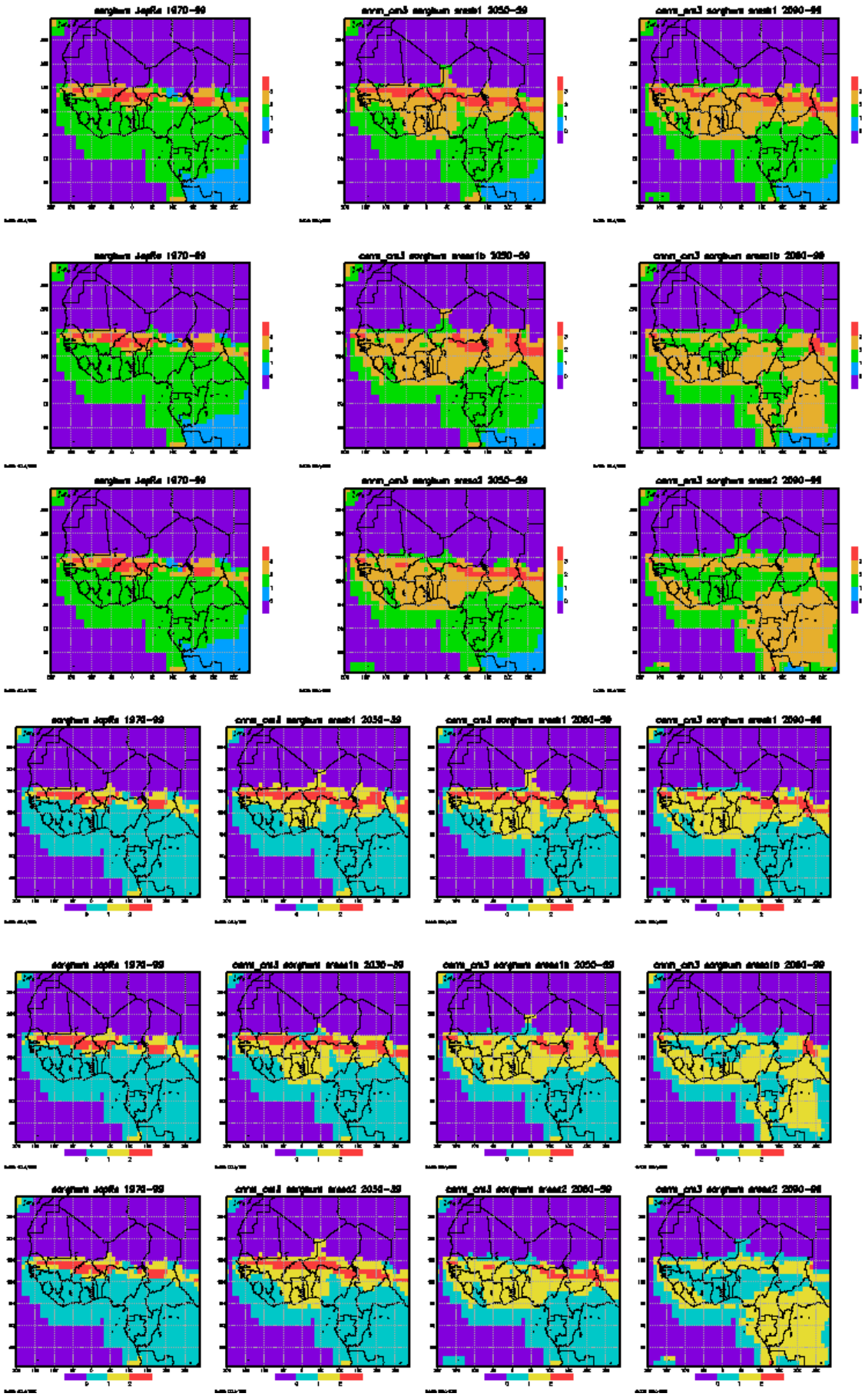

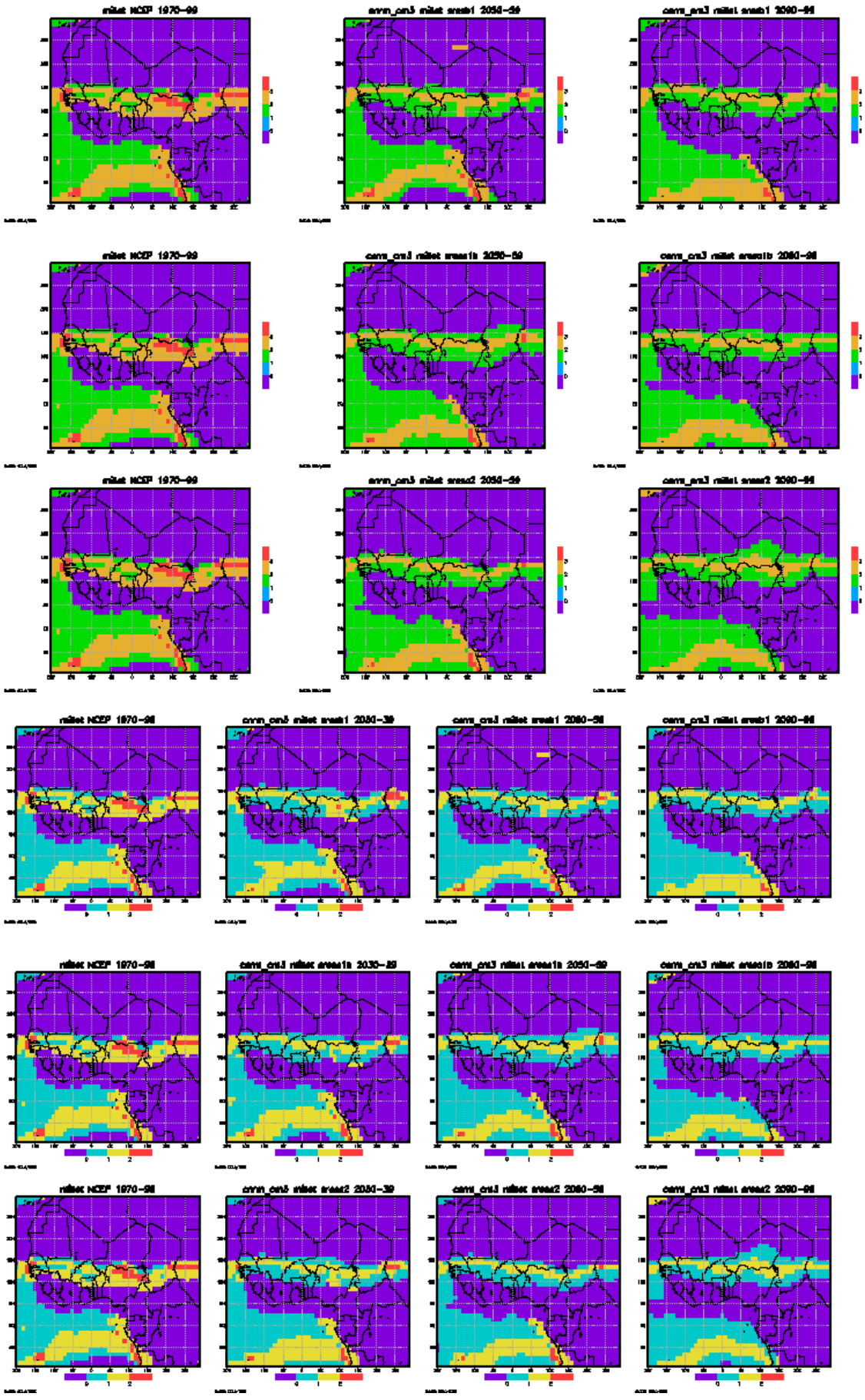
millet NCEP 1970–99
cnrm_cm3 millet sreal1 2030–39
cnrm_cm3 millet sreal1 2060–99
millet NCEP 1970–99
cnrm_cm3 millet sreal1b 2030–39
cnrm_cm3 millet sreal1b 2060–99
millet NCEP 1970–99
cnrm_cm3 millet sreal2 2030–39
cnrm_cm3 millet sreal2 2060–99
millet NCEP 1970–99
cnrm_cm3 millet sreal1 2030–39
cnrm_cm3 millet sreal1 2060–99
cnrm_cm3 millet sreal1 2060–99
millet NCEP 1970–99
cnrm_cm3 millet sreal1b 2030–39
cnrm_cm3 millet sreal1b 2060–99
cnrm_cm3 millet sreal1b 2060–99
millet NCEP 1970–99
cnrm_cm3 millet sreal2 2030–39
cnrm_cm3 millet sreal2 2060–99
cnrm_cm3 millet sreal2 2060–99

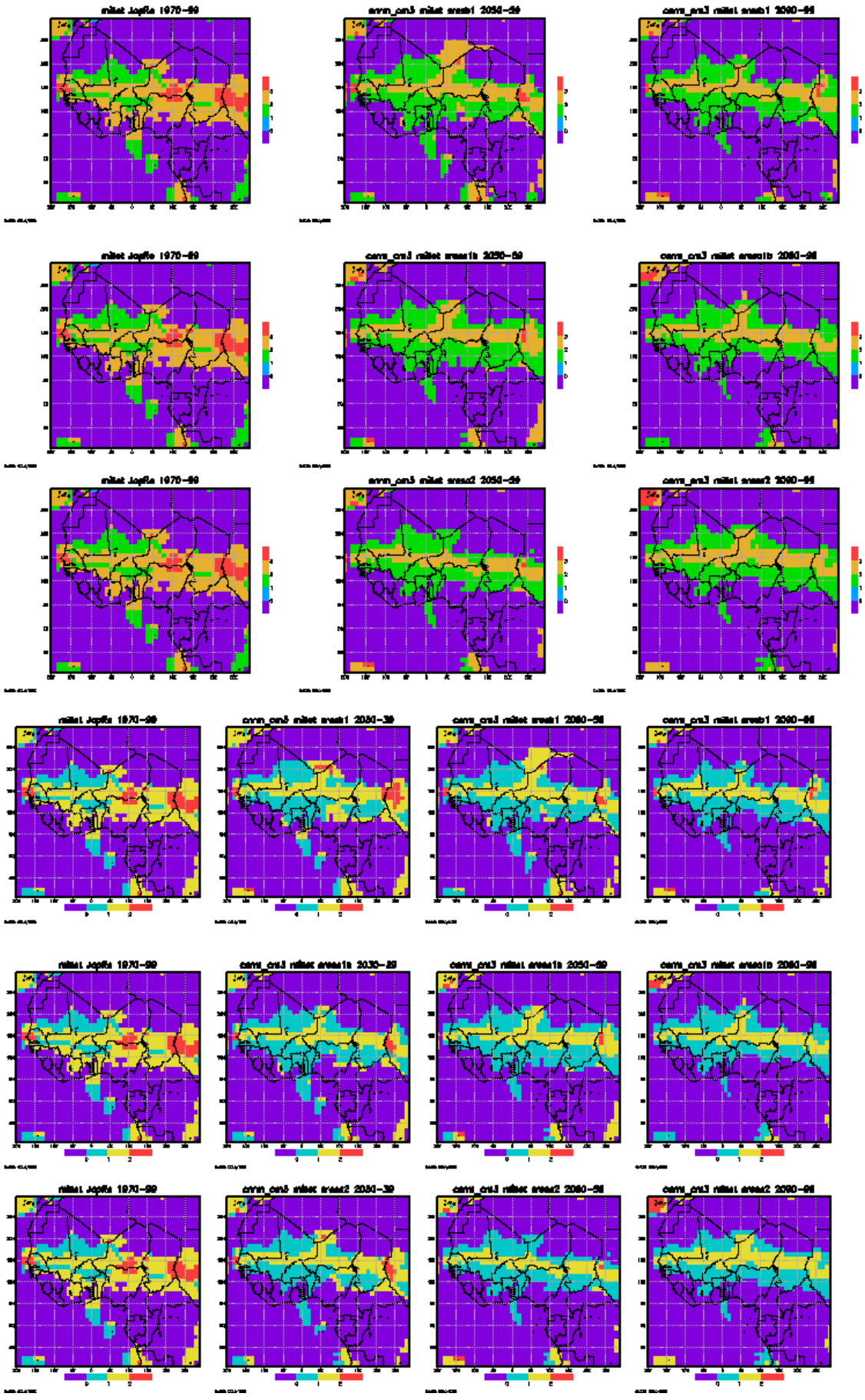

c. CSIRO

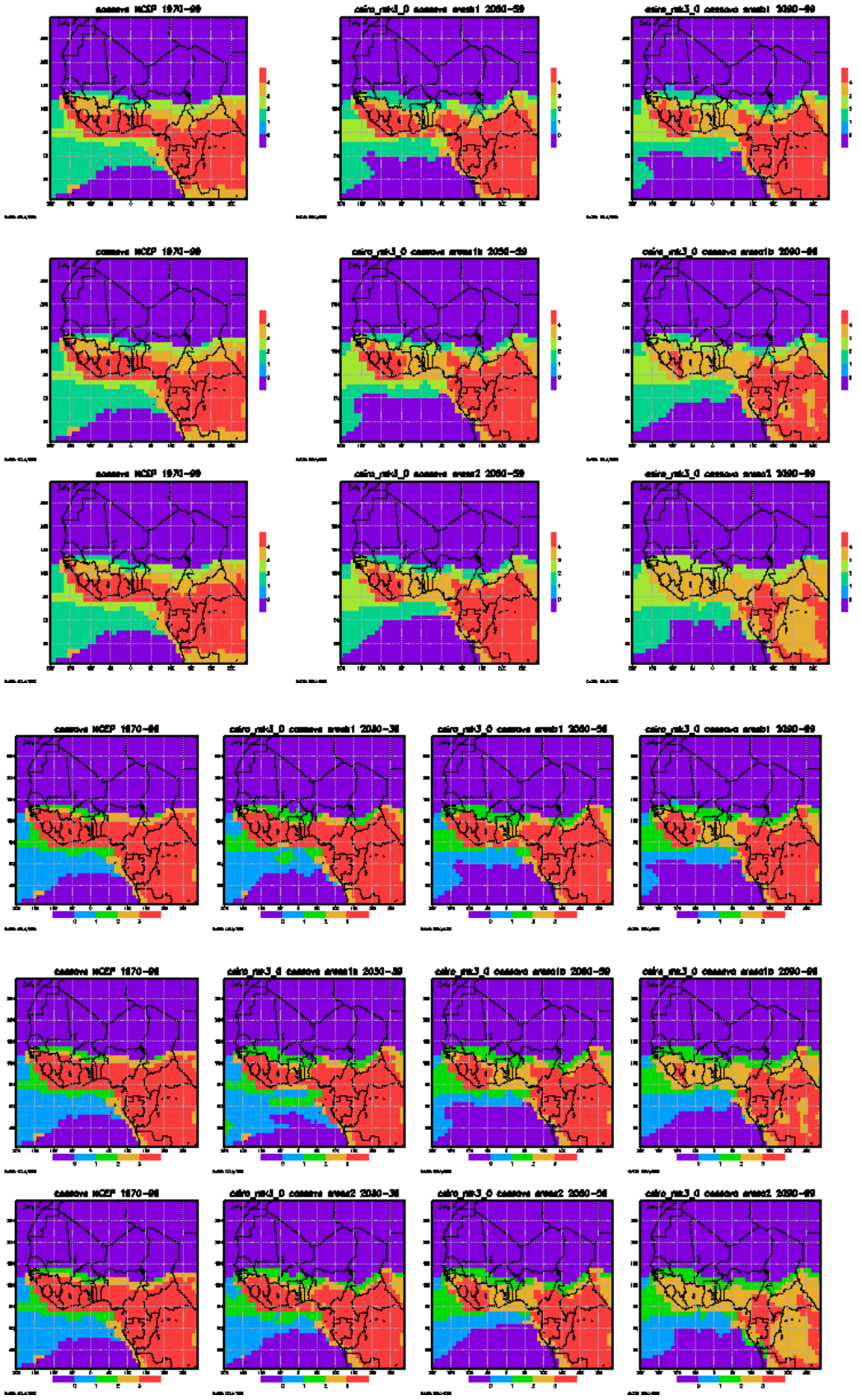

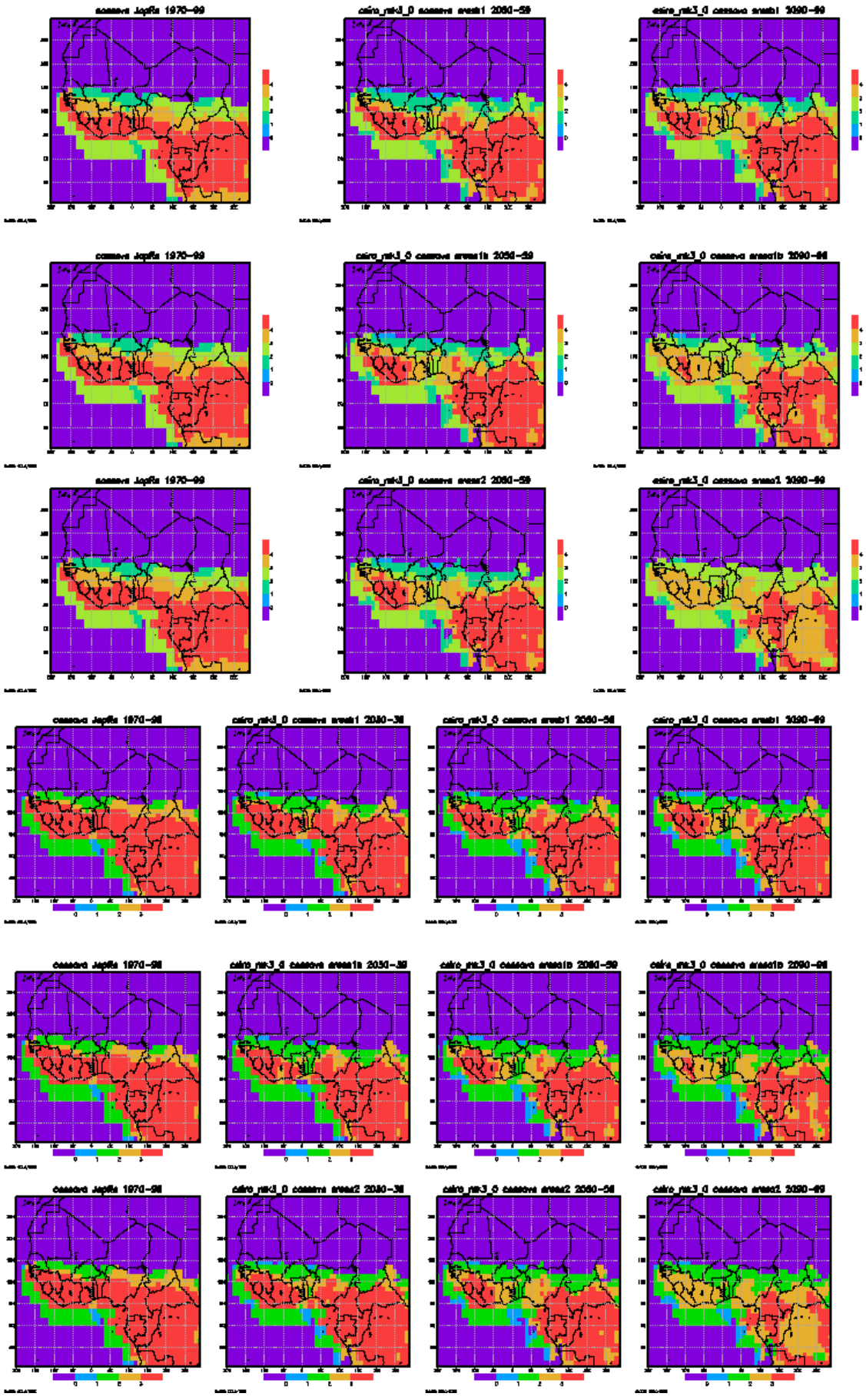

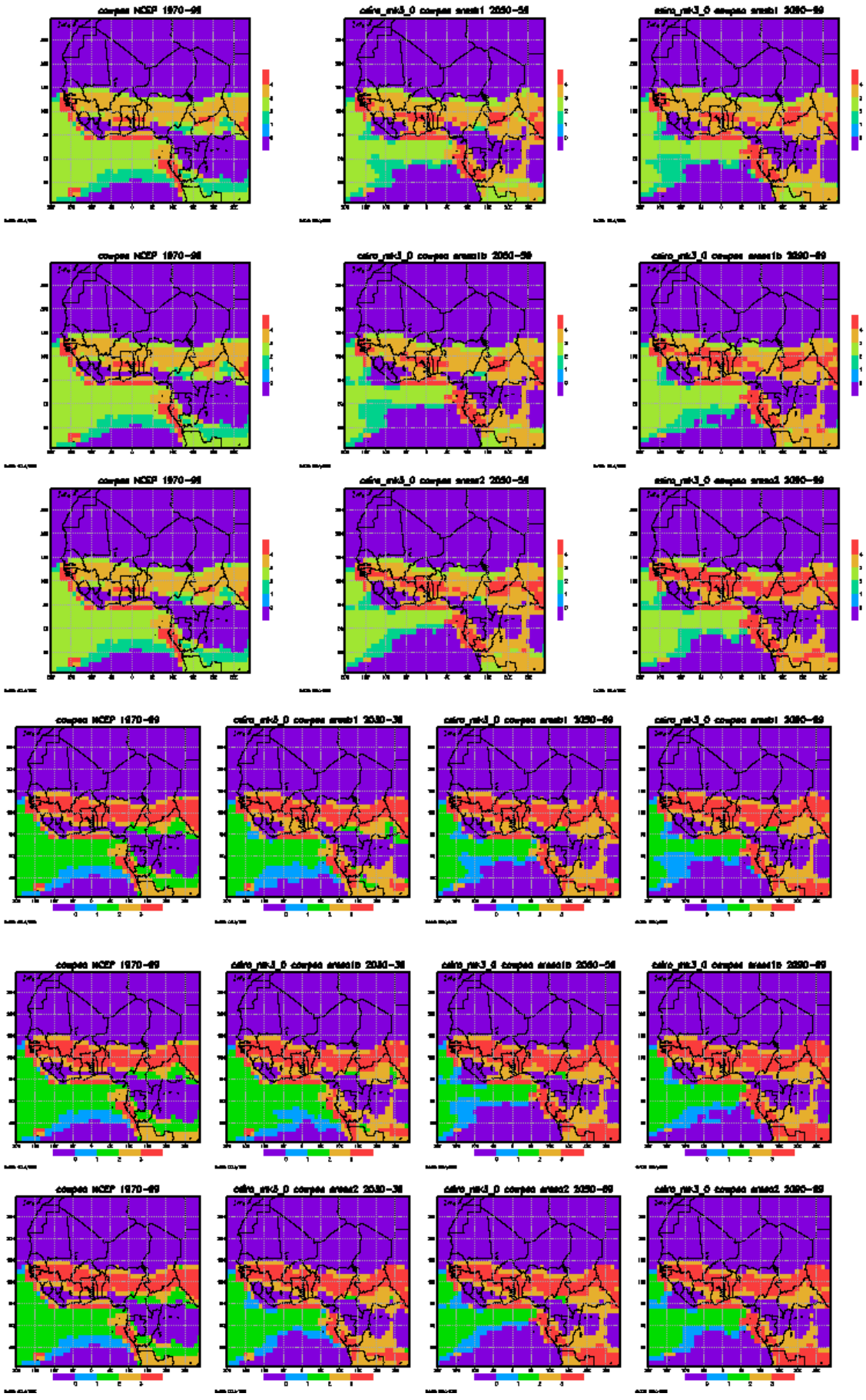

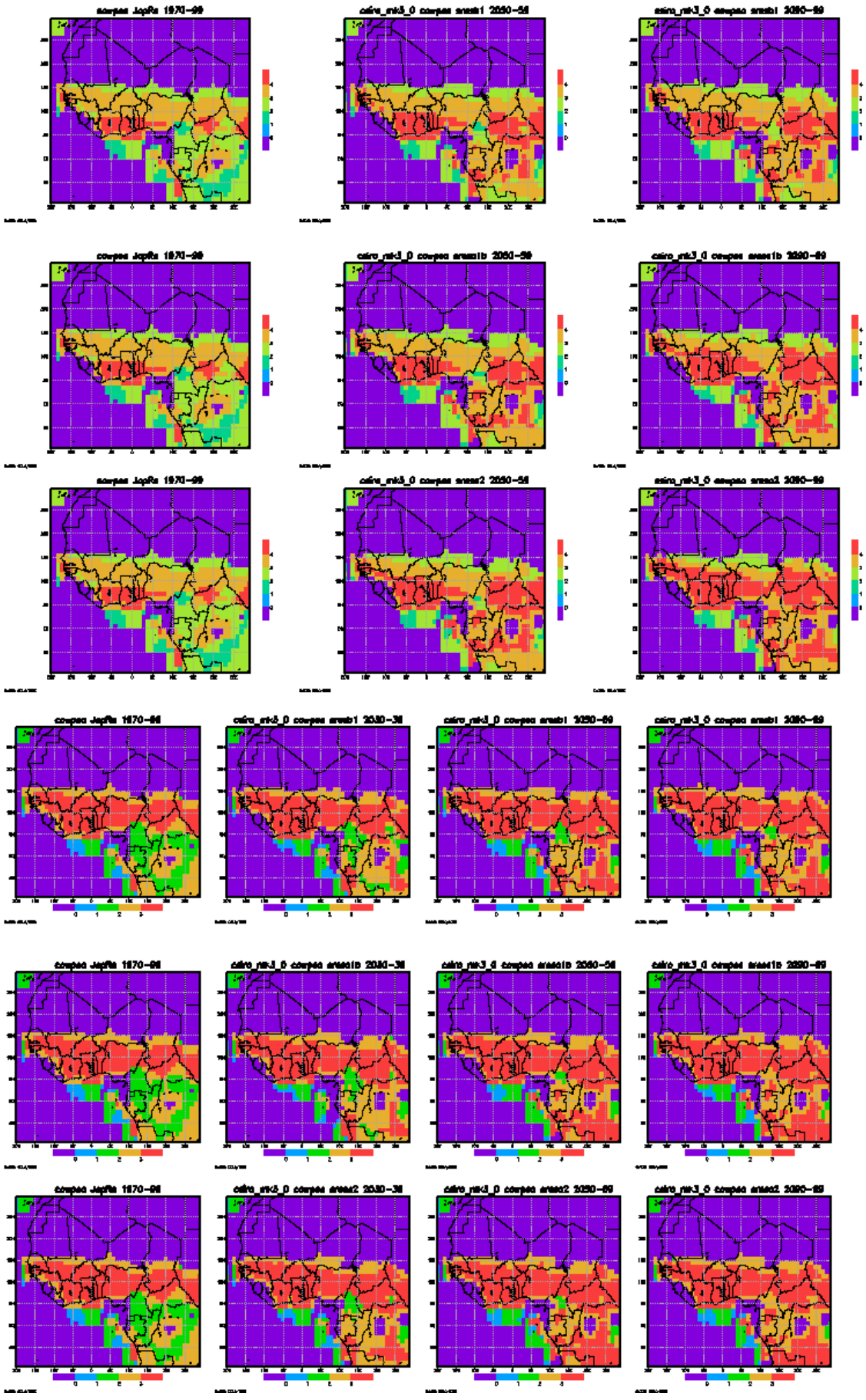

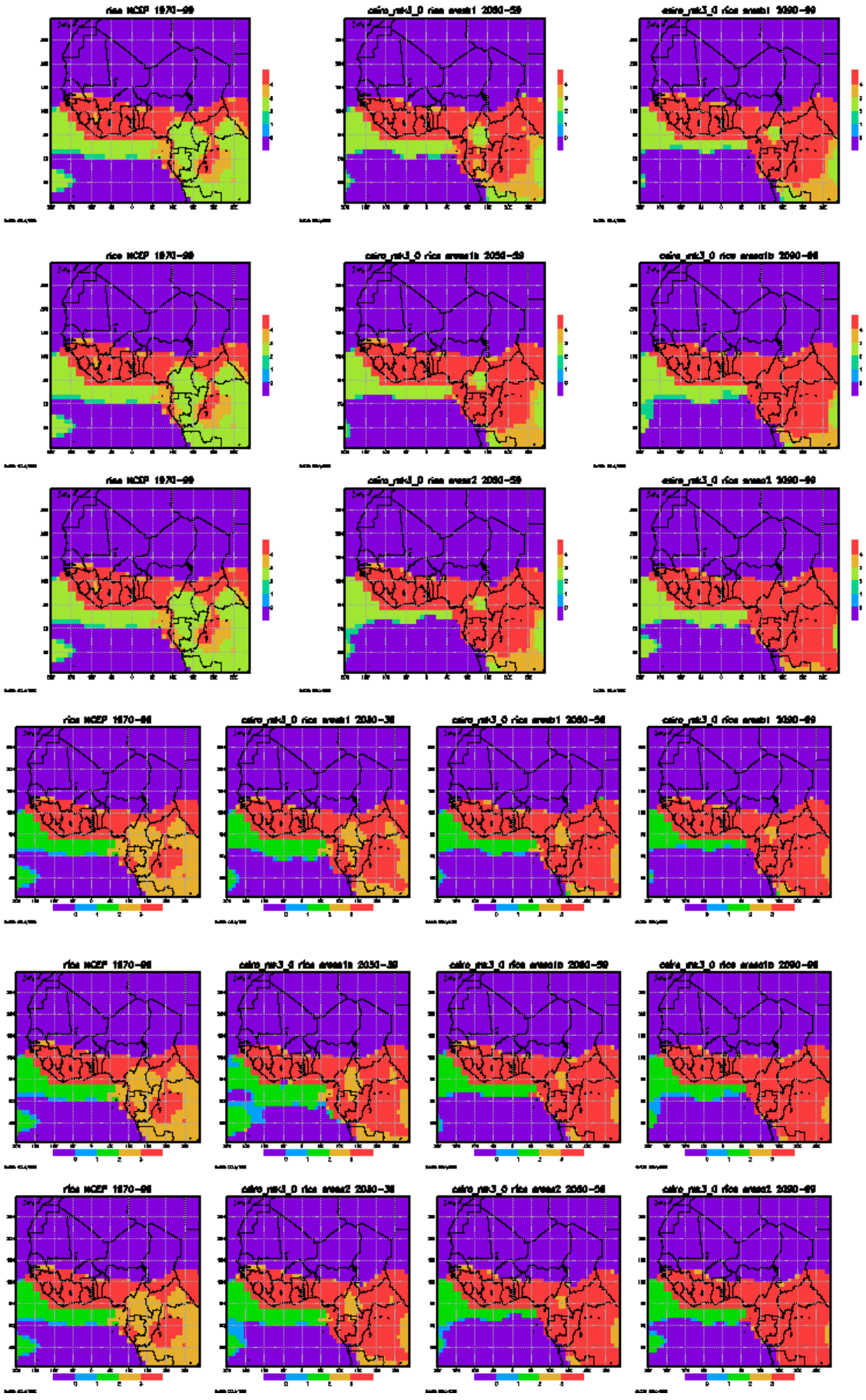

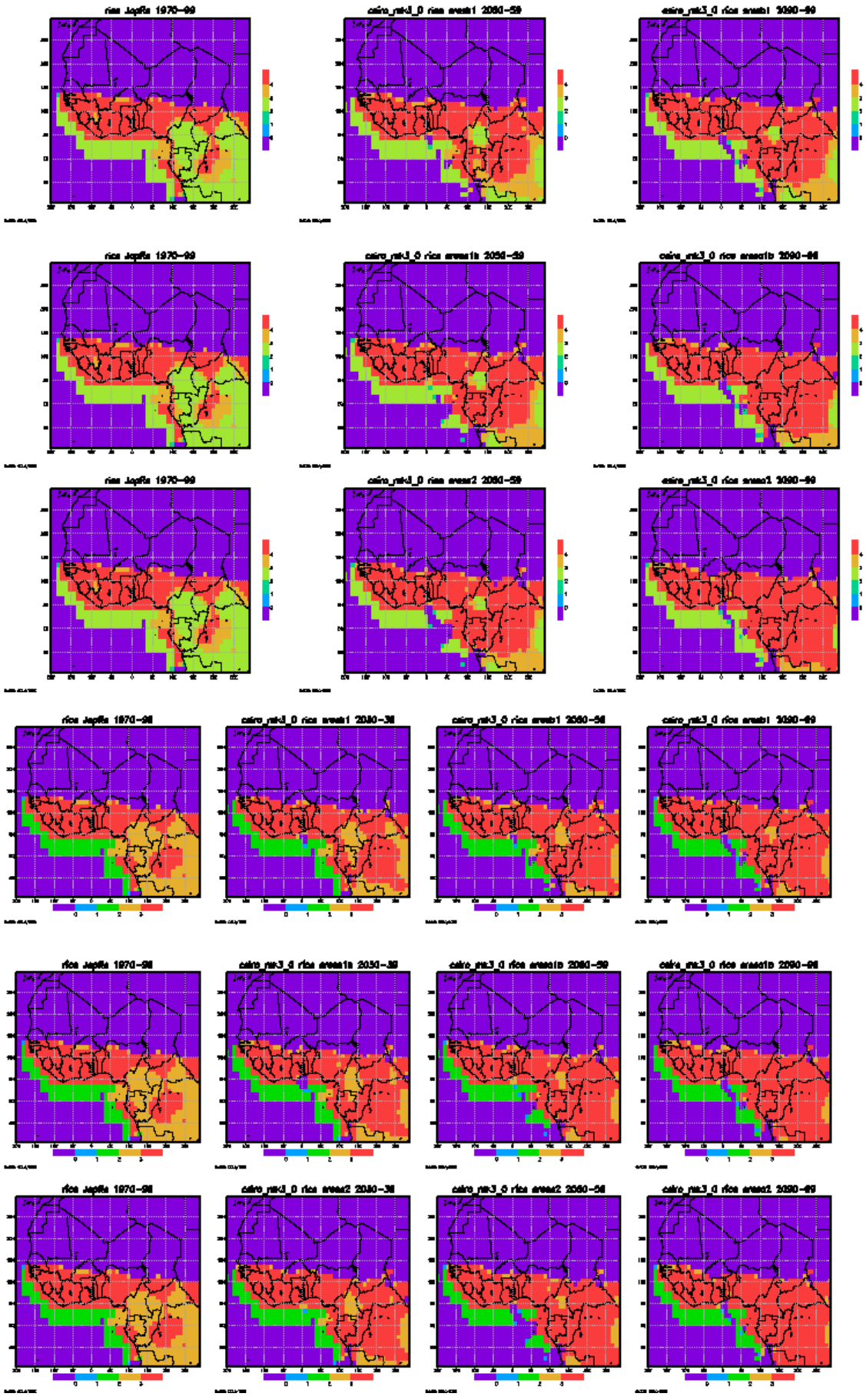

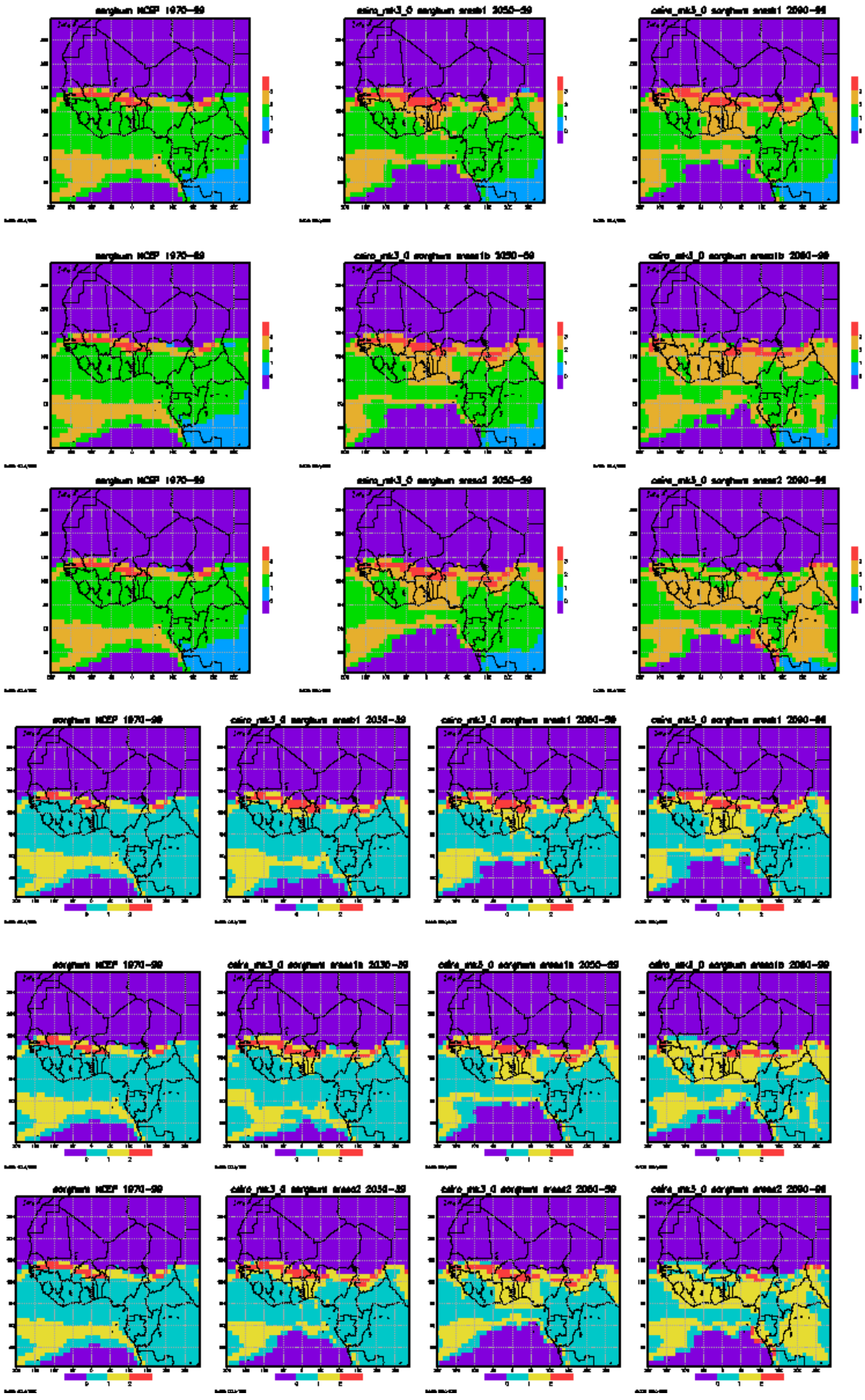

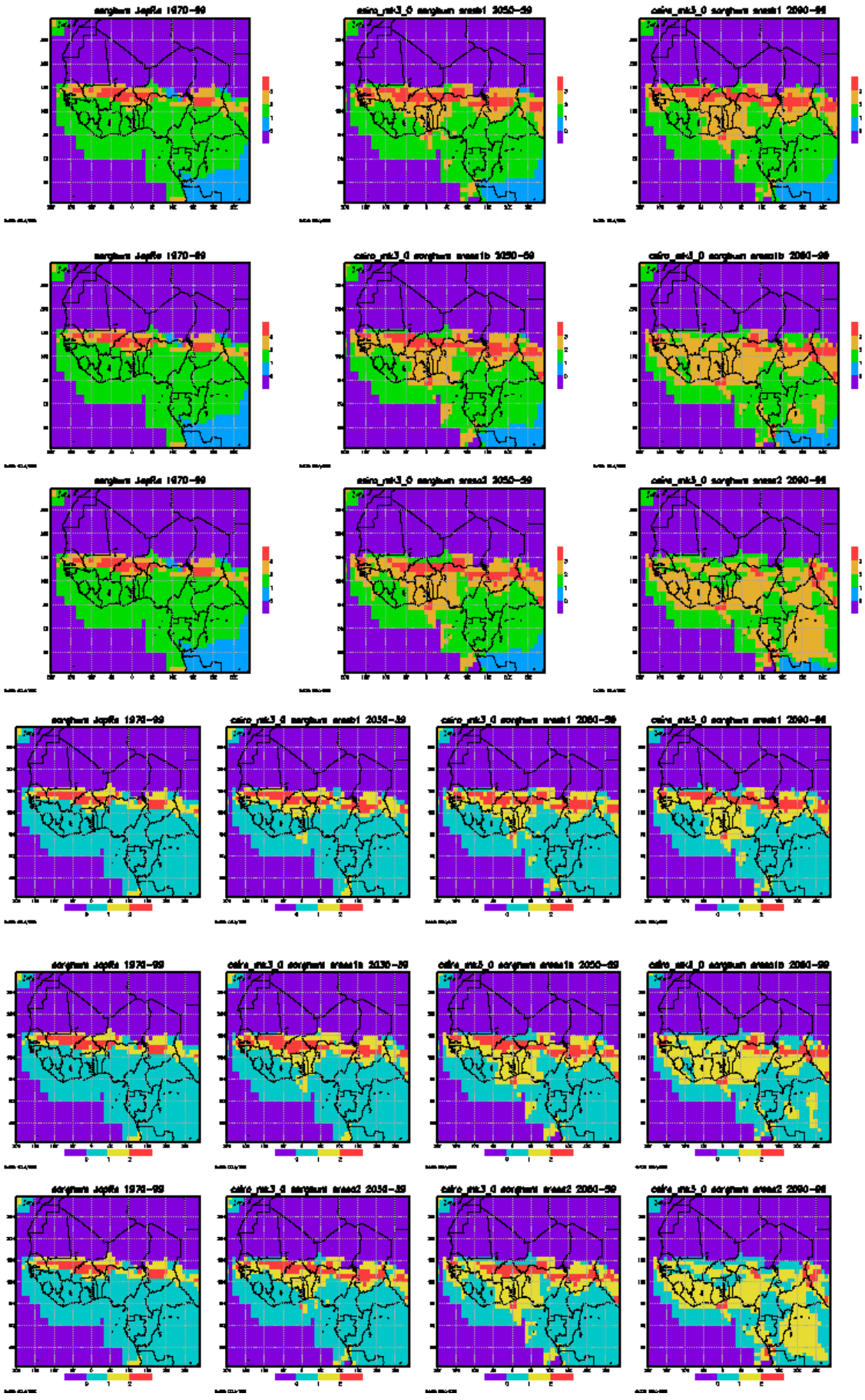

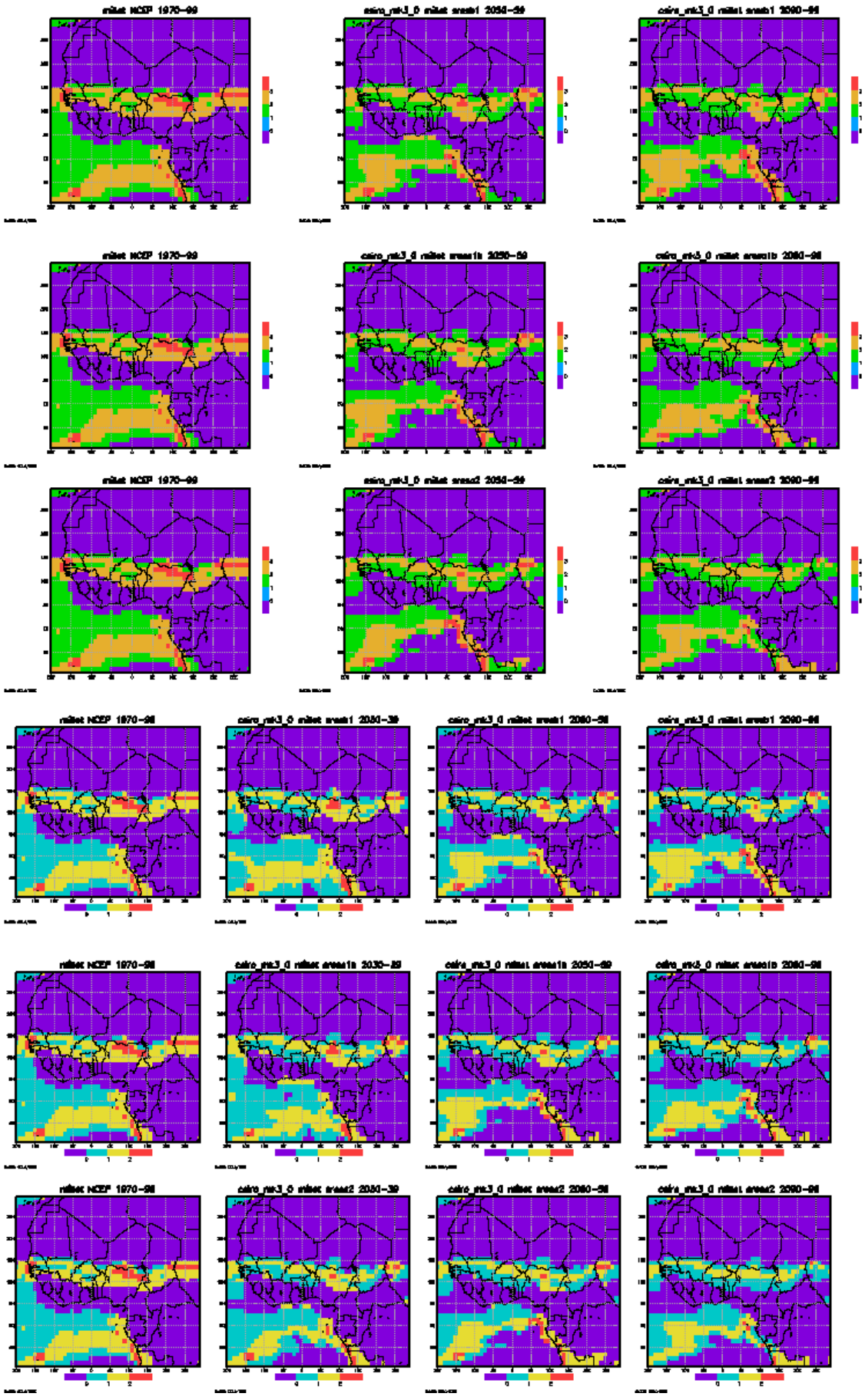

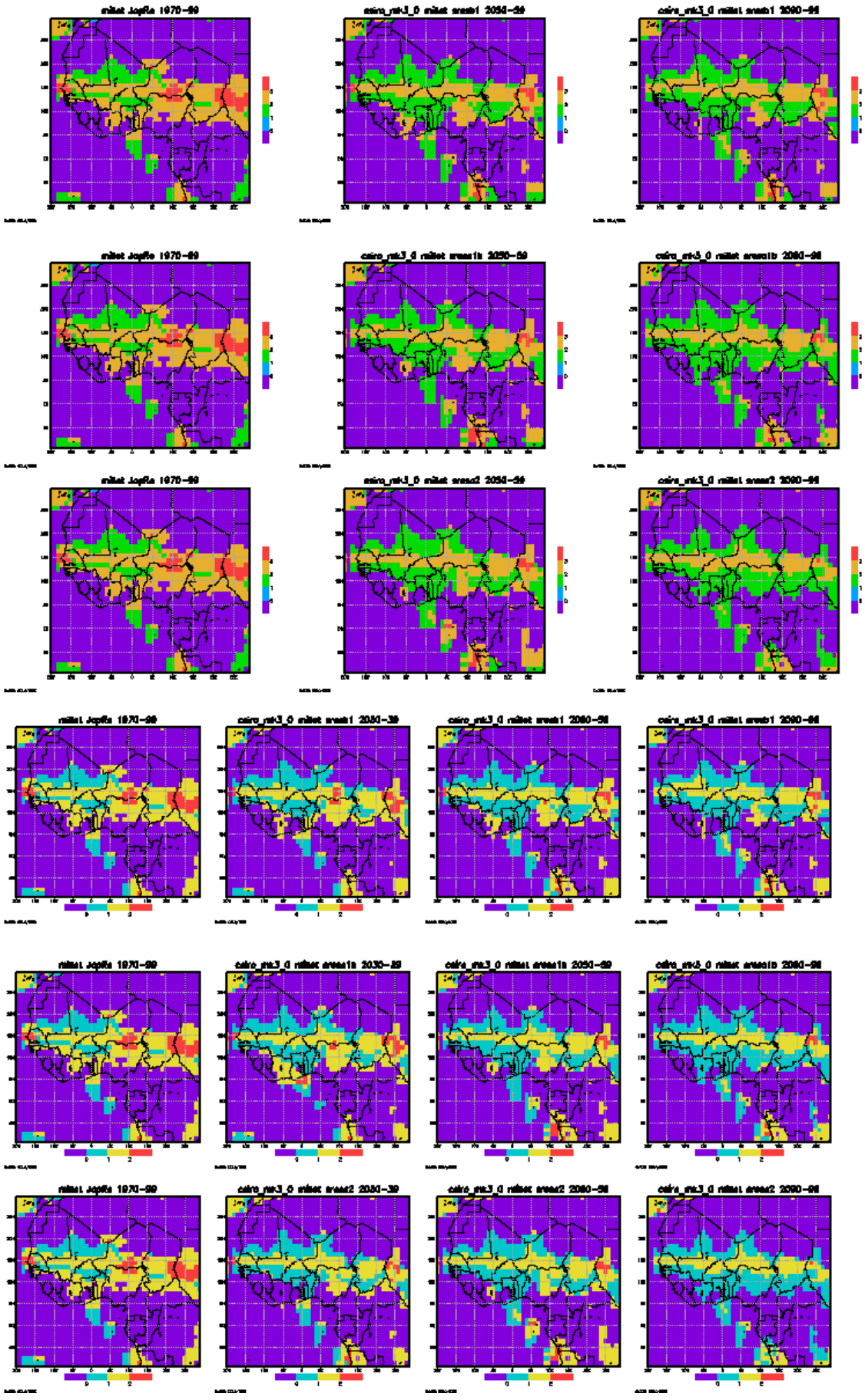

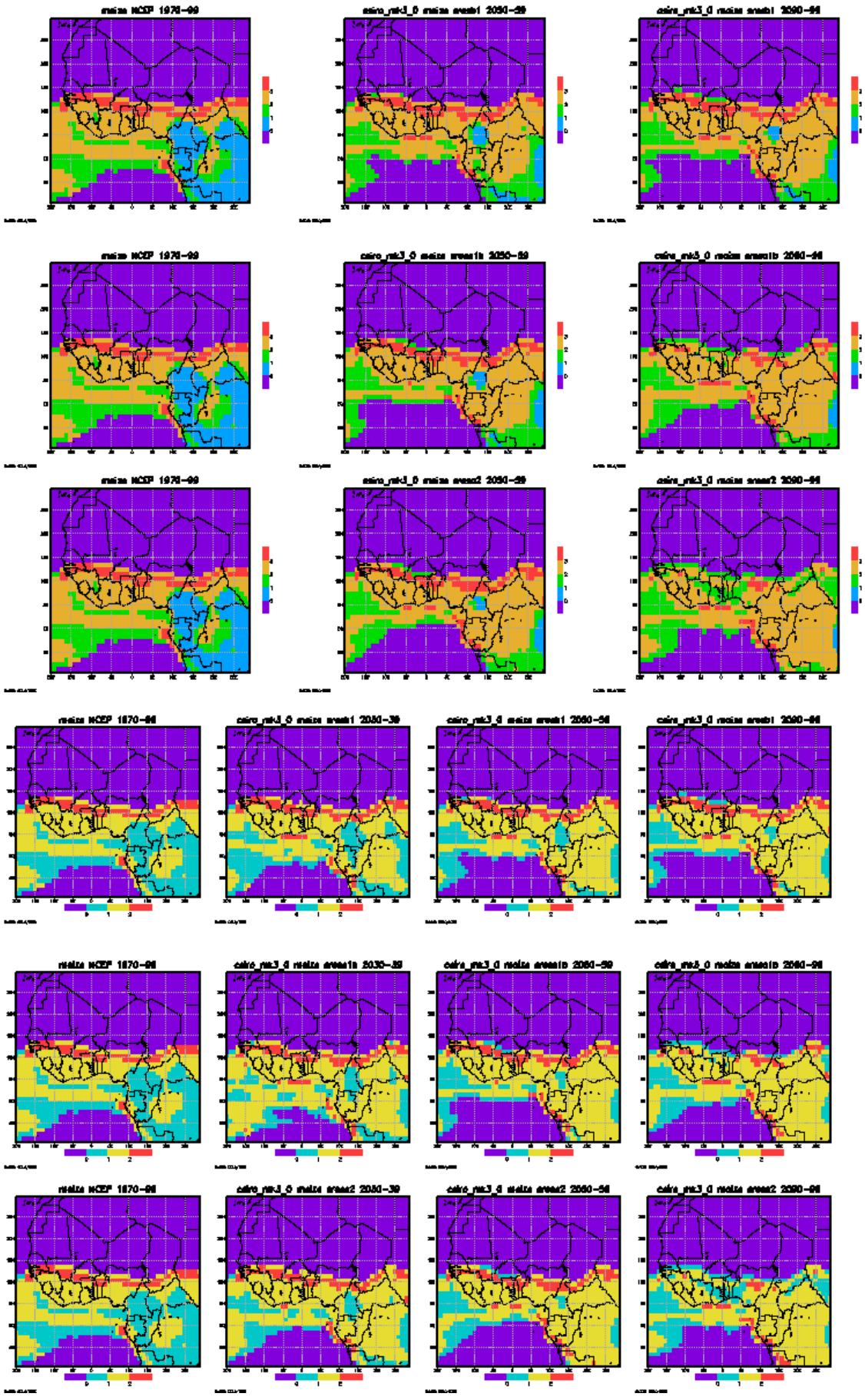

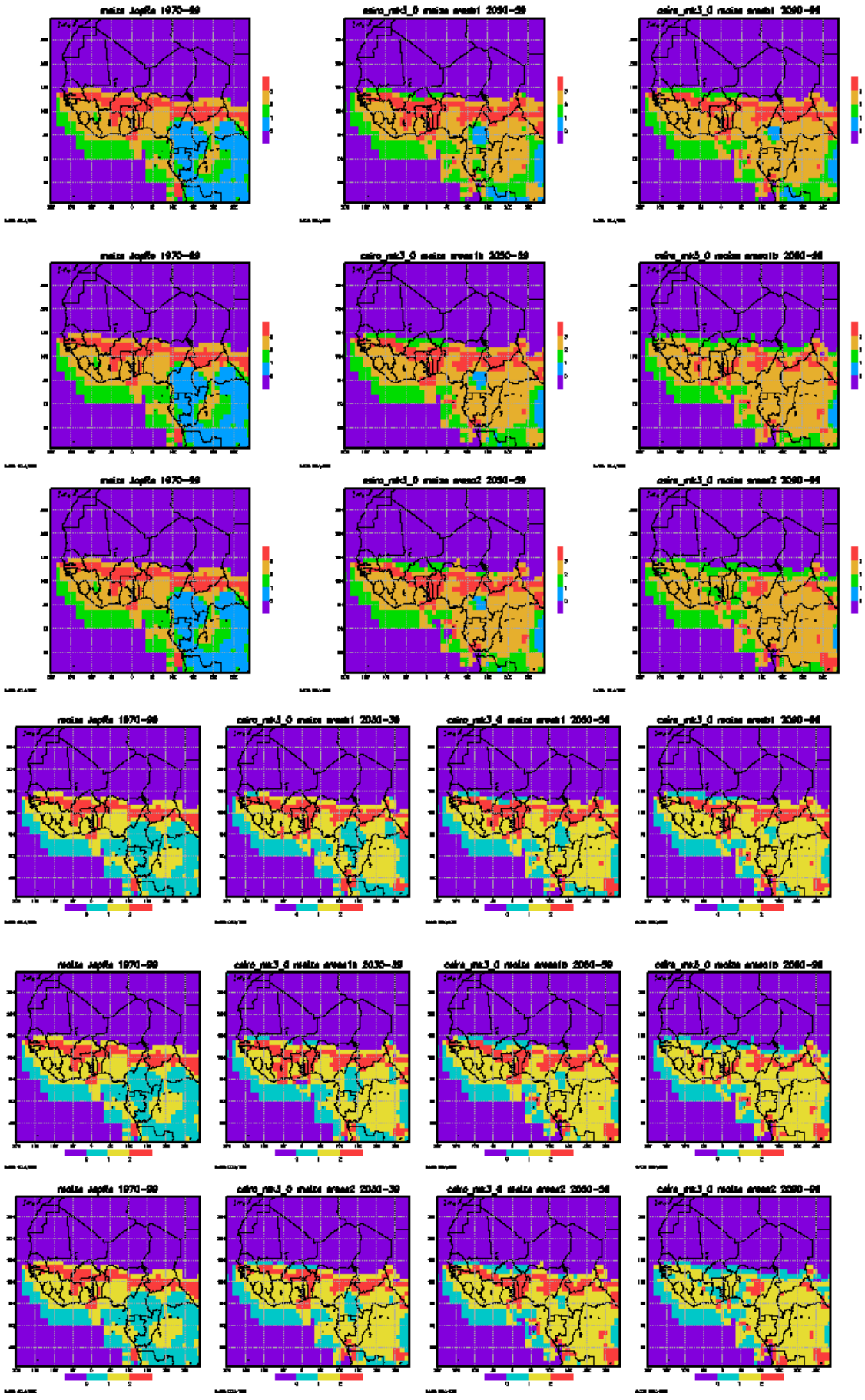

d. GFDL

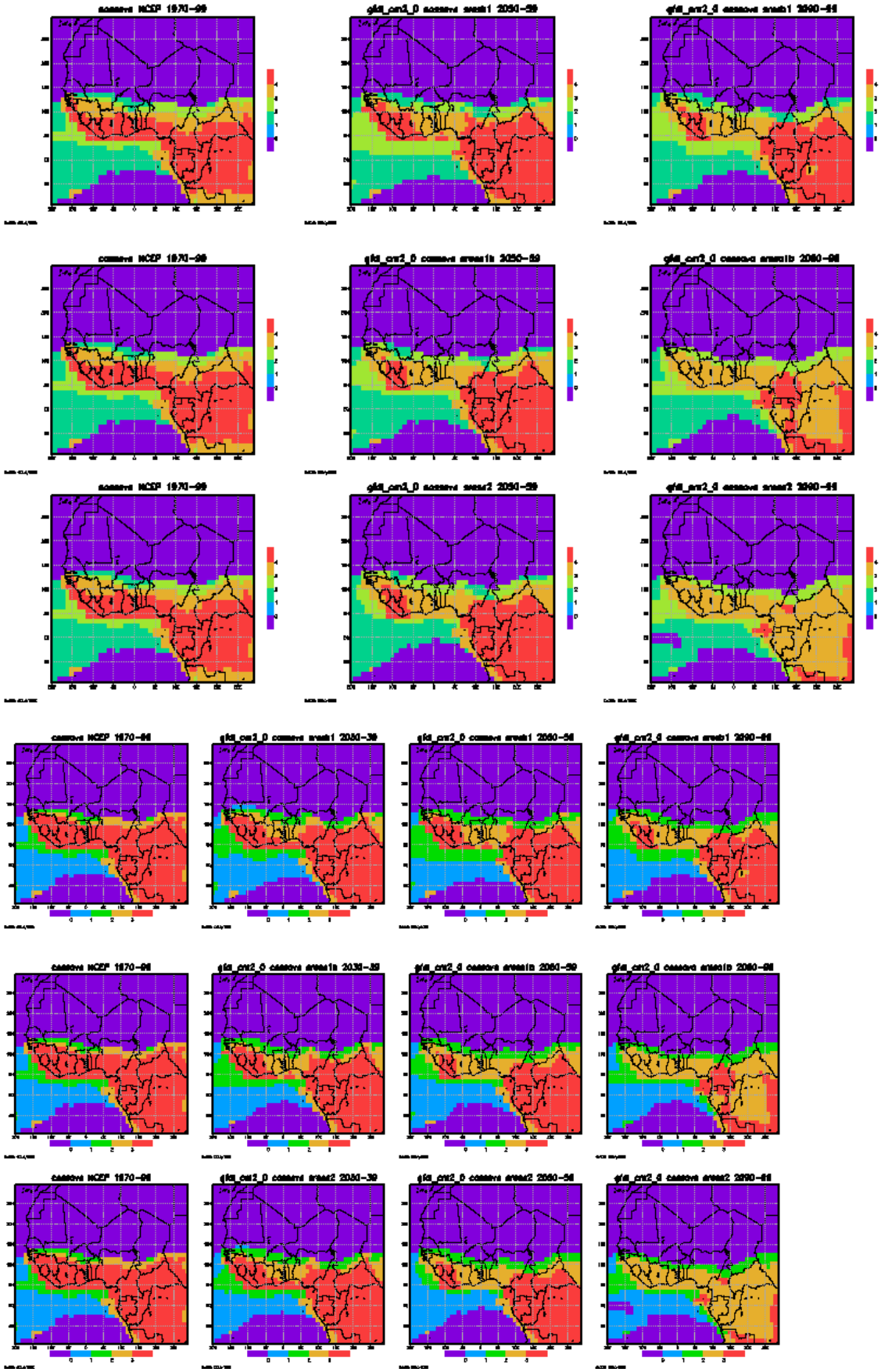

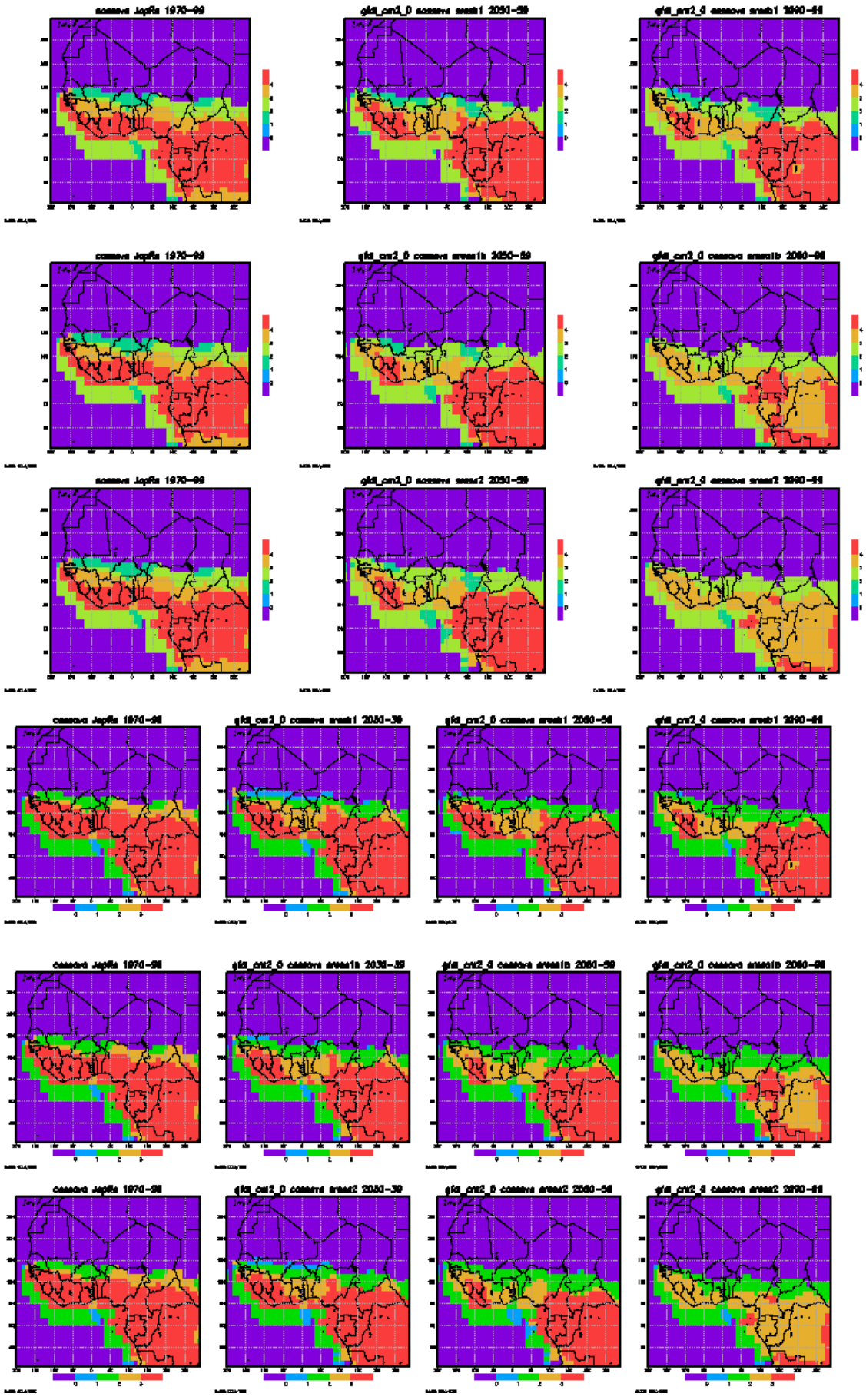

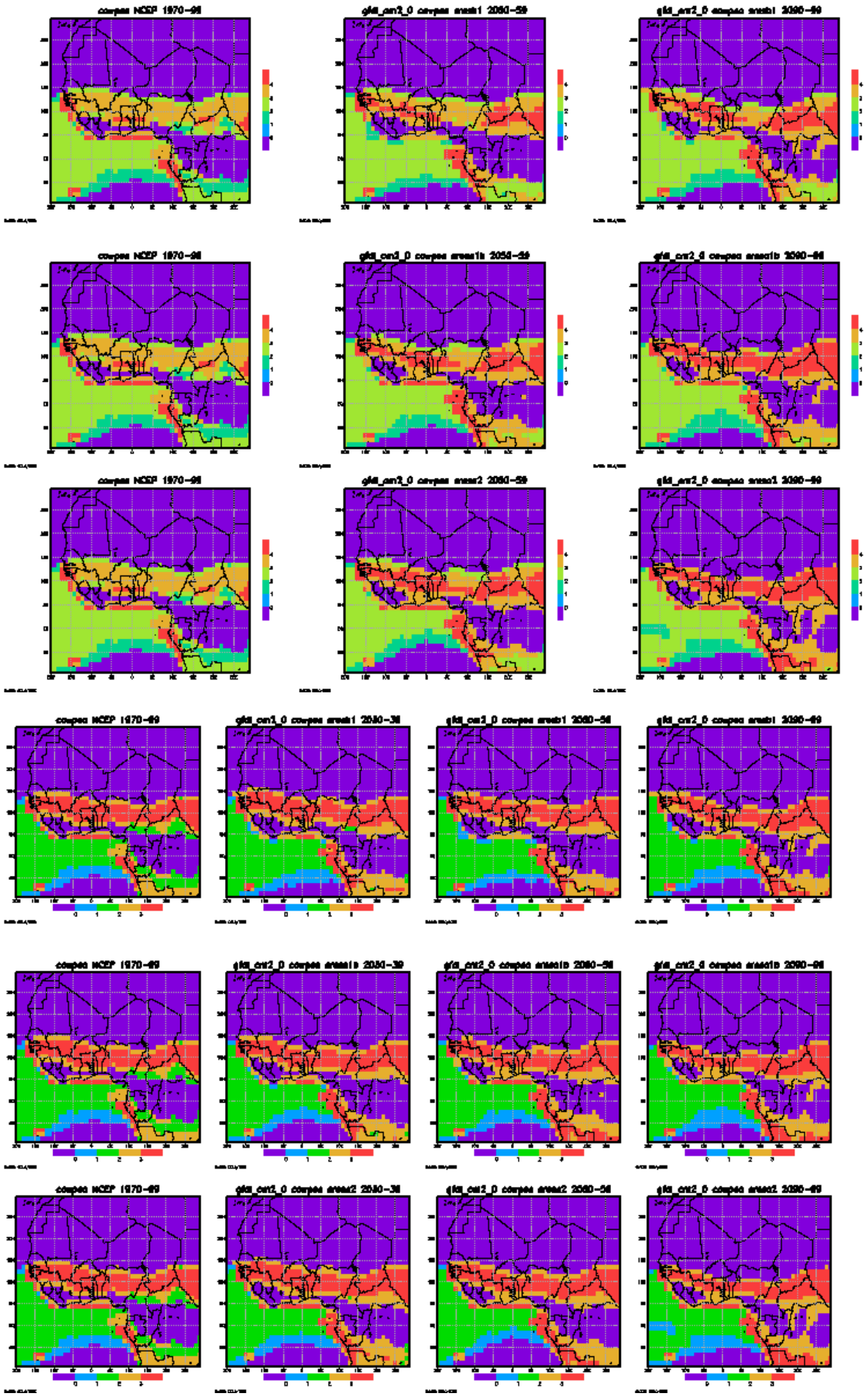

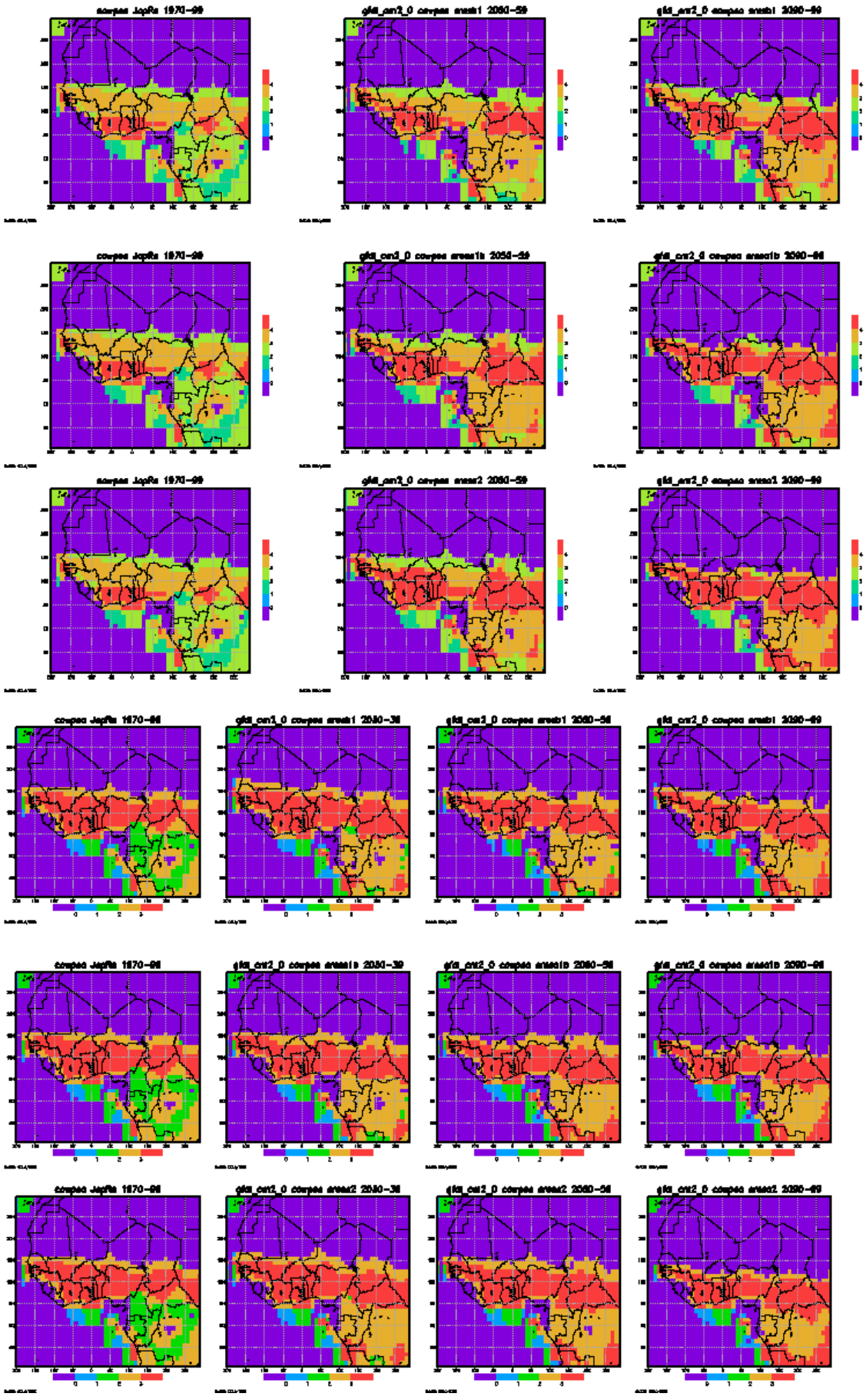

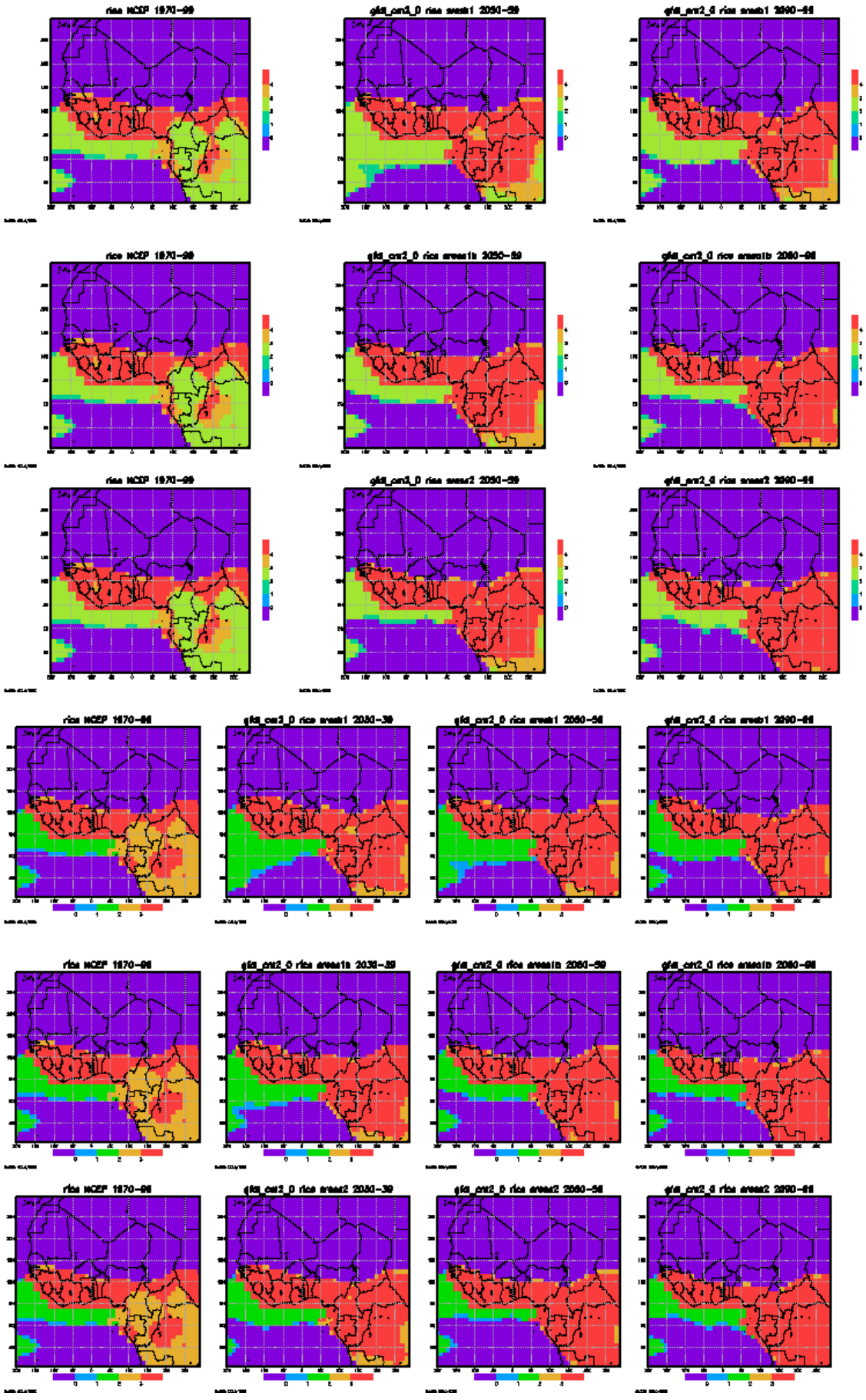

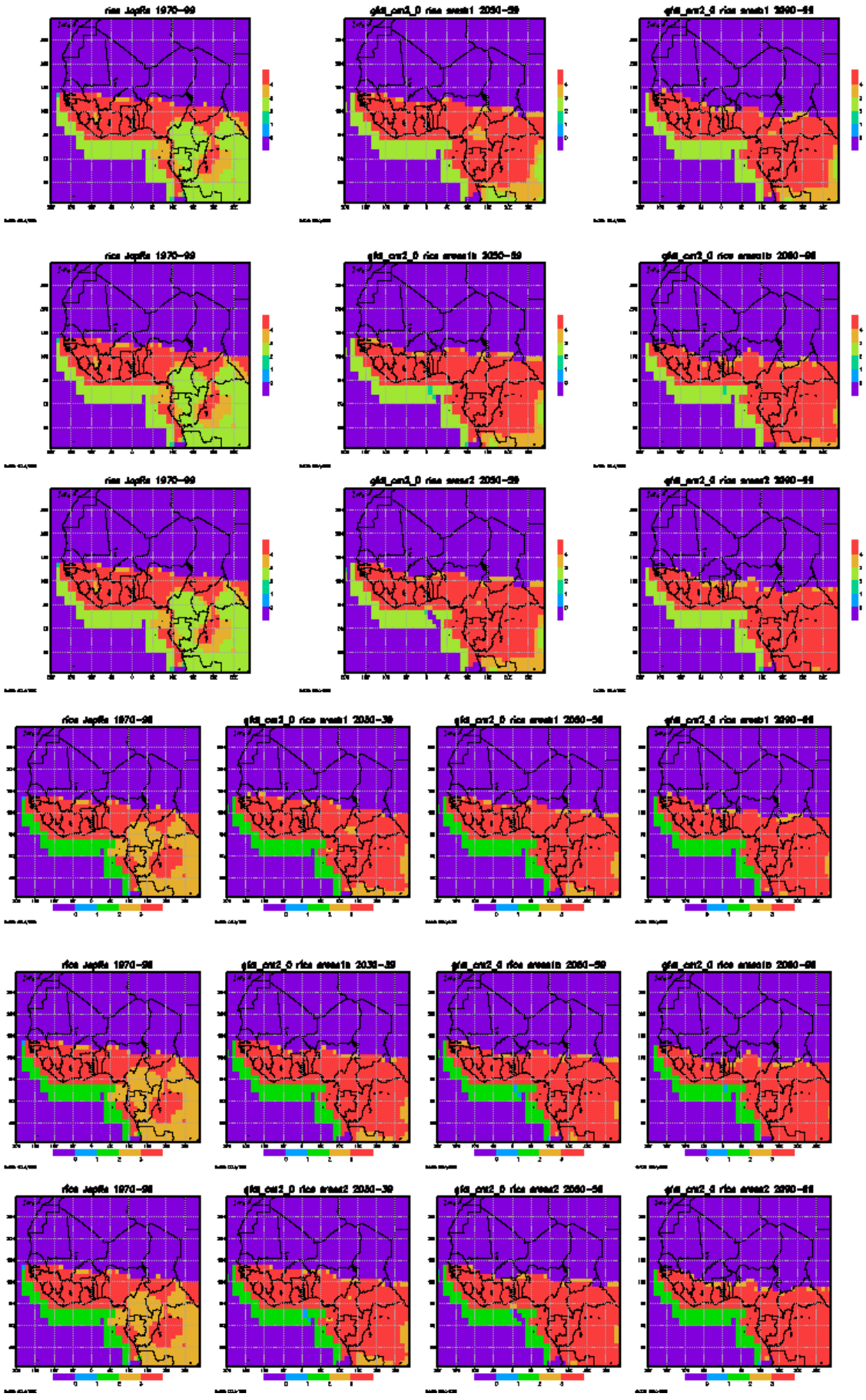

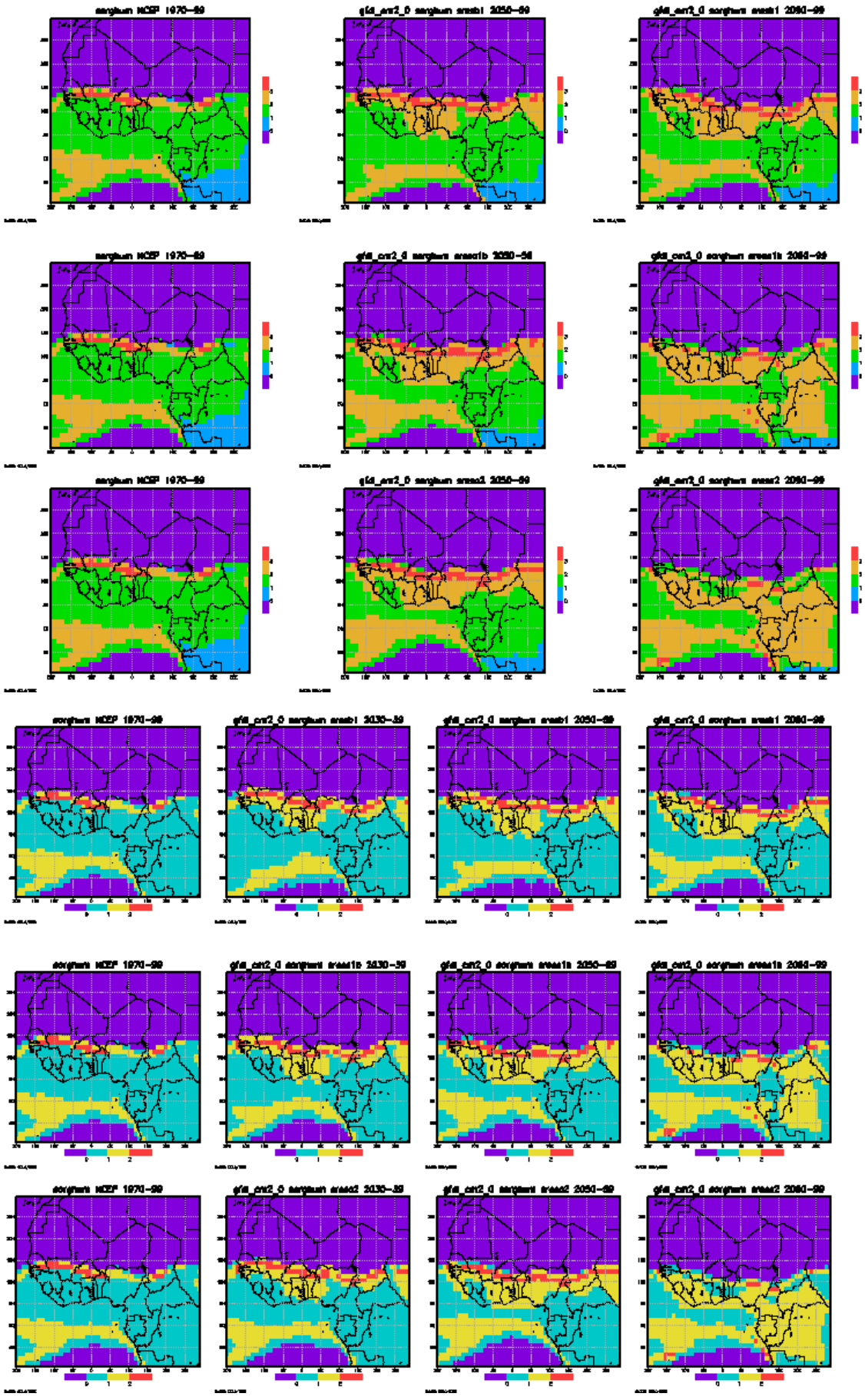

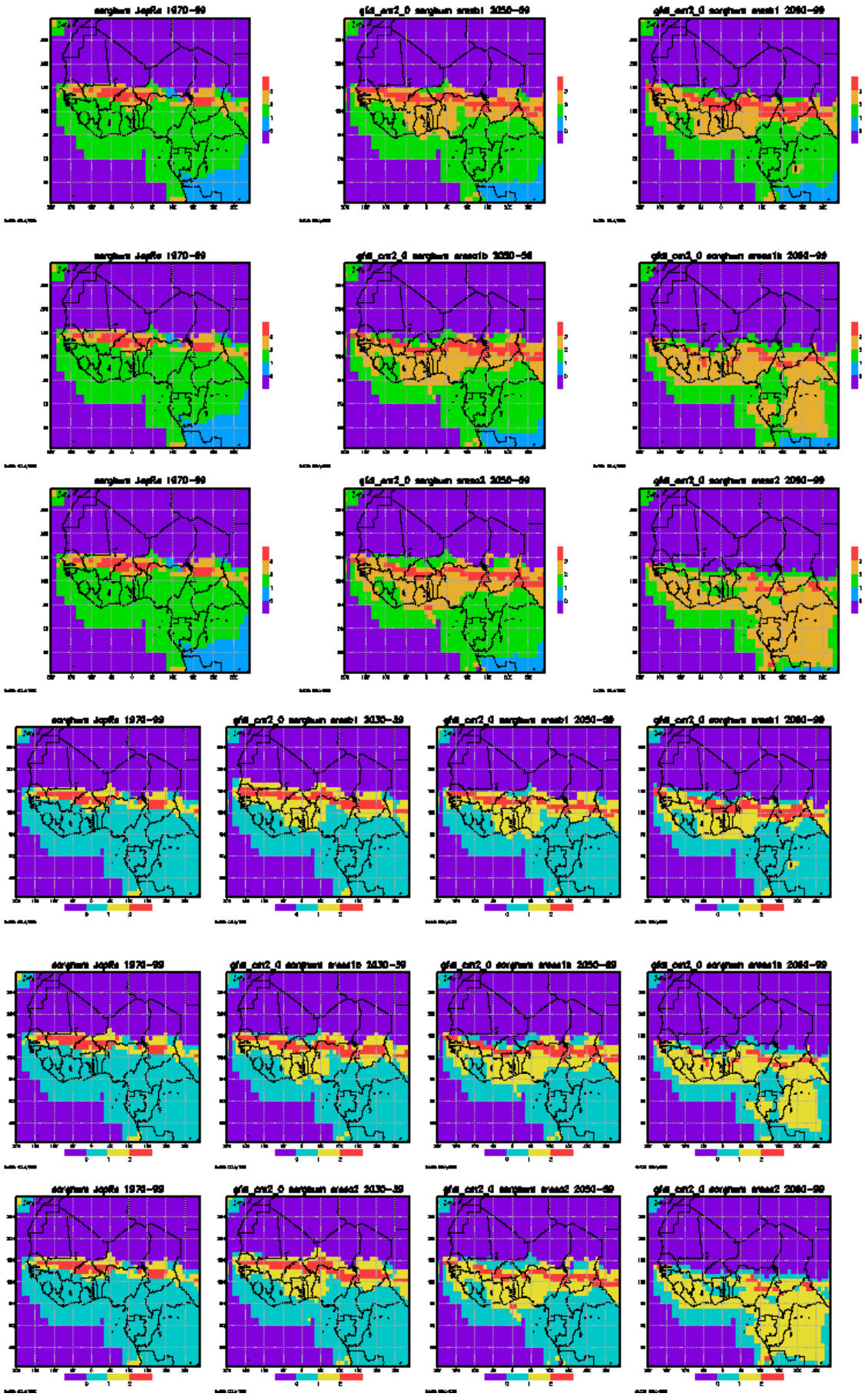

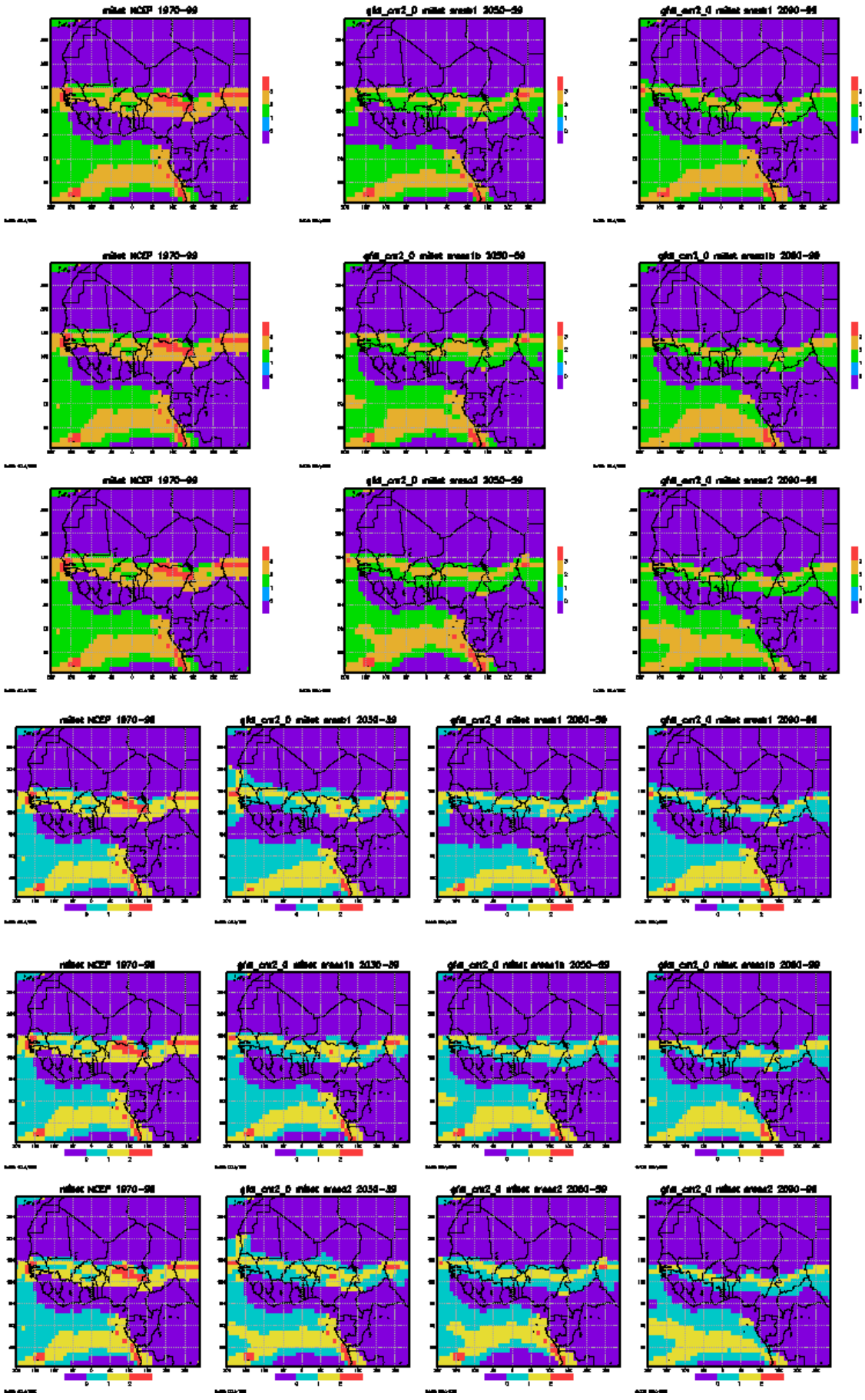

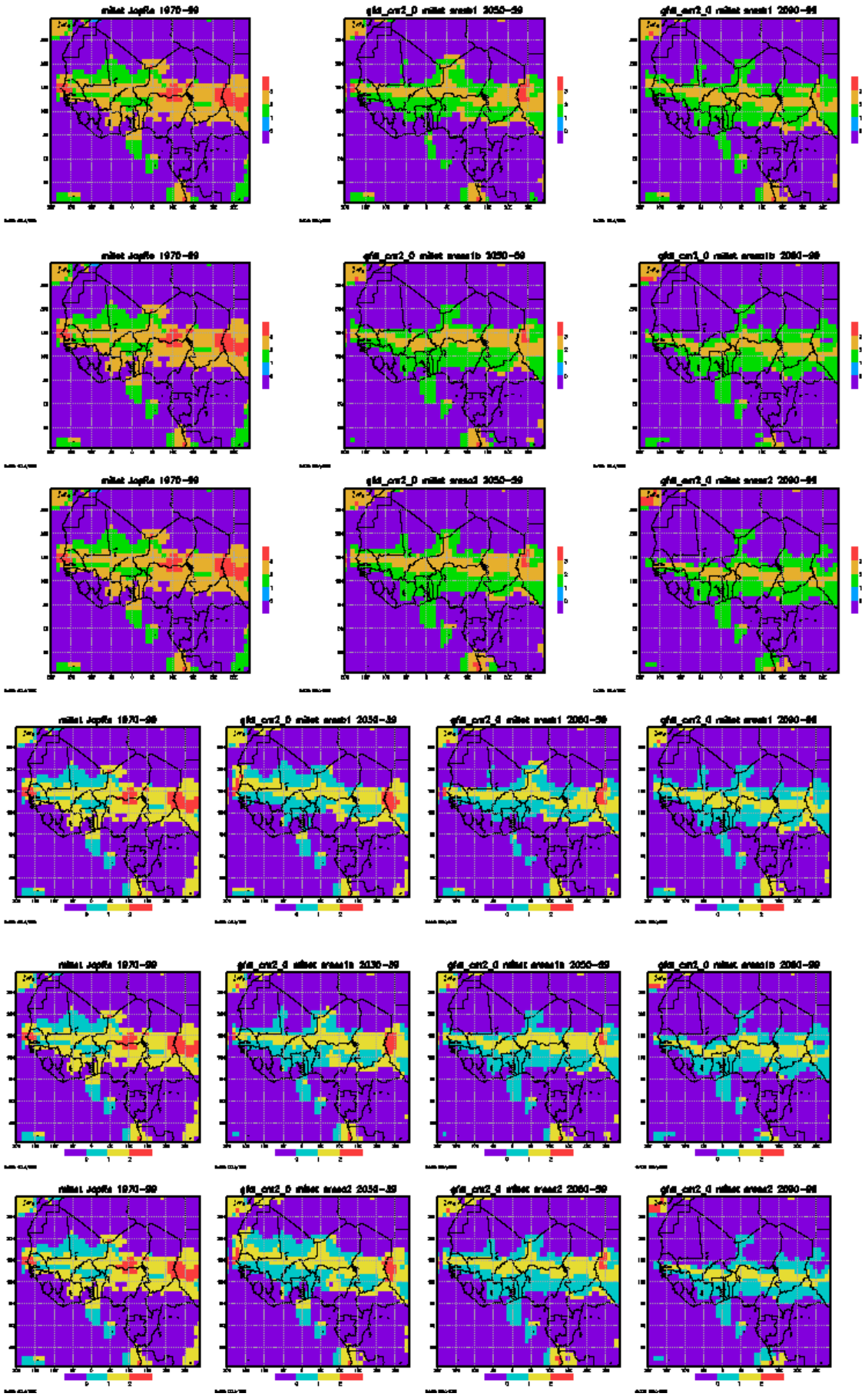

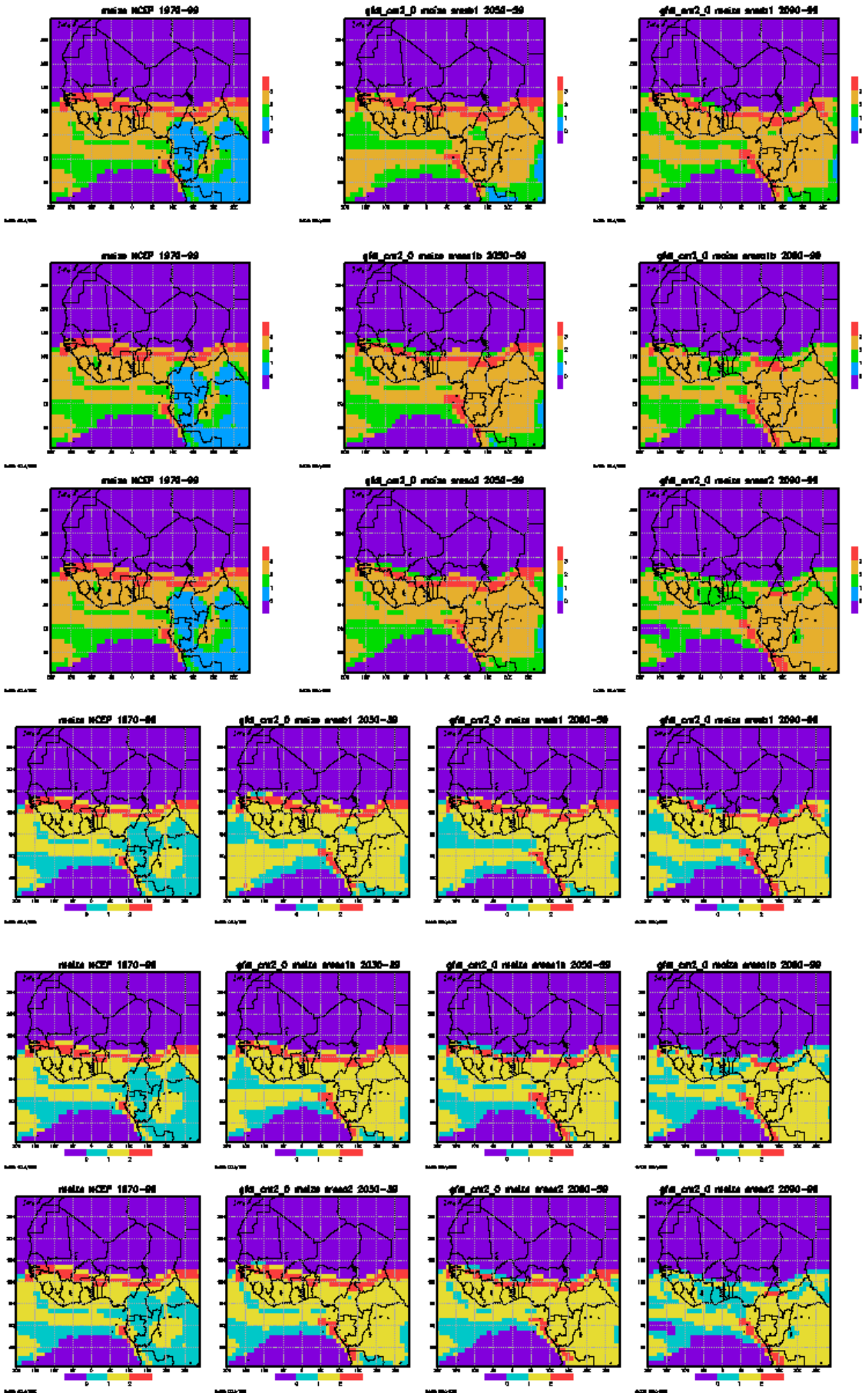

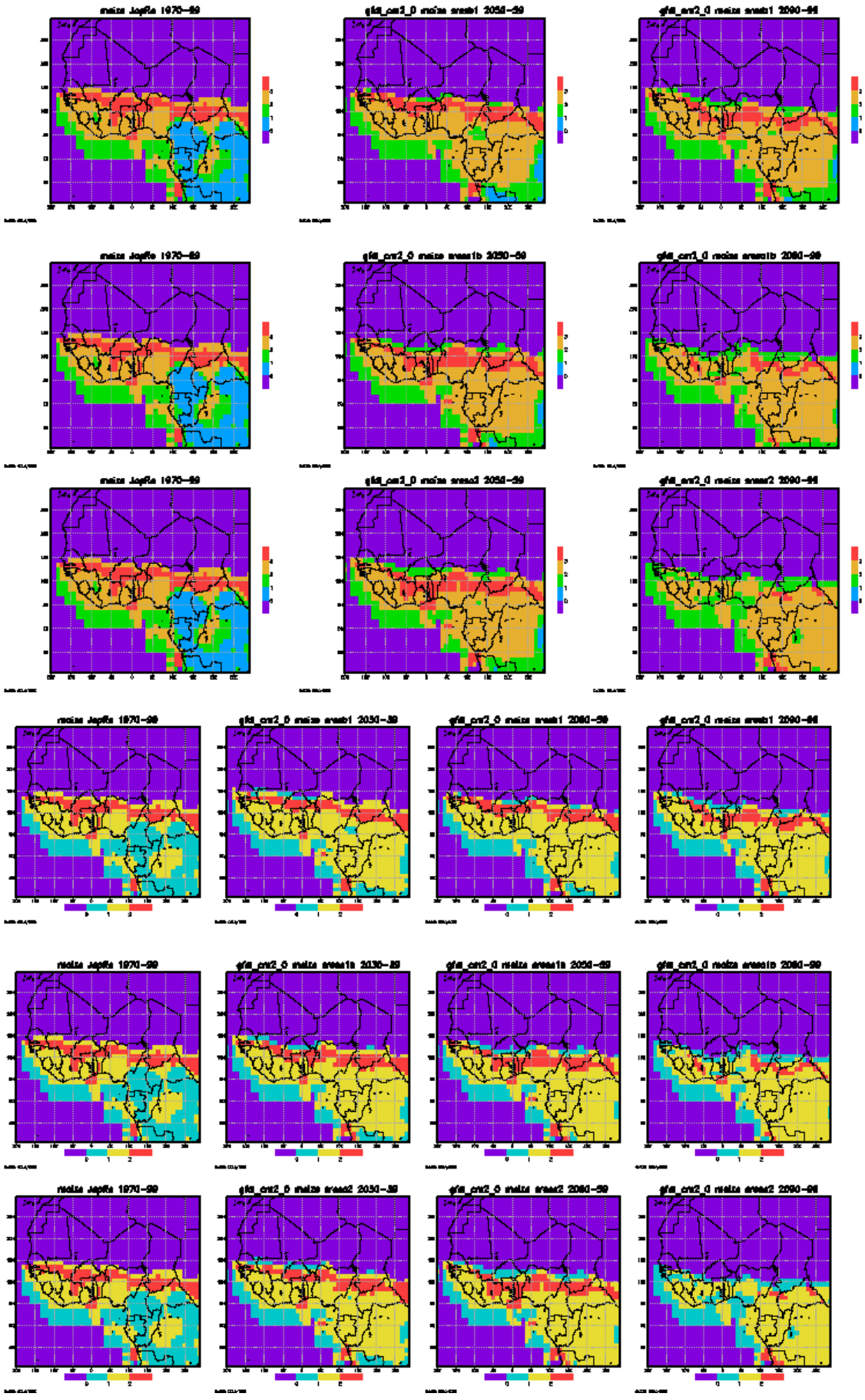

e. MIUB

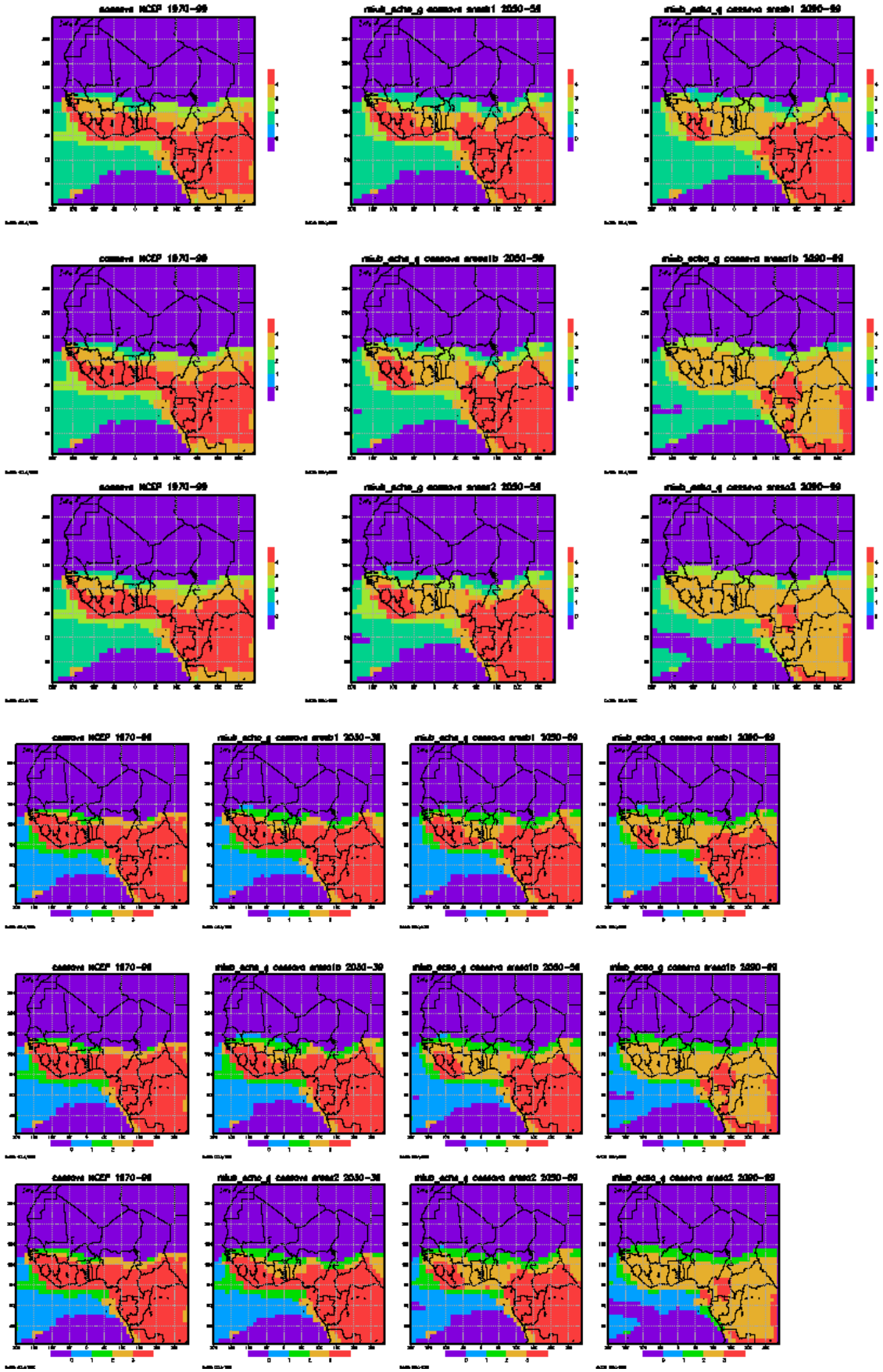

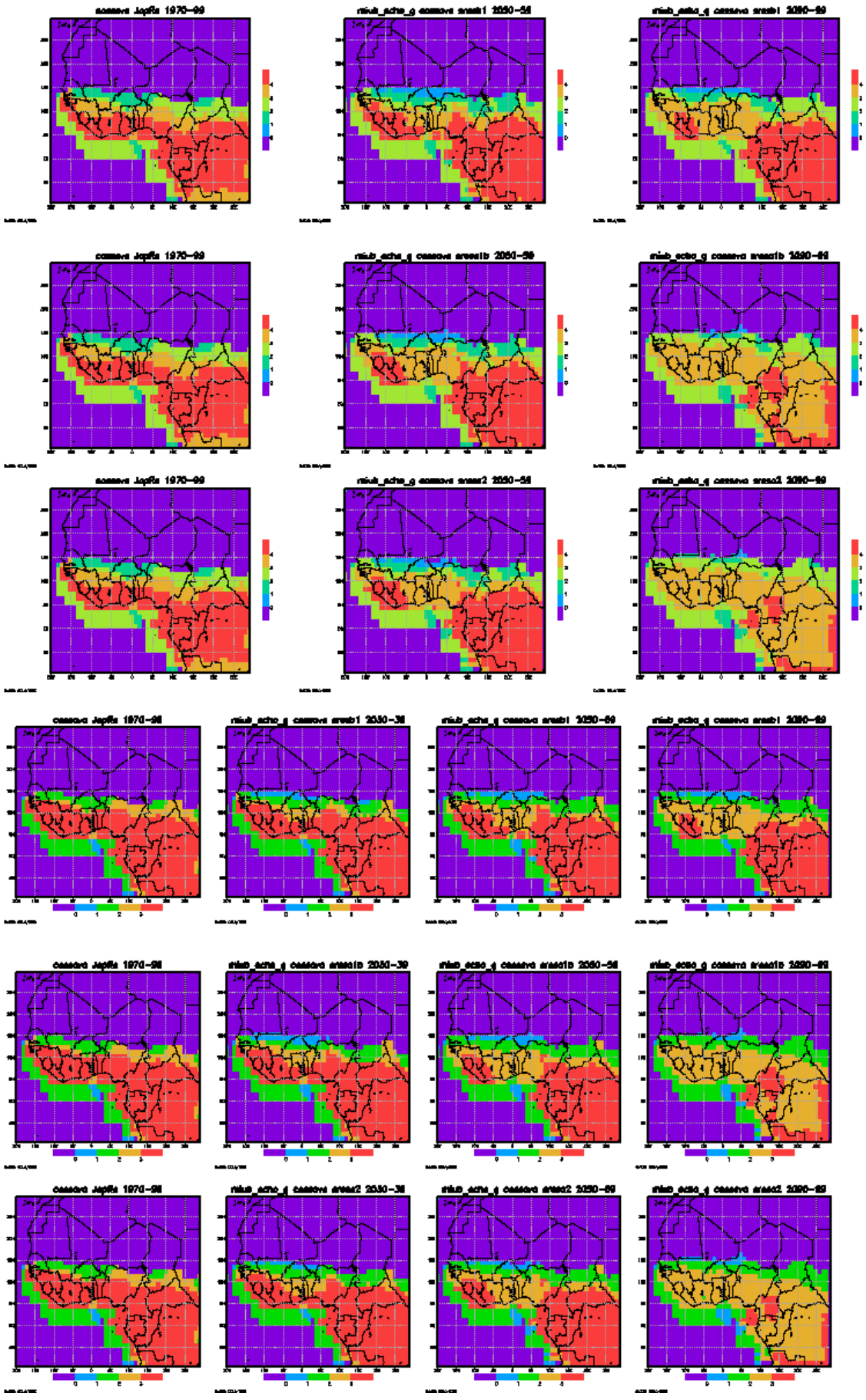

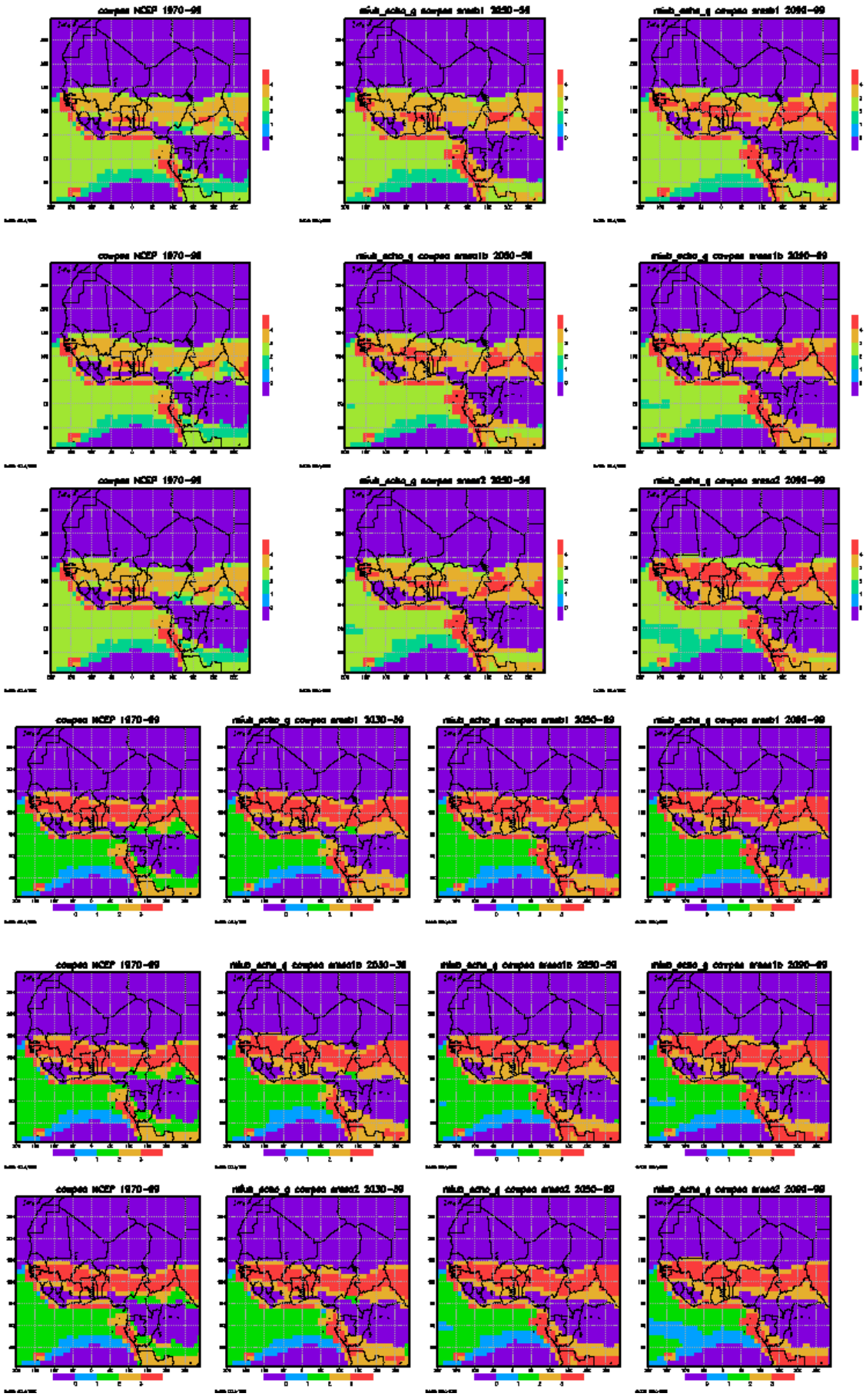

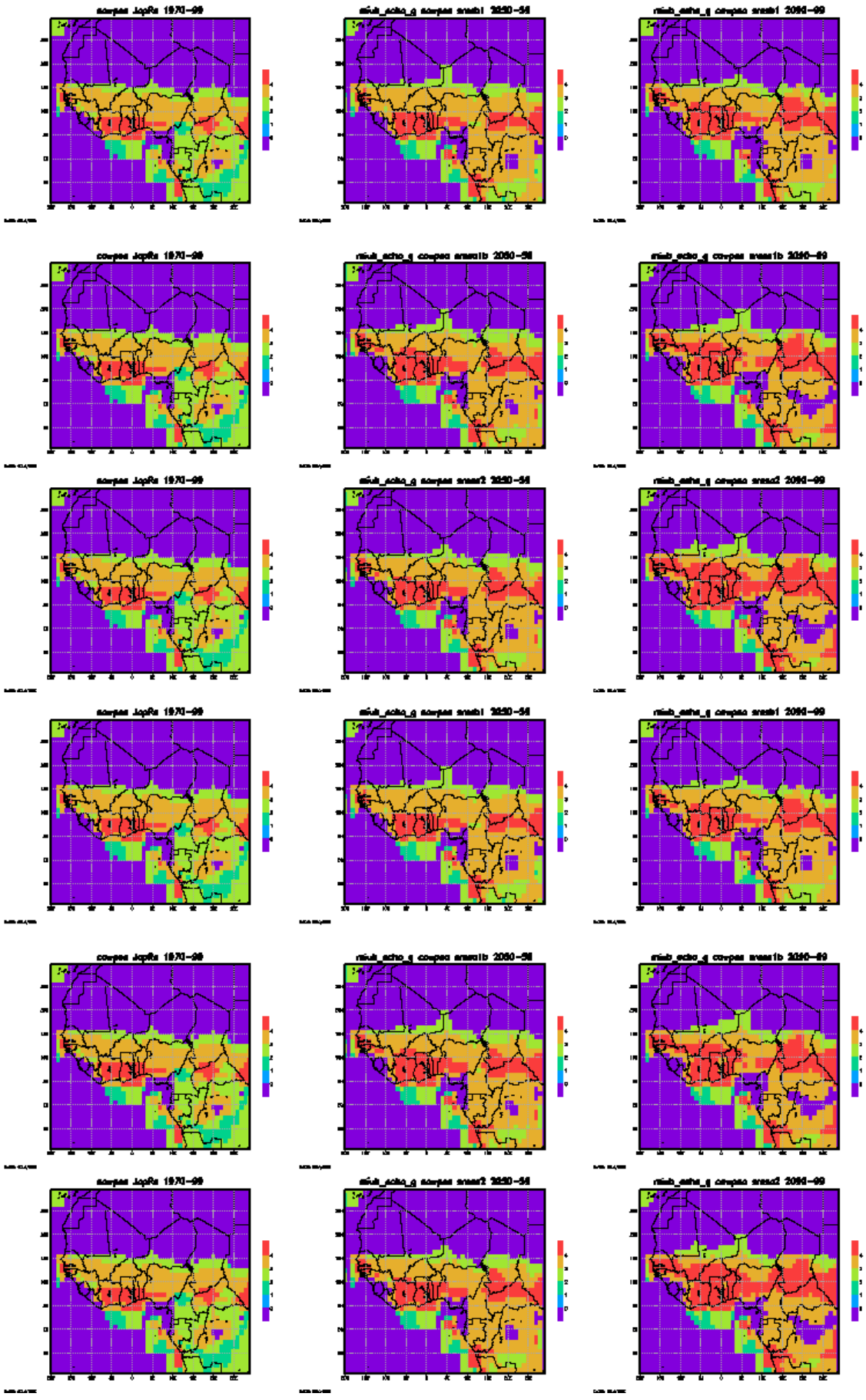

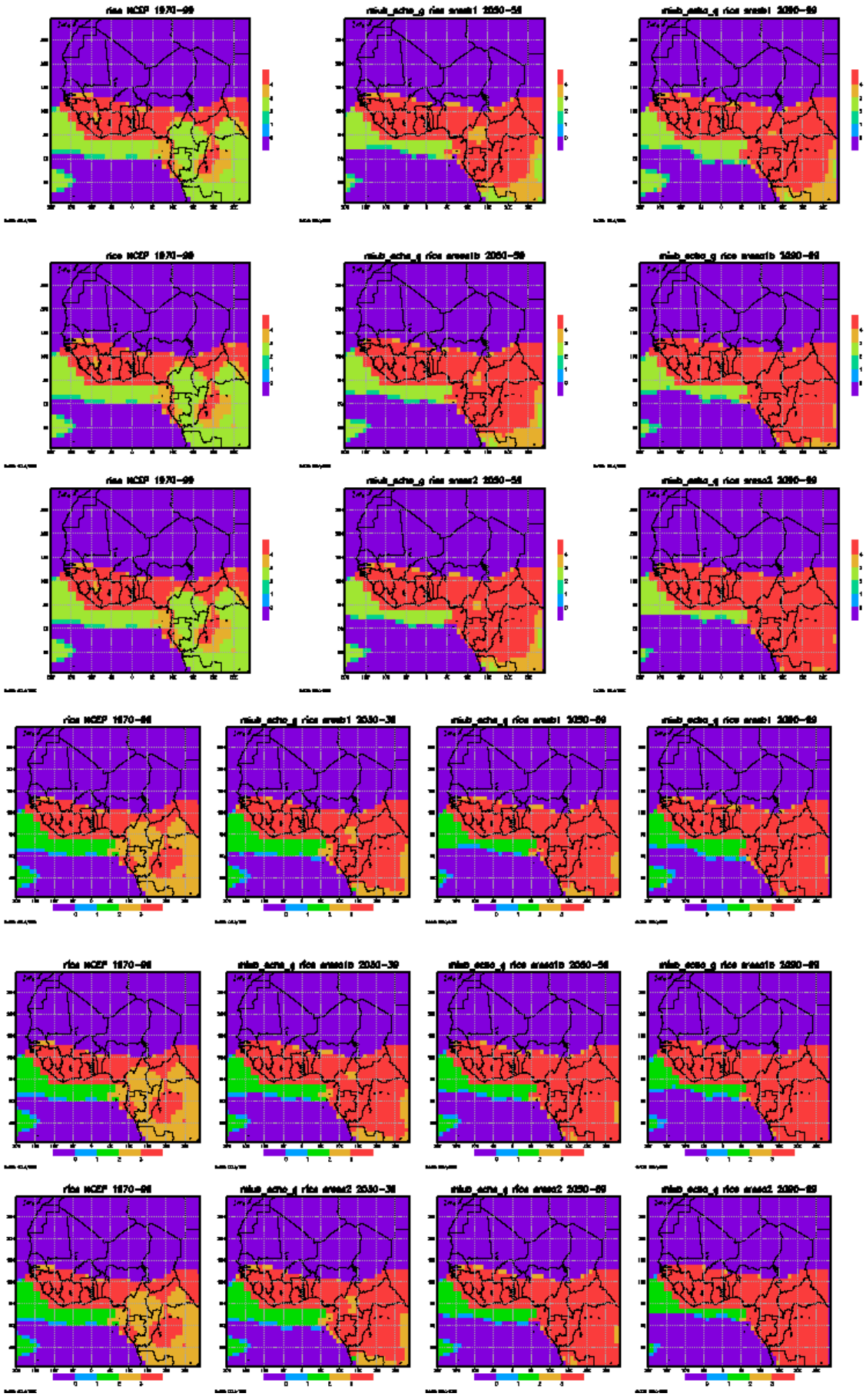

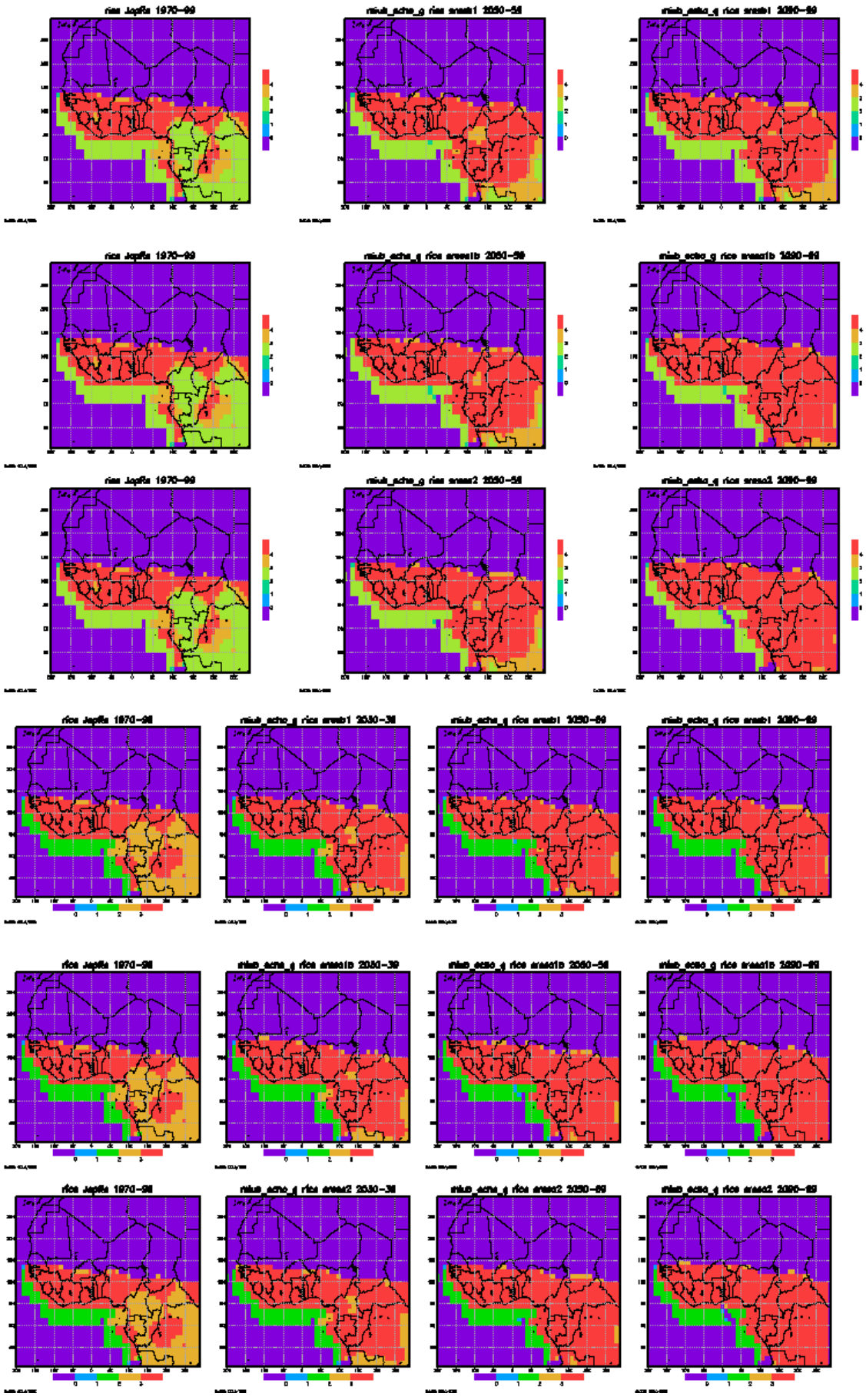

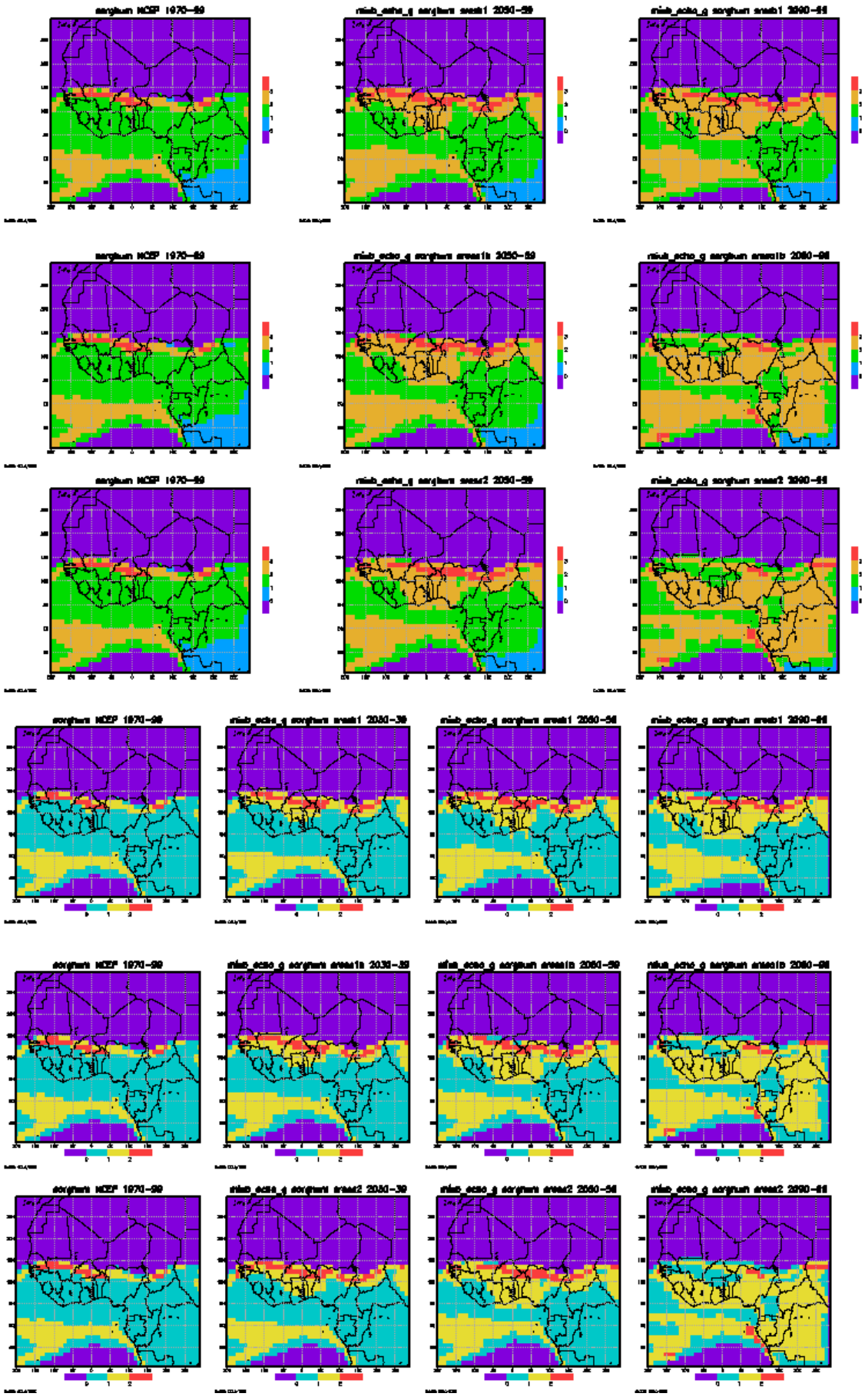

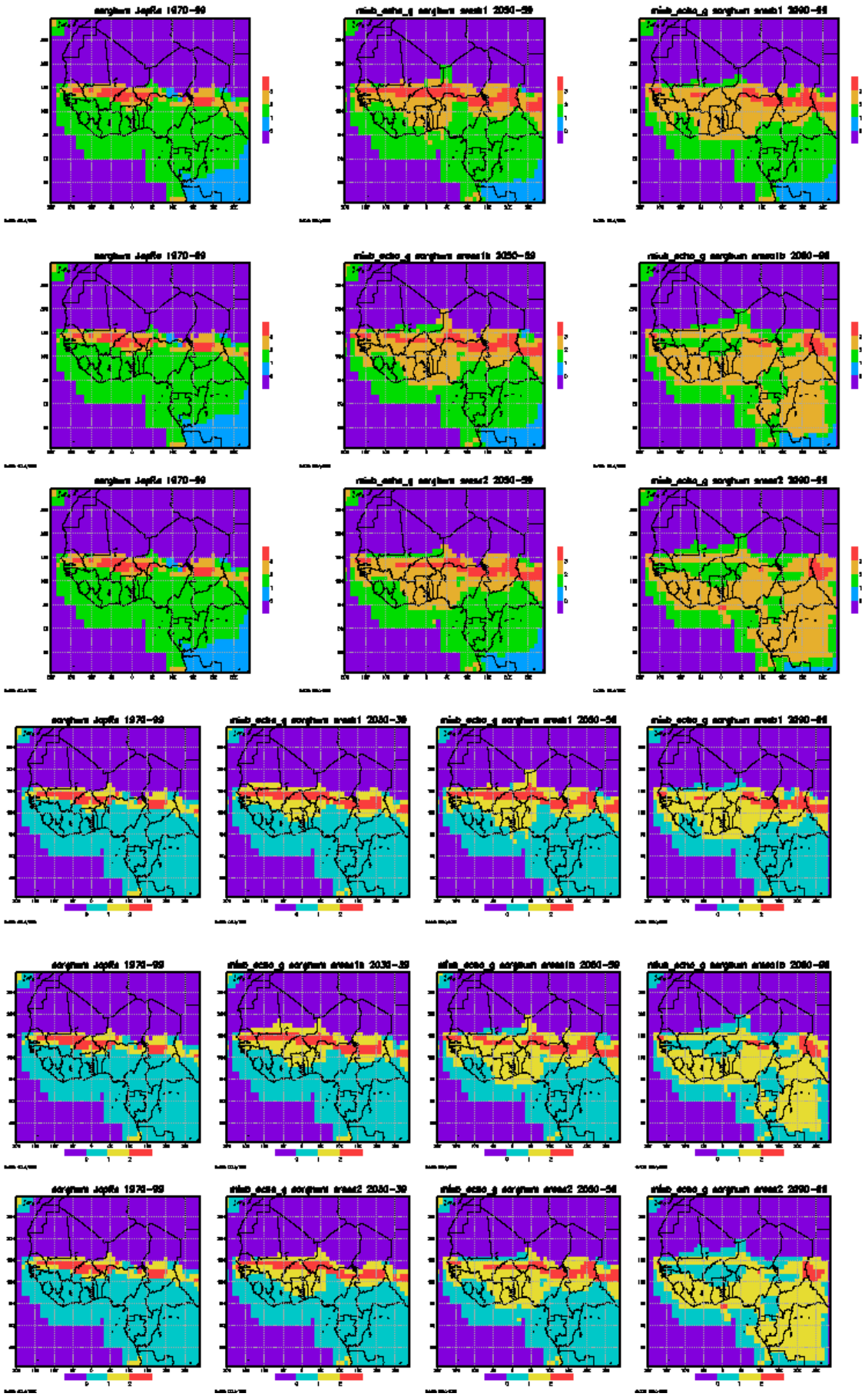

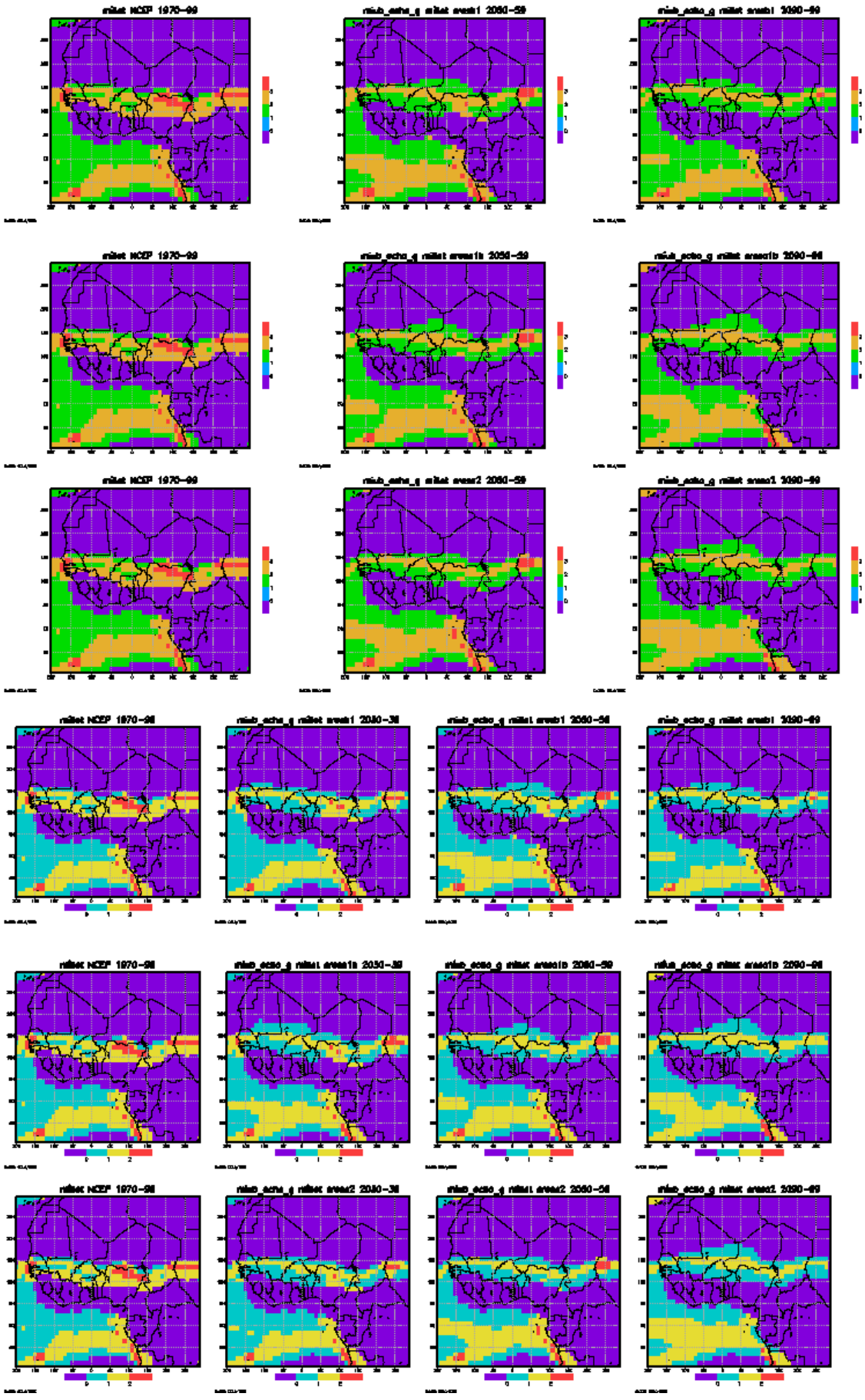

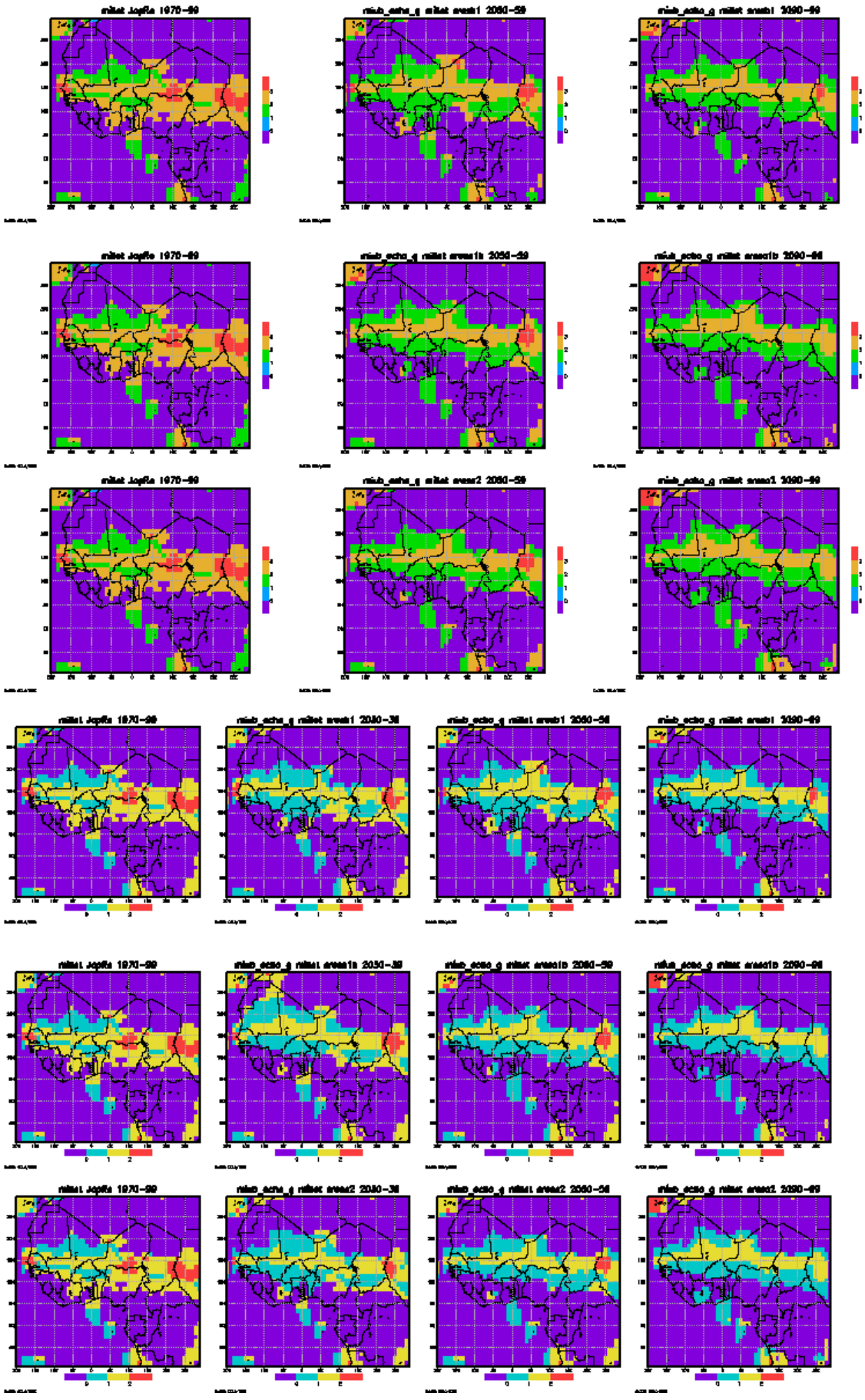

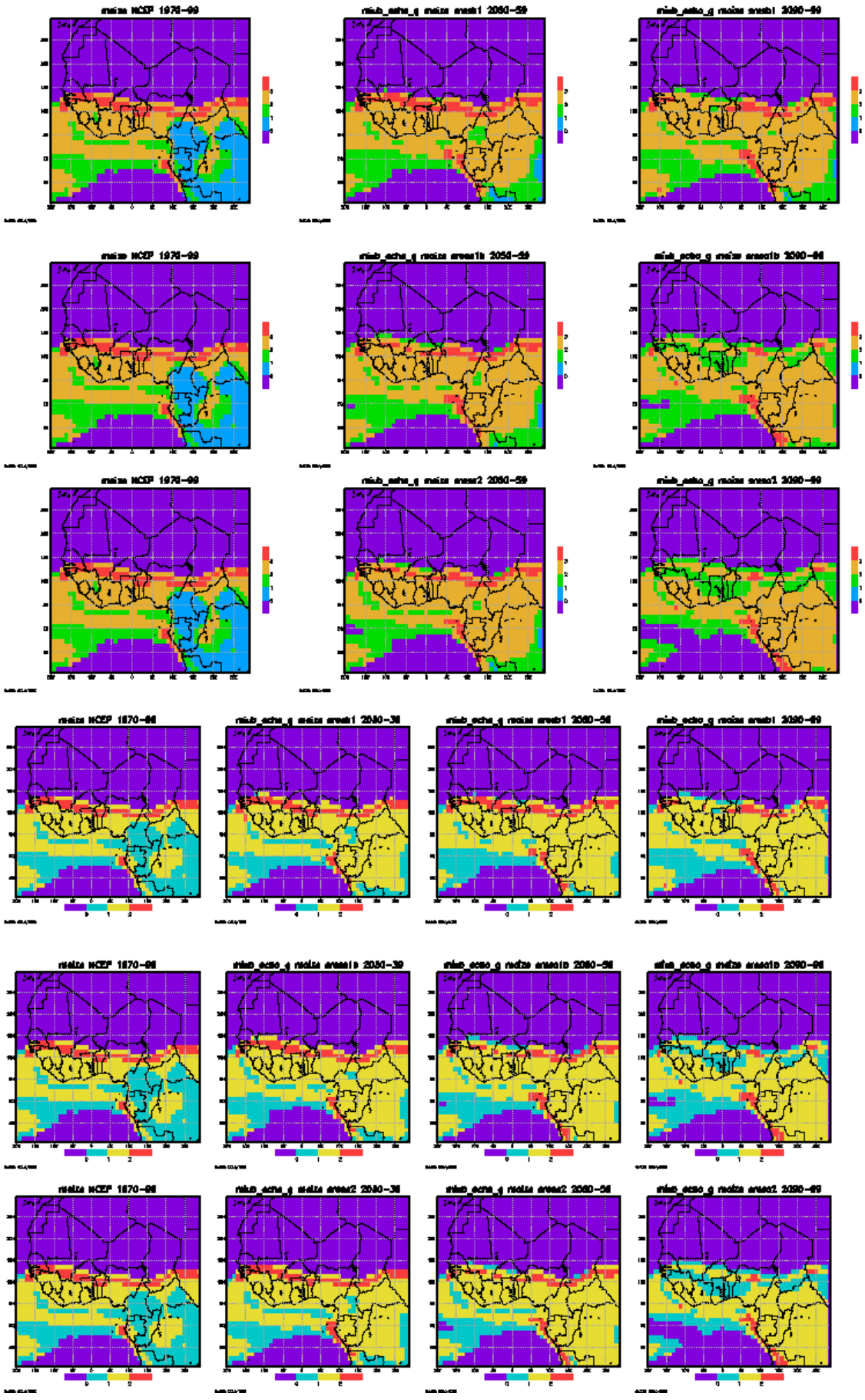

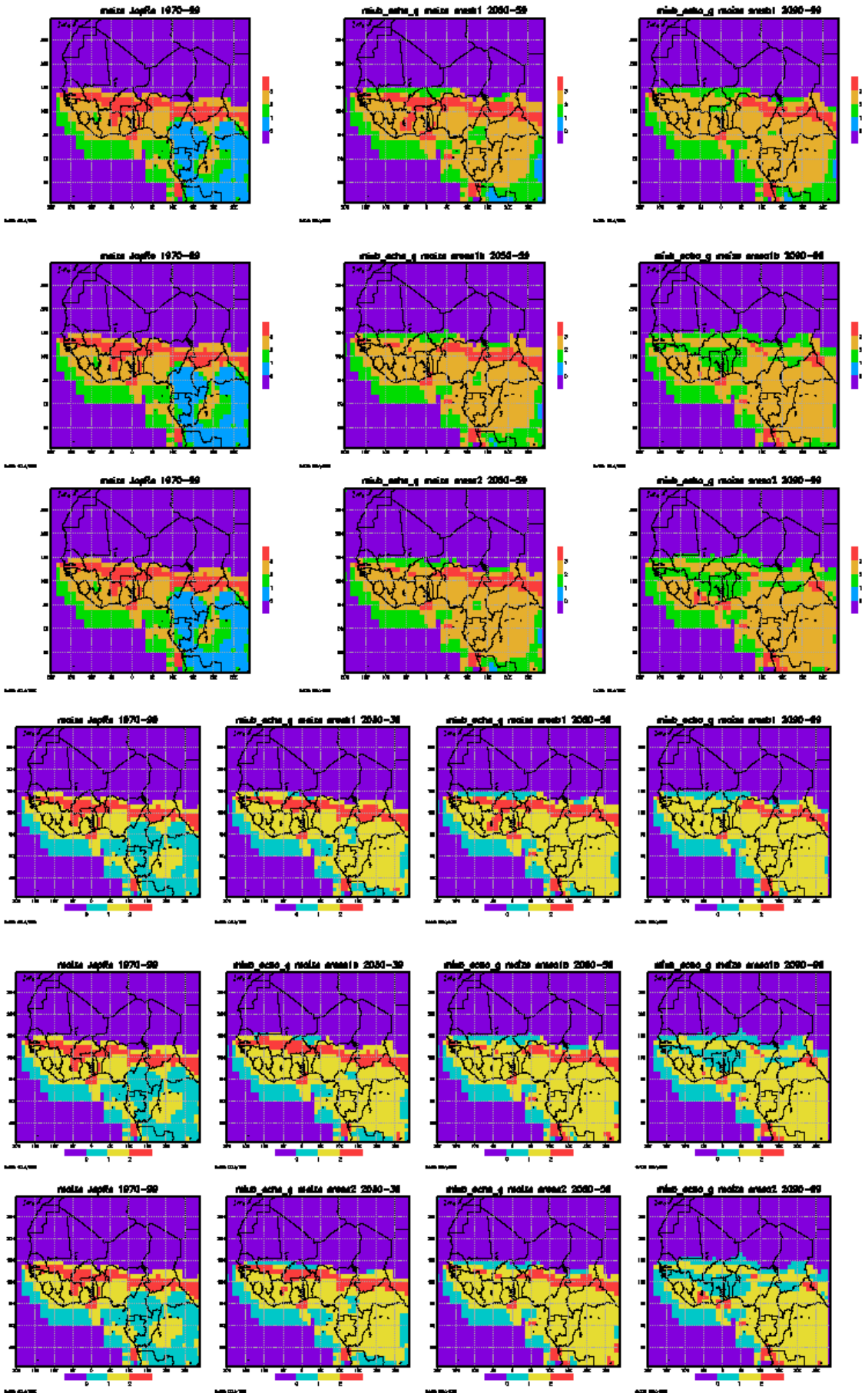

f. MPI

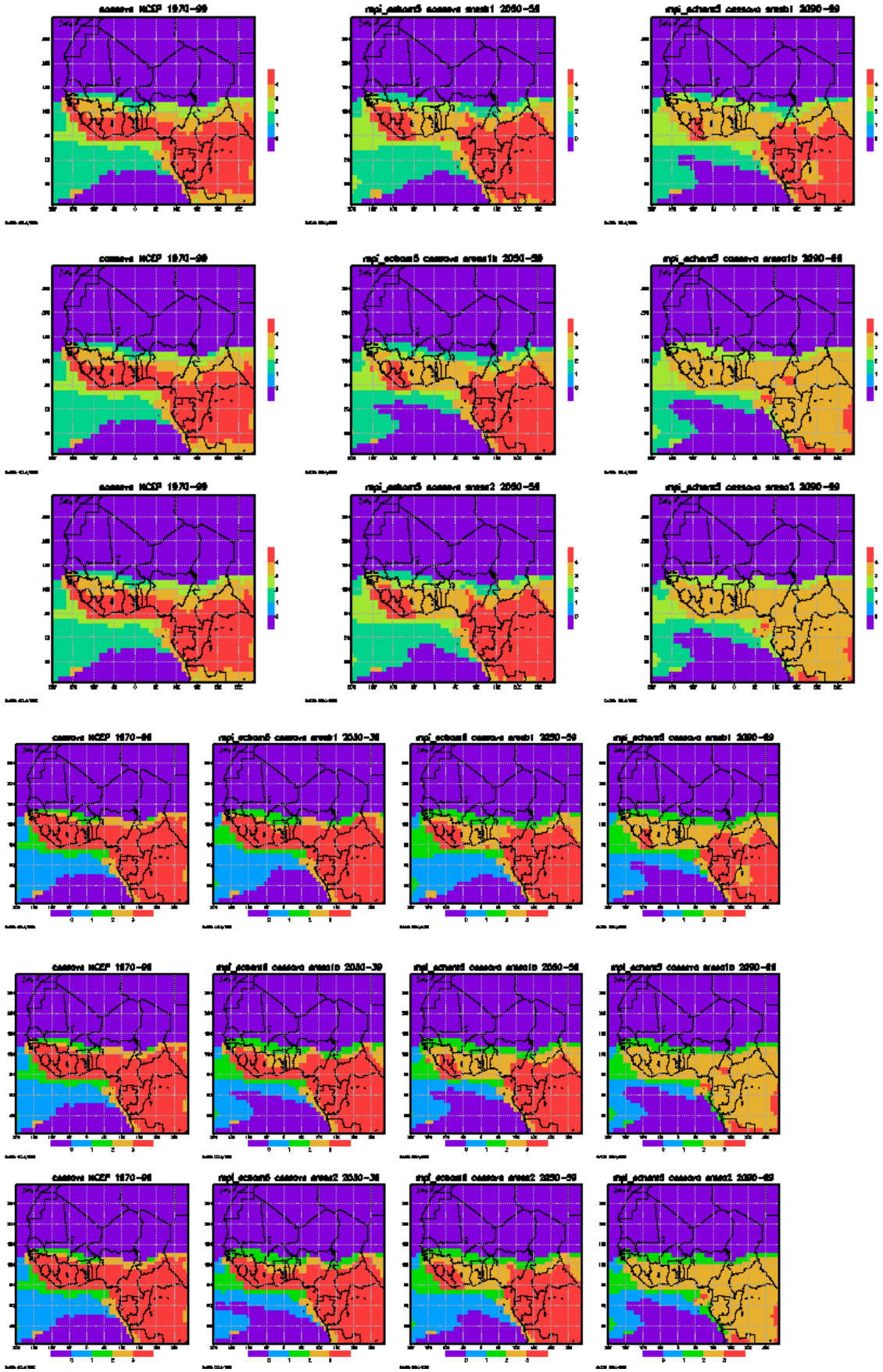

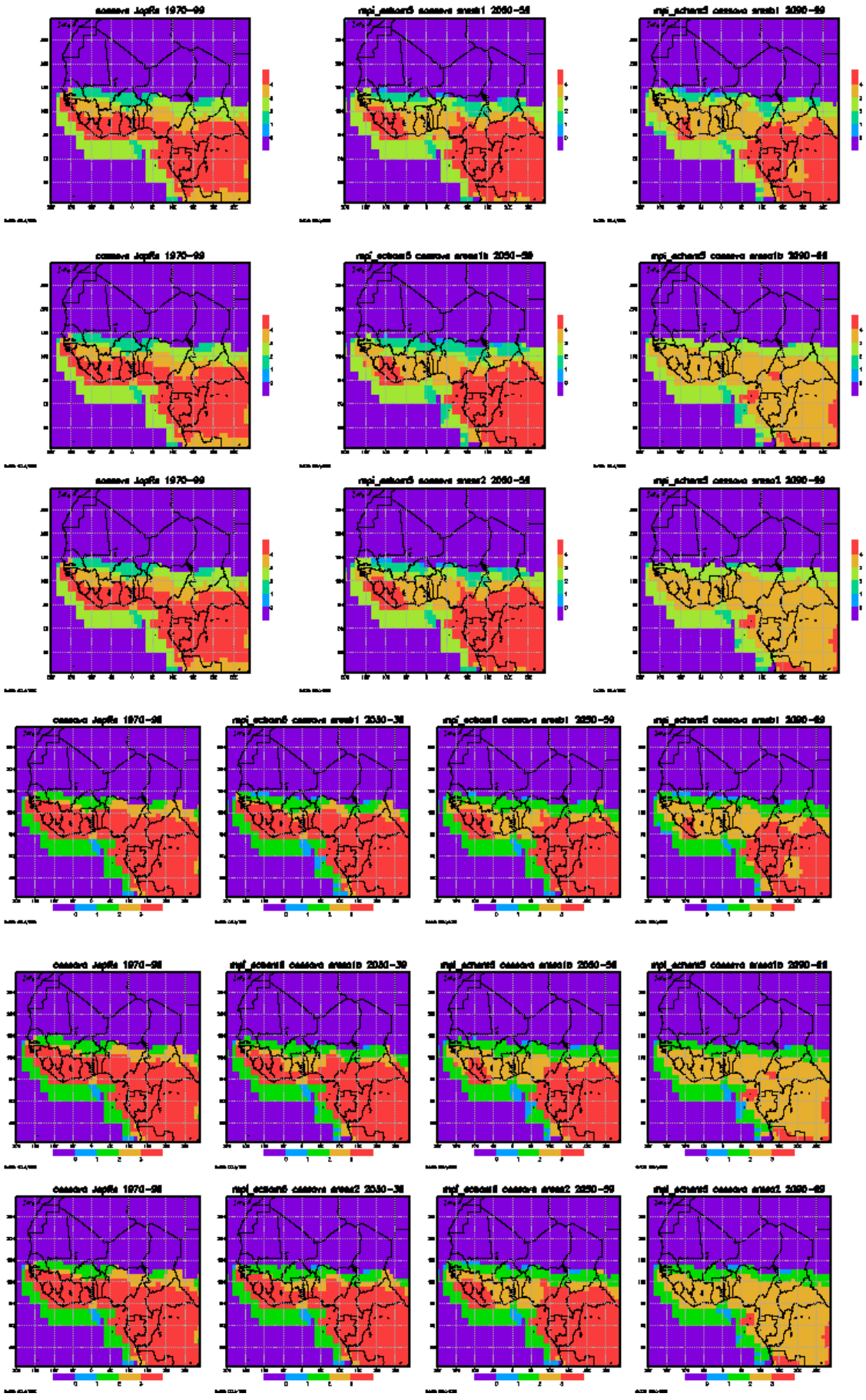

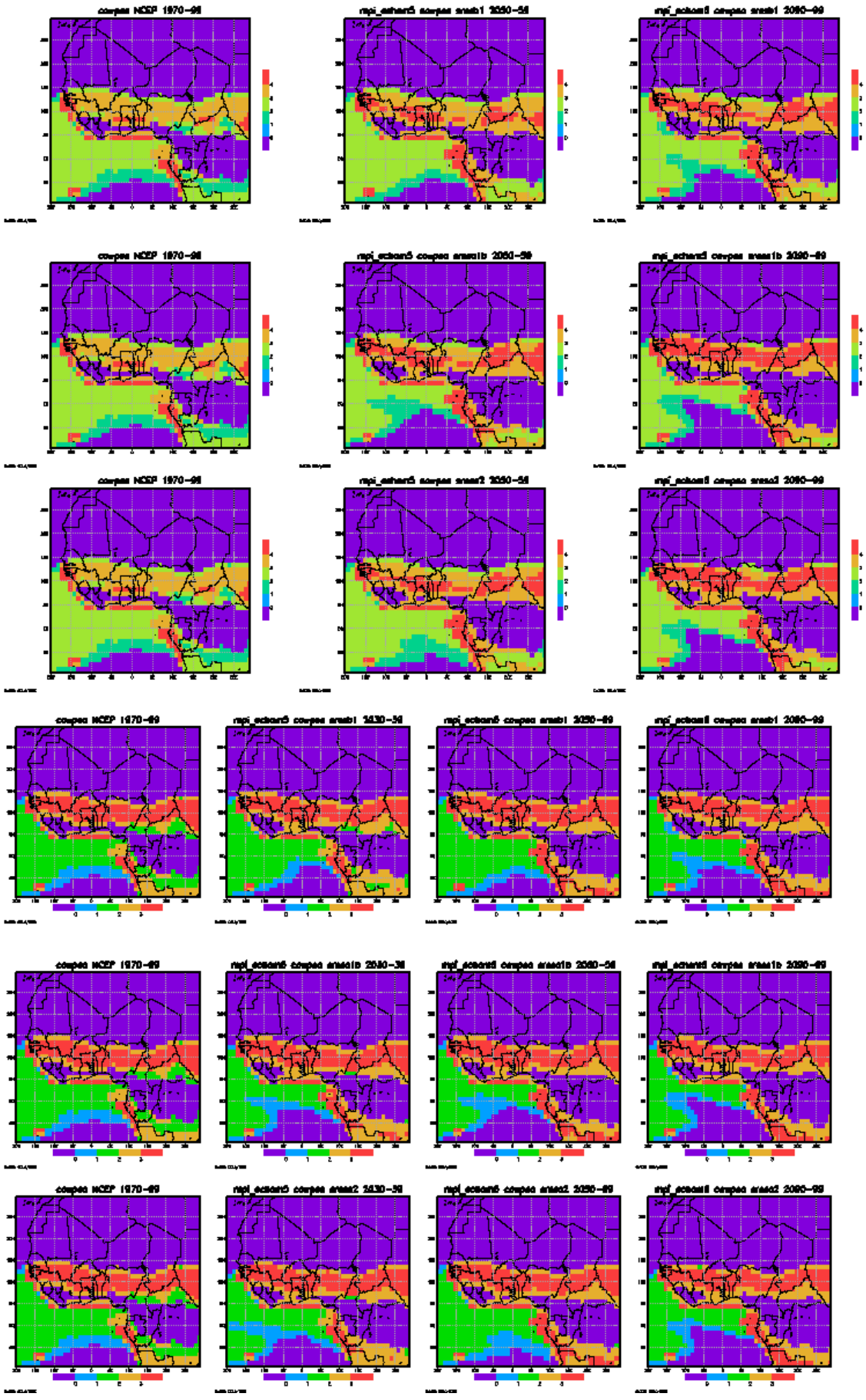

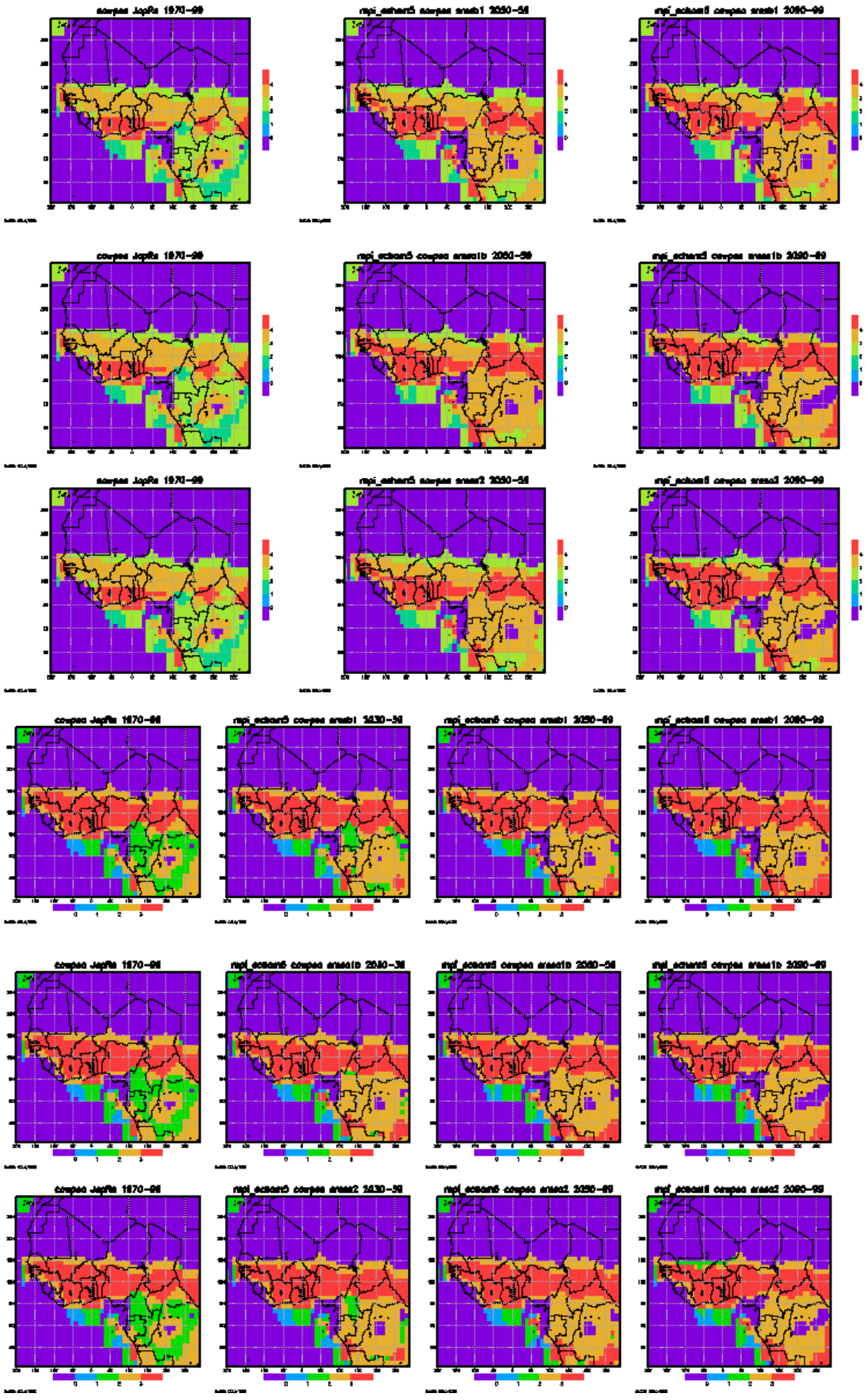

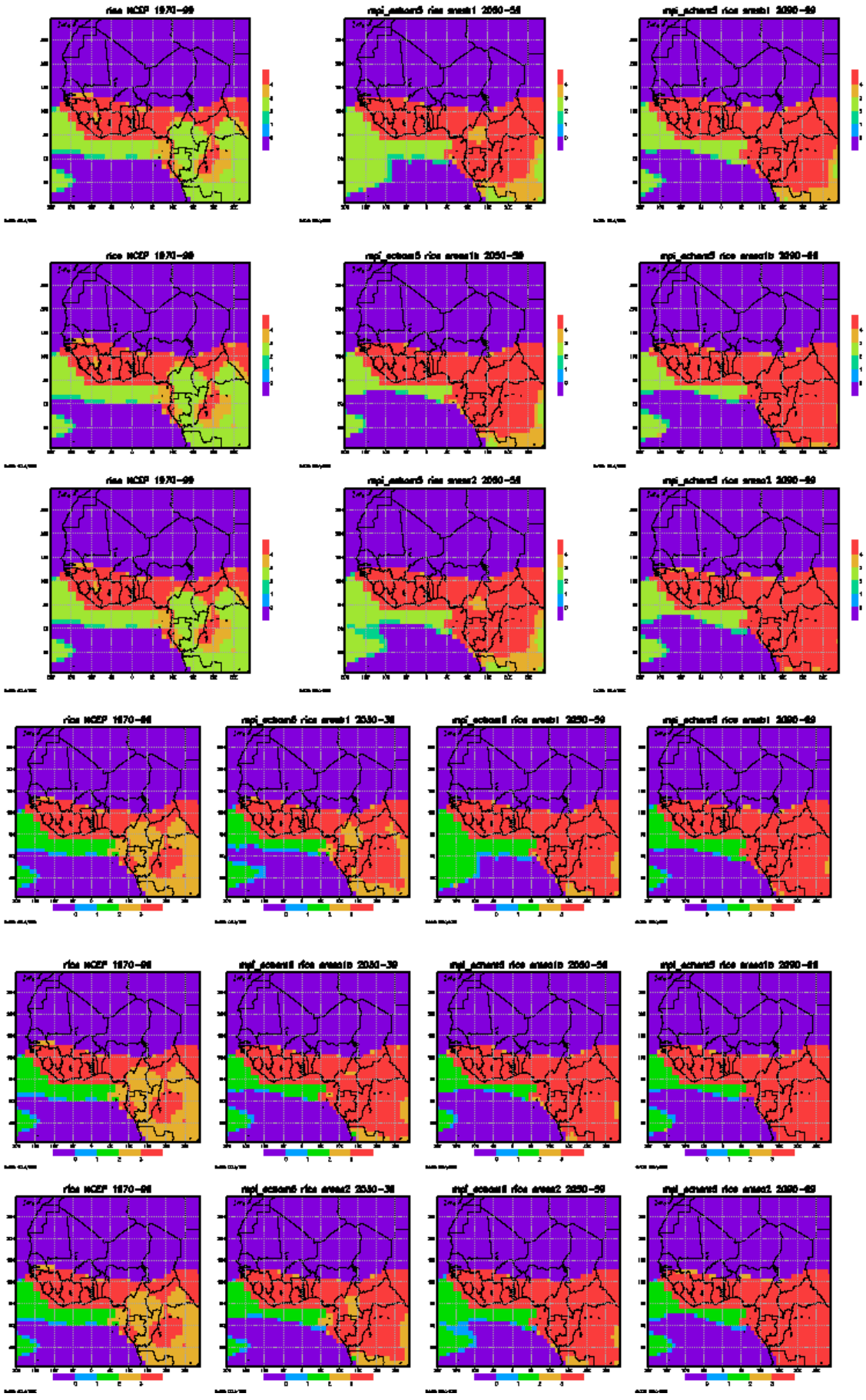
rice NCEP 1971–99
mpi_echam5 rice areal1 2050–58
mpi_echam5 rice areal1 2090–99
rice NCEP 1971–99
mpi_echam5 rice areal1b 2050–58
mpi_echam5 rice areal1b 2090–99
rice NCEP 1971–99
mpi_echam5 rice areal2 2050–58
mpi_echam5 rice areal2 2090–99
rice NCEP 1970–99
mpi_echam5 rice areal1 2030–39
mpi_echam5 rice areal1 2050–59
mpi_echam5 rice areal1 2090–99
rice NCEP 1970–99
mpi_echam5 rice areal1b 2030–39
mpi_echam5 rice areal1b 2050–59
mpi_echam5 rice areal1b 2090–99
rice NCEP 1970–99
mpi_echam5 rice areal2 2030–39
mpi_echam5 rice areal2 2050–59
mpi_echam5 rice areal2 2090–99

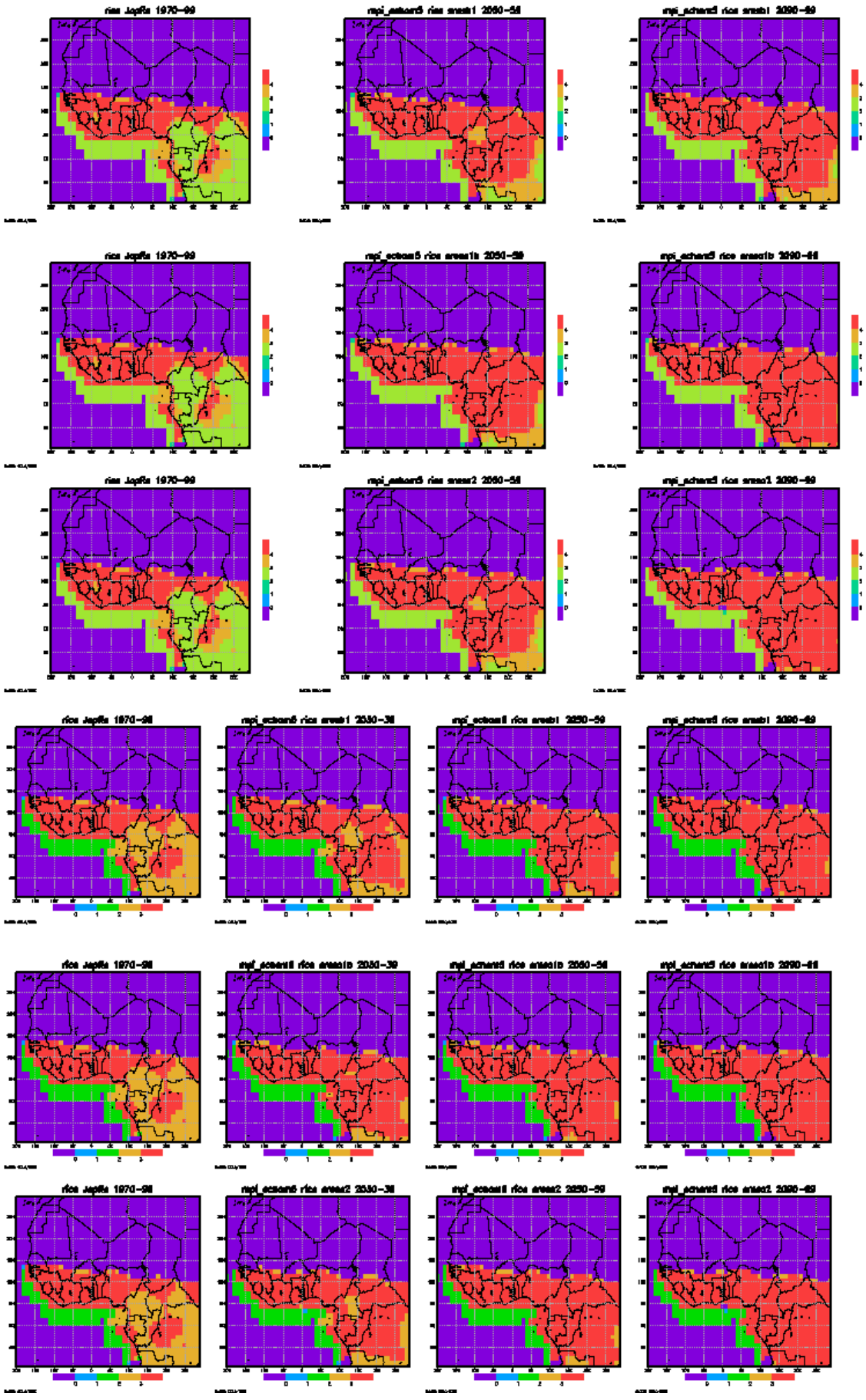

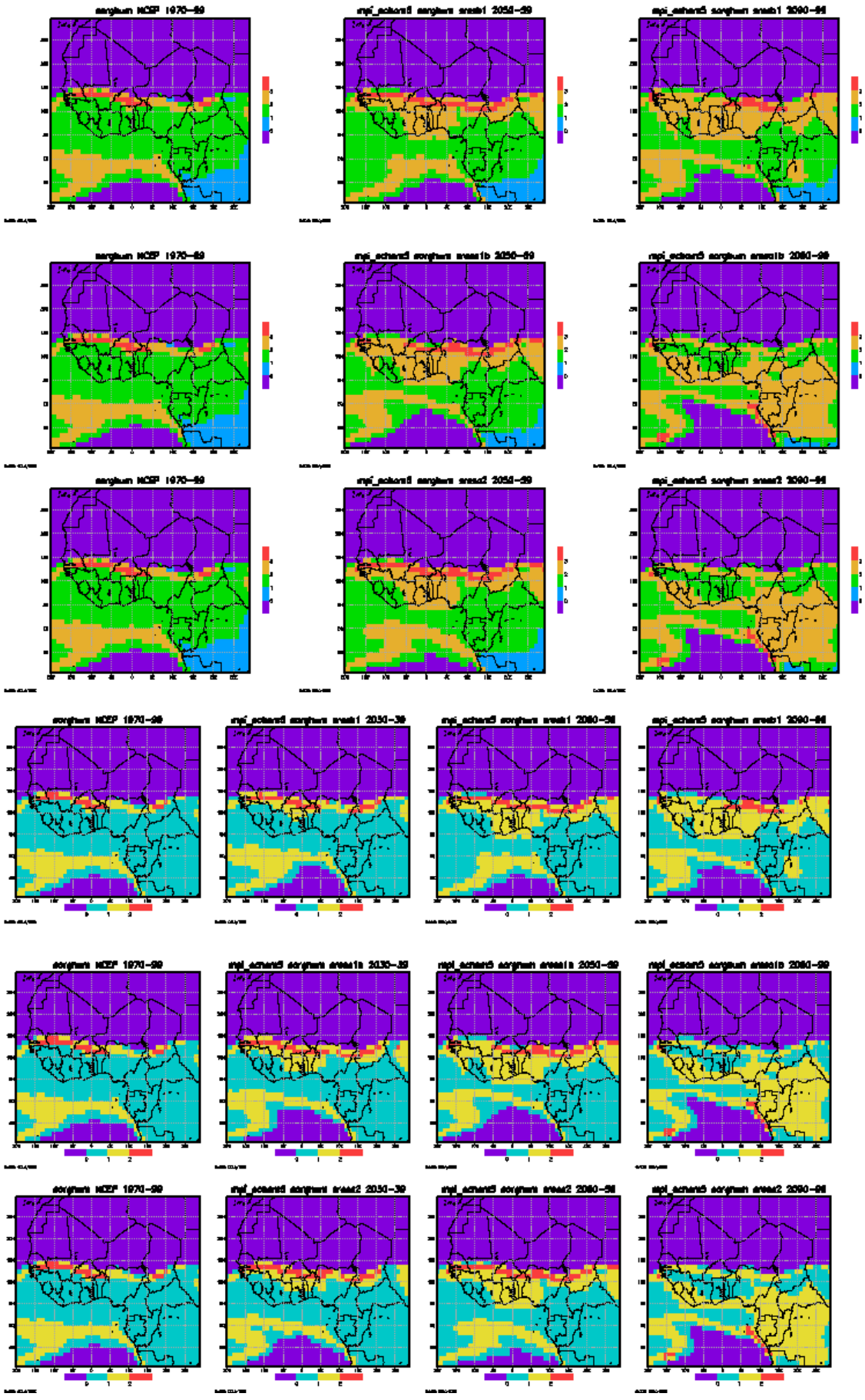

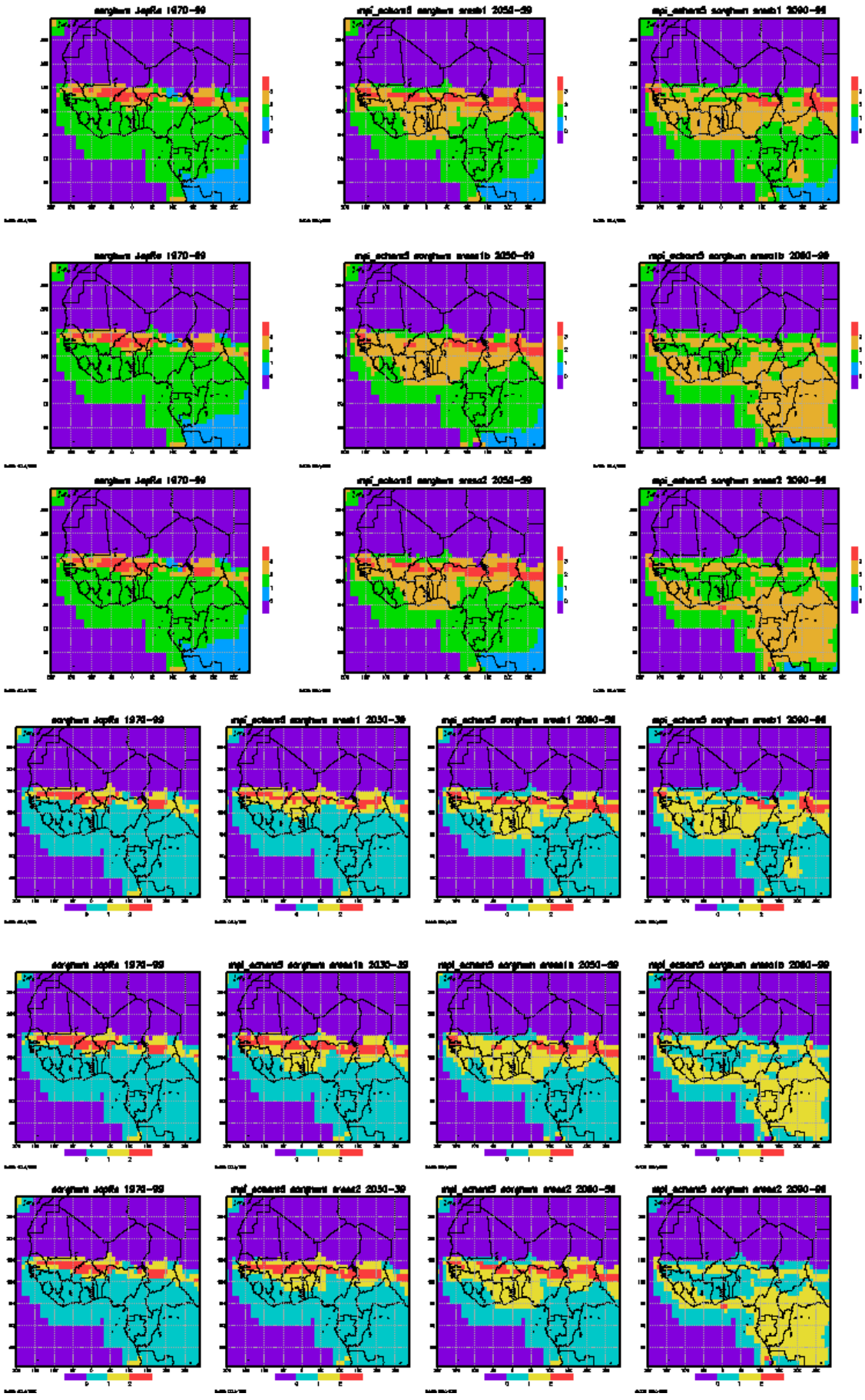

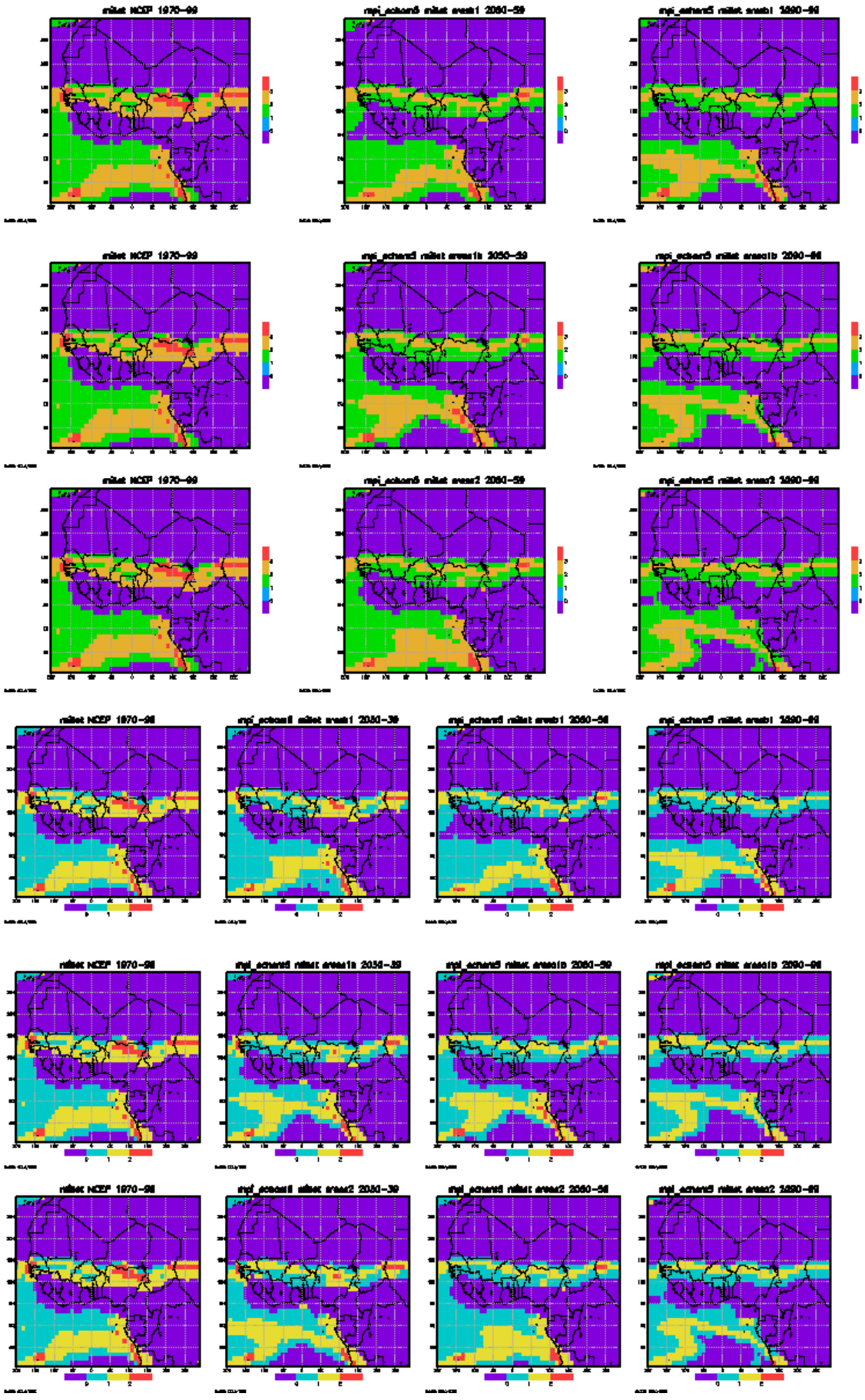

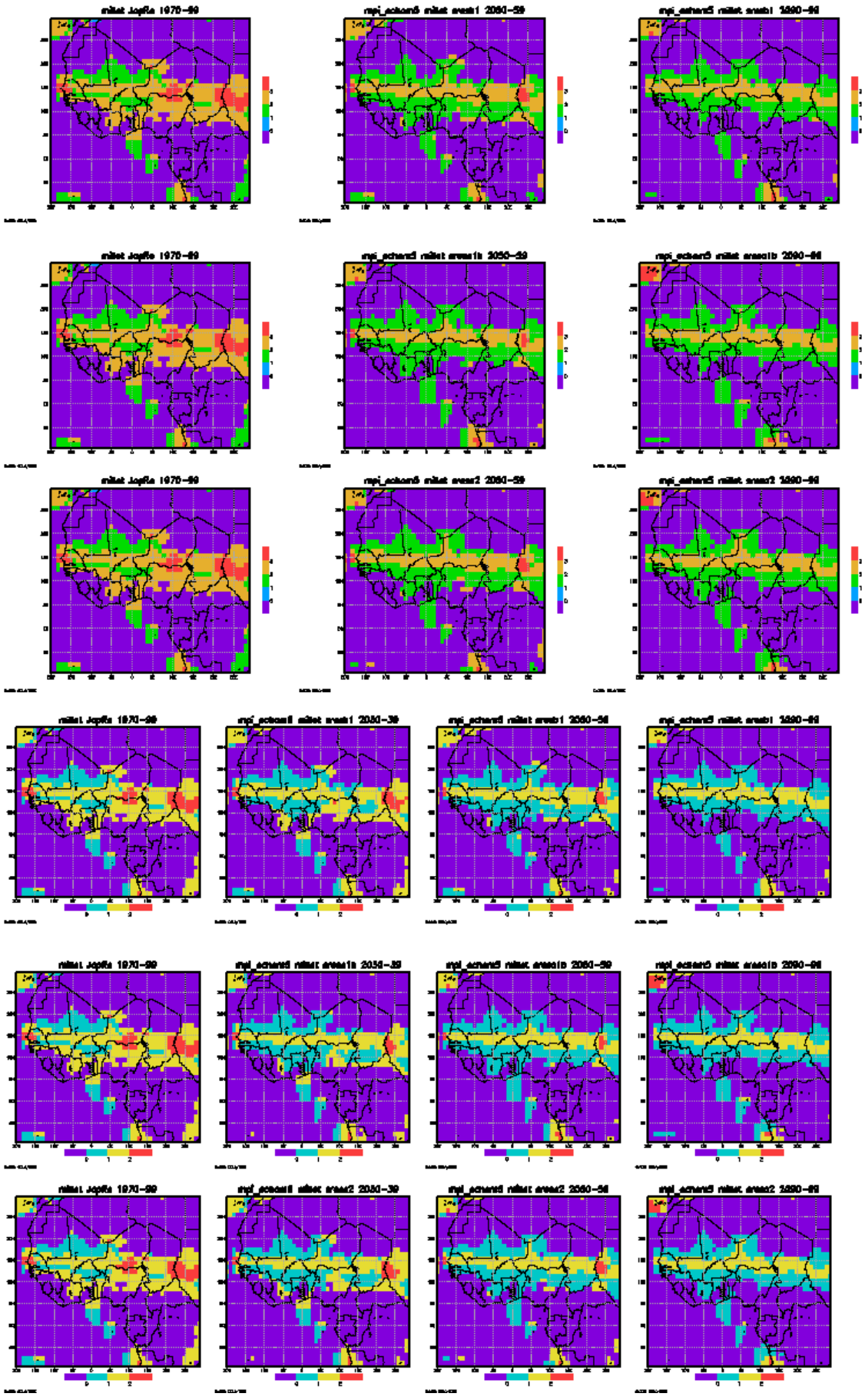

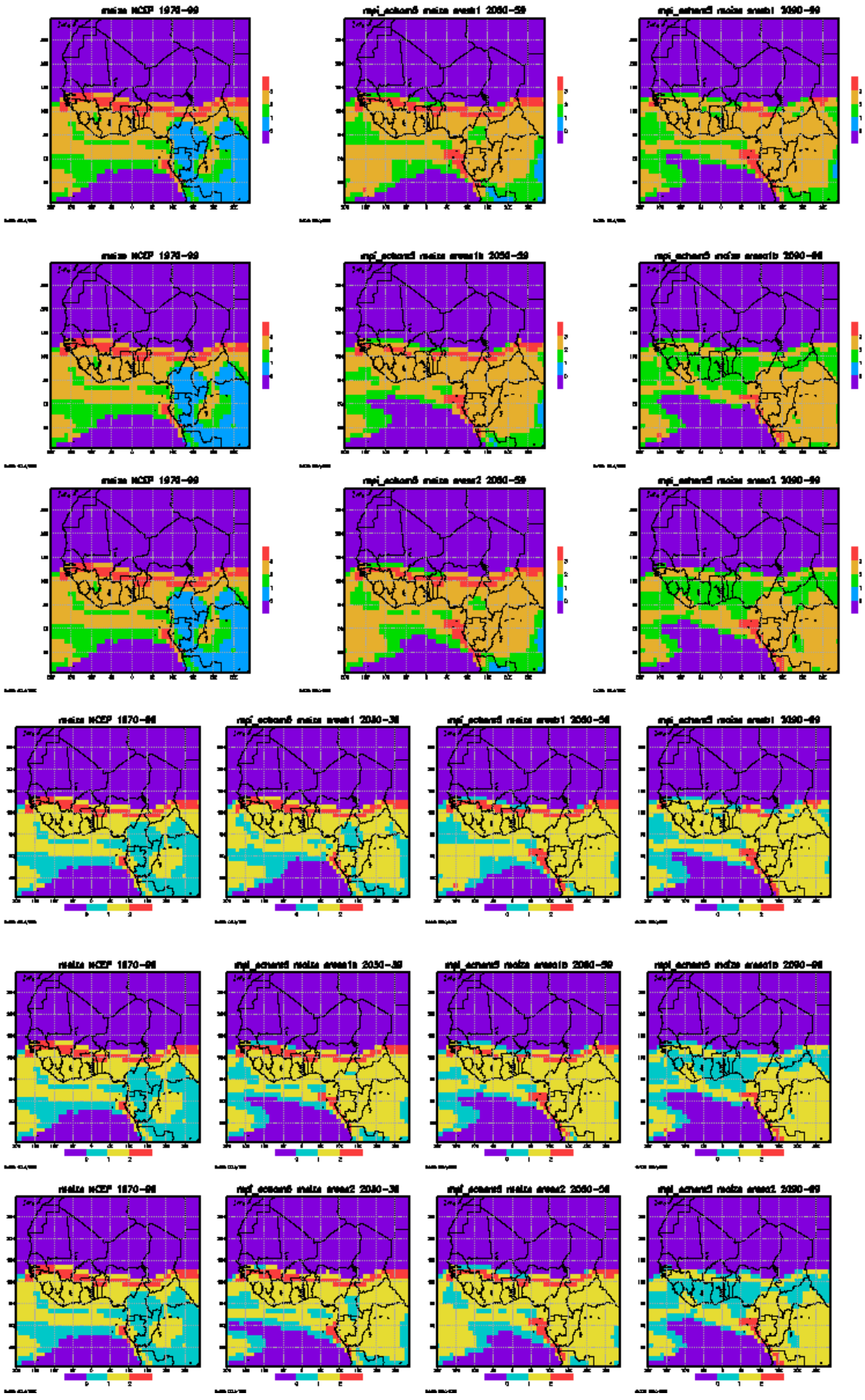

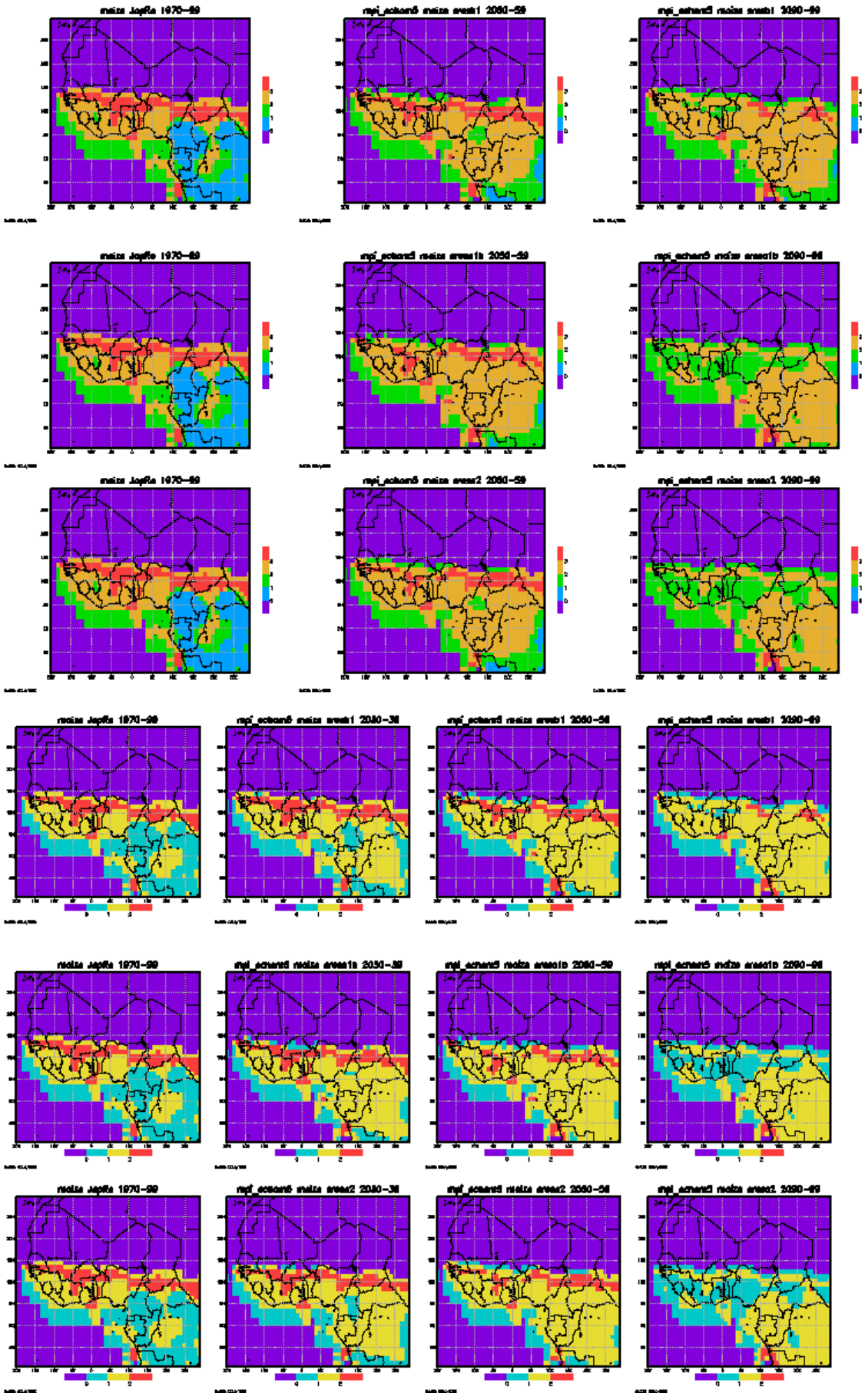

g. MRI

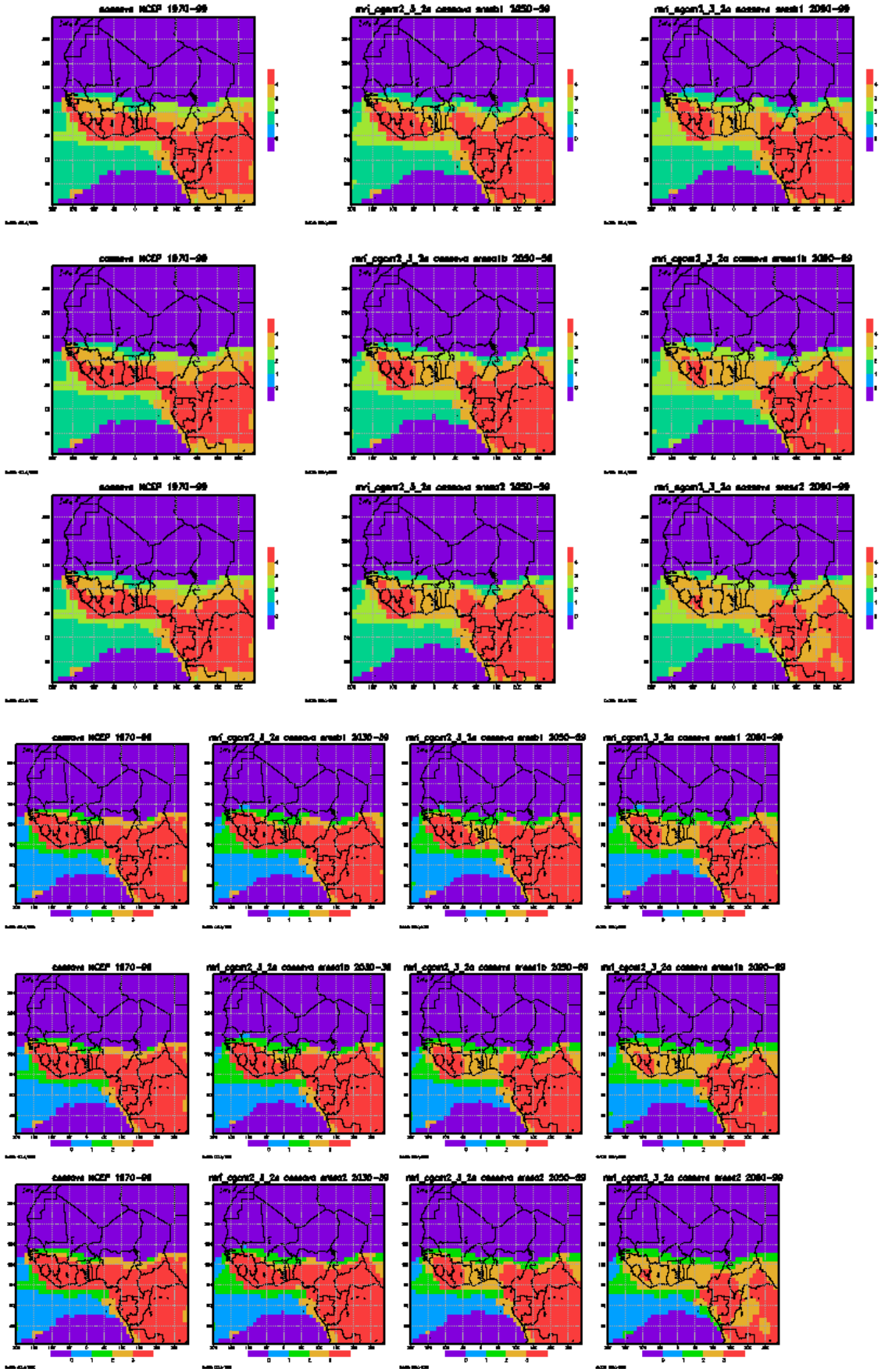

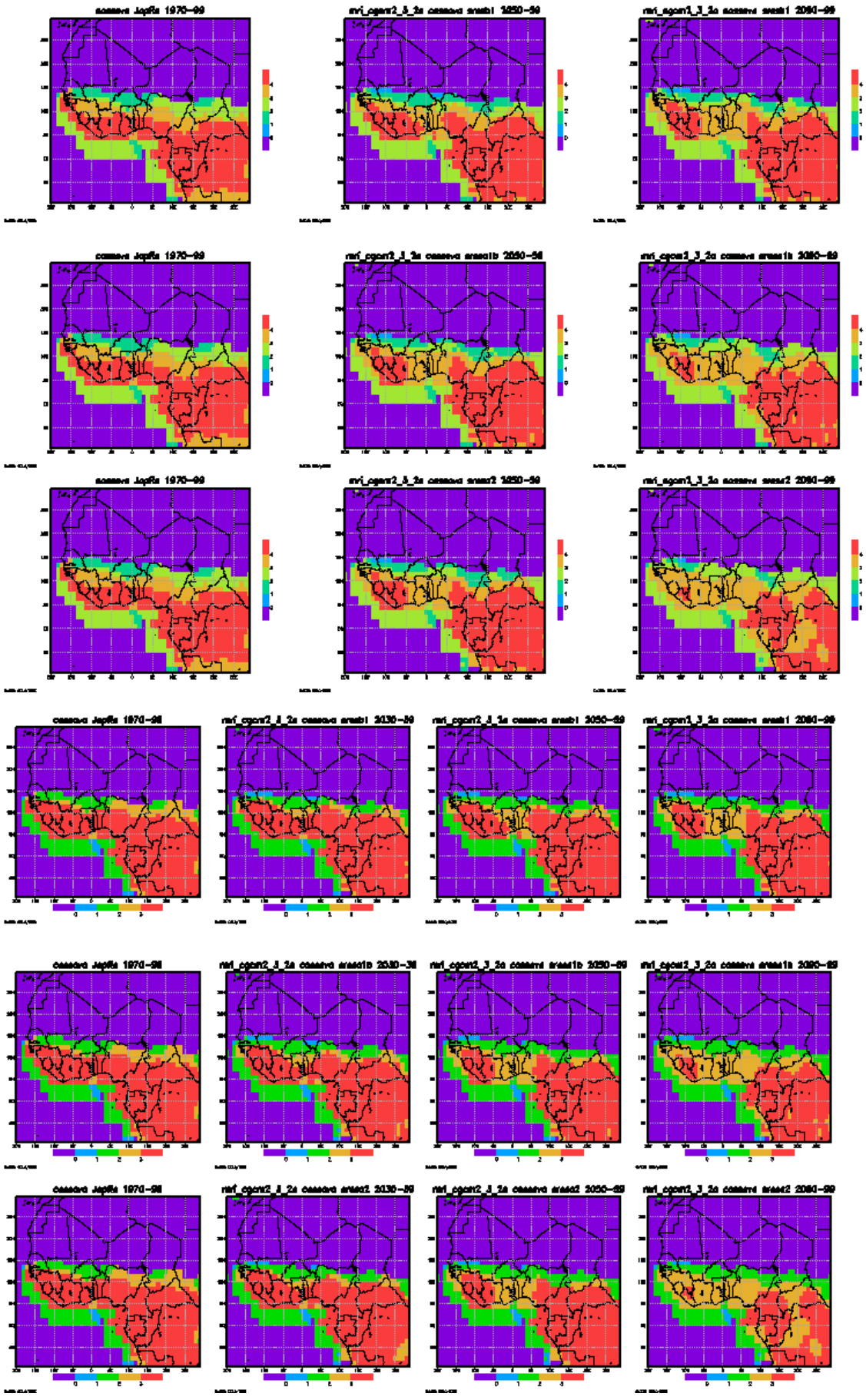

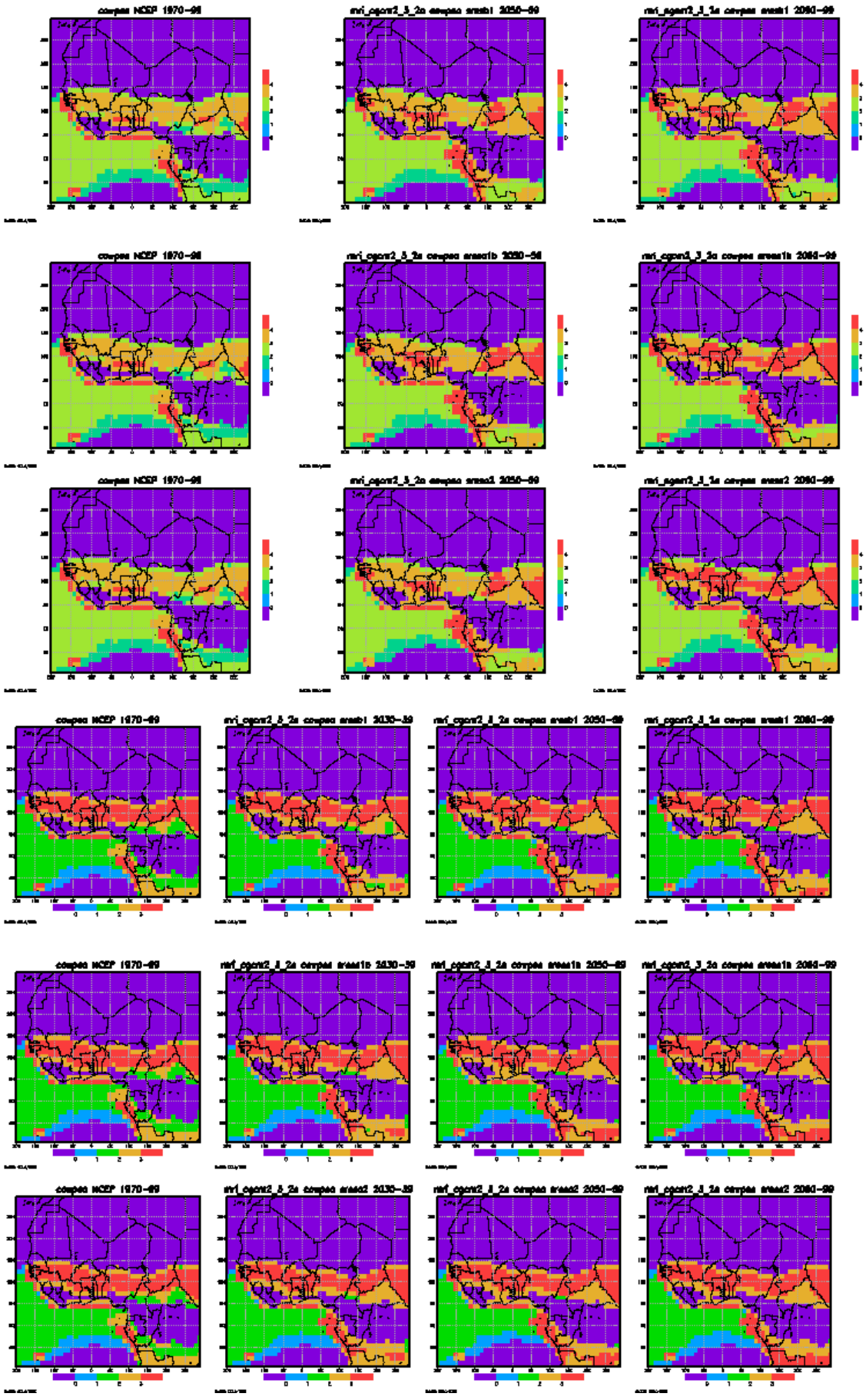

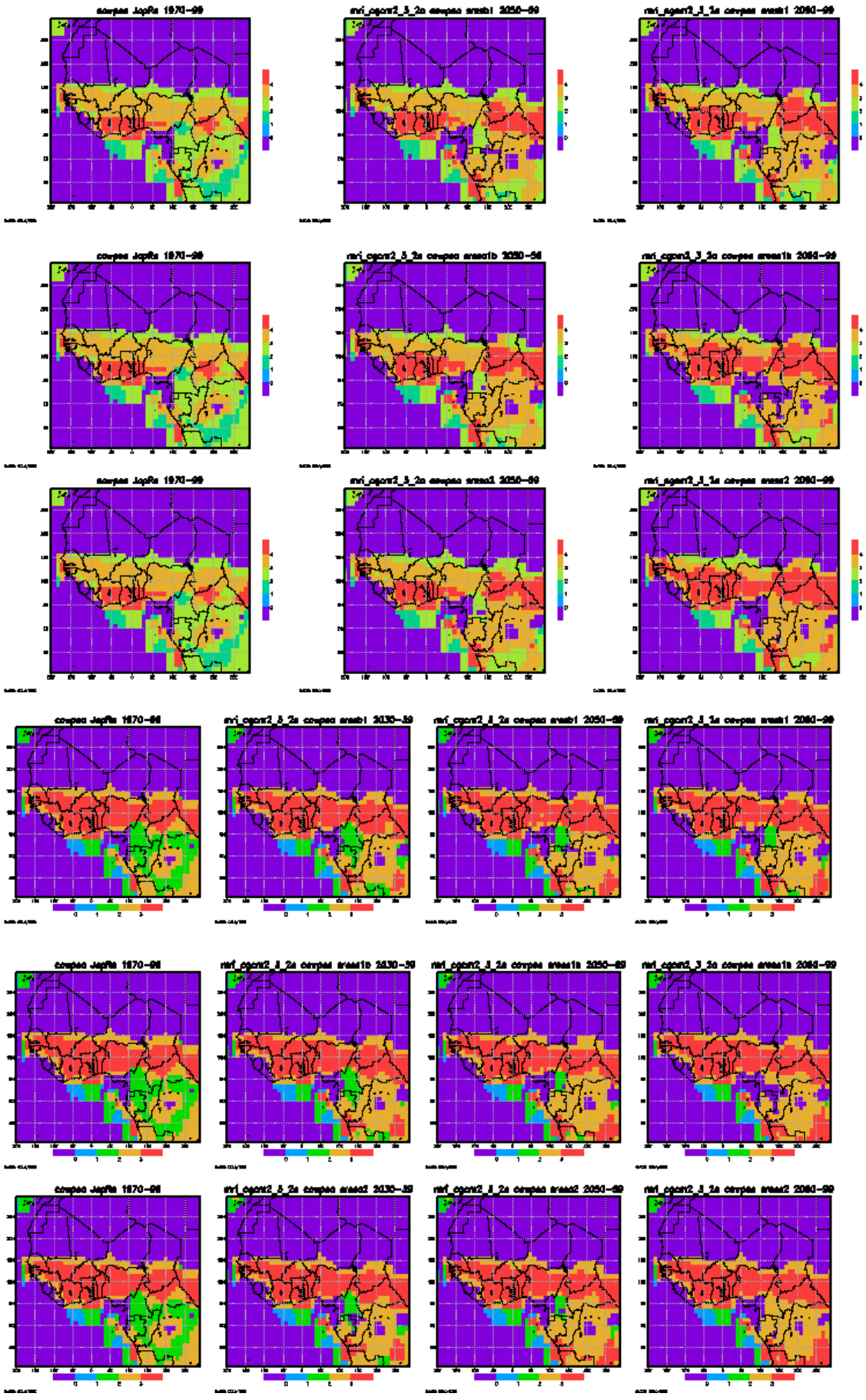

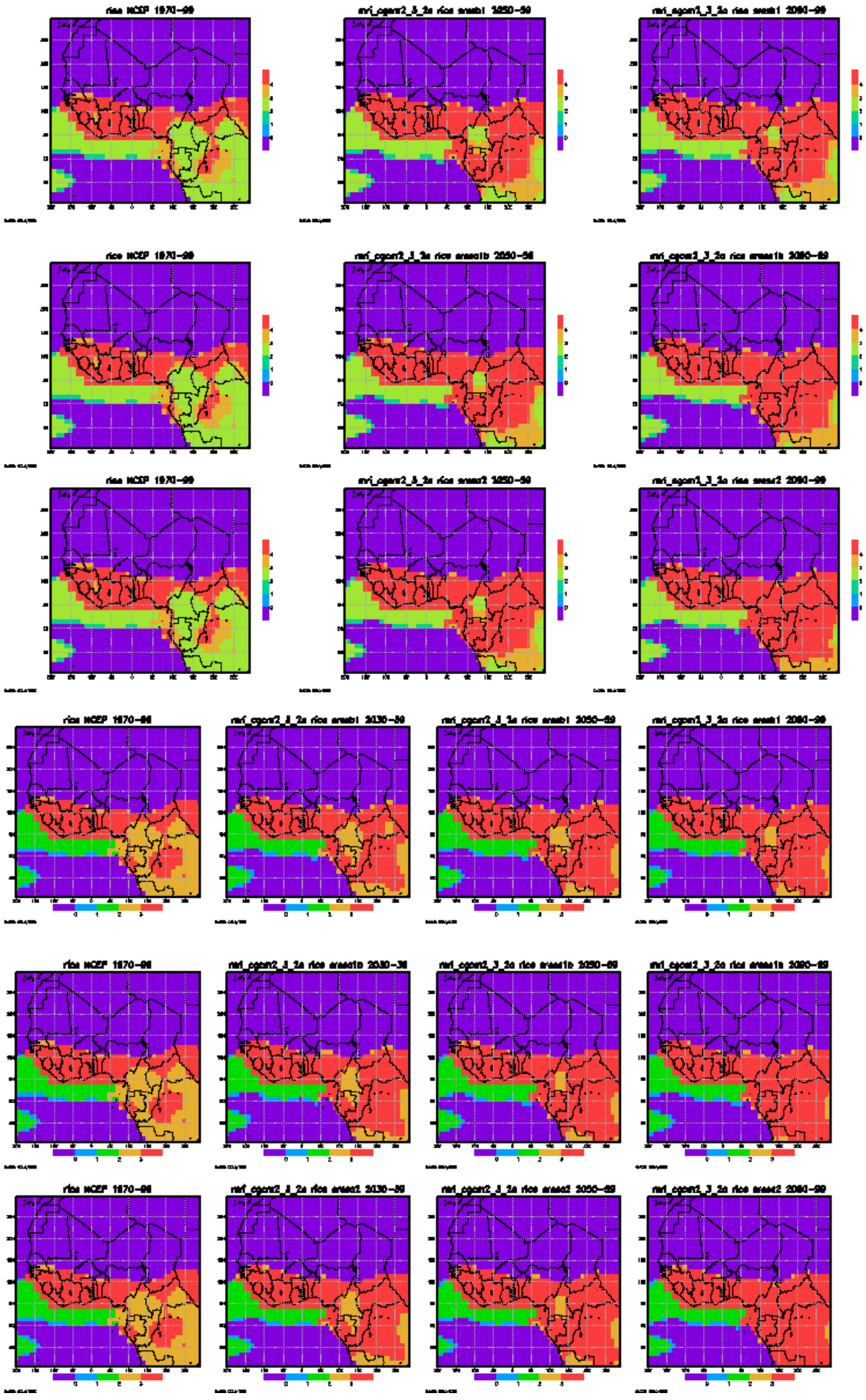

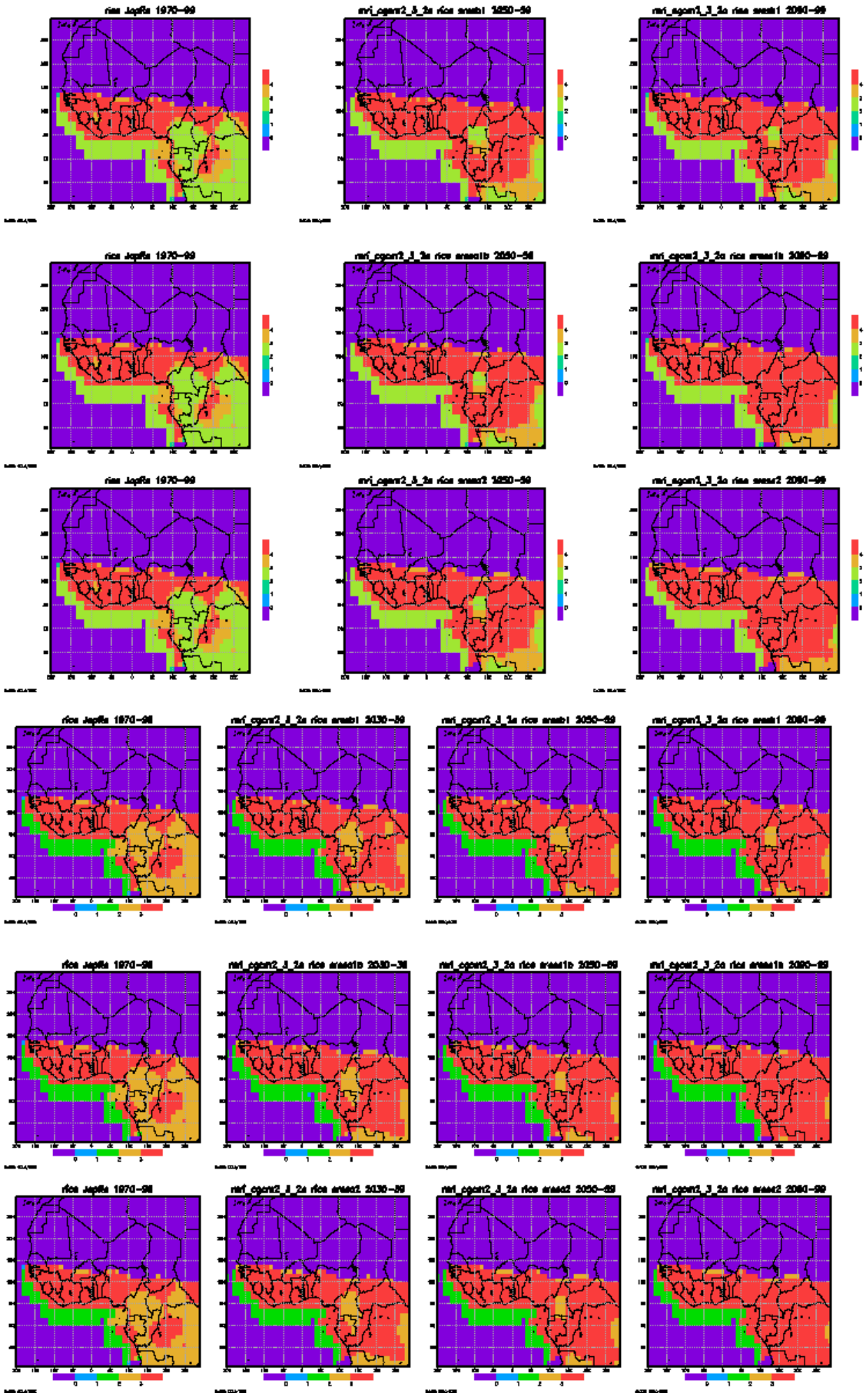

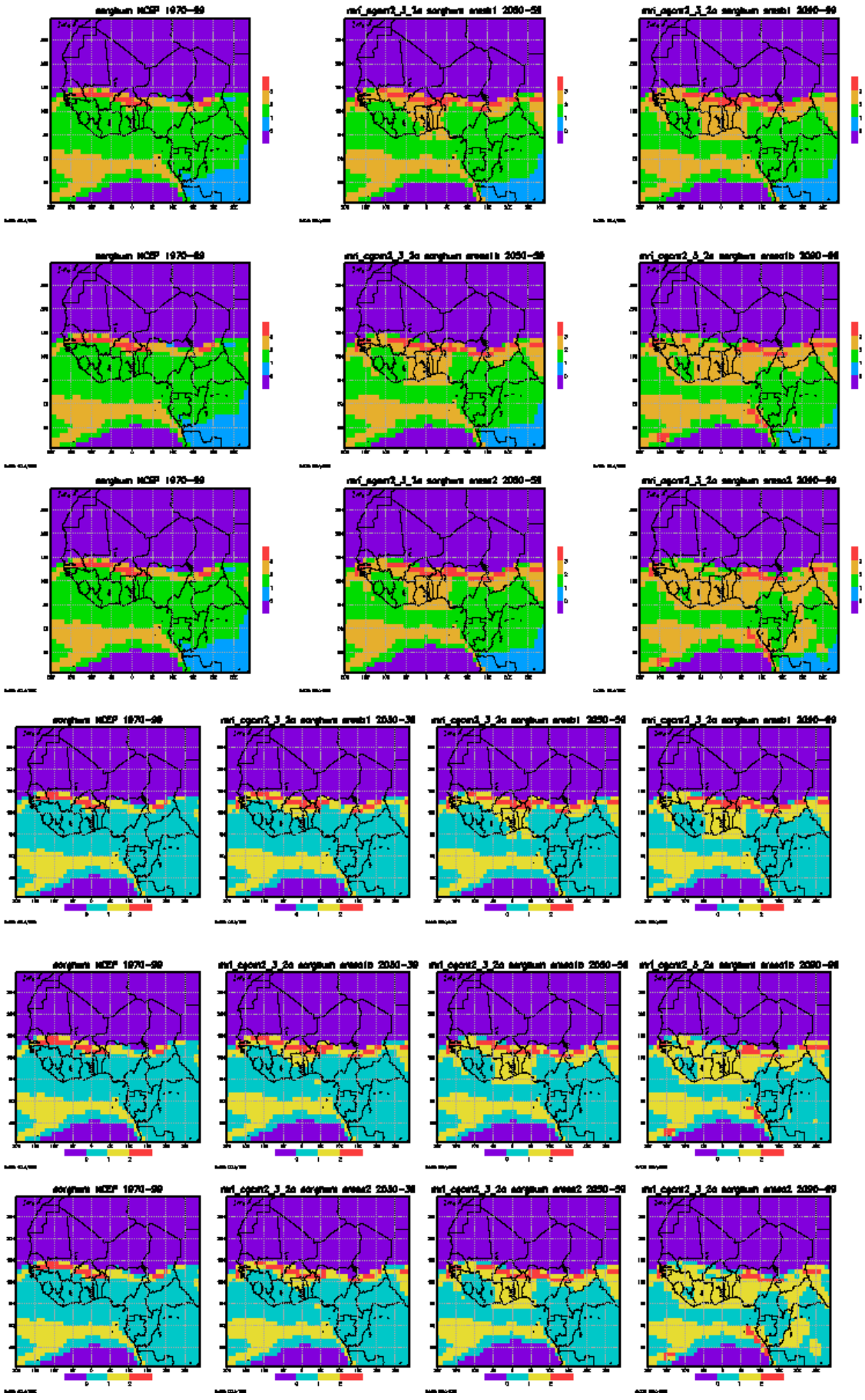

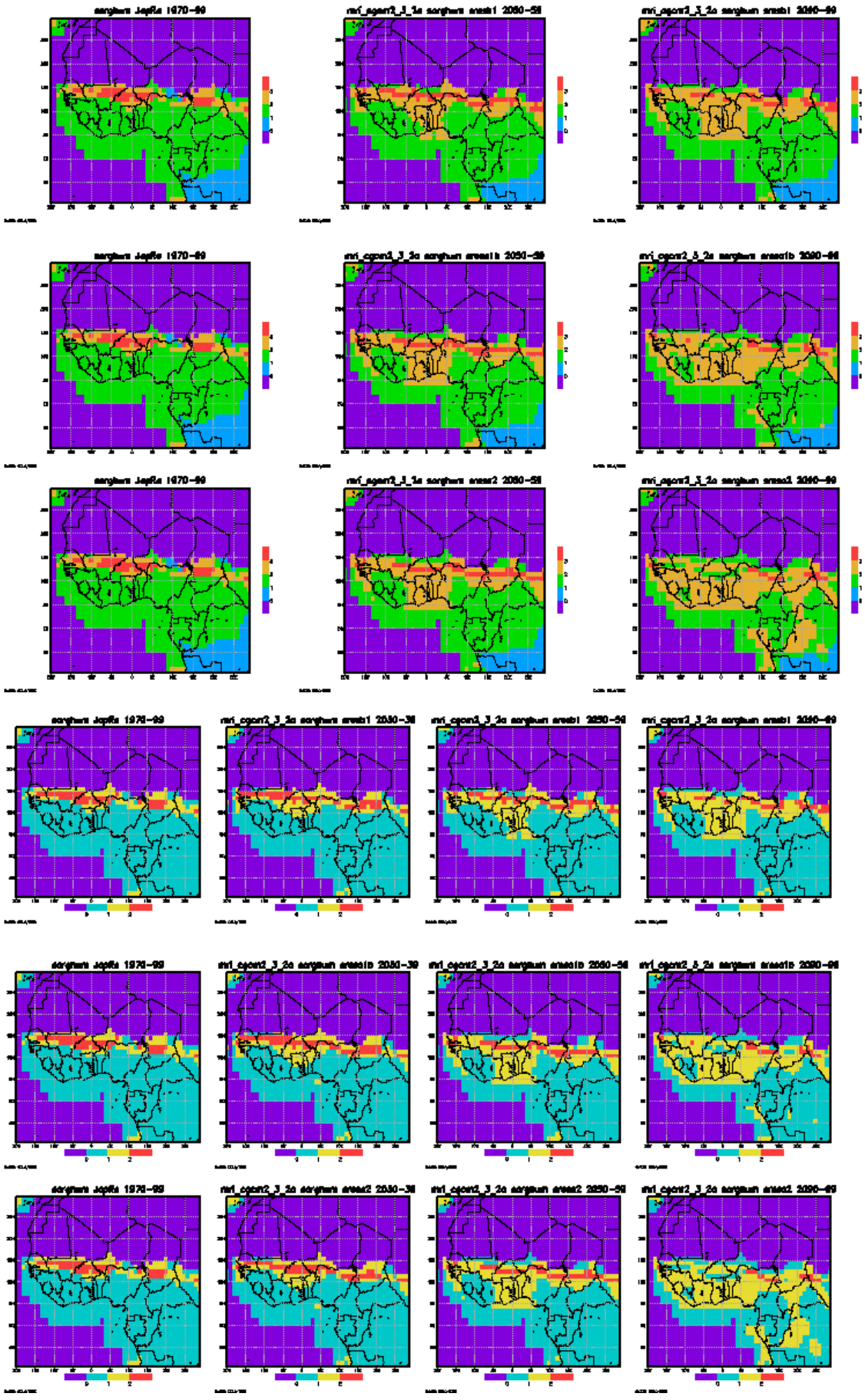

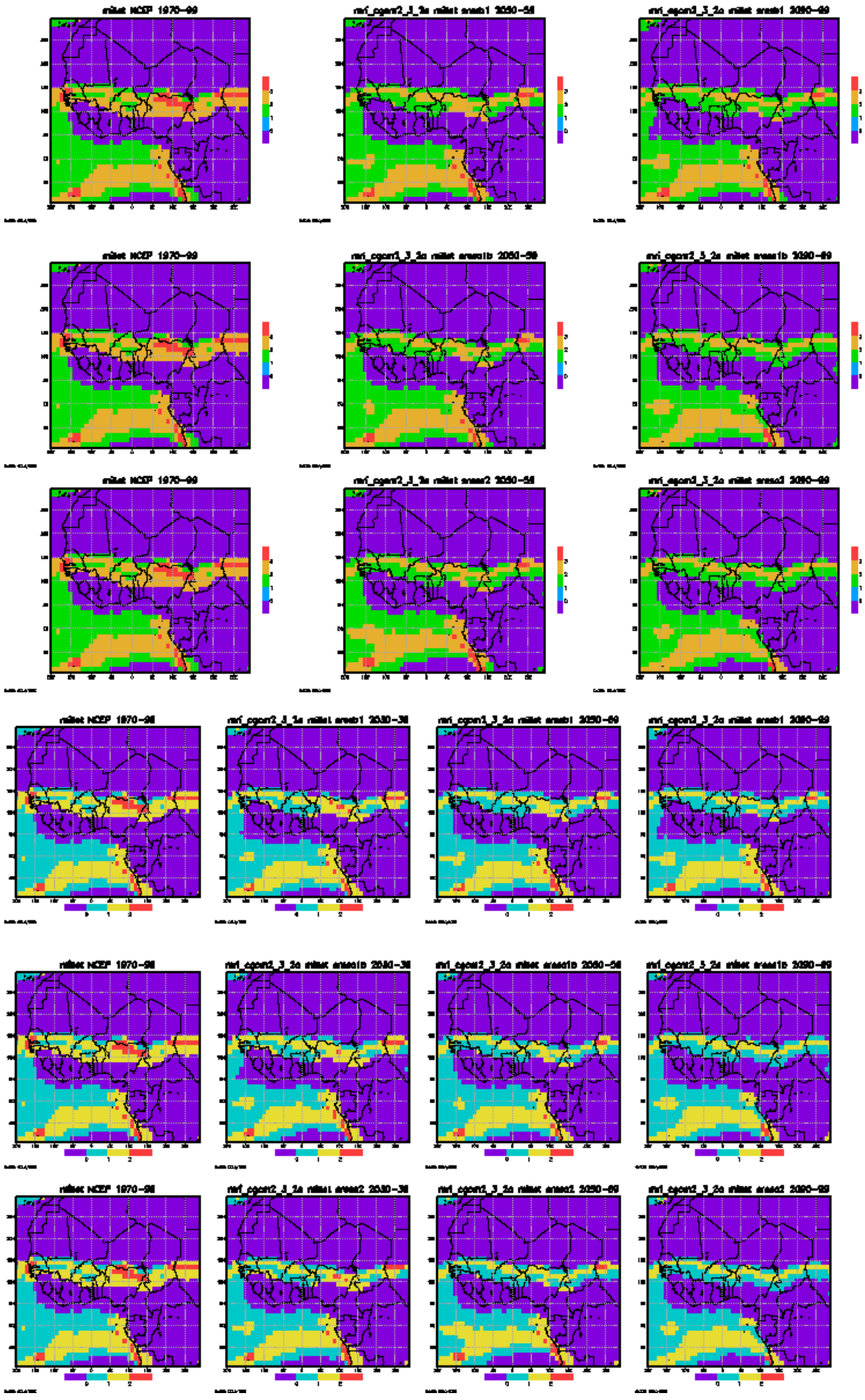

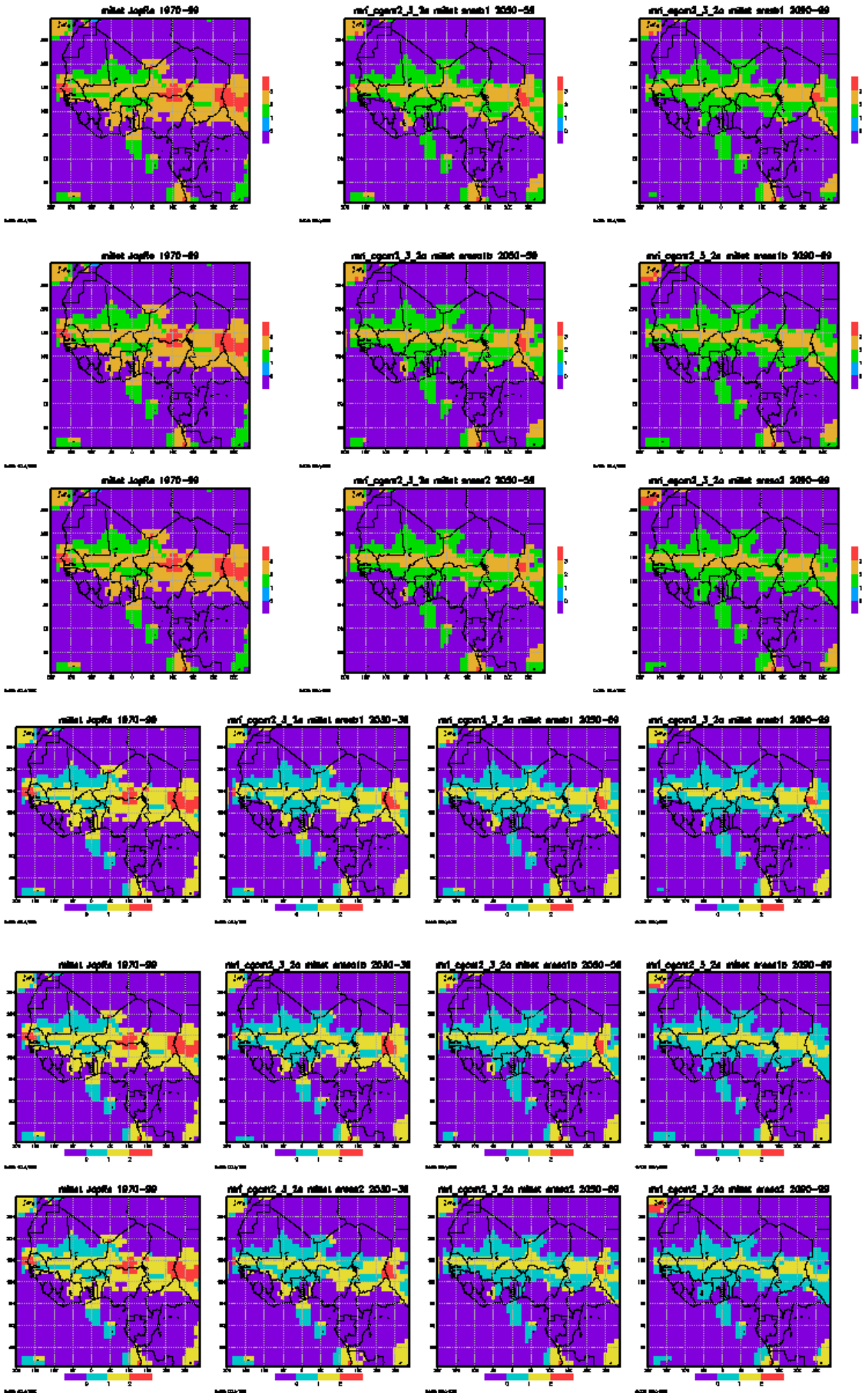

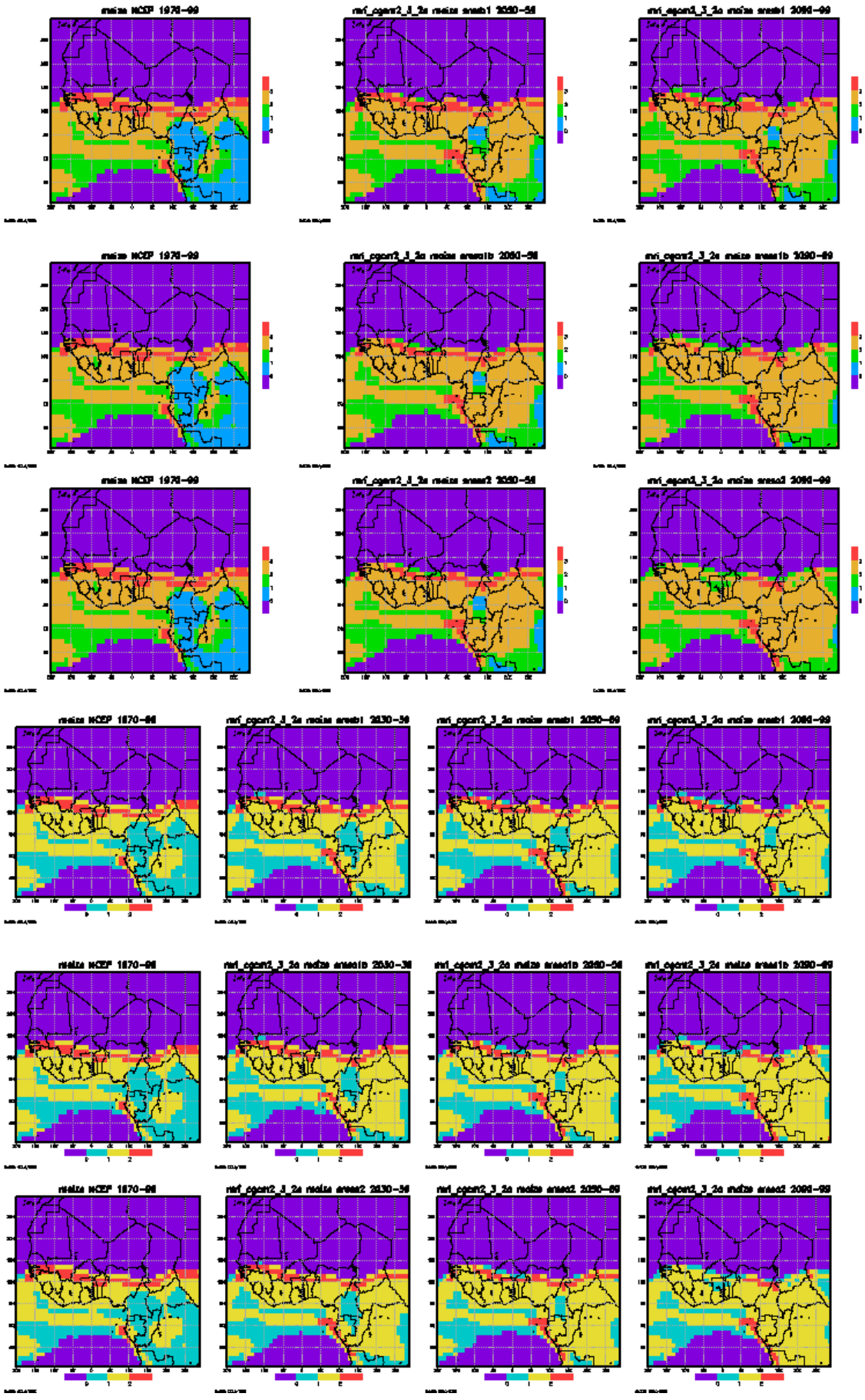

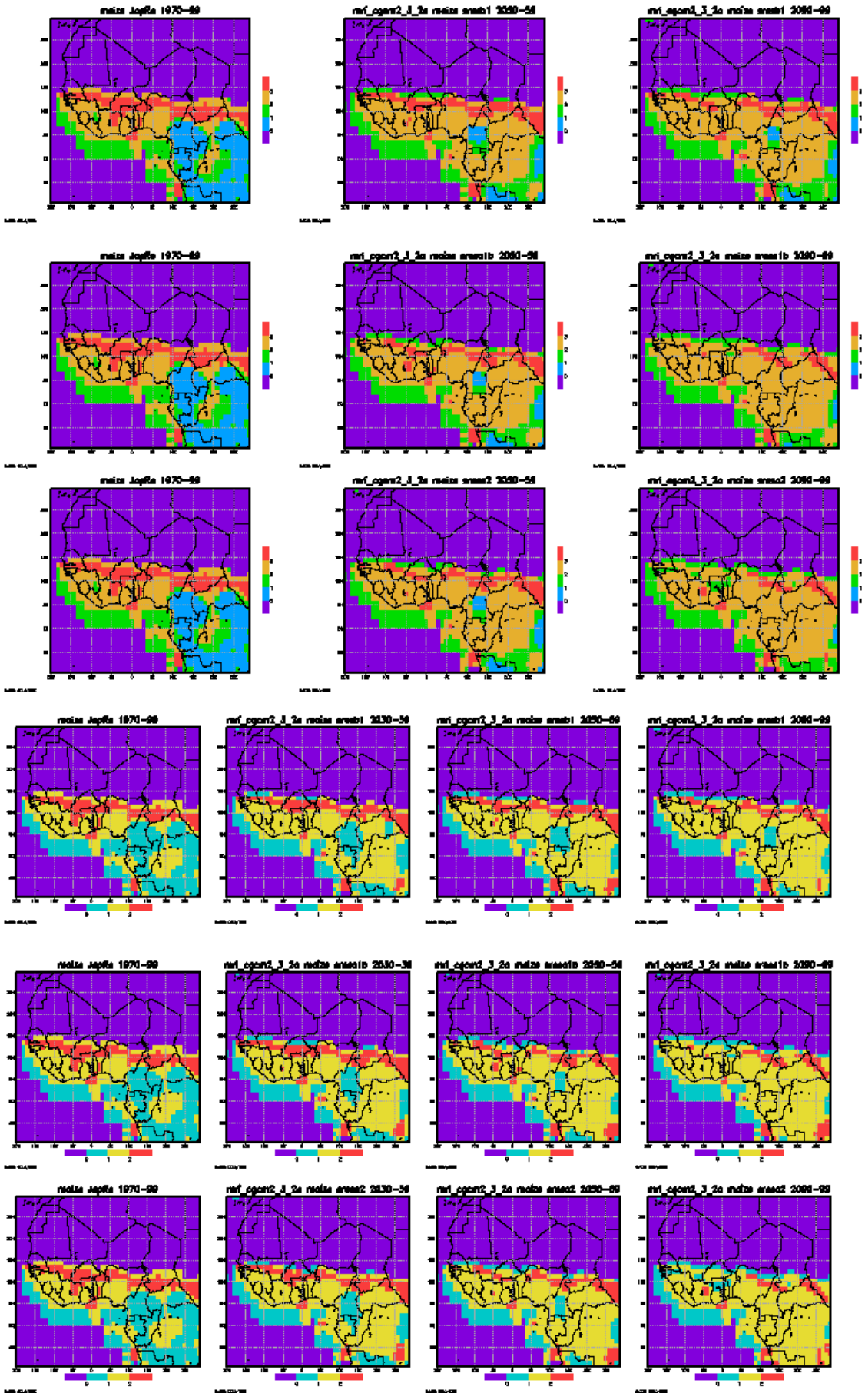

References

Alexander L, et al. 2006. Global observed changes in daily climate extremes of temperature and precipitation. *Journal of Geophysical Research* 111: D05109.

Ati O, et al. 2002. A comparison of methods to determine the onset of the growing season in northern Nigeria. *International Journal of Climatology* 22: 731–742.

Biasutti M, Giannini A. 2006a. Robust Sahel drying in response to late 20th century forcings. *Geophysical Research Letters* 11: L11706.

Biasutti M, Giannini A. 2006b. The impact of decadal-scale Indian Ocean sea surface temperature anomalies on Sahelian rainfall and the North Atlantic Oscillation. *Geophysical Research Letters* 30: 2169.

Biasutti M, et al. 2008. SST forcings and Sahel rainfall variability in simulations of the twentieth and twenty-first centuries. *Journal of Climate* 21: 3471-3486.

Biasutti M, et al. 2009. The role of the Sahara low in summertime Sahel rainfall variability and change in the CMIP3 models. *Journal of Climate* 22: 5755-5771.

Biasutti M, Sobel A. 2009. Delayed Sahel rainfall and global seasonal cycle in a warmer climate. *Geophysical Research* 36: L23707.

Brown S, et al. 2008. Global changes in extreme daily temperature since 1950. *Journal of Geophysical Research* 113: D05115.

Caesar J, et al. 2006. Large-scale changes in observed daily maximum and minimum temperatures: Creation and analysis of a new gridded data set. *Journal of Geophysical Research* 111: D05101.

Caminade C, Terray L. 2009. Twentieth century Sahel rainfall variability as simulated by the ARPEGE AGCM, and future changes. *Climate Dynamics* 35: 75-94.

Chen C, Knutson T. 2008. On the verification and comparison of extreme rainfall indices from climate models. *Journal of Climate* 21: 1605–1621.

Chou C, Neelin J. 2004. Mechanisms of global warming impacts on regional tropical precipitation. *Journal of Climate* 17(13): 2688–2701.

Cook K. 2008. Climate science: the mysteries of Sahel droughts. *Nature Geoscience* 1(10): 647–648.

Cook K, Vizy E. 2008. Coupled model simulations of the West African monsoon system: Twentieth and twenty first century simulations. *Journal of Climate* 19: 3681-3703.

Dai A. 2006. Precipitation characteristics in eighteen coupled climate models. *Journal of Climate* 19: 4605–4630.

Dai A, et al. 2004. The recent Sahel drought is real. *International Journal of Climatology* 24: 1323–1331.

Delworth T, et al. 2006. GFDL's CM2 global coupled climate models. Part I: Formulation and simulation characteristics. *Journal of Climate* 19: 643–674.

Dingkuhn M, et al. 2006. Past, present and future criteria to breed crops for water-limited environments in West Africa. *Agricultural Water Management* 80(1 – 3): 241 – 261.

Dodd D, Jolliffe T. 2001. Early detection of the start of the wet season in semiarid tropical climates of western Africa. *International Journal of Climatology* 21: 1251–1262.

Druyan L. 2010. Studies of 21st-century precipitation trends over West Africa. *International Journal of Climatology* 31: 1415-1424.

Easterling D, et al. 2003. CCI/CLIVAR Workshop to develop priority climate indices. *Bulletin of the American Meteorological Society* 84: 1403–1407.

Flato G, Boer G. 2001. Warming asymmetry in climate change simulations. *Geophysical Research Letters* 28: 195-198.

Folland C, et al. 1986. Sahel rainfall and worldwide sea temperatures, 1901–85. *Nature* 320: 602–607.

Fontaine B, et al. 2002. Spring to summer changes in the West African monsoon through NCEP/NCAR reanalyses (1968–1998). *Journal of Geophysical Research* 107: 4186-4195.

Fontaine B, Louvet S. 2006. Sudan–Sahel rainfall onset: Definition of an objective index, types of years, and experimental hindcast. *Journal of Geophysical Research* 111: D20103.

Fontaine B, et al. 2010. Recent changes in precipitation, ITCZ convection and northern tropical circulation over North Africa (1979–2007). *International Journal of Climatology* 31: 633–648.

Frei C, et al. 2006. Future change of precipitation extremes in Europe: Intercomparison of scenarios from regional climate models, *Journal of Geophysical Research* 111: D06105.

Frei C, Schar C. 2001. Detection probability of trends in rare events: theory and application to heavy precipitation in the alpine region. *Journal of Climate* 14: 1568–1584.

Giannini A. 2010. Mechanisms of climate change in the semiarid African Sahel: the local view. *Journal of Climate* 23: 743–756.

Giannini A, et al. 2008. A global perspective on African climate change. *Climatic Change* 90: 359-383.

Giannini A, et al. 2008. A climate model-based review of drought in the Sahel: Desertification, the re-greening and climate change. *Global and Planetary Change* 64: 119–128.

Gleckler P, et al. 2008. Performance metrics for climate models. *Journal of Geophysical Research* 113: D06104.

Gnanadesikan A, et al. 2006. GFDL's CM2 global coupled climate models. Part II: The baseline ocean simulation. *Journal of Climate* 19: 675-697.

Gordon H, et al. 2002. *The CSIRO Mk3 Climate System Model*. CSIRO Atmospheric Research Technical Paper no. 60. Aspendale: CSIRO Atmospheric Research.

Grist J, Nicholson S. 2001. A study of the dynamic factors influencing the rainfall variability in the West African Sahel. *Journal of Climate* 14: 1337–1359.

Grodsky S, et al. 2003. Near surface westerly wind jet in the Atlantic ITCZ. *Geophysical Research Letters* 30: 2009-2012.

Gu G, Adler R. 2004. Seasonal evolution and variability associated with the West African monsoon system. *Journal of Climate* 17: 3364-3377.

Haarsma R, et al. 2005: Sahel rainfall variability and response to greenhouse warming. *Geophysical Research Letters* 32: L17702.

Hagos S, Cook K., 2007. Dynamics of the West African monsoon jump. *Journal of Climate* 20: 5264–5284.

Hagos S, Cook K. 2008. Ocean warming and late-twentieth-century Sahel drought and recovery. *Journal of Climate* 21(15): 3797–3814.

Hastenrath S. 1984. Interannual variability and the annual cycle: Mechanisms of circulation and climate in the tropical Atlantic sector. *MonthlyWeather Review* 112(6): 1097–1107.

Held I, et al. 2005. Simulation of Sahel drought in the 20th and 21st centuries. *Proceedings of the National Academy of Sciences* 102(50): 17891–17896.

Hewitson B, Crane R. 2006. Consensus between GCM climate change projections with empirical downscaling: precipitation downscaling over South Africa. *International Journal of Climatology* 26: 1315–1337.

Hirabayashi Y, et al. 2008. A 59-year (1948-2006) global near-surface meteorological data set for land surface models. Part I: Development of daily forcing and assessment of precipitation intensity. *Hydrological Research Letters* 2: 36-40.

Hoerling M, et al. 2006. Detection and attribution of 20th century northern and southern African rainfall change. *Journal of Climate* 19(16): 3989–4008.

Hulme M. 1992. A 1951-80 global land precipitation climatology for the evaluation of general circulation models. *Climate Dynamics* 7: 57–72.

[IPCC] Intergovernmental Panel on Climate Change. 2007. *Climate Change 2007: The Physical Science Basis. Contribution of Working Group I to the Fourth Assessment Report of the Intergovernmental Panel on Climate Change.* Solomon S, et al., eds.

Janicot S. 1992. Spatiotemporal variability of Wet African rainfall. Part 1: regionalizations and typings. *Journal of Climate* 5: 489–497.

Janowiak J. 1988. An investigation into interannual rainfall variability in Africa. *Journal of Climate* 1: 240-255.

Kalnay E, et al. 1996. The NCEP/NCAR 40-year reanalysis project. *Bulletin of the American Meteorological Society* 77: 437-471.

Kamga A, et al. 2005. Evaluating the National Center for Atmospheric Research climate system model over West Africa: Present-day and the 21st century A1 scenario. *Journal of Geophysical Research* 110: D03106.

Kharin V, Zwiers F. 2005. Estimating extremes in transient climate change simulations. *Journal of Climate* 18: 1156-1173.

Kharin V, et al. 2007. Changes in temperature and precipitation extremes in the IPCC ensemble of global coupled model simulations. *Journal of Climate* 20: 1419-1444.

Kiktev D, et al. 2003. Comparison of modeled and observed trends in indices of daily climate extremes. *Journal of Climate* 16: 3560–3571.

Klein Tank A, Können G. 2003. Trends in indices of daily temperature and precipitation extremes in Europe, 1946–1999. *Journal of Climate* 16: 3665–3680.

Knight J, et al. 2006. Climate impacts of the Atlantic multidecadal oscillation. *Geophysical Research Letters* 33: L17706.

Konare A, et al. 2008. A regional climate modeling study of the effect of desert dust on the West African monsoon. *Journal of Geophysical Research* 113: D12206.

Lamb P. 1978. Case studies of Tropical Atlantic surface circulation patterns during recent Sub-Saharan weather anomalies: 1967 and 1968. *Monthly Weather Review* 106: 482–491.

Lamb P. 1978. Large-scale tropical Atlantic surface circulation patterns associated with sub-Saharan weather anomalies. *Tellus* 30: 240–251.

Laux P, et al. 2008. Predicting the regional onset of the rainy season in West Africa. *International Journal of Climatology* 28: 329–342.

Lavaysse C, et al. 2009. Seasonal evolution of the West African heat low: a climatological perspective. *Climate Dynamics* 33(2–3): 313–330.

Le Barbé L, Lebel T. 1997. Rainfall climatology of the HAPEX-Sahel region during the years 1950–1990. *Journal of Hydrology* 188–189: 43–73.

Le Barbé L, et al. 2002. Rainfall variability in West Africa during the years 1950–1990. *Journal of Climate* 15: 187–202.

Lebel T, Ali A. 2009. Recent trends in the Central and Western Sahel rainfall regime (1990–2007) *Journal of Hydrology* 375(1-2): 52-64.

Lebel T, et al. 2003. Seasonal cycle and interannual variability of the Sahelian rainfall at hydrological scales. *Journal of Geophysical Research* 108: 1401–1411.

Lebel T, et al. 2009. AMMA-CATCH studies in the Sahelian region of West-Africa: an overview. *Journal of Hydrology* 375(1–2): 3–13.

Legutke S, Voss R. 1999. *The Hamburg Atmosphere-Ocean Coupled Circulation Model ECHO-G.* Technical Report 18. Hamburg: Deutsches Klimarechenzentrum.

Lu J, Delworth T. 2005. Oceanic forcing of the late 20th century Sahel drought. *Geophysical Research Letters* 32: L22706.

Marteau R, et al. 2009. Spatial coherence of monsoon onset over western and central Sahel (1950–2000). *Journal of Climate* 22: 1313-1324.

Mathon V, et al. 2002: Mesoscale convective system rainfall in the Sahel. *Journal of Applied Meteorology* 41: 1081–1092.

Mathon V, Laurent H. 2001. Life cycle of Sahelian mesoscale convective cloud systems. *Quarterly Journal of the Royal Meteorological Society* 127: 377–406.

McFarlane N, et al. 2005. *The CCCma third generation atmospheric general circulation model*. CCCma Internal Report. (Available from http://www.cccma.ec.gc.ca/papers/jscinocca/AGCM3_report.pdf) (Accessed 13 February 2012).

Meehl G, et al. 2000. Trends in extreme weather and climate events: Issues related to modeling extremes in projections of future climate change. *Bulletin of the American Meteorological Society* 81: 427–436.

Meehl G, et al. 2007. The WCRP CMIP3 multimodel dataset: A new era in climate change research. *Bulletin of the American Meteorological Society* 88(9): 1383–1394.

Min S, et al. 2009. Signal detectability in extreme precipitation changes assessed from twentieth century climate simulations. *Climate Dynamics* 32(1): 95-111.

Mitchell T, Jones P. 2005. An improved method of constructing a database of monthly climate observations and associated high-resolution grids. *International Journal of Climatology* 25: 693-712.

Moberg A, Jones P. 2005. Trends in indices for extremes in daily temperature and precipitation in central and western Europe, 1901–99. *International Journal of Climatology* 25: 1149–1171.

Mohino E, et al. 2010. Sahel rainfall and decadal to multi-decadal sea surface temperature variability. *Climate Dynamics* 37: 419-440.

Mohr K, Thorncroft C. 2006. Intense convective systems in West Africa and their relationship to the African easterly jet. *Quarterly Journal of the Meteorological Society* 132: 163–176.

Murphy J. 1999. An evaluation of statistical and dynamical techniques for downscaling local climate. *Journal of Climate* 12: 2256–2284.

Neelin J, et al. 2003. Tropical drought regions in global warming and El Niño teleconnections. *Geophysical Research Letters* 30(24): 2275.

Nicholson S. 1980. The nature of rainfall fluctuations in sub-tropical West-Africa. *Monthly Weather Review* 108: 473–487.

Nicholson S. 2000. Land surface processes and Sahel climate. *Reviews of Geophysics* 38: 117–139.

Nicholson S. 2001. Climatic and environmental change in Africa during the last two centuries. *Climate Research* 17: 123–144.

Nicholson S. 2009. A revised picture of the structure of the "monsoon" and land ITCZ over West Africa. *Climate Dynamics* 32: 1155-1171.

Nicholson S, Grist J. 2003. The seasonal evolution of the atmospheric circulation over West Africa and Equatorial Africa. *Journal of Climate* 16: 1013–1030.

Nicholson S, et al. 2000. An analysis on recent rainfall conditions in West Africa, including the rainy season of 1997 ENSO year. *Journal of Climate* 13: 2628–2640.

Nicholson S, et al. 1998. Desertification, drought and surface vegetation: an example from the West African Sahel. *Bulletin of the American Meteorological Society* 79: 815–829.

Omotosho J. 1990. Onset of thunderstorms and precipitation over northern Nigeria. *International Journal of Climatology* 10: 849–860.

Omotosho J. 1992. Long-range prediction of the onset and end of the rainy season in the West African Sahel. *International Journal of Climatology* 12: 369–382.

Paeth H, Thamm H. 2007. Regional modeling of future African climate north of 15 degrees S including greenhouse warming and land degradation. *Climatic Change* 83(3): 401–427.

Paeth H, et al. 2008. Climate change and food security in tropical West Africa—a dynamic-statistical modelling approach. *Erdkunde* 62: 101–115.

Paeth H, et al. 2009. Regional climate change in tropical and Northern Africa due to greenhouse forcing and land use changes. *Journal of Climate* 22: 114–132.

Paeth H. 2010. Postprocessing of simulated precipitation for impact research in West Africa. Part I: model output statistics for monthly data. *Climate Dynamics* 36(7-8): 1321-1336.

Patricola C, Cook K. 2010a. Northern African Climate at the end of the 21st Century: integrated application of regional and global climate models. *Climate Dynamics* 35: 193-212.

Patricola C, Cook K. 2010b. Sub-Saharan Northern African climate at the end of the twenty-first century: forcing factors and climate change processes. *Climate Dynamics* 37: 1165-1188.

Philippon N, et al. 2010. Skill, reproducibility and potential predictability of the West African monsoon in coupled GCMs. *Climate Dynamics* 35(1): 53-74.

Prospero J, Lamb P. 2003. African droughts and dust transport to the Caribbean: Climate change implications. *Science* 302: 1024–1027.

Pu B, Cook K. 2010. Dynamics of the West African Westerly Jet. *Journal of Climate* 23: 6263-6276.

Ramel R, et al. 2006. On the northward shift of the West African monsoon. *Climate Dynamics* 26: 429–440.

Roeckner E, et al. 2006. Sensitivity of simulated climate to horizontal and vertical resolution in the ECHAM5 atmosphere model. *Journal of Climate* 19: 3771-3791.

Rotstayn L, Lohmann U. 2002. Tropical rainfall trends and the indirect aerosol effect. *Journal of Climate* 15(15): 2103–2116.

Rowell D, et al. 1995. Variability of summer rainfall over tropical North Africa (1906–1992): observations and modelling. *Quarterly Journal of the Royal Meteorological Society* 121: 669–704.

Salas y Melia D, et al. 2005. *Description and validation of CNRM-CM3 global coupled climate model.* Note de centre GMGEC (internal publication), CNRM, 103.

Schmidt G, et al. 2005. Present day atmospheric simulations using GISS ModelE: Comparison to in-situ, satellite and reanalysis data. *Journal of Climate* 19: 153-192.

Sijikumar S, et al. 2006. Monsoon onset over Sudan–Sahel: simulation by the regional scale model MM5. *Geophysical Research Letters* 33: L03814.

Sivakumar M. 1988. Predicting rainy season potential from the onset of rains in southern Sahelian and Sudanian climatic zones of West Africa. *Agricultural and Forest Meteorology* 42: 295–305.

Sillmann J, Roeckner E. 2008. Indices for extreme events in projections of anthropogenic climate change. *Climatic Change* 86: 83–104.

Sivakumar M, et al. 2000. Agrometeorology and sustainable agriculture. *Agricultural and Forest Meteorology* 103: 11-26.

Stern R, et al. 1981: The start of the rains in West Africa. International Journal of Climatology 1: 59–68.

Stouffer R, et al. 2006. GFDL's CM2 Global Coupled Climate Models. Part IV: Idealized Climate Response. *Journal of Climate* 19: 723-740.

Sultan B, Janicot S. 2003. The West African monsoon dynamics. Part II. The “preonset” and “onset” of the summer monsoon. *Journal of Climate* 16(21): 3407–3427.

Sultan B, et al. 2005. Agricultural impacts of the large-scale variability of the West African monsoon. *Agricultural and Forest Meteorology* 128: 93–110.

Sultan B, et al. 2010. Multi-scales and multi-sites analyses of the role of rainfall in cotton yields in West Africa. *International Journal of Climatology* 30: 58–71.

Sylla M, et al. 2009. High resolution simulations of West Africa climate using Regional Climate Model (RegCM3) with different lateral boundary conditions. Theoretical and Applied Climatology 98: 293-314.

Sylla M. 2009. Multiyear simulation of the African climate using a regional climate model (RegCM3) with the high resolution ERA-interim reanalysis. *Climate Dynamics* 35: 231-247.

Tadross M, et al. 2005. The interannual variability of the onset of the maize growing season over South Africa and Zimbabwe. *Journal of Climate* 18: 3356–3372.

Tapiador F, Sanchez E. 2008. Changes in the European precipitation climatologies as derived by an ensemble of regional models. *Journal of Climate* 21: 2540-2557.

Tebaldi C, et al. 2006. Going to the extremes: An intercomparison of model-simulated historical and future changes in extreme events. *Climatic Change* 79: 185-211.

Ting M, et al. 2009. Forced and internal twentieth-century SST trends in the North Atlantic. *Journal of Climate* 22(6): 1469–1481.

Trenberth K. 2010. Changes in precipitation with climate change. *Climate Research* 47: 123-138.

Trenberth K, et al. 2003. The changing character of precipitation. *Bulletin of the American Meteorological Society* 84: 1205-1217.

Turner A, et al. 2009. Modelling monsoons: understanding and predicting current and future behaviour. In: Chang CP, et al. (eds.) *The global monsoon system: research and forecast.* Singapore: World Scientific Publishing. p 421-454.

Uppala S, et al. 2005. The ERA-40 reanalysis. *Quarterly Journal of the Royal Meteorological Society* 131: 2961–3012.

Vavrus S, et al. 2006. The behavior of extreme cold air outbreaks under greenhouse warming. *International Journal of Climatology* 26: 1133-1147.

Vizy E, Cook K. 2001. Mechanism by which Gulf of Guinea and eastern North Atlantic sea surface temperature anomalies can influence African rainfall. *Journal of Climate* 15: 795–821.

Vizy E, Cook K. 2002. Development and application of a mesoscale climate model for the tropics: Influence of sea surface temperature anomalies on the West African monsoon. *Journal of Geophysical Research* 107: 4023-4044.

Walter M. 1967. Length of rainy season in Nigeria. *Nigerian Geography Journal* 10: 123–128.

Ward M. 1998. Diagnosis and short lead time prediction of summer rainfall in Tropical North Africa at interannual and multidecadal timescales. *Journal of Climate* 11: 3167-3191.

Webb M, et al.2006. On the contribution of local feedback mechanisms to the range of climate sensitivity in two GCM ensembles. *Climate Dynamics* 27: 1–22.

Wilby R. 2009. *Review of Recent Trends and Projected Climate Changes for Niger, West Africa.* (Available from http://www.worldwaterweek.org/documents/WWW_PDF/Resources/2009_WnC/Niger-SS_Technical_Brief_R_Wilby.pdf) (Accessed 13 February 2012).

Wittenberg A, et al. 2006. GFDL's CM2 Global Coupled Climate Models. Part III: Tropical Pacific Climate and ENSO. *Journal of Climate* 19: 698-722.

Xue Y, et al. 2010. The West African Monsoon Modeling and Evaluation project (WAMME) and its first model intercomparison experiment. *Bulletin of the American Meteorological Society.*

Yoshioka M, et al. 2007. Impact of desert dust radiative forcing on Sahel precipitation: relative importance of dust compared to sea surface temperature variations, vegetation changes and greenhouse gas warming. *Journal of Climate* 20: 1445–1467.

Yukimoto S, et al. 2001. A new Meteorological Research Institute coupled GCM (MRI-CGCM2) - its climate and variability. *Papers in Meteorology and Geophysics* 51: 47-88.

Zhang R, Delworth T. 2006. Impact of Atlantic multidecadal oscillations on India/Sahel rainfall and Atlantic hurricanes. *Geophysical Research Letters* 33: L17712.

Zhou T, et al. 2008. Ocean forcing to changes in global monsoon precipitation over the recent half-century. *Journal of Climate* 21: 3833–3852.